

ISTANBUL TECHNICAL UNIVERSITY ★ GRADUATE SCHOOL OF SCIENCE
ENGINEERING AND TECHNOLOGY

**DETERMINING OPTIMUM SULPHUR CONTENT AS AN ALTERNATIVE
BINDER ADDITIVE IN ASPHALTIC CONCRETE PAVEMENTS**

Ph.D. THESIS

Abdulgazi GEDIK

Civil Engineering Department

Transport Engineering Program

FEBRUARY 2016

ISTANBUL TECHNICAL UNIVERSITY ★ GRADUATE SCHOOL OF SCIENCE
ENGINEERING AND TECHNOLOGY

**DETERMINING OPTIMUM SULPHUR CONTENT AS AN ALTERNATIVE
BINDER ADDITIVE IN ASPHALTIC CONCRETE PAVEMENTS**

Ph.D. THESIS

**Abdulgazi GEDIK
(501082404)**

Civil Engineering Department

Transport Engineering Program

Thesis Advisor: Prof. Dr. Abdullah Hilmi LAV

FEBRUARY 2016

İSTANBUL TEKNİK ÜNİVERSİTESİ ★ FEN BİLİMLERİ ENSTİTÜSÜ

**ESNEK YOL ÜSTYAPILARINDA BİTÜM İLE BİRLİKTE BAĞLAYICI
OLARAK OPTİMUM SÜLFÜR ORANININ VE PERFORMANSININ
BELİRLENMESİ**

DOKTORA TEZİ

**Abdulgazi GEDİK
(501082404)**

İnşaat Mühendisliği Anabilim Dalı

Ulaştırma Mühendisliği Programı

Tez Danışmanı: Prof. Dr. Abdullah Hilmi LAV

ŞUBAT 2016

Abdulgazi GEDIK, a Ph.D. student of ITU Graduate School of Science Engineering and Technology student ID **501082404**, successfully defended the thesis entitled "**DETERMINING OPTIMUM SULPHUR CONTENT AS AN ALTERNATIVE BINDER ADDITIVE IN ASPHALTIC CONCRETE PAVEMENTS**", which he prepared after fulfilling the requirements specified in the associated legislations, before the jury whose signatures are below.

Thesis Advisor : **Prof. Dr. Abdullah Hilmi LAV**
Istanbul Technical University

Jury Members : **Prof. Dr. Hulusi OZKUL**
Istanbul Technical University

Prof. Dr. Reha ARTAN
Istanbul Technical University

Prof. Dr. Necati KULOGLU
Firat University

Assoc. Prof. Dr. Mehmet YILMAZ
Firat University

Date of Submission : 04 January 2016
Date of Defense : 15 February 2016

To my father,

FOREWORD

I would like to express my deepest appreciation and gratitude to my supervisor Prof. Dr. Abdullah Hilmi LAV for his constant encouragement, guidance, and suggestions, without whose knowledge and assistance this study would not have been possible. Always, he has been there supporting, guiding, and teaching me not only in this study but also in every part of my life. We spent a long time working together, and I promise not to forget him. I thank the lecturers and staff at Firat University Civil Engineering Department for their remarkable help in conducting my experimental laboratory test through my thesis. I thank Assoc. Prof. Dr. Mehmet YILMAZ for sharing his expertise in pavement engineering with me and providing me recommendations for my thesis. Last but certainly not least, I extend my sincere appreciation and love to my parents, my workmates, and friends for their great love, support, and understanding. I am greatly indebted to my parents who have given me love, encouragement, and confidence. Special thanks to my chief engineer Suat OZBAY for his worthy support and help. I will be always remembering great contributions of Fatih DEMIRELLI and Engin TUTAR who are skillful technician at General Directorate of Highways, Republic of Turkey.

January 2016

Abdulgazi GEDIK
(Civil Engineer)

TABLE OF CONTENTS

	<u>Page</u>
FOREWORD.....	ix
TABLE OF CONTENTS.....	xi
ABBREVIATIONS	xiii
LIST OF TABLES	xv
LIST OF FIGURES	xix
SUMMARY	xxvii
ÖZET.....	xxix
1. INTRODUCTION.....	1
2. THE PURPOSE OF THIS THESIS	11
3. PROPERTIES OF SULPHUR AND ITS USE.....	13
3.1 Sulphur Review	13
3.2 Physical and Chemical Properties of Sulphur	17
3.3 Sulphur Resources.....	18
3.3.1 Natural sulphur resources.....	19
3.3.2 Other resources	22
3.4 Sulphur in Turkey.....	22
4. UTILIZATION OF SULPHUR IN HIGHWAY CONSTRUCTION	25
5. EXPERIMENTAL STUDY.....	29
5.1 First Generation Tests	29
5.1.1 Penetration test.....	29
5.1.2 Softening point temperature test	32
5.1.3 Penetration index.....	34
5.1.4 Specific gravity test.....	40
5.1.5 Viscosity test	43
5.1.6 Aging and loss on heating test	46
5.2 SUPERPAVE Tests.....	67
5.2.1 Rotational viscometer (RV) test.....	68
5.2.2 Dynamic shear rheometer (DSR) test	72
5.2.3 Rolling thin film oven test (RTFOT)	81
5.2.4 Pressure aging vessel (PAV)	81
5.2.5 Bending beam rheometer (BBR) test	81
5.3 Morphology Analysis.....	88
6. EXPERIMENTAL RESULTS.....	91
6.1 First Generation Test Results	91
6.1.1 Penetration test results	91
6.1.2 Softening point temperature test results	95
6.1.3 Penetration index results	101
6.1.4 Specific gravity results.....	105
6.2 SUPERPAVE Test Results	108
6.2.1 Mass change results	108

6.2.2 Viscosity test results.....	112
6.2.3 Dynamic shear rheometer (DSR) results.....	138
6.2.4 Bending beam rheometer (BBR) results	278
6.3 Morphology Analysis Results	287
7. COST ANALYSIS.....	301
8. CONCLUSIONS.....	303
REFERENCES	305
APPENDICES	315
APPENDIX A	316
CURRICULUM VITAE	365

ABBREVIATIONS

AASHTO	: American Association of State Highway and Transportation Officials
AC	: Asphalt Cement
ACP	: Asphalt Concrete Pavement
AI	: Aging Index
ASTM	: American Society for Testing and Materials
BBR	: Bending Beam Rheometer
BRRC	: Belgian Road Research Center
BST	: Bituminous Surface Treatment
DSR	: Dynamic Shear Rheometer
DTT	: Direct Tensile Test
EN	: European Standard
GRFT	: German Rotating Flask Test
GSF	: Granular Sulphur
HMA	: Hot Mix Asphalt
H-PAT	: High Pressure Aging Test
HRTEM	: High Resolution Transmission Electron Microscopy
ITS	: Indirect Tensile Test
LPG	: Liquefied Petroleum Gas
M-GRFT	: Modified German Rotating Flask Test
M-RAT	: Modified Rotavapor Aging Test
M-RTFOT	: Modified Rolling Thin Film Oven Test
N-RTFOT	: Nitrogen Rolling Thin Film Oven Test
R	: Rheological index
RCAT	: Rotating Cylinder Aging Test
REM	: Reflection Electron Microscope
RPM	: Round Per Minute
RTD	: Resistance Thermal Detector
RTFOT	: Rolling Thin Film Oven Test
RV	: Rotational Viscometer
PAV	: Pressure Aging Vessel
PI	: Penetration Index
POV	: Pressure Oxidation Vessel
PVN	: Penetration Viscosity Number
SEP	: Sulphur Extended Pavement
SHRP	: Strategic Highway Research Program
SUPERPAVE	: Superior PERforming Asphalt PAVEmnts
SEB	: Sulphur Extended Binder
SEM	: Scanning Electron Microscope
SG	: Specific Gravity
STEM	: Scanning Transmission Electron Microscope
SPT	: Softening Point Temperature
TEM	: Transmission Electron Microscope

TFOT : Thin Film Oven Test
TUPRAS : Turkish Petroleum Refineries Company

LIST OF TABLES

	<u>Page</u>
Table 3.1 : Estimated global reservoirs of sulphur.	16
Table 3.2 : Sulphur resources.....	19
Table 3.3 : Sulphur production of TUPRAS.....	23
Table 3.4 : Sulphur consumption in Turkey.....	24
Table 5.1 : Advantages and disadvantages of a penetration test.....	30
Table 5.2 : Typical specific gravity of bitumens at 25°C.....	41
Table 5.3 : Ways to measure specific gravity of bitumens	41
Table 5.4 : Summary to of aging indicators.....	53
Table 5.5 : Comparison of TFOT and RTFOT	57
Table 5.6 : SUPERPAVE tests.....	68
Table 5.7 : Applied stress, plate diameter and plate gap in this study	77
Table 6.1 : Penetration values of SEBs	94
Table 6.2 : Softening point temperature of SEBs	99
Table 6.3 : Penetration index of SEBs	105
Table 6.4 : Specific gravity of SEBs	107
Table 6.5 : Mass change of neat bitumens and SEBs	111
Table 6.6 : Viscosity values	113
Table 6.7 : Showing the equiviscous temperatures of B50/70-0%GSF.....	119
Table 6.8 : Showing the equiviscous temperatures of B50/70-10%GSF.....	119
Table 6.9 : Showing the equiviscous temperatures of B50/70-20%GSF.....	120
Table 6.10 : Showing the equiviscous temperatures of B50/70-30%GSF.....	120
Table 6.11 : Showing the equiviscous temperatures of B50/70-40%GSF	121
Table 6.12 : Showing the equiviscous temperatures of B50/70-50%GSF	121
Table 6.13 : Showing the equiviscous temperatures of B70/100-0%GSF	124
Table 6.14 : Showing the equiviscous temperatures of B70/100-10%GSF	124
Table 6.15 : Showing the equiviscous temperatures of B70/100-20%GSF	125
Table 6.16 : Showing the equiviscous temperatures of B70/100-30%GSF	125
Table 6.17 : Showing the equiviscous temperatures of B70/100-40%GSF	126
Table 6.18 : Showing the equiviscous temperatures of B70/100-50%GSF	126
Table 6.19 : Showing the equiviscous temperatures of B100/150-0%GSF	129
Table 6.20 : Showing the equiviscous temperatures of B100/150-10%GSF	129
Table 6.21 : Showing the equiviscous temperatures of B100/150-20%GSF	130
Table 6.22 : Showing the equiviscous temperatures of B100/150-30%GSF	130
Table 6.23 : Showing the equiviscous temperatures of B100/150-40%GSF	131
Table 6.24 : Showing the equiviscous temperatures of B100/150-50%GSF	131
Table 6.25 : Showing the equiviscous temperatures of B160/220-0%GSF	133
Table 6.26 : Showing the equiviscous temperatures of B160/220-10%GSF	134
Table 6.27 : Showing the equiviscous temperatures of B160/220-20%GSF	134
Table 6.28 : Showing the equiviscous temperatures of B160/220-30%GSF	135

Table 6.29 : Showing the equiviscous temperatures of B160/220-40%GSF	135
Table 6.30 : Showing the equiviscous temperatures of B160/220-50%GSF	136
Table 6.31 : Aging indices for short-term aged SEBs at different temperatures and 1.59Hz.....	142
Table 6.32 : Aging indices for long-term aged SEBs at different temperatures and 1.59Hz.....	143
Table 6.33 : Values of rheological parameters for the B50/70 base bitumen and SEB groups at 0.1Hz before aging.	146
Table 6.34 : Relative changes in complex modulus for the B50/70 base bitumen and SEB groups at 0.1Hz before aging.	148
Table 6.35 : Values of rheological parameters at 0.1Hz following RTFOT aging. 149	
Table 6.36 : Relative changes in complex modulus and aging index at 0.1Hz following short-term aging.....	151
Table 6.37 : Values of rheological parameters at 0.1Hz following PAV aging..... 152	
Table 6.38 : Relative changes in complex modulus and aging index at 0.1Hz following long-term aging.....	153
Table 6.39 : Values of rheological parameters for the B50/70 base bitumen and SEB groups at 0.2517Hz before aging.	154
Table 6.40 : Relative changes in complex modulus for the B50/70 base bitumen and SEB groups at 0.2517Hz before aging.	156
Table 6.41 : Values of rheological parameters for the B50/70 base bitumen and SEB groups at 0.2517Hz after short-term aging.	157
Table 6.42 : Relative changes in complex modulus and aging index at 0.2517Hz following short-term aging.....	159
Table 6.43 : Values of rheological parameters for the B50/70 base bitumen and SEB groups at 0.2517Hz after long-term aging.	160
Table 6.44 : Relative changes in complex modulus and aging index at 0.2517Hz following long-term aging.....	162
Table 6.45 : Values of rheological parameters for the B50/70 base bitumen and SEB groups at 0.6329Hz before aging.	163
Table 6.46 : Relative changes in complex modulus for the B50/70 base bitumen and SEB groups at 0.6329Hz before aging.	165
Table 6.47 : Values of rheological parameters for the B50/70 base bitumen and SEB groups at 0.6329Hz after short-term aging.	166
Table 6.48 : Relative changes in complex modulus and aging index at 0.6329Hz following short-term aging.....	168
Table 6.49 : Values of rheological parameters for the B50/70 base bitumen and SEB groups at 0.6329Hz after long-term aging.	169
Table 6.50 : Relative changes in complex modulus and aging index at 0.6329Hz following long-term aging.....	171
Table 6.51 : Values of rheological parameters for the B50/70 base bitumen and SEB groups at 4.0Hz before aging.	172
Table 6.52 : Relative changes in complex modulus for the B50/70 base bitumen and SEB groups at 4.0Hz before aging.	174
Table 6.53 : Values of rheological parameters for the B50/70 base bitumen and SEB groups at 4.0Hz after short-term aging.	175
Table 6.54 : Relative changes in complex modulus and aging index at 4.0Hz following short-term aging.....	177
Table 6.55 : Values of rheological parameters for the B50/70 base bitumen and SEB groups at 4.0Hz after long-term aging.	178

Table 6.56 : Relative changes in complex modulus and aging index at 4.0Hz following long-term aging.....	180
Table 6.57 : Stiffness values at different temperatures and 1.59Hz (10rad/sn) for B70/100 base bitumen and SEB groups with various GSF content before aging.....	181
Table 6.58 : Stiffness values at different temperatures and 1.59Hz (10rad/sn) for B70/100 base bitumen and SEB groups with various GSF content after short-term aging.....	184
Table 6.59 : Stiffness values at different temperatures and 1.59Hz (10rad/sn) for B70/100 base bitumen and SEB groups with various GSF content after long-term aging.....	187
Table 6.60 : Values of rheological parameters for the B70/100 base bitumen and SEB groups at 0.1Hz before aging.....	188
Table 6.61 : Relative changes in complex modulus for the B70/100 base bitumen and SEB groups at 0.1Hz before aging.....	190
Table 6.62 : Values of rheological parameters for the B70/100 base bitumen and SEB groups at 0.1Hz after short-term aging.....	191
Table 6.63 : Relative changes in complex modulus and aging index at 0.1Hz following short-term aging.....	193
Table 6.64 : Values of rheological parameters at 0.1Hz following sulphur extension.....	194
Table 6.65 : Relative changes in complex modulus and aging index at 0.1Hz following long-term aging.....	196
Table 6.66 : Values of rheological parameters for the B70/100 base bitumen and SEB groups at 0.2517Hz before aging.....	197
Table 6.67 : Relative changes in complex modulus for the B70/100 base bitumen and SEB groups at 0.2517Hz before aging.....	199
Table 6.68 : Values of rheological parameters for the B70/100 base bitumen and SEB groups at 0.2517Hz after short-term aging.....	200
Table 6.69 : Relative changes in complex modulus and aging index at 0.2517Hz following short-term aging.....	202
Table 6.70 : Values of rheological parameters for the B70/100 base bitumen and SEB groups at 0.2517Hz after long-term aging.....	203
Table 6.71 : Relative changes in complex modulus and aging index at 0.2517Hz following long-term aging.....	204
Table 6.72 : Values of rheological parameters for the B70/100 base bitumen and SEB groups at 0.6329Hz before aging.....	206
Table 6.73 : Relative changes in complex modulus for the B70/100 base bitumen and SEB groups at 0.6329Hz before aging.....	208
Table 6.74 : Values of rheological parameters for the B70/100 base bitumen and SEB groups at 0.6329Hz after short-term aging	209
Table 6.75 : Relative changes in complex modulus and aging index at 0.6329Hz following short-term aging.....	211
Table 6.76 : Values of rheological parameters for the B70/100 base bitumen and SEB groups at 0.6329Hz after long-term aging.....	212
Table 6.77 : Relative changes in complex modulus and aging index at 0.6329Hz following long-term aging.....	214
Table 6.78 : Values of rheological parameters for the B70/100 base bitumen and SEB groups at 4.0Hz before aging	215

Table 6.79 : Relative changes in complex modulus for the B70/100 base bitumen and SEB groups at 4.0Hz before aging.	218
Table 6.80 : Values of rheological parameters for the B70/100 base bitumen and SEB groups at 4.0Hz after short-term aging.	219
Table 6.81 : Relative changes in complex modulus and aging index at 4.0Hz following short-term aging.	221
Table 6.82 : Values of rheological parameters for the B70/100 base bitumen and SEB groups at 4.0Hz after long-term aging.	223
Table 6.83 : Relative changes in complex modulus and aging index at 4.0Hz following long-term aging.	226
Table 6.84 : Changes in phase angle (δ) at 0.1 and 1.59Hz following GSF replacement and aging.	229
Table 6.85 : Changes in complex modulus (G^*) at 0.2517 and 4.0Hz following GSF replacement and aging.	238
Table 6.86 : Showing the changes in complex modulus at 0.2517 and 4.0Hz following RTFOT and PAV aging.	241
Table 6.87 : Changes in phase angle (δ) at 0.2517 and 4.0Hz following GSF extension and aging.	246
Table 6.88 : Values of rheological parameters for the B100/150 base bitumen and SEB groups at 0.6329Hz before aging.	247
Table 6.89 : Relative changes in complex modulus for the B100/150 base bitumen and SEB groups at 0.6329Hz before aging.	249
Table 6.90 : Values of rheological parameters for the B100/150 base bitumen and SEB groups at 0.6329Hz after short-term aging.	250
Table 6.91 : Relative changes in complex modulus and aging index following short-term aging at 0.6329Hz.	252
Table 6.92 : Values of rheological parameters for the B100/150 base bitumen and SEB groups at 0.6329Hz after long-term aging.	252
Table 6.93 : Relative changes in complex modulus and aging index following long-term aging at 0.6329Hz.	254
Table 6.94 : Rheological values of B160/220 base bitumen and B160/220-sulphur -extended-binders at a reference temperature of 25°C before aging, after RTFOT- and PAV-aging.	255
Table 6.95 : Rheological values of B160/220 base bitumen and B160/220-sulphur -extended-binders at a reference temperature of 30°C before aging, after RTFOT- and PAV-aging.	261
Table 6.96 : Rheological values of B160/220 base bitumen and B160/220-sulphur -extended-binders at a reference temperature of 40°C before aging, after RTFOT- and PAV-aging.	267
Table 6.97 : Rheological values of B160/220 base bitumen and B160/220-sulphur -extended-binders at a reference temperature of 50°C before aging, after RTFOT- and PAV-aging.	273
Table 6.98 : A-short-brief of BBR results.	279
Table 6.99 : Element analyses for the series of B50/70 before and after aging.	290
Table 6.100 : Element analyses for the series of B70/100 before and after aging.	294
Table 6.101 : Element analyses for the series of B100/150 before and after aging.	296
Table 6.102 : Element analyses for the series of B160/220 before and after aging.	299

LIST OF FIGURES

	<u>Page</u>
Figure 1.1 : Products of crude oil.....	2
Figure 1.2 : Classification of bitumen.....	4
Figure 1.3 : Refinery process of crude oil.....	6
Figure 3.1 : Natural sulphur and pyrite	14
Figure 3.2 : Pyrite and crushed sulphur	14
Figure 3.3 : Granule sulphur and granular sulphur	15
Figure 3.4 : Block sulphur.....	15
Figure 5.1 : A typical penetrometer	32
Figure 5.2 : A softening point temperature test apparatus	34
Figure 5.3 : Nomograph for penetration index (SP/pen)	37
Figure 5.4 : Nomograph for penetration index (pen/pen)	38
Figure 5.5 : The relationship between chemical composition and the PI	39
Figure 5.6 : The effect of temperature and loading time on stiffness of a high PI bitumen.....	40
Figure 5.7 : Mechanical response of elastic, viscous and viscoelastic materials.....	44
Figure 5.8 : Influence of the initial molecular weight on durability	51
Figure 5.9 : Influence of the time on aging index	51
Figure 5.10 : Equipment of TFOT	56
Figure 5.11 : Pouring the bitumen into an empty jar	59
Figure 5.12 : RTFOT equipment	59
Figure 5.13 : The same RTFOT jar after aging, before aging, and empty.....	60
Figure 5.14 : The German rotating flask test (GRFT) equipment	62
Figure 5.15 : Equipment of PAV	64
Figure 5.16 : A-bitumen-poured pan of PAV	65
Figure 5.17 : Equipment of RCAT.....	66
Figure 5.18 : Illustration of SUPERPAVE tests	68
Figure 5.19 : Typical equiviscosity curve for bitumen	69
Figure 5.20 : Brookfield rotational viscometer	70
Figure 5.21 : Schematic view of rotational viscometer	71
Figure 5.22 : Elastic and viscous part of G^*	76
Figure 5.23 : DSR and its major components	78
Figure 5.24 : Upper and lower plates (the left one in 25-mm diameter and the right one in 8-mm diameter) DSR and its major components.....	79
Figure 5.25 : DSR silicone molds	79
Figure 5.26 : Bitumen sample shape after trimming and after final setting of gap ..	80
Figure 5.27 : The major components of BBR.....	82
Figure 5.28 : Bituminous binder specimen mold	83
Figure 5.29 : Pouring the bitumen into the mold	84
Figure 5.30 : A schematic drawing of the operation.....	85
Figure 5.31 : A typical BBR sample output.....	85

Figure 5.32 : Graphs of BBR test.....	87
Figure 5.33 : Picture of the used BBR	88
Figure 5.34 : Picture of SEM	89
Figure 6.1 : Showing penetration grades of (B50/70+GSF) at unaged, short-term and long-term aged stages.....	92
Figure 6.2 : Showing penetration grades of (B70/100+GSF) at unaged, short-term and long-term aged stages	92
Figure 6.3 : Showing penetration grades of (B100/150+GSF) at unaged, short-term and long-term aged stages	93
Figure 6.4 : Showing penetration grades of (B160/220+GSF) at unaged, short-term and long-term aged stages	93
Figure 6.5 : Showing softening point temperature of (B50/70+GSF) at unaged, short-term and long-term aged stages	97
Figure 6.6 : Showing softening point temperature of (B70/100+GSF) at unaged, short-term and long-term aged stages	97
Figure 6.7 : Showing softening point temperature of (B100/150+GSF) at unaged, short-term and long-term aged stages	98
Figure 6.8 : Showing softening point temperature of (B160/220+GSF) at unaged, short-term and long-term aged stages	98
Figure 6.9 : Showing penetration index of (B50/70+GSF) at un-aged, short-term and long-term aged stages.....	102
Figure 6.10 : Showing penetration index of (B70/100+GSF) at un-aged, short-term and long-term aged stages	102
Figure 6.11 : Showing penetration index of (B100/150+GSF) at un-aged, short-term and long-term aged stages	103
Figure 6.12 : Showing penetration index of (B160/220+GSF) at un-aged, short-term and long-term aged stages	103
Figure 6.13 : Showing mass change of (B50/70+GSF) and (B70/100+GSF) between un-aged and short-term stage respectively	110
Figure 6.14 : Showing mass change of (B100/150+GSF) and (B160/220+GSF) between un-aged and short-term stage respectively	110
Figure 6.15 : Showing viscosity values of (B50/70+GSF) at unaged and short-term stage respectively	114
Figure 6.16 : Showing viscosity values of (B70/100+GSF) at unaged and short-term stage respectively	114
Figure 6.17 : Showing viscosity values of (B100/150+GSF) at unaged and short-term stage respectively	115
Figure 6.18 : Showing viscosity values of (B160/220+GSF) at unaged and short-term stage respectively	115
Figure 6.19 : Showing the equiviscosity curve and its equation for B50/70-0%GSF.....	119
Figure 6.20 : Showing the equiviscosity curve and its equation for B50/70-10%GSF	119
Figure 6.21 : Showing the equiviscosity curve and its equation for B50/70-20%GSF	120
Figure 6.22 : Showing the equiviscosity curve and its equation for B50/70-30%GSF.....	120
Figure 6.23 : Showing the equiviscosity curve and its equation for B50/70-40%GSF.....	121

Figure 6.24 : Showing the equiviscosity curve and its equation for B50/70-50%GSF.....	121
Figure 6.25 : Showing the equiviscosity curve and its equation for B70/100-0%GSF.....	124
Figure 6.26 : Showing the equiviscosity curve and its equation for B70/100-10%GSF.....	124
Figure 6.27 : Showing the equiviscosity curve and its equation for B70/100-20%GSF.....	125
Figure 6.28 : Showing the equiviscosity curve and its equation for B70/100-30%GSF.....	125
Figure 6.29 : Showing the equiviscosity curve and its equation for B70/100-40%GSF.....	126
Figure 6.30 : Showing the equiviscosity curve and its equation for B70/100-50%GSF.....	126
Figure 6.31 : Showing the equiviscosity curve and its equation for B100/150-0%GSF.....	129
Figure 6.32 : Showing the equiviscosity curve and its equation for B100/150-10%GSF.....	129
Figure 6.33 : Showing the equiviscosity curve and its equation for B100/150-20%GSF.....	130
Figure 6.34 : Showing the equiviscosity curve and its equation for B100/150-30%GSF.....	130
Figure 6.35 : Showing the equiviscosity curve and its equation for B100/150-40%GSF.....	131
Figure 6.36 : Showing the equiviscosity curve and its equation for B100/150-50%GSF.....	131
Figure 6.37 : Showing the equiviscosity curve and its equation for B160/220-0%GSF.....	133
Figure 6.38 : Showing the equiviscosity curve and its equation for B160/220-10%GSF.....	134
Figure 6.39 : Showing the equiviscosity curve and its equation for B160/220-20%GSF.....	134
Figure 6.40 : Showing the equiviscosity curve and its equation for B160/220-30%GSF.....	135
Figure 6.41 : Showing the equiviscosity curve and its equation for B160/220-40%GSF.....	135
Figure 6.42 : Showing the equiviscosity curve and its equation for B160/220-50%GSF.....	136
Figure 6.43 : $G^*/\sin \delta$ measured at 1.59Hz (10rad/s) as a function of temperature for B50/70 extended with various GSF amount before aging	139
Figure 6.44 : Loss modulus measured (G'') at 1.59Hz (10rad/s) as a function of temperature for SEB samples before aging	140
Figure 6.45 : Storage modulus measured (G') at 1.59Hz (10rad/s) as a function of temperature for SEB samples before aging	141
Figure 6.46 : Complex modulus (G^*) at 1.59Hz (10rad/s) as a function of temperature for B50/70 bitumen and its extensive binders before aging.....	144
Figure 6.47 : Complex modulus (G^*) at 1.59Hz (10rad/s) as a function of temperature for B50/70 bitumen and its extensive binders after short-term aging	145

Figure 6.48 : Complex modulus (G^*) at 1.59Hz (10rad/s) as a function of temperature for B50/70 bitumen and its extensive binders after long-term aging	145
Figure 6.49 : Isochronal plots at 0.1Hz for SEB made of B50/70 bitumen before aging. (a) Complex modulus and (b) Phase angle	147
Figure 6.50 : Isochronal plots at 0.1Hz for SEB made of B50/70 bitumen after short-term aging. (a) Complex modulus and (b) Phase angle.....	150
Figure 6.51 : Isochronal plots at 0.1Hz for SEB made of B50/70 bitumen after long-term aging. (a) Complex modulus and (b) Phase angle.....	153
Figure 6.52 : Isochronal plots at 0.2517Hz for SEB made of B50/70 bitumen before aging. (a) Complex modulus and (b) Phase angle	155
Figure 6.53 : Isochronal plots at 0.2517Hz for neat B50/70 bitumen and SEB groups made of B50/70 bitumen after short-term aging. (a) Complex modulus and (b) Phase angle	158
Figure 6.54 : Isochronal plots at 0.2517Hz for neat B50/70 bitumen and SEB groups made of B50/70 bitumen after short-term aging. (a) Complex modulus and (b) Phase angle	161
Figure 6.55 : Isochronal plots at 0.6329Hz for neat B50/70 bitumen and SEB groups made of B50/70 bitumen before aging. (a) Complex modulus and (b) Phase angle	163
Figure 6.56 : Isochronal plots at 0.6329Hz for neat B50/70 bitumen and SEB groups made of B50/70 bitumen after short-term aging. (a) Complex modulus and (b) Phase angle	167
Figure 6.57 : Isochronal plots at 0.6329Hz for neat B50/70 bitumen and SEB groups made of B50/70 bitumen after long-term aging. (a) Complex modulus and (b) Phase angle	170
Figure 6.58 : Isochronal plots at 4.0Hz for neat B50/70 bitumen and SEB groups made of B50/70 bitumen before aging. (a) Complex modulus and (b) Phase angle.....	173
Figure 6.59 : Isochronal plots at 4.0Hz for neat B50/70 bitumen and SEB groups made of B50/70 bitumen after short-term aging. (a) Complex modulus and (b) Phase angle	175
Figure 6.60 : Isochronal plots at 4.0Hz for neat B50/70 bitumen and SEB groups made of B50/70 bitumen after long-term aging. (a) Complex modulus and (b) Phase angle	179
Figure 6.61 : $G^*/\sin\delta$ measured at 1.59Hz (10rad/s) as a function of temperature for B70/100 base bitumen and SEB groups with various GSF content before aging.....	181
Figure 6.62 : $G^*/\sin\delta$ measured at 1.59Hz (10rad/s) as a function of temperature for B70/100 base bitumen and SEB groups with various GSF content after short-term aging	183
Figure 6.63 : Showing a typical fatigue cracking	184
Figure 6.64 : $G^*\sin\delta$ measured at 1.59Hz (10rad/s) as a function of temperature for B70/100 base bitumen and SEB groups with various GSF content after long-term aging	186
Figure 6.65 : Isochronal plots at 0.1Hz for neat B70/100 bitumen and SEB groups made of B70/100 bitumen before aging (a) Complex modulus (b) Phase angle	189

Figure 6.66 : Isochronal plots at 0.1Hz for neat B70/100 bitumen and SEB groups made of B70/100 bitumen after short-term aging. (a) Complex modulus and (b) Phase angle.....	192
Figure 6.67 : Isochronal plots at 0.1Hz for neat B70/100 bitumen and SEB groups made of B70/100 bitumen after long-term aging. (a) Complex modulus and (b) Phase angle.....	195
Figure 6.68 : Isochronal plots at 0.2517Hz for neat B70/100 bitumen and SEB groups made of B70/100 bitumen before aging. (a) Complex modulus and (b) Phase angle	198
Figure 6.69 : Isochronal plots at 0.2517Hz for neat B70/100 bitumen and SEB groups made of B70/100 bitumen after short-term aging. (a) Complex modulus and (b) Phase angle.....	201
Figure 6.70 : Isochronal plots at 0.2517Hz for neat B70/100 bitumen and SEB gousps made of B70/100 bitumen after long-term aging. (a) Complex modulus and (b) Phase angle.....	204
Figure 6.71 : Isochronal plots at 0.6329Hz for neat B70/100 bitumen and SEB groups made of B70/100 bitumen before aging. (a) Complex modulus and (b) Phase angle	207
Figure 6.72 : Isochronal plots at 0.6329Hz for neat B70/100 bitumen and SEB groups made of B70/100 bitumen after short-term aging. (a) Complex modulus and (b) Phase angle.....	210
Figure 6.73 : Isochronal plots at 0.6329Hz for neat B70/100 bitumen and SEB groups made of B70/100 bitumen after long-term aging. (a) Complex modulus and (b) Phase angle.....	213
Figure 6.74 : Isochronal plots at 4.0Hz for neat B70/100 bitumen and SEB groups made of B70/100 bitumen before aging. (a) Complex modulus and (b) Phase angle	216
Figure 6.75 : Isochronal plots at 4.0Hz for neat B70/100 bitumen and SEB groups made of B70/100 bitumen after short-term aging. (a) Complex modulus and (b) Phase angle.....	220
Figure 6.76 : Isochronal plots at 4.0Hz for neat B70/100 bitumen and SEB groups made of B70/100 bitumen after long-term aging. (a) Complex modulus and (b) Phase angle.....	224
Figure 6.77 : Isochronal plots at 0.1Hz for un-aged, RTFOT and PAV aged B100/150 with various GSF amount (o), (r) and (p) respectively	228
Figure 6.78 : Isochronal plots at 1.59Hz for un-aged, RTFOT and PAV aged B100/150 with various GSF amount (o), (r) and (p) respectively	232
Figure 6.79 : Isochronal plots at 0.2517Hz for un-aged B100/150 with various GSF amount	235
Figure 6.80 : Isochronal plots at 4.0Hz for un-aged B100/150 with various GSF amount	235
Figure 6.81 : Isochronal plots at 0.2517Hz for RTFOT-aged B100/150 with various GSF amount	241
Figure 6.82 : Isochronal plots at 4.0Hz for RTFOT-aged B100/150 with various GSF amount	242
Figure 6.83 : Isochronal plots at 0.2517Hz for PAV-aged B100/150 with various GSF amount	244
Figure 6.84 : Isochronal plots at 4.0Hz for PAV-aged B100/150 with various GSF amount	245

Figure 6.85 : Isochronal plots at 0.6329Hz for neat B100/150 bitumen and SEB groups made of B100/150 bitumen before aging. (a) Complex modulus and (b) Phase angle	248
Figure 6.86 : Isochronal plots at 0.6329Hz for neat B100/150 bitumen and SEB groups made of B100/150 bitumen after short-term aging. (a) Complex modulus and (b) Phase angle.....	251
Figure 6.87 : Isochronal plots at 0.6329Hz for neat B100/150 bitumen and SEB groups made of B100/150 bitumen after long-term aging. (a) Complex modulus and (b) Phase angle.....	253
Figure 6.88 : The isochronal plots of complex modulus and phase angle versus loading frequency for B160/220 and B160/220-sulphur-extended-binders at a reference temperature of 25°C (loading frequency sweep, 0.1-4.0Hz). (a) and (b) Before aging. (c) and (d) After RTFOT-aging. (e) and (f) After PAV-aging.....	258
Figure 6.89 : The isochronal plots of complex modulus and phase angle versus loading frequency for B160/220 and B160/220-sulphur-extended-binders at a reference temperature of 30°C (loading frequency sweep, 0.1-4.0Hz). (a) and (b) Before aging. (c) and (d) After RTFOT-aging. (e) and (f) After PAV-aging.....	264
Figure 6.90 : The isochronal plots of complex modulus and phase angle versus loading frequency for B160/220 and B160/220-sulphur-extended-binders at a reference temperature of 40°C (loading frequency sweep, 0.1-4.0Hz). (a) and (b) Before aging. (c) and (d) After RTFOT-aging. (e) and (f) After PAV-aging.....	270
Figure 6.91 : The isochronal plots of complex modulus and phase angle versus loading frequency for B160/220 and B160/220-sulphur-extended-binders at a reference temperature of 50°C (loading frequency sweep, 0.1-4.0Hz). (a) and (b) Before aging. (c) and (d) After RTFOT-aging. (e) and (f) After PAV-aging.....	276
Figure 6.92 : Showing BBR results of (B50/70+GSF) residues at 0°C	280
Figure 6.93 : Showing BBR results of (B50/70+GSF) residues at -6°C.....	281
Figure 6.94 : Showing BBR results of (B70/100+GSF) residues at 0°C	282
Figure 6.95 : Showing BBR results of (B70/100+GSF) residues at -6°C.....	282
Figure 6.96 : Showing BBR results of (B100/150+GSF) residues at 0°C	283
Figure 6.97 : Showing BBR results of (B100/150+GSF) residues at -6°C.....	284
Figure 6.98 : Showing great deflection of (B160/220+GSF) residues at 0°C	285
Figure 6.99 : Showing BBR results of (B160/220+GSF) residues at 0°C	285
Figure 6.100 : Showing BBR results of (B160/220+GSF) residues at -6°C.....	286
Figure A.1 : Showing images of B50/70-0% GSF (o1 and o2 at the un-aged stage, r1, r2 and r3 at the RTFOT-aged stage and p1, p2 and p3 at the PAV-aged stage)	317
Figure A.2 : Showing element analysis of B50/70-0% GSF	318
Figure A.3 : Showing images of B50/70-10% GSF (o1 and o2 at the un-aged stage, r1, r2 and r3 at the RTFOT-aged stage and p1, p2 and p3 at the PAV-aged stage)	319
Figure A.4 : Showing element analysis of B50/70-10% GSF	320
Figure A.5 : Showing images of B50/70-20% GSF (o1, o2 and o3 at the un-aged stage, r1, r2 and r3 at the RTFOT-aged stage and p1, p2 and p3 at the PAV-aged stage)	321
Figure A.6 : Showing element analysis of B50/70-20% GSF	322

Figure A.7 : Showing images of B50/70-30%GSF (o1, o2 and o3 at the un-aged stage, r1, r2 and r3 at the RTFOT-aged stage and p1, p2 and p3 at the PAV-aged stage)	323
Figure A.8 : Showing element analysis of B50/70-30%GSF	324
Figure A.9 : Showing images of B50/70-40%GSF (o1 and o2 at the un-aged stage, r1, r2 and r3 at the RTFOT-aged stage and p1 and p2 at the PAV-aged stage)	325
Figure A.10 : Showing element analysis of B50/70-40%GSF	326
Figure A.11 : Showing images of B50/70-50%GSF (o1, o2 and o3 at the un-aged stage, r1, r2 and r3 at the RTFOT-aged stage and p1, p2 and p3 at the PAV-aged stage)	327
Figure A.12 : Showing element analysis of B50/70-50%GSF	328
Figure A.13 : Showing images of B70/100-0%GSF (o1, o2 and o3 at the un-aged stage, r1, r2 and r3 at the RTFOT-aged stage and p1, p2 and p3 at the PAV-aged stage)	329
Figure A.14 : Showing element analysis of B70/100-0%GSF	330
Figure A.15 : Showing images of B70/100-10%GSF (o1, o2 and o3 at the un-aged stage, r1, r2 and r3 at the RTFOT-aged stage and p1, p2 and p3 at the PAV-aged stage)	331
Figure A.16 : Showing element analysis of B70/100-10%GSF	332
Figure A.17 : Showing images of B70/100-20%GSF (o1, o2 and o3 at the un-aged stage, r1, r2 and r3 at the RTFOT-aged stage and p1, p2 and p3 at the PAV-aged stage)	333
Figure A.18 : Showing element analysis of B70/100-20%GSF	334
Figure A.19 : Showing images of B70/100-30%GSF (o1, o2 and o3 at the un-aged stage, r1, r2 and r3 at the RTFOT-aged stage and p1, p2 and p3 at the PAV-aged stage)	335
Figure A.20 : Showing element analysis of B70/100-30%GSF	336
Figure A.21 : Showing images of B70/100-40%GSF (o1, o2 and o3 at the un-aged stage, r1, r2 and r3 at the RTFOT-aged stage and p1, p2 and p3 at the PAV-aged stage)	337
Figure A.22 : Showing element analysis of B70/100-40%GSF	338
Figure A.23 : Showing images of B70/100-50%GSF (o1, o2 and o3 at the un-aged stage, r1, r2 and r3 at the RTFOT-aged stage and p1, p2 and p3 at the PAV-aged stage)	339
Figure A.24 : Showing element analysis of B70/100-50%GSF	340
Figure A.25 : Showing images of B100/150-0%GSF (o1, o2 and o3 at the un-aged stage, r1, r2 and r3 at the RTFOT-aged stage and p1, p2 and p3 at the PAV-aged stage)	341
Figure A.26 : Showing element analysis of B100/150-0%GSF	342
Figure A.27 : Showing images of B100/150-10%GSF (o1, o2 and o3 at the un-aged stage, r1, r2 and r3 at the RTFOT-aged stage and p1, p2 and p3 at the PAV-aged stage)	343
Figure A.28 : Showing element analysis of B100/150-10%GSF	344
Figure A.29 : Showing images of B100/150-20%GSF (o1, o2 and o3 at the un-aged stage, r1, r2 and r3 at the RTFOT-aged stage and p1, p2 and p3 at the PAV-aged stage)	345
Figure A.30 : Showing element analysis of B100/150-20%GSF	346

Figure A.31 : Showing images of B100/150-30%GSF (o1, o2 and o3 at the un-aged stage, r1, r2 and r3 at the RTFOT-aged stage and p1, p2 and p3 at the PAV-aged stage)	347
Figure A.32 : Showing element analysis of B100/150-30%GSF	348
Figure A.33 : Showing images of B100/150-40%GSF (o1, o2 and o3 at the un-aged stage, r1, r2 and r3 at the RTFOT-aged stage and p1, p2 and p3 at the PAV-aged stage)	349
Figure A.34 : Showing element analysis of B100/150-40%GSF	350
Figure A.35 : Showing images of B100/150-50%GSF (o1, o2 and o3 at the un-aged stage, r1, r2 and r3 at the RTFOT-aged stage and p1, p2 and p3 at the PAV-aged stage)	351
Figure A.36 : Showing element analysis of B100/150-50%GSF	352
Figure A.37 : Showing images of B160/220-0%GSF (o1, o2 and o3 at the un-aged stage, r1, r2 and r3 at the RTFOT-aged stage and p1, p2 and p3 at the PAV-aged stage)	353
Figure A.38 : Showing element analysis of B160/220-0%GSF	354
Figure A.39 : Showing images of B160/220-10%GSF (o1, o2 and o3 at the un-aged stage, r1, r2 and r3 at the RTFOT-aged stage and p1, p2 and p3 at the PAV-aged stage)	355
Figure A.40 : Showing element analysis of B160/220-10%GSF	356
Figure A.41 : Showing images of B160/220-20%GSF (o1, o2 and o3 at the un-aged stage, r1, r2 and r3 at the RTFOT-aged stage and p1, p2 and p3 at the PAV-aged stage)	357
Figure A.42 : Showing element analysis of B160/220-20%GSF	358
Figure A.43 : Showing images of B160/220-30%GSF (o1, o2 and o3 at the un-aged stage,r1, r2 and r3 at the RTFOT-aged stage and p1, p2 and p3 at the PAV-aged stage)	359
Figure A.44 : Showing element analysis of B160/220-30%GSF	360
Figure A.45 : Showing images of B160/220-40%GSF (o1, o2 and o3 at the un-aged stage, r1, r2 and r3 at the RTFOT-aged stage and p1, p2 and p3 at the PAV-aged stage)	361
Figure A.46 : Showing element analysis of B160/220-40%GSF	362
Figure A.47 : Showing images of B160/220-50%GSF (o1, o2 and o3 at the un-aged stage, r1, r2 and r3 at the RTFOT-aged stage and p1, p2 and p3 at the PAV-aged stage)	363
Figure A.48 : Showing element analysis of B160/220-50%GSF	364

DETERMINING OPTIMUM SULPHUR CONTENT AS AN ALTERNATIVE BINDER ADDITIVE IN ASPHALTIC CONCRETE PAVEMENTS

SUMMARY

A by-product of crude oil, about 50 million tons of bitumen are manufactured annually, with the majority of this production directed towards pavement construction. The world's mounting population means that in coming decades the current oil reserves will no longer meet needs, causing a rise in the price of bitumen, and thus in the price of pavements as well. Used as the primary binder in asphaltic concrete production, the high financial costs of bitumen, coupled with the constricting amounts needed have been forcing pavement engineers to search for an alternative material that can at least partially be used as a substitute.

Sulphur ranks as the tenth most abundant chemical element in the universe and the thirteenth in the earth's crust. Apart from its natural existence, the strict environmental regulations of developed countries have also led to the acquisition of an abundant amount of elemental sulphur during desulphurization processes of natural gas and petroleum. Therefore instead of discarding sulphur, it can be utilized in road pavements. Although many important studies were conducted in the 1970s on the use of sulphur in asphalt pavements, there is still a deficiency of additional information due to the lack of multi-sided assessments and contemporary SUPERPAVE tests. The purpose of this paper is to provide an in-depth explanation of the integrated studies relative to sulphur utilization with current binders.

In this study, a set of both laboratory experiments is conducted on different types of neat bitumen and sulphur-extended-binders. Bitumen types classified by penetration grades (B50/70, B70/100, B100/150, and B160/220) are used to investigate the effectiveness of sulphur. Each neat bitumen type is then replaced with 10, 20, 30, 40, and 50% granular sulphur by weight. It is important to note here that the granular sulphur proportion in the replacement process is a weight percentage of the entire mixture. During the blending, careful attention is paid to the sulphur replacement and the blending process is performed in accordance with relevant specifications to maximize the rheological properties, minimize the bitumen degradation, obtain a homogenous blend, create chemical bonds, and prevent possible crystallization and the emission of poisonous SO₂ and H₂S gases. After the completion of the blending, the new binders are placed in small containers, and the mixtures are allowed to cool to room temperature. The mixtures are sealed with aluminium foil against possible oxidation and aging. Finally, they are stored for the following experiments:

The basic properties of neat bitumen, prior to any extension, are determined so that they can be compared with resultant sulphur-extended-binders. Monitoring of the molecular and intermolecular (microstructure) levels of these new binders is carried out by scanning electron microscope. Physical and rheological tests specified in many binder specifications are also examined to determine penetration, softening

point, penetration index, specific gravity, rotational viscometer, dynamic shear rheometer, and bending beam rheometer.

Re-monitoring of a new morphology is performed to understand the matrix of bitumen phase and sulphur phase by scanning electron microscope. All physical experiments mentioned above are conducted so as to validate the effectiveness of differing amounts of sulphur on each bitumen sample. A dynamic shear rheometer test is conducted at different frequencies and temperatures to calculate the complex modulus and phase angle. To simulate the aging mechanism of the new binders, they are first aged via a rolling thin film oven test and then a pressure aging vessel.

All physical experiments on short-term aged and long-term aged specimens are performed to examine the behavior of aged new binder specimens that are simulating the performance of itself during typical compaction and service life.

The morphology, mechanical, and rheological engineering properties investigated demonstrated that the addition of sulphur not only lowers total costs, but also increases the performance of the binder.

ESNEK YOL ÜSTYAPILARINDA BİTÜM İLE BİRLİKTE BAĞLAYICI OLARAK OPTIMUM SÜLFÜR ORANININ VE PERFORMANSININ BELİRLENMESİ

ÖZET

Karayolu üstyapıları esasen esnek ve rijit olmak üzere iki gruba ayrılır. Farklı tabakalardan meydana gelen esnek üstyapı kaplamalarında alttan itibaren, sırasıyla binder ve aşınma tabakaları vardır. Bu tabakalarda belirlenmiş gradasyonlarda hazırlanmış iri agrega, ince agrega ve filler bitüm ile birlikte plentlerde (asfalt üretim tesisleri) karıştırılarak projesinde belirtilen kalınlıklarda sıkıştırılır. Bu tür karışımlar "Bitümlü Sıcak Karışımlar, BSK, Asfalt Betonu" olarak adlandırılır. Bunun yanında, yol yüzeyine ince bir bitüm tabakasının püskürtülmesi ve üzerine agrega serilip sıkıştırılması sonucu elde edilen, "Yüzeysel (sathi) Kaplama" olarak adlandırılan yöntemler de mevcuttur. Dolayısıyla, asfalt betonu ve yüzeysel kaplamalarda bağlayıcı olarak "bitüm" kullanılmakta ve ülkemizin karayollarında tamamına yakınında yukarıdaki iki türden bir tanesi, yolun trafik miktarı da göz önüne alınarak uygulanmaktadır.

Bitüm ham petrolün rafinerilerde ayrıştırılması sonucu elde edilir, yani ham petrolün fraksiyonlarından biridir. İlerleyen teknoloji petrolün; bitüm, benzin ve motorin gibi daha kıymetli olan fraksiyonlarına çevrilmesine olanak sağlamıştır. Ham petrolün ithal edildiği de göz önüne alındığında, esnek üstyapılarda bitüm kullanımının azaltılmasının ülke ekonomisine faydası aşıkârdır. Bitümlü sıcak karışımlara olan talep azalmadığından, bu bağlamda yapılacak uygulama bitümün yerine daha uygun bir bağlayıcı kullanmaktır. Bu nedenle bitümün yerine kullanılacak bağlayıcının bitümün özelliklerine sahip olması gerekmektedir. Bitüm'ün esnek üstyapılarda kullanılmasına olanak sağlayan en önemli iki özelliği adezyon (agregalara yapışabilme) ve kohezyondur (esnek bir biçimde şekil değiştirebilme). Epoksi bir tür bağlayıcı olup bitümün yerine kullanılabilmektedir ve bu tür uygulamalar "epoksi asfalt" olarak adlandırılmaktadır. Ancak epoksi asfaltın maliyeti çok yüksek olup, çelik köprü kaplamaları gibi çok özel uygulamalarda kullanılmaktadır. Bu nedenle bitüm yerine kullanılacak bağlayıcının aynı zamanda karışımın maliyetini artırmaması elzemdir.

Doğada yaygın olarak bulunan ve "küükür" olarak da bilinen sülür, yukarıda belirtilen özellikleri nedeniyle bitüm yerine kullanılabilecek bir bağlayıcıdır. Doğada bulunmasının yanı sıra birçok endüstride yan ürün olarak da elde edilmektedir. Ülkemiz sülür yatakları bakımından birbirinden farklı, büyük rezervlere sahip olup, bunlar çeşitli şekillerde işletilmektedir. Dolayısıyla, asfalt betonu üretiminde sülür kullanılması, birim fiyatı ve ülke ekonomisine katkısı yönünden bitüme göre daha uygun olabilmektedir. Ülke ekonomisine yapacağı katının ve bitümün önemli özelliklerine sahip olmanın yanı sıra, sülür kullanılarak hazırlanan asfalt betonlarının kalıcı deformasyonlara direncinin yüksekliği ve karışımlarda işlenebilirliği olumlu yönde etkilemesi, yani mekanik özelliklerinin üstünlüğü de söz konusu uygulamalarda kullanımını cazip kılmaktadır. Ancak yapılan araştırmalar,

en azından günümüzde, sülfürün bitümün yerine tamamen değil de kısmen kullanılabileceği doğrultusunda sonuçlar vermektedir. Arazideki uygulamalarda, sülfür bitümle birlikte asfalt betonu üretiminde iki şekilde kullanılabilir. Bunlar:

- Harman tipi (batchtype) asfalt plentlerinde debitüm ve agrega ile birlikte, mikserde aynı anda karıştırmak
- Rafinerilerde veya karışım tesislerinde bitümle önceden karıştırılarak plentlerde kullanıma hazır hale getirmek

Bu tezin danışmanın daha önce yaptırmış olduğu, granüler sülfür kullanılarak bitümlü sıcak karışımlar hazırlanması ve performansının incelenmesi konusundaki doktora çalışmasının sonuçlarından da faydalılarak, sülfürün bitümün yerine tamamen kullanılmasının istenilen performansı sağlamayaceği düşüncesine varılmıştır. Ayrıca mezkur çalışmada sülfür agrega ile karıştırılarak, yani asfalt plentlerindeki uygulamanın benzeri asfalt betonu numuneleri hazırlanarak sülfür kullanımının karışım üzerine etkisi incelenmiştir. Dolayısıyla, sülfürün bitümle birlikte bağlayıcı olarak performansı, diğer bir deyişle rafinerilerde veya karışım tesislerinde bitümle önceden karıştırılarak hazırlanması sonucu üretilen bağlayıcının performansı incelenmiş ve sonuçları değerlendirilmiştir.

Bu bağlamda ve laboratuvar ölçünginde yapılan çalışmalarla esas olarak, ülkemizde yaygın olarak kullanılan penetrasyon dereceli bitümler belirli oranlarda granüler sülfürle karıştırılarak reolojik, mekanik ve morfolojik özelliklerini karşılaştırılmıştır. Reolojik, mekanik ve morfolojik deneyler sülfür ilave edilmemiş, asfalt betonu yapımında kullanılan bitümlere de uygulanarak, bu bağlayıcılar "kontrol grubu" olarak kabul edilmiştir. Bu şekilde sülfür ilave edilerek özellikleri değiştirilen bağlayıcıların geleneksel olarak kullanılan bağlayıcılara göre performansı karşılaştırılmıştır. Çalışmada sırasıyla B50/70, B70/100, B100/150, B160/220 penetrasyon dereceli bitümler kullanılmıştır. Bağlayıcılardan B160/220 genellikle yüzeysel kaplamalarda, B50/70 sıcak bölgelerde, diğerleri ise ülkenin değişik kesimlerindeki uygulamalarda kullanılmaktadır. Öncelikle bu bitümlerin temel özellikleri belirlenmiş, Penetrasyon İndeksleri hesaplanmıştır. Daha sonra, %10 oranından başlayarak, sırasıyla %20, %30, %40 ve %50 oranlarında sülfür bitüm ile karıştırılarak numuneler hazırlanmıştır. Bitüm ve sülfürün birim hacim ağırlıkları farklı olduğundan, ilave edilen sülfür miktarı ağırlıkça, yani 10 gram bitüm yerine 10 gram sülfür ilave edilmiştir. Oranların bu şekilde belirlenmesi, yukarıda sözü edilen ve diğer deneysel çalışmaların göz önüne alınması sonucunda verilmiş bir karardır. Karışımlar hazırlanırken homojen bir karışım elde edilmesi doğrultusunda gerekli her tedbir alınış, bitümün bozulması kristalleşme oluşumu önlenmiştir. Hazırlandıktan sonra ortam sıcaklığında soğumaya bırakılan numuneler, alüminyum folyeye sarılarak çevresel etkilerden olumsuz etkilenmesi önlenmiştir.

Asfalt betonu hazırlanırken, serilip ve sıkıştırılırken, ayrıca hizmet ömrü süresince bitüm oksitlenir, yani yaşlanır. Yaşlanmış bağlayıcıların performanslarının incelenmesi amacıyla, hazırlanan karışımlar kısa ve uzun süreli yaşlandırılmaları sırasıyla, Dönel İnce Film Halinde Isıtma Deneyi ve Basınçlı Yaşlandırma Kabini cihazları kullanılarak gerçekleştirilmiştir. Temel bitüm deneyleri yaşlandırılan numunelere de uygulanmıştır. Temel deneylerin üzerine, bağlayıcının çeşitli ortamlardaki davranışını belirleyen gelişmiş SUPERPAVE bağlayıcı deneyleri uygulanmıştır. Bunlar Dönel Viskometre bağlayıcının uygulama sıcaklığındaki vizkozitesini, Dinamik Kesme Reometresi farklı sıcaklıklardaki rijitlik özelliğini ve Kiriş Eğilme Reometresi özellikle düşük sıcaklıklarda sünme rijitliğini belirleyen deneylerdir. Bütün bu deneylerin gerçekleştirilmesi sonucunda, farklı oranlarda sülfür ilave edilen bağlayıcıların hem kendi aralarında hem de geleneksel olarak

kullanılan bağlayıcılara nazaran, yaşılanma özellikleri de göz önüne alınarak tüm performans özelliklerini incelemiştir ve değerlendirilmiştir.

Sülfür kullanılarak hazırlana karışımın performansları değerlendirilirken, bitümle sülfürün birlikte kullanılması halinde aralarındaki uyumluluk son derece önemlidir. Genel olarak bitümle sülfür arasındaki ilişki, düşük oranlarda sülfürün bir kısmının bitümle kimyasal reaksiyona girmesi biçimindedir. Bitüme ilave edilen sülfür oranı arttırıldıkça sülfürün bir kısmının bitüm içerisinde çözülmesi ve geriye kalanının kristalleşmesi şeklindedir. Bütün bu ilişkinin karışımın performansı açısından önemi göz önüne alındığında, numunelerin yaşlandırılmadan önce ve sonraki morfolojisi SEM (Scanning Electron Microscopy) yardımıyla belirlenmiştir. Böylelikle sülfürün bitüm içerisinde dağılımı ve oluşturduğu yapılanmalar gözlemlenmiştir. İlave olarak, yapılan kimyasal analizlerle karışılardaki Karbon ve Sülfür oranları hem ağırlık hem de atomik yüzde cinsinden hesaplanmıştır. Böylelikle standart ve SUPERPAVE bitüm deneylerinden elde edilen sonuçların görsel olarak da karşılaştırılması ve yorumlanması sağlanmıştır.

Sonuç olarak, sülfür ilave edilen bitümlerin kalıcı deformasyonlara karşı daha dirençli olduğu, viskozite özellikleri nedeniyle daha düşük sıcaklıklarda karıştırılıp sıkıştırılacağı düşüncesine varılmıştır. Yapılan ekonomik analiz de göz önüne alındığında bağlayıcılarda bitüm yerine %30 ve/veya %40 oranında sülfür kullanıldığında hem daha ekonomik hem de performansı daha yüksek bitümlü karışımının elde edilebileceği kanaatine varılmıştır.

1. INTRODUCTION

The history of transportation dates back to around 3500 BCE with the invention of fixed-wheeled carts. From this fledgling beginning to the present day, mankind has had the constant need to move either themselves and/or their goods from one place to another in a process universally termed "transportation". And even though there are many modes of transportation today, highway transportation remains the most preferred in most of the world. Effective highways are necessary to meet this demand, and these motorways require substantial investments in infrastructure and pavement materials. It has only been in the last two centuries, however, that the importance of pavement materials has been understood and/or taken into account. Pavement materials are now considered vital components of highway construction and longevity.

The first known implementations of pavement materials in road building history were those of Pierre-Marie-Jérôme Trésaguet (1716-1796, France) and John Loudon MacAdam (1756-1836, Scotland). Trésaguet developed a pavement consisting of three layers of stone of differing sizes. MacAdam's pavement, whose total depth was 250 mm, was made of angular hand broken gravel. He filled the voids between the aggregate with stone dust. His became a very popular method and was popularly used until the 1950s in most parts of the world, particularly in the United Kingdom. However, due to such various factors as the lack of binders, the compulsory requirement to roll the surface, and – of course – the substantially increasing axle loads, highway engineers found themselves facing the need to design stronger pavements methods and materials (Yayla, 2002).

Today there are three types of pavement designs: rigid, flexible and composite pavements. This classification is based on pavement behavior under traffic loads. Flexible pavement is the most preferred type in Turkey, as well as in many other countries. This kind of pavement is produced by blending different size aggregates with "a small amount" of binder, a kind of glue used to hold aggregates together (Amsterdam, 2008). A unique binder (at least for the time being) made of bitumen

materials is used to hold and bind these discrete aggregates together. "A small amount" of binder in pavements indicates an amount that can range from 3% to 5% by weight as per international specifications. It is these small amounts of binders that are the primary determinants of both the performance and the cost of flexible pavements.

Bitumen, a by-product of crude oil, is a sticky, black, and mostly viscous liquid, or semi-solid. According to the 2010 statistics published by the Turkish Petroleum Refineries Company (TUPRAS), the Republic of Turkey then had four refineries with a total capability of refining 28.1 million tons of crude oil per year. In that same year, the United States had 149 active refineries with a 940 million ton crude oil capacity. As shown in Figure 1.1, using an approximate approach, one unit of crude oil provides 43% gas, 18% fuel oil and gas oil, 11% liquefied petroleum gas (LPG), 9% jet fuel, 5% bitumen and 14% other products.

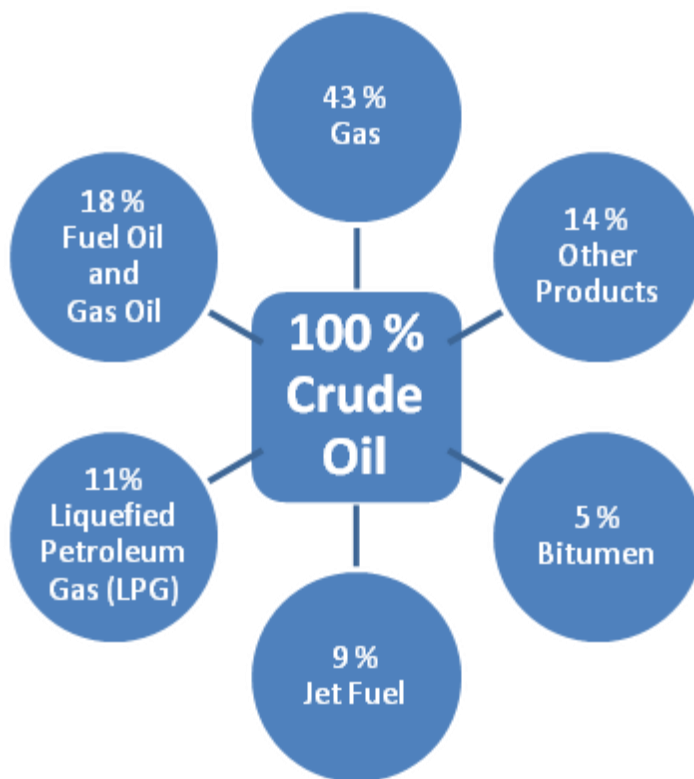


Figure 1.1 : Products of crude oil.

Corresponding to the proportions shown in Figure 1.1, in 2010, 1.4 million and 47 million tons of bitumen were fabricated in Turkey and the USA respectively.

Bitumen is a rheological material whose properties undergo deforming changes caused not only by the effects of physical loads, but also by loading durations and

variations of temperature. These mechanical, technical, and chemical properties will be discussed later. In fact, the word "bitumen" is often misused because the material referred to as bitumen is not a "specific product", but rather a group of materials of slightly different properties that are classed together as "bituminous product". In any case, many people – including engineers – refer to the binders as bitumen instead of asphalt and/or tar, both of which are bituminous materials. Figure 1.2 explains this issue. Today we see that the utilization of tar as a binder is gradually being replaced by asphalt due to environmental concerns and regulations.

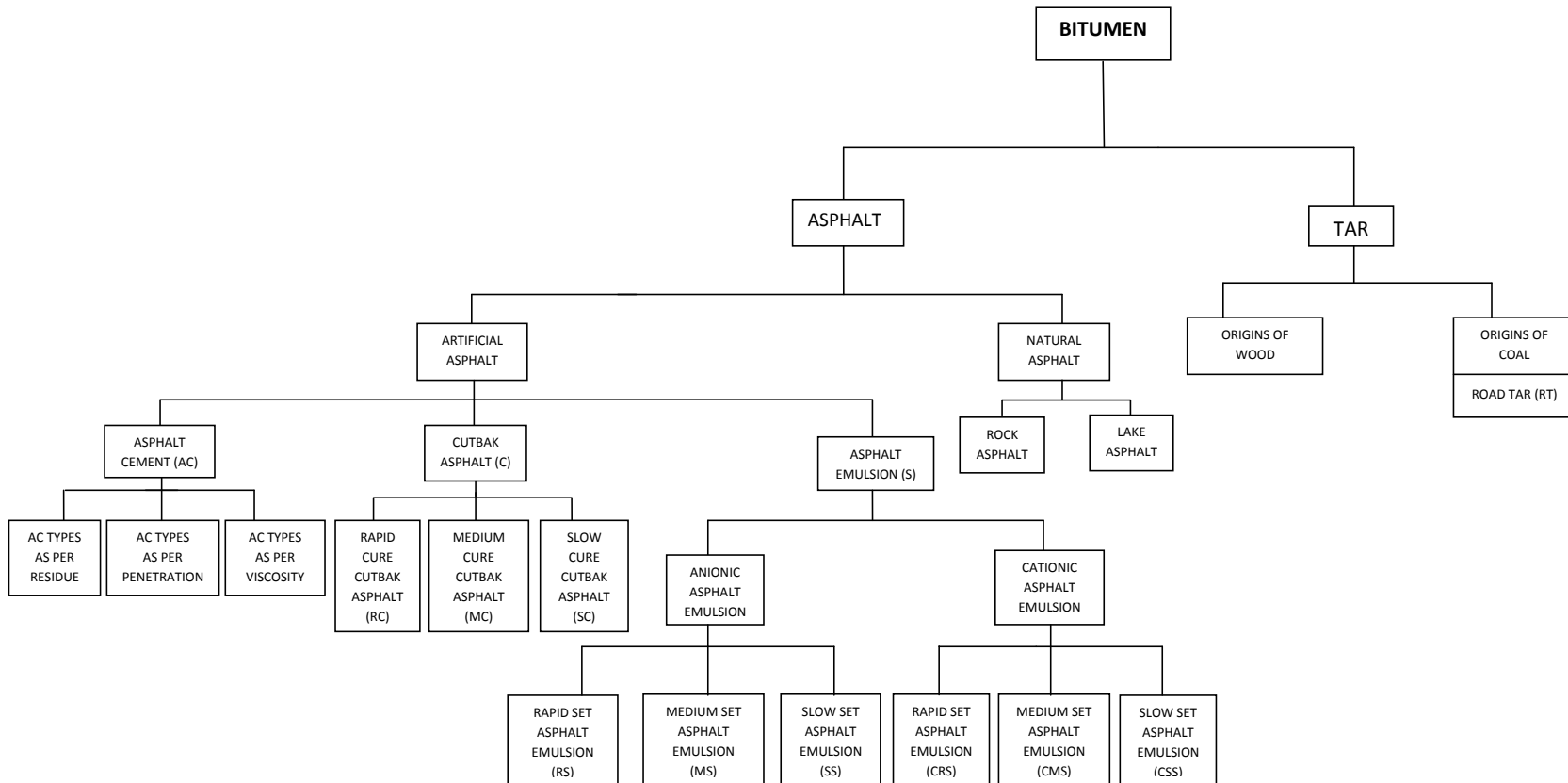


Figure 1.2 : Classification of bitumen.

There are two types of asphalt: natural and refinery manufactured. These are illustrated in Figure 1.2. Natural asphalt occurs in rocks and lakes. Rock asphalt is obtained from porous limestone or sandstone that contains up to 10% of natural asphalt. Lake asphalt is excavated from fresh water lakes, partially refined by heating up to 160°C to remove water, and then is filtered. Both rock and lake asphalt are not available, or plentiful, enough to be used directly on highways, and due to their substantial hardness, they must be blended with refinery manufactured asphalt when they are used.

Artificial asphalt is the most prevalently used world binder. This asphalt is a residual material produced after the refinery of crude oil as shown in Figure 1.3 (Illston and Domone, 2001). Although this asphalt has many applications, such as roofing, insulation and others, it is most widely utilized in road pavements in the hot mix asphalt (HMA) and bituminous surface treatment (BST).

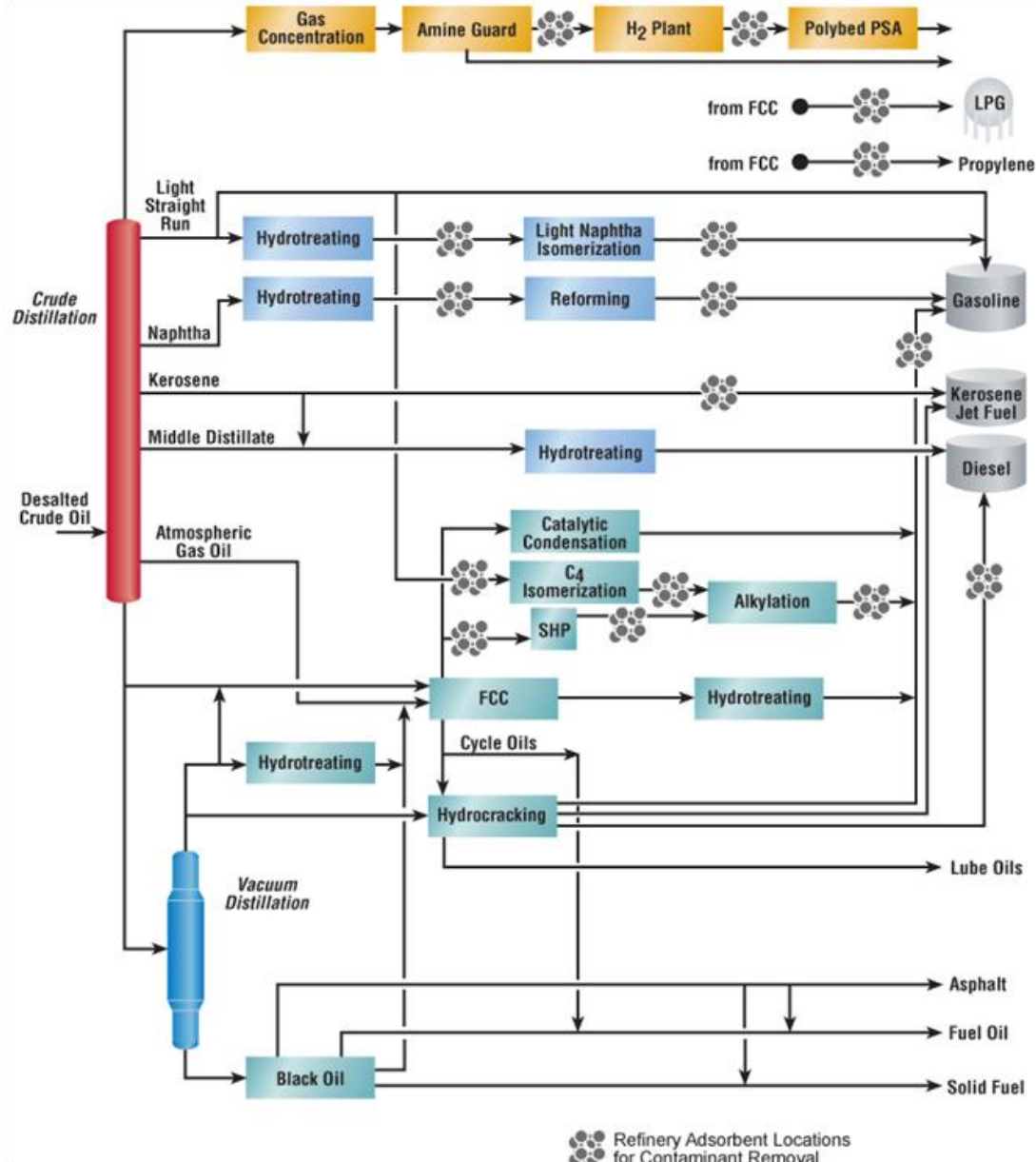


Figure 1.3 : Refinery process of crude oil.

Since bitumen is a by-product of crude oil, refineries in the past regarded it as a residual material of little or no commercial value and, as such, specific attention was not paid to its manufacture. Refineries operating prior to modern innovations had high levels of production flexibility. Gradually, these refineries began to acknowledge bitumen as a more valuable material, and reassessed their processes (Anderson et al., 2000). The crude oil refinery process has also changed in line with rising concerns about the impacts of environmental pollution and has modified its processes so as to eliminate hazardous components. These changes have resulted in a reduction of air pollution and acid rain. However, despite these ameliorations, it remains still nearly impossible to produce asphalt with such desirable properties as

sustainable resistance to aging, temperature, fatigue, and different types of cracks and rutting. While there are several known ways or interventions that aid in overcoming these problems and lead to the production of desired qualities of asphalt, including the establishing of discrete refining facilities, use of high-quality crude petroleum, or altering the entire refining process, these processes are very expensive and require substantial refinery investments (Ishai and Yuval, 2002).

The durability of flexible pavements to traffic loads and environmental conditions is mainly dependent on the kind and chemical composition of the bitumen used. In the past, pavements made of neat bitumen met the required specifications and performed satisfactorily under the then-prevalent axle loads. However, the substantial increase in traffic loads, traffic volumes, and tire pressure began to impede the performance of neat bitumen, and even resulted in additional detrimental distresses in pavements with straight bitumen binders.

Typical distresses include rutting, shoving, stripping, and fatigue cracks, all of which are caused by both traffic loads and weather conditions. Unfortunately, various cracks can be observed in even perfectly constructed-traffic free pavement when it is exposed to severe weather conditions. These distress types may result not only in poor ride quality, but also in higher maintenance cost and – even – the failure of the entire pavement (Taha et al., 1998). Since, as mentioned above, fabricating bitumen of an expected chemical composition is both a difficult and expensive process, producers are looking for ways to enhance the properties of their neat bitumen by coming-up with convenient, practical and cost effective engineering processes that are, at once, economical, environmentally friendly, and – particularly – compatible with current international specifications. Beginning in the early 1970s producers and scientists have been demonstrating great interest in this matter, and numerous modifications have been suggested as ways to improve the properties of bitumen. These modifications are fundamentally categorized depending on their inclusion of either polymer (elastomers and plastomers) and non-polymer additives (filler, extender, anti-striping and anti-oxidation agents). In addition, another less-prevalent chemical reactive modification has also been suggested (Elseifi et al., 2003).

The main goals of all these bitumen-modification attempts may be summarized as:

- Changing its consistency in order to resist rutting, particularly in hot weather, and to avoid cracking in cold conditions.
- Obtaining high adhesion between bitumen and aggregates in order to prevent any possible stripping and raveling in case of the presence of water (Taha et al., 1998).

As indicated previously, today the world depends primarily on a "unique" binder derived from crude oil for both its HMA (hot-mix asphalt) and BST (bitumen surface treatment) pavements.

When the world's mounting population is taken into consideration, it becomes evident that in the following decades the current oil reserves will be unable to meet supply needs. This means that the price of bitumen material will rise, making the construction of flexible pavements even more expensive. Frequent political events between oil and non-oil producing countries are also exacerbating oil prices and ultimately bitumen. Therefore, the world has recognized that it has to find binders that can be used in place of bitumen – or that can at the very least replace some part of the bitumen used. Substitute binders should be cheaper than our current product, should be environmentally friendly, and should meet or exceed determined performance requirements.

In the past, a limited number of studies have been conducted on the utilization of sulphur as a modifier and as an extender in both binders and hot mixtures. The first attempt to this end was made in the 1970s by The US Bureau of Mines and The Federal Highway Department. However, serious concerns about health, safety, storage, and performance arose after prolonged exposure of the sulphur to the bitumen at elevated temperatures (Strickland et al., 2008). Sulphur may be used as a non-polymer modifier by blending it with bitumen to enhance its mechanical and rheological properties. As an extender, it can also be used as an extender by replacing it, either partially or completely, for both straight and modified bitumen (Asphalt Institute, 2007). Cost ranks as one of its positive features as it is approximately five or six times cheaper than bitumen. In addition to its lower cost feature, sulphur can also be attained substantially and readily both from natural sources and also from blast furnaces. Thermal plants represent another high potential. Instead of discarding residual sulphur, it is now being recognized that it can be utilized in road pavements (Deniz, 2009). Due to lack of several assessments,

however, sulphur is still not widely used, neither in Turkey nor in the rest of the world. The goal of this study is to investigate the potential applicability of sulphur as a binder that may replace bitumen, and correspondingly to investigate its potential and wide use in HMA.

2. THE PURPOSE OF THIS THESIS

In this study, a set of laboratory experiments is conducted on different types of neat bitumen and Sulphur-Extended-Binders (SEBs). The morphology, mechanical, and rheological engineering properties are then investigated to understand how sulphur affects bitumen's behavior. Bitumen types classified by penetration grades (B50/70, B70/100, B100/150, and B160/220) are used to investigate the effectiveness of sulphur. Most of Turkey prefers to use B50/70, B70/100, and B100/150 as typical binders for HMA, while B160/220 is commonly chosen in BST. Due to its low degree of penetration, B50/70 penetration bitumen is generally used in the highways and roofing industries of hot climatic regions. In this work, the basic properties of neat bitumen, prior to any extension, are determined so that they can be compared with resultant SEBs. Monitoring of the molecular and intermolecular (microstructure) levels of these new binders is carried out by Scanning Electron Microscope (SEM). Physical and rheological tests specified in many binder specifications are also examined to determine Penetration, Softening Point, Penetration Index (PI), Specific Gravity, Rotational Viscometer (RV), Dynamic Shear Rheometer (DSR), and Bending Beam Rheometer (BBR).

The new binder samples, SEBs were prepared using a digital high shear mixer (EUROSTAR made by IKA). First, each type of neat bitumen (400g) was heated until fluid in an iron container. Each neat bitumen type is then replaced with 10, 20, 30, 40, and 50% granular sulphur (GSF) by weight. It is important to note here that the GSF proportion in the replacement process is a weight percentage of the entire mixture. For instance, a 10% GSF replacement means that 10% of the bituminous binder is replaced by 10g of GSF; the resultant SEB totals 100 grams. Each blending process was performed at 140°C under high-speed shear mixing for 60 minutes, with a shear speed of 1000rpm. During the blending, careful attention is paid to the GSF replacement and the blending process is performed in accordance with relevant specifications to maximize the rheological properties, minimize the bitumen degradation, obtain a homogenous blend, create chemical bonds, and prevent

possible crystallization and the emission of poisonous SO₂ and H₂S gases. After the completion of the blending, the new binders are placed in small containers, and the mixtures are allowed to cool to room temperature. The mixtures are sealed with aluminum foil against possible oxidation and aging. The samples were marked according to type of neat bitumen, the amount of replaced GSF and their age. As an example, "R-B70/100-40%GSF" stands for short-term aged SEB whose virgin bitumen is B70/100 and replaced 40%GSF by weight. The three letters are used to define the age of the SEBs: O, R, and P representing original age, short- and long-term aging respectively. Finally, they are stored for the following experiments:

Re-monitoring of a new morphology is performed to understand the matrix of bitumen phase and sulphur phase by SEM. In light of the results, the available micro-mechanical models such as those developed by Drs. Einstein, Mooney, Nielsen, and Kerner (the Kernel Model) are adapted to predict the complex shear modulus of the new composite. All physical experiments mentioned above are conducted so as to validate the effectiveness of differing amounts of GSF on each bitumen sample. A DSR test is conducted at different frequencies and temperatures to calculate the complex modulus and phase angle. These values are compared with values computed from the empirical model and the correlation between them are investigated. To simulate the aging mechanism of the new binders, they are first aged via a Rolling Thin Film Oven Test (RTFOT) and then a Pressure Aging Vessel (PAV).

All physical experiments on short-term aged and long-term aged specimens are performed to examine the behavior of aged new binder specimens that are simulating the performance of itself during typical compaction and service life (Short-term aging and long-term aging are ensured via Rolling Thin Film Oven (RTFO) and Pressure Aging Vessel (PAV) respectively).

3. PROPERTIES OF SULPHUR AND ITS USE

3.1 Sulphur Review

Sulphur ranks as the tenth and thirteenth most abundant chemical element in the universe and in the earth's crust respectively (Stevenson, 1986; Trudinger, 1975). In today's world, sulphur and sulphuric acid directly or indirectly play a major role in all fields of our lives, and is a compulsory component for all living cells without which everyday life would be extremely difficult.

The history of sulphur dates back to ancient times and was used in ancient Greece, China, and Egypt. Today the element is used in mainly two applications: In cultivation as a fertilizer, and in the production of sulphuric acid, which is considered a fundamental industrial chemical. Secondary utilization areas of sulphur are used in matches, insecticides, and fungicides (Kutney, 2007).

Sulphur is mainly distributed in the earth's crust as a pure element, in the form of sulfides, and as sulfates, but represents only about 0.1% by weight. The definition of the typical forms of sulphur are given below (Özgüner, 2005);

Natural sulphur: Pure sulphur existing in nature as an element.

Recovered sulphur: A by-product type of sulphur recovered from H₂S, contaminated by natural gas and oil-refinery gases.

Pyrite: An iron sulfide with formula: FeS₂. This is the most common type of the sulfide minerals.

Elemental sulphur: A bright yellow crystalline solid at room temperature. Its crystals are sought after by mineral collectors for their brightly colored polyhedron shapes.

Frasch sulphur: This sulphur is obtained by extracting melted sulphur from underground deposits after superheated water is pumped into sulphur deposits.

Crude sulphur: Sulphur ore containing between 99 to 99.9% pure sulphur.

Brimstone sulphur: Also known as crude sulphur.

Crushed sulphur: Achieved by crushing crude sulphur into 8inch (20.32mm) size pieces.

Granule sulphur: Sulphur shaped as lumps subsequent to cooling with water.

Granular sulphur: Its main components are SO₂, H₂S and Carbon Black. It is blended with bitumen to a granular shape.

Block sulphur: Subsequent to cooling sulphur with water or air, block sulphur is obtained by pelletizing and compressing.

Bright sulphur: A type of sulphur that is a bright yellow color.

Wet sulphur: A kind of sulphur that easily disperses in water.

Figures 3.1, 3.2, 3.3 and 3.4 show various photographs of these varieties:



Figure 3.1 : Natural sulphur and pyrite.



Figure 3.2 : Pyrite and crushed sulphur.



Figure 3.3 : Granule sulphur and granular sulphur.



Figure 3.4 : Block sulphur.

Elemental and organic sulphur, gypsum ($\text{CaSO}_4 \cdot 2\text{H}_2\text{O}$), pyrite(FeS_2), and other base metal sulphides are mainly found in the lithosphere of the Earth's crust. The hydrosphere (especially the oceans) is the main reservoir of sulphate and a small amount of sulphur also exists in the pedosphere. Even smaller amounts of sulphur are found in the atmosphere, despite the fact that the high mobility and short mean residence time of sulphur compounds in this environment make it a remarkably important component in the global sulphur cycle (Zhao et al., 1996). The estimated global reservoirs of sulphur are displayed in Table 3.1.

Table 3.1 : Estimated global reservoirs of sulphur (Stevenson, 1986).

Reservoir	Amount of Sulphur (ton)
Atmosphere	4.8×10^6
Lithosphere	24.3×10^{15}
Hydrosphere	
Sea	1.3×10^{15}
Fresh water	3.0×10^9
Marine organisms	2.4×10^8
Pedosphere	
Soil	2.4×10^{11}
Soil organic matter	1.0×10^{10}
Land plants	7.6×10^8

In practice, there is a cycle of sulphur between these various reservoirs. The industrial revolution ushered in with it a mounting realization of the importance of the global sulphur cycle. These budding industries learned how to extract a great amount of various sulphur-containing minerals from these reservoirs.

In addition to its existence in nature, sulphur is also recovered as a by-product from such industries as coal and natural gas. Up until the twentieth century, elemental sulphur was obtained by extracting it from salt domes, where it sometimes occurs in almost pure form. In today's world, nearly all elemental sulphur is obtained as a by-product in the removal of sulphur-containing contaminants from natural gas and petroleum. When compared with its natural reservoirs, a relatively greater amount of sulphur is obtained as a recovery from these sources.

The marked variations in the annual production of sulphur in various world countries is due both to the the various sulphur-containing reservoirs of that country and its level of industrialization. Hence, the level of sulphur production of any country is dependent on not only natural resources but also on market factors (SAIMM, 2015).

Today, the world annually consumes approximately 55 to 60 million tons of the various types of sulphur. Its main use is in the fertilizer industry, but it is also used in the chemical, dye, paper, agrochemical, gunpowder, safety match, iron-steel, and oil industries. The total amount of recovered sulphur as a by-product of oil, natural gas, and smoke-stack gas has been increasing daily. Various associations, especially industrial, academic, civil and governmental organizations, are worried about the growing amount of by-product sulphur and they are investigating new potential areas in which it can be utilized. These include:

- As a binder in highway pavements,
- In the production of alloys,
- As a foam due to its insulation properties and high pressure resistance,
- As a construction material used in concrete, mortar, and aggregate.

3.2 Physical and Chemical Properties of Sulphur

Pure sulphur occurring in rhombic crystals is a yellow, tasteless, odorless, solid and nonmetallic element. Its melting, combustion and boiling points are 112.8, 270.0 and 444.6°C respectively. Its hardness is about 1.5–2.5, while its density has a range of 2.03 – 2.06g/cm³. Sulphur is not good at conducting heat and electricity, however, when rubbed, it takes on a negative charge. Its diverse physical properties are due to its complex molecular structure. Several different varieties of molecules can be observed in both its liquid and vapor states. This element does not dissolve in water when exposed to the weather, but rather it oxidizes gradually and becomes slightly acid (Texas Gulf Sulphur Company, 1957).

After its initial melting, sulphur becomes a thin liquid of a light yellow color. With subsequent heating, especially at 159.5°C, the sulphur becomes very fluid and its color gets darker. Interestingly, it gets harder at 200°C. Its viscosity starts to decrease over 250°C (approximately), and it becomes a thin liquid at 400°C (Maden Tetkik ve Arama Enstitüsü, 1984).

Sulphur, a fascinating element, can be found in multitude of forms. Normally, it exists as a solid in its familiar yellow form as either rhombic or monoclinic crystals, or as a dark amorphous, moldable mass referred to as plastic sulfur. Sulphur has the chemical symbol of "S" and atomic number of 16; its atomic weight is: 32.064. Similar to oxygen, it rapidly reacts with particularly metals, and as a chemical compound its chemical value is within -2 and +6. Sulphur is capable of reacting with nearly all elements except the noble gases and nitrous (N). Sulphur can chemically react as either an oxidant or reducing agent and it oxidizes most metals and several non-metals such as carbon, leading to its negative charge in many sulphur compounds. It reduces several strong oxidants, such as oxygen and fluorine (Cremlyn, 1996). It is noteworthy to point out that SO₂ and H₂S gas are poisonous.

In all its forms sulphur presents as molecules of eight-membered, (S_8) crown-shaped rings. At room temperature sulphur is stable in its rhombic form and this form turns to monoclinic form at 95.5°C. Just above this temperature, (especially at 114.6°C) it melts to a transparent, pale yellow mobile liquid. At a little below 160°C, the crown-shaped rings are about to break into chains and about 160°C, the ring-bonded form of sulphur is largely lost to a much darker, reddish-brown, viscous linear polymeric form, where "n", the number of bonded sulphur atoms is notably more than eight. While sulphur vapour consists of S_8 molecules at the boiling point, S_8 molecules convert to S_6 at higher temperature, and ultimately these molecules convert to S_2 at temperatures over 650°C (Maden Tetkik ve Arama Enstitüsü, 1984; Özgüler, 2005).

3.3 Sulphur Resources

Sulphur is one of the most abundant materials existing in the earth's crust. It is found in its elemental state in nature, as well as an organic compound and a sulphide after reacting with other elements.

Despite the plentiful natural sulphur resources, few of them are easily obtainable. The cost of the sulphur extracted from these reservoirs is higher than that of sulphur obtained as a by-product from an oil and natural gas refinery (Şener and Özgüler, 2000; Er, 2003; Sulphur Institute, 2011; Deniz, 2009). Table 3.2 shows the availability of sulphur resources.

Table 3.2 : Sulphur resources.

Natural Resources	Other Resources
Natural pure sulphur ore bed	Natural gas (includes H ₂ S and SO ₂)
Sulphite ore bed (such as pyrites and copper pyrites)	Power plant and industrial flue gas (includes SO ₂)
Sulphate ore bed (such as gypsum and alunite)	Oil and bituminous sand
	Coal and bituminous shale

3.3.1 Natural sulphur resources

Due to the high costs involved, only a few natural sulphur resources are convenient for mining and operations. The largest natural sulphur ore beds are found in Poland, the USA, Russia, Iraq, Mexico, China and Italy, while the largest pyrite ore beds exist in China, Russia, Spain and South Africa. Rich volcanic sulphur reservoirs are located in Turkey and Japan (Jimenez and Stokes, 1981; Şener and Özgüler, 2000; Er, 2003).

In addition to the sulphur found in its elemental state, sulphur that has reacted with various elements now exists as sulphate and organic compounds in sedimentary, metamorphic, volcanic rock and all fossil-originated fuels.

Based on origin, natural sulphur ore beds can be classified in three ways;

Sedimentary sulphur ore bed: Found in intermediate layers with gypsum or embodied in gypsum. The largest natural sedimentary sulphur ore beds are found in Poland, the USA, Russia, Iraq, Mexico, China and Italy.

Volcanic sulphur ore bed: This ore bed is massive and is incorporated in porous and volcanic rocks. Pyritic and clayish zones spread outward from the center of the rocks around the sulphur ore. Volcanic H₂S and SO₂ gas surfaces from faults and generate sulphur sublimation and crust on the ground.

Hydrothermal sulphur ore bed: Sulphur flowers are spherical or elliptical shapes that cover faults and cracks and powdered crack embankments. Sulphur is mostly seen in the intersections of the faults.

Elemental sulphur: This type of sulphur is recovered from salt dome sediments located in the Isthmus of Tehuantepec of Mexico and the gulf shores of the US. It is also recovered from west Texas (USA), Poland, Sicily, Russia and Iraq's evaporite basin sediments. Moreover, elemental sulphur is supplied from 12 different countries' volcanogenic natural sulphur ores. It is for this reason that fifty countries, including Canada, France, the U.S., Japan, West European countries, and Middle Eastern oil-producing countries forbid the release of poisonous H₂S and SO₂ gases.

Thirty countries, including Russia, Japan and Spain, have produced large amounts of pyrites. Both the U.S. and Russia rank as the world's the largest sulphur producers, as well as its greatest consumers. Canada and Poland are the third and fifth largest sulphur producers and the first and second sulphur exporters respectively.

Elemental sulphur is utilized in large quantities by the agricultural sector due to its needs for sulphuric acid. Sulphuric acid is also derived from pyrites, chimney gas, gypsum and anhydrides.

Although there are several sulphur production processes, the primary processes are the Frasch, Melting and Flotation Processes (Kenneppohl et al., 1975; Şener and Özgüner, 2000; Sulphur Institute, 2011).

Frasch Process:

The Frasch process, which extracts sulphur from underground deposits, is the only economical method of recovering sulphur from elemental deposits (Nehb and Vydra, 2006). This process depends on the pumping of superheated water into the sulphur deposits to melt and extract the high purity sulphur. Three concentric tubes are first drilled and inserted into the sulphur deposit. Superheated water under high pressure (165°C, 2.5-3MPa) is injected into the deposit via the outermost tube. The sulphur then begins to melt and flow into the middle tube. Water pressure alone is not enough to force the sulphur to the surface due to the molten sulphur's greater density, so hot air is also introduced via the innermost tube to froth the sulphur, making it less dense, and pushing it to the surface (Nehb and Vydra, 2006).

A light yellow and very pure (99.7-99.8%) sulphur can be obtained with this method. However, when contaminated by organic compounds, it can be dark-colored. Further purification is not economic, but usually required.

The Frasch process can be used on deposits that are 50 to 800 meters deep. This method, however, requires 3 to 38 cubic meters of superheated water to recover every ton of sulphur, making the associated energy costs significant (Nehb and Vydra, 2006).

Up until the late 20th century most of the world's sulphur was obtained this way. The United States used this method to produce 3.89 million tons of sulphur in 1989, and Mexico produced 1.02 million tons of sulphur in 1991 with this method (Nehb and Vydra, 2006). Once, however, sulphur started to be recovered from petroleum and gas sources (recovered sulphur), the Frasch method became less popular. As of 2011, the only operating Frasch mines worldwide were in Poland and since 2010 in Mexico. The last Frasch mine operating in the United States was closed in 2000 (Sulphur Institute, 2011).

Melting process:

In this process, rich sulphur ore is crushed into 2cm pieces then transferred to melting pools, where a blender is used to very rapidly melt the sulphur ore. After being separated from the unmelted coarse sulphur with a sieve, the liquid sulphur is sent to a second pool. Subsequent to filtration, highly purified liquid sulphur (99.8%) is stockpiled in a third pool.

Flotation Process:

In this method, ores with lesser amounts of sulphur are crushed and sent to the concentrator. The sulphur foam that collects on the surface of the concentrator is separated and the pyrites settled. Once its moisture is lowered to 15 to 20%, the concentrated sulphur ore is converted to a liquid state in hot melting pools. Ultimately the liquid, 99.8% pure sulphur is stockpiled in another pool via filtered-pumping (Şener and Özgüner, 2000; Er, 2003).

When the bitumen in bituminous shale, sand, and coal is melted or hydrogenated, the resulting liquid or gas state of H₂S can then be converted to elemental sulphur. When Turkey's Keciborlu Sulphur Enterprise was still in operation, it used this flotation

process to produce sulphur (Şener and Özgüler, 2000; Devlet Planlama Teşkilatı, 2001).

3.3.2 Other resources

Natural sulphur represents only a small amount of the world's total consumed sulphur. Today almost all sulphur and its derivates are extracted with various methods from the wide array of industrial smokestacks. In recent years the amount of sulphur obtained as a by-product has surpassed that found in the plentiful natural reservoirs. For instance, in spite of the fact that it does not have an oil reservoir, Japan is the second elemental sulphur supplier via recovery from oil refineries.

The main resources include the smokestacks of oil refineries, natural gas operating foundations, thermal power stations and iron producing blast furnaces. Sulphur exists in an unbound state, as a compound of H₂S and SO₂ in natural gas, and it exists as an organic compound in crude oil. Desulphurization is the method used to recover sulphur from natural gas and oil. During the refinement process, the hydrogenation process converts some of the gas into H₂S. This gas is then passed through a solution to separate H₂S and CO₂. Following this process, the H₂S in the solution remains as concentrated H₂S gas.

Sulphur recovered from flue gas is a by-product of oil refineries located in different parts of the world. In addition to oil refineries, sulphur is also produced in the smokestacks of natural gas facilities found mainly in Canada, France and more than 10 other countries (Kennepohl et al., 1975; Şener and Özgüler, 2000; Devlet Planlama Teşkilatı, 2001).

3.4 Sulphur in Turkey

In addition to pyrite and gypsum, Turkey also has plentiful elemental sulphur reservoirs. Turkey's only operable natural sulphur ore bed is located in the province of Isparta-Keciborlu. In 1992 a total of 22,700 tons of elemental sulphur was sourced from 100,750 tons of raw sulphur ore in this bed. One year later, 650,000 tons of raw sulphur ore remained. However, ETIBANK (an enterprise bank that was established in 1935 to finance the Turkish natural resources economy) operated this sulphur ore bed until 1995, and then closed it due to its expired economic life. At this point Turkey started to produce its elemental sulphur through TUPRAS (Turkey's largest

petrochemical company, with a 28.1 m ton crude processing capacity petrochemical facility). Considering that crude oil consists of 2% sulphur, more than a total of 500,000 tons of sulphur are expected to be recovered annually from Turkey's refineries. However, due to the plant's 59% productivity inefficiency rates, the maximum volume of producible sulphur is actually 300,000 tons. Since half of this amount is required to produce sulphuric acid, Turkey currently has the potential capability of producing 150,000 tons of elemental sulphur in its refineries.

TUPRAS has four main refineries and these are located in the provinces of Izmit, Izmir, Kirikkale and Batman. However, sulphur is currently being recovered from only three of these (Izmit, Izmir and Kirikkale). These refineries' average daily sulphur production capacities are shown in Table 3.3.

Table 3.3 : Sulphur production of TUPRAS (Deniz, 2009).

Refinery	Production Capacity of Sulphur (m ³ /day)
Izmit	137
Izmir	113
Kirikkale	83

Once these Turkish refineries begin to operate sulphur recycling processes, the volume of sulphur being recovered will rise considerably, eliminating Turkey's need for sulphur importation. For instance, the U.S. increased its volumes of recovered sulphur to 84% between the years of 1981 through 1991 by operationalizing additional recovery units (Sulphur Institute, 2011). Sulphur consumption ratios in Turkey are shown in Table 3.4.

Table 3.4 : Sulphur consumption in Turkey.

Sector	Percentage (%)
Agriculture	65.2
Paper	10
Defence Industry	9
Chemical Industry	5.7
Textile Industry	5.5
Detergent Industry	2.1
Rubber Industry	1.2
Others	1.3
Total	100

The total amount of consumed sulphur in Turkey includes the elemental sulphur produced at the Keciborlu Sulphur Enterprise, the sulphur recovered from the Izmit, Ipras, and Kirikkale refineries and the sulphur imported from abroad. During the years between 1988 and 1992, sulphur consumption ranged between 140,000 and 200,000 tons. Because Turkey's Keciborlu Sulphur Enterprise halted its production of elemental sulphur in 1995, Turkey has been currently importing more than 75% of the sulphur it needs to meet its demands (Er, 2003).

4. UTILIZATION OF SULPHUR IN HIGHWAY CONSTRUCTION

Faced by the facts that bitumen is a by-product of oil refining, is expensive, and that its volume does not meet demands, pavement engineers assumed the responsibility of finding a binder they could use as an alternative to bitumen. Prior to the global economic crisis of the 1970s, the price of bitumen was approximately 25 to 30 dollars per ton. In the following decade this price rose to 175 to 200 dollars per ton. After researching several different kinds of materials, these engineers began to focus on sulphur owing to its promising abundance, accessibility, cost, compatibility, and ecological impacts. Elemental sulphur began to be used as a replacement for a considerable portion of the conventional bitumen. Typically up to 50 percent by weight of sulphur is substituted for bitumen to generate sulphur-extended-pavements (SEP). However the term "SEP" was used to refer not only to binder, but also to paving mixture and pavements. Extensive laboratory, field work, and analytical investigations were conducted on several SEPs to find a feasible alternative to ordinary asphalt-concrete-pavements (ACP).

In the 1970's deep interest began increasing the utilization of SEP, especially in North America, Canada, Europe, and the Middle East. Although many studies of this issue were completed in the past, the SUPERPAVE (SUperior PERforming Asphalt PAVEments) system that gave pavement engineers the opportunities they need to design pavements that will perform better under extreme conditions such as high temperatures and heavy traffic loads had not yet been developed. Thanks to the Strategic Highway Research Program (SHRP), the SUPERPAVE system was introduced in 1992 in order to provide engineers with new ways to test and analyze binder behavior and performance. A new binder specification based on performance grades (PG) was also generated.

These SUPERPAVE investigations and tests, as well as sulphur's ready availability from natural gas, oil sands and refineries, rather than from natural reservoirs, have recently led pavement engineers to reestablish sulphur as an excellent binder.

Many-sided assessments have concluded that there are no remarkable overall differences in either laboratory and field performance between SEP and ACP. Additionally, these assessments also determined that SEP has both lower temperature susceptibility and higher resistance to moisture susceptibility than ACP. SEP also has less of a tendency to succumb to destructive distresses, particularly fatigue cracking and rutting. Prior to mentioning these previous investigations in detail, some of studies are briefly summarized below.

Kennepohl et al. investigated samples of hot mix asphalt with binders of 50% sulphur and 50% conventional bitumen, and with a 85-100 penetration grade by weight. They presented the Marshall stability and flow, stiffness, and fatigue results of the samples. The results revealed that Marshall Stability increased proportionally with mounting sulphur content, while no considerable loss in flow values was observed. He also observed that the sulphur had no unfavorable effects in terms of fatigue life (Kennepohl et al., 1975).

In his comparisons of SEP and ACP performances, *Lytton et al.* employed the VESYS IIM software program, which is capable of analyzing viscoelastic pavement designs. His results demonstrated that SEP was clearly less prone to rutting compared to ACP, and even had a more preferable serviceability index. However, SEP's high susceptibility to moisture was not also overlooked (Lytton et al., 1977).

Kennedy et al. conducted a full-scale laboratory project aimed at monitoring the engineering properties of sulphur-extended mixtures. As a binder, three different percentages of sulphur (0, 20 and 50%) by weight were substituted for two different bituminous binders with penetration grades of 40-50 and 85-100. He loaded the prepared specimens under static and repetitive loads to reveal their Indirect Tensile Test (ITS) results at the temperatures of 10, 24, 38 and 52°C. His results confirmed considerable improvement in the modulus of elasticity, fatigue life, and tensile strength when the substituted sulphur increased to 50% percentage (Kennedy et al., 1977).

In their efforts to monitor material characterization, *Al Otaishan and Terrell* conducted a field study on four different highways paved with SEP in Nevada, Texas and Louisiana (USA). These researchers performed Marshall Stability and flow, modulus of elasticity, creep and fatigue test under static and repetitive loads on the

SEP specimens. They claimed that SEP and ACP showed similar performance in service, however, SEP had higher tendencies to rapid loss in stability, modulus of elasticity, and fatigue resistance (Al-Otaishan and Terrel, 1980).

Mc Bee et al. also conducted a similar full-scale experimental study on SEP specimens. They stated that SEP specimens whose bituminous binder was substituted with 26% sulphur by weight was said to have performed similarly with ACP specimens. They observed preferable stability and stiffness when the sulphur was increased (McBee et al., 1980).

These studies agree that SEP applications will serve to preserve limited bitumen resources, and provide promising and low-cost pavements blended at low temperature.

During the course of study on the thesis, "A State of the Art" this researcher wrote a paper providing detailed background information about "Utilization of Sulphur in Highway Construction". It was sent to one of ASCE's conferences. The paper was accepted by the scientific committee of the ASCE conference. The paper titled *Sulphur Utilization in Asphaltic Concrete Pavements* was verbally presented at the Airfield & Highway Pavement Conference held in Los Angeles, California on June 9 – 12, 2013.

5. EXPERIMENTAL STUDY

Numerous experiments classified as first generation and SUPERPAVE tests have been performed on bituminous binders.

The First Generation Tests include:

Penetration Test, Softening Point Temperature Test, Penetration Index, Specific Gravity Test, Viscosity Test, aging and Loss on Heating Test, Storage Stability Test, Solubility Test, Frash Breaking Test, Elastic Recovery Test, Flash and Fire Point Test, Ductility Test, Float Test and Water Content Test.

This study conducts the first six tests on this list.

5.1 First Generation Tests

5.1.1 Penetration test

This test is the most commonly used method of measuring the consistency and hardness of a bituminous material under specified standards of load, temperature, and time. Standards are met by utilizing a 100 gram weight, a standard sewing needle, a 5 second loading duration at 25°C. It should be noted that this test may occasionally be conducted at 0°C with a 200g load for 60 seconds or/and at 46.1°C with a 50g weight for 5 seconds (Fwa, 2005). The penetration grade is determined by a standard sewing needle vertically penetrating the bitumen in tenths of a millimeter increments. A bitumen penetration grade of 50 indicates that the needle penetrates 5mm. Since bitumen is viscoelastic, the penetration grade depends not only on elastic deformation, but also on viscosity. It is clear that due to changes in viscosity at different temperatures, different bitumens may have the same hardness at a temperature of 25°C, but different hardnesses at other temperatures (Illston and Domone, 2001).

One way to classify a bituminous binder is by grading its penetration value, even though this value is not related to its quality (Pavement Interactive, 2012). Although

grades of penetration range between 20 to 330, typical bitumen binders in Turkey, as well as in many countries, have a grade range of 40 to 220 (B40/60, B50/70, B70/100, B100/150, and B160/220).

The penetration of a bitumen binder is inversely proportional to its consistency. While hard bitumen has a low penetration, soft bitumen has a high penetration value. Therefore, these "soft" bituminous binders with high penetration numbers are used in colder climates while "hard" binders with low penetration numbers are typically used in warmer climates.

Even though this test empirically correlates binder performance in terms of viscosity, there are some disadvantages as well. Table 5.1 explains the advantages and disadvantages of this test (Roberts et al., 1996).

Table 5.1 : Advantages and disadvantages of a penetration test.

Advantages	Disadvantages
The test is performed at 25°C, which is reasonably close to a typical pavement service temperature.	The test is empirical and does not give any hints about quality and fundamental engineering parameters such as viscosity.
May also provide a better correlation with low-temperature asphalt binder properties than the viscosity test, which is performed at 60°C.	Shear rate is variable and high during the test. Since bituminous binders typically behave as a non-Newtonian fluid at 25°C, this will affect test results.
To understand the temperature susceptibility of the bitumen binder, the test can be carried out at different temperatures.	Temperature susceptibility cannot be figured out by a single test at 25°C.
The test is practical and cheap. Hence, it can readily be conducted in the both laboratory and field.	The test does not represent behaviour of binder at mixing and compaction temperatures.

The process of the "Standard Test Method for Penetration of Bituminous Materials" is specified in AASHTO T49 and ASTM D5, and is as follows;

- Stored bitumen is heated in an oven until it becomes fluid.
- Flowable bitumen is poured into a 55mm diameter and 35mm height container. It is then cooled to room temperature (approximately 25°C) for at

least 60 minutes (Any possible air bubbles are removed from the specimen by vacuum or vibration).

- The prepared specimen is kept in a 25°C water bath for at least 60 minutes.
- The standard sewing needle is cleaned and a 100g weight is placed above the needle.
- The needle is carefully mounted on the bitumen specimen, so that it just touches the surface of bitumen.
- The needle is allowed to penetrate freely for 5 seconds.

An average of at least three readings will result in the penetration grade of the bitumen sample (A typical penetrometer is shown in Figure 5.1).

The penetration depths are very sensitive to both test conditions and the prepared bitumen samples; therefore, all of the specified requirements should be completely fulfilled. The maximum difference between the highest and lowest readings should not be higher than (Diew, 2001a):

Penetration (d-mm)	0-49	50-149	150-249	250-500
Maximum difference (d-mm)	2	4	12	20



Figure 5.1 : A typical penetrometer.

5.1.2 Softening point temperature test

Unlike ordinary materials, due to its viscoelastic behavior, a bituminous binder does not melt at a definite temperature. As the temperature rises, this binder gradually changes from its brittle consistency behavior to a less viscous liquid. The softening point must be determined by using a fixed and closely defined method. The softening point test (also known as ring and ball test) is a method used to determine the softening point of not only bituminous binders, but also such thick films as joint and crack fillers and roofing materials, which range from 30 to 150°C (Diew, 2001b). This test is also an indirect measure of viscosity or, rather, the temperature at which a given viscosity is evident. A high softening point bitumen has less susceptibility to temperature and can flow in various rates. In addition to viscosity, it was observed that when bitumen is at its softening point it has a grade of approximately 800. However this approach is only an approximation and it can differ from one bitumen

to another owing to its non-Newtonian behavior and the different shear rates used by different methods (Chen and Richard Liew, 2002). The primary goal of the test is to evaluate the temperature at which a bituminous binder is too soft to carry two steel balls (each weighing 3.5g and falling from 25mm).

A softening point temperature test apparatus is shown in Figure 5.2. The process of the "Standard Test Method for Softening Point of Bitumen" is specified in ASTM D36 and AASHTO T53 and is summarized as follows:

- Subsequent to heating, fluid bitumen is poured into two pre-heated brass rings.
- The bitumen-filled rings are placed on a pre-treated plate with a release agent and allowed to cool to room temperature for least 30 minutes (60 minutes in this study).
- When the specimens have cooled, excess bitumen is cleanly cut away with a slightly heated knife or spatula, so that each disk is flush and level with the top of the ring.
- Bath liquids and thermometers are prepared (Although there are other baths such as USP Glycerin and Ethylene Glycol, the most widely used is boiled distilled water and is used in this study).
- The apparatus with the rings, thermometer, and ball guides are assembled into position.
- A beaker is filled with the distilled water at a temperature $5.0\pm0.5^{\circ}\text{C}$ per minute.
- The liquid is stirred and heated to a temperature of $5.0\pm0.5^{\circ}\text{C}$ per minute.
- The bituminous binder is heated until it softens enough to allow the ball to pass through the ring.
- Two temperature readings for each ball touching the bottom are recorded. Then the softening point of the binder is calculated as the mean of these two records (It is crucial to note that if the difference between the two temperatures exceeds 1°C , the test must be repeated).



Figure 5.2 : A softening point temperature test apparatus.

5.1.3 Penetration index

Since all bituminous binders behave thermoplastically, they become softer when heated, and stiffer when cooled. They should never become softer than the softening point expected under traffic during its service life. Even though there are several equations that create a relationship between consistency and temperature, the most prevalent and widely accepted one is that proposed by Pfeiffer and Van Doormaal.

Non-blown bitumens exhibit a linear relationship between the logarithm of the penetration grade and temperature when below the softening point temperature. This is depicted in Equation 5.1.

$$\log P = AT + K \quad (5.1)$$

where:

P = penetration at temperature (T)

A = temperature sensitivity (or temperature susceptibility)

K = constant

Slope A is a measurement of a given bitumen's temperature susceptibility and is calculated by measuring the penetration grade at two different temperatures (T_1 and T_2) as shown in Equation 5.2.

$$A = \frac{\log(\text{pen at } T_1) - \log(\text{pen at } T_2)}{(T_1 - T_2)} \quad (5.2)$$

The value of A varies from 0.015 to 0.06, meaning that there may be a significant difference in temperature susceptibility. Because these values make it difficult for a road engineer to determine temperature susceptibility, Pfeiffer and Van Doormaal have devised an equation of temperature susceptibility that has a penetration index (PI) assuming a "normal" 200 penetration. Mexican bitumen has a 0 (zero) PI and other bituminous binders are then compared to this standard. The PI is calculated as follows in Equation 5.3.

$$PI = \frac{20(1 - 25A)}{(1 + 50A)} \quad (5.3)$$

where:

PI: penetration index

A: temperature susceptibility

The value of PI ranges from around -3 for high temperature susceptible bitumens to around +7 for highly blown low-temperature susceptible (high PI) bitumens. Initially, a bitumen having a PI less than zero was accepted as being inferior in terms of temperature susceptibility. However, current binders are considered acceptable if they have a PI that ranges between -1 and +1 (Brennan and O'Flaherty, 2002). J.M. Illston and Domone say that a PI range of -2 to +2 is also preferable. They also claim that low-PI-bitumens behave more Newtonian and become very brittle at low temperatures. In contrast to low-PI-bitumen, high-PI bitumens have a tendency to exhibit time-dependent elastic properties and have more resistance to permanent deformation (Illston and Domone, 2001).

The consistency of bitumen at the softening point can be expressed in terms of penetration by linear extrapolation of a logarithm of penetration versus temperature, as well as by a direct measurement with an extra-long penetration needle at the

softening point temperature. *Pfeiffer and Van Doormaal* claimed that almost all bitumens had a penetration grade of 800 at their softening point. Instead of T_2 and penetration at T_2 , softening point temperatures and 800d-mm are respectively utilized in Equation 5.2 and then can be converted a new equation (Equation 5.4) and depicted as follows;

$$A = \frac{\log(\text{pen at } T_1) - \log 800}{T_1 - \text{SPT}} \quad (5.4)$$

where:

SPT: Softening Point Temperature ($^{\circ}\text{C}$)

Since, typically, the standard penetration test is conducted at 25°C , T_1 can be replaced by 25 and by substituting the new equation in the equation for PI (Equation 5.4 and 5.3) the final equation (Equation 5.5) calculating the penetration index (PI) of a given bitumen can ultimately be obtained as follows:

$$\text{PI} = \frac{1952 - 500 * \log(\text{pen at } 25^{\circ}\text{C}) - 20 * (\text{SPT})}{50 * \log(\text{pen at } 25^{\circ}\text{C}) - \text{SPT} - 120} \quad (5.5)$$

It should be noted assuming a penetration of 800 at SPT is not always valid for all bitumen. To obtain a more precise PI, a penetration test at two different temperatures (T_1 and T_2) should be performed.

To draw an easier interpretation, two different nomographs are generated for an approximate measurement of PI by either the penetration at 25°C and the SPT, or the penetration of the bitumen at two different temperatures (T_1 , T_2). The nomographs and how to use them are shown in Figure 5.3 and 5.4.

Draw a line between the softening point (line A) and penetration (line B) values. The intercept on line C is the PI of the bitumen

Penetration
at 25 °C : dmm
B

Softening point
(IP): C
A

150

140

130

120

110

100

90

80

70

60

50

40

30

Penetration
index
C

800

700

600

500

400

300

200

100

90

80

70

60

50

40

30

20

10

9

8

7

6

5

4

3

2

1

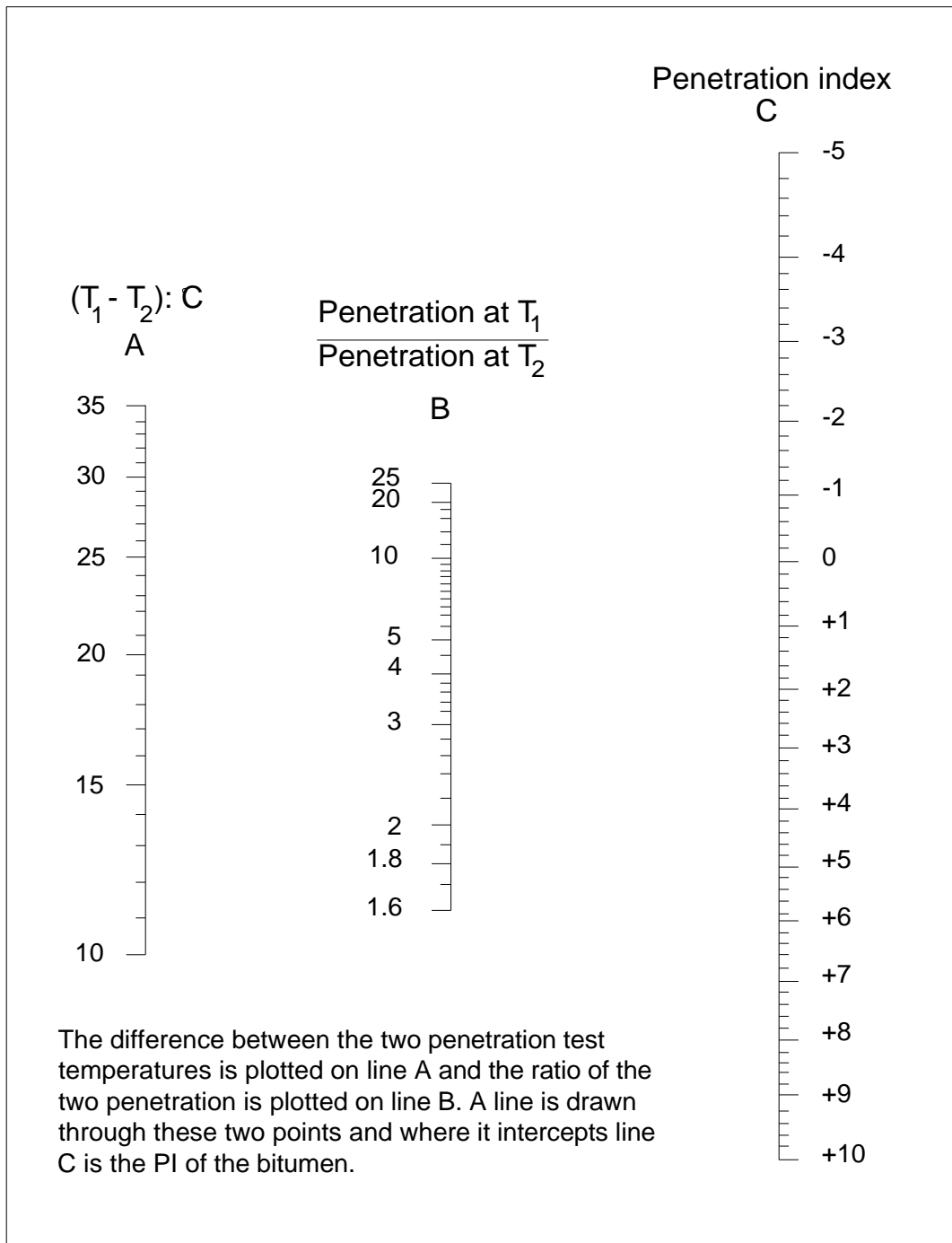


Figure 5.4 : Nomograph for penetration index (pen/pen) (Read and Whiteoak, 2003).

Lubbers pointed out that the chemical composition of bitumen has a major effect on its temperature susceptibility, as depicted in Figure 5.5. Lubbers also says that PI generally increases when excessive asphaltenes override the aromatics (Lubbers, 1985).

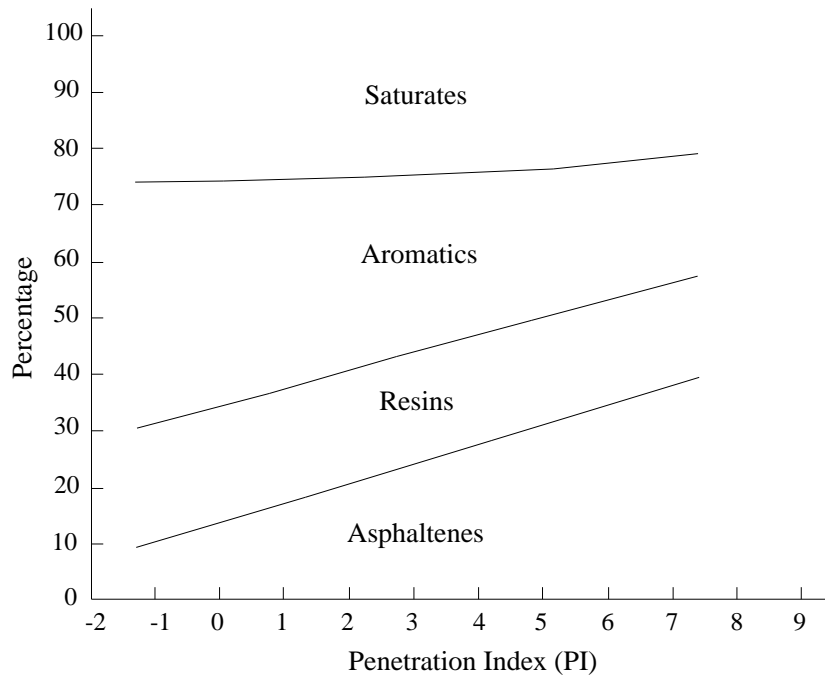


Figure 5.5 : The relationship between chemical composition and the PI (Lubbers, 1985).

In addition to temperature susceptibility, PI is also utilized to predict the stiffness of a given bitumen for an analytical pavement design. It can also, to a limited extent, be used to identify a particular type of bituminous binder. One deficiency of the PI test system is that it utilizes the changes in bitumen properties over a relatively small range of temperatures to characterize bitumen. Extrapolations of the extremes of the behavior can sometimes be misleading. This test can give a good approximation of the behavior to be expected, but confirmation using stiffness or viscosity measurements is desirable (Pfeiffer and Van Doornmal, 1936; Heukelom, 1973; Diew, 2001a; Brennan and O'Flaherty, 2002; Read and Whiteoak, 2003).

The effects of temperature and loading time on stiffness of a high PI bitumen are shown in Figure 5.6.

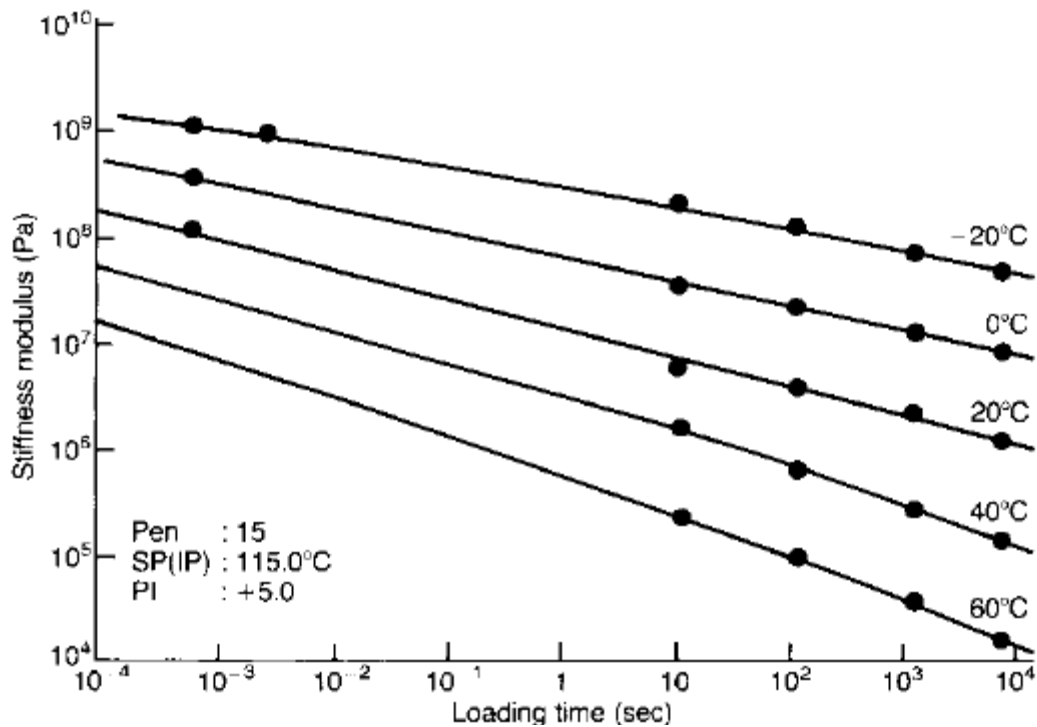


Figure 5.6 : The effect of temperature and loading time on stiffness of a high PI bitumen (Read and Whiteoak, 2003).

5.1.4 Specific gravity test

Specific gravity refers to the ratio of mass of a given volume of any material of known content to the mass of an equal volume of pure water at 25°C . The specific gravity can be calculated by using either a pycnometer or by using a prefabricated cube specimen of known volume and mass. In pavement design, particularly in HMA, the specific gravity of a binder is very important because when used with aggregates its weight is converted to volume using its density values. In other words, the determination of the effective bitumen content and the percentage of air voids in compacted bituminous hot mixture specimens and compacted pavements is vital (Asphalt Institute, 1998; Mathew and Rao, 2006).

The specific gravity of bitumen strongly depends on its chemical composition, its grade, and the temperature (Read and Whiteoak, 2003). As stated in previous sections, there are four different constituents in asphalt, and their molecular weights are totally different. The fractional volume of these constituents affects not only the bitumen grade but also its density. In general, the specific gravity of any bitumen typically varies from 1.00 to 1.04 at 25°C and its thermal expansion coefficient is about 0.00061 per $^\circ\text{C}$ (Brennan and O'Flaherty, 2002). In addition to the grade of bitumen, temperature also plays a major role in the specific gravity. Since bitumen

expands and contracts at elevated and lower temperature respectively, the volume of a given amount of bitumen is not always the same; its volume becomes greater at elevated temperatures than it does at lower ones. Therefore, it is impossible to maintain bitumen volume and, consequently, its density at constant rates (Asphalt Institute, 1998). Typical values of specific gravities for a range of grades of bitumen are given in Table 5.2.

Table 5.2 : Typical specific gravity of bitumens at 25°C (Read and Whiteoak, 2003).

Penetration Grade	Typical Specific Gravity at 25 °C
40/60	1.025-1.035
50/70	1.020-1.030
70/100*	1.020-1.030*
100/150	1.020-1.030
160/220	1.015-1.025

** is not originally stated in the table; however it is supposed and added.*

Methods used to measure the specific gravity of bitumen depend on its type. These are depicted below in Table 5.3.

Table 5.3 : Ways to measure specific gravity of bitumens.

Method	Type of bitumen
Hydrometer	Thin fluid bitumen
Pycnometer	Viscous fluid, semi-solid bitumens and emulsions
Displacement	Hard, solid bitumens

The pycnometer method is utilized in this study by referencing Specific Gravity and Density of Semi-Solid Bituminous Materials specified as in AASHTO T 228 and ASTM D 70.

The main stages of this method are:

- The dried and cleaned pycnometer and its stopper are weighed and expressed as "a";
- The pycnometer is filled with freshly boiled distilled water and its stopper is firmly inserted. The complete equipment is then immersed in the water bath

and is maintained at 25°C at for at least half hour (Air bubbles must be avoided).

- The pycnometer should be checked to ensure that the meniscus of water in the bore of stopper is at the same level as the top of the stopper. If there is insufficient water, the bore should be filled. In case of excess water, the excess should be removed. The outer surfaces of the pycnometer should be wiped after removing it from the water bath.
- The pycnometer is filled with distilled water, is weighed, and expressed as "b".
- The pycnometer is emptied and kept in the oven until all the distilled water has evaporated.
- The pycnometer is filled approximately half full with pre-heated bitumen. The bitumen should not be allowed to contaminate the sides of the pycnometer above the top level of the bitumen and no air bubbles should be allowed to form.
- The bitumen-filled pycnometer is allowed to cool at room temperature for at least a half hour then weighed. This value is expressed as "c".
- The rest part of the pycnometer is filled with fresh distilled water and its stopper is inserted. The equipment is then immersed in the water bath (maintained at 25°C) for at least half hour. No air bubbles are allowed to form.
- The third stage is repeated and the pycnometer is filled with bitumen and fresh distilled water then weighed and expressed as "d".

In brief:

a = weight of empty pycnometer with its stopper (g)

b = weight of pycnometer filled with distilled water (g)

c = weight of pycnometer filled with bitumen (g)

d = weight of pycnometer filled with bitumen and distilled water (g)

G = Specific Gravity

The Specific Gravity (G) of bitumen at 25°C is calculated as follows in Equation 5.6 (Kett, 1998):

$$G = \frac{(c-a)}{(b-a)-(d-c)} \quad (5.6)$$

5.1.5 Viscosity test

The mechanical response of any rheological material under loading depends upon such applied external conditions as stress, strain, timescale and temperature. The science focusing on the rheological materials is known as rheology. Bituminous binder, a rheological material, plays a major role on both quality and performance of HMA pavements.

Because it exhibits both elastic and viscous behavior, bituminous binder is classified as a viscoelastic material. A material's elastic, viscous, and viscoelastic responses to an applied load totally differ from one another. When exposed to a constant load, the deformation of elastic material is recoverable. When the constant (or creep) load is removed, the deformation disappears and the material immediately returns to its initial shape. However, if a viscous material subjected to a constant load the deformation will occur at a constant rate up to the removal of the load is removed. However, even though the load is removed, the deformation remains constant. In this case it is said that a viscous material has experienced "non-recoverable deformation" (Anderson et al., 1994).

When subjected to a creep load, viscoelastic material, which – as its name implies – exhibits both elastic and viscous behavior, undergoes an immediate deformation followed by a continued time-dependent deformation. The immediate deformation and the time-dependent deformation represent the material's elastic and viscous responses respectively. Once the load is removed, the viscous-induced deformation immediately halts, but the deformation it has experienced up to then is not recoverable. The postponed elastic deformation, however, is slowly recovered at a decreasing rate. Hence, a viscoelastic material experiences only a partial recovery of a deformation resulting from creep loading (Zaniewski and Pumphrey, 2004).

Figure 5.7 briefly depicts the behaviors defined above:

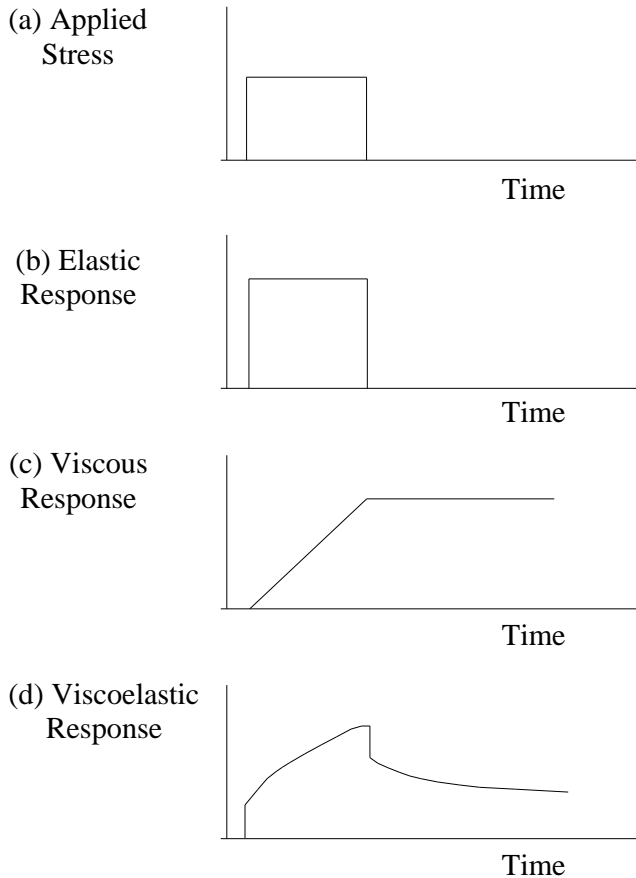


Figure 5.7 : Mechanical response of elastic, viscous and viscoelastic materials (Zaniewski and Pumphrey, 2004).

Resistance of any fluid to shear or tensile stress is defined as "viscosity". In general, viscosity is substantially related to consistency and less-viscous fluids have less consistency or vice-versa. The tendency of a fluid's movement is mainly dependent on its internal friction, thereby its viscosity. In reality all fluids have more or less resistance to deformation and movement and, therefore, all are viscous. When bitumen, a viscoelastic material, is at low temperatures its elastic behavior is dominant and it acts like a solid; hence, it obeys Hooke's law (stress-strain relationship). On the other hand, at high temperatures bitumen behaves like a liquid and exhibits fluid flow properties, namely viscosity. Therefore, the viscosity of bitumen at elevated temperatures must be investigated. In addition to the temperature, the behavior of bitumen is also related to the duration of loading. Under shorter loading time it behaves as a solid, whereas under longer loading time it acts as a fluid. In brief, bitumen exhibits discrete properties depending upon temperature and loading duration.

The viscous parameter of bitumen must also be investigated by determining HMA performance. When the volume of viscous binder is low, HMA pavements can be susceptible to rutting and bleeding, while HMA pavements consisting of a more viscous binder can be susceptible to thermal cracking.

There are two common viscosities of bitumen: absolute (dynamic) viscosity and kinematic viscosity. Since HMA pavement surfaces in the USA and in many countries face a maximum temperature of 60°C, absolute (dynamic) viscosity of bitumen is measured at this temperature. Physically, it means the resistance of bitumen to flow and can be formulated as the ratio of shear stress to shear rate at 60°C in Equation 5.7.

$$\mu = \frac{\tau}{\gamma} \quad (5.7)$$

where:

μ = viscosity (in cgs units of poise). poise = dyne-sec/cm² = g/cm-sec (the SI unit of viscosity is the Pa-sec = N-sec/m² = 10 poise)

τ = shear stress

γ = shear rate

The basic absolute viscosity is fundamentally based on the calculated time it takes for a fixed volume of bitumen binder to be vacuumed through a capillary tube under closely controlled conditions of vacuum and temperature (ASTM, 2001). The process for absolute viscosity test is specified in both AASHTO T202 and ASTM D2171 "Standard Method of Test for Viscosity of Asphalts by Vacuum Capillary Viscometer".

Although it may seem as if the absolute viscosity is more advanced than empirical tests such as penetration test, this test cannot fully explain the behavior of bitumen due to its lack of consistency over the expected range of construction and service conditions.

A viscosity grade at 60°C can also be utilized to categorize bitumen, although bitumen is typically classified according to its penetration grade. ASTM D3381 specifies six different unaged bitumen binders: AC-2.5, AC-5, AC-20, AC-30 and AC-40. Viscosity is measured with various types of viscometers and rheometers and

stated in "poise". The first character (A) stands for unaged Asphalt Cement while the second (C) stands for the viscosity of a hundred times of poises. For instance, AC-2.5 has a viscosity of 250 poises at 60°C. AC-30 is therefore softer than AC-40. There is also another type of viscosity grading system based on the short-term aged residue viscosity grading system or AR viscosity grading system. This system classifies bitumen using aged residue from a rolling thin film oven test (RTFOT). Similar to the AC viscosity grading system, the viscosity of RTFOT aged bitumen is measured at 60°C. However, this system describes five different asphalt cements according to their viscosity grades: AR-1000, AR-2000, AR-4000, AR-8000 and AR-16000. An AR-1000 grade refers to an RTFOT aged bitumen with a viscosity of 1000 poises at 60°C. The AR viscosity grading system is primarily used by western countries (Zaniewski and Pumphrey, 2004).

Another viscosity standard is kinematic; this is measured at 135°C, the temperature at which bitumen is fluid enough to flow through a capillary tube under its own weight. This temperature can also be used to simulate the mixing and compaction temperatures of HMA construction.

The kinematic viscosity test is based on the calculated time it takes for a fixed volume of bitumen binder to pass through a capillary viscometer under closely controlled conditions of heat and temperature. A liquid's kinematic viscosity is equal to the ratio of its absolute (dynamic) viscosity to its density (ASTM, 2001).

"Standard Method of Test for Kinematic Viscosity of Bitumen" is stated in both AASHTO T201 and ASTM D2170.

5.1.6 Aging and loss on heating test

Here the term durability designates the ability to survive, sustain, and perform at permissible levels. When used as an attribute of bitumen, it is defined as the degree to which bitumen preserves its physical properties under changing circumstances, particularly aging (Illston and Domone, 2001). Durability ranks as one of the most desired properties of a hot bituminous mixture. To ensure this, the bitumen and aggregate must be preheated prior to the manufacturing of a hot mix asphalt. After it is prepared, the mixture is transported to a job site to be poured and compacted. By the time the compacted mixture begins to cool to the normal pavement temperatures, the bitumen has already substantially aged. The typical properties of the ultimate

bitumen in service differ greatly from those of the initial bitumen. Unfortunately, bitumen gets more viscous, stiffer, and more brittle as a result of the aging process, and worse still, this process is inevitable. Since the role of the aged binder is much more important than that of the initial binder in the overall desired performance of the mixture, the mechanism of aging and its progression must be carefully investigated (Chen and Richard Liew, 2002).

Aging is caused by mainly:

Oxidation: Oxygen physically diffuses into the bitumen, where it causes several chemical reactions. When bitumen is subjected to atmospheric conditions, resin, one of lower molecular weight constituents, latches onto the oxygen molecules and turns into asphaltenes. This causes an increase in the polar high molecular weight fraction and will result in high viscosity. In addition to viscosity, the bitumen becomes unstable because of the discontinuity that forms between the saturates and other constituents. This is the reason both for the loss of cohesion in the bitumen and the occurrence of cracking. Oxidation mainly occurs during the blending process in the plant and the paving in the field (Illston and Domone, 2001). Oxidation is affected primarily by temperature, time, and the thickness of the bitumen film, as well as by fractional constituents and the structure of the bitumen (Shui et al., 1998). Here temperature plays two major roles. On the one hand, it accelerates the oxygen diffusion rate by softening the bitumen and, secondly, it paves the way for chemical reactions (Hagos, 2008). Different studies have revealed that the oxidation sensitivity of bitumen not only depends on the source of the original binder but also on the annual atmospheric cycle, such as temperature variations, rain/water, and ultraviolet light and so on. The aging rate of bitumen is greatly affected by both daily and seasonal pavement temperatures. This susceptibility of the binder aging rate to the temperature is binder specific. Binders from different sources may also demonstrate different aging dependencies. The degree of aging of bitumen may also be related to the energy of the solar influx depending on the cut-off angle of the sun's radiation (Anderson et al., 1994).

Volatilization: The volatilization of bitumen is fundamentally related to its integrity and fumigation. At elevated temperatures, especially during the manufacture of hot mix asphalt, lighter components of bitumen evaporate and the bitumen starts to fume. The loss of volatiles is relatively small after the bituminous material has been laid

(Illston and Domone, 2001). Less volatile bitumen is also less sensitive to alterations of its rheological properties, and is therefore more stable than highly volatile bitumen (Hagos, 2008).

Polymerisation: This effect is caused by a combination of like molecules forming larger molecules resulting in a progressive hardening. At low temperatures the rate of association is considered slow as a result of the higher viscosity of the binder (Peterson, 2000).

Thixotropy: This is caused by hydrophilic suspended particles forming a lattice structure in bitumen. This makes bitumen more viscous, thereby harder (Exxon, 1997).

Syneresis: Shrinkage and/or rearrangement occur in bitumen via physical and/or chemical changes over time. Consequently, less viscous constituents separate from the more viscous bituminous binder molecular structure and this viscosity loss affects the overall bitumen and ultimately makes bitumen harder. This circumstance is a form of bleeding (Exxon, 1997).

Separation: This mainly depends on the sort of aggregate that is used with bitumen. Use of some porous aggregates, oily constituents, resins or asphaltenes are removed by absorption.

Bitumen has a tendency to harden during the blending process due to its exposure to high temperature in the plant. This hardening decelerates after the paving process in line with relatively low temperatures and also the accessibility of oxygen molecules. This tendency is limited by the impermeability of the hot mix asphalt. Dense bituminous materials have higher impermeability, with the effect that it becomes difficult for the oxygen molecules to penetrate the mixture. On the other hand, when the bituminous mixtures are more open-textured, such as Macadams, air can easily access the interconnected voids and this is the reason why there is an improvement in the aging of bitumen. However, in either cases, aging improves more rapidly at the top layer than at the internal layers due to its continual presence of air and exposure of higher temperatures (Illston and Domone, 2001).

Hardening of bitumen is important for pavement engineers. Several aging indicators were developed to quantify the aging of bitumen. These are explained below (Roberts et al., 1996).

Penetration Indicator: In general, a penetration grade of fresh bitumen can fall from 50 to 40 or 30 depending on the duration of the blending and the range of temperatures. When accounting for high temperature storage, the initial penetration grade can drop by as much as half (Illston and Domone, 2001). Indicators for penetration grades are depicted in Equation 5.8.

$$\% \Delta P = \frac{P_a}{P_o} * 100 \quad (5.8)$$

where:

ΔP = Retained penetration (%)

P_a = Penetration of aged binder (d-mm)

P_o = Penetration of original binder (d-mm)

Softening Point Indicator: In order to determine the changes occurring at the softening point temperature, we measure the difference between the softening point of fresh and aged bitumen. This indicator is expressed in Equation 5.9.

$$\Delta T_{SPT} = T_1 - T_0 \quad (5.9)$$

where:

ΔT_{SPT} = Change in softening point temperature ($^{\circ}\text{C}$)

T_0 = Softening point temperature of fresh bitumen ($^{\circ}\text{C}$)

T_1 = Softening point temperature of aged bitumen ($^{\circ}\text{C}$)

In order to estimate the effect of aging vs. time on penetration and softening point temperatures, several numerical models were generated by extracting a large number of binders from pavements that had been in service for more than 10 years. These equations (5.10, 5.11, and 5.12) explain the long-term effects of aging on the penetration grade and softening point and are depicted as follows (COST 333, 1999):

$$Pen(t) = 11.9925 - 1.2586 * \sqrt{t} + 0.3322 * Pen(0) - 2.9965 * V_v * X(t) + 0.765 * Pen(0) * X(t) \quad (5.10)$$

$$T_{SPT}(t) = 64.448 + 1.5755 * \sqrt{t} + 0.2531 * Pen(0) + 0.5518 * V_v \quad (5.11)$$

$$X(t) = \frac{1}{\sqrt{t} + 1} \quad (5.12)$$

where:

t = Duration that the binder has been in place in the pavement (months),

$\text{Pen}(0)$ = Penetration at 25°C of the original bitumen (d-mm),

$\text{Pen}(t)$ = Penetration at 25°C of the aged bitumen (d-mm),

$T_{\text{SPT}}(t)$ = Softening point temperature of the aged bitumen (°C)

V_v = Voids content in the mixture (%)

Mass Change Indicator: There are several reasons why a bitumen loses or gains mass as it ages. Thus, after the aging process, a change in mass should be observed as demonstrated above.

Mass loss/gain = mass of the fresh bitumen – mass of the short-term aged bitumen

Aging Index Indicator: We know that the initial viscosity of fresh bitumen and the ultimate viscosity of aged bitumen differ and that the viscosity of the bitumen immediately after the mixture is paved in the field is usually 2 to 4 times the viscosity of the initial fresh bitumen. Bituminous binder continues to age during its service life. Ultimately, viscosity can escalate as high as 10 to 20 times the initial bitumen's viscosity (Chen and Richard Liew, 2002).

The microfilm durability test measures bitumen's resistance to hardening (Griffin et al., 1955). The test consists of aging 5 microns thick films of bitumen on glass plates in an oven at 107.22°C (225°F) for two hours. These two different viscosities are measured by the sliding plate microviscometer. The resulting ratio is accepted as their aging index (Illston and Domone, 2001). Higher values of the aging index (AI) show a high level of bitumen aging. Isaccson and Lu specified that this indicator can be used for both pure bitumen and certain modified bitumen exhibiting no remarkable changes in the polymer aging (Isaccson and Lu, 1999). The absolute viscosity of aged bitumen measured at 60°C is often used as a parameter in the classification of long-term aging and in determining the durability of different bitumens (Bell and Sosnovske, 1994). Figure 5.8 displays the degree of effect of the initial molecular weight of the bitumen on the aging index.

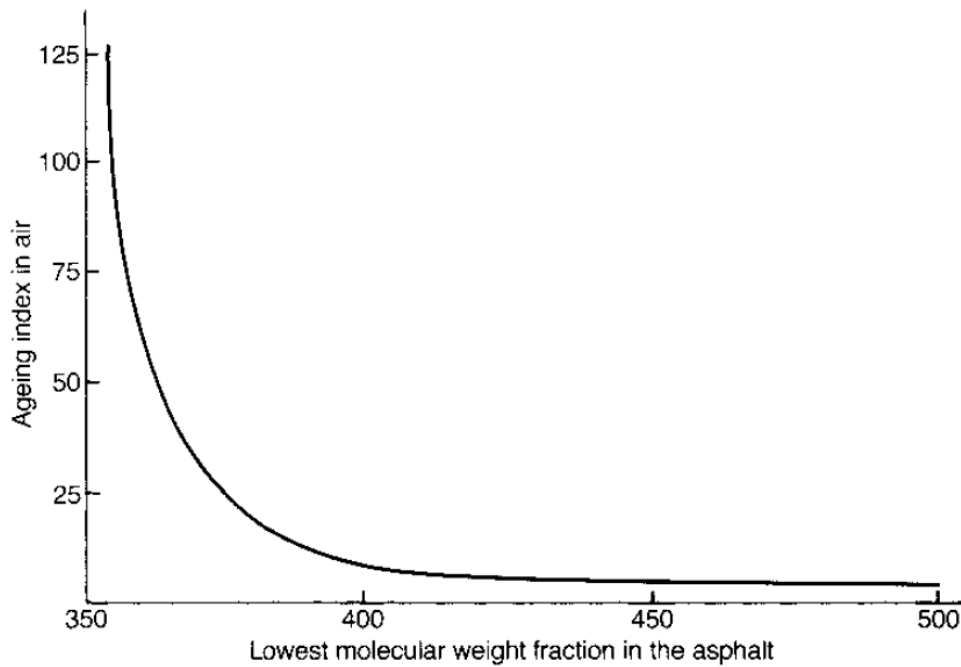


Figure 5.8 : Influence of the initial molecular weight on durability (Griffin et al., 1955).

The aging index is inversely proportional to low molecular weight in the bitumen, as depicted in Figure 5.8. A desirable durability (aging index less than 10) can be obtained if constituents with a molecular weight less than 400 are eliminated (Illston and Domone, 2001). Figure 5.9 demonstrates how the aging index of bitumen changes over time.

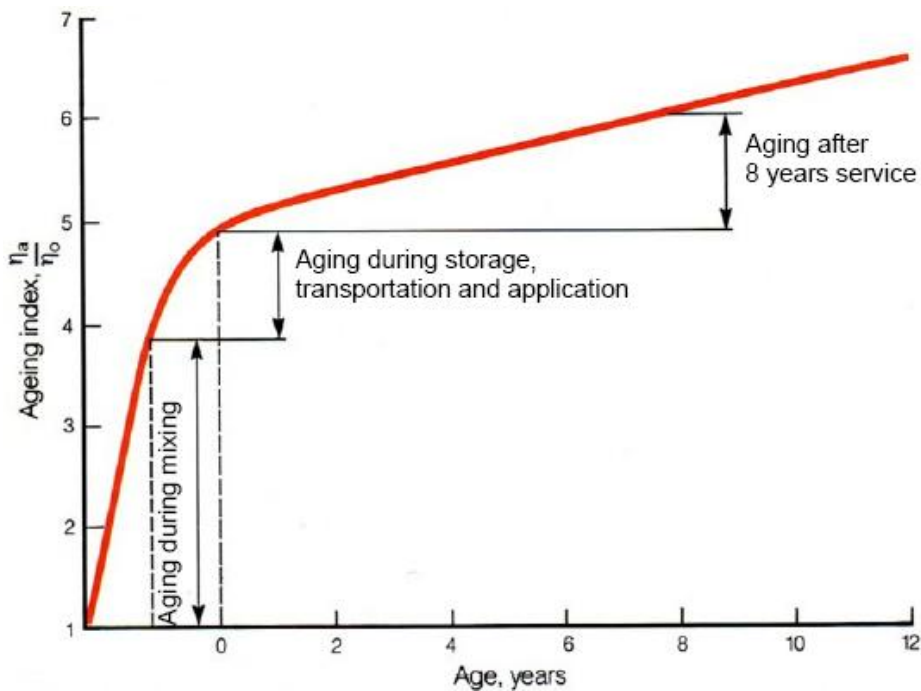


Figure 5.9 : Influence of the time on aging index (Read and Whiteoak, 2003).

Chemical Composition Indicator: Aging also influences the chemical constituents of bitumen. The Gaestel Index (IC) was developed to refer to the change of bitumen contents in terms of its internal colloidal structure (Ishai et al., 1988). The Gaestel Index (IC) measures the ratio of the sum of the asphaltenes and saturates to the sum of the aromatics and resins. This is displayed in Equation 5.13.

$$IC = \frac{\text{Asphaltenes} + \text{Saturates}}{\text{Aromatics} + \text{Resins}} \quad (5.13)$$

Rheological Index Indicator: Previous studies have demonstrated that aging has a major effect on the behavior of bitumen, which differs greatly from its original condition. It is for the following reasons, however, that current research into the empirical properties of short or long-term aged bitumen with the consideration of such properties as penetration, ductility, softening point have not provided full understanding of this behavior:

1. These tests are generally conducted in confined conditions and according to fixed standards. Such results, then, are limited in their ability to provide a full simulation of the initial bitumen or the changes the complex behavior of bitumen viscoelastic properties after aging.
2. These tests are eventually empirical, as they can not accurately represent any other fundamental rheological properties of the aged binder.

From this we understand that focusing our attention on rheology will be more beneficial. As we said earlier, bitumen is a viscoelastic material and aging has a great affect on its complex modulus and phase angle. The rheological index (R) and temperature dependency therefore deserve a thorough investigation. R is defined as indicator of the rheological type and is calculated as the difference between the logarithm of the glassy modulus and the logarithm of the dynamic complex modulus at the cross over frequency. It is explained numerically in Equation 5.14 (Bahia et al., 2001).

$$R = \log(G_g \text{ at } \omega) - \log(G_d \text{ at } \omega) \quad (5.14)$$

where:

G_g = Glassy modulus (Pa)

G_d = Dynamic complex modulus (Pa)

ω_c =Cross-over frequency (rad/s)

Cross-over frequency (ω_c) is the frequency where the phase angle is close to 45 degrees and is an indicator of the hardness of the binder. It is shown in Equation 5.15:

$$\omega_c = \frac{1}{t_c} \quad (5.15)$$

where:

t_c = the corresponding loading time (sn)

In this study, penetration, softening point, mass change and rheological index indicator are evaluated to fully understand the role of aging on bitumen. Other indicators include: tensile/creep strength, critical (cracking) temperature, increment in carbon+sulfoxide area (infra-red spectra test), and change in molecular weight distribution (GPC test).

Briefly, the impacts of aging on rheological, mechanical and chemical properties of bitumen can be observed by aging indicators as demonstrated in Table 5.4.

Table 5.4 : Summary of aging indicators (Hagos, 2008).

AGING INDICATORS		
RHEOLOGY	CHEMICAL	MECHANICAL
Retained Penetration	Gaestel Index	Critical (Cracking) Temperature
Change in Softening Point Temperature	Increment in Carbonyl and Sulfoxide Area	
Mass Change	Change in Molecular Weight Distribution	
Aging Index (Viscosity Ratio)		
Rheological Index		
Tensile/Creep Strength		

These indicators are beneficial if used with specifications to limit the level of distress in pavements. It should be noted that they are variable with respect to pavement structure, location, mixture type, environment and origin of the binder.

Excessive aging may cause the bitumen to partially lose its adhesion and cohesion, and subsequently it may cause raveling or graveling (progressive disintegration of

the mixture and a separation of the aggregates from it) in the mixture. Aging is a kind of providence in that a certain amount of aging is beneficial. If a bitumen has not aged sufficiently, it may be too soft during the paving. Compaction of the tender mixture will not be easy and it will have a low resistance to rutting in its service life. If the softness of a mixture disappears within a few weeks after paving, the trouble was most probably caused by a slow setting asphalt. This kind of bitumen needs a much longer duration to "set up" after it heated up and returned to normal service temperature. Bitumen, having less than 10 percent asphaltenes, tends to have a higher probability of being a slow-setting mixture (Chen and Richard Liew, 2002).

Usually bitumen aging can be classified in two ways: On one hand it ages during the manufacture process itself. The second aging is experienced during the in-service life of the pavement. Since the first aging occurs rapidly it is termed "short-term." The second process continues for years and is accepted as "long-term." All aging, but most particularly the short-term type, play major roles on the field performance of the pavement (Zhang et al., 2010).

Short-Term Aging

Short-term aging is primarily caused by oxidation and volatilization. These occur when bitumen encounters hot aggregates in the plant, during the hauling, the paving, and final compaction of the bituminous material. *Roberts et al.* showed that the amount of aging is even dependent on the type of manufacturing plant. The presence of water vapor in the mixing drum reduces oxidation. Age hardening in a drum-mix plant appears to be less severe than in a batch plant (Roberts et al., 1996). Once the bituminous mixture is laid, oxidation and volatilization are remarkably slow but never cease, continuing at a slower rate.

Simulation of Short-Term Aging:

Short-term aging can be simulated in the laboratory by heating the bitumen to 163°C, which is similar to the blending temperature in actual practice. The main goals of these simulations are to increase temperature, decrease bitumen film thickness, and increase bitumen surfaces exposed to oxygen.

Short-time aging can be achieved by using the thin film oven test (TFOT) and rolling thin film oven test (RTFOT). The progression of these two experiments will be given in detail in following sections.

Thin Film Oven Test (TFOT)

In the past, the TFOT was very commonly used, with a history that dates back to the 1940s. The test was also validated by AASHTO and ASTM in 1959 and 1969 respectively. It is conducted to approximate the effect of short-term aging during the blending process. The test stages should comply with the criteria of AASHTO T179 and ASTM D1754 "Standard Method of Test for Effect of Heat and Air on Asphalt Materials, Thin-Film Oven Test". It is open to discussion as to whether both TFOT and RTFOT are kinds of aging processes themselves, rather than conventional bitumen tests.

Even though TFOT is still commonly used in some western countries, RTFOT, which was adopted by SUPERPAVE, is currently superior to TFOT due to reasons as shown in Table 5.5.

TFOT, the equipment of which is shown in Figure 5.10, is performed as follows:

- A 50g bitumen sample is placed on a cylindrical flat-bottom pan at a depth of approximately 3.2mm.
- The pan is then placed on a shelf that rotates at 5 to 6 revolutions per minute in a ventilated oven maintained at 163°C for 5 hours.
- The sample is considered short-term aged after it is removed from the oven.
- The sample is then tested in accordance with the specification requirements (Fwa, 2005).



Figure 5.10 : Equipment of TFOT.

Rolling Thin Film Oven Test (RTFOT)

The basic main goals of RTFOT are (1) to calculate the loss of mass, specifically to learn how many constituents have evaporated from the bitumen sample, and (2) to simulate the field hardening process in order to prepare the aged specimens for further experiments. It is open to discussion to whether both TFOT and RTFOT are a kind of aging process rather than conventional bitumen tests.

Even though TFOT is still prevalent in some western countries, RTFOT was adopted by SUPERPAVE, is currently superior to TFOT due to reasons as shown in Table 5.5.

Table 5.5 : Comparison of TFOT and RTFOT.

TFOT	RTFOT
Test takes 5 hours	Test duration is less than 85 minutes
No rolling nor movement of jars	Rolling and movement of jars simulates the bitumen in the plant
Due to lack of rolling, whole bitumen cannot be exposed to heat and air flow	Heat and air flow can penetrate overall bitumen via rolling
Modified or extended bitumen cannot keep its homogeneity	Rolling lets extender or modifier remain dispersed in the bitumen
Free-rolling aging is not able to cause agitation consequently aging is limited to top layer	Agitation prevents the formation of a surface skin on the bitumen.
Thickness of bitumen film on the jar is 3.2mm	It is 1.25mm

RTFOT requires a flow meter and thermometer.

The progression of RTFOT is outlined in AASHTO T240 "Tests on Residue from Rolling Thin Film Oven" and ASTM D2872 "Standard Test Method for Effect of Heat and Air on a Moving Film of Asphalt (Rolling Thin-Film Oven Test)" and can be summarized as follows:

- Prior to the test, the oven of the RTFOT is heated at least 16 hours. When fully loaded and the air is on, the oven should return to $163 \pm 0.5^\circ\text{C}$ within 10 minutes of the warm up period.
- 300g of bitumen is heated to a maximum of 163°C (150°C is preferred).
- 35 ± 0.5 grams of the liquid bitumen is poured into each specified glass jar as shown in Figure 5.11. Eight jars are required, two of which are used for the measurement of the mass changes.
- Two labelled and empty jars are first weighed ("a" and "b"), and then the bitumen filled jars ("c" and "d") are re-weighed separately. For a precise calculation, a 0.001g digital scale is required.
- The bitumen filled jars are placed in the carriage and the oven door is closed securely.
- The carriage is set to rotate at the rate of 15 ± 0.2 revolutions per minute and the air blower is set to flow at 4000ml/minute for 85 minutes as shown in Figure 5.12.

- After completion of the test, two of the labelled jars are allowed to air cool and are then weighed to measure the aged bitumen ("e" and "f"). The change in mass is calculated as follows:

$$\text{change in mass}(\%) = \frac{c - a}{e - a} \quad \text{change in mass}(\%) = \frac{d - b}{f - b}$$

- a: weight of the first empty jar (g)
- b: weight of the second empty jar (g)
- c: weight of the fresh bitumen filled first jar (g)
- d: weight of the fresh bitumen filled second jar (g)
- e: weight of the aged bitumen filled first jar (g)
- f: weight of the aged bitumen filled second jar (g)

A typical RTFOT empty jar, before aging and after aging, is pictured in Figure 5.13.

The change in mass is the mean of the first and second samples. However, it should be noted there is no rule that the changes in mass always occur in terms of loss after the RTFOT. Instead, since the air penetrates into the samples, any base bitumen or modified bitumen can be oxidized and can gain mass.

- All of the residues left in the jars are immediately poured into a spout container and sealed to be used for the following tests.

A typical question raised in regard to this test is: "Why is the aging process set at 85 minutes?" The answer lies in the fact that this time is used to categorize all bitumens to the same extent of aging produced in the TFOT. The actual time of aging varies from a few minutes in the case of hot-in-place recycling to several hours in the case of plant mixing and long distance hauling or paving delays. Nonetheless, researchers have indicated that a duration of 85 minutes produces the aging effects comparable to the average field conditions. It is, however, true that bitumen exposed to heat and oxygen will result in hardening patterns that are substantially different from those produced in 85 minutes (Shalaby, 2001).

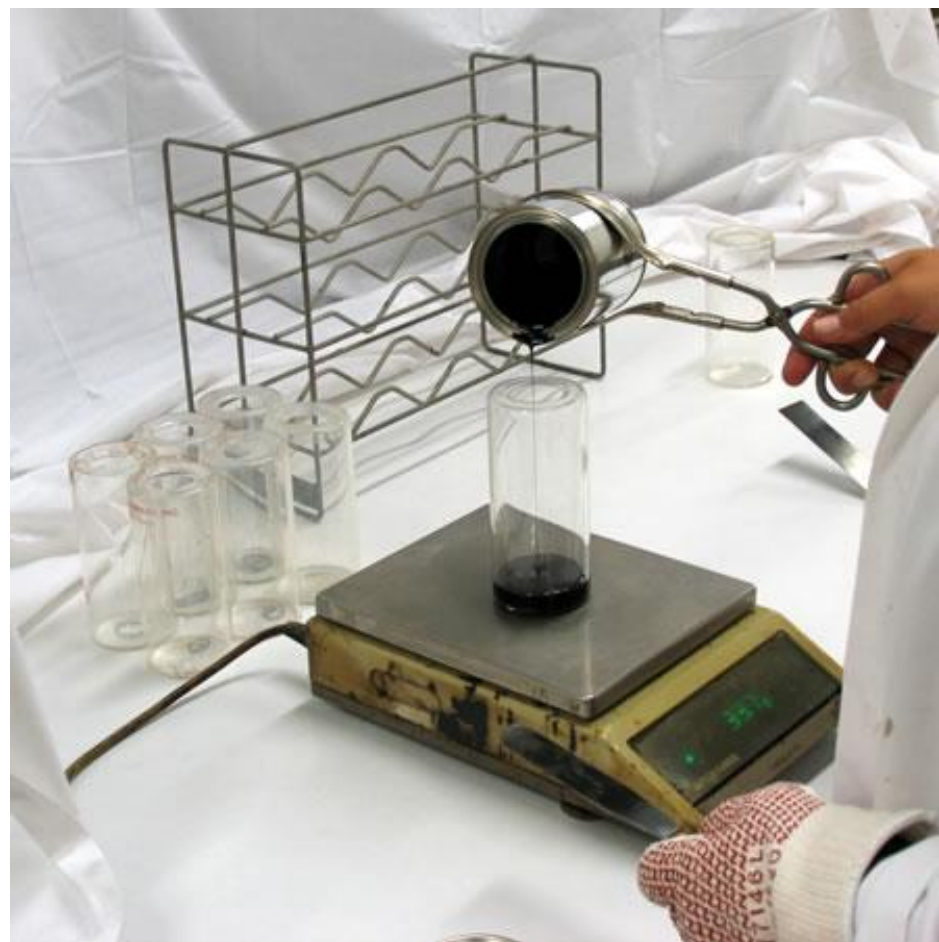


Figure 5.11 : Pouring the bitumen into an empty jar.

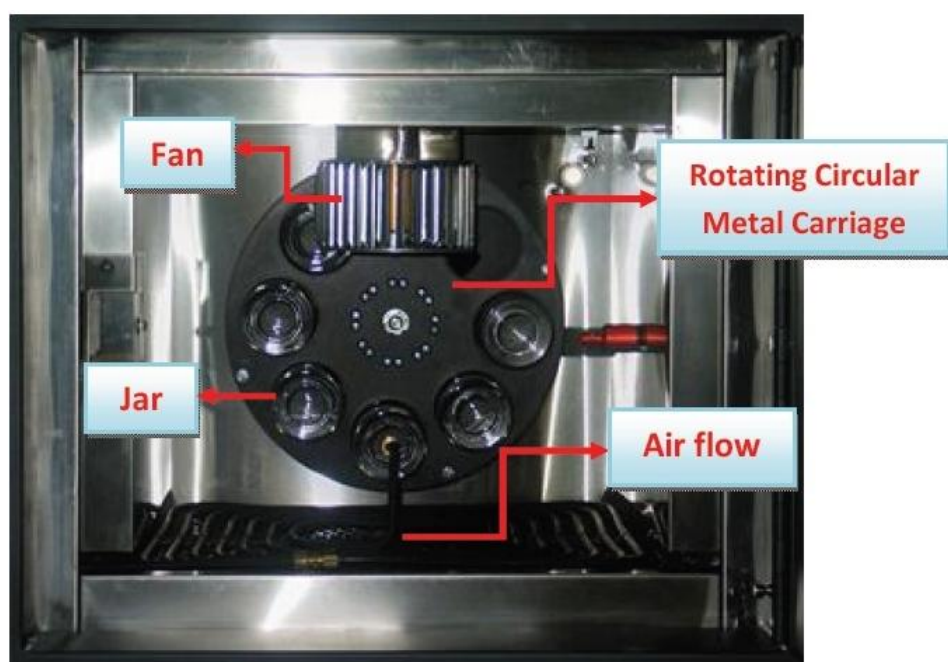


Figure 5.12 : RTFOT equipment.



Figure 5.13 : The same RTFOT jar after aging, before aging, and empty.

While the RTFOT and TFOT have generally worked well on base bitumens, problems are experienced in the testing of modified bitumen. Such modified bitumen, particularly with those crumb rubber and SBR, demonstrate the tendency to spill out of the RTFOT jars during the RTFOT process. When the TFOT is used on these kinds of modified binders, a thin skin tends to develop on the top layer of the modified bitumen; this skin reduce the homogeneity and the aging of the samples.

Modified Rotavapor Aging Test (M-RAT)

The modified rotavapor aging procedure appears to be a feasible alternative to the RTFOT and TFOT in the testing of modified bitumens (Sirin et al., 1998). The rotavapor apparatus, which was initially used for the recovery of asphalt from a solution (ASTM D5404), was later improved to run as an aging device for bitumen. The binder is placed in a rotating flask, which is then immersed in a temperature-controlled oil bath. An air pump is used to provide a controlled air flow to the flask. Different aging effects can be obtained by using different combinations of process temperatures, process durations and sample sizes. One of them resembles RTFOT by aging a 200g bitumen at 163°C and during 165 minutes of the test (Chen and Richard Liew, 2002).

The other aging processes for modified bitumens can be described as follows:

Modified Rolling Thin Film Oven Test (M-RTFOT)

Due to variations in the viscosity in base bitumen and modified bitumen, RTFOT is not capable of achieving the same oxidation levels. The traditional RTFOT was modified so as to eliminate the effects of the variations in viscosity. A set of 127mm long and a 6.4mm diameter steel rods were placed inside each of the rolling jars in order to achieve uniform aging (Bahia et al., 1998). The objective of the rods is to prevent the spilling-over of the binder. While first developed by *Oliver and Tredrea*, subsequent studies concluded that these rods did not improve the aging of modified and base bitumen, hence the test has been widely rejected (Oliver and Tredrea, 1997).

The Nitrogen Rolling Thin Film Oven Test (N-RTFOT)

Parmeggiani improved the conventional RTFOT to include the physical and chemical reactions occurring during the simulation of bituminous mixtures, including evaporation and oxidation. He suggested replacing the blowing of hot air on the bitumen with an inert gas. Here, nitrogen is used to assess the extent of evaporation of the lighter molecules in the bituminous mixture. The main goal of the test is to determine the extent of both evaporation and oxidation. Since the loss of oily components is so vital in the subsequent performance of the binder, the test is meaningful in terms of its ability to distinguish the sensitivity of different binders to aging (Parmeggiani, 2000).

The German Rotating Flask Test (GRFT)

Since static type aging testing methods demonstrate such drawbacks as skin formation and separation, a dynamic aging process was explored to enable the short term aging of modified bitumen binders. Some researchers have claimed that GRFT can simulate the long-term aging mechanism (Hagos, 2008). In this test 100g bitumen is poured into a spherical flask. This flask is inclined and submerged in a 165°C oil bath as depicted in Figure 5.14. The flask rotates at a speed of 20rpm while 500cc/min of air diffuses to flask. The test is conducted for 150 minutes in a closed vessel, allowing control of the type and volume of air diffusing to the bitumen. By rotating the vessel, bitumen turns over during the test, a representative bitumen film is maintained, and – more importantly – the formation of skin is prevented. Since the test is conducted at 165°C, oil, which allows the sample to heat rapidly, is required

for the bath. This step solves the radiant heating problems encountered in some ovens. Airey has indicated that GRFT is roughly one-third as strong as the TFOT and RTFOT in producing volatiles, which mean less aging (Gordon, 2003a).

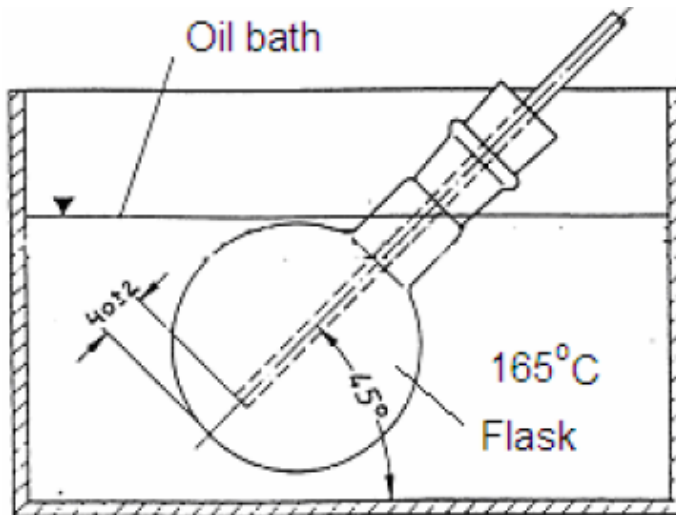


Figure 5.14 : The German rotating flask test (GRFT) equipment (Hagos, 2008).

Modified German Rotating Flask Test (M-GRFT)

In this test, 200g bitumen is poured into a 2000ml flask attached to a rotary evaporator that is allowed to rotate for 210 minutes at 165°C with 2000ml/min of air being diffused. Rotated at 20rpm, steel balls may also be added to the flask so as to cause a fresh bitumen film. The main goal of the M-GRFT is to provide more aged bitumen while, similar to the RTFOT method, maintaining the same degree of aging of the bitumen (Hagos, 2008). When compared with RTFOT, M-GRFT shows better agreement on base and modified bitumen with an exception in the level of mass loss. *Ramaiah et al.* pointed out that the mass loss in the RTFOT was a bit higher than that of the GRFT (Ramaiah et al., 2004).

Long-Term Aging

While a significant percentage of bitumen hardening is developed at the short-term stage, and, despite the fact that the speed of aging diminishes, the aging process itself never stops and will continue at a slower speed after the bituminous mixture is finally laid. A long-duration test is needed to realize the effects of hardening on the behavior of bitumen during its service life. Similar to short-term aging, long-term aging is mainly caused by oxidation. In addition to oxidation, other factors, especially environmental conditions, type, and origin of binders should be considered.

Even though long-term service life binder aging occurs at relatively lower temperatures (approximately 50-60°C) than short-term aging, its simulation in a laboratory is carried out at higher temperatures (90-110°C). This can result in differences in the long-term aging results of the laboratory and field processes.

The Simulation of Long-Term Aging:

Pressure Aging Vessel (PAV)

The Pressure Aging Vessel (PAV) is a SUPERPAVE test developed by SHRP to simulate long-term aging of bitumen in service. *Bahia and Anderson* specified that PAV aged bitumen typically represents the binder of a hot mixture asphalt that has been in service from 5 to 10 years (Bahia and Anderson, 1994).

Since it will be used to present the behavior of long-term aged bitumen, the PAV used sample should have been previously short-term aged by using either the TFOT or RTFOT methods. This process is specified in detail in AASHTO PP1 and ASTM D6521 "Standard Practice for Accelerated Aging of Asphalt Binder Using a Pressurized Aging Vessel (PAV)" and is summarized as follows:

A 50g sample of bitumen is poured into a preheated 140mm diameter pan that is placed on a shelf rack with a capacity of 10 pans. As many as 10 pans can be utilized and it is expected that a bitumen film having an approximately 3.2mm thickness will occur in each pan. The test is typically conducted at temperatures between 90 and 110°C and at a pressure of $2.1 \pm 0.1 \text{ MPa}$ during the 20 hours of the test. The PAV temperature to be used in the laboratory is dependent on the climatic conditions of the region where the binders will be used. Long-term aging of bitumen is not only temperature dependent but also pressure and geometry dependent. Past research has revealed that aging is variable at a constant temperature (Domke et al., 1997). A higher PAV temperature can create a warmer climatic condition, while a lower temperature may present a colder climatic condition. However, aging temperatures below 100°C are generally recommended in order to achieve similar chemical changes as in field aging. The confined loss of volatiles and the oxidation process at these elevated temperatures are some of the PAV advantages (Chen and Richard Liew, 2002). Despite this, due to some of the test drawbacks, some researchers have questioned the results of PAV. For instance, since it is performed at temperatures above the actual pavement temperatures, the properties of the tested bitumen are

more vulnerable than the bitumen actually in service. Since PAV is a static test, air cannot penetrate homogeneously and thus the aging varies between the surface and the bulk of the specimen. When the top and bottom parts of the aged modified bitumen are investigated, modifier migration is inevitable during the PAV (Verhasselt, 2002). Nonetheless, PAV is fairly well accepted by the scientific community as a functional simulation of the long term, in-service aging of bitumen.

Typical PAV equipment and its pan are depicted in Figure 5.15 and Figure 5.16.

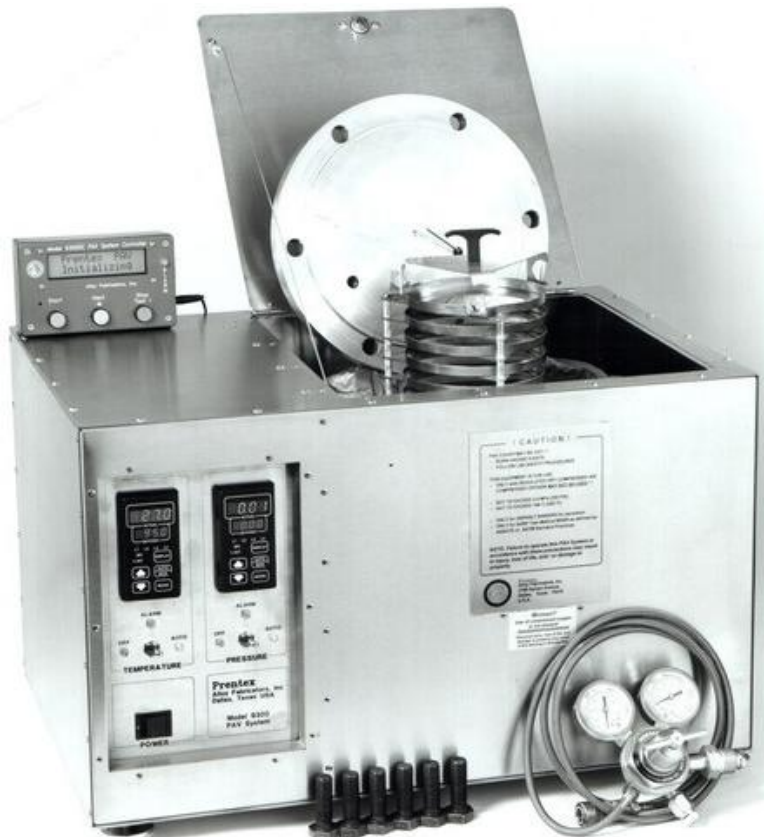


Figure 5.15 : Equipment of PAV.

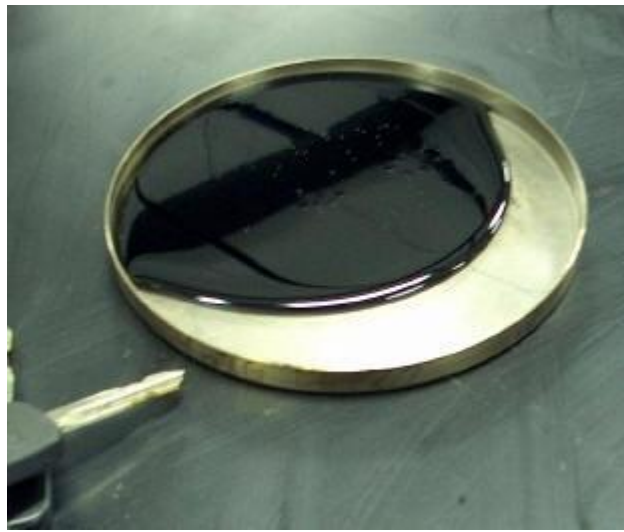


Figure 5.16 : A-bitumen-poured pan of PAV.

High Pressure Aging Test (H-PAT)

The H-PAT is performed by using the PAV equipment. However, it is carried out at a relatively low temperature (85°C) and a longer aging duration (65 hours) compared with PAV.

Pressure Oxidation Vessel (POV)

POV, another a long-term aging test, is performed in a stainless steel reactor. The samples are immersed in a temperature-controlled water-triethylene glycol bath. During the POV, a rack with a 40 tray capacity (55mm diameter each) is put in-place. 7.6g of bitumen is placed in each of the trays. A binder film of approximately 3.2mm thickness is subjected to aging. Although there are some differences between POV and PAV – such as heating mechanisms and the amount of trays – *Domke et al.* pointed out that similar aging results were observed from the same sample exposed separately to POV and PAV (*Domke et al., 1997*).

The Rotating Cylinder Aging Test (RCAT)

The Belgian Road Research Center (BRRC) established the RCAT as a means of performing both the short and the long term aging of bitumen. While this test takes longer to perform than other long-term aging tests, it is dynamic in nature, allowing the monitoring of all the aging properties of the bitumen at different intervals. Both short-term and long-term aging can be performed by using the same specimens and using the same equipment. This means that the researcher need only create one sample, saving both time and resources (*Verhasselt, 2002*).

It should be noted that in the case of short-term aging, the rotation and an air flow is set at 5rpm and 4liters/min respectively during the complete test (235 ± 5 minutes – 4 hours – at 163°C). The values for the RTFOT are: 15 ± 0.2 rpm, 4l/min, 85 min, at 163°C (Verhasselt, 2002). In cases of long-term aging, the progress of RCAT is specified in the draft standard CEN TC336 WG3 and states:

- Approximately 500-550g of preheated bitumen is poured into a stainless steel cylinder as depicted in Figure 5.17.
- The cylinder is set to rotate at the rate of 1rpm.
- A grooved, stainless steel roller is inserted into the cylinder to press and distribute the binder film (having about 3mm thickness) against the inner wall of the cylinder so as to constantly provide a fresh surface. This allows the homogenization of the binder sample.
- A constant flow rate of 4.5l/h of oxygen is set to diffuse and renew the environment inside the cylinder.
- A temperature of 85°C is suggested, but 90°C can be used to reduce the test duration. The test is performed for a duration of 240 hours at 85°C , or 144 hours at 90°C .

Mes proved that the properties of the RCAT aged bitumens are similar to those of bitumen extracted from various pavements. He interpreted this good correlation as a result of the relatively slow aging process, prevention of skin formation, and uniform aging of the binder compared to PAV aging which is also performed at the same temperature (Mes, 2003).

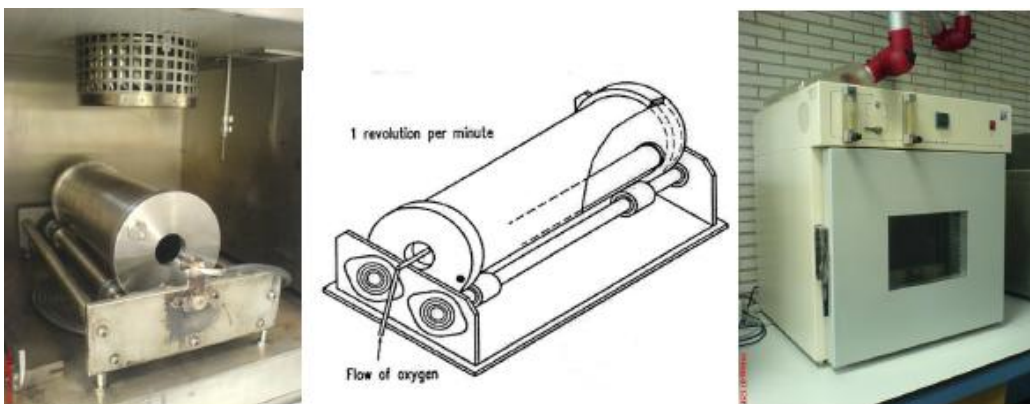


Figure 5.17 : Equipment of RCAT (Hagos, 2008).

The Aging of Bituminous Mixtures

Such fundamental properties of bituminous mixtures as stiffness, stability, fracture, toughness and relaxation can be affected by aging. Although, aging has the greatest effect on the binder, attention should also be paid to aggregate-binder composition in terms of the binder's adhesive characteristics. This is required because in the field, raveling is a result of both cohesive and adhesive failure mechanisms. The density and porosity of a mixture greatly affect on aging. For instance, due to their high void content, porous mixtures are much susceptible to aging, and, therefore, raveling. A bituminous mixture with aged bituminous becomes brittle and vulnerable to cracking at low temperatures. Since this thesis is specifically focused on the aging of bituminous binders, this background information about aging of bituminous mixture is sufficient for the moment.

5.2 SUPERPAVE Tests

The viscoelastic aspect of bituminous binder plays a predominant role in the mechanical behavior of HMA mixtures. Until the 1990s, the viscoelastic behavior of a binder was determined by such basic empirical consistency tests as penetration, softening point etc. However, in line with increases in traffic volume, axle loadings and tire pressures, it quickly became apparent that these tests were not capable of fully characterizing the viscoelastic properties of bitumen and of predicting the mechanical behavior of HMA under these high loads and conditions.

Cognizant of the shortcomings of the binder specifications of that era, the Strategic Highway Research Program (SHRP) assumed responsibility for this issue. In 1987 they initiated a \$50 million research program aimed at introducing new performance-based binder specifications. Called SUPERPAVE (**S**Uperior **P**ERforming asphalt **P**AVEMENTs), this program presented a new set of tests and testing equipment that allowed pavement engineers to gain the ability of correlating bitumen chemistry and physical properties with its performance. In addition to an analytical approach to its performance, the program also allows the testing to monitor the three types of pavement deteriorating: permanent deformation, fatigue and low temperature cracking. Figure 5.18 and Table 5.6 explain these new generation SUPERPAVE tests.

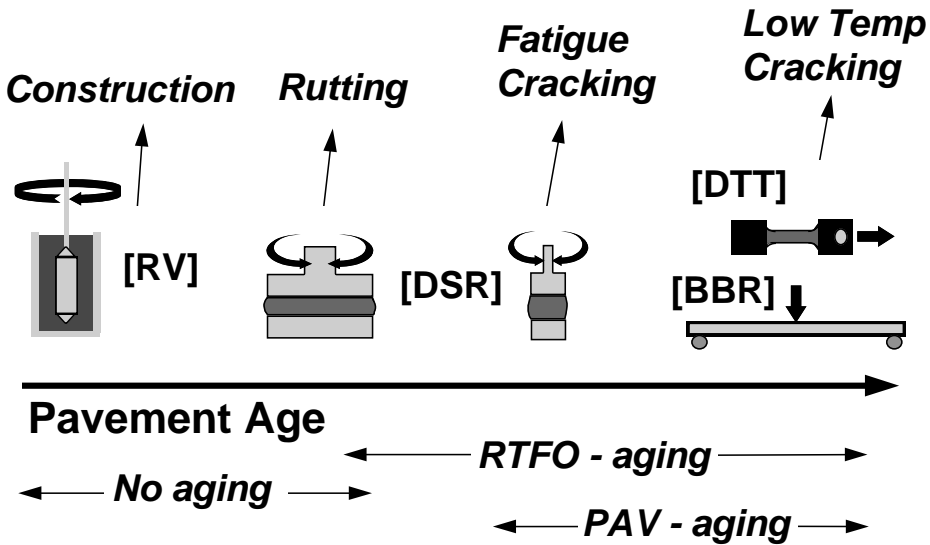


Figure 5.18 : Illustration of SUPERPAVE tests.

Table 5.6 : SUPERPAVE tests.

Test	Target
Rotational Viscometer (RV)	Measure binder pumpability and workability
Dynamic Shear Rheometer (DSR)	Measure binder properties at intermediate and high service temperatures (performed on original binder, RTFO-aged binder and PAV residue)
Rolling Thin Film Oven (RTFO)	Simulate binder aging during HMA production, laying and compaction
Pressure Aging Vessel (PAV)	Simulate oxidative aging that occurs in the binder of HMA during its service life
Bending Beam Rheometer (BBR)	Measure binder properties at low service temperatures
Direct Tensile Test (DTT)	Measure binder properties at low service temperatures (complementary test in case of failure of BBR criteria)

5.2.1 Rotational viscometer (RV) test

The Strategic Highway Research Program (SHRP) deployed the Rotational Viscosity test to determine the workability of bitumen at elevated temperatures. Before such processes as plant mixing, field placement, and compaction of HMA can begin, the bitumen to be employed has to be checked to determine that it has enough fluid and is pumpable (Roberts et al., 1996). In general, any unaged bitumen can meet these requirements at 135°C.

Accordingly, SHRP assigned the bitumen binders' viscosity at a maximum of 3.0Pa·s at 135°C. Although a minimum viscosity range is not specified in the performance-

graded system, ASTM 3381 specifies minimum viscosities ranging from 0.08Pa·s to 3.0Pa·s at 135°C to control bitumen drain-down during storage and hauling (Zaniewski and Pumphrey, 2004).

The rotational viscometer is also utilized to appoint equiviscous temperature ranges to determine convenient mixing and compaction temperatures. Viscosities at two different temperatures are plotted on the log-log viscosity vs. log temperature graph. The equiviscous temperature range for mixing and compaction correspond to the point at which the plotted line passes through the respective viscosity range (Zaniewski and Pumphrey, 2004). A typical log-log viscosity vs. log temperature graph is depicted in Figure 5.19 (Asphalt Institute, 2003).

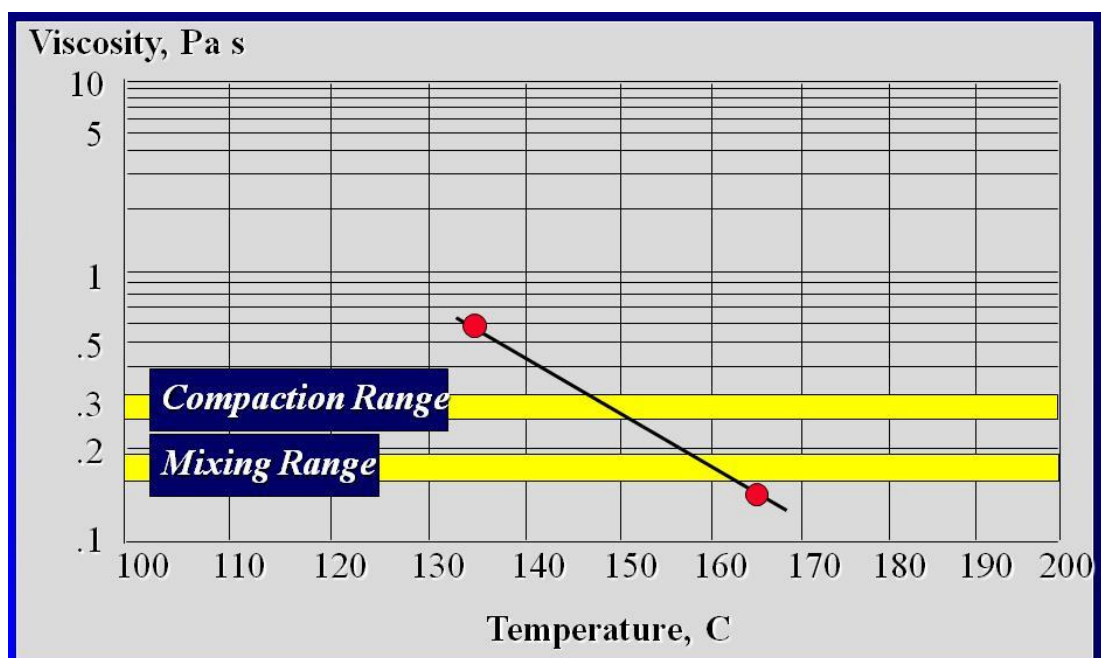


Figure 5.19 : Typical equiviscosity curve for bitumen (Asphalt Institute, 2003).

Although there are many devices to measure viscosity, the most widely used is the Brookfield apparatus, a rotational coaxial cylinder viscometer that is also known as the "Brookfield Viscosity Test." In this experimental study, "Brookfield Rotational Viscometer DV III Ultra" was used and it is shown in Figure 5.20.

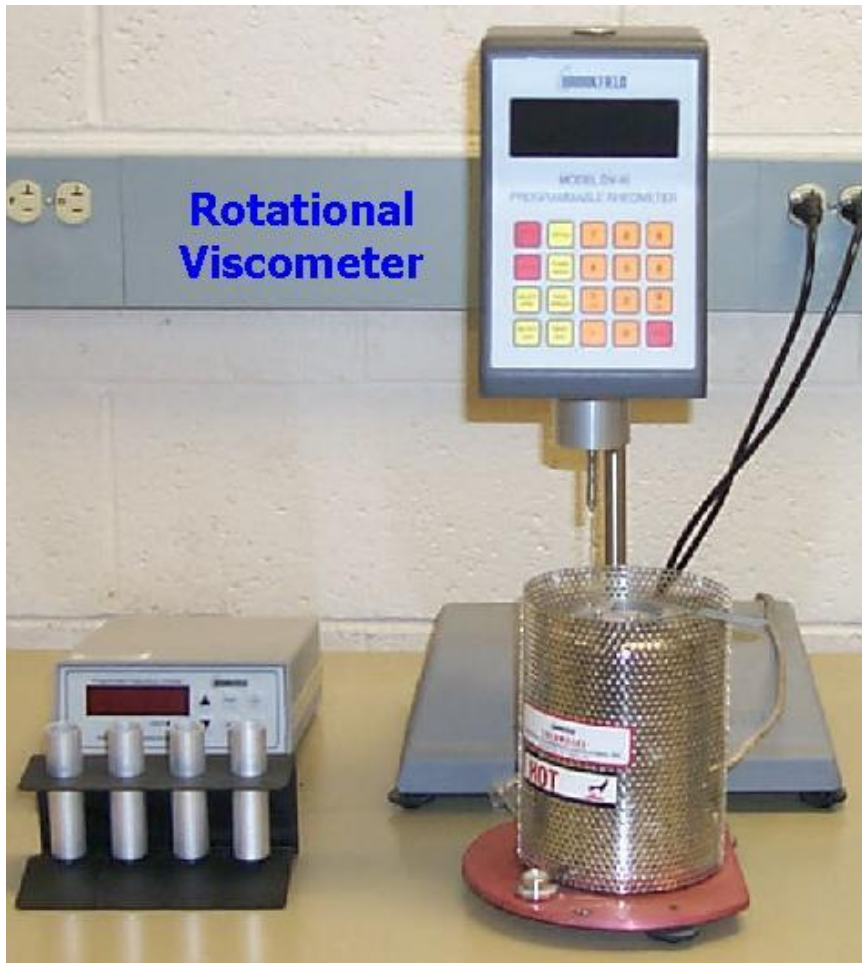


Figure 5.20 : Brookfield rotational viscometer.

A typical rotational viscometer system consists of a rotating spindle-type viscometer, temperature controller, thermo-chamber, and a computer. The main components of the viscometer are the rheometer head and base unit. The rheometer head unit consists of a motor, rotational transducer, spindle, digital readout display and a control panel. The base unit builds a bridge between the rheometer head and the computer. The thermo-chamber is a heating chamber that houses the bitumen sample holder during the test. The temperature within the thermo-chamber is monitored by a Resistance Thermal Detector (RTD) and is controlled by the temperature controller unit (Zaniewski and Pumphrey, 2004).

Test Process

Viscosity at 135°C expresses the pumpability and workability of the bitumen. However, the Asphalt Institute recommends two viscosity grades at two different temperatures (135 and 165°C) to draw viscosity-temperature graphs for establishing equiviscous temperature ranges. Determining bitumen viscosities at both 135 and

165°C are promising in terms of determining equiviscous temperatures via interpolation but not extrapolation (Asphalt Institute, 2001). In addition to these temperatures, in this study, a viscosity at 105°C is also measured due to presence of sulphur.

Since it takes less time to elevate the temperature of a sample than to cool it down, the measurements start at a lower temperature and progress upward (105, 135 and 165°C respectively). Prior to performing the tests, the thermo-chamber needs to be preheated at the lower temperature first. Similarly, the sample holder and spindle should be preheated in an oven heated to the lower temperature (105°C) as well.

Viscosity is derived from the torque required to keep the speed of the rotational coaxial cylinder (spindle) constant while it is submerged in a bitumen at a constant temperature as shown in Figure 5.21 (Petersen et al., 1994).

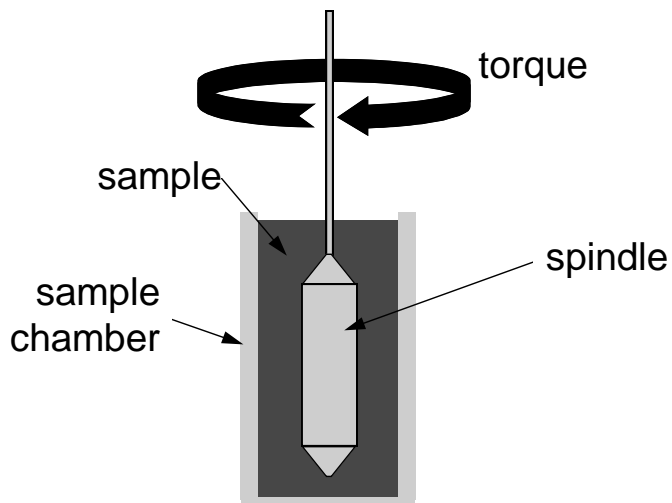


Figure 5.21 : Schematic view of rotational viscometer (Petersen et al., 1994).

The constant speed of the spindle is 20rpm and the required torque is directly related to the viscosity of the bitumen binder sample. A rotational transducer inside the rheometer head measures the torque required to maintain a constant speed of 20rpm. The electronic circuitry inside the base automatically converts the measured torque to viscosity and sends the results to the computer. The data are given in poise units (Zaniewski and Pumphrey, 2004). The viscosity of a typical bitumen varies between 0.01Pa-s (0.1poise) and 200Pa-s (2000poise) and should not exceed 3.0Pa-s at 135°C. Viscosity measurements should be noted at one minute intervals for at least three readings (Petersen et al., 1994).

The process of the test is explained in AASHTO TP48, "Viscosity Determination of Asphalt Binders Using (a) Rotational Viscometer".

Analysis

When heated to temperatures exceeding 100°C, most bitumen loses its elastic properties and starts to behave as Newtonian fluids (Bahia and Anderson, 1995a). Therefore the viscosity of the bitumen should be measured at elevated temperatures (exceeding 100°C) in terms of its workability during the mixing and construction. The current equations make sense of the shear stress and shear rate to torque and shear rate respectively. They are given below as Equation 5.16 and 5.17 (Petersen et al., 1994; Whorlow, 1980).

$$\text{Shear Rate (s}^{-1}\text{)} \quad \gamma = \omega \frac{2R_c^2}{(R_c^2 - R_s^2)} \quad (5.16)$$

$$\text{Shear Stress (dynes/cm}^2\text{)} \quad \tau = \frac{M}{2\pi R_s^2 L} \quad (5.17)$$

where:

ω = angular velocity of spindle (rad/s)

R_c = radius of sample holder (cm)

R_s = radius of spindle (cm)

M = applied torque (dyne-cm)

L = effective length of spindle (cm)

The viscosity is eventually calculated by the following relationship in Equation 5.18;

$$\mu = \frac{\tau}{\gamma} \quad (5.18)$$

5.2.2 Dynamic shear rheometer (DSR) test

Asphalt concrete pavement has a high tendency to wheel path rutting shortly after it is laid. Repeated traffic loads trigger the consolidation of the pavement structure after construction, thus resulting in rutting predominantly in right-sided traffic lanes where heavy-loaded vehicles typically travel. Rutting is a typical permanent deformation

and reduces driving comfort and safety. Although there are several parameters influencing the rutting potential of pavement such as the quality of compaction, mix design, aggregate angularity and texture, the role of bituminous binder should be taken into consideration. Since the bitumen gets more fluid with increasing temperatures, rutting commonly occurs at high service temperatures (Bahia and Anderson, 1995b; Roberts et al., 1996; Zaniewski and Pumphrey, 2004).

However, the rutting potential of HMA decreases over time due to the fact that bitumen gets stiffer by aging. On the other hand, once put into service, pavements will experience fatigue cracking in due time. In addition to repeated load-based stresses, the properties of bituminous binder are crucial in the fatigue life of HMA pavements. The fatigue life of HMA pavements is very dependent on the amount of bituminous binder hardening that occurs.

In order to reduce rutting and fatigue cracking, bitumen must be sufficiently stiff, elastic, and flexible. The bitumen needs to be adequately stiff at service temperatures to prevent the creeping of the bituminous layers that cause rutting. In order to withstand fatigue cracking, it also needs to be sufficiently soft at low temperatures.

SHRP developed the dynamic shear rheometer (DSR) to evaluate the binder's performance in terms of rutting and fatigue cracking. By evaluating the viscoelastic behavior of bitumen, DSR guides pavement engineers to control its rutting resistance at high service temperatures in the early stages of the pavement and to control its fatigue cracking resistance at all service temperatures in the later stages of its service life.

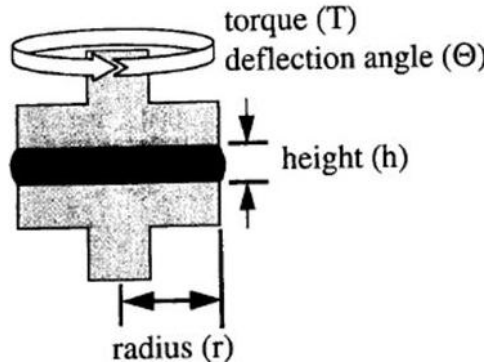
DSR gives pavement engineers an opportunity to qualify the viscoelastic properties of bituminous binder by evaluating its complex modulus and phase angle at variable temperatures and frequencies when exposed to oscillatory (sinusoidal) stresses. The complex modulus (G^*) is a measurement of the total resistance of a material to deformation under cyclic loading conditions while the phase angle (δ) is an indicator of the relative amount of recoverable and non-recoverable deformation.

Although G^* and δ are commonly measured at a single temperature and frequency, a large range of temperatures and frequencies can be performed to determine the time (frequency) dependency of the modulus of bituminous binders. The common frequency of 1.59Hz (10rad/sec) has been related to a traffic speed of 100km/hr. However, slower moving traffic such as heavy-loaded trucks traveling at speeds no

higher than 40-50km/hr exist side-by-side with faster moving traffic. For slower moving traffic, a lower frequency should be used to simulate low traffic speeds and vice versa. Moreover, pavement is subjected to different temperatures during its service life. In this study, four distinct temperatures (25, 30, 40, and 50°C) and five distinct frequencies (0.10, 0.25, 0.63, 1.59, and 4.00Hz) will be applied to all specimens.

In this test, a bitumen sample with 1-to 2mm thickness is typically placed between two parallel circular plates. The bottom plate is fixed and the top plate is oscillated by a computer controlled electronic motor. While the top plate is oscillating with an angular velocity, the shear stress or shear strain can be evaluated from the measured torque and angle of rotation (Chen and Richard Liew, 2002). The test can be applied in both stress-controlled and strain-controlled studies. In this study, all specimens will be subjected to stress-controlled DSR test.

The angular rotation (Θ) and applied torque (τ) and the complex modulus (G^*) are calculated via the following equations: (Equation 5.19, 5.20, 5.21 and 5.22) (Kennedy et al., 1994).

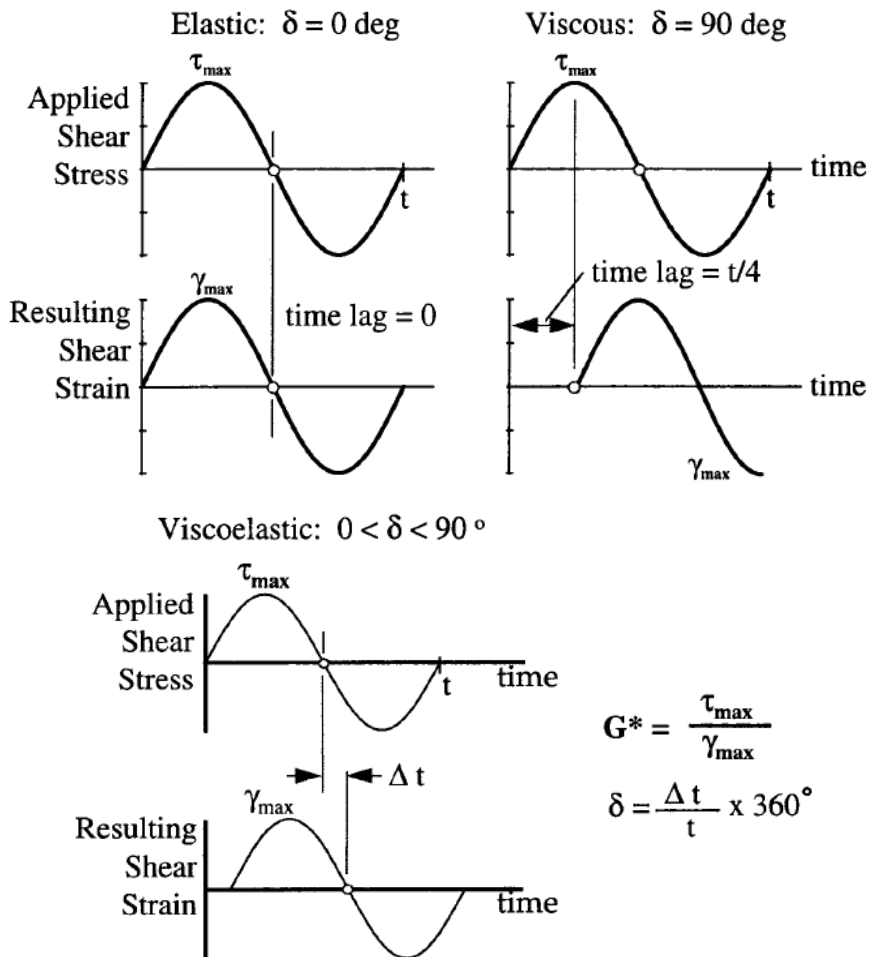


$$G^* = \frac{\tau_m}{\gamma_m} \quad (5.19)$$

$$\tau = \frac{2T}{\pi r^3} \quad (5.20)$$

$$\gamma = \frac{\Theta r}{h} \quad (5.21)$$

$$G^* = \frac{\tau_{\max}}{\gamma_{\max}} \quad (5.22)$$



where:

G^* = the complex shear stiffness modulus, kPa,

τ_m = maximum shear stress (peak to peak), kPa, and

γ_m = maximum shear strain (peak to peak).

τ = shear stress

γ = shear strain

T = applied torque

r = radius of the plate

Θ = deflection or angle of rotation

The phase angle (δ) is referred to as the time delay between the applied torque and angular rotation in the stress-controlled DSR test or between the induced shear strain and the required shear stress in a strain-controlled DSR test. It can be calculated in degrees or radians using the Equations 5.23 and 5.24 respectively:

$$\delta = 360 \frac{\Delta t}{t} \quad (5.23)$$

$$\delta = 2\pi \frac{\Delta t}{t} \quad (5.24)$$

where:

Δt = time shift

t = cycle time (Kennedy et al., 1994).

A complex shear modulus (G^*) has two components: elastic (G') and viscous(G''), as shown in Figure 5.22.

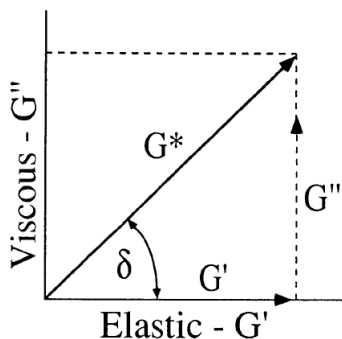


Figure 5.22 : Elastic and viscous part of G^* .

$$G' = G^* \cos(\delta)$$

$$G'' = G^* \sin(\delta)$$

G^* : Complex Shear Modulus

G' : Elastic part of G^*

G'' : Viscous part of G^*

Generally speaking, bitumen behaves elastically at low temperatures, and viscously at very high temperatures. An ideal elastic material exhibits a phase angle equal to zero ($\delta=0$), however an ideal viscous material exhibits a phase angle equal to 90° .

In terms of size, there are currently two parallel plates used; one of them is 8mm the other is 25mm in diameter. Typically the 8mm diameter plates are utilized at intermediate pavement temperatures (from 4 to 40°C) and in the event that applied stress is 1.00 and 2.20kPa for the original and RTFOT-aged bitumen respectively. The 25mm diameter plates are utilized to evaluate the bitumen's behavior at high pavement temperatures (from 46 to 82°C) and in the event that applied stress is 5.00MPa.

SHRP recommends the following use of type of plate and plate gap according to G^* :

- 8mm parallel plates with a 2mm gap when $0.1 \text{ MPa} < G^* < 30 \text{ MPa}$.

- 25mm parallel plates with a 1mm gap when $1.0\text{kPa} < G^* < 100\text{kPa}$.
- 50mm parallel plates when $G^* < 1\text{kPa}$.

The specific plate diameter and sample thickness (plate gap) used in testing a given asphalt depend more on the modulus of the binder than on temperature. Table 5.7 explains the applied stress, plate types and plate gaps utilized in this study.

Table 5.7 : Applied stress, plate diameter and plate gap in this study.

State of Bitumen	Applied Stress (kPa)	Plate Diameter (mm)	Plate Gap (mm)
Original	1.00	25	1
RTFOT-Aged	2.20	25	1
PAV-Aged	2.20	25	1

Regardless of the stress or strain-control, typical DSR equipment is composed of three major components: rheometer, controller, and computer.

The rheometer normally consists of a housing or frame, a motor for applying the strain or stress to the specimen, a transducer for calculating the response of the specimen, and a temperature control and measurement system.

The controller is simply an interface between the rheometer and the computer and includes the data acquisition and signal conditioning hardware for the motors and transducers used in the rheometer.

The computer operates and programs the rheometer. The DSR utilized in this thesis is demonstrated in Figure 5.23.



Figure 5.23 : DSR and its major components.

The stages of "Standard Method of Test for Determining the Rheological Properties of Asphalt Binder Using a Dynamic Shear Rheometer (DSR)" are discussed in AASHTO T-315-08 and ASTM D 7175 as follows:

Prior to placing the bitumen between the plates, the zero plate gap setting is set up at the test temperature to prevent the changing dimensions with temperature changes. The bitumen is heated to 130-140°C in the oven until it is sufficiently fluid to pour. The bitumen is prepared as follows:

- An adequate amount of fluid bitumen is poured on the lower plate. It may be poured directly onto the lower plate of the rheometer, after which the two plates are closed to the final gap plus 50µm. It should be noted that before or during the process of squeezing the bitumen between the plates, the fixed plate (liquid bath) or the chamber (air oven) should be heated to approximately 40-45°C to provide enough adhesion between bitumen and plates. In this study the fixed plate was always heated to 40°C.
- The second option is to pour fluid bitumen on the portable upper plate. It may be poured directly onto the upper plate with the upper plate removed from the rheometer and at room temperature. Then the plate is immediately replaced in the rheometer with the fixed plate that had already heated up to

approximately 40-45°C. This is done to provide enough adhesion between bitumen and the plates. Both upper and lower plates both having both 8mm and 25mm diameters are shown in the Figure 5.24.



Figure 5.24 : Upper and lower plates (the left one in 25-mm diameter and the right one in 8-mm diameter) DSR and its major components.

- Instead of pouring the bitumen onto into the upper or lower plate, a practical silicone mold can also be employed. Fluid bitumen is poured into this mold and allowed to cool to room temperature. Before chilling the mold, the bitumen sample is removed and positioned on the fixed plate that had already been heated to approximately 40-45°C. This step will provide sufficient adhesion between the bitumen and plates. Two typical (8 and 25mm in diameter) molds are demonstrated in Figure 5.25.

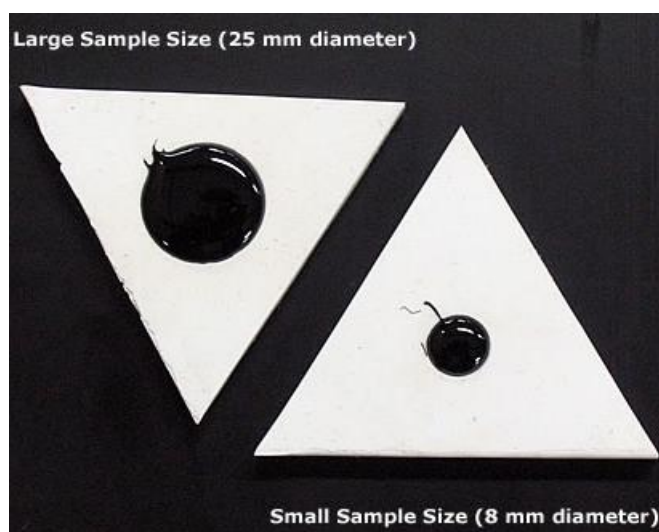


Figure 5.25 : DSR silicone molds.

In this study, silicone molds are also utilized.

Subsequent to placing bitumen, the gap between the plates decreases to the final gap plus 50 μm . Then the sandwiched bitumen between the plates is trimmed flush with the edge of the plate.

After trimming, the final adjustment is set to the target gap (2.0mm gap for the 8mm diameter plate, and 1.0mm gap for the 25mm diameter plate). This process causes a slight bulge in the bitumen specimen, which is the desired configuration. It is noteworthy to say that as the temperature changes, the periphery of the bitumen retains a convex (bulging outward) shape as the temperature changes. The sample should not shrink to the point where the edge becomes concave. The initial and final shapes of the bitumen samples are depicted in Figure 5.26. After these processes, the test begins.

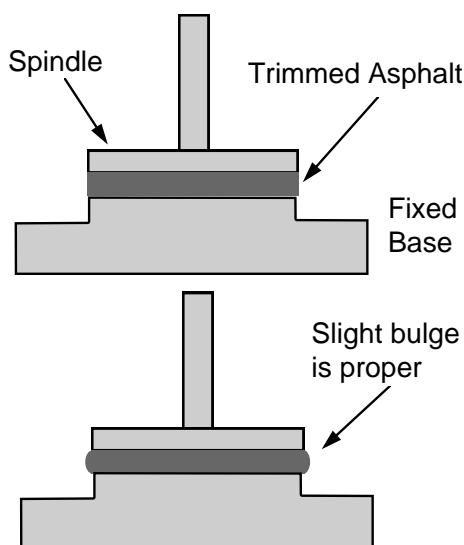


Figure 5.26 : Bitumen sample shape after trimming and after final setting of gap.

In order to prevent rutting and fatigue cracking, SHRP developed a specification by using the DSR results.

The results are used to calculate the specification parameters as follows:

- To minimize rutting:
 - The stiffness value ($G^*/\sin\delta$) of the original binder must be greater than or equal to 1.0kPa at 10rad/s.
 - The stiffness value ($G^*/\sin\delta$) of RTFOT-aged binder must be greater than or equal to 2.2kPa at 10rad/s.

- To minimize fatigue cracking:
 - The stiffness value ($G^*\sin\delta$) of PAV-aged binder must be less than or equal to 5.0MPa at 10rad/s.

5.2.3 Rolling thin film oven test (RTFOT)

This test was comprehensively mentioned in section of 5.1.6 "Aging and loss on heating test" with sub-titles: *Short-Term Aging* and *Simulation of Short-Term Aging*.

5.2.4 Pressure aging vessel (PAV)

This test was mentioned in detail in section of 5.1.6 "Aging and loss on heating test" with the sub-titles: *Long-Term Aging* and *Simulation of Long-Term Aging*.

5.2.5 Bending beam rheometer (BBR) test

In addition to traffic loads, adverse environmental conditions initiate cracking in the asphalt layers. An asphalt pavement contracts when it is subjected to low temperatures in cold weather. The magnitude of the tensile stress occurred due to shrinkage depends on the stiffness of the bituminous binder, its resistance to deformation, and its ability to relax by dissipating energy via permanent flow. If the tensile stress exceeds the tensile strength at any possible points crack propagation will occur in the asphalt layers. These types of cracks occur primarily during a single cycle of low temperatures, but can also develop from several low temperature cycles.

The binder plays a key role in low temperature cracking. In most cases, hard bituminous binders have a higher tendency of low temperature cracking than do soft asphalt binders. Cracking of hard asphalt pavement is inevitable at low temperatures. In regions of cold climates, pavement engineers should use a bituminous binder that is both softer and less prone to hardening.

Since the binder, or rather its stiffness, plays a major and direct role in the thermal cracking potential of HMA pavement, SHRP developed a method to measure the stiffness of the binder and evaluate its potential for thermal cracking. The specifications of the method, "Bending Beam Rheometer" is given below (Bahia and Anderson, 1995a; Roberts et al., 1996; Zaniewski and Pumphrey, 2004).

The Bending Beam Rheometer (BBR) test which has been designed to measure the stiffness of a small asphalt beam specimen under a creep load is based upon the beam

theory. The creep load is applied so as to simulate the stresses progressively occurring in a pavement as the temperature drops (Asphalt Institute, 1998).

In this test the two main parameters – creep stiffness and creep rate – are measured and calculated via the BBR test. Creep stiffness is a measurement of the binder's resistance to a constant load, while the creep rate is typically known as "m value," a measurement of the differentiation of the binder stiffness as loads are applied (Read and Whiteoak, 2003).

High creep stiffness most probably allows asphalt layers to behave in a brittle way; therefore cracking will be unavoidable. On the contrary, a high value of creep rate means that the binder will be more prone to disperse energy due to its rapid changing stiffness.

The process of the BBR test is explained in AASHTO TP1 "Determining the Flexural Creep Stiffness of Asphalt Binder Using the Bending Beam Rheometer (BBR)".

Details of the test are:

Test Equipment

The major components of the BBR are a loading frame, controlled temperature fluid bath, computer control, data acquisition system, and specimen molds. These items are depicted in Figure 5.27 and Figure 5.28 respectively.

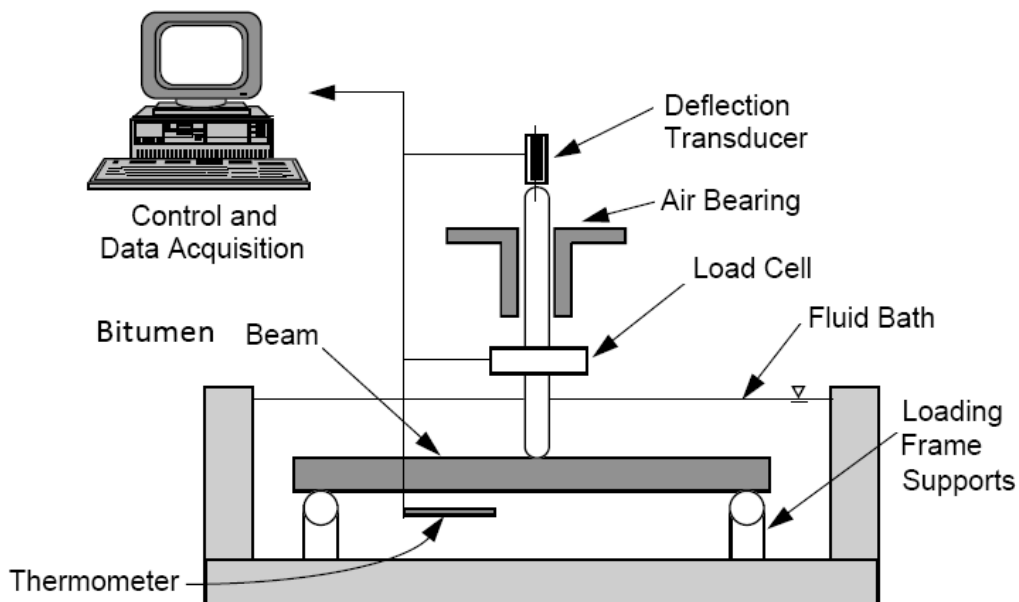


Figure 5.27 : The major components of BBR.

The bitumen beam supported at two locations is exposed to a midpoint load provided by a-blunt-nosed shaft. A mounted-load-cell is used to decrease any frictional resistance during the load application. The applied load is provided by pneumatic pressure and the regulators are used to adjust the load applied through the loading shaft. A deflection transducer is located on the shaft to monitor deflections.

Typical bath fluids include ethanol, methanol, and glycol-methanol mixtures. To prevent the beam from floating, it is important that the mass of the fluid is not greater than 1.05g/cm^3 at the testing temperature. The best fluid bath includes: 60% glycol, 15% methanol, and 25% water.

The data acquisition system requires a computer connected to the BBR test system to control the test parameters and the loads, and to evaluate the deflection test results.

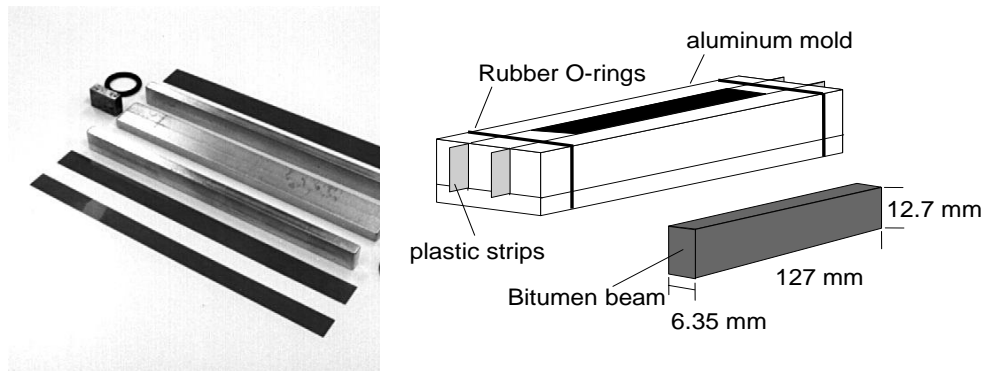


Figure 5.28 : Bituminous binder specimen mold.

Specimen Preparation

Since low temperature cracking is primarily seen in aged pavements, the BBR test is carried out on bitumen samples that are already RTFOT and PAV aged. The aged bitumen is heated until it gets fluid enough to pour. During the heating, the sample is covered and occasionally stirred to remove any air bubbles and to ensure homogeneity. The sample is then poured into two aluminum BBR molds as shown in Figure 5.29. Parts of the aluminum mold are coated with petroleum jelly. Plastic strips are then placed against the greased faces. The end parts are treated with a paste-like glycerin and talc release agent.

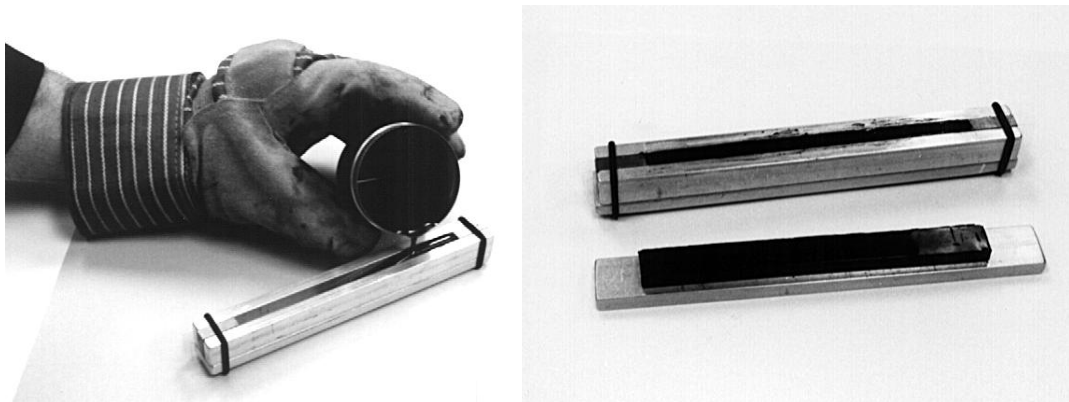


Figure 5.29 : Pouring the bitumen into the mold.

After cooling, the excessive bitumen is trimmed from the upper surface via a hot spatula. To de-mold the beam, the sample is placed in a freezer or ice bath. Then the beam is placed in the BBR fluid bath for 60 minutes. It is important to complete the whole test within 4 hours after the bitumen is poured (Zaniewski and Pumphrey, 2004).

Process of the Test

Prior to testing, it is important to check the test device and system calibration. Once the bitumen beam is thermally conditioned for at least 60 minutes, it is carefully placed on the supports. A $30 \pm 5\text{mN}$ magnitude preload is applied to ensure that the beam is firmly in contact with the supports. Then, a 980mN magnitude seating load is applied for one second by the rheometer software. Subsequent to this seating stage, the load is automatically decreased to the preload for a 20 second recovery period. A constant 980mN test load is applied and maintained for 240 seconds. While the bitumen beam is being deflected under the 980mN load, the deflection transducer is measuring the movement. The software program leads the computer to record both load and deflection.

The deflection of the beam is recorded during this period, and the operator will be able to obtain creep stiffness and m -value at the end of the 240 second duration test. Figure 5.30 and 5.31 depict a schematic of the operation and a typical BBR sample respectively.

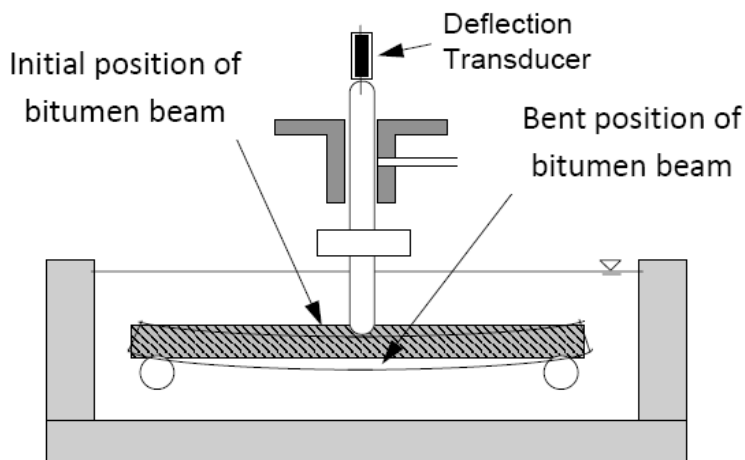


Figure 5.30 : A schematic drawing of the operation.

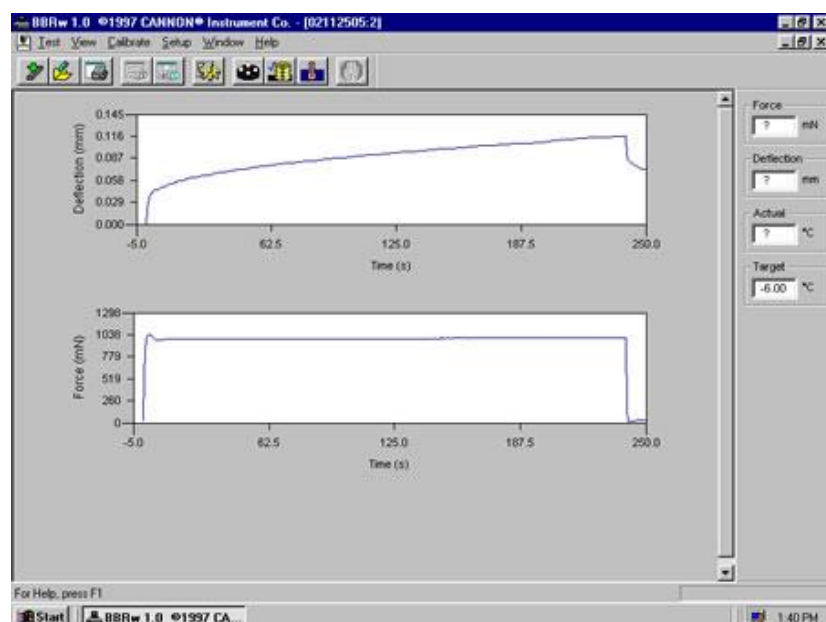


Figure 5.31 : A typical BBR sample output (Pavement Interactive, 2012).

Theory of the Test

Anderson et al. claimed that the convenience of the selected beam dimensions makes the elementary Bernoulli-Euler theory suitable for the analysis of the test (*Anderson et al.*, 1994). According to this theory, the maximum deflection of a beam in three-point loading is expected to occur at the beam midspan.

The deflection of the beam, δ , is measured as follows in the Equation 5.25:

$$\delta = \frac{PL^3}{48EI} \quad (5.25)$$

where:

P = applied load (N)

L= span length (mm)

E = modulus of elasticity (Pa)

I = moments of inertia of section (mm⁴)

When the extensional creep compliance, D(t), is taken into account, the modulus of elasticity, E, is given according to Equation 5.26:

$$E = \frac{1}{D(t)} \quad (5.26)$$

The inverse of the extensional creep compliance is equivalent to the time dependent creep stiffness, S(t), of a viscoelastic material. According to the elastic-viscoelastic correspondence theory, the way of stress distribution in a viscoelastic beam is similar to that of an elastic beam under the same loading. Hence, the time-dependent strains and displacements of a bitumen specimen can be derived from the elementary bending theory for elastic materials when S(t) is used instead of E. Thus, Equation 5.25 can be converted to Equation 5.27:

$$\delta(t) = \frac{PL^3}{48S(t)I} \quad (5.27)$$

Based on the rules of strength of materials, the moment of inertia of a beam whose cross-section is rectangular is defined as follows in Equation 5.28

$$I = \frac{bh^3}{12} \quad (5.28)$$

Where:

b = width of the beam (mm)

h = height of the beam (mm)

In conclusion, when Equation 5.27 and Equation 5.28 are combined, the final Equation (5.29) will be beneficial for pavement engineers to evaluate the S(t).

$$S(t) = \frac{PL^3}{4bh^3\delta(t)} \quad (5.29)$$

Despite the fact that software is able to calculate and give all required outputs, an operator can also manually calculate these parameters from the graphs. Two typical graphs are given below in the Figure 5.32.

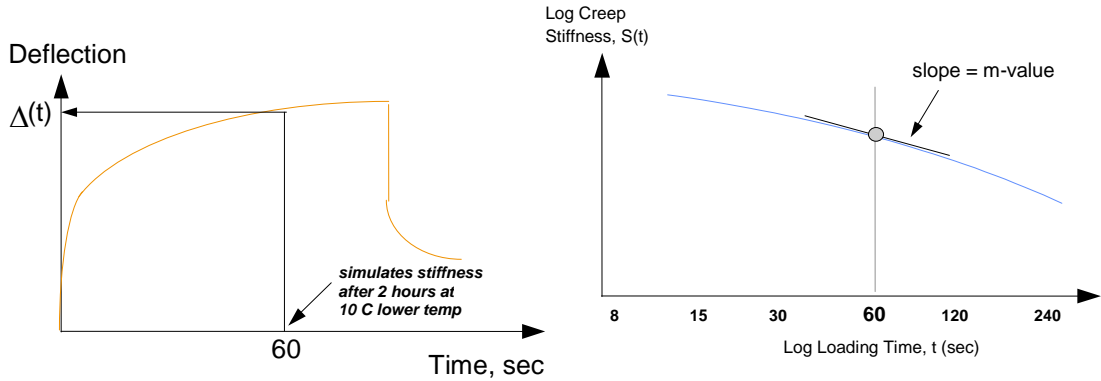


Figure 5.32 : Graphs of BBR test.

The desired critical stiffness and m -value at the minimum pavement design temperature are expected to be obtained after a 2-hour loading. However, instead of long time loading, SHRP researchers realized that a 60-second loading would be adequate to obtain these two parameters if the test temperature is raised 10°C. Their approach was based upon the theory time-temperature superposition (Fwa, 2005).

SHRP specifications recommend a maximum value of 300MPa for creep stiffness and a minimum value of 0.30 for the m -value is necessary to minimize low-temperature cracking (Marasteanu et al., 2006). If both criteria are met, no additional testing is required. Otherwise other SUPERPAVE tests such as direct tension test (DTT) should be carried out on the samples to check the convenience.

The BBR utilized in this thesis is demonstrated in following Figure 5.33.



Figure 5.33 : Picture of the used BBR.

5.3 Morphology Analysis

Conventional methods to determine the phase behavior of any additive and bitumen include the use of optical and electron microscopy. However, most researchers prefer electron microscopy due to the fact that it provides a clear view of a material in the raw state (Blanco et al., 1996; Michler, 1996; Lesueur et al., 1998; Jian-Shiu Chen et al., 2002).

Although there are several major types of electron microscopes: Scanning Electron Microscope (SEM), Reflection Electron Microscope (REM), Transmission Electron Microscope (TEM), Scanning Transmission Electron Microscope (STEM), and others, the first one, in other words, the Scanning Electron Microscope (SEM) is more commonly used. SEM is a microscopy technique in which a beam of electrons is transmitted through an ultra-thin specimen, interacting with the specimen as it passes through. An image is formed from the interaction of the electrons transmitted through the specimen; the image is magnified and focused onto an imaging device, such as a fluorescent screen, on a layer of photographic film, or is set up so that it is detected by a sensor such as a CCD camera (Wikipedia, 2014). This study utilized a

high-resolution scanning electron model (SEM, JEOL JSM-7,001 F) microscopy, an imaging mode of the SEM allowing direct imaging of the atomic structure of the sample, and then images were focused onto a CCD camera. Its picture is shown in Figure 5.34.



Figure 5.34 : Picture of SEM.

Since the compatibility between sulphur and bitumen is expected to play a key role on the properties of SEBs, their morphology was investigated using the SEM by characterizing the distribution and the dispersion of sulphur in bitumen matrix. Previous studies showed that the major effect of aging on the morphology of the

modified binders was to homogenize the dispersion of any modifier in bitumen matrix. Due to the severe degradation of the modifier, the compatibility between the modifier and bitumen was prone to significantly improve with further aging (Zhang et al., 2010). Hence, in order to understand how both short and long-time aging affect the morphology and compatibility between sulphur and bitumen, not only unaged, but also R and P-SEBs were also observed.

Chen and Huang added sulphur as a vulcanizing agent to polymer-modified-bitumen to enhance the storage stability and the solubility of the polymer in the bitumen. They revealed that micrographs obtained from a TEM demonstrated that the addition of sulphur led to the asphalt particles losing size diametrically, which means a remarkable improvement in compatibility through a process called vulcanization (Chen and Huang, 2007).

Nonconductive samples tend to charge when scanned by the electron beam, and especially in secondary electron imaging mode, this causes scanning faults and other image artifacts. SEBs were therefore coated with an ultrathin coating of gold. This technique provides clues as to how the microstructure differences between sulphur and bitumen in SEB should be analyzed.

6. EXPERIMENTAL RESULTS

6.1 First Generation Test Results

6.1.1 Penetration test results

It was found that the penetration value of the all O and R-SEBs increases when 10% of the conventional bitumen is replaced with sulphur. An additional sulphur content increase of more than 10% resulted in a variable decrease in the value. The penetration value of the all O and R-SEBs with a 50% sulphur content, excepting B100/150, is lower than that of its pure bitumen. On the other hand, despite the fact that no change found in P-SEBs regarding variable amount of sulphur content, any additional sulphur quantity promises to decrease their penetration grade.

The penetration values of all SEBs at the three different phases are given graphically in the following figures (Figure 6.1, Figure 6.2, Figure 6.3, and Figure 6.4):

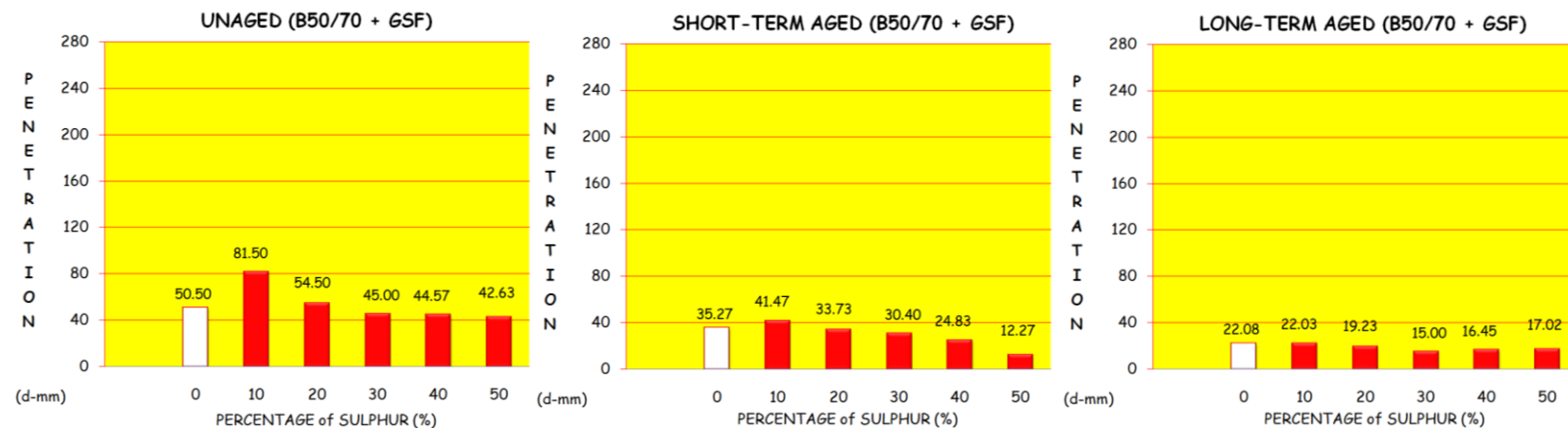


Figure 6.1 : Showing penetration grades of (B50/70+GSF) at unaged, short-term and long-term aged stages.

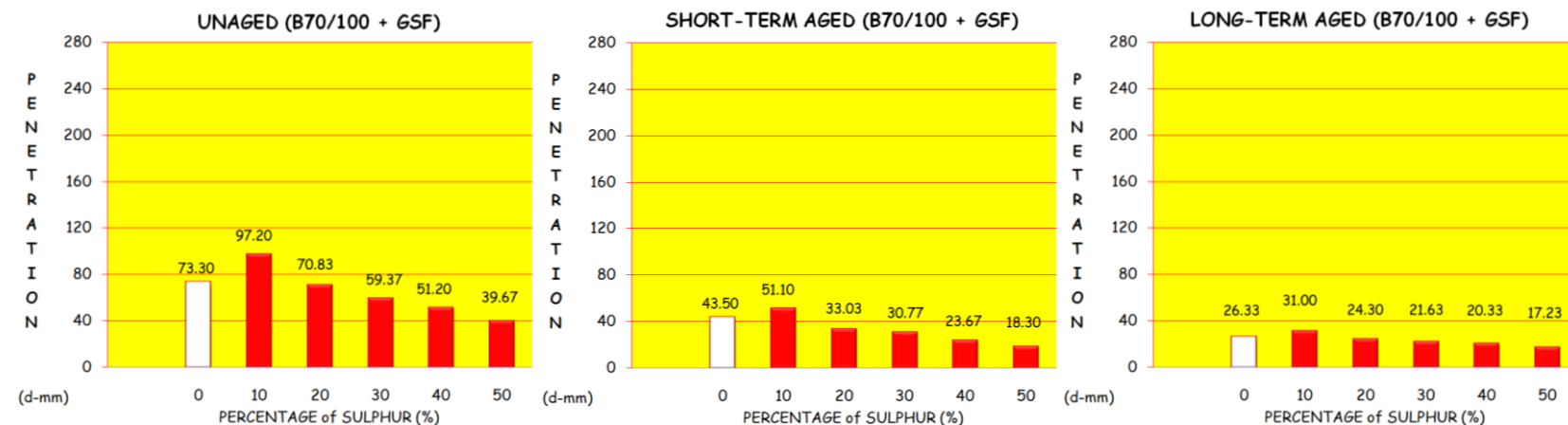


Figure 6.2 : Showing penetration grades of (B70/100+GSF) at unaged, short-term and long-term aged stages.

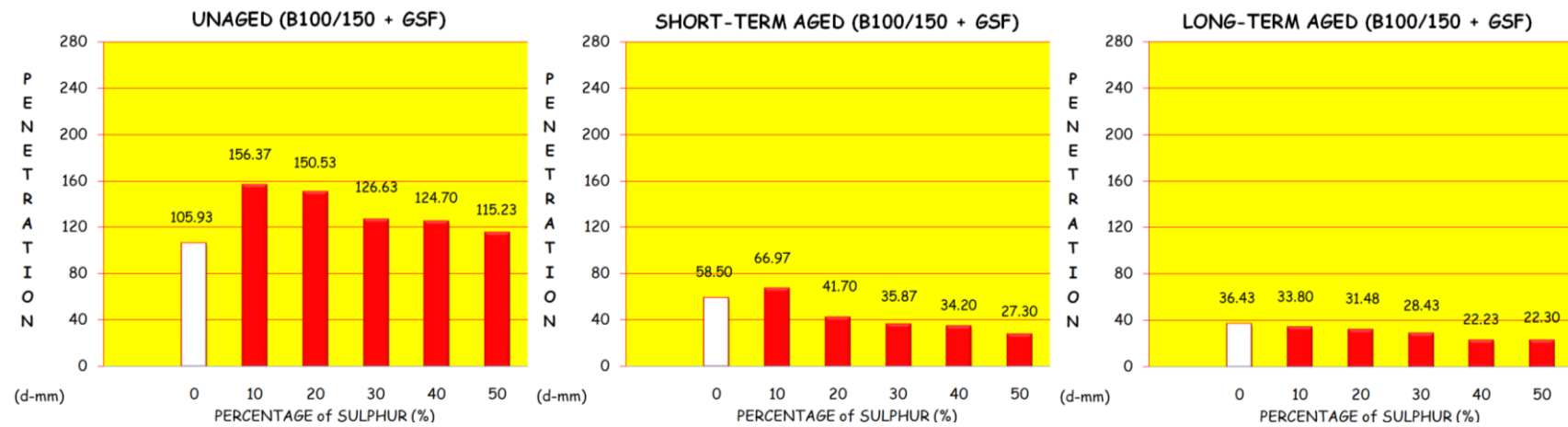


Figure 6.3 : Showing penetration grades of (B100/150+GSF) at unaged, short-term and long-term aged stages.

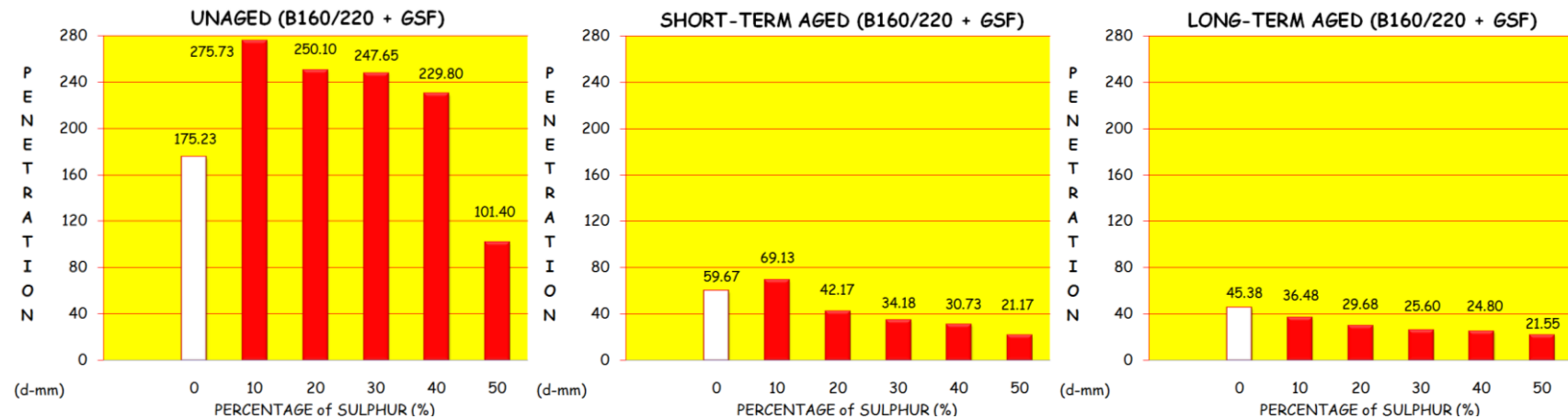


Figure 6.4 : Showing penetration grades of (B160/220+GSF) at unaged, short-term and long-term aged stages.

The penetration values of all SEBs at the three different phases are summarized in the following table (Table 6.1):

Table 6.1 : Penetration values of SEBs.

Sample	Penetration (d mm)			Penetration Change (%)		
	O	R	P	$\Delta O-R$	$\Delta R-P$	$\Delta O-P$
B50/70-0%GSF	50.50	35.27	22.08	30.16	37.40	56.28
B50/70-10%GSF	81.50	41.47	22.03	49.12	46.88	72.97
B50/70-20%GSF	54.50	33.73	19.23	38.11	42.99	64.72
B50/70-30%GSF	45.00	30.40	15.00	32.44	50.66	66.67
B50/70-40%GSF	44.57	24.83	16.45	44.29	33.75	63.09
B50/70-50%GSF	42.63	12.27	17.02	71.22	-38.71	60.08
B70/100-0%GSF	73.30	43.50	26.33	40.65	39.47	64.08
B70/100-10%GSF	97.20	51.10	31.00	47.43	39.33	68.11
B70/100-20%GSF	70.83	33.03	24.30	53.37	26.43	65.69
B70/100-30%GSF	59.37	30.77	21.63	48.17	29.70	63.57
B70/100-40%GSF	51.20	23.67	20.33	53.77	14.11	60.29
B70/100-50%GSF	39.67	18.30	17.23	53.87	5.85	56.57
B100/150-0%GSF	105.93	58.50	36.43	44.77	37.73	65.61
B100/150-10%GSF	156.37	66.97	33.80	57.17	49.53	78.38
B100/150-20%GSF	150.53	41.70	31.48	72.30	24.51	79.09
B100/150-30%GSF	126.63	35.87	28.43	71.67	20.74	77.55
B100/150-40%GSF	124.70	34.20	22.23	72.57	35.00	82.17
B100/150-50%GSF	115.23	27.30	22.30	76.31	18.32	80.65
B160/220-0%GSF	175.23	59.67	45.38	65.95	23.95	74.10
B160/220-10%GSF	275.73	69.13	36.48	74.93	47.23	86.77
B160/220-20%GSF	250.10	42.17	29.68	83.14	29.62	88.13
B160/220-30%GSF	247.65	34.18	25.60	86.20	25.10	89.66
B160/220-40%GSF	229.80	30.73	24.80	86.63	19.30	89.21
B160/220-50%GSF	101.40	21.17	21.55	79.12	-1.79	78.75

O, R, and P representing original age, short-term (RTFOT-aged) and long-term (PAV-aged) aging respectively.

- When compared to pure B50/70 bitumen, the penetration grades are found to be 61.3% higher for B50/70-10%GSF and 15.5% lower for B50/70-50%GSF at the unaged stage. At the short-term aged stage, they are found to be 17.5% higher for B50/70-10%GSF and 65.2% lower for B50/70-50%GSF and at the long-term aged stage, it is found to be 32.0% lower for B50/70-30%GSF.
- When compared to pure B70/100 bitumen, the penetration grades are found to be 32.6% higher for B70/100-10%GSF and 45.8% lower for B70/100-50%GSF at the unaged stage. At the short-term aged stage, they are found to be 17.4% higher for B70/100-10%GSF and 57.9% lower for B70/100-

50%GSF. At the long-term aged stage, they are found to be 17.7% higher by for B70/100-10%GSF and 34.5% lower for B70/100-50%GSF.

- When compared to pure B100/150 bitumen, the penetration grades are found to be 47.6% higher for B100/150-10%GSF and 8.7% higher for B100/150-50%GSF respectively at the unaged stage. At the short-term aged stage, they are found to be 14.4% higher for B100/150-10%GSF and 55.3% lower for B100/150-50%GSF. At the long-term aged stage, it is found to be 38.9% lower for B100/150-40%GSF.
- When compared to pure B160/220 bitumen, penetration grades are found to be 57.3% higher for B160/220-10%GSF and 42.1% lower for B160/220-50%GSF at the unaged stage. At the short-term aged stage, they are found to be 15.8% higher for B160/220-10%GSF and 64.5% lower for B160/220-50%GSF and at the long-term aged stage, it is found to be 52.5% lower for B160/220-50%GSF.

Considering the penetration grade of O, R and P-SEBs, as expected, the utmost penetration loss is observed between O and P stages of the same samples. When the penetration loss between O and R stage of the same sample is compared with its penetration loss between O and P, it is lower, but still remarkable. The biggest difference in the penetration value for both types between O-R and O-P stage specifically occurred in the SEB samples that are derivatives of B160/200. The reason why they are so high is (supposedly) that B160/220 already has a wide range of penetration values.

On the other hand, no higher penetration loss between the R and P phases of the same samples has been detected. This becomes more meaningful when the sulphur content of the SEBs is increased. Compared with bitumen, sulphur's sensitivity to aging is different and in accordance with the increase in sulphur content, the penetration loss decreases after the same SEB in both short-term and long-term aging.

6.1.2 Softening point temperature test results

It was found that the softening point temperature (SPT) of the SEBs including 10% sulphur, decreases at both the unaged and short-term aged stages. However, the SPT

of the long-term aged SEBs had a tendency to decrease when the sulphur content was raised to 20%.

Further sulphur content increases more than 10% for O and R and 20% for P-SEBs, which resulted in a slow increase in the values.

The SPT points of all SEBs at the three different phases are given graphically in Figures 6.5, 6.6, 6.7, and 6.8.

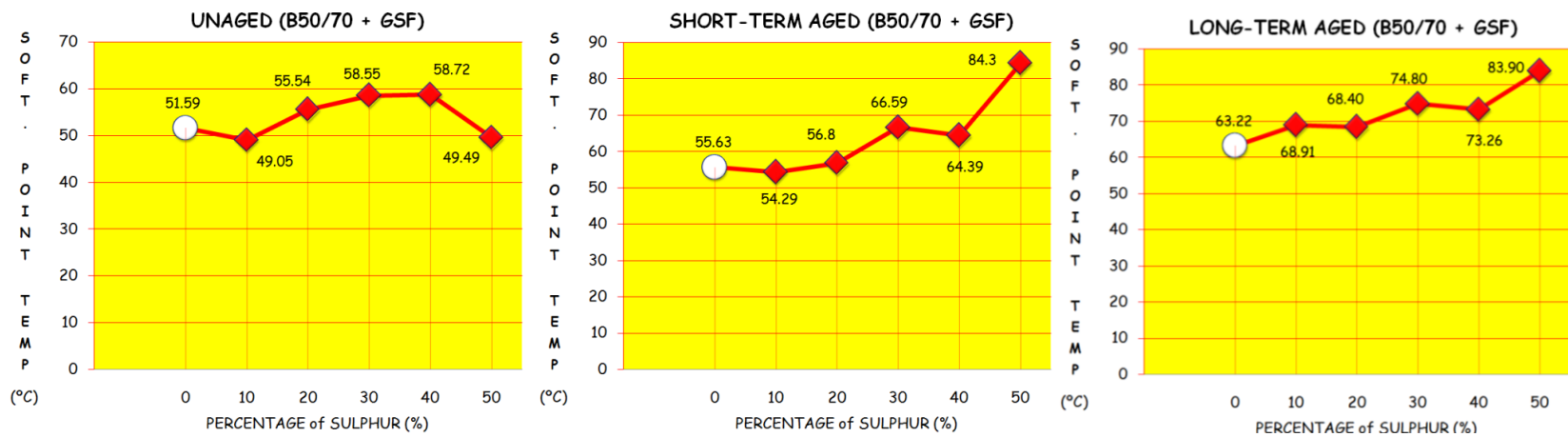


Figure 6.5 : Showing softening point temperature of (B50/70+GSF) at unaged, short-term and long-term aged stages.

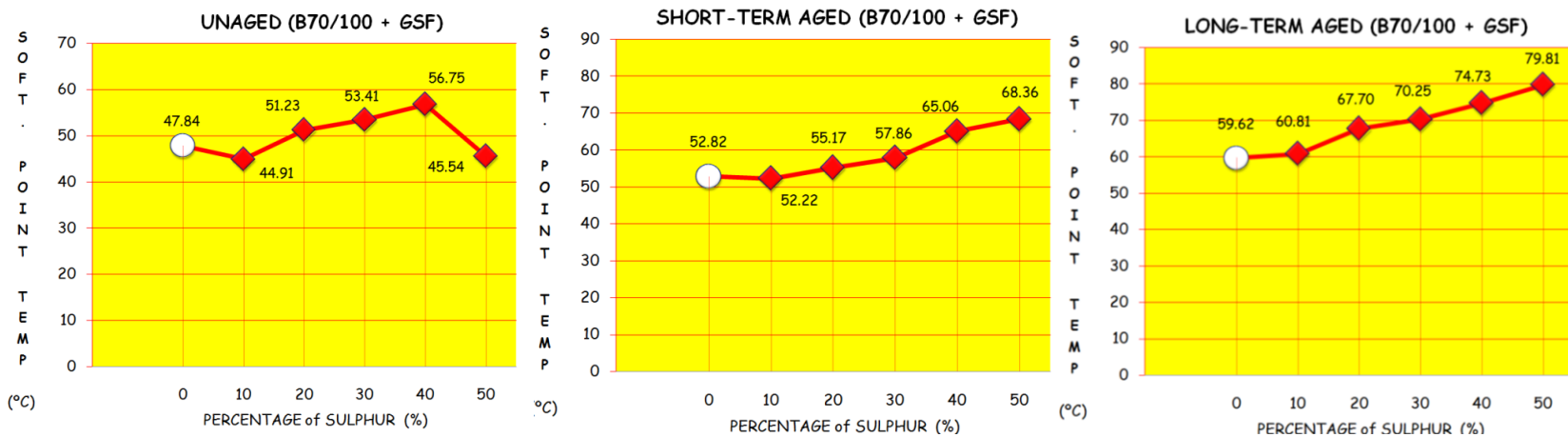


Figure 6.6 : Showing softening point temperature of (B70/100+GSF) at unaged, short-term and long-term aged stages.

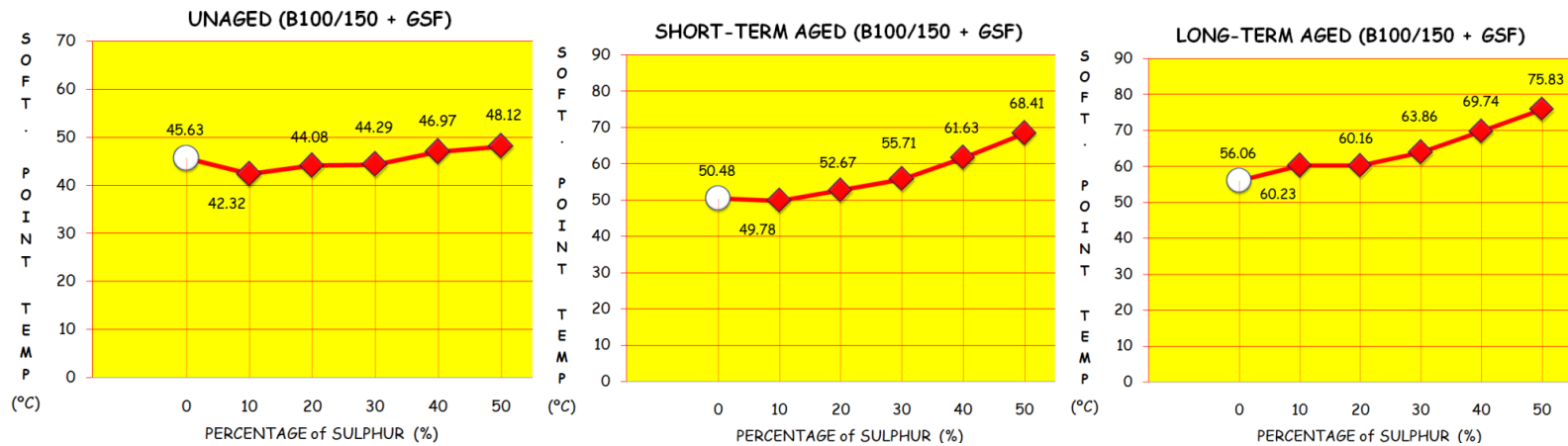


Figure 6.7 : Showing softening point temperature of (B100/150+GSF) at unaged, short-term and long-term aged stages.

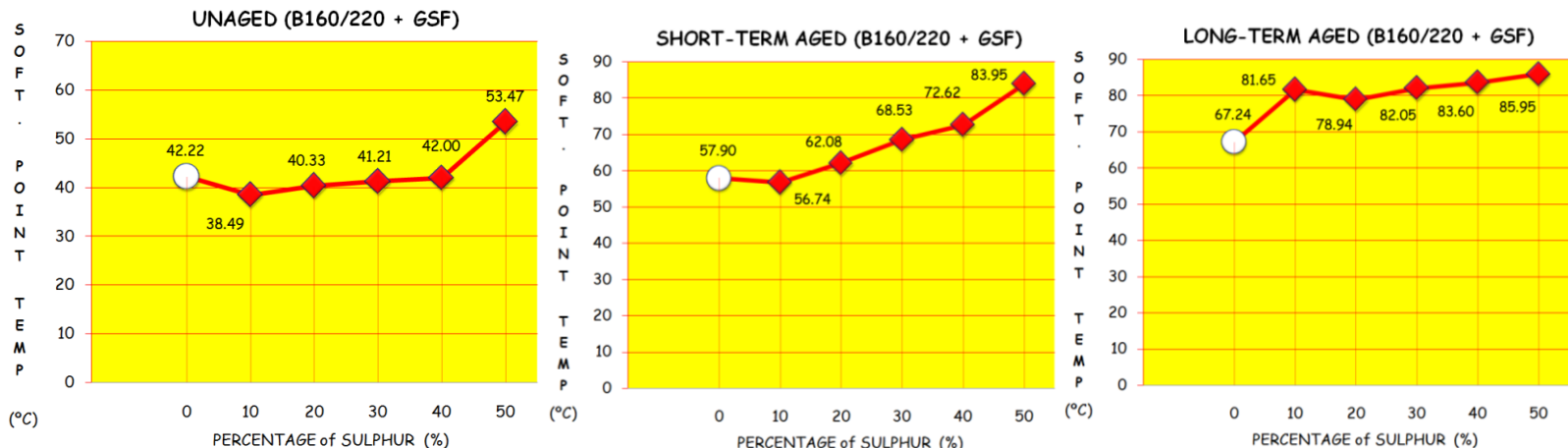


Figure 6.8 : Showing softening point temperature of (B160/220+GSF) at unaged, short-term and long-term aged stages.

The SPT points of all SEBs at the three different phases are given in Table 6.2.

Table 6.2 : Softening point temperature of SEBs.

Sample	Softening Point (°C)			Softening Point Change (%)		
	O	R	P	Δ O-R	Δ R-P	Δ O-P
B50/70-0%GSF	51.59	55.63	63.22	7.83	13.64	22.54
B50/70-10%GSF	49.05	54.29	68.91	10.68	26.93	40.49
B50/70-20%GSF	55.54	56.80	68.40	2.27	20.42	23.15
B50/70-30%GSF	58.55	66.59	74.80	13.73	12.33	27.75
B50/70-40%GSF	58.72	64.39	73.26	9.66	13.78	24.76
B50/70-50%GSF	49.49	84.30	83.90	70.34	-0.47	69.53
B70/100-0%GSF	47.84	52.82	59.62	10.41	12.87	24.62
B70/100-10%GSF	44.91	52.22	60.81	16.28	16.45	35.40
B70/100-20%GSF	51.23	55.17	67.70	7.69	22.71	32.15
B70/100-30%GSF	53.41	57.86	70.25	8.33	21.41	31.53
B70/100-40%GSF	56.75	65.06	74.73	14.64	14.86	31.68
B70/100-50%GSF	45.54	68.36	79.81	50.11	16.75	75.25
B100/150-0%GSF	45.63	50.48	56.06	10.63	11.05	22.86
B100/150-10%GSF	42.32	49.78	60.23	17.63	20.99	42.32
B100/150-20%GSF	44.08	52.67	60.16	19.49	14.22	36.48
B100/150-30%GSF	44.29	55.71	63.86	25.78	14.63	44.19
B100/150-40%GSF	46.97	61.63	69.74	31.21	13.16	48.48
B100/150-50%GSF	48.12	68.41	75.83	42.17	10.85	57.59
B160/220-0%GSF	42.22	57.90	67.24	37.14	16.13	59.26
B160/220-10%GSF	38.49	56.74	81.65	47.41	43.90	112.13
B160/220-20%GSF	40.33	62.08	78.94	53.93	27.16	95.74
B160/220-30%GSF	41.21	68.53	82.05	66.29	19.73	99.10
B160/220-40%GSF	42.00	72.62	83.60	72.90	15.12	99.05
B160/220-50%GSF	53.47	83.95	85.95	57.00	2.38	60.74

O, R, and P representing original age, short-term (RTFOT-aged) and long-term (PAV-aged) aging respectively.

- When compared to pure B50/70 bitumen, the softening point temperatures are found to be lower by 4.9% for B50/70-10%GSF and 13.8% higher for B50/70-40%GSF at the unaged stage. At the short-term aged stage, they are 2.4% lower for B50/70-10%GSF and 51.5% higher for B50/70-50%GSF. At the long-term aged stage, they are 32.7% higher for B50/70-50%GSF.
- When compared to pure B70/100 bitumen, the softening point temperatures are 6.1% lower for B70/100-10%GSF and 18.6% higher for B70/100-40%GSF at the unaged stage. At the short-term aged stage, they are found to be 1.1% lower for B70/100-10%GSF and 29.4% higher for B70/100-50%GSF. At the long-term aged stage it is 33.8% higher for the B70/100-50%GSF.
- When compared to pure B100/150 bitumen, the softening point temperatures are 7.2% lower for B100/150-10%GSF and 5.4% higher for B100/150-

50%GSF at the unaged stage. At the short-term aged stage, they are 1.3% lower for B100/150-10%GSF and 35.5% higher for B100/150-50%GSF. At the long-term aged stage, it is 35.2% higher for the B100/150-50%GSF.

- When compared to pure B160/220 bitumen, the softening point temperatures are 8.8% lower for B160/220-10%GSF and 26.6% higher for B160/220-50%GSF at the unaged stage. At the short-term aged stage, they are 2.0% lower for B160/220-10%GSF and 44.9% higher for B160/220-50%GSF. At the long-term aged stage, it is 27.8% higher for B160/220-50%GSF.

While the observed results are not surprising, they are meaningful. As already stated in the penetration results, the penetration grades of both O and R-aged SEBs including 10%GSF were also seen to increase. Therefore the SPT and penetration grades of those SEBs are closely related to each other, and regardless of its type, any bitumen replaced with 10%GSF has a lower hardness at both the unaged and short-aged stages. In addition to their inter-corporation, both SPT and penetration grades are undoubtedly corresponding to the viscosity of the binder. To understand this correlation comprehensively, we looked at what happens when sulphur is added to a conventional binder.

Adding sulphur to a conventional bitumen results in three typical events: A certain amount of the sulphur reacts with the bitumen, another dissolves in the bitumen, while the rest forms a crystalline structure (Kennepohl and Miller, 1978; Rennie, 1979). The reaction of sulphur and bitumen leads to physical and chemical variations in the SEB over time. Studies have demonstrated that all three states of the sulphur in bitumen, i.e., reacting, dissolving, and crystallizing, have a positive impact on the properties of the SEB (Bencowitz and Boe, 1938; Petrossi et al., 1972; Imants, 1977). The amount of dissolution of sulphur in bitumen depends on both the method used in the mixing and in the bitumen type. Micrographic images show that the sulphur dissolved in the bitumen has a colloidal form (Kennepohl et al., 1974; Kennepohl et al., 1975). If the amount of the sulphur in this new binder exceeds 30% (by weight), the colloidal particles condense, grow, and transform into needle-like sulphur crystals. It was found that untransformed, but reacted and dissolved sulphur particles of 5-10 μ m in diameter have a homogenous distribution and characterize the basic morphology of the SEB (Fairbrother et al., 1955). However, when the sulphur content is higher than 30%, needle-like, coarse sulphur crystals of a heterogeneous

structure form clusters in the matrix (Courval and Akili, 1982). While no problems arise from low crystallization, the coarsening of the crystals does affect the properties and behavior of the sulphur in the SEB. The dissolution of the sulphur in bitumen is closely related with the temperature and the dissolution efficiency of the sulphur (Petrossi et al., 1972).

6.1.3 Penetration index results

The temperature susceptibility of any bituminous binder is generally evaluated by the penetration index (PI) and penetration viscosity number (PVN) (Awanti et al., 2008). Since PI is more common than PVN as proposed by *Mcleod* in 1976, it is used in this study to determine the temperature susceptibilities of SEBs.

The penetration index of all SEBs at the three different phases are displayed graphically in Figures 6.9, 6.10, 6.11, and 6.12.

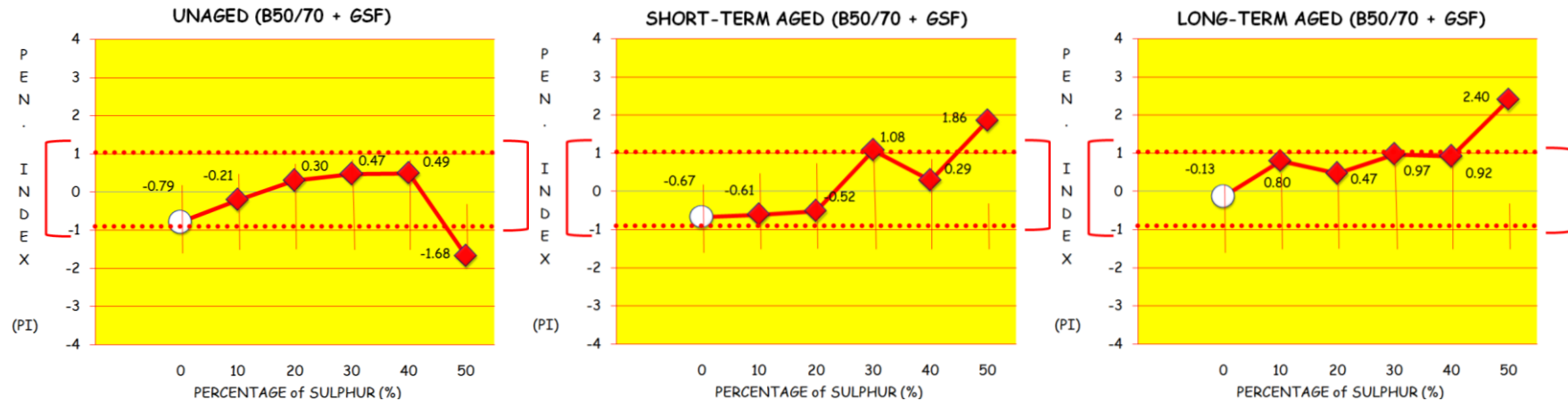


Figure 6.9 : Showing penetration index of (B50/70+GSF) at un-aged, short-term and long-term aged stages.

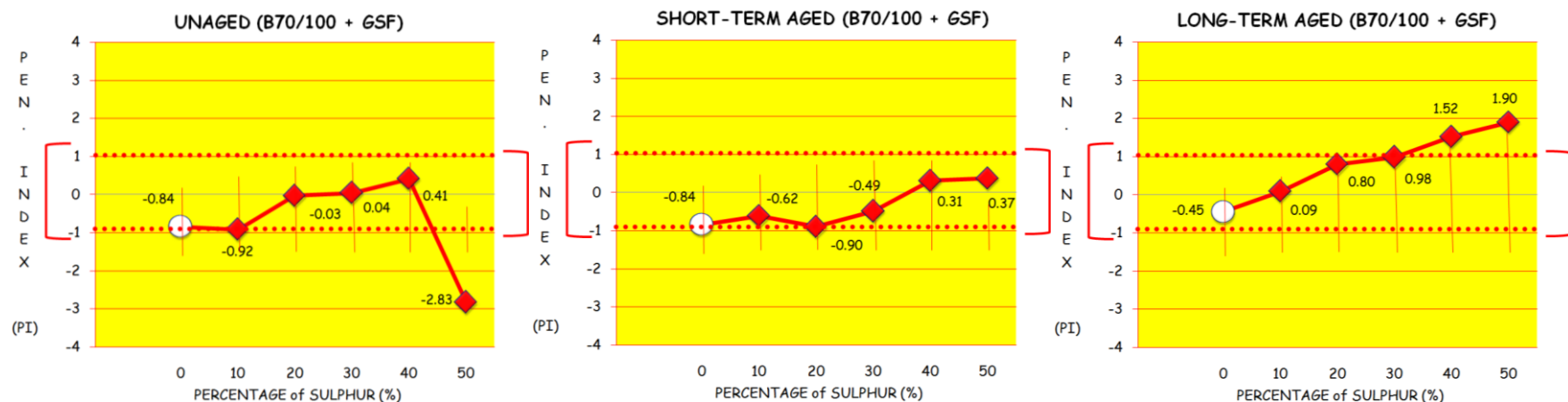


Figure 6.10 : Showing penetration index of (B70/100+GSF) at un-aged, short-term and long-term aged stages.

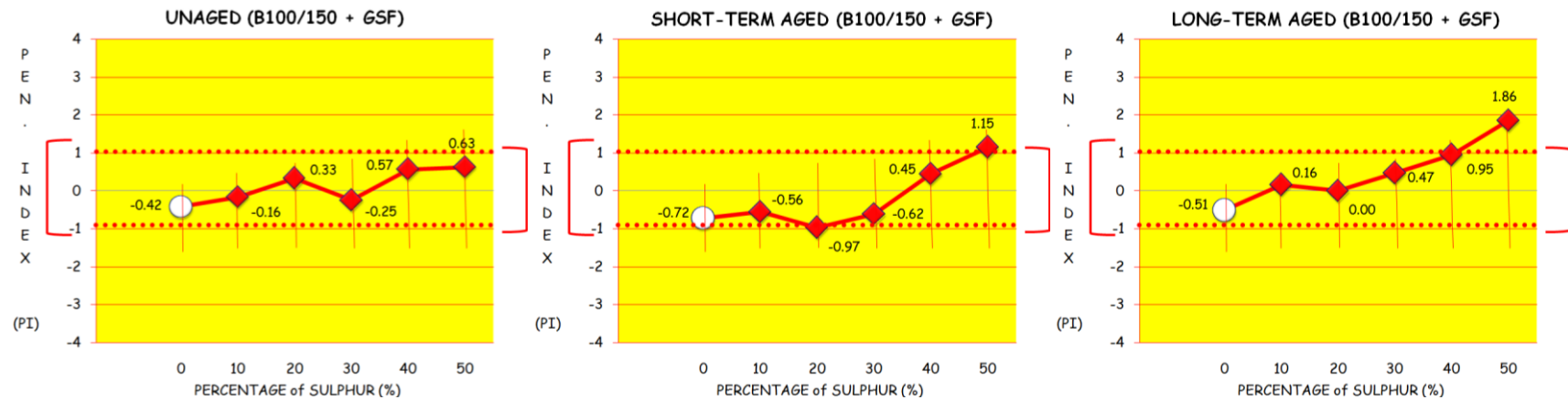


Figure 6.11 : Showing penetration index of (**B100/150+GSF**) at un-aged, short-term and long-term aged stages.

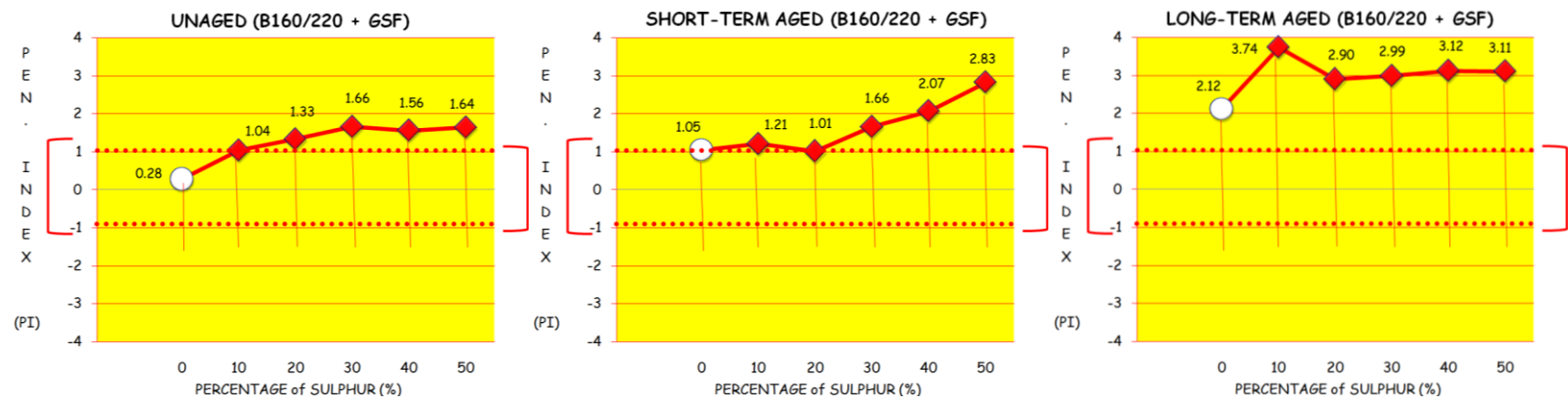


Figure 6.12 : Showing penetration index of (**B160/220+GSF**) at un-aged, short-term and long-term aged stages.

- ***At the un-aged stage;*** Since the PI of SEBs extended from both B50/70 and B70/100 and included 10, 20, 30, or 40%GSF as a variable between -1 and +1, those SEBs meet required temperature susceptibility. However, at a 50% sulphur level, they become more sensitive to temperature when compared to the reference Mexican bitumen whose PI is equal to zero. No matter what percentage of sulphur they contain, all derivatives of B100/150 are expected to have a performance well in accordance with temperature susceptibility because of their -1 and +1 PI range. In contrast to B100/150, all SEBs extended from B160/220 are very sensitive to temperature due to their PI grades, which are close to that of Mexican bitumen.

- ***At the short-term aged stage;*** Excepting B50/70-30%GSF, B50/70-50%GSF, B100/150-50%GSF and each derivative of B160/220, all SEBs are still acceptable.

- ***At the long-term aged stage;*** Excepting B50/70-50%GSF, B70/100-40%GSF, B70/100-50%GSF, B100/150-50%GSF and each derivative of B160/220, all SEBs are still promising.

The penetration index of all SEBs at the three different phases are illustrated in Table 6.3.

Table 6.3 : Penetration index of SEBs.

Sample	Penetration Index			Penetration Index Change (%)		
	O	R	P	$\Delta O-R$	$\Delta R-P$	$\Delta O-P$
B50/70-0%GSF	-0.79	-0.67	-0.13	15.2	80.6	83.5
B50/70-10%GSF	-0.21	-0.61	0.80	-190.5	231.1	481.0
B50/70-20%GSF	0.30	-0.52	0.47	-273.3	190.4	56.7
B50/70-30%GSF	0.47	1.08	0.97	129.8	-10.2	106.4
B50/70-40%GSF	0.49	0.29	0.92	-40.8	217.2	87.8
B50/70-50%GSF	-1.68	1.86	2.40	210.7	29.0	242.9
B70/100-0%GSF	-0.84	-0.84	-0.45	0.0	46.4	46.4
B70/100-10%GSF	-0.92	-0.62	0.09	32.6	114.5	109.8
B70/100-20%GSF	-0.03	-0.90	0.80	-2900.0	188.9	2766.7
B70/100-30%GSF	0.04	-0.49	0.98	-1325.0	300.0	2350.0
B70/100-40%GSF	0.41	0.31	1.52	-24.4	390.3	270.7
B70/100-50%GSF	-2.83	0.37	1.90	113.1	413.5	167.1
B100/150-0%GSF	-0.42	-0.72	-0.51	-71.4	29.2	-21.4
B100/150-10%GSF	-0.16	-0.56	0.16	-250.0	128.6	200.0
B100/150-20%GSF	0.33	-0.97	0.00	-393.9	100.0	-100.0
B100/150-30%GSF	-0.25	-0.62	0.47	-148.0	175.8	288.0
B100/150-40%GSF	0.57	0.45	0.95	-21.1	111.1	66.7
B100/150-50%GSF	0.63	1.15	1.86	82.5	61.7	195.2
B160/220-0%GSF	0.28	1.05	2.12	275.0	101.9	657.1
B160/220-10%GSF	1.04	1.21	3.74	16.3	209.1	259.6
B160/220-20%GSF	1.33	1.01	2.90	-24.1	187.1	118.0
B160/220-30%GSF	1.66	1.66	2.99	0.0	80.1	80.1
B160/220-40%GSF	1.56	2.07	3.12	32.7	50.7	100.0
B160/220-50%GSF	1.64	2.83	3.11	72.6	9.9	89.6

O, R, and P representing original age, short-term (RTFOT-aged) and long-term (PAV-aged) aging respectively.

6.1.4 Specific gravity results

The specific gravity (SG) of sulphur is in the range of 2.03–2.08. It is approximately twice as high as the SG of conventional bitumen (Gardner and Frankel, 1956). The SG of granular sulphur utilized in this study is equal to 2.07; hence, when the same weights of sulphur and bitumen are blended, the volume of the sulphur is half of the bitumen. Consequently, the SG value of SEB is expected to increase as the sulphur content rises.

In addition to experimental methods for measurement of SG as stated in chapter 5.1.4, there is also a mathematical approach to evaluate the SG of SEBs by following equation (Equation 6.1).

$$SG_{SEB} = \frac{100}{\frac{R_s}{SG_s} + \frac{R_b}{SG_b}} \quad (6.1)$$

Where:

SG_{SEB} = Specific gravity of SEB

SG_s = Specific gravity of sulphur

SG_b = Specific gravity of bitumen

R_s = Ratio of sulphur by weight (%)

R_b = Ratio of bitumen by weight (%)

The SG of all SEBs at the three different stages has been evaluated by using the pycnometer method at 25°C and the above equation was also used to calculate the SG values of unaged SEBs mathematically. Then the correlation coefficient was computed for each SEB class to describe how strongly the units in the same group resemble each other.

The value of the correlation coefficient (r) is such that $-1 \leq r \leq +1$. The "+" and "-" signs represent the positive and negative linear correlations, respectively. Positive correlation means that if two parameters have a strong positive linear correlation, r is converging to +1. An r value of exactly +1 indicates a perfect positive fit. Positive values indicate a relationship between two parameters such as that values for the one increase, values for the other also increase or vice versa.

Negative correlation means that if two parameters have a strong negative linear correlation, r is converging to -1. An r value of exactly -1 indicates a perfect negative fit. Negative values indicate a relationship between two parameters such as that values for the one increase, values for the other decrease or vice versa.

If r diverges from -1 and +1 and converges to 0, there is no linear correlation or a weak linear correlation. A value near zero indicates that there is a random, nonlinear relationship between the two parameters. Here, it is noteworthy to specify that r is a dimensionless quantity; that is, it does not depend on the units employed.

An excellent correlation of ± 1 occurs only when the data points all lie exactly on a straight line. If r is equal to +1, the slope of this line is positive. If r is equal to -1, the slope of this line is negative.

To sum up, a correlation greater than 0.8 is generally accepted as being "strong," whereas a correlation less than 0.5 is generally accepted as "weak."

Table 6.4 : Specific gravity of SEBs.

SAMPLE	Calculated Specific Gravity at the "O" Stage					Experimental Specific Gravity at the "O, R, P" Stage			Corr. Coeff. Between Cal. O and Exp. O
	R _S	R _B	SG _S	SG _B	SG _{SEB} (O)	O	R	P	
B50/70-0%GSF	0	100	2.07	1.024	1.024	1.024	1.031	1.033	0.743
B50/70-10%GSF	10	90	2.07	1.024	1.078	1.071	1.068	1.064	
B50/70-20%GSF	20	80	2.07	1.024	1.139	1.111	1.113	1.113	
B50/70-30%GSF	30	70	2.07	1.024	1.207	1.117	1.194	1.121	
B50/70-40%GSF	40	60	2.07	1.024	1.283	1.095	1.157	1.150	
B50/70-50%GSF	50	50	2.07	1.024	1.370	1.115	1.401	1.347	
B70/100-0%GSF	0	100	2.07	1.016	1.016	1.016	1.022	1.026	0.970
B70/100-10%GSF	10	90	2.07	1.016	1.071	1.068	1.058	1.062	
B70/100-20%GSF	20	80	2.07	1.016	1.131	1.122	1.106	1.107	
B70/100-30%GSF	30	70	2.07	1.016	1.199	1.149	1.154	1.144	
B70/100-40%GSF	40	60	2.07	1.016	1.276	1.347	1.323	1.169	
B70/100-50%GSF	50	50	2.07	1.016	1.363	1.381	1.216	1.246	
B100/150-0%GSF	0	100	2.07	1.012	1.012	1.012	1.000	1.020	0.835
B100/150-10%GSF	10	90	2.07	1.012	1.067	1.060	1.054	1.060	
B100/150-20%GSF	20	80	2.07	1.012	1.127	1.117	1.101	1.098	
B100/150-30%GSF	30	70	2.07	1.012	1.195	1.121	1.154	1.136	
B100/150-40%GSF	40	60	2.07	1.012	1.272	1.124	1.202	1.172	
B100/150-50%GSF	50	50	2.07	1.012	1.359	1.128	1.332	1.253	
B160/220-0%GSF	0	100	2.07	1.030	1.030	1.030	1.035	1.047	0.869
B160/220-10%GSF	10	90	2.07	1.030	1.084	1.081	1.075	1.074	
B160/220-20%GSF	20	80	2.07	1.030	1.145	1.134	1.124	1.122	
B160/220-30%GSF	30	70	2.07	1.030	1.213	1.154	1.174	1.163	
B160/220-40%GSF	40	60	2.07	1.030	1.289	1.174	1.220	1.213	
B160/220-50%GSF	50	50	2.07	1.030	1.376	1.158	1.289	1.329	

O, R, and P representing original age, short-term (RTFOT-aged) and long-term (PAV-aged) aging respectively.

Considering the obtained results shown in Table 6.4, it is clear that:

- For the unaged derivative binders of B50/70, SG is generally prone to increase with the mounting sulphur content up to 30%. After this point, since there is no homogeneity phase between the sulphur and bitumen, SG is variable. As expected, after aging, the SG values of both short-term and long-term, generally increase. The r value for calculated and experimental SG at the O phase is 0.743, meaning that their inter-relationships are promising.
- For the extended of B70/100, SG increases with the rising sulphur content at the unaged stage. Regardless of short-term and long-term aging, SG values still increased depending on increased sulphur content, excepting R-B70/100-50%GSF. When compared with the values of the O phase, SG grades of R

and P phase did not regularly change. Some of them increased, while some of them decreased after aging. The r value for calculated and experimental SG at the O phase is 0.970, meaning that the correlation is "strong".

- For the derivative binders of B100/150, regardless of aging, SG increases with the rising sulphur content at the unaged as well as both short and long-term ages. The r value for the calculated and experimental SG at the O phase is 0.835 meaning that relationship between them is "strong".
- For the unaged extended of B160/220, SG increases with the rising sulphur content except in O-B160/220-50%GSF. Regardless of short-term and long-term aging, SG values increased depending on the increased sulphur content. However, when compared with those of the O phase, SG grades of R and P phase did not regularly change. Some of them increased, while some of them decreased after aging. The r value for calculated and experimental SG at the O phase is 0.869, which means that the correlation is "strong".

To conclude, since the r values for derivative binders of B70/100, B100/150, and B160/220 are greater than 0.8 there is a strong relationship between the experimental and calculated SG at the unaged stage, and that both methods are proper.

6.2 SUPERPAVE Test Results

6.2.1 Mass change results

Mass change in bitumen (either a decrease or increase) occurs as a result of short-term aging. The change of mass after aging is determined according to EN 12607-1 (RTFOT). This is calculated as the mass difference between unaged bitumen and RTFOT-aged residue. The final result is the absolute percentage of mass difference between the sample before and after the aging test (Błażejowski et al., 2014). Although many different parameters play a major role in the mass change after short-term aging, the key factors are a loss in mass due to the loss of volatile compounds and a gain in mass due to oxidation. In this study, several percentages of granular sulphur were replaced by bitumen and then new SEBs were exposed to short-term aging. When compared with bitumen, sulphur is more vulnerable to aging due to its chemical structure. In addition to bitumen's role, sulphur will also influence a total

mass change of SEBs. The mass changes of all SEBs after RTFOT aging are given in Figure 6.13 and 6.14 and summarized in Table 6.5.

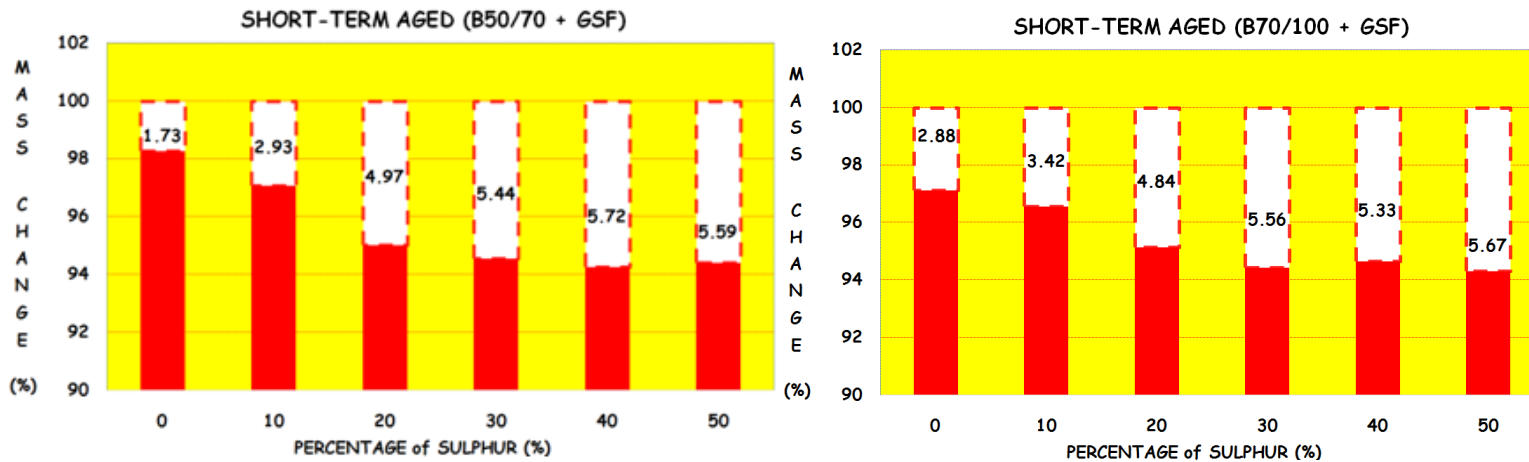


Figure 6.13 : Showing mass change of (B50/70+GSF) and (B70/100+GSF) between un-aged and short-term stage respectively.

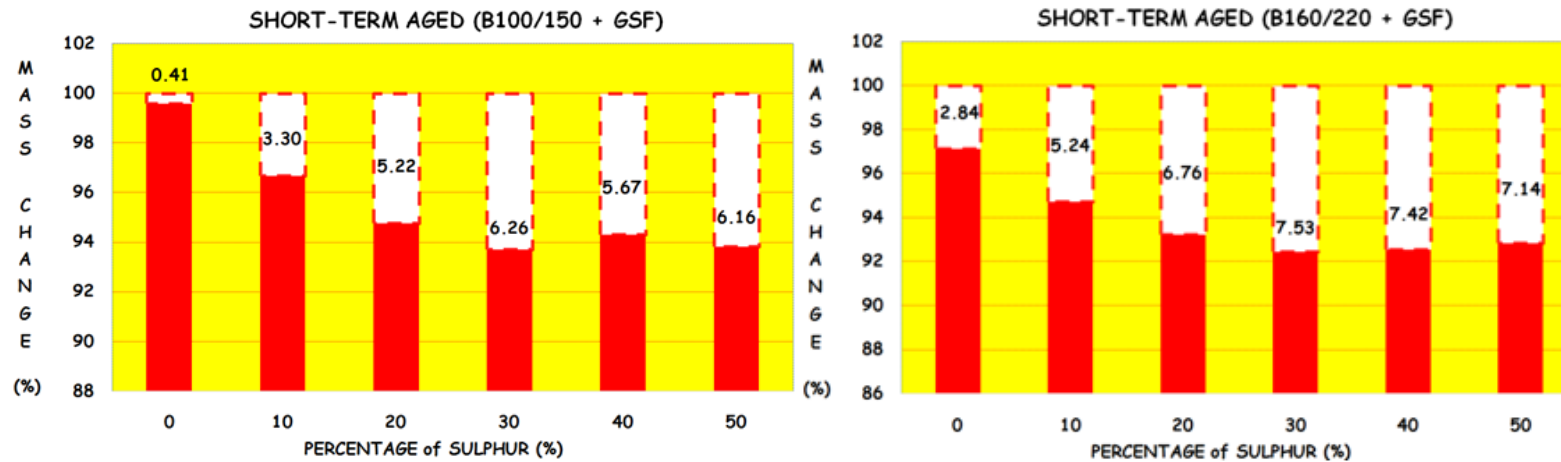


Figure 6.14 : Showing mass change of (B100/150+GSF) and (B160/220+GSF) between un-aged and short-term stage respectively.

Table 6.5 : Mass change of neat bitumens and SEBs.

Sample	Mass Change (%) O-R	Sample	Mass Change (%) O-R
B50/70-0%GSF	1.731	B100/150-0%GSF	0.414
B50/70-10%GSF	2.927	B100/150-10%GSF	3.297
B50/70-20%GSF	4.968	B100/150-20%GSF	5.222
B50/70-30%GSF	5.438	B100/150-30%GSF	6.262
B50/70-40%GSF	5.722	B100/150-40%GSF	5.670
B50/70-50%GSF	5.590	B100/150-50%GSF	6.158
B70/100-0%GSF	2.881	B160/220-0%GSF	2.844
B70/100-10%GSF	3.424	B160/220-10%GSF	5.240
B70/100-20%GSF	4.842	B160/220-20%GSF	6.759
B70/100-30%GSF	5.564	B160/220-30%GSF	7.525
B70/100-40%GSF	5.328	B160/220-40%GSF	7.420
B70/100-50%GSF	5.670	B160/220-50%GSF	7.137

O and *R* representing the original age and short-term (RTFOT-aged) aging respectively.

Since it is more apparent compared with mass gain, all net mass changes point to mass loss in this study.

When the replaced sulphur is increased, the mass loss of derivative binders of B50/70 is shown to rise. A 40% sulphur replacement is the maximum mass loss of SEB. Although B50/70 bitumen is the hardest binder among bitumens used in this study, contrary to expectations, minimum mass losses were not seen on its derivative SEBs.

Mass loss of the SEBs originating from both B70/100 and B100/150 is raised with increased sulphur amounts up to 30%. A further sulphur replacement first decreases and then increases the mass loss. For the extended of B70/100, the maximum mass loss is seen at 50% sulphur replacement. This also occurs at 30% sulphur replacement for the extended of B100/150.

Since it is already a soft bitumen and – regardless of the sulphur amount mass loss of SEBs originating from B160/220 – it exceeds those of other SEBs. Similar to the SEBs of B70/100 and B100/150, mass loss increased with an increased sulphur content up to 30%. After the mass loss peaks at 30%, a further increase in the sulphur content results in a slow increase in the value.

Under the light of observed results, it was found that the mass loss values of SEBs are much greater than those of pure bitumen and, furthermore, they are quite distant from the limits of the existing standards.

However, when the following are taken into account:

- Current standards are arranged to current binders and they do not specifically include these new SEBs.
- RTFOT is carried out at 163°C to age the current binders, and this high temperature can be sufficiently extreme to age SEBs.
- According to previous results, it was clear that replacing the bitumen with a specific sulphur amount resulted in SEBs with less hardness. Using SEBs as a binder will pave the way for "warm asphalt" production. When compared with the hot mix asphalt presently used, its laying and compaction temperatures will be reduced, as will mass loss.

The mass loss values of SEBs obtained at 163°C are promising.

6.2.2 Viscosity test results

Viscosity is a very common property when evaluating bituminous binder, given that it has to be sufficiently workable to coat chippings (Murphy et al., 2001). The viscosity value of an original binder in the range of 80 and 3000cP at 135°C is considered as a proper range for workability, including easy utilization of binder in the HMA and the hauling, spreading and compaction of the mixture (Zaniewski and Pumphrey, 2004).

In this study, in addition to being tested at 135°C, the viscosity test was conducted at two other temperatures as well: 105 and 165°C. These tests were carried out on all samples both before and after short-term aging. The Brookfield Rotational Viscometer DV III Ultra was used to measure the viscosity of all SEBs at the constant speed of spindle 20rpm and then compared with the viscosity results of base B50/70, B70/100, B100/150 and B160/220 penetration grade bitumen. The obtained results are summarized in Table 6.6 and graphically presented in Figures 6.15 to 6.18.

Table 6.6 : Viscosity values.

Temperature Sample	105 °C			135 °C			165 °C		
	O	R	ΔV (%)	O	R	ΔV (%)	O	R	ΔV(%)
B50/70-0%GSF	2675	4004	49.68	463	646	39.52	150	175	16.67
B50/70-10%GSF	1592	3613	126.95	250	558	123.20	100	167	67.00
B50/70-20%GSF	1600	2513	57.06	213	388	82.16	63	125	98.41
B50/70-30%GSF	1975	4842	145.16	263	404	53.61	63	104	65.08
B50/70-40%GSF	2067	4796	132.03	250	421	68.40	81	125	54.32
B50/70-50%GSF	1913	UR*	-	213	933	338.03	69	208	201.45
B70/100-0%GSF	1896	2892	52.53	338	475	40.53	113	146	29.20
B70/100-10%GSF	1167	2546	118.17	275	517	88.00	75	133	77.33
B70/100-20%GSF	1238	2338	88.85	175	333	90.29	88	100	13.64
B70/100-30%GSF	950	3492	267.58	169	363	114.79	63	100	58.73
B70/100-40%GSF	2458	4984	102.77	219	475	116.89	81	100	23.46
B70/100-50%GSF	1896	6413	238.24	192	613	219.27	79	146	84.81
B100/150-0%GSF	1625	2183	34.34	286	404	41.26	104	121	16.35
B100/150-10%GSF	950	1796	89.05	225	363	61.33	88	113	28.41
B100/150-20%GSF	1975	1588	-19.59	179	263	46.93	63	88	39.68
B100/150-30%GSF	1363	2167	58.99	154	263	70.78	63	75	19.05
B100/150-40%GSF	1184	2738	131.25	175	308	76.00	71	75	5.63
B100/150-50%GSF	1834	4834	163.58	150	475	216.67	67	96	43.28
B160/220-0%GSF	1617	5671	250.71	346	783	126.30	113	188	66.37
B160/220-10%GSF	1275	4279	235.61	233	638	173.82	88	163	85.23
B160/220-20%GSF	1246	2909	133.47	188	396	110.64	75	113	50.67
B160/220-30%GSF	1875	4400	134.67	146	354	142.47	63	88	39.68
B160/220-40%GSF	1367	7855	474.62	188	471	150.53	63	100	58.73
B160/220-50%GSF	1304	UR*	#VALUE!	163	783	380.37	71	163	129.58

UR: unreadable viscosity result

O and R representing original age and short-term (RTFOT-aged) aging respectively.

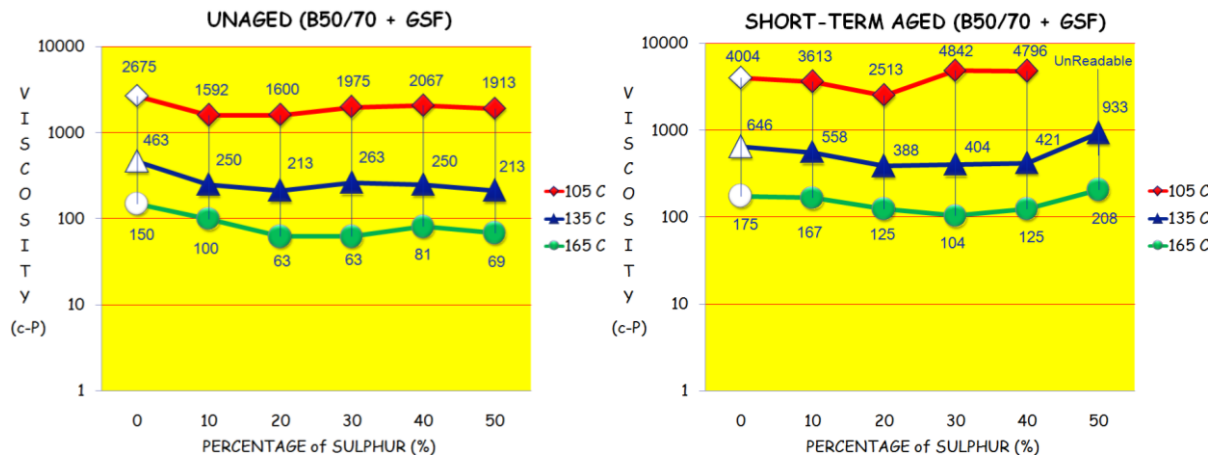


Figure 6.15 : Showing viscosity values of (B50/70+GSF) at unaged and short-term stage respectively.

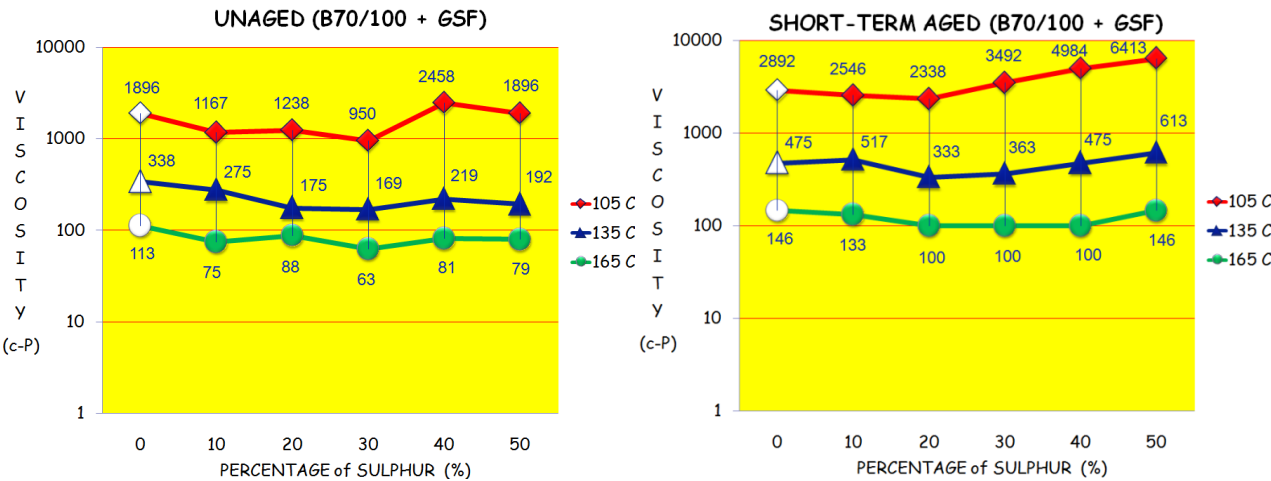


Figure 6.16 : Showing viscosity values of (B70/100+GSF) at unaged and short-term stage respectively.

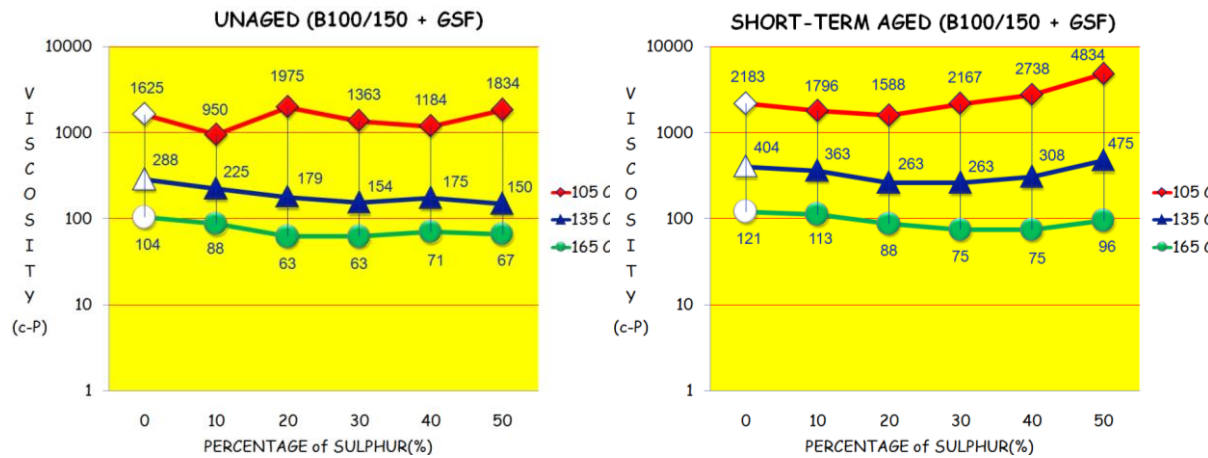


Figure 6.17 : Showing viscosity values of (B100/150+GSF) at unaged and short-term stage respectively.

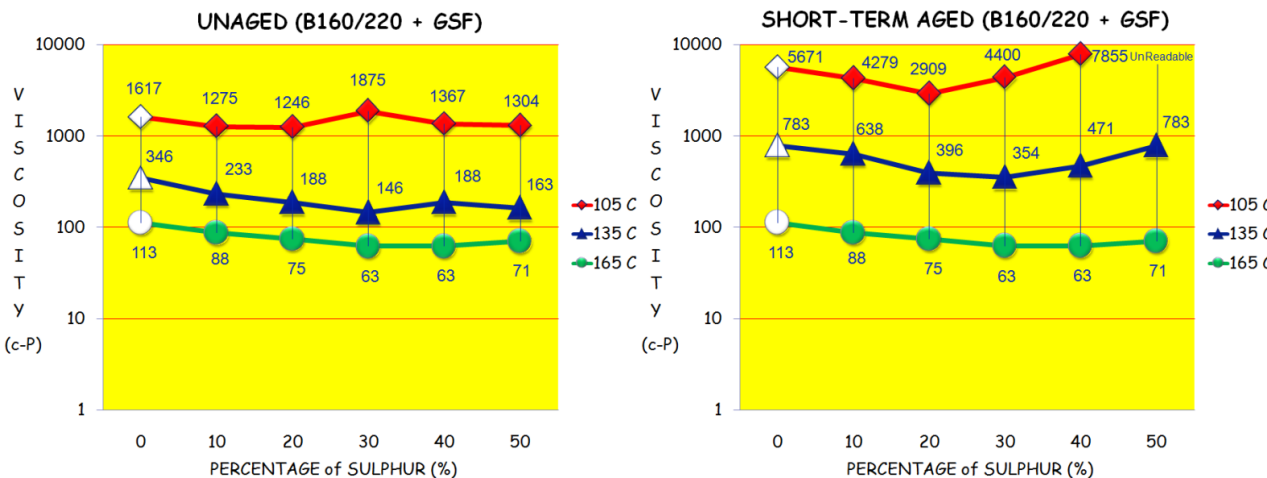


Figure 6.18 : Showing viscosity values of (B160/220+GSF) at unaged and short-term stage respectively.

Equiviscous temperature ranges were deployed to determine optimum laboratory mixing and compaction temperatures. These have been used by asphalt mix design procedures for a long time.

In 1974, the Asphalt Institute's Mix Design Methods for Asphalt Concrete and Other Hot-Mix Types (MS-2) manual suggested viscosity ranges of 170 ± 20 and 280 ± 30 centistokes for mixing and compaction temperatures respectively when carrying out a Marshall mix design. Twenty years later, though the centistoke was converted to Pascal-second ($1\text{Pascal-second} = 1000\text{centipoise}$) the ranges were not altered and, in fact, were also used for Superpave mixture design.

The aim of applying equiviscous mixing and compaction temperatures during the mix design procedure is to optimize the bituminous binder stiffness on mixture volumetric properties. As a consequence, a specific asphalt mixture of the same aggregate gradation will display volumetric properties that are very similar to those of a softer bituminous binder, such as a B160/220, as with a harder bituminous binder, such as B50/70. In this manner, based on these ranges, a hot-mix plant could achieve the same coating and compaction obtained with a softer bituminous binder in those cases when the mix temperature was increased with a stiffer bituminous binder. These equiviscous ranges used in Marshall mix design and currently in Superpave mix design were actually assigned for neat or unmodified bituminous binders, but were not specified for other specific binders such as new SEB. However, it is assumed that they will also work well with SEBs (Asphalt Institute, 2006).

We should point out that one of our aims here is that the temperatures used in the application of this procedure will not only be used for laboratory production but will also be utilized in the field. However, it must be remembered that the mixing temperature is significantly affected by such critical parameters as gradation (fine content) of the mixture, the type of plant, and the mixing time. This implies that the actual field mixing temperature for convenient coating may be 10 to 30°C lower than the laboratory temperature assigned by this method.

On the other hand, although the actual field compaction temperature is dependent on many parameters, including air temperature, base temperature, wind speed, haul distance, roller type and lift thickness, its range is very close to that of laboratory compaction (Asphalt Institute, 2006).

Owing to their viscosity reads at three different temperatures, the equiviscosity curves of all original SEBs were drawn and equation and correlation coefficients were determined. Following this, the mixing and compaction temperature ranges for each were calculated.

At the unaged stage, regardless of GSF proportion, all SEBs had lower viscosity values than base B50/70 penetration bitumen had at 105, 135, and 165°C. Parallel to other hardness test results obtained (penetration and softening point temperature test), 10%GSF replacement led to lower viscosity at each three temperatures for both unaged and short-term aged original B50/70, as did hardness. Hence, in terms of stiffness, a relatively softer binder, B50/70-10%GSF, is formed.

At 105°C none of the SEBs had viscosities similar to that of original B50/70 penetration bitumen. However, the viscosity change between the SEBs containing 10% and 20 proportion of GSF was extremely low. Furthermore, B50/70-30%GSF, B50/70-40%GSF, B50/70-50%GSF had close viscosity values: 1975, 2067, and 1913 cP respectively.

At 135°C a 10%GSF replacement led a nearly half (46.00%) reduction of the viscosity of original B50/70 bitumen. The SEBs with higher amounts of GSF replacement achieved closer viscosity grades, while the SEBs of 20% and 50%GSF had the same viscosity measurements, 213cP. Viscosities of all SEBs at 135°C fulfilled the desired range (80 to 3000cP) of SHRP requirements.

At 165°C the SEBs with GSF replacement exceeding 10% had nearly the same viscosity values varying 63-81cP and was still less than that of base B50/70, 150cP.

In order to understand how aging affects the permanent viscosity grades of derivatives of B50/70, the test was again performed on all short-term aged residues at 105, 135, and 165°C. No surprising levels of permanent viscosity loss occurred depending on bitumen and sulphur amount.

The viscosity of R-B50/70-50%GSF could not be measured at 105°C due to the fact that it already has a relatively hard ancestor bitumen (B50/70), a proportion of 50%GSF and was determined by RTFOT to being short-term aged. The value was unreadable since it exceeded the machine's maximum available viscosity grade, 12500cP. According to obtained results, at 105°C the maximum permanent viscosity loss was observed for the R-B50/70-50%GSF (?%), the minimum permanent

viscosity loss observed for the short-term aged base B50/70 bitumen residue (49.68%), and then for the R-B50/70-20%GSF residue (57.06%) respectively.

The viscosities of short-term aged SEB residues at 135 and 165°C generally tend to be higher than the base B50/70, but the trend was reversed in the case of 50%GSF replacement.

Since as a binder itself is already a relatively hard bitumen, the HMA made of B50/70 is expected to have a high temperature range for both mixing and compaction. As seen in the Table 6.7 showing the equiviscous temperatures, its mixing range varies between 157.62 to 163.55°C, and its compaction range varies 146.01 to 151.01°C respectively. It is evident that a huge amount of fuel will have to be consumed to reach this high mixing temperature range. This will, in turn, clearly produce a significant amount of hazardous gas emissions. Moreover, at these high mixing and compaction temperatures, B50/70 penetration bitumen will be exposed to excessive aging in both the hot mix plant and in the field; therefore, its initial viscosity grade and stiffness will not be protected. On the other hand, all derivative SEBs of B50/70, including even the B50/70-50%GSF, have relatively lower mixing and compaction temperature ranges as seen in Table 6.8 to 6.12. Under these circumstances, all derivative SEBs of B50/70 promise utilization for "warm-asphalt" production corresponding to their viscosity grades. This is displayed in Figures 6.20 to 6.24.

Table 6.7 : Showing the equiviscous temperatures of B50/70-0%GSF.

B50/70-0%GSF	Viscosity	Temperature
Mixing Range	150	163.55
170±20	190	157.62
Compaction Range	250	151.01
280±30	310	146.01

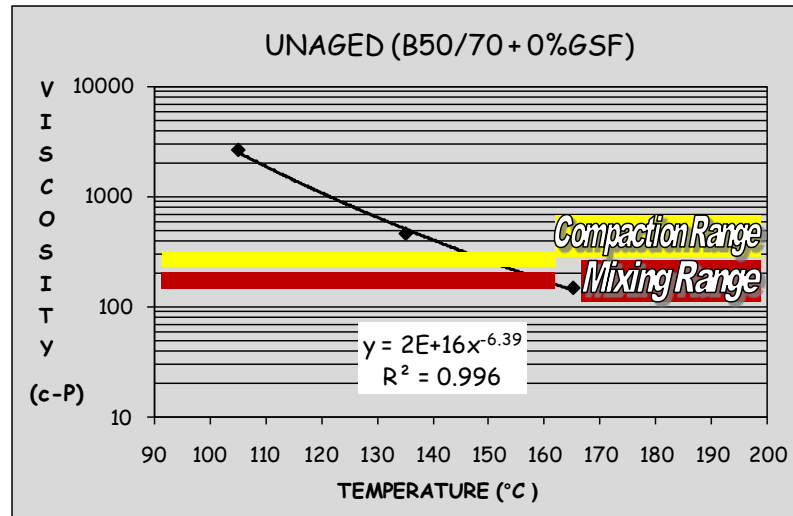


Figure 6.19 : Showing the equiviscosity curve and its equation for B50/70-0%GSF.

Table 6.8 : Showing the equiviscous temperatures of B50/70-10%GSF.

B50/70-10%GSF	Viscosity	Temperature
Mixing Range	150	151.65
170±20	190	145.95
Compaction Range	250	139.61
280±30	310	134.83

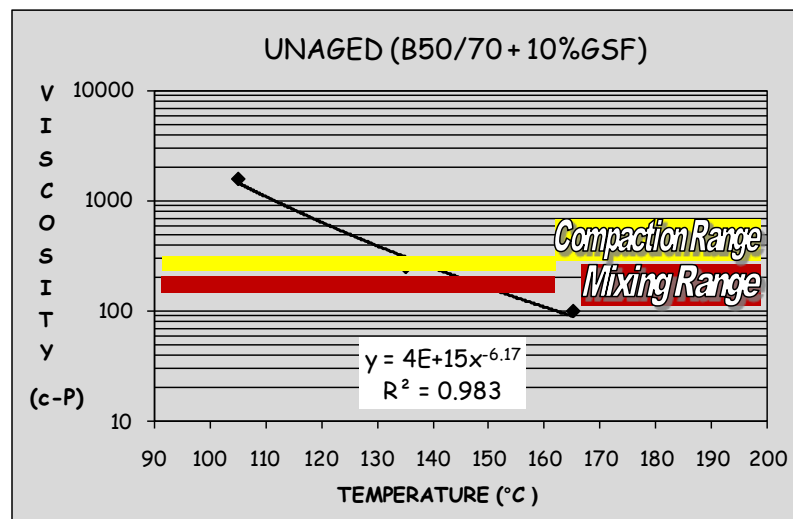


Figure 6.20 : Showing the equiviscosity curve and its equation for B50/70-10%GSF.

Table 6.9 : Showing the equiviscous temperatures of B50/70-20%GSF.

B50/70-20%GSF	Viscosity	Temperature
Mixing Range	150	144.62
170±20	190	139.94
Compaction Range	250	134.70
280±30	310	130.74

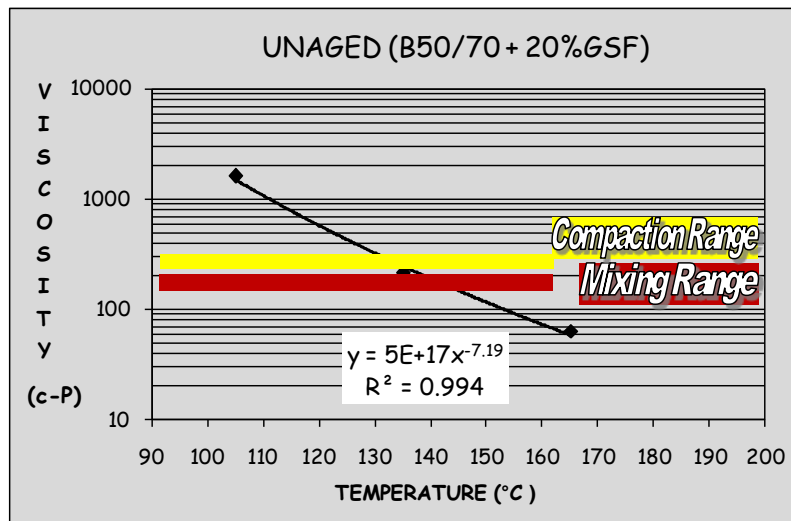


Figure 6.21 : Showing the equiviscosity curve and its equation for B50/70-20%GSF.

Table 6.10 : Showing the equiviscous temperatures of B50/70-30%GSF.

B50/70-30%GSF	Viscosity	Temperature
Mixing Range	150	146.57
170±20	190	142.10
Compaction Range	250	137.09
280±30	310	133.28

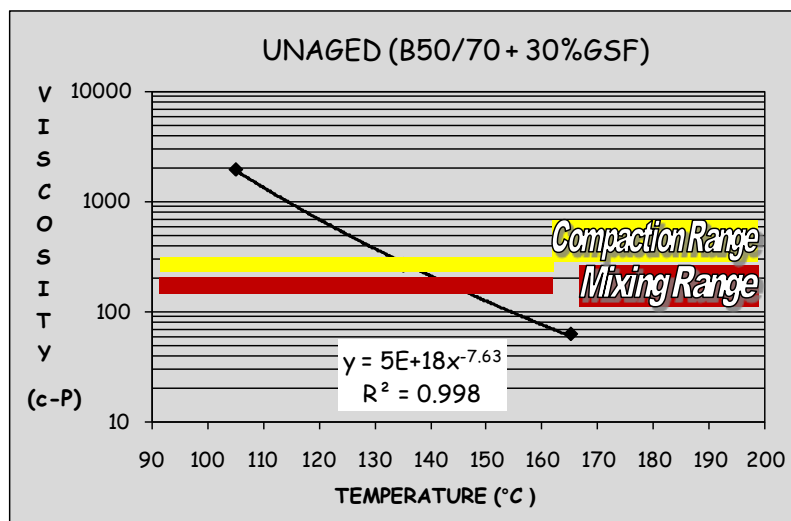


Figure 6.22 : Showing the equiviscosity curve and its equation for B50/70-30%GSF.

Table 6.11 : Showing the equiviscous temperatures of B50/70-40%GSF.

B50/70-40%GSF	Viscosity Temperature	
Mixing Range	150	149.10
170±20	190	144.30
Compaction Range	250	138.91
280±30	310	134.84

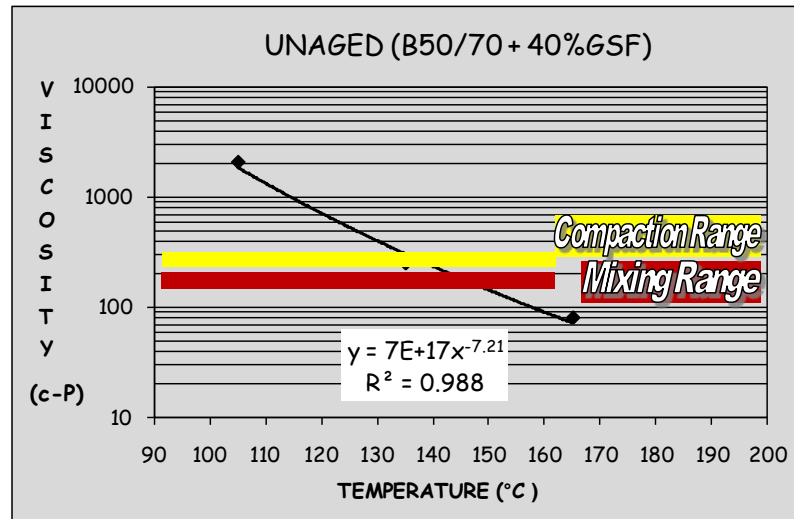


Figure 6.23 : Showing the equiviscosity curve and its equation for B50/70-40%GSF.

Table 6.12 : Showing the equiviscous temperatures of B50/70-50%GSF.

B50/70-50%GSF	Viscosity Temperature	
Mixing Range	150	146.02
170±20	190	141.43
Compaction Range	250	136.29
280±30	310	132.39

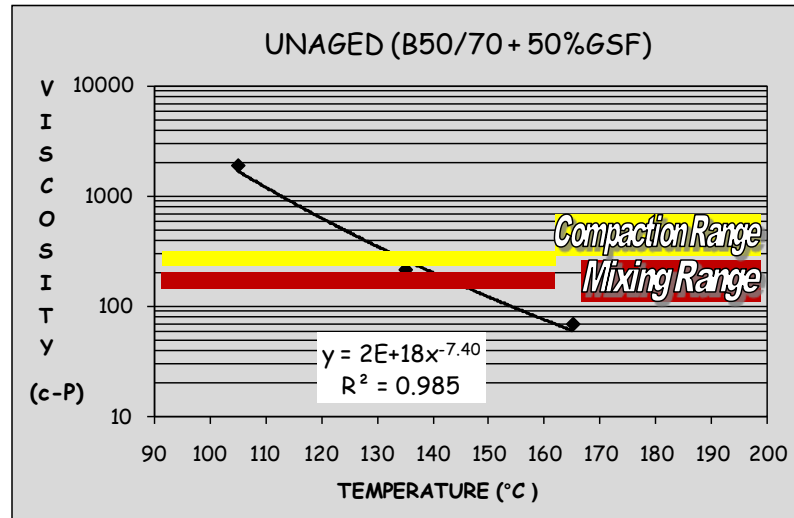


Figure 6.24 : Showing the equiviscosity curve and its equation for B50/70-50%GSF.

Rotational viscometer test was also conducted on derivatives of B70/100 penetration bitumen.

In accordance with SHRP requirements that the viscosity grade of unaged bitumen be lower than 3000cP and greater than 80cP at 135°C, all unaged extensions of B70/100 met this specification.

At 105°C, viscosity fell to 1167cP when the GSF content was 10%, indicating a decrease in stiffness. When the amount of replaced GSF increased to 20% and 30%, viscosity values of 1238 and 950cP were respectively observed. When 40%GSF replaced pure B70/100, the viscosity grade seemed to exceed the pure bitumen's initial viscosity; however, when the proportion of GSF was increased up to 50%, the viscosity value decreased and reached initial grade, 1896cP. Hence, when comparing the results with that of B70/100 penetration grade bitumen, among all GSF replacements, 50%GSF had the most similar viscosities to that of B70/100 penetration grade bitumen at 105°C.

Not surprisingly, a decrease in viscosity with increasing temperature from 105 to 135°C was apparent for all unaged extensions of B70/100. In general, each GSF replacement gave relatively lower results at 135°C. When compared to original B70/100 bitumen, the viscosity grades were found to be lower by 18.63%, 48.22%, and 50.00% for B70/100-10%GSF, B70/100-20%GSF, B70/100-30%GSF respectively, where little change is evident when the amount of GSF is increased from 20 to 30%. Additional GSF replacement first led the viscosity grade to increase to 219cP and then decrease to 192cP.

Similar to measurements at 135°C, all viscosity values of SEBs at 165°C were relatively lower than that of original bitumen; all of them were in the 63–88cP range indicating that unremarkable variation had occurred among the different SEBs.

In addition to viscosity results at the unaged stage, permanent viscosity grades of RTFOT-aged SEB residues were measured again at 105, 135 and 165°C. As expected, the permanent viscosity grades of all short-term aged residues were distinctively increased.

At 105°C the general trend for all short-term aged SEBs excepting R-B70/100-10%GSF appears to be an increase in viscosity (increasing stiffness) parallel to an increase of GSF. A replacement of 10%GSF caused the viscosity to fall to 2546cP

and for 20%GSF, the result was 2338cP. After this, the permanent viscosity values started to increase with additional increase in GSF proportion.

Although they are short-term aged via RTFOT at 163°C for 85 minutes, the permanent viscosity grade of B70/100 and of all its derivatives still met the desired ranges at 135°C (more and less than 80cP and 3000cP respectively). While it had been expected that R-B70/100-10%SF residue would have had a lower permanent viscosity grade than that of pure R-B70/100, the opposite occurred, with a greater value of 517cP demonstrated. However, no remarkable viscosity gap between R-B70/100-20%GSF and R-B70/100-30%GSF was observed, and when compared to pure R-B70/100 the values were lower, indicating less hardness. When GSF replacement increased to 40%, the permanent viscosity grade reached that of R-B70/100, 475cP. The maximum permanent viscosity loss at 135°C, 219.27%, was observed for the SEB residue including 50%GSF. Its viscosity grade seemed to exceed that of pure short-term aged B70/100, indicating it had become harder.

After the pure B70/100 penetration bitumen was short-term aged, its permanent viscosity at 165°C increased from 113 to 146cP. After aging, the viscosity of B70/100-10%GSF increased from 75 to 133cP, indicating that its permanent viscosity loss was equal to 77.33%. In terms of permanent viscosity measured at 165°C no gap was observed among B70/100-20%GSF, B70/100-30%GSF, and B70/100-40%GSF. This trio had the same grade, 100cP. The utmost permanent viscosity loss, 84.81%, was observed for the SEB including 50%GSF and its viscosity grade was equal to that of the residue of base B70/100 pen bitumen.

The aim of the replacement of varying amounts of GSF was to decrease the mixing and compaction temperature ranges. Fortunately, this aim appears to have been met, for as shown in Table 6.13 to 6.18 (originally got from Figure 6.25 to 6.30), both temperature ranges decrease, indicating lower energy consumption and hazardous gas emission when compared to base B70/100 penetration bitumen.

Table 6.13 : Showing the equiviscous temperatures of B70/100-0%GSF.

B70/100-0%GSF	Viscosity	Temperature
Mixing Range	150	156.25
170±20	190	150.47
Compaction Range	250	144.02
280±30	310	139.16

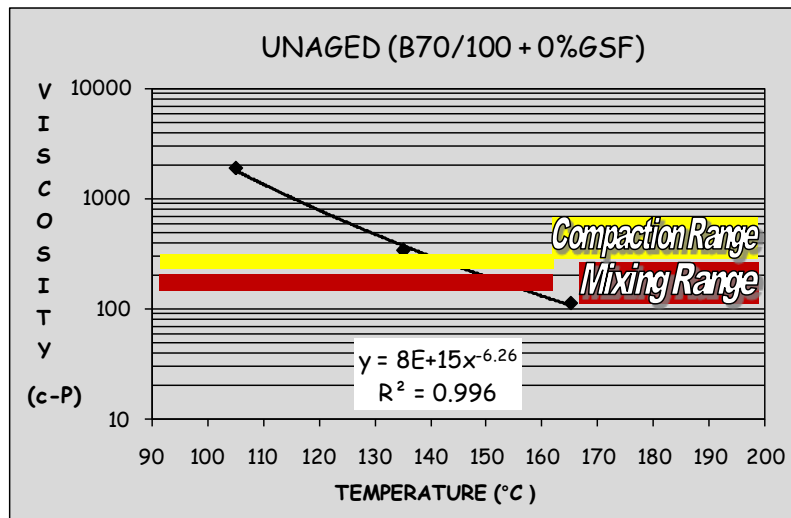


Figure 6.25 : Showing the equiviscosity curve and its equation for B70/100-0%GSF.

Table 6.14 : Showing the equiviscous temperatures of B70/100-10%GSF.

B70/100-10%GSF	Viscosity	Temperature
Mixing Range	150	149.31
170±20	190	144.14
Compaction Range	250	138.14
280±30	310	133.44

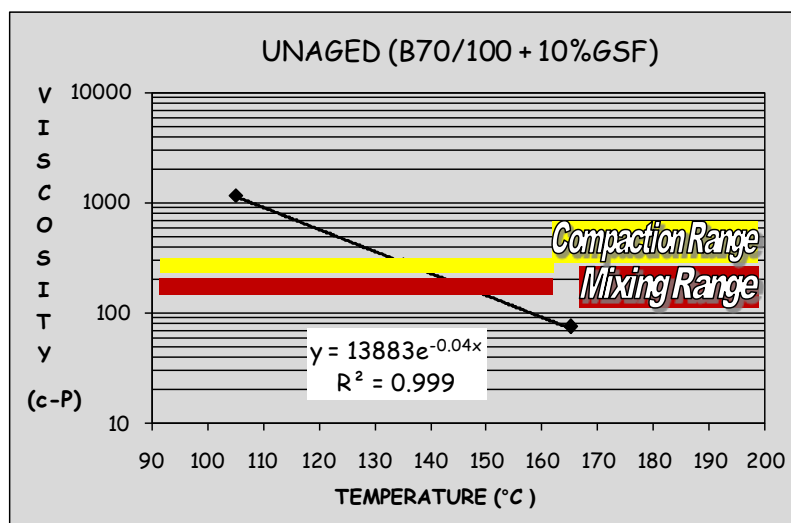


Figure 6.26 : Showing the equiviscosity curve and its equation for B70/100-10%GSF.

Table 6.15 : Showing the equiviscous temperatures of B70/100-20%GSF.

B70/100-20%GSF	Viscosity	Temperature
Mixing Range	150	146.31
170±20	190	140.59
Compaction Range	250	134.23
280±30	310	129.45

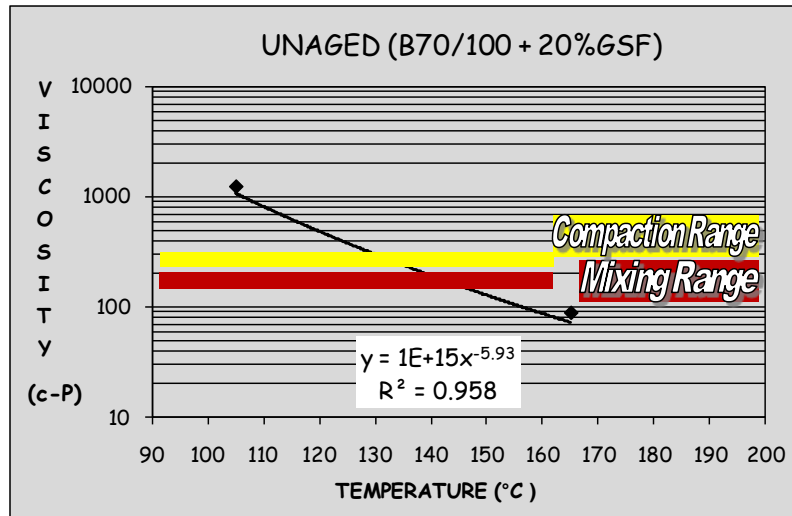


Figure 6.27 : Showing the equiviscosity curve and its equation for B70/100-20%GSF.

Table 6.16 : Showing the equiviscous temperatures of B70/100-30%GSF.

B70/100-30%GSF	Viscosity	Temperature
Mixing Range	150	141.02
170±20	190	135.61
Compaction Range	250	129.59
280±30	310	125.06

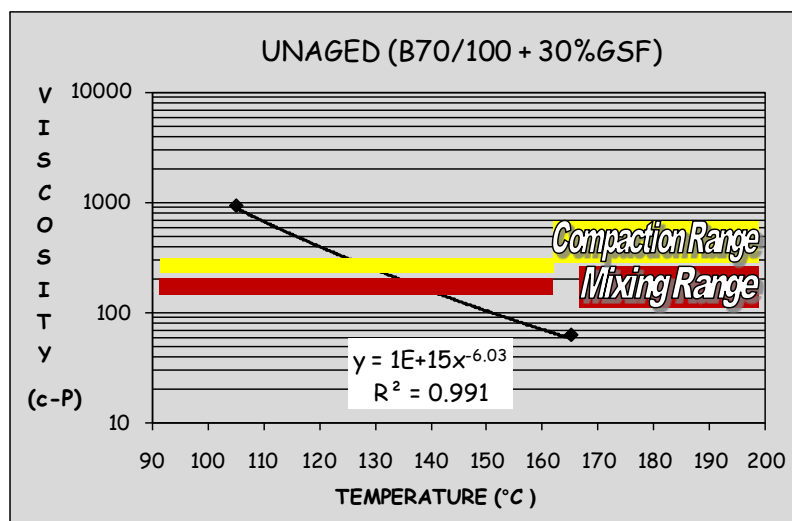


Figure 6.28 : Showing the equiviscosity curve and its equation for B70/100-30%GSF.

Table 6.17 : Showing the equiviscous temperatures of B70/100-40%GSF.

B70/100-40%GSF		Viscosity Temperature
Mixing Range	150	148.42
170±20	190	143.90
Compaction Range	250	138.82
280±30	310	134.96

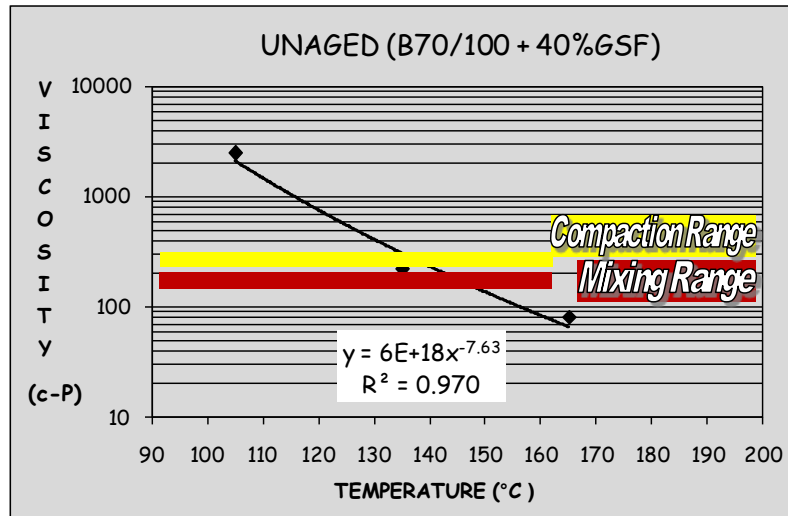


Figure 6.29 : Showing the equiviscosity curve and its equation for B70/100-40%GSF.

Table 6.18 : Showing the equiviscous temperatures of B70/100-50%GSF.

B70/100-50%GSF		Viscosity Temperature
Mixing Range	150	146.75
170±20	190	141.95
Compaction Range	250	136.58
280±30	310	132.52

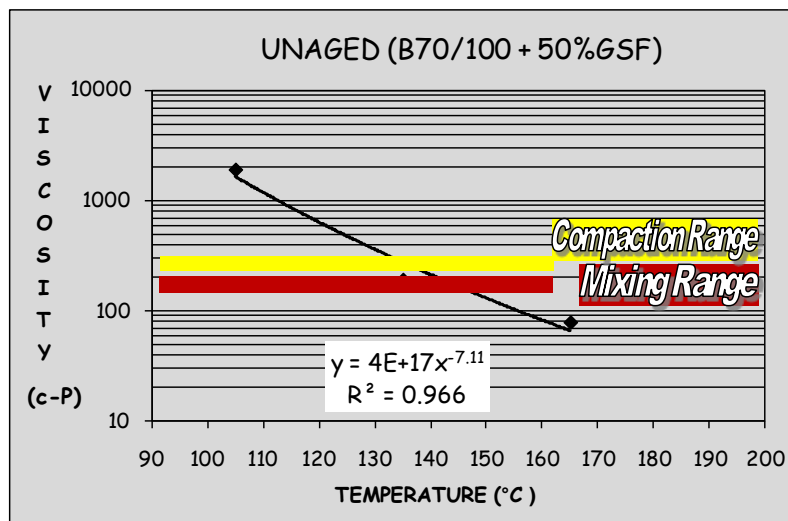


Figure 6.30 : Showing the equiviscosity curve and its equation for B70/100-50%GSF.

According to viscosity measurements obtained at 105°C, none of extended binders of B100/150 had the same viscosity measurement of the original B100/150 penetration bitumen. Some GSF proportion replacements caused higher values, while some caused lower values: B100/150-20%GSF and B100/150-50%GSF had 1975 and 1834cP respectively, which are higher than that of pure B100/150 with its grade of 1625cP. On the other hand, other SEBs including 10, 30 and 40%GSF proportions had lower viscosity grades of 950, 1363 and 1184cP respectively.

Viscosity decreased at a temperature of 135°C, and there was also a general decrease in viscosity when levels of sulphur were increased. All GSF replacements tended to soften the original B100/150 bitumen, but an increase in GSF proportion did not cause a regular change in viscosity. The viscosities of the all B100/150 and GSF combinations are lower than that of original bitumen and they all meet the SHRP's required range at 135°C. Among these SEBs, B100/150-10%GSF exhibited the highest viscosities of all five. The separate SEBs including 20 and 40%GSF achieved nearly the same results (179 and 175cP respectively), whereas B100/150-30%GSF and B100/150-50%GSF exhibited viscosity results that were similar to each other (154 and 150cP respectively).

Compared to base B100/150, at 165°C viscosity values for the SEBs remained relatively lower and nearly the same as each other, in the range 63-88cP.

After aging via RTFOT, the permanent viscosity loss was evaluated for each residue of extended binders of B100/150. The general trend first appeared to be a reduction and then an increase in permanent viscosity grade in line with an increase in the proportion of GSF.

Considering the permanent viscosity values at 105°C, the SEBs containing 10% and 20%GSF separately, whose viscosities are 1796 and 1588cP respectively, had values that were lower than conventional control B100/150 penetration bitumen. When the sulphur proportion was increased to 30%, the permanent viscosity value also started to increase, becoming almost equal to the sole use of 100-150 penetration bitumen. This value continued to increase with a further increase of sulphur content, reaching a maximum value when sulphur was 50%.

Under normal conditions, a significant amount of permanent viscosity loss was expected to occur due to aging. On the contrary, however, and interestingly enough, after short-term aging, B100/150-20%GSF did not lose any fluidity and softened instead. It is assumed that this unexpected state occurred during and immediately

after the initial blending. It is assumed that the GSF increasingly and gradually dissolved in the pure bitumen, causing a softer result of B100/150-20%GSF.

Parallel to viscosity readings obtained at 105°C, it was found that the permanent viscosity grade at 135°C decreased when 10 to 20% of the conventional binder was replaced with granular sulphur. The value did not change, however, when the sulphur content was further increased to 30% (still 263cP). A 40% sulphur replacement started to increase the permanent viscosity grade of the SEB, but the value 308cP was still lower than that of pure aged B100/150 penetration bitumen. When the amount increased to 50%, the viscosity of SEB reached 475cP, indicating that it had exceeded that of conventional B100/150 bitumen at 135°C.

Similar to results obtained at 105 and 135°C, an increasing sulphur content also first decreased and then again increased the permanent viscosity values at 165°C. However, contrary to its high readings at 105 and 135°C, R-B100/150-50%GSF did not demonstrate a permanent viscosity that exceeded that of short-term aged B100/150. Of the SEB residues tested at 165°C, the minimum permanent viscosity loss was 5.63%, a result yielded by R-B100/150-40%GSF; whereas the maximum was 43.28%, a result yielded by R-B100/150-50%GSF.

As shown in Tables 6.19 to 6.24 (originally taken from Figures 6.31 to 6.36), the replacement of varying amounts of the amount of GSF first decreased and then increased both the mixing and compaction temperature ranges. However, none of the SEB temperatures surpassed that of pure control B100/150 penetration bitumen. Therefore, both temperature ranges appeared to decrease, indicating lower energy consumption and lower hazardous gas emissions.

Table 6.19 : Showing the equiviscous temperatures of B100/150-0%GSF.

B100/150-0%GSF		Viscosity Temperature
Mixing Range	150	153.46
170±20	190	147.64
Compaction Range	250	141.16
280±30	310	136.28

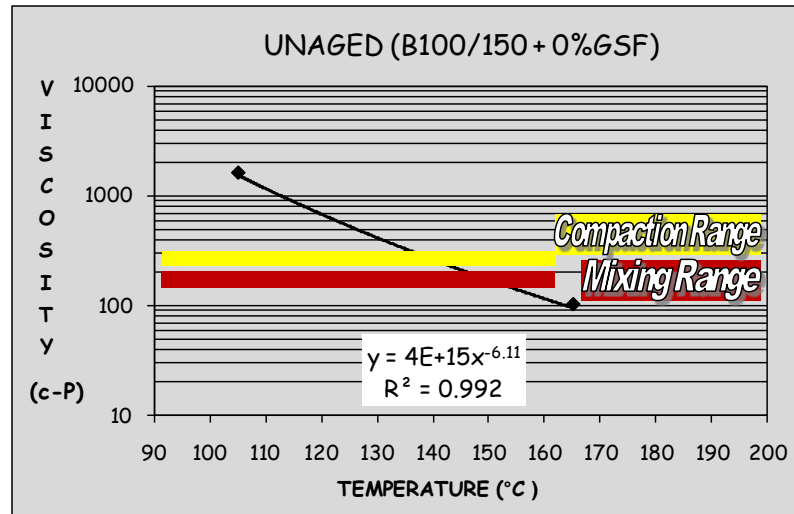


Figure 6.31 : Showing the equiviscosity curve and its equation for B100/150-0%GSF.

Table 6.20 : Showing the equiviscous temperatures of B100/150-10%GSF.

B100/150-10%GSF		Viscosity Temperature
Mixing Range	150	147.93
170±20	190	141.46
Compaction Range	250	134.30
280±30	310	128.94

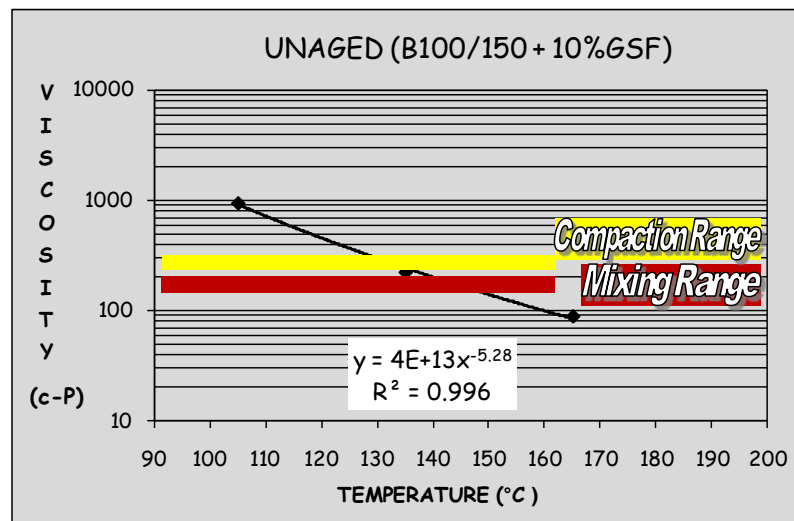


Figure 6.32 : Showing the equiviscosity curve and its equation for B100/150-10%GSF.

Table 6.21 : Showing the equiviscous temperatures of B100/150-20%GSF.

B100/150-20%GSF Viscosity Temperature		
Mixing Range	150	144.03
170±20	190	139.68
Compaction Range	250	134.79
280±30	310	131.07

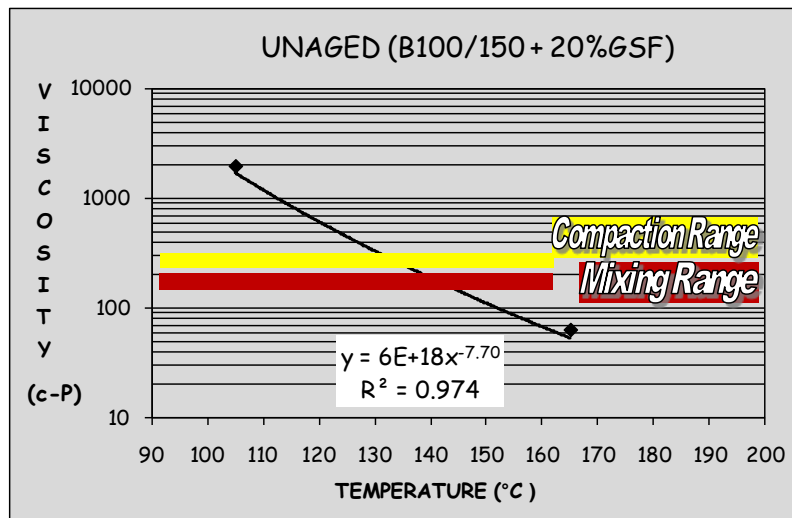


Figure 6.33 : Showing the equiviscosity curve and its equation for B100/150-20%GSF.

Table 6.22 : Showing the equiviscous temperatures of B100/150-30%GSF.

B100/150-30%GSF Viscosity Temperature		
Mixing Range	150	141.82
170±20	190	137.03
Compaction Range	250	131.67
280±30	310	127.61

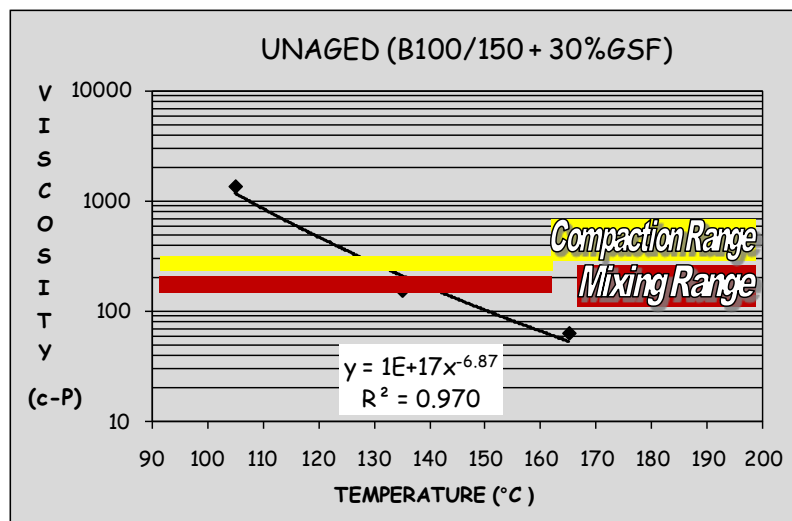


Figure 6.34 : Showing the equiviscosity curve and its equation for B100/150-30%GSF.

Table 6.23 : Showing the equiviscous temperatures of B100/150-40%GSF.

B100/150-40%GSF Viscosity Temperature		
Mixing Range	150	143.52
170±20	190	138.22
Compaction Range	250	132.31
280±30	310	127.86

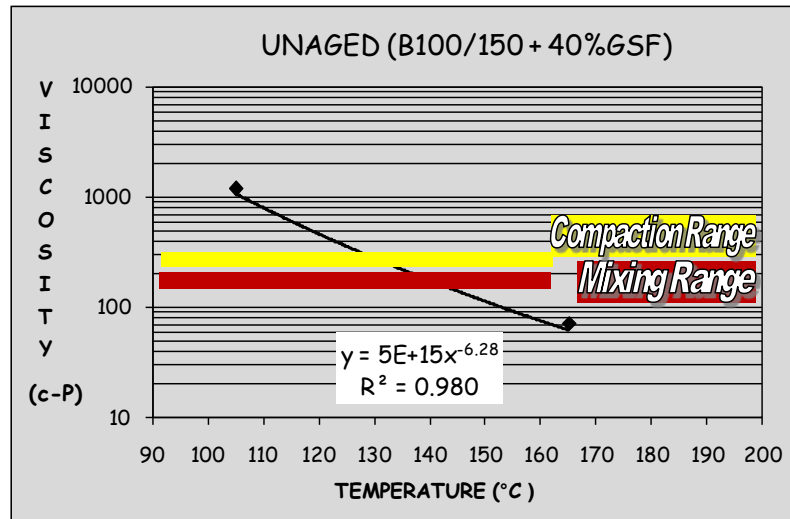


Figure 6.35 : Showing the equiviscosity curve and its equation for B100/150-40%GSF.

Table 6.24 : Showing the equiviscous temperatures of B100/150-50%GSF.

B100/150-50%GSF Viscosity Temperature		
Mixing Range	150	143.24
170±20	190	138.75
Compaction Range	250	133.72
280±30	310	129.91

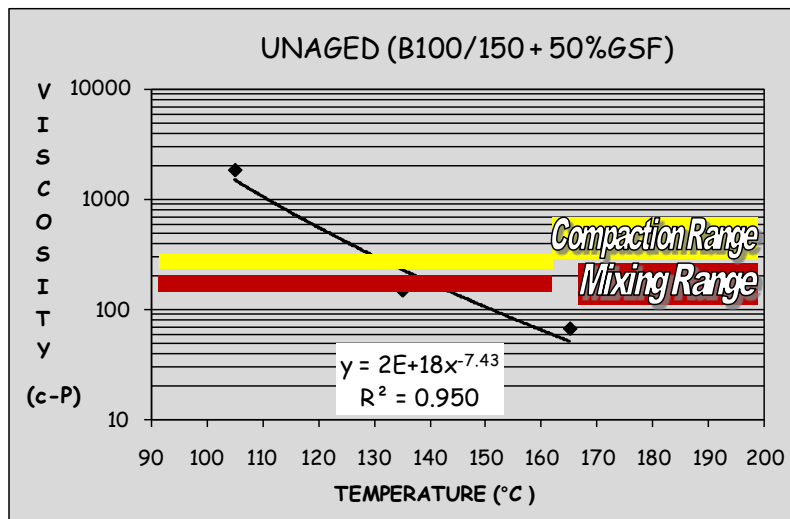


Figure 6.36 : Showing the equiviscosity curve and its equation for B100/150-50%GSF.

Rotational viscometer tests were also conducted on the SEBs where various GSF were proportionally replaced in base B160/220 penetration bitumen.

The viscosities of the unaged SEBs at 105°C generally tend to be lower than the original B160/220, but the scenario is reversed in the case of unaged B160/220-30%GSF. Its viscosity, 1875cP, is found to be 15.95% higher. Regardless of their GSF contents, the other SEBs had close and even nearly the same viscosity grades: 1275, 1246, 1367 and 1304cP for 10, 20, 40, and 50%GSF replacement respectively. At 135°C, GSF proportions did not result in a regular viscosity change in the SEBs; however, up to a 30% amount they decreased the viscosity of original B160/220. When the GSF content was either 20% or 40%, the same viscosity value of 188cP was observed. The B160/220-50%GSF had nearly half the viscosity value of pure bitumen, but it still met the desired viscosity range at 135°C. According to obtained viscosity results, all derivatives of B160/220 are very promising in respect to lower energy consumption and hazardous gas emissions.

As was expected, increasing the temperature to 165°C softened the pure B160/220 bitumen and its SEB series, indicating a decrease in stiffness as also a result in viscosity. When 10%GSF was replaced, viscosity decreased to 88cP and then fell to 75cP in the case of 20%GSF. The same viscosity values of 63cP were then observed for both B160/220-30%GSF and B160/220-40%GSF. When the amount of GSF was increased to a proportion of 50% the value increased to 71cP.

At very high temperatures such as 165°C, every SEB in each series had close viscosity measurements, regardless of the pure bitumen type and GSF proportions.

Viscosity measurements at the same three temperatures were also again performed on the derivative SEBs of B160/220 after they were RTFOT-aged. In the previous paragraphs it was stated that B160/220 penetration bitumen itself was already a soft bitumen and after it was replaced with GSF of various GSF proportions the resultant SEBs were also softer and had less stiffness. Aging undoubtedly hardens the bitumen considerably compared to its original stage. Hence, considering the other SEBs in other series, these SEBs were also expected to demonstrate minimal permanent viscosity loss. Just the opposite occurred, as very high permanent viscosity losses were demonstrated. This happened most probably due to these reasons: Since these SEBs were softer due to their GSF proportions they were more sensitive to RTFOT aging at 163°C. During the aging, the resin in the SEB, one of lower molecular weight constituents, might have been converted into asphaltene after bonding with

the oxygen molecules. The evaporation of other soft components of SEB might also have resulted in this relatively substantial loss of permanent viscosity.

As seen in Tables 6.25 to 6.30 showing the equiviscous temperatures, (as well as in Figures 6.37 to 6.42) mixing and compaction temperature ranges generally tend to decrease in the case of GSF replacement. However, it should be noted that great care must be taken to prevent such pavement disorders as rutting, bleeding, raveling and stripping, especially in warm climates , if an HMA made of these SEBs is applied.

Table 6.25 : Showing the equiviscous temperatures of B160/220-0%GSF.

B160/220-0%GSF	Viscosity Temperature
Mixing Range	150 156.65
170±20	190 150.49
Compaction Range	250 143.65
280±30	310 138.50

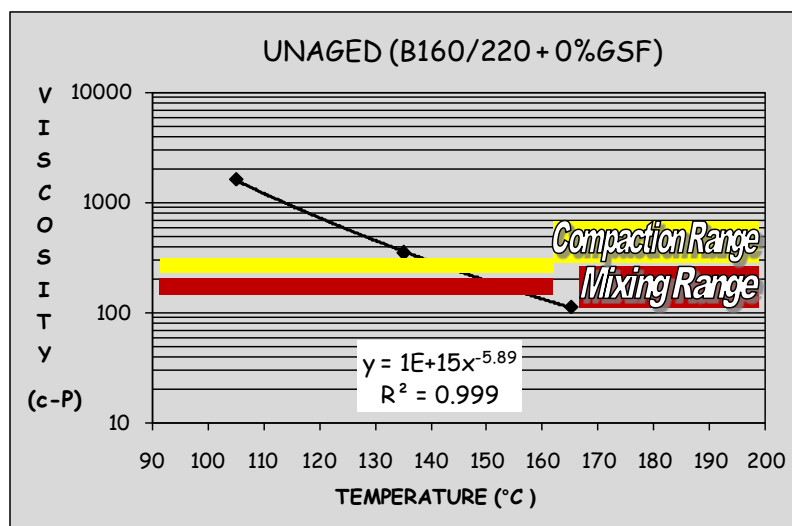


Figure 6.37 : Showing the equiviscosity curve and its equation for B160/220-0%GSF.

Table 6.26 : Showing the equiviscous temperatures of B160/220-10%GSF.

B160/220-10%GSF Viscosity Temperature		
Mixing Range	150	148.87
170±20	190	143.07
Compaction Range	250	136.62
280±30	310	131.77

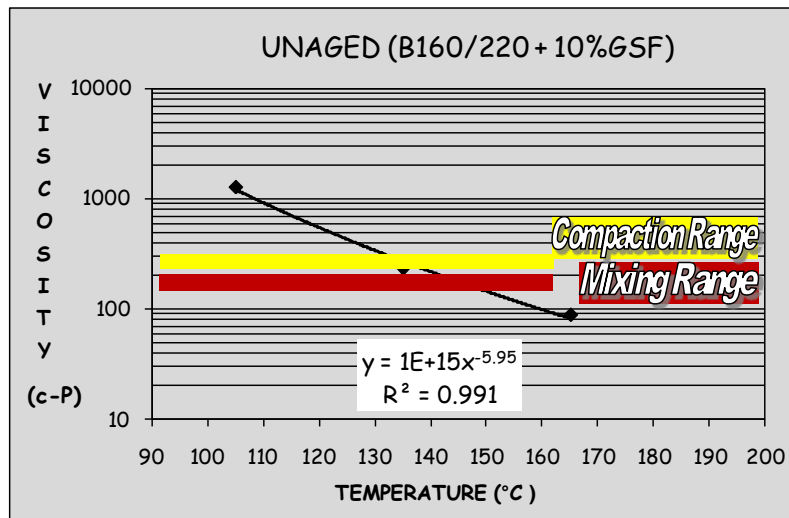


Figure 6.38 : Showing the equiviscosity curve and its equation for B160/220-10%GSF.

Table 6.27 : Showing the equiviscous temperatures of B160/220-20%GSF.

B160/220-20%GSF Viscosity Temperature		
Mixing Range	150	144.90
170±20	190	139.54
Compaction Range	250	133.56
280±30	310	129.06

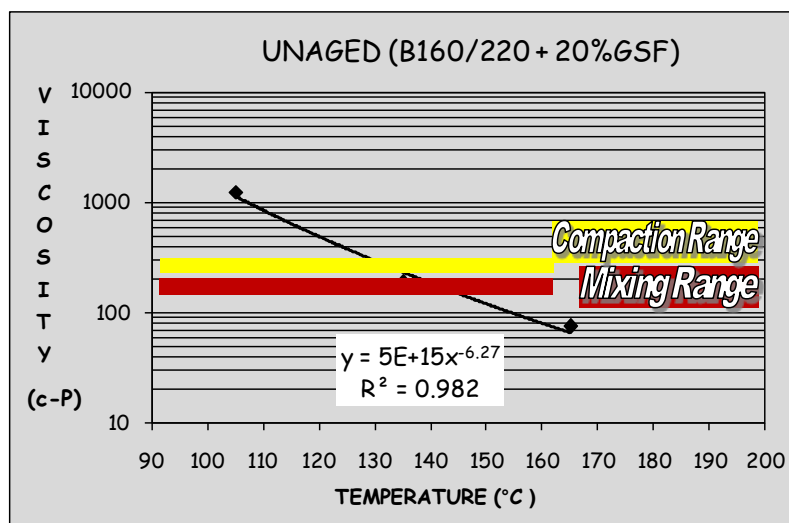


Figure 6.39 : Showing the equiviscosity curve and its equation for B160/220-20%GSF.

Table 6.28 : Showing the equiviscous temperatures of B160/220-30%GSF.

B160/220-30%GSF Viscosity Temperature		
Mixing Range	150	142.56
170±20	190	138.20
Compaction Range	250	133.31
280±30	310	129.60

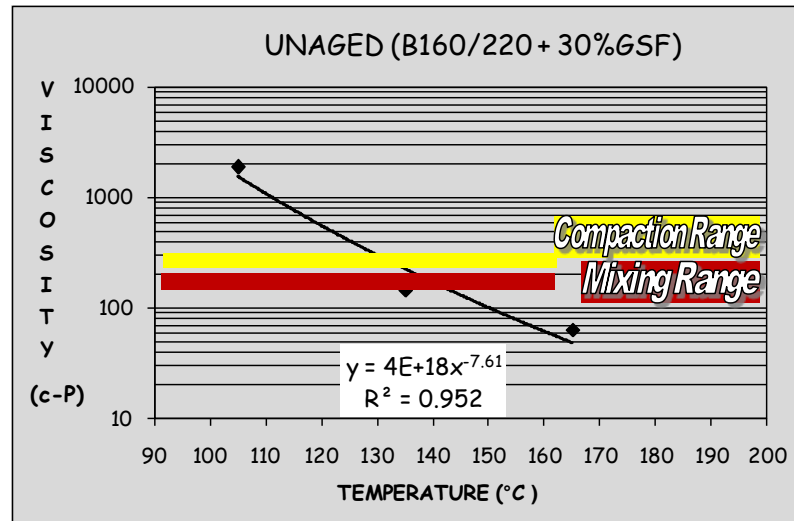


Figure 6.40 : Showing the equiviscosity curve and its equation for B160/220-30%GSF.

Table 6.29 : Showing the equiviscous temperatures of B160/220-40%GSF.

B160/220-40%GSF Viscosity Temperature		
Mixing Range	150	143.26
170±20	190	138.40
Compaction Range	250	132.97
280±30	310	128.86

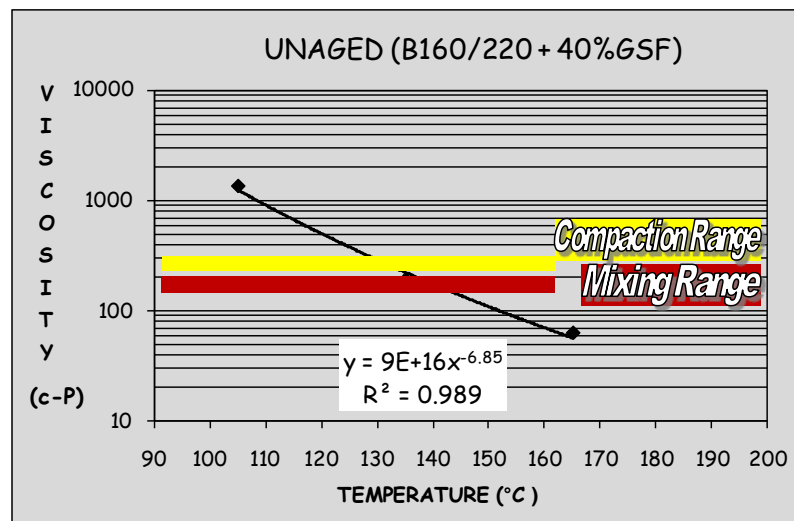


Figure 6.41 : Showing the equiviscosity curve and its equation for B160/220-40%GSF.

Table 6.30 : Showing the equiviscous temperatures of B160/220-50%GSF.

B160/220-50%GSF Viscosity Temperature		
Mixing Range	150	143.31
170±20	190	138.20
Compaction Range	250	132.50
280±30	310	128.20

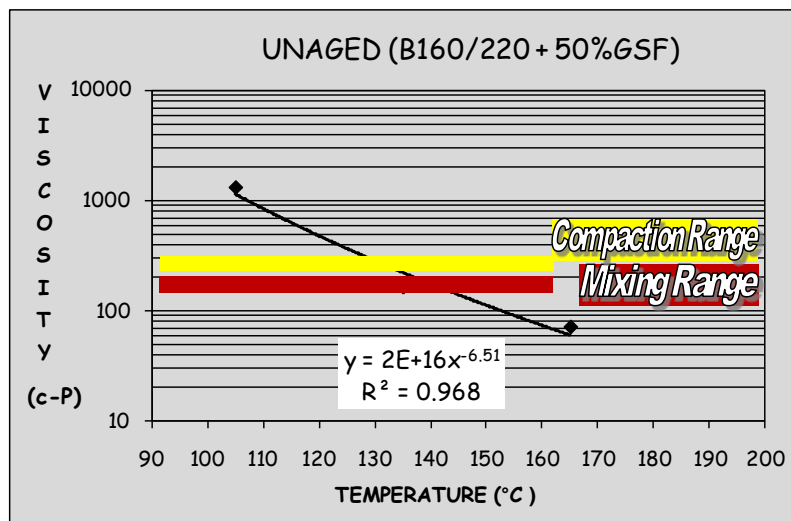


Figure 6.42 : Showing the equiviscosity curve and its equation for B160/220-50%GSF.

To conclude, a range of granular sulphur amount was tested to evaluate its potential effect on viscosity for use as an extender in place of conventional bitumen. Viscosity measurements at 105, 135 and 165°C were performed on all SEBs in distinct series before and after they aged.

In general, it was seen that viscosity reduced as temperatures were increased. Also apparent was the fact that higher levels of SEB GSF also had higher viscosity levels. Analysis of the corresponding tables and figures showed that increasing sulphur content led to an irregular viscosity change at 105°C; in other words, some fluctuations in viscosity measurements were observed and SEBs could not gain adequate fluidity and pumpability at 105°C, a relatively low temperature. On the other hand, at both 135°C and 165°C increasing GSF replacement generally caused regular change in the SEBs, and all unaged SEBs demonstrated lower viscosity values than conventional bitumen. From the data in Table 6.6, it can be seen that regardless the percentage of GSF, each unaged SEB passed the SHRP's limiting conditions at 135°C (viscosity less than 3000cP and greater than 80cP).

Both softening point temperature and penetration value are closely related with the viscosity and hardness of the binder and the obtained viscosity results confirm these hardness test results. The decreases in the viscosity and hardness are caused partially from the dissolution of the sulphur in bitumen and partially from its reaction with bitumen. Meanwhile, it is also believed that when the amount of sulphur exceeds 50%, a crystallization of a different phase occurs, thus increasing the values of viscosity and hardness. Results have also demonstrated that SEB provides workable fluidity, hardness, and pumpability properties. It is promising in its utilization as a coating of the aggregates in the preparation of hot mix, and the resultant mixture provides easy hauling, spreading and compaction. Overall, the substitution of each conventional binder with 10%GSF was the most similar to the neat bitumen in terms of fluidity at 135 and 165°C.

It is obvious that the aging effect has a major role on the viscosity of a binder. Today, most short-term aging is being carried out by RTFOT under SUPERPAVE's specifications: exposure to aging during 85-minute at 163°C. However previous studies on alternative binders revealed that RTFOT at 163°C was not useful as it resulted in significant damage to the binder's structure, especially its modifiers (Peralta et al., 2012). This state can be also valid for SEB developed from varying amount of GSF and conventional bitumen. Hence, in short-term aging, the temperature employed should not exceed 140°C as some of the compounds are very volatile. Moreover, the results obtained in this work make it clear that replacing the bitumen with a specific sulphur amount resulted in softer SEBs. Namely, using SEBs as a binder will pave the way for "warm asphalt" production, thus eliminating the need for RTFOT performance at 163°C.

Tables 6.7 to 6.30 and Figure 6.19 to 6.42 reveal that the replacement of varying amounts of GSF significantly influences mixing and compaction temperature ranges. No SEB in distinct series, regardless of their GSF percentages, had higher mixing and compaction temperature ranges than each conventional bitumen. This means that the utilization of SEB as a binder significantly reduces energy consumption and, thus, a huge amount of hazardous gas emissions. Hence, in terms of viscosity, there is a considerable potential utilization of SEBs as a binder, especially in "warm asphalt" production.

6.2.3 Dynamic shear rheometer (DSR) results

B50/70 and its derivatives

SEBs composed of B50/70 and variable amounts of GSF at 1.59Hz;

Shortly after being laid, asphalt concrete pavement begins demonstrating a high tendency to wheel path rutting. Repeated traffic loads trigger the consolidation of the pavement structure after construction, thus resulting in rutting, predominantly in right-sided traffic lanes where heavy-loaded vehicles typically travel. Rutting is a typical permanent deformation and reduces both driving comfort and safety. Although several parameters, such as the quality of compaction, mix design, aggregate angularity and texture influence the rutting potential of pavement, bituminous binder plays the leading role in this kind of deformation. Since bitumen becomes more fluid with increasing temperatures, rutting commonly occurs at high service temperatures (Bahia and Anderson, 1995b; Roberts et al., 1996; Zaniewski and Pumphrey, 2004).

To evaluate the binder's rutting performance, SHRP developed the specification property of $G^*/\sin\delta$ (where: G^* , the complex modulus, a measurement of the total resistance of a material to deformation under cyclic loading conditions and δ , the phase angle, an indicator of the relative amount of recoverable and non-recoverable deformation) (Maccarrone et al., 1995)).

In this work, this parameter, which indicates rutting resistance in the Superpave specification, has been calculated for each SEB and the values are displayed in Figure 6.43. Excepting the temperature of 40°C, 10%GSF extended SEB showed less rutting resistance value than neat 50/70 grade bitumen. Previous studies proved that following its addition to neat bitumen, a certain amount of sulphur reacted with the bitumen leading gradually to both physical and chemical variations (Kennepohl and Miller, 1978; Rennie, 1979). The resulting decrease in stiffness and decrease in viscosity for this SEB most probably stem from these ongoing reactions. Regardless of temperature, further GSF replacement did not cause the rutting resistance to exceed the value of neat bitumen, while it even decreased the stiffness of neat bitumen. This result is also in agreement with previously reported viscosity results, suggesting that the addition of GSF up to 20% results in a less stiff binder. Although the 30%GSF extension yields an increase in rutting deformation at increasing temperatures, the effect is not as marked as that seen for temperature of 25°C.

However, for each temperature, a remarkable increase in the parameter of $G^*/\sin\delta$ takes place when the amount of extended GSF is 40%, reaching a value that is clearly higher than that found for neat bitumen. This fact suggests that, rather than chemical reactions, the appreciable sulphur-bitumen bonds developed during the mixing process are such that they are capable of leading to a remarkable of rutting stiffness at every temperature. Figure 6.43 also shows that at each temperature, 50% utilization of GSF with a 50/70 penetration bitumen resulted in a binder that has almost the same kind of viscoelastic behavior as that containing no GSF (neat bitumen). Hence, the observed results demonstrate that 40%GSF extension for 50/70 penetration bitumen will be favorable in the case of heavy traffic at high temperatures.

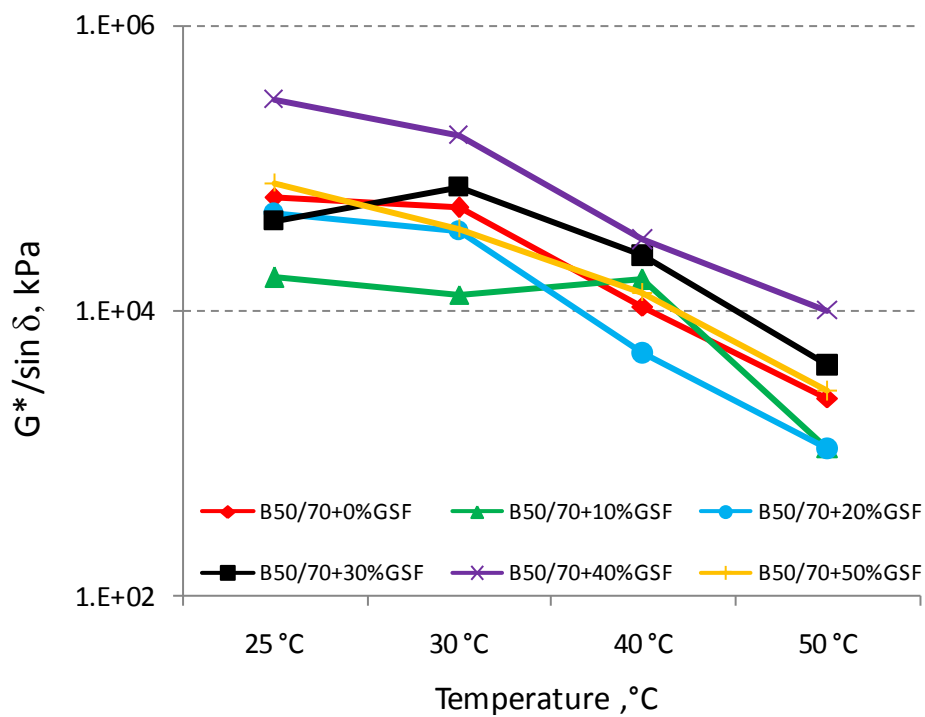


Figure 6.43 : $G^*/\sin\delta$ measured at 1.59Hz (10rad/s) as a function of temperature for B50/70 extended with various GSF amount before aging.

Deformation Resistance

The storage and loss modulus in bituminous binder is a kind of measurement of stored energy, indicating the elastic portion the energy dissipated as heat and the viscous portion respectively (Meyers and Chawla, 1999). As a viscoelastic material, bituminous binder is expected to have a large value of storage modulus (G'), especially at high temperatures, for deformation endurance due to the fact that G' represents the binder elasticity (Lu and Isacsson, 1997). However, as is commonly

understood, since it becomes brittle at low temperatures, bitumen should demonstrate low elasticity and high viscosity for energy dissipation in order for cracking to be prevented (Kumar et al., 2010). The loss modulus (G'') and storage modulus (G') of SEB samples at different temperatures are given in Figures 6.44 and 6.45 respectively.

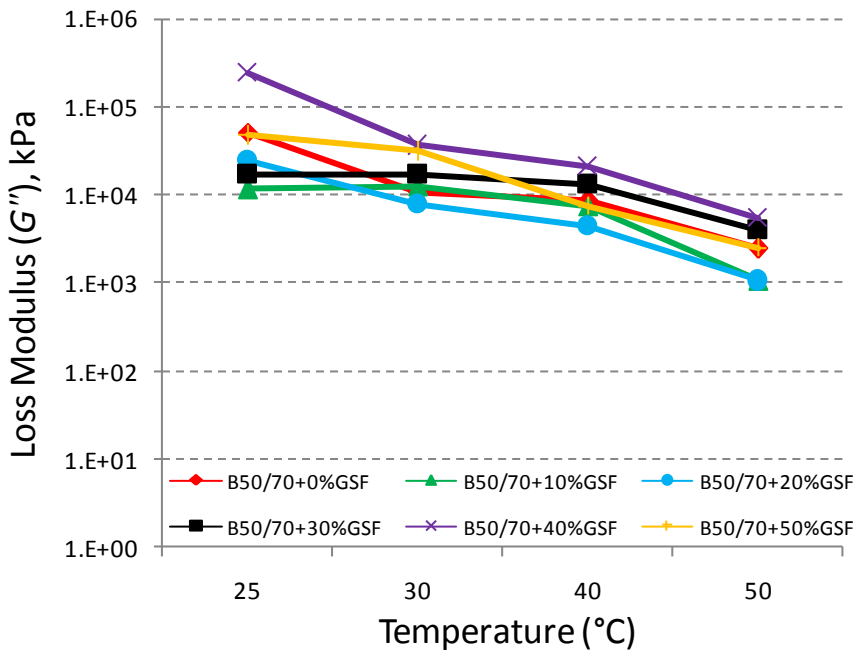


Figure 6.44 : Loss modulus measured (G'') at 1.59Hz (10rad/s) as a function of temperature for SEB samples before aging.

It is clear that as the temperature increases, the loss modulus of every SEB decreases, as shown in Figure 6.44. Consistent with the trend observed in the viscosity results, the values of G'' for extended binders with 10% and 20%GSF are lower than that of neat bitumen and this gap is more distinctive particularly in case of 20%GSF utilization. A further increase in sulphur content is seen to cause an increase in the value, and then the viscous behavior shown by SEB with 30%GSF becomes nearly similar to that of neat B50/70 grade bitumen excepting low temperature. Regardless of temperature, the loss modulus is found with most value for the SEB with 40%GSF indicating that this percentage of sulphur provides the highest viscous effect in binder. Contrary to expectations, a further increase in the amount of GSF does not further increase the rutting deformation. A decline in G'' is obvious in case of 50%GSF extension, but the value is still comparable to that of the 50/70 penetration bitumen.

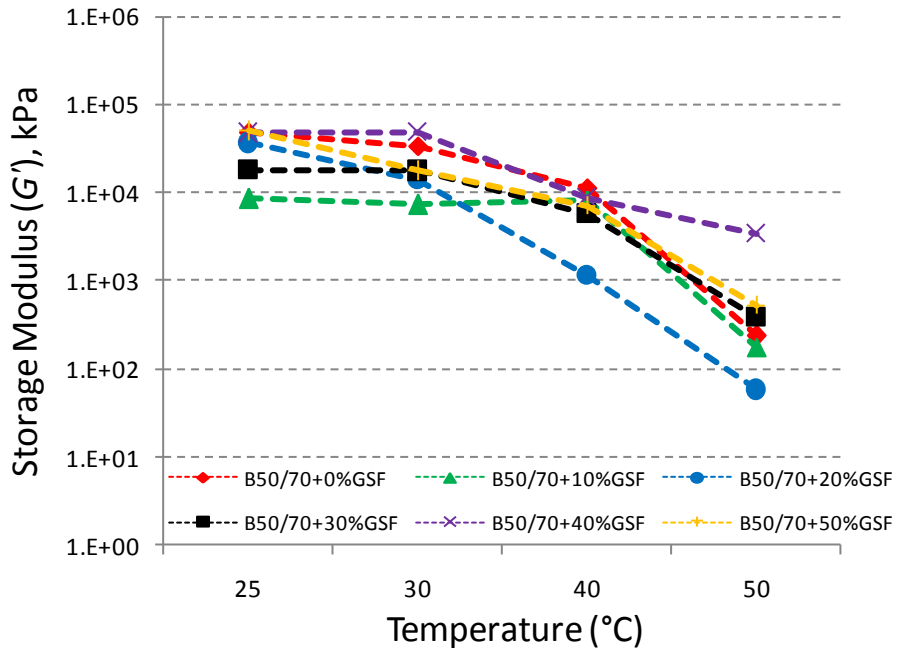


Figure 6.45 : Storage modulus measured (G') at 1.59Hz (10rad/s) as a function of temperature for SEB samples before aging.

Under the same experimental conditions, the line of the linear evolution of storage modulus is significantly higher at every temperature for neat bitumen than it is for 10% and 20%GSF extended bitumen, as can be seen in Figure 6.45. For the B50/70 bitumen extended with 10%GSF, temperatures up to 40°C do not affect the value and the slope is nearly equal to 0. It is only the 40%GSF extension that leads to an increase in G' in the 1.59Hz frequency in relation to neat bitumen. This fact underlines the fact that the higher increase in storage modulus (which provides information on the elastic response of binder) shown by the 40%GSF extended bitumen may not yield a better performance of the binder, especially at low temperatures. Therefore, these laboratory based tests demonstrate that a SEB with 10 and 20%GSF will be more durable in terms of low temperature cracking. However, it should be noted that the results in the field may have a slight variation.

Aging Effect

It is clear that aging seriously affects the behavior of bitumen, changing it almost totally from its original state. Bitumen aging is most often evaluated by calculating an aging indicator that measures the ratio of one parameter of the aged bitumen to that of the original bitumen. According to a simple general approach, it may be assumed that a higher aging indicator also indicates a higher degree of bitumen hardening (Lu and Isacsson, 1998). Many indicators, including rheological,

mechanical or chemical indicators, can also be used to evaluate the influence of aging on bitumen hardening. Rheological aging indicators include retained penetration, a change in softening point temperature, mass change, viscosity ratio, rheological index and tensile/creep strength. In this study, rheological index values were measured to reveal the effect of aging on the SEB samples.

Here, an evaluation of the rheological index obtained from the ratio of the complex modulus (G^*) of aged (via RTFOT and PAV) binder to the complex modulus of unaged binder was conducted. The values of rheological index at 1.59Hz frequency and four different temperatures for the neat B50/70 grade bitumen and SEBs are listed in Tables 6.31 and 6.32. Table 6.31 shows the rheological index by presenting the correlation between unaged and short-term aged samples, whereas Table 6.32 shows the rheological index by presenting the correlation between unaged and long-term aged samples.

Table 6.31 : Aging indices for short-term aged SEBs at different temperatures and 1.59Hz.

Short-term aging indices (G^*/G^*_o) at temperature				
Sample	25 °C	30 °C	40 °C	50 °C
50/70 Bitumen	0.44	1.19	1.72	2.61
50/70+10%GSF	2.07	1.85	1.09	3.41
50/70+20%GSF	9.12	4.51	2.57	4.87
50/70+30%GSF	0.57	0.72	0.80	1.98
50/70+40%GSF	2.01	6.96	1.91	1.65
50/70+50%GSF	5.54	3.62	2.02	3.93

As can be deduced from Table 6.31, the aging index is greater than 1 at each temperature (25-50°C) and 1.59Hz for the all extended binders, excepting the one containing 30%GSF, which points out hardening of these SEBs during short-term aging (via RTFOT). This increase in the rheological index is due to oxidation, that is, transformation of light particles such as aromatics into resins and these into asphaltens, which develops a considerable bitumen hardening (Lepe et al., 2003). In addition to this oxidation phenomenon, ongoing bonds between sulphur particles and bitumen compounds during the aging processed are believed to contribute substantially to SEB hardening. However, for neat 50/70 grade bitumen this value is

lower than 1 at low temperature (25°C), and for the 30%GSF SEB it is lower at both low and moderate temperatures ($25\text{-}40^{\circ}\text{C}$).

Table 6.32 : Aging indices for long-term aged SEBs at different temperatures and 1.59Hz .

Long-term aging indices ($G^*_{\text{p}}/G^*_{\text{o}}$) at temperature				
Sample	25°C	30°C	40°C	50°C
50/70 Bitumen	0.72	2.17	1.58	5.98
50/70+10%GSF	3.22	1.59	1.30	14.98
50/70+20%GSF	0.85	1.27	3.39	11.17
50/70+30%GSF	2.00	3.08	0.91	3.71
50/70+40%GSF	1.08	5.35	2.09	2.73
50/70+50%GSF	1.10	1.85	5.54	12.34

According to Table 6.32, as the temperature increased to 50°C , the sharply rising rheological index reveals that the influence of long-term aging has become more distinctive and dominant.

As per the values of both rheological indexes, the obtained test results reveal that the aging index indicator for extended binders is almost always higher than 1, and only rarely lower than 1. This variation is dependent on several parameters: the neat bitumen type, the amount of sulphur, temperature, and frequency, and highly dependent on the aging process.

Figures 6.46-6.48 demonstrate the variation in complex modulus in temperatures ranging from 25 to 50°C and at the frequency of 1.59Hz before aging and after both short and long-term aging. Regardless of aging phenomenon and sample type, the complex modulus appears to decrease as the temperature increases. This differentiation is more pronounced at the point at which the temperature is converging to 50°C . Figure 6.46 shows that prior to aging, the 40%GSF extended bitumen has the highest complex modulus compared with other SEBs and also neat bitumen in terms of increasing the temperature.

After short-term aging, the G^* values of SEBs with 10% and 30%GSF appeared to be less sensitive to any changes in temperature when compared to the other SEBs. Figure 6.47 also illustrates that the viscoelastic responses of these two samples are

comparable both with each other and also with neat bitumen, even though these binders were extended with different levels of GSF.

According to Figure 6.48, as expected, long-term aging ensures a further increase in complex modulus over changes in temperature range due to a relatively large stiffening by PAV. The promising improvement in the complex modulus of the PAV residual binder is most probably consistent with two scenarios: the further loss of the lighter compounds of the bitumen and the further dissolution and dispersion of sulphur particles in bitumen phase through pressure aging (Huang, 2008).

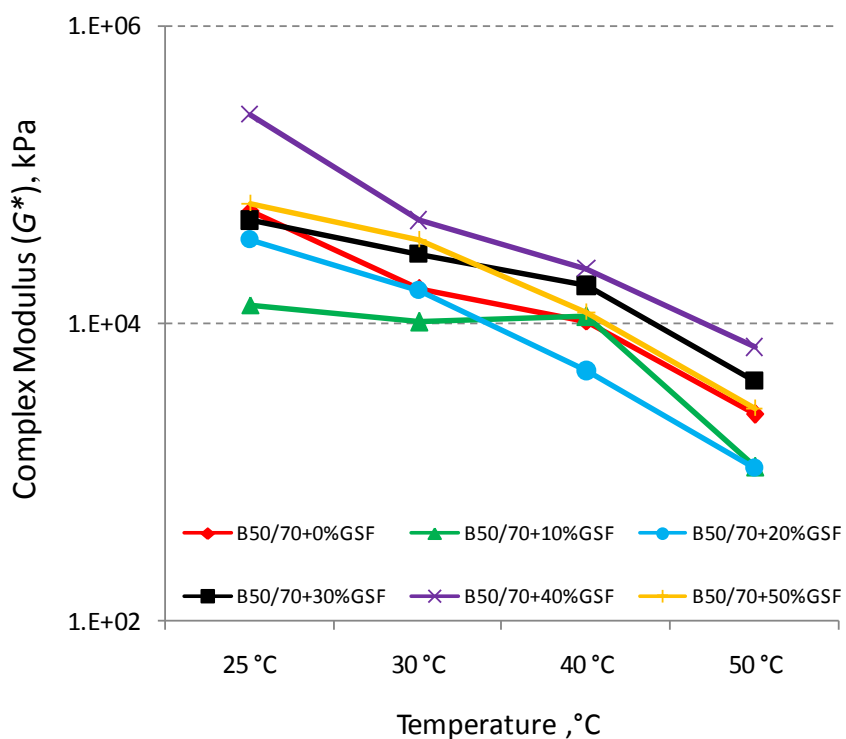


Figure 6.46 : Complex modulus (G^*) at 1.59Hz (10rad/s) as a function of temperature for B50/70 bitumen and its extensive binders before aging.

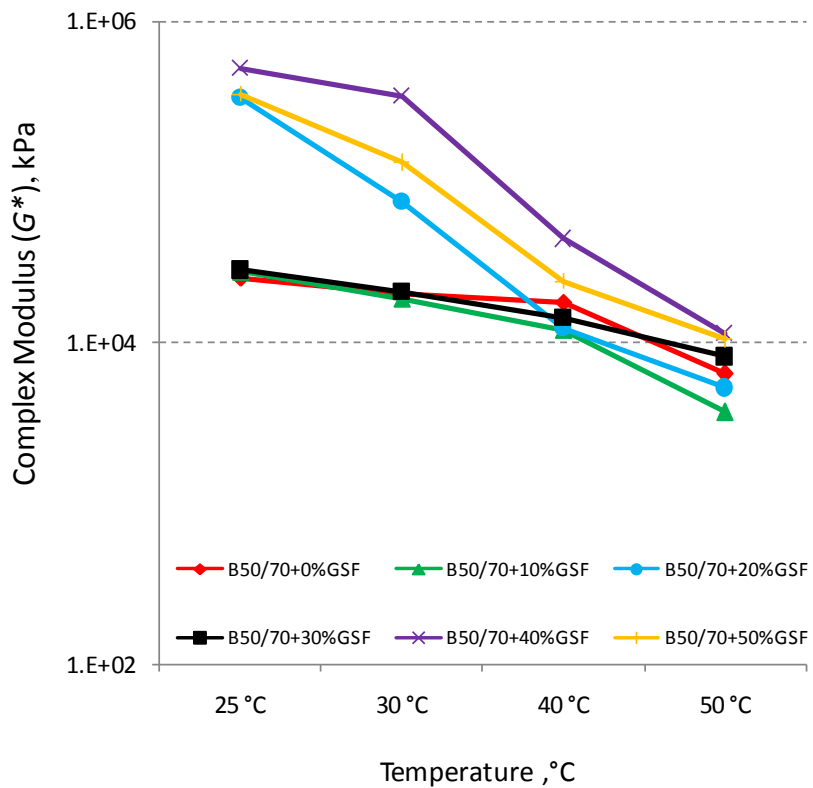


Figure 6.47 : Complex modulus (G^*) at 1.59Hz (10rad/s) as a function of temperature for B50/70 bitumen and its extensive binders after short-term aging.

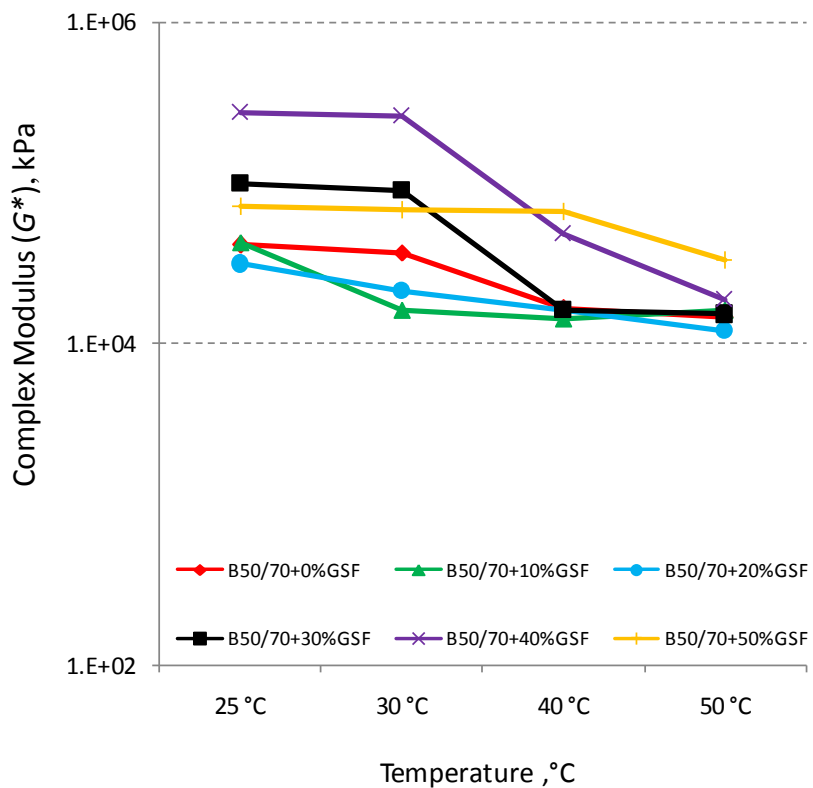


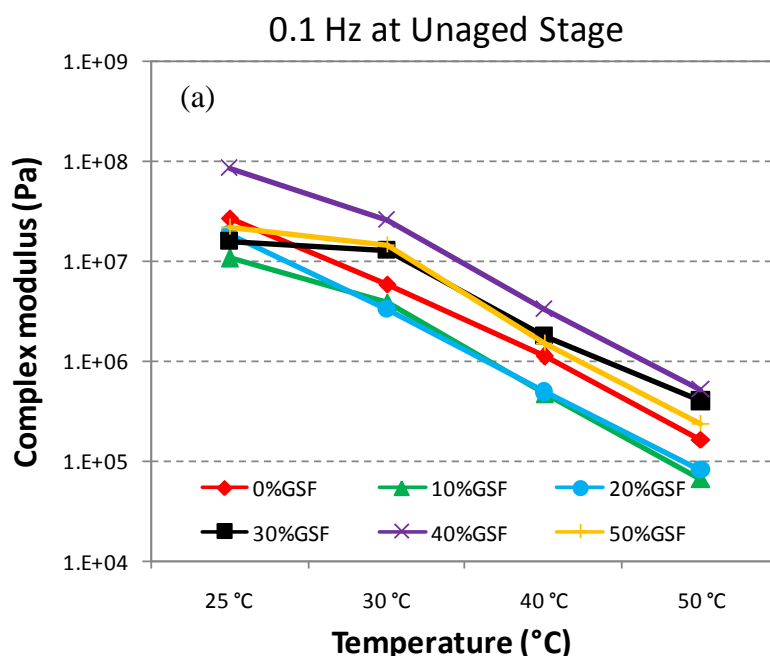
Figure 6.48 : Complex modulus (G^*) at 1.59Hz (10rad/s) as a function of temperature for B50/70 bitumen and its extensive binders after long-term aging.

SEBs composed of B50/70 and variable amounts of GSF at 0.1Hz;

Rheological parameter values at 0.1Hz for the unaged 50/70 penetration bitumen and SEBs are presented in Table 6.33. In addition, the isochronal plots of complex modulus (G^*) and phase angle (δ) versus temperature at 0.1Hz for both are shown in Figure 6.49 (a) and (b) respectively. The obtained results indicate that extended-binders with low sulphur level (10 and 20%) show a decrease in the complex modulus compared to the origin bituminous binder regardless of test temperatures. In case of 10% sulphur extension, the decrease in G^* is relatively large, particularly at 25, 40 and 50°C. High level sulphur extension (40%) greatly increases the elasticity of base 50/70 penetration grade bitumen at each test temperature, as measurements indicate a considerable increase in complex modulus (Table 6.33).

Table 6.33 : Values of rheological parameters for the B50/70 base bitumen and SEB groups at 0.1Hz before aging.

GSF	Stage	Complex Modulus at 0.1 Hz (Pa)				Phase Angel at 0.1 Hz (degree)			
		25 °C	30 °C	40 °C	50 °C	25 °C	30 °C	40 °C	50 °C
0%	o	2.72E+07	5.85E+06	1.11E+06	1.61E+05	73.54	80.28	86.62	88.08
10%	o	1.06E+07	3.85E+06	4.64E+05	6.66E+04	76.14	76.41	86.09	87.69
20%	o	1.81E+07	3.32E+06	4.88E+05	8.15E+04	71.33	77.30	82.16	81.75
30%	o	1.58E+07	1.29E+07	1.80E+06	3.95E+05	49.02	64.82	78.59	81.04
40%	o	8.57E+07	2.59E+07	3.26E+06	5.20E+05	46.10	59.39	80.26	83.12
50%	o	2.18E+07	1.45E+07	1.49E+06	2.37E+05	52.45	73.44	81.91	86.95



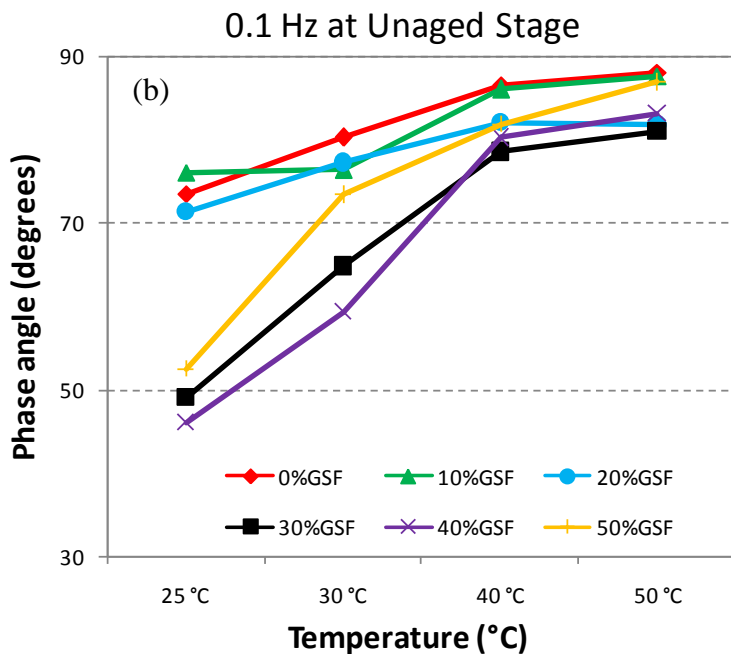


Figure 6.49 : Isochronal plots at 0.1Hz for SEB made of B50/70 bitumen before aging. (a) Complex modulus and (b) Phase angle.

This observation acts as supporting evidence for the conjecture that a more extended network is developed when this base bitumen is extended with 40%GSF. This same magnitude has not been observed at either 30 or 50%GSF level. This is an indication that 40% sulphur extension is an optimum content and yields a desirable viscoelastic behavior at low loading frequency (0.1Hz). As can be observed in Figure 6.49 (a), the slope of the G^* curve of each SEB is nearly identical to that of the neat bitumen, indicating that temperature sensitiveness of G^* at 0.1Hz for unaged binders is independent of sulphur extension.

Both Figure 6.49 (b) and Table 6.33 illustrate the changes of phase angle δ as the function of temperature, which also indicates that the addition of 10% sulphur to 50/70 penetration bitumen first increases the phase angle at the low temperature region, and then slightly decreases the phase angle with increasing test temperature. The considerable decrease in phase angle evidently starts even at 20% sulphur, which is not consistent with complex modulus values. For this above-mentioned SEB (B50/70-20%GSF), the complex modulus values appear relatively lower than those of original neat bitumen. Therefore, it is worth noting that it is the chemical composition of the binder, rather than G^* values, that has a greater impact on the phase angle. Further increases in amounts of sulphur lead to improved elastic behavior when the decrease in phase angle is considered. This phenomenon,

consistent with the G^* values, is clearly more pronounced, particularly in the case of 40%GSF utilization.

The extension indices of G^* ($G^*_{SEB}/G^*_{B50/70}$) indicating relative changes in complex modulus for all five SEBs have been recorded at each temperature and 0.1Hz in Table 6.34.

Table 6.34 : Relative changes in complex modulus for the B50/70 base bitumen and SEB groups at 0.1Hz before aging.

Binder	Stage	Extension Indices ($G^*_{SEB}/G^*_{B50/70}$) at 0.1Hz			
		25 °C	30 °C	40 °C	50 °C
B50/70	o	1.00	1.00	1.00	1.00
B50/70-10%GSF	o	0.39	0.66	0.42	0.41
B50/70-20%GSF	o	0.67	0.57	0.44	0.51
B50/70-30%GSF	o	0.58	2.21	1.62	2.45
B50/70-40%GSF	o	3.16	4.43	2.95	3.22
B50/70-50%GSF	o	0.80	2.47	1.35	1.47

The influences of sulphur-extension on the increase of G^* follows the extension indices factors of 3.16, 4.43, 2.95, and 3.22 for SEB with 40%GSF, at 25, 30, 40, and 50°C respectively; whereas the effects of the extension of sulphur results in variation of G^* by decreased extension indices factor of 0.39, 0.66, 0.42, and 0.41 for SEB with 10%GSF at 25, 30, 40, and 50°C respectively.

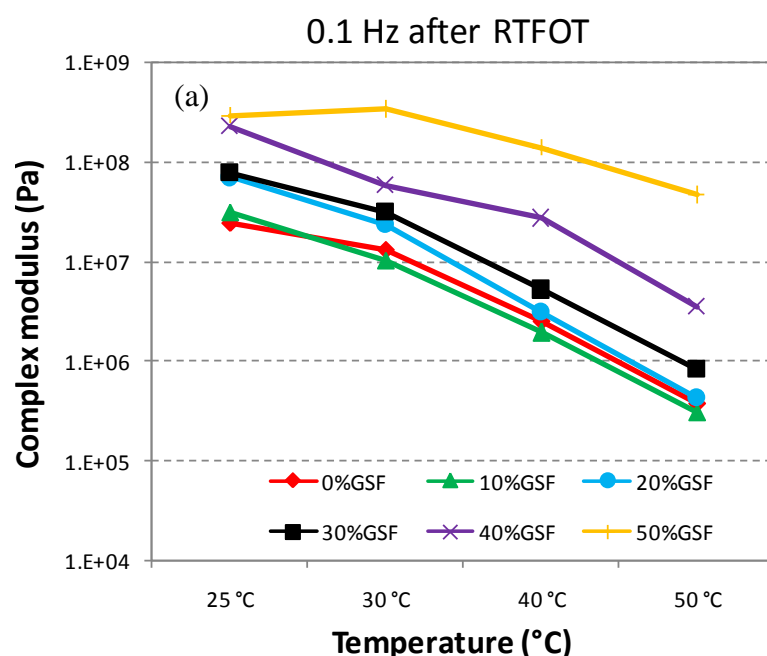
These lead us to unhesitatingly hypothesize that the sulphur-extended-binder can be treated as a type of two-phase composite material with granular sulphur particles dispersed, dissolved, and crystallized in bitumen matrix, which is similar to particulate-filled composite materials (Wu et al., 2007). Moreover, several chemical interactions are expected to occur between bitumen compounds and sulphur particles. Consequently, at high level of GSF, an increase in the complex modulus of SEBs can be expected based on the rule-of-mixture's methods. Owing to its varying levels in bitumen, the ratio of dispersed, dissolved, crystallized, and reacted amount of sulphur differs each time and as a result, the G^* values of each SEB are expected to also differ in magnitude, as does the base bitumen. This has been demonstrated by the experimental data obtained. To sum up, in combination with reducing δ and increasing G^* , it is clear that the inclusion of granular sulphur at high levels (particularly 40%) into 50/70 penetration bitumen leads to a significant increase in

elastic component, thus underlining that a considerable shift of rheological behavior from visco-like to a more elastic-like body will occur.

The rheological parameter values at 0.1Hz belonging to both short-term aged 50/70 penetration bitumen and short-term aged SEB groups reveal the effects of aging. These are given in Table 6.35. In addition, the isochronal plots of complex modulus (G^*) and phase angle (δ) versus temperature at 0.1Hz for both SEBs are shown in Figure 6.50 (a) and (b) respectively. The effects of short-term aging of RTFOT indicate that laboratory simulations of aging increases G^* . When the lowest test temperature (25°C) do not surpass a certain value, even the RTFOT-aged SEB with 10%GSF exhibits higher G^* values compared with the RTFOT-aged base sample. The general hierarchy of the curves (Figure 6.50 (a)) indicates that at the short-term aged stage, the binders become more elastic parallel to an increase in the sulphur content. Here, R-B50/70-50%GSF, whose curve is drawn at the top of graph, is significantly more elastic compared to its respective aged base bitumen.

Table 6.35 : Values of rheological parameters at 0.1Hz following RTFOT aging.

GSF	Stage	Complex Modulus at 0.1 Hz (Pa)				Phase Angle at 0.1 Hz (degree)			
		25 °C	30 °C	40 °C	50 °C	25 °C	30 °C	40 °C	50 °C
0%	r	2.49E+07	1.33E+07	2.54E+06	3.86E+05	58.85	73.13	79.99	86.14
10%	r	3.15E+07	1.04E+07	1.94E+06	3.08E+05	61.74	75.33	80.70	85.30
20%	r	7.07E+07	2.38E+07	3.12E+06	4.30E+05	55.09	63.85	73.38	80.72
30%	r	7.90E+07	3.14E+07	5.28E+06	8.29E+05	42.06	53.12	65.88	76.67
40%	r	2.28E+08	5.80E+07	2.73E+07	3.52E+06	45.90	53.12	53.06	68.64
50%	r	2.91E+08	3.40E+08	1.38E+08	4.70E+07	40.88	48.46	51.12	60.68



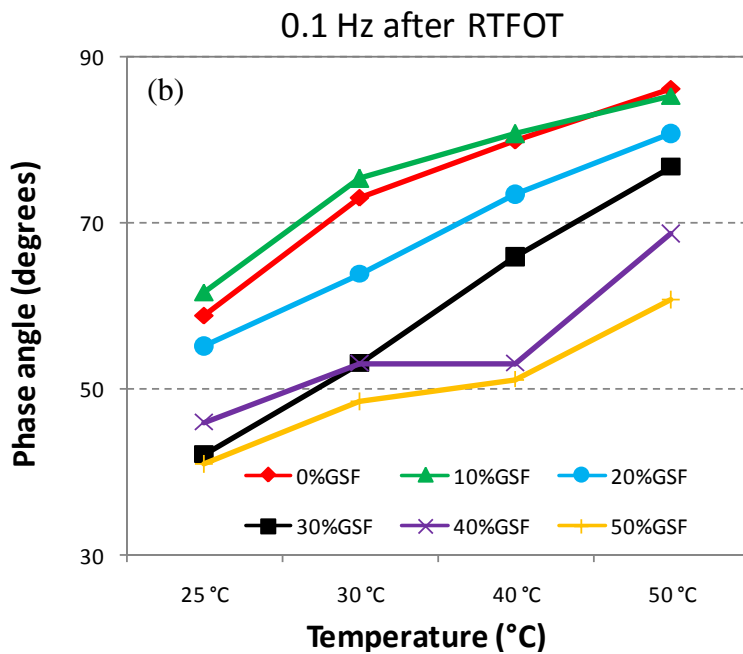


Figure 6.50 : Isochronal plots at 0.1Hz for SEB made of B50/70 bitumen after short-term aging. (a) Complex modulus and (b) Phase angle.

After short-term aging, sulphur extension continues to significantly increase the elasticity of base 50/70 penetration bitumen at 20, 30, 40, and 50%GSF levels, as measured by the reduction in phase angle (Figure 6.50 (b)). This observation represents supporting evidence for the conjecture that a more extended network is developed when this base bitumen is extended with GSF. This approach supports the argument that rutting resistance is improved by increasing the amounts of sulphur after aging. In the case of 50% sulphur extension, a remarkable reduction in the phase angle is confirmed by the increased G^* values observed at each test temperature. The phase angle data for this SEB at 0.1Hz, which is shown in the Figure 6.50 (b), also appear to reinforce the argument that resistance to rutting would be improved.

A more illustrative way of comparison is to represent the relevant factors in changes of G^* for both base asphalt (BA) and SEBs after short-term aging, as listed in Table 6.36. Several important observations can be derived from these listed values. For instance, after short-term aging, the extension indices ($G^*_{SEB}/G^*_{50/70}$) are much higher than those at the unaged stage. This indicates that sulphur extension is more pronounced by the aging effect. On the other hand, being subjected to only short-term aging simulation does not cause the extension of 10% sulphur to exceed its extension indices factor 1.00 at 30, 40, and 50°C.

Table 6.36 : Relative changes in complex modulus and aging index at 0.1Hz following short-term aging.

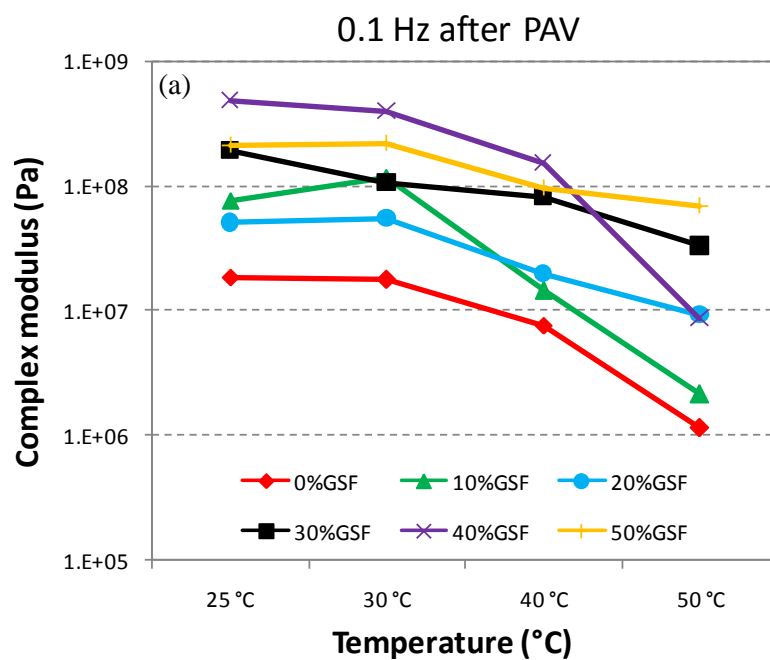
Binder	Stage	Extension Indices ($G^*_{SEB}/G^*_{B50/70}$) at 0.1 Hz				Aging Index (G^*_{RTFOT}/G^*_{UNAGED}) at 0.1 Hz			
		25 °C	30 °C	40 °C	50 °C	25 °C	30 °C	40 °C	50 °C
B50/70	r	1.00	1.00	1.00	1.00	0.92	2.28	2.30	2.40
B50/70-10%GSF	r	1.26	0.78	0.76	0.80	2.96	2.70	4.18	4.63
B50/70-20%GSF	r	2.84	1.79	1.23	1.12	3.90	7.17	6.39	5.28
B50/70-30%GSF	r	3.17	2.36	2.08	2.15	4.99	2.43	2.94	2.10
B50/70-40%GSF	r	9.15	4.35	10.72	9.13	2.66	2.24	8.35	6.78
B50/70-50%GSF	r	11.67	25.53	54.39	121.69	13.31	23.51	92.67	198.34

The effects of short-term aging of RTFOT indicate that laboratory aging simulations increase G^* , as proved by their aging index parameter (G^*_{RTFOT}/G^*_{UNAGED}). Generally speaking, there is a significant difference between unaged and aged binders in their G^* values for both base bitumen and SEBs. In particular, for the SEB with 50%GSF the influences of aging on the increase of G^* follows the aging index factors of 13.31, 23.51, 92.67, and 198.34, at 25, 30, 40, and 50°C respectively as listed in Table 6.36.

The impacts of long-term aging on the rheological behavior of the neat B50/70 bitumen and SEB groups are shown in Figure 6.51 (a) and (b) and their values are given in Table 6.37. After PAV aging, a continuous shift of the curve towards higher complex modulus can be seen over the entire temperature range. There are two major reasons for this phenomenon: On the one hand, the sulphur particles dispersed in 50/70 penetration bitumen rearranged and then finely decomposed after long-term aging; as a result, these small size particles interacted more easily with bitumen components. Secondly, the elasticity of bitumen matrix, no doubt, increased significantly owing to the obvious elevated level of hard bituminous components (such as asphaltene) in the prolonged aging process of PAV aging. However it should be noted that the hierarchy of the G^* curves after PAV aging is lost and also loses the similarity to that observed after RTFOT aging. For instance, even though the long-term aged SEB with 50%GSF appears to have the highest G^* values at high temperature ranges (40-50°C), the P-B50/70-40%GSF binder seems to have the highest complex modulus values at low and moderate temperature ranges (25-40°C). In other words, after PAV-aging the magnitude of increase in G^* values did not vary in a regular fashion with varying amounts of sulphur.

Table 6.37 : Values of rheological parameters at 0.1Hz following PAV aging.

GSF	Stage	Complex Modulus at 0.1 Hz (Pa)				Phase Angle at 0.1 Hz (degree)			
		25 °C	30 °C	40 °C	50 °C	25 °C	30 °C	40 °C	50 °C
0%	p	1.88E+07	1.78E+07	7.63E+06	1.15E+06	67.19	70.12	75.19	81.03
10%	p	7.72E+07	1.17E+08	1.45E+07	2.15E+06	64.84	67.24	68.50	73.31
20%	p	5.11E+07	5.49E+07	2.00E+07	9.24E+06	53.87	58.50	52.05	68.28
30%	p	1.93E+08	1.07E+08	8.25E+07	3.33E+07	56.74	58.98	65.88	70.46
40%	p	4.91E+08	3.97E+08	1.55E+08	8.79E+06	49.47	52.28	54.59	68.48
50%	p	2.13E+08	2.21E+08	9.62E+07	7.00E+07	61.17	53.02	63.26	64.73



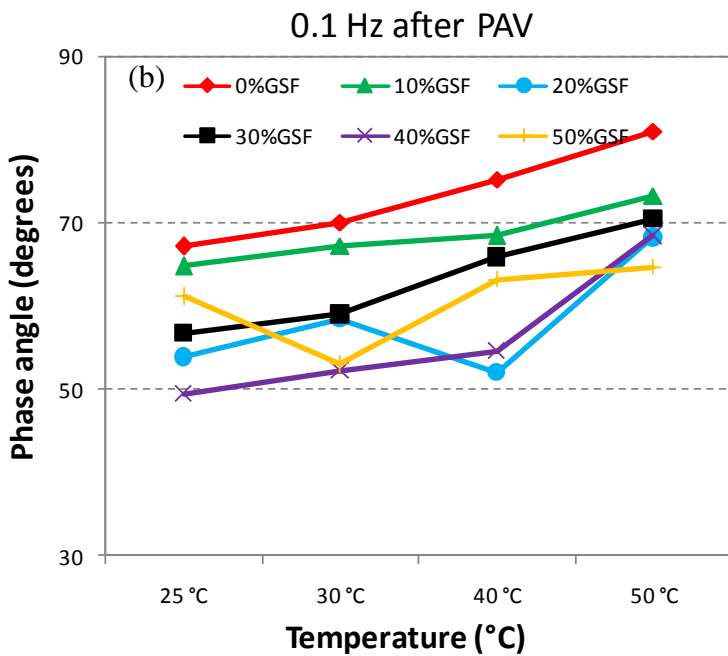


Figure 6.51 : Isochronal plots at 0.1Hz for SEB made of B50/70 bitumen after long-term aging. (a) Complex modulus and (b) Phase angle.

The extension indices and long-term aging index parameter (G^*_{PAV}/G^*_{UNAGED}) are given in Table 6.38. The effects of long-term aging of PAV emphasize that the laboratory aging simulations tend to increase G^* . Generally, there is a significant change among unaged, RTFOT-aged and PAV- aged binders in their G^* values for both base bitumen and SEBs. The influences of aging on an increase of G^* follow the greatest extension indices factors of 26.14, 22.29 and 20.30 for the SEB with 40%GSF, at 20, 30, and 40°C and 29.01 for the SEB with 20%GSF at 50°C respectively, whereas long-term aging has a distinctive impact, particularly on the SEB with 50%GSF in terms of variation of G^* by increased aging index factors of 64.45 and 295.52 at 40 and 50°C.

Table 6.38 : Relative changes in complex modulus and aging index at 0.1Hz following long-term aging.

Binder	Stage	Extension Indices ($G^*_{SEB}/G^*_{B50/70}$) at 0.1 Hz				Aging Index (G^*_{PAV}/G^*_{UNAGED}) at 0.1 Hz			
		25 °C	30 °C	40 °C	50 °C	25 °C	30 °C	40 °C	50 °C
B50/70	p	1.00	1.00	1.00	1.00	0.69	3.05	6.90	7.13
B50/70-10%GSF	p	4.11	6.57	1.90	1.87	7.26	30.38	31.28	32.30
B50/70-20%GSF	p	2.72	3.09	2.61	8.05	2.82	16.53	40.86	113.44
B50/70-30%GSF	p	10.29	6.04	10.81	29.01	12.22	8.31	45.90	84.29
B50/70-40%GSF	p	26.14	22.29	20.30	7.66	5.73	15.34	47.47	16.92
B50/70-50%GSF	p	11.35	12.40	12.60	60.95	9.77	15.26	64.45	295.52

It can be clearly seen from both the complex viscosity and phase angle plots versus temperature depicted above that the rheological behavior of the SEBs depends strongly on the effect of sulphur level compared with the base bitumen after long-term aging.

SEBs composed of B50/70 and variable amount of GSF at 0.2517Hz;

In order to clarify the effects of frequency change on both the base bitumen and SEB groups, the rheological properties of each sample before aging was investigated at a relatively higher frequency, 0.2517Hz. These obtained results are presented in Table 6.39, while the isochronal plots of complex modulus (G^*) and phase angles (δ) versus temperature domain are demonstrated in Figure 6.52 (a) and (b) respectively. Increasing the loading test frequency from 0.1 to 0.2517Hz did not change the viscoelastic behavior of unaged SEB with 10%GSF. Excepting low temperature (25°C), this binder insisted on displaying relatively more viscous behavior in terms of its lower G^* values compared to respective base bitumen. Besides, this well-defined trend is also true for the SEB with 20%GSF since sulphur extension at this level made the base bitumen exhibit more sol-like (viscous and less structured) behavior at 0.2517Hz.

Table 6.39 : Values of rheological parameters for the B50/70 base bitumen and SEB groups at 0.2517Hz before aging.

GSF	Stage	Complex Modulus at 0.2517 Hz (Pa)				Phase Angel at 0.2517 Hz (degree)			
		25 °C	30 °C	40 °C	50 °C	25 °C	30 °C	40 °C	50 °C
0%	o	3.43E+07	2.11E+07	2.59E+06	4.08E+05	70.02	75.64	82.22	87.92
10%	o	3.94E+07	1.17E+07	1.11E+06	1.64E+05	79.55	81.97	85.95	88.48
20%	o	2.34E+07	1.02E+07	1.11E+06	1.87E+05	70.65	76.31	82.12	83.05
30%	o	3.91E+07	2.75E+07	3.77E+06	8.56E+05	34.95	46.86	80.40	81.19
40%	o	8.71E+07	2.71E+07	9.78E+06	1.19E+06	30.95	52.03	76.48	84.94
50%	o	4.48E+07	2.59E+07	3.71E+06	5.72E+05	39.60	49.71	79.34	87.05

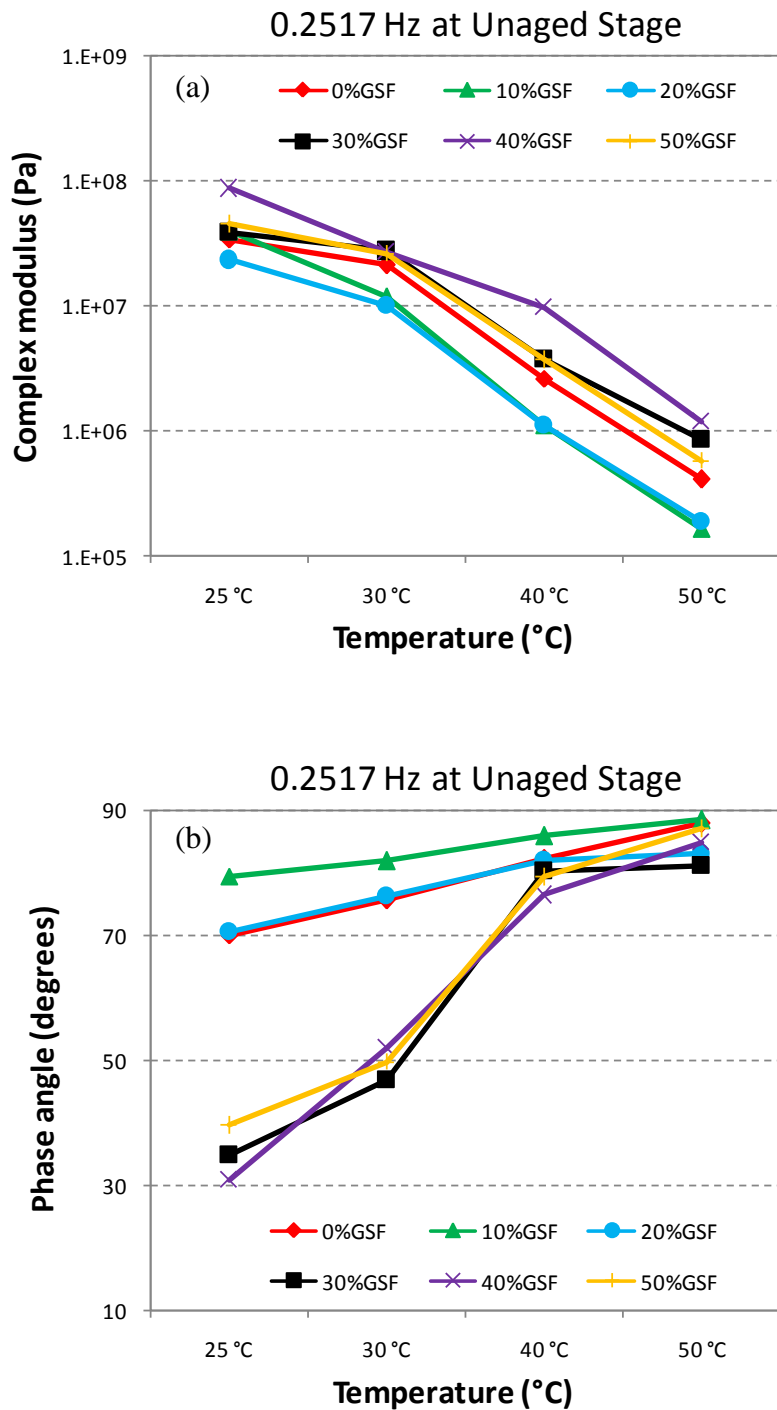


Figure 6.52 : Isochronal plots at 0.2517Hz for SEB made of B50/70 bitumen before aging. (a) Complex modulus and (b) Phase angle.

Even though the chemical structure of these binders are totally different, they have similar G^* plots versus temperature, as shown in Figure 6.52 (a). The change towards a more viscous behavior after 10 and/or 20% sulphur extension at both 0.1 and 0.2517Hz due to the decrease in G^* confirms the assumption that a low amount of sulphur generates viscous networks in bitumen matrix.

The other unaged SEBs with further extended GSF appear to have higher G^* values and, as a result, they are expected to display more gel-like (elastic and more structured) behavior at 0.2517Hz compared with 50/70 pen base bitumen.

Compared with the base bitumen, SEBs with 20%GSF demonstrated almost the same variation in phase angle. However, due to its structural characteristics, the change of the phase angle of the SEB with 10%GSF was not similar to that of the base bitumen and its phase angle curve is seen to have been drawn above that of neat bitumen. For the other SEBs with increasing amounts of GSF (30, 40, and 50%), increasing the temperature up to 40°C plays a major role on their phase angle due to sharp changes in their curve slopes. However, it was found that SEBs with 20 and 30%GSF demonstrate a plateau region to phase angle in cases of the high temperatures ranging approximately from 40 to 50°C, as illustrated in Figure 6.52 (b).

The extension indices of G^* ($G^*_{SEB}/G^*_{B50/70}$) measuring relative changes in complex modulus for all five SEBs have been recorded at each temperature and at 0.2517Hz and are shown in Table 6.40.

Table 6.40 : Relative changes in complex modulus for the B50/70 base bitumen and SEB groups at 0.2517Hz before aging.

Binder	Stage	Extension Indices ($G^*_{SEB}/G^*_{B50/70}$) at 0.2517 Hz			
		25 °C	30 °C	40 °C	50 °C
B50/70	o	1.00	1.00	1.00	1.00
B50/70-10%GSF	o	1.15	0.56	0.43	0.40
B50/70-20%GSF	o	0.68	0.48	0.43	0.46
B50/70-30%GSF	o	1.14	1.30	1.45	2.10
B50/70-40%GSF	o	2.54	1.28	3.78	2.91
B50/70-50%GSF	o	1.31	1.23	1.43	1.40

Among all of the SEBs, that with 40%GSF had the highest extension indices values (except 30°C), implying that sulphur extension of B50/70 at 40% level generates desirable viscoelastic behavior in terms of increased complex modulus. Contrary to expectations, increasing sulphur amount up to 50% offered no further improvements to elastic behavior; conversely, related extension indices started to converge to 1.00 as listed in Table 6.40.

The short-term aging dependence of rheological behavior for base bitumen and SEB groups has been assessed at 0.2517Hz. The obtained results are presented in Table

6.41, while the isochronal plots of complex modulus (G^*) and phase angles (δ) versus temperature domain are demonstrated in Figure 6.53 (a) and (b) respectively. Similar to its rheological behavior at unaged stage, the same conclusion can be drawn for the RTFOT-aged SEB with 10%GSF as shown by the slight changes in the complex modulus. Even after short-term aging this SEB has lower G^* values compared to base bitumen. On the other hand, the results are very different for the SEB with 20%GSF. Even though it had lower G^* values than that of neat bitumen prior to aging, the elasticity of the sulphur dispersed in bitumen sufficiently increased by the RTFOT aging, as shown in its increased G^* values. The rest of the SEBs remarkably enhanced rheological behaviors owing to their increased G^* values. This benefit is due to two major reasons: On the one hand, increasing the test frequency from 0.1 to 0.2517Hz led to an increase in their G^* values. On the second hand, it is clear that aging via RTFOT markedly contributed to an improved viscoelastic behavior since the sulphur particles are assumed to have gained favorable compatibility with bitumen compounds after aging.

The higher phase angle curve can be observed for base bitumen across the entire temperature range after RTFOT aging, which emphasizes the fact that neat bitumen, in the absence of sulphur, is more susceptible to oxidization. Inconsistent with its complex modulus results, the phase angle values of SEB with 10%GSF are lower than those of neat bitumen after aging. This paradox can be related to the strong sensitivity of phase angle on chemical composition. Previous researchers have pointed out that the measurement of δ was generally considered to be more sensitive to the chemical structure and therefore extension and/or modification of bitumen than complex modulus (Gordon, 2003b).

Table 6.41 : Values of rheological parameters for the B50/70 base bitumen and SEB groups at 0.2517Hz after short-term aging.

GSF	Stage	Complex Modulus at 0.2517 Hz (Pa)				Phase Angel at 0.2517 Hz (degree)			
		25 °C	30 °C	40 °C	50 °C	25 °C	30 °C	40 °C	50 °C
0%	r	5.12E+07	3.55E+07	5.48E+06	9.29E+05	57.29	64.17	78.89	86.62
10%	r	4.81E+07	2.13E+07	4.14E+06	7.11E+05	42.86	60.22	78.27	83.90
20%	r	1.14E+08	1.05E+08	6.73E+06	9.48E+05	51.64	52.94	64.62	80.13
30%	r	9.94E+07	7.68E+07	1.17E+07	1.75E+06	49.03	45.91	51.23	74.80
40%	r	2.82E+08	4.64E+07	3.97E+07	8.13E+06	42.49	28.26	73.92	74.04
50%	r	1.04E+08	1.38E+08	3.10E+07	1.54E+07	27.18	55.58	53.66	67.29

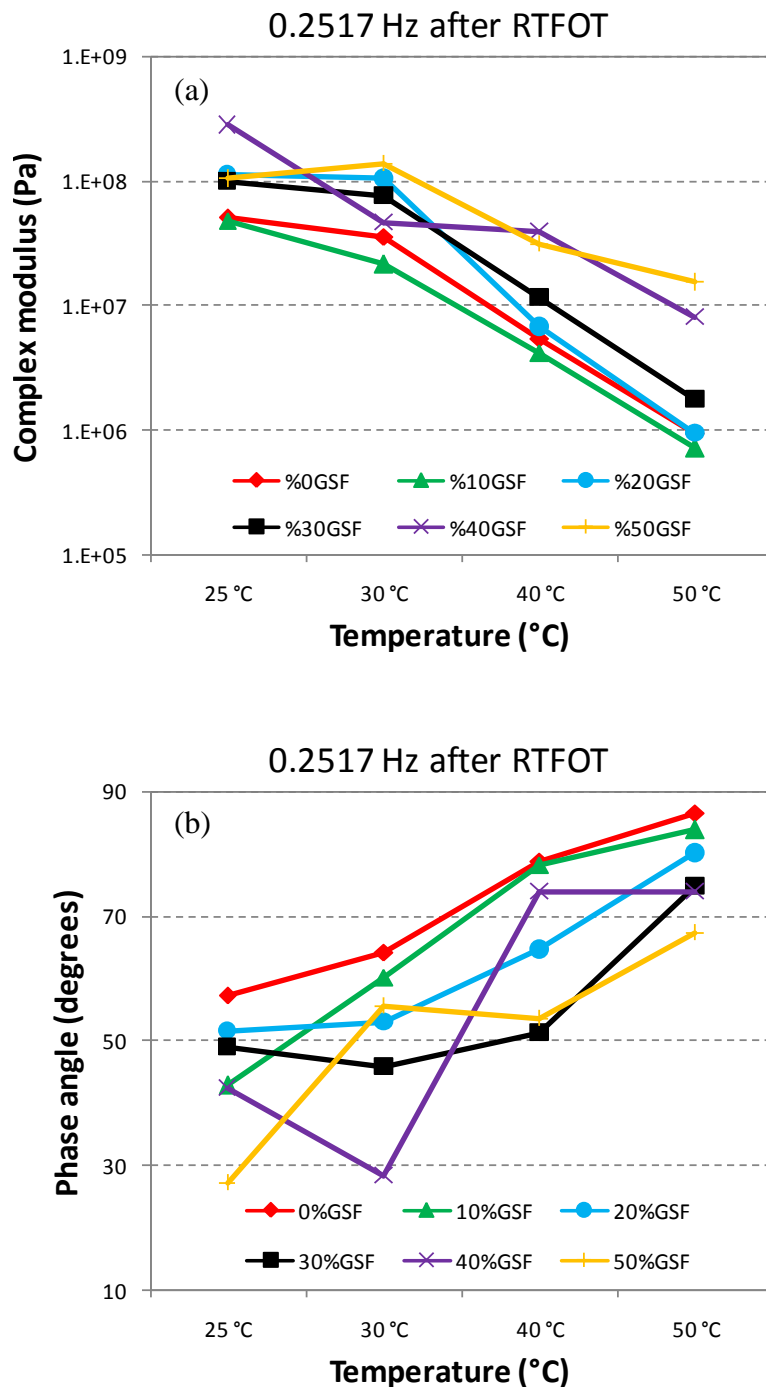


Figure 6.53 : Isochronal plots at 0.2517Hz for neat B50/70 bitumen and SEB groups made of B50/70 bitumen after short-term aging. (a) Complex modulus and (b) Phase angle.

In order to understand both the effects of sulphur extension and short-term aging, extension indices ($G^*_{SEB}/G^*_{B50/70}$) and aging index parameter (G^*_{RTFOT}/G^*_{UNAGED}) are evaluated at 0.2517Hz and given in Table 6.42. The extension indices for each sample show that there is a kind of competition between the SEB with 40%GSF and the SEB with 50%GSF. At 25 and 40°C, SEB with 40%GSF has the highest values, whereas at 30 and 50°C, SEB with 50%GSF has the highest values. One of the most

probable reasons for this is that aging results in more interactions between high amount of sulphur particles and bitumen components, especially through thermal and oxidative effects.

As compared with those at 0.1Hz, aging index values at 0.2517Hz are not remarkable high, but are still greater than 1.00. This gap between binders' aging index is no doubt related to magnitude of loading frequency; therefore, one can observe that as loading frequency is increased, the influence of aging plays a minor role on the complex modulus values.

Table 6.42 : Relative changes in complex modulus and aging index at 0.2517Hz following short-term aging.

Binder	Stage	Extension Indices ($G^*_{SEB}/G^*_{B50/70}$) at 0.2517 Hz				Aging Index (G^*_{RTFOT}/G^*_{UNAGED}) at 0.2517 Hz			
		25 °C	30 °C	40 °C	50 °C	25 °C	30 °C	40 °C	50 °C
B50/70	r	1.00	1.00	1.00	1.00	1.49	1.68	2.11	2.28
B50/70-10%GSF	r	0.94	0.60	0.76	0.77	1.22	1.81	3.73	4.33
B50/70-20%GSF	r	2.23	2.94	1.23	1.02	4.88	10.27	6.05	5.08
B50/70-30%GSF	r	1.94	2.16	2.13	1.89	2.54	2.79	3.10	2.05
B50/70-40%GSF	r	5.51	1.30	7.26	8.75	3.24	1.71	4.06	6.84
B50/70-50%GSF	r	2.03	3.87	5.66	16.61	2.32	5.31	8.35	26.97

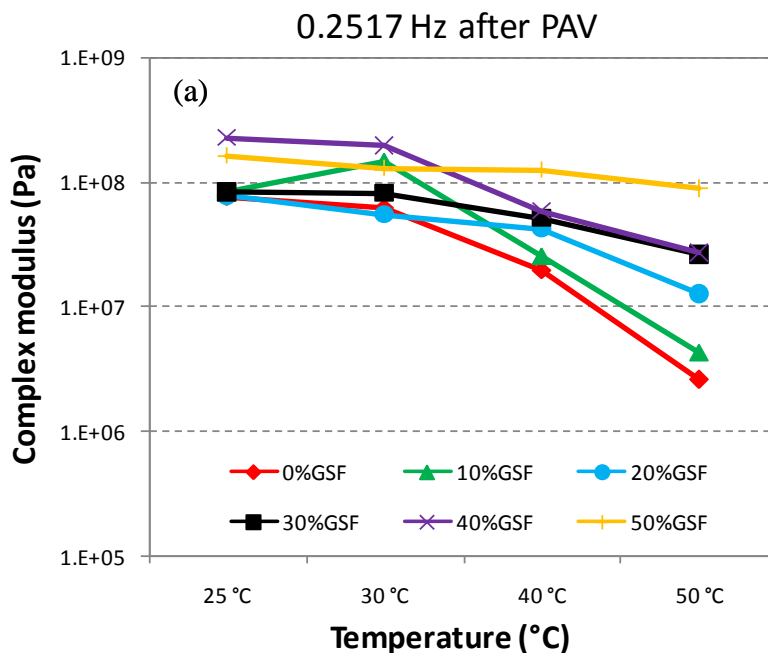
To sum up, it is clear that sulphur extension, in particular at intermediate and/or high levels, can improve both the low and high temperature performance of 50/70 penetration bitumen significantly. In addition, this improved performance also can be retained after short-term aging.

In order to investigate the influence of long-term aging on both the base bitumen and SEB groups, the dynamic shear rheometer (DSR) test was performed again on each PAV-aged sample at the same frequency, 0.2517Hz. The obtained results are presented in Table 6.43 and the isochronal plots of complex modulus (G^*) and phase angles (δ) versus temperature domain are demonstrated in Figure 6.54 (a) and (b) respectively. Nowadays, dynamic mechanic analysis is considered to be an important rheological approach for the evaluation of the temperature performance of binders, especially so the high-temperature performance and thus is used widely. In this study, the DSR test has been used to study the SEBs complex modulus as a fundamental viscoelastic indicator and to express the contribution of both bitumen matrix and sulphur phase to permanent deformation after long-term aging. The changes in complex modulus values after RTFOT and PAV aging are very different

for the samples. As can be seen in Table 6.43, the evident increase in G^* at most temperatures after PAV aging is understandably greater than after RTFOT aging due to the prolonged aging process in the PAV. However this impact is not regularly seen at the lowest test temperature (25°C), particularly for the SEB with 20, 30, 40, and 50%GSF. Rather than an increase in their G^* values, a distinctive decline was observed. The most probable reason for this decline at 25°C after PAV aging is due to the breakdown of the elastic sulphur networks during pressure aging. As illustrated in Figure 6.54 (a) studies of temperature dependency reveal that all long-term aged samples, including the base, show a plateau region to complex modulus over the low temperature range approximately from 25 to 30°C , which indicates a kind of G^* stability.

Table 6.43 : Values of rheological parameters for the B50/70 base bitumen and SEB groups at 0.2517Hz after long-term aging.

GSF	Stage	Complex Modulus at 0.2517 Hz (Pa)				Phase Angel at 0.2517 Hz (degree)			
		25 °C	30 °C	40 °C	50 °C	25 °C	30 °C	40 °C	50 °C
0%	p	7.58E+07	6.30E+07	1.98E+07	2.58E+06	52.05	72.18	74.22	79.74
10%	p	8.34E+07	1.49E+08	2.59E+07	4.28E+06	45.11	60.19	67.55	71.66
20%	p	7.73E+07	5.48E+07	4.18E+07	1.27E+07	49.90	63.20	70.18	71.89
30%	p	8.33E+07	8.15E+07	5.12E+07	2.61E+07	42.89	52.31	65.97	69.00
40%	p	2.25E+08	1.95E+08	5.89E+07	2.69E+07	42.07	44.08	51.94	57.40
50%	p	1.64E+08	1.28E+08	1.25E+08	8.91E+07	46.21	58.48	59.56	59.81



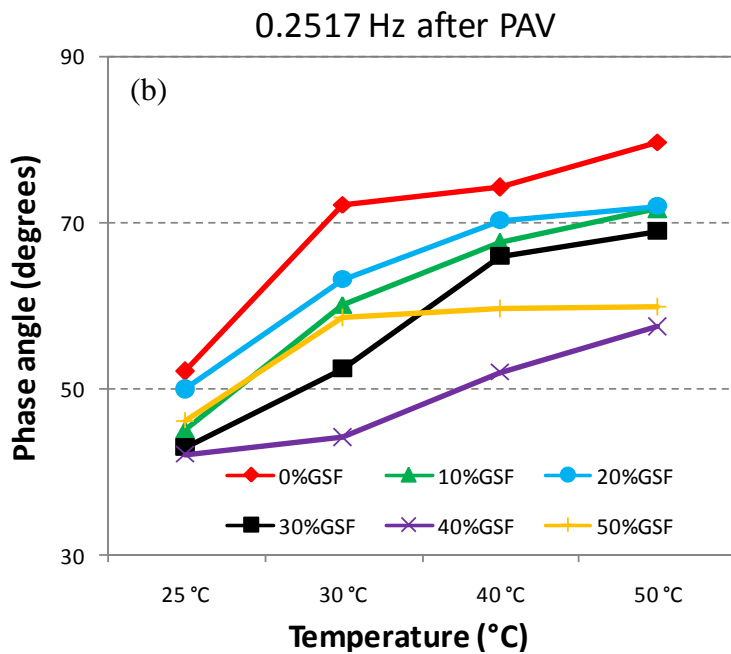


Figure 6.54 : Isochronal plots at 0.2517Hz for neat B50/70 bitumen and SEB groups made of B50/70 bitumen after short-term aging. (a) Complex modulus and (b) Phase angle.

Phase angle isochrones at 0.2517Hz for long-term aged binders are presented in Figure 6.54 (b) and the absolute values are also listed in Table 6.43. A measurement of δ is generally considered to be more sensitive to the chemical and physical structure than complex modulus when the modification and/or extension of straight bitumen is considered. The general shape of the phase angle curves indicates that the binders become more elastic as the frequency is increased from 0.1 to 0.2517Hz and after being subjected to long-term aging. Furthermore, the same graph (Figure 6.54 (b)) clearly illustrates the improved elastic response (reduced phase angles) of the SEBs compared to the base binder. The phase angles of the base bitumen are comparatively greater and therefore predominantly show viscous behavior with increasing temperature. Sulphur extension significantly improves the elastic response at high temperature, which can be attributed to the viscosity of the base bitumen being low enough to allow the elastic network of the sulphur particles to influence the mechanical properties of the sulphur-extended-binders.

The differences among the phase angle curves become more and more evident in shape and absolute values when a greater quantity of sulphur is utilized. For instance, the curve of P-B50/70-50%GSF shows a sort plateau in δ at intermediate and high temperatures; this strongly highlights how this high quantity of sulphur affects the properties of the base bitumen after long-term aging. The presence and nature of the

plateau and sulphur network is an outcome of the chemical and physical interactions of the sulphur and base 50/70 penetration bitumen after PAV-aging.

The extension indices ($G^*_{SEB}/G^*_{B50/70}$) and long-term aging index parameter (G^*_{PAV}/G^*_{UNAGED}) are given in Table 6.44. The extension indices of long-term aged samples remarkably differ from both those of unaged samples and short-term aged samples and they are generally higher at 50°C, as well as slightly higher for the SEB with 50%GSF.

Table 6.44 : Relative changes in complex modulus and aging index at 0.2517Hz following long-term aging.

Binder	Stage	Extension Indices ($G^*_{SEB}/G^*_{B50/70}$) at 0.2517 Hz				Aging Index (G^*_{PAV}/G^*_{UNAGED}) at 0.2517 Hz			
		25 °C	30 °C	40 °C	50 °C	25 °C	30 °C	40 °C	50 °C
B50/70	p	1.00	1.00	1.00	1.00	2.21	2.99	7.66	6.32
B50/70-10%GSF	p	1.10	2.36	1.31	1.66	2.12	12.68	23.35	26.10
B50/70-20%GSF	p	1.02	0.87	2.11	4.91	3.30	5.39	37.52	67.87
B50/70-30%GSF	p	1.10	1.29	2.58	10.13	2.13	2.96	13.60	30.50
B50/70-40%GSF	p	2.97	3.10	2.97	10.44	2.58	7.20	6.03	22.65
B50/70-50%GSF	p	2.16	2.04	6.28	34.57	3.65	4.94	33.58	155.75

Comparisons of the aging index values at 0.1 and 0.2517Hz highlight that PAV aging at lower frequency, where the increased stiffness of the base bitumen is dominated by the influence of the sulphur network, is much more influential than PAV aging at higher frequency of 0.2517Hz.

SEBs composed of B50/70 and variable amount of GSF at 0.6329Hz:

In order to investigate the effects of further increases in loading frequency on both the base bitumen and SEB groups, the dynamic shear rheometer (DSR) test was performed again on each unaged sample at the frequency of 0.6329Hz. Then obtained results are presented in Table 6.45 and isochronal plots of complex modulus (G^*) and phase angles (δ) versus temperature domain are demonstrated in Figure 6.55 (a) and (b) respectively.

Table 6.45 : Values of rheological parameters for the B50/70 base bitumen and SEB groups at 0.6329Hz before aging.

GSF	Stage	Complex Modulus at 0.6329 Hz (Pa)				Phase Angel at 0.6329 Hz (degree)			
		25 °C	30 °C	40 °C	50 °C	25 °C	30 °C	40 °C	50 °C
0%	o	6.98E+07	1.99E+07	6.04E+06	9.84E+05	35.79	41.41	82.30	87.92
10%	o	5.78E+07	1.24E+07	2.69E+06	4.06E+05	40.79	52.37	83.08	89.09
20%	o	5.30E+07	1.43E+07	2.80E+06	4.30E+05	38.86	46.33	84.13	87.18
30%	o	2.35E+07	2.22E+07	1.21E+07	1.93E+06	29.42	45.20	74.45	80.63
40%	o	2.59E+08	3.13E+07	2.56E+07	2.67E+06	36.15	35.50	44.54	84.98
50%	o	5.84E+07	2.19E+07	1.92E+07	1.35E+06	38.48	55.97	69.99	85.57

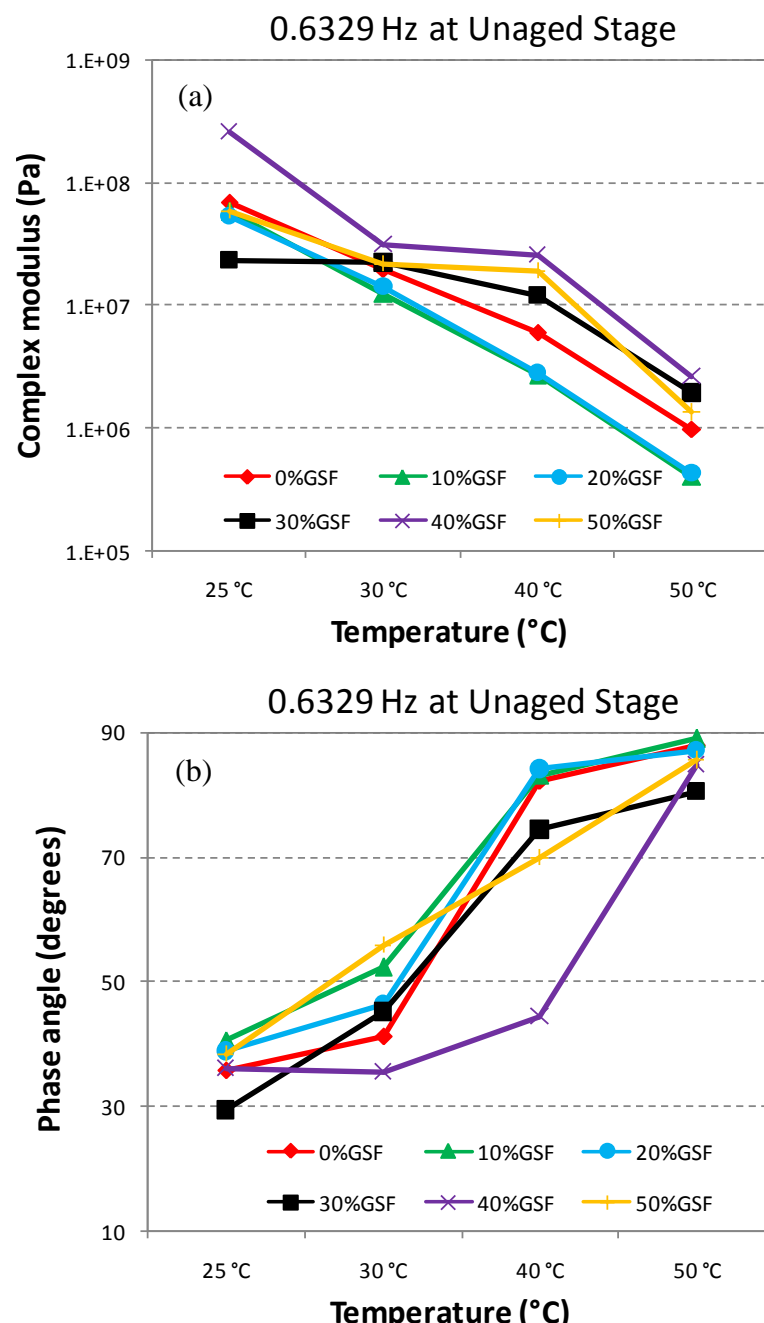


Figure 6.55 : Isochronal plots at 0.6329Hz for neat B50/70 bitumen and SEB groups made of B50/70 bitumen before aging. (a) Complex modulus and (b) Phase angle.

The unaged SEB with 10%GSF binder exhibits lower complex modulus values compared with the unaged base. Furthermore, this well-defined trend is also clear for the SEB at 20% sulphur level as illustrated in Figure 6.55 (a). Even though it has different chemical composition due to its low sulphur content, the curve of SEB with 10%GSF appears almost superposed over that of SEB with 20%GSF and only small differences are appreciable at complex modulus values between 25 and 50°C. Hence it is worthy to point out that regardless of magnitude in loading test frequency (0.1, 0.2517 and 0.6329Hz) the inclusion of granular sulphur at low level (10 and 20%) into 50/70 penetration bitumen yields a significant amount of increase in viscous component.

The differences among the G^* curves become increasingly evident in both shape and absolute values when a greater quantity of sulphur is utilized. From a qualitative point of view, the elastic behavior gradually increases when the amount of sulphur further increased. However the magnitude of increase in values does not exhibit a regular change; for instance, the curve at 40%GSF level is placed at the top of the graph. The curve of SEB with 30%GSF at low temperature range and the curves of both the SEB with 40 and 50%GSF at medium temperatures show a sort of intermediate plateau in G^* which strongly highlights how the sulphur affects the properties of the base bitumen.

The phase angle isochrones clearly illustrate that even the introduction of a low amount of GSF (10 and/or 20%) has a remarkable influence on the rheological properties of base bitumen in terms of gaining a significant viscous property. Consistent with the decline in complex modulus values, the increase in phase angle is meaningful. The shift of the curve towards lower complex modulus and the shift of the curve towards higher phase angles indicate the softening of neat bitumen with sulphur extension at low content. Despite the fact that with decreasing phase angle the performance of the bituminous binder will be improved, particularly at high-temperatures, the viscous behavior that might be gained by sulphur extension can be desirable at cold temperatures. On the other hand, the decreasing phase angle resulting from further increases in sulphur level is expected to be favorable as it reflects a promising rutting resistance at high temperatures.

The extension indices of G^* ($G^*_{SEB}/G^*_{B50/70}$) measuring relative changes in complex modulus for all five SEBs have been recorded at each temperature and at 0.6329Hz

in Table 6.46. The decline in the extension indices for the SEB with 10 and 20%GSF emphasizes the loss in rutting resistance at unaged stages. On the other hand, B50/70-40%GSF, which represents the highest extension indices at each test temperature displays considerable rutting resistance compared to other SEBs before aging.

Table 6.46 : Relative changes in complex modulus for the B50/70 base bitumen and SEB groups at 0.6329Hz before aging.

Binder	Stage	Extension Indices ($G^*_{SEB}/G^*_{B50/70}$) at 0.6329 Hz			
		25 °C	30 °C	40 °C	50 °C
B50/70	o	1.00	1.00	1.00	1.00
B50/70-10%GSF	o	0.83	0.62	0.45	0.41
B50/70-20%GSF	o	0.76	0.72	0.46	0.44
B50/70-30%GSF	o	0.34	1.12	2.00	1.96
B50/70-40%GSF	o	3.71	1.57	4.24	2.71
B50/70-50%GSF	o	0.84	1.10	3.17	1.37

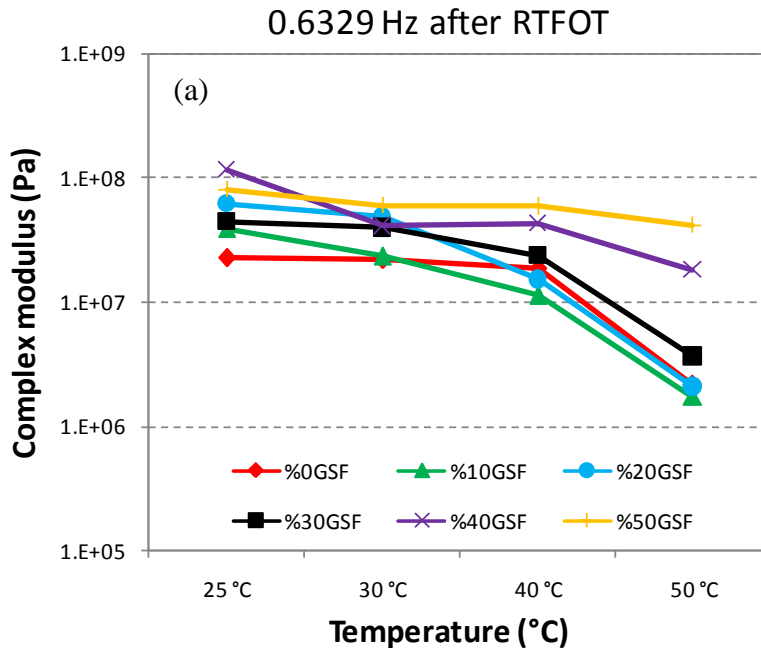
High temperature rutting and low temperature cracking restrict the performance of bituminous binder and/or the coating layer. In fact, it should be noted that the performance of asphaltic concrete pavement strongly depends on the properties of aged binders. In this sense, in order to evaluate the influence of short-term aging at 0.6329Hz on rheological behavior, the dynamic shear rheometer (DSR) test was again carried out on the RTFOT-aged samples. The rheological parameter values at 0.6329Hz belonging to both the short-term aged base 50/70 bitumen and short-term aged SEB groups are given in Table 6.47. In addition, the isochronal plots of complex modulus (G^*) and phase angle (δ) versus temperature at 0.6329Hz for both are shown in Figure 6.56 (a) and (b) respectively.

An increase in complex modulus values generally occurred after short-term aging, which indicates an improvement in elasticity (For instance, for the 40%GSF SEB, the increase is from 2.35E+07 to 4.38E+07Pa at 25°C, from 2.22E+07 to 3.95E+07Pa at 30°C, from 1.21E+07 to 2.34E+07Pa at 40°C, and from 1.93E+06 to 3.63E+06Pa at 50°C). What is more noticeable from the obtained results is that rheological behaviors of the 10 and/or 20%GSF SEBs completely differ from those found at their unaged stages. As can be seen from Figure 6.56 (a), the isochronal plots of these two SEBs are drawn just over that of neat bitumen at low and medium

temperature ranges. However there is only a minor increase in their G^* values up to 40°C and these binders persist in displaying relatively more viscous behavior at high temperature compared to respective base bitumen.

Table 6.47 : Values of rheological parameters for the B50/70 base bitumen and SEB groups at 0.6329Hz after short-term aging.

GSF	Stage	Complex Modulus at 0.6329 Hz (Pa)				Phase Angle at 0.6329 Hz (degree)			
		25 °C	30 °C	40 °C	50 °C	25 °C	30 °C	40 °C	50 °C
0%	r	2.24E+07	2.16E+07	1.87E+07	2.13E+06	46.81	50.92	70.02	85.13
10%	r	3.87E+07	2.31E+07	1.12E+07	1.70E+06	48.72	54.91	72.60	85.58
20%	r	6.22E+07	4.81E+07	1.51E+07	2.05E+06	44.55	46.32	65.85	81.72
30%	r	4.38E+07	3.95E+07	2.34E+07	3.63E+06	35.27	46.21	66.58	72.32
40%	r	1.17E+08	4.08E+07	4.29E+07	1.81E+07	30.25	48.77	54.00	71.95
50%	r	8.04E+07	5.97E+07	5.88E+07	4.13E+07	32.50	39.61	48.00	52.56



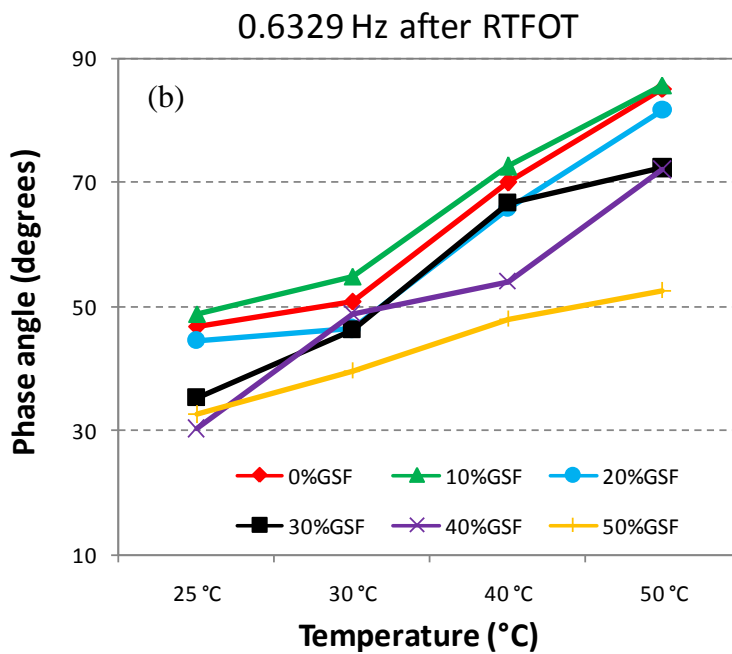


Figure 6.56 : Isochronal plots at 0.6329Hz for neat B50/70 bitumen and SEB groups made of B50/70 bitumen after short-term aging. (a) Complex modulus and (b) Phase angle.

Compared with that of control 50/70 penetration bitumen, SEB with 10, 20 and 30%GSF displayed a similarity in their slope of G^* curves after aging. However, most probably due to their structural characteristics, SEBs with further GSF (40 and 50%) showed somewhat different behavior in terms of flatter slopes of G^* curves. The plateau regions and increased G^* values at nearly all temperature ranges are synonymous with the independency of temperature defined for the SEB with 40 and 50%GSF, and illustrate the ability of the high content sulphur to generate a continuous elastic network in bituminous phase particularly after short-term aging.

Phase angle isochrones at 0.6329Hz after short-term aging illustrate enhanced elastic response (reduced phase angles) of the binders compared to their initial behavior at unaged stages. However, as shown in Figure 6.56 (b), the introduction of 10%GSF still has distinctive influence on the base bitumen in terms of elevated phase angles at each test temperature, in spite of being subjected to RTFOT aging. As listed in Table 6.47, the phase angles of the control 50/70 penetration bitumen and particularly SEB with 10%GSF approach 90° and therefore predominantly show viscous behavior in line with increasing temperature; further increases in the amount of GSF significantly improve the elastic response at high temperature. This phenomenon can be dedicated to the declined viscosity of the base bitumen by both sulphur extension and short-

term aging, which allows the elastic networks of the sulphur particles to affect the mechanical characteristics of SEBs.

In order to understand the effects of both sulphur extension and short-term aging, extension indices ($G^*_{SEB}/G^*_{B50/70}$) and aging index parameter (G^*_{RTFOT}/G^*_{UNAGED}) are evaluated and given in Table 6.48.

Compared to those at unaged stages, increased extension indices prove that sulphur extension at 0.6329Hz is generally more influential on rheological properties after RTFOT aging. Among all the short-term aged SEBs, those with 10%GSF at 25 and 30°C and the one with 20%GSF at 40 and 50°C show the closest rheological behavior to that of neat bitumen as shown by the closest extension indices values (1.72 and 1.07; 0.81 and 0.96 respectively).

Table 6.48 : Relative changes in complex modulus and aging index at 0.6329Hz following short-term aging.

Binder	Stage	Extension Indices ($G^*_{SEB}/G^*_{B50/70}$) at 0.6329 Hz				Aging Index (G^*_{RTFOT}/G^*_{UNAGED}) at 0.6329 Hz			
		25 °C	30 °C	40 °C	50 °C	25 °C	30 °C	40 °C	50 °C
B50/70	r	1.00	1.00	1.00	1.00	0.32	1.09	3.09	2.16
B50/70-10%GSF	r	1.72	1.07	0.60	0.80	0.67	1.87	4.15	4.20
B50/70-20%GSF	r	2.77	2.23	0.81	0.96	1.17	3.36	5.39	4.77
B50/70-30%GSF	r	1.95	1.83	1.25	1.70	1.86	1.78	1.94	1.88
B50/70-40%GSF	r	5.20	1.89	2.29	8.48	0.45	1.30	1.67	6.77
B50/70-50%GSF	r	3.58	2.77	3.14	19.39	1.38	2.72	3.07	30.59

As presented in Table 6.48, aging index values for the SEB with 10 and 20%GSF appear greater than that of neat bitumen, showing that low amounts of sulphur extension makes 50/70 grade bitumen more susceptible to aging. However, the same results were not observed with further amount of sulphur utilization due to the irregularity in aging index values.

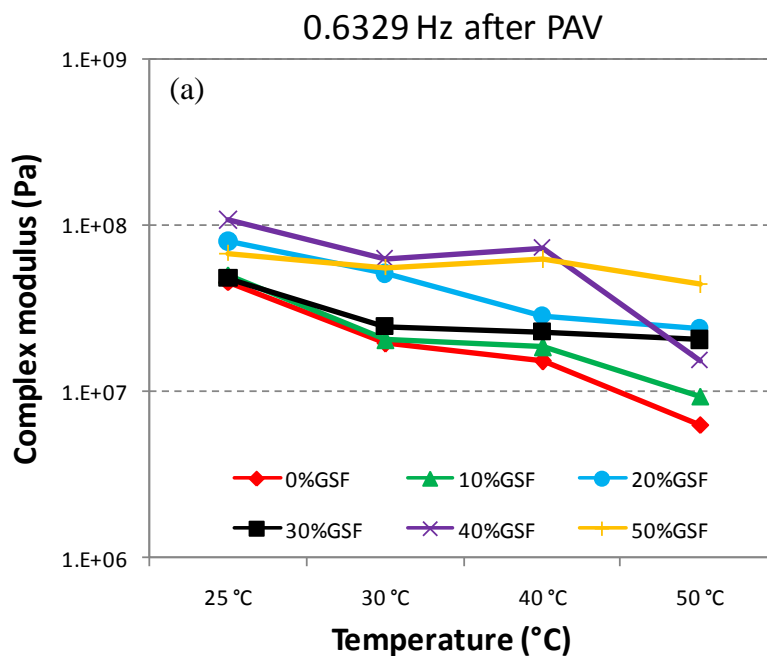
The rheological properties of the five SEBs and control neat bitumen after PAV long-term aging were compared by producing isochronal plots at a reference loading temperature frequency of 0.6329Hz with increasing temperature as shown in Figure 6.57 (a) (complex modulus) and (b) (phase angle). The absolute values are given in Table 6.49.

As listed in Table 6.49, G^* values of both 10 and 20%GSF SEB eventually exceeded those of the control bitumen after long-term aging. The viscous effect of low amount

of sulphur introduction at either original or RTFOT-aged stage was converted to elastic response by long-term aging. As explained in morphological analysis, a crystalline structure formed in bitumen phase by prolonged aging was believed to have been the major responsible factor for the increased resistance to rutting (Chapter 6.3 Morphology Analysis Results and pg. 320; Figure A.5 shows images of B50/70-20%GSF).

Table 6.49 : Values of rheological parameters for the B50/70 base bitumen and SEB groups at 0.6329Hz after long-term aging.

GSF	Stage	Complex Modulus at 0.6329 Hz (Pa)				Phase Angel at 0.6329 Hz (degree)			
		25 °C	30 °C	40 °C	50 °C	25 °C	30 °C	40 °C	50 °C
0%	p	4.60E+07	1.95E+07	1.52E+07	6.31E+06	24.07	48.98	66.48	70.86
10%	p	5.03E+07	2.05E+07	1.86E+07	9.40E+06	26.10	51.15	62.24	77.11
20%	p	7.98E+07	5.10E+07	2.84E+07	2.40E+07	24.82	46.48	62.61	61.69
30%	p	4.83E+07	2.47E+07	2.29E+07	2.05E+07	20.70	39.58	51.39	57.03
40%	p	1.07E+08	6.31E+07	7.32E+07	1.55E+07	28.69	33.81	54.48	68.16
50%	p	6.75E+07	5.60E+07	6.23E+07	4.41E+07	39.34	43.38	53.85	65.49



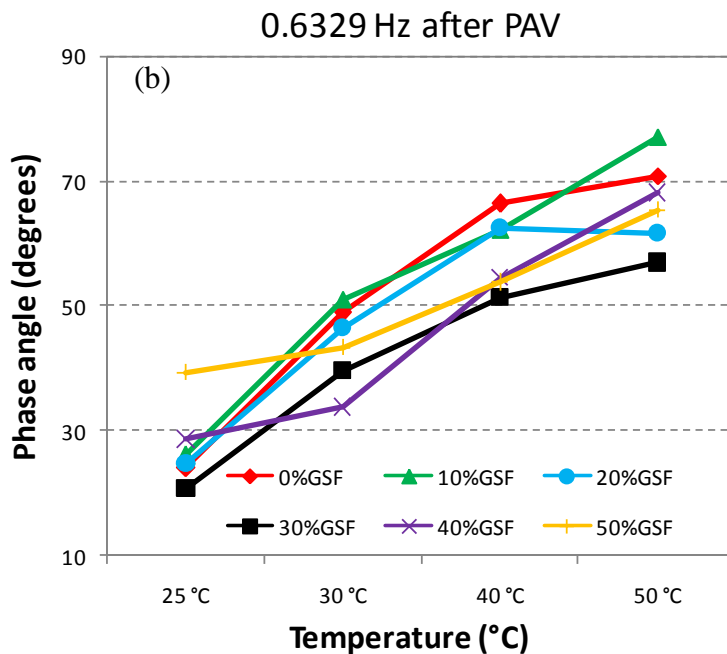


Figure 6.57 : Isochronal plots at 0.6329Hz for neat B50/70 bitumen and SEB groups made of B50/70 bitumen after long-term aging. (a) Complex modulus and (b) Phase angle.

Overall, aging demonstrated a stiffening effect by increasing the complex modulus and flattening out the plateau effect for the modulus as displayed in Figure 6.57 (a). As an example, 50% GSF content SEB demonstrates a large increase of the complex modulus, most probably due to a considerably larger amount of melting of the sulphur in bitumen matrix. A corresponding plateau effect for the same sample appeared very clearly in terms of complex modulus. This is a desirable phenomenon and an indication of improved elasticity, possibly causing an enhanced resistance to deformation of an asphaltic concrete pavement.

The decrease in phase angle, particularly at high temperature ranges, for all PAV-aged SEBs containing different amounts of GSF points out higher elasticity. This leads us to believe that the introduced sulphur forms a kind of crystal, gel, or network structure in the bitumen matrix after long-term aging. This becomes more evident when comparing DSR analysis at a lower frequency of 0.1Hz. Hence, the contribution of higher frequency to elastic behavior should be also taken into consideration.

A comparison was made among the properties of the long-term aged base bitumen by long-term aged SEBs with five different sulphur levels as shown in Table 6.50.

Owing to extension indices ($G^*_{SEB}/G^*_{B50/70}$), which are very close to 1.00, one can conclude that a small amount of GSF (10%) had almost no effect on the complex modulus of long-term aged base bitumen (1.09, 1.05, 1.22 and 1.49 at 25, 30, 40 and 50°C respectively).

Table 6.50 : Relative changes in complex modulus and aging index at 0.6329Hz following long-term aging.

Binder	Stage	Extension Indices ($G^*_{SEB}/G^*_{B50/70}$) at 0.6329 Hz				Aging Index (G^*_{PAV}/G^*_{UNAGED}) at 0.6329 Hz			
		25 °C	30 °C	40 °C	50 °C	25 °C	30 °C	40 °C	50 °C
B50/70	p	1.00	1.00	1.00	1.00	0.66	0.98	2.51	6.41
B50/70-10%GSF	p	1.09	1.05	1.22	1.49	0.87	1.65	6.89	23.16
B50/70-20%GSF	p	1.73	2.62	1.87	3.80	1.50	3.56	10.13	55.73
B50/70-30%GSF	p	1.05	1.27	1.51	3.25	2.05	1.11	1.90	10.64
B50/70-40%GSF	p	2.32	3.23	4.82	2.45	0.41	2.02	2.85	5.80
B50/70-50%GSF	p	1.47	2.87	4.11	6.98	1.16	2.55	3.25	32.66

Aging index (G^*_{PAV}/G^*_{UNAGED}) values shown in Table 6.50 clarify that at low temperature ranges PAV-aging had minimal influence on the rheological properties of both 50/70 penetration bitumen and SEB groups. However, increasing the temperature to over 40°C led the long-term aging to have a significant effect on the rheological properties of samples, which can be proved by the elevated aging index values.

SEBs composed of B50/70 and variable amount of GSF at 4.0Hz;

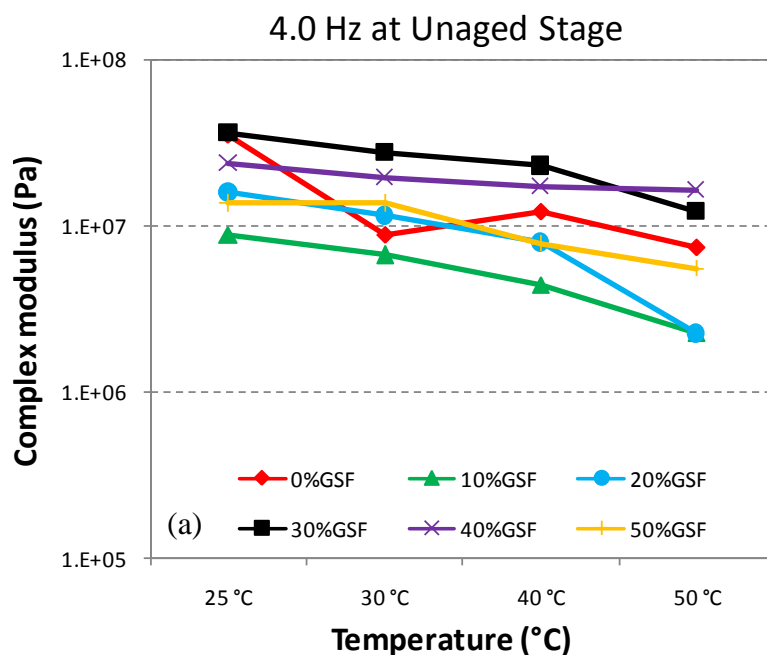
In order to investigate the effects of ultimate loading frequency (in this study) on both the base bitumen and SEB groups, the dynamic shear rheometer (DSR) test was performed at a frequency of 4.0Hz on each unaged sample. The obtained results are presented in Table 6.51 and the isochronal plots of complex modulus (G^*) and phase angles (δ) versus temperature domain are demonstrated in Figure 6.58 (a) and (b) respectively.

Increasing the loading frequency up to 4.0Hz led to the utmost increase in complex modulus values, which were more significant at elevated temperatures; the G^* curves became flatter over a wide range of tested temperatures as displayed in Figure 6.58 (a). This result indicates that increasing loading frequency served to maintain and even improve the elasticity of the SEBs and even make them less susceptible to any changes in temperature. This desirable effect is most probably due to the

development of both physically and chemically cross-linked networks of sulphur particles in the extended 50/70 penetration bitumen.

Table 6.51 : Values of rheological parameters for the B50/70 base bitumen and SEB groups at 4.0Hz before aging.

GSF	Stage	Complex Modulus at 4.0 Hz (Pa)				Phase Angle at 4.0 Hz (degree)			
		25 °C	30 °C	40 °C	50 °C	25 °C	30 °C	40 °C	50 °C
0%	o	3.57E+07	8.83E+06	1.23E+07	7.42E+06	39.74	66.38	71.75	80.29
10%	o	8.88E+06	6.66E+06	4.44E+06	2.28E+06	24.39	49.07	55.09	63.85
20%	o	1.58E+07	1.14E+07	7.95E+06	2.24E+06	31.77	48.80	68.52	76.59
30%	o	3.66E+07	2.75E+07	2.30E+07	1.22E+07	30.67	48.55	50.97	62.68
40%	o	2.37E+07	1.97E+07	1.72E+07	1.66E+07	20.52	16.24	33.28	54.21
50%	o	1.37E+07	1.37E+07	7.83E+06	5.55E+06	29.46	57.02	62.07	73.61



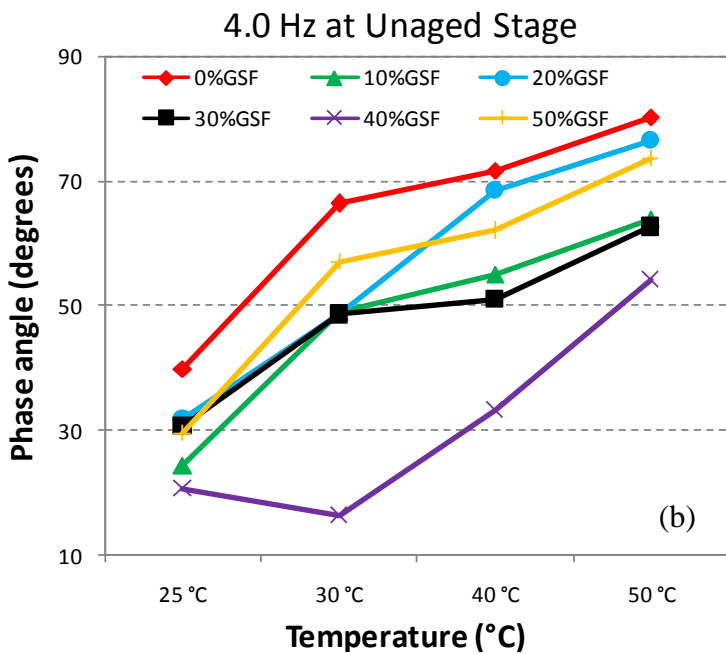


Figure 6.58 : Isochronal plots at 4.0Hz for neat B50/70 bitumen and SEB groups made of B50/70 bitumen before aging. (a) Complex modulus and (b) Phase angle.

On the other hand, rheological evaluation of the unaged binders with each other at 4.0Hz reveals that 10 and/or 20% sulphur-extended binders show little sharp tendency as compared with corresponding sulphur-free bitumen, indicating that these SEBs had relatively higher viscous responses. The differences in rheological properties might be attributed to a change in morphologies due to sulphur-extension. The introduction of low quantity GSF might facilitate the forming of viscous networks in bitumen phase, leading to the viscous improvement of the binder.

As illustrated in Figure 6.58 (b), the phase angle of the straight bitumen converges to 90°C with increasing temperatures. In this case, it displays almost pure viscous liquid behavior with scant elasticity due to insufficient stored energy per cycle of deformation. However, the varying trend of δ was slowed with even low amounts of sulphur extension. As mentioned before, 10 and/or 20%GSF SEBs led to a decline in complex modulus of the base bitumen. This paradox between decreased G^* and decreased δ once more again reveals the major role of the chemical structure on the sensitiveness of phase angle. As recorded in Table 6.51, with a further increase of sulphur quantity (30%), the δ values of the extended binder remained very close to that of the previous (10%GSF SEB). What is more noticeable is that the sequence of δ curves is not similar to the sequence seen for the G^* curves. This means that

varying amount of sulphur in straight bitumen could not cause a regular variation in phase angle values.

Since the rheology of sulphur-extended bitumen is strongly dependent on utilized content of GSF, the extension indices of G^* ($G^*_{SEB}/G^*_{B50/70}$) measuring relative changes in complex modulus for all five SEBs have been recorded at each temperature and at 4.0Hz in Table 6.52.

As also previously proved by its G^* curve drawn at the top of graph (Figure 6.58 (a)), the 30%GSF SEB has the maximum extension indices among the all extended binders (except at 50°C). Furthermore, its values greater than 1.00 at each test temperature again emphasize the enhanced elastic-like behavior compared with the neat bitumen.

Table 6.52 : Relative changes in complex modulus for the B50/70 base bitumen and SEB groups at 4.0Hz before aging.

Binder	Stage	Extension Indices ($G^*_{SEB}/G^*_{B50/70}$) at 4.0 Hz			
		25 °C	30 °C	40 °C	50 °C
B50/70	o	1.00	1.00	1.00	1.00
B50/70-10%GSF	o	0.25	0.75	0.36	0.31
B50/70-20%GSF	o	0.44	1.30	0.65	0.30
B50/70-30%GSF	o	1.03	3.12	1.87	1.64
B50/70-40%GSF	o	0.67	2.23	1.40	2.23
B50/70-50%GSF	o	0.38	1.55	0.64	0.75

The DSR test was conducted on the RTFOT-aged samples in order to investigate the changes in both complex modulus and phase angle after short-term aging. The isochronal plots of G^* and δ at 4.0Hz for both base bitumen and SEB group in their RTFOT-aged conditions are shown in Figure 6.59 (a) and (b) and the measured values are listed in Table 6.53.

Table 6.53 : Values of rheological parameters for the B50/70 base bitumen and SEB groups at 4.0Hz after short-term aging.

GSF	Stage	Complex Modulus at 4.0 Hz (Pa)				Phase Angle at 4.0 Hz (degree)			
		25 °C	30 °C	40 °C	50 °C	25 °C	30 °C	40 °C	50 °C
0%	r	5.58E+07	3.66E+07	1.29E+07	9.83E+06	33.61	42.59	64.11	67.60
10%	r	2.97E+08	4.21E+07	2.67E+07	1.03E+07	23.21	33.76	58.51	63.97
20%	r	6.63E+07	6.39E+07	5.78E+07	9.91E+06	27.22	34.96	61.58	66.08
30%	r	5.48E+07	4.94E+07	4.19E+07	1.01E+07	26.54	27.82	34.88	60.81
40%	r	1.10E+08	2.36E+07	1.63E+07	1.54E+07	28.95	28.22	20.74	29.96
50%	r	1.57E+08	3.66E+07	1.62E+07	1.83E+07	25.84	28.03	30.80	47.58

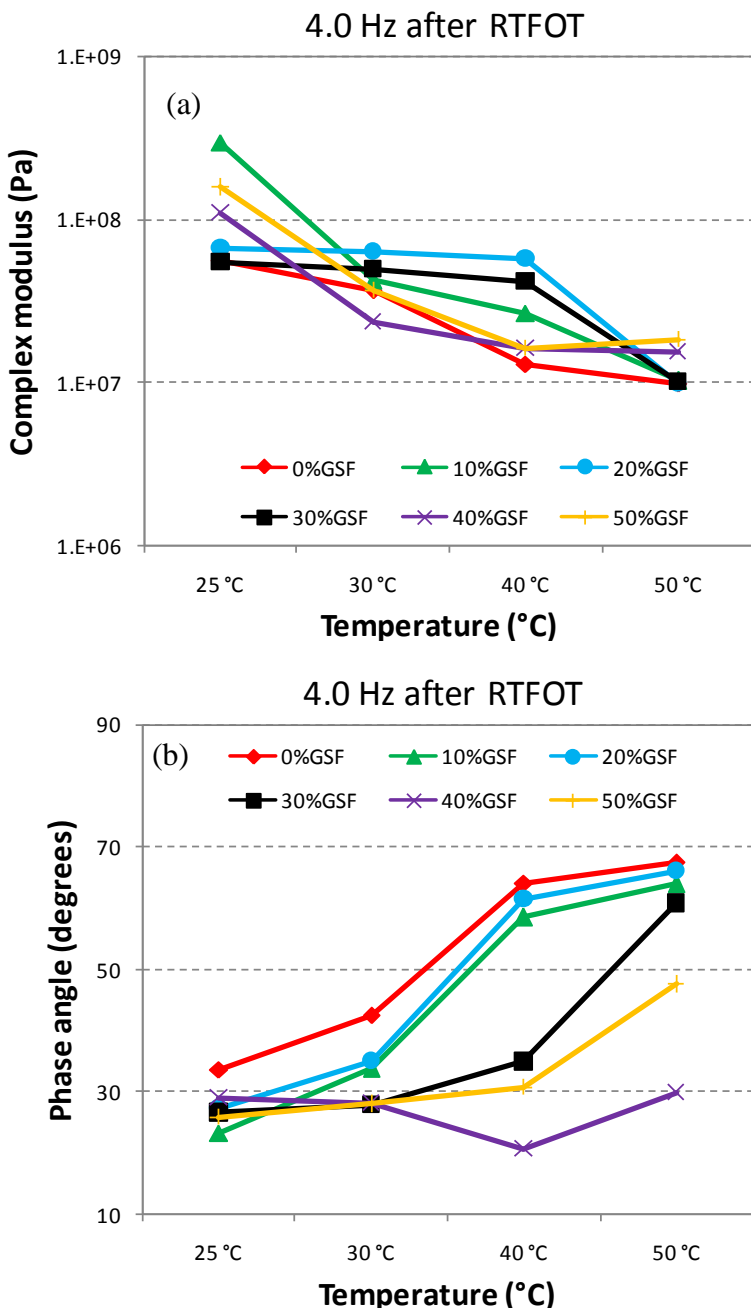


Figure 6.59 : Isochronal plots at 4.0Hz for neat B50/70 bitumen and SEB groups made of B50/70 bitumen after short-term aging. (a) Complex modulus and (b) Phase angle.

Figure 6.59 (a) demonstrates that the viscous effect of low sulphur amount (10 and 20%) on unaged neat bitumen was completely changed by short-term aging. It is assumed that the initial sulphuric viscous networks became elastic during the RTFOT process. The same figure also illustrates that increasing the sulphur quantity from 20 to 30% in aged neat bitumen does not remarkably change the complex modulus.

According to results listed in Table 6.53, G^* of the RTFOT residues are substantially higher than G^* of the unaged binders. In this sense, the significance of sulphur extension increases with aging. This approach reinforces the hope that the practical application of sulphur-extended binders might be convenient, particularly for hot climatic regions where the main aim is to increase as much as possible the restricted bitumen capability to endure high service temperatures with minimal permanent deformation.

As illustrated in Figure 6.59 (b), the δ curve of aged-neat bitumen is laid out at the top and its phase angle value is approaching 70° with increasing temperature. The presence of low sulphur quantity (up to 20%) caused a slight decrease in the δ values of the aged-neat bitumen. However, there is no distinctive variation between the curves of the 10 and 20%GSF SEBs after short-term aging. Their almost superimposed δ curves confirm their very close phase angle values, as listed in Table 6.53. The expected decrease in phase angle and as a result the increase in elasticity is observed after short-term aging and this trend becomes very apparent with increasing sulphur level. The enhanced elasticity can be attributed to more polysulfide bonds developed during RTFOT process which restricts the free movement of sulphur particles in bitumen phase.

In order to investigate the effect of short-term aging on the level of sulphur extension the extension indices of G^* ($G^*_{SEB}/G^*_{B50/70}$) measuring relative changes in viscoelastic response for all five SEBs have been recorded at each temperature and 4.0Hz and the outcomes are displayed in Table 6.54. Having been subjected to RTFOT aging, the SEB with 50%GSF had nearly the same viscoelastic behavior with its respective straight bitumen, particularly at intermediate temperature range (1.00 and 1.26 at 30 and 40°C respectively).

Table 6.54 : Relative changes in complex modulus and aging index at 4.0Hz following short-term aging.

Binder	Stage	Extension Indices ($G^*_{SEB}/G^*_{B50/70}$) at 4.0 Hz				Aging Index (G^*_{RTFOT}/G^*_{UNAGED}) at 4.0 Hz			
		25 °C	30 °C	40 °C	50 °C	25 °C	30 °C	40 °C	50 °C
B50/70	r	1.00	1.00	1.00	1.00	1.51	5.60	0.48	0.19
B50/70-10%GSF	r	5.32	1.15	2.07	1.04	3.73	0.94	2.14	4.50
B50/70-20%GSF	r	1.19	1.75	4.49	1.01	4.67	5.90	3.40	4.41
B50/70-30%GSF	r	0.98	1.35	3.26	1.03	2.97	2.51	0.55	0.24
B50/70-40%GSF	r	1.97	0.65	1.27	1.57	7.26	1.20	0.07	0.93
B50/70-50%GSF	r	2.81	1.00	1.26	1.86	15.58	4.31	0.76	2.15

The aging index showing the changes in the rheological characteristics of 50/70 penetration bitumen and SEB group after aging are also listed in Table 6.54. The aging index showing the changes in the rheological characteristics of 50/70 penetration bitumen and SEB group after aging is listed in Table 6.54. The aging index for 20%GSF SEB is 1.00 greater at each test temperature. This demonstrates that short-term aging had triggered the viscoelastic behavior of this SEB so that it demonstrates more elasticity (4.67, 5.90, 3.40 and 4.41 at 25, 30, 40, and 50°C respectively). Although the other specimens were also subjected to the same laboratory simulation of short-term aging via RTFOT, they could not increase their G^* values at each temperature.

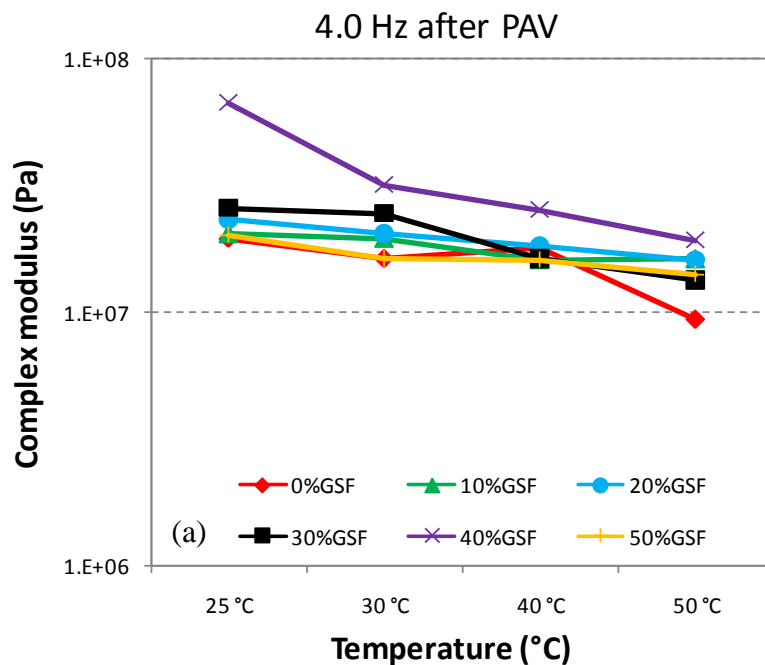
The change in viscoelastic behavior after PAV aging differs from both RTFOT aging and unaged condition. The values from the DSR test conducted on long-term aged samples are given in Table 6.55 and the isochronal plots of complex modulus and phase angle at 4.0Hz are displayed in Figure 6.60 (a) and (b) respectively.

The DSR analysis illustrates the significant influence of long-term aging on the rheological behavior of SEBs. It is believed that PAV-aging initiated the dissolution of a large portion of the sulphur particles in bitumen. It was this that led to the increase in the elastic behavior. Maximum G^* values were found in the 40%GSF SEB. An insignificant difference was noted in the complex modulus of other SEBs and neat bitumen particularly at 40°C (1.79E+07, 1.62E+07, 1.82E+07, 1.62E+07, and 1.62E+07Pa for neat bitumen, SEB with 10, 20, 30, and 50%GSF respectively). This reveals that the aforementioned SEBs have similar viscoelastic responses with each other after prolonged aging, as does neat bitumen at an intermediate temperature. However, when the test temperature is increased to 50°C, a remarkable drop in elastic behavior is clearly detected for the aged-free sulphur bitumen while

each SEB maintained its stiffness. These results suggest that 50/70 penetration bitumen is comparable to sulphur-extended binders at low and/or intermediate temperatures, but not at high temperatures (*where rutting is most likely probable*), due to the lack of polysulfide bonds.

Table 6.55 : Values of rheological parameters for the B50/70 base bitumen and SEB groups at 4.0Hz after long-term aging.

GSF	Stage	Complex Modulus at 4.0 Hz (Pa)				Phase Angle at 4.0 Hz (degree)			
		25 °C	30 °C	40 °C	50 °C	25 °C	30 °C	40 °C	50 °C
0%	p	1.96E+07	1.62E+07	1.79E+07	9.36E+06	65.12	71.99	64.82	84.96
10%	p	2.04E+07	1.95E+07	1.62E+07	1.62E+07	53.51	64.38	64.46	76.56
20%	p	2.32E+07	2.04E+07	1.82E+07	1.62E+07	24.32	37.15	58.19	69.28
30%	p	2.58E+07	2.45E+07	1.62E+07	1.33E+07	28.40	33.54	42.04	64.37
40%	p	6.73E+07	3.19E+07	2.54E+07	1.92E+07	29.55	38.31	55.66	73.40
50%	p	2.02E+07	1.62E+07	1.62E+07	1.42E+07	12.61	35.12	23.17	58.43



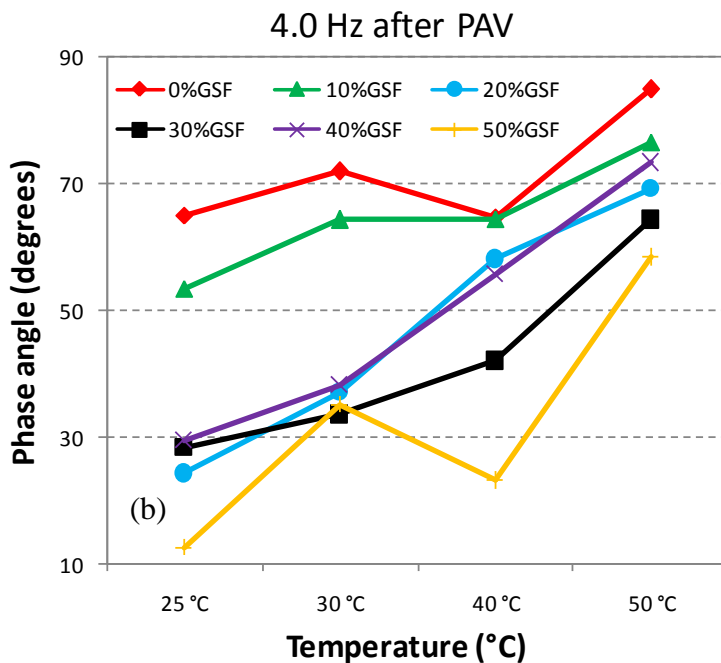


Figure 6.60 : Isochronal plots at 4.0Hz for neat B50/70 bitumen and SEB groups made of B50/70 bitumen after long-term aging. (a) Complex modulus and (b) Phase angle.

When we consider the phase angle values we see that the sequence noted for G^* curves has been lost for the δ curves. For instance, δ curve of SEB with 40%GSF is moderately placed among the other curves; however, as previously mentioned, its G^* curve is drawn at the top. What is more interesting about this SEB is that in spite of having been composed of a further extended sulphur level, it has almost the same phase angle values with the SEB with 20%GSF after long-term aging. This inconsistency once more emphasizes that the phase angle is much more dependent on the chemical composition of binders and aging phenomenon than are the G^* values.

A comparison was made among the properties of the long-term aged base bitumen with long term aged SEBs of five different sulphur levels, as shown in Table 6.56. Extension indices of SEB with 50%GSF are very close to 1.00, meaning that after prolonged aging this SEB is comparable to straight 50/70 penetration bitumen in terms of G^* values (1.03, 1.00, 0.90, and 1.51 at 25, 30, 40, and 50°C respectively). This case was also previously proved by its G^* curve, which is nearly superposed on that of neat bitumen.

Table 6.56 : Relative changes in complex modulus and aging index at 4.0Hz following long-term aging.

Binder	Stage	Extension Indices ($G^*_{SEB}/G^*_{B50/70}$) at 4.0 Hz				Aging Index (G^*_{PAV}/G^*_{UNAGED}) at 4.0 Hz			
		25 °C	30 °C	40 °C	50 °C	25 °C	30 °C	40 °C	50 °C
B50/70	p	1.00	1.00	1.00	1.00	0.53	2.48	0.67	0.18
B50/70-10%GSF	p	1.04	1.20	0.90	1.73	0.26	0.43	1.30	7.12
B50/70-20%GSF	p	1.19	1.26	1.01	1.73	1.64	1.88	1.07	7.21
B50/70-30%GSF	p	1.32	1.51	0.90	1.42	1.40	1.24	0.21	0.31
B50/70-40%GSF	p	3.44	1.97	1.42	2.05	4.43	1.62	0.11	1.16
B50/70-50%GSF	p	1.03	1.00	0.90	1.51	2.01	1.91	0.76	1.66

The impact of long term aging at 4.0Hz on the rheological behaviors with neat bitumen and sulphur extended binders are shown in Table 6.56. Despite the fact that a great benefit of long-term aging was expected on the PAV-aged samples, the resultant index values are not always greater than 1.00; conversely a few are even less than 1.00. The loss in G^* values is most likely due to the break-down of polysulfide bonds during pressure aging.

B70/100 and its derivatives

SEBs composed of B70/100 and variable amount of GSF at 10rad/sn (1.59Hz);

Developed to replace older and conventional bitumen tests, the Strategic Highway Research Program (SHRP) tests sought to take advantage of the recent rheological evaluations in order to analyze the ultimate properties of bituminous materials used in road pavements (Fu et al., 2007). To this end, the SHRP generated a specification based on the DSR results in order to prevent rutting and fatigue cracking. As mentioned previously in Section 5.2.2, in order to resist rutting, an unaged binder is expected to have a stiffness value ($G^*/\sin\delta$) greater than or at least equal to 1.0kPa at 1.59Hz (10rad/s). Moreover after short-term aging, the same sample is expected to have a stiffness value ($G^*/\sin\delta$) greater than, or at least equal to, 2.2kPa at 1.59Hz (10rad/s). In order to minimize fatigue cracking, a binder in service simulated by long-term aging should have a stiffness value ($G^*\sin\delta$) less than, or maximum equal to, 5.0MPa at 1.59Hz (10rad/s).

Curves of $G^*/\sin\delta$ versus temperature for base and sulphur-extended bitumen at 10 rad/s before aging are shown in Figure 6.61 and their stiffness values are given in Table 6.57.

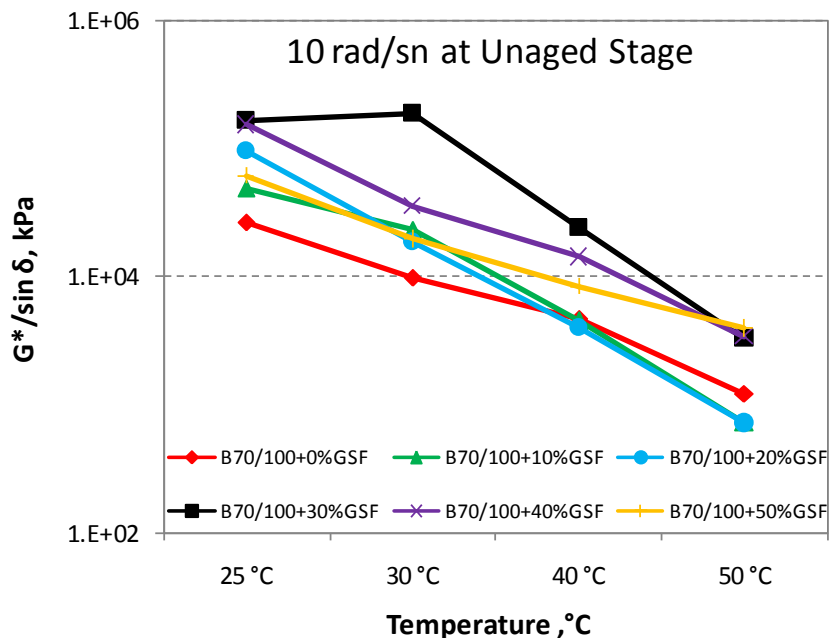


Figure 6.61 : $G^*/\sin \delta$ measured at 1.59Hz (10rad/s) as a function of temperature for B70/100 base bitumen and SEB groups with various GSF content before aging.

As can be deduced from Figure 6.61, the first two SEBs show similar linear viscoelastic behavior and functions over temperature range since their curves are very close to each other. The curves of the SEBs with 30, 40, 50%GSF are higher than those of base bitumen. In this case, this threesome demonstrates a remarkable resistance to rutting due most probably to the presence of sulphur networks in bitumen.

Table 6.57 : Stiffness values at different temperatures and 1.59Hz (10rad/sn) for B70/100 base bitumen and SEB groups with various GSF content before aging.

Binder	Stage	Stiffness Values, $G^*/\sin \delta$, (kPa)			
		25 °C	30 °C	40 °C	50 °C
B70/100	o	2.68E+04	1.00E+04	4.74E+03	1.22E+03
B70/100-10%GSF	o	4.92E+04	2.36E+04	4.52E+03	7.33E+02
B70/100-20%GSF	o	9.74E+04	1.90E+04	4.02E+03	7.22E+02
B70/100-30%GSF	o	1.68E+05	1.91E+05	2.46E+04	3.36E+03
B70/100-40%GSF	o	1.56E+05	3.59E+04	1.43E+04	3.41E+03
B70/100-50%GSF	o	6.24E+04	1.98E+04	8.41E+03	3.98E+03

As shown in Table 6.57, regardless of GSF proportion each SEB had a stiffness value greater than SHRP's requirement, 1kPa, as a criterion for the unaged binders. Since it is clear that the values for SEB groups already surpass the minimum requirement at 50°C, when $G^*/\sin \delta$ is equal to 1000Pa the temperature of each SEB

will undoubtedly significantly exceed 50°C. When compared to the stiffness values of the base bitumen, even though the first two SEBs (10 and 20%GSF) seem to have higher values at 25 and 30°C, their values dramatically decrease with increasing temperature and are relatively low at high temperatures. With regard to other hardness test results, these measurements are meaningful. This decrease in stiffness can be related to a low amount of GSF acting as a dispersed and dissolved agent instead of forming a network structure in neat bitumen. As GSF content increases, $G^*/\sin\delta$ of the SEBs increases at each temperature, which becomes apparent when the GSF content is 30%. At this content, the sulphur particles are believed to form a continuous network throughout the bituminous compounds. However, at GSF content over 30%, the magnitude of increase in $G^*/\sin\delta$ starts to decrease slightly. Hence, 30% sulphur extension can significantly improve resistance to rutting deformation and B70/100-30%GSF can be used at the highest service temperature. Despite this, it should be noted that these results are based on laboratory measurements and there is still a long way left to go and a lot to do in order to fully understand the rheology of SEB in the field.

It was considered quite important to re-check the rutting resistance of base B70/100 bitumen and SEB samples after short-term aging. Curves of $G^*/\sin\delta$ versus temperature for base and sulphur-extended bitumens at 10rad/s after RTFOT aging are shown in Figure 6.62 and their stiffness values are given in Table 6.58. According to Table 6.58, the stiffness values of all short-term aged SEBs at 10rad/s exceeded the desired minimum limitation (2.2kPa) and were in accordance with SHRP methodology. Similar to its behavior at unaged stage, the 10%GSF content SEB again demonstrated lower stiffness values at 25 and 30°C after aging. Besides these temperatures, this SEB was also observed to have lower rutting resistance at high temperature (50°C), when compared to the values of neat bitumen.

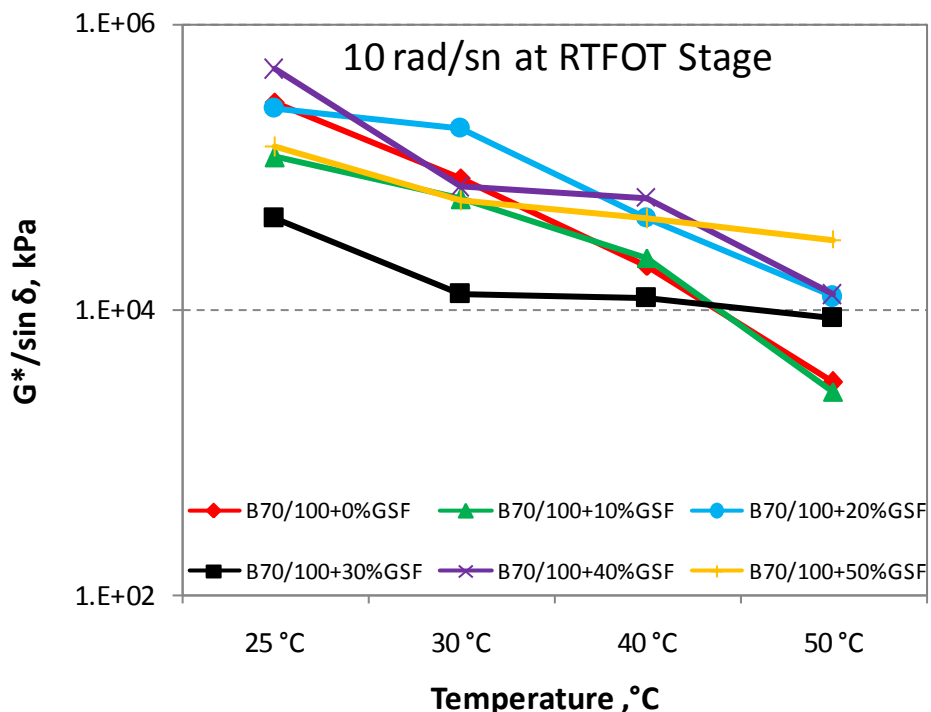


Figure 6.62 : $G^*/\sin\delta$ measured at 1.59Hz (10rad/s) as a function of temperature for B70/100 base bitumen and SEB groups with various GSF content after short-term aging.

As can be deduced from Figure 6.62, the curve of this sample remains very close to that of the B70/100-50%GSF at low temperature range (25 to 30°C); however, at moderate and high temperature range (30 to 50°C) it remains very close to that of neat bitumen. On the other hand, after short term aging, another low content GSF (20%) SEB virtually elevated its $G^*/\sin\delta$ curve and its values significantly surpassed those of neat B70/100 bitumen. This suggests that short-term aging improved the rutting resistance of the B70/100-20%GSF sample since it caused it to have a relatively high service temperature. However after same short-term aging process, a somewhat marked change is observed in the 30%GSF content SEB. Even though this sample was observed to have the highest stiffness values at the unaged stage, excepting at the highest temperature ranges RTFOT aging led to a decrease in stiffness values and the $G^*/\sin\delta$ curve became flatter over a wide range of tested temperatures. This indicates that for B70/100-30%GSF, the impact of RTFOT aging had a negative effect on reduced rutting resistance. This worsening influence of short-term aging on this sample can be attributed to the breakage of initial formed sulphur networks during RTFOT aging.

The further increases of sulphur levels in short-term aged SEBs did not cause a regular change in the stiffness value at increasing temperature. The $G^*/\sin\delta$ value of

short-term aged SEB at 40%GSF level is about 4 times higher than that of the short-term aged neat bitumen, whereas at 50% sulphur level it is nearly ten times higher than that of RTFOT-aged neat bitumen.

Table 6.58 : Stiffness values at different temperatures and 1.59Hz (10rad/sn) for B70/100 base bitumen and SEB groups with various GSF content after short-term aging.

Binder	Stage	Stiffness Values, $G^*/\sin\delta$, (kPa)			
		25 °C	30 °C	40 °C	50 °C
B70/100	r	2.81E+05	8.41E+04	2.03E+04	3.07E+03
B70/100-10%GSF	r	1.17E+05	5.93E+04	2.31E+04	2.68E+03
B70/100-20%GSF	r	2.54E+05	1.85E+05	4.36E+04	1.22E+04
B70/100-30%GSF	r	4.33E+04	1.30E+04	1.21E+04	8.80E+03
B70/100-40%GSF	r	4.81E+05	7.17E+04	6.05E+04	1.26E+04
B70/100-50%GSF	r	1.37E+05	5.76E+04	4.32E+04	3.04E+04

Fatigue cracking, also called crocodile cracking or alligator cracking, is a common type of distress in asphalt concrete pavements. This distress is termed "crocodile cracking" because the interconnecting or interlaced cracking in the asphalt layer resembles the hide of a crocodile, as illustrated in Figure 6.63 (University of Washington, 2010).



Figure 6.63 : Showing a typical fatigue cracking.

This common distress in asphalt pavements is most often triggered by surface failure brought on by several parameters. Although many parameters currently play major

roles in fatigue cracking, environmental effects, traffic loading, and unquestionably the binder in the pavement remain the direct causes. Since this study only focuses on revealing binder effects, here the effects of sulphur levels on base bitumen is studied in terms of fatigue cracking.

In order to investigate the resistance of SEB to fatigue cracking, pre-aged (via RTFOT) samples were exposed to long-term aging, then the dynamic shear rheometer (DSR) test was again conducted on these PAV-aged samples at 1.59Hz. Similar to the test process for RTFOT-aged samples, these long-term aged samples were conducted at 2.20kPa applied stress. Curves of $G^*\sin\delta$ versus temperature for base and sulphur-extended bitumens at 1.59Hz (10rad/s) after PAV aging are shown in Figure 6.64 and Table 6.59 lists their stiffness values at each test temperature.

As depicted in Figure 6.64, for the long-term aged neat bitumen, as test temperature decreases, the stiffness value increases in a sort of linear way. However, this linearity seems to disappear for the low GSF (10 and 20%) SEBs. Both of their curves are entirely higher than that of the neat bitumen. At further GSF extensions (30%), the $G^*\sin\delta$ curve became flatter over a wide range of tested temperatures, indicating that the stiffness values of this SEB change only very slightly with changing temperatures.

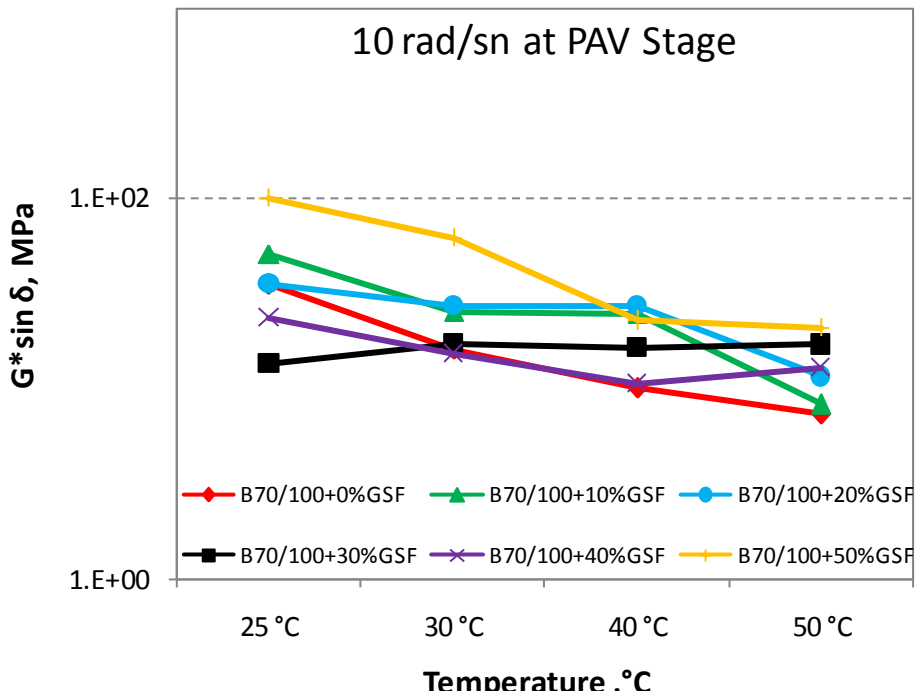


Figure 6.64 : $G^* \sin \delta$ measured at 1.59Hz (10rad/s) as a function of temperature for B70/100 base bitumen and SEB groups with various GSF content after long-term aging.

At 40%GSF content, the isochronal plot of $G^* \sin \delta$ does indicate a negligible difference in resistance to fatigue cracking between the base bitumen and the SEB, particularly at the upper and lower ends of the temperature domain at the frequency of 1.59Hz. However, from 40 to 50%GSF level, the SEB begins to act in a completely different rheological way.

Listed in Table 6.59, all PAV-aged extensions of B70/100 met the obligatory specification even at the lowest test temperature (25°C), as SHRP requires long-term aged binder's stiffness values ($G^* \sin \delta$) to be less than 5.0MPa in order to prevent fatigue cracking. Hence there is no doubt that when $G^* \sin \delta$ is equal to 5.0MPa, the temperature of each SEB will be much lower than 25°C .

The DSR results and calculations in this study show that 70/100 penetration bitumen containing low level sulphur (10 and 20%) both showed higher values for fatigue cracking parameter $G^* \sin \delta$ than the free-sulphur-bitumen at temperature domain according to SHRP specifications. Extending neat bitumen to 20%GSF significantly increased the value of this parameter, although this was higher for 10%GSF than it was for 20%GSF at low temperatures.

Table 6.59 : Stiffness values at different temperatures and 1.59Hz (10rad/sn) for B70/100 base bitumen and SEB groups with various GSF content after long-term aging.

Binder	Stage	Stiffness Values, $G^* \sin\delta$, (MPa)			
		25 °C	30 °C	40 °C	50 °C
B70/100	p	3.50E+01	1.61E+01	1.00E+01	7.29E+00
B70/100-10%GSF	p	5.08E+01	2.52E+01	2.47E+01	8.23E+00
B70/100-20%GSF	p	3.57E+01	2.74E+01	2.73E+01	1.15E+01
B70/100-30%GSF	p	1.35E+01	1.73E+01	1.65E+01	1.70E+01
B70/100-40%GSF	p	2.34E+01	1.54E+01	1.06E+01	1.30E+01
B70/100-50%GSF	p	9.99E+01	6.20E+01	2.27E+01	2.08E+01

Although the behavior of P-B70/100-40%GSF relative to its respective base bitumen seems to be different, the stiffness values at 30 and 40°C are almost identical. Increasing the amount of GSF up to 50% in neat bitumen resulted in a noticeable difference for the fatigue cracking parameter at each test temperature (increase from 35.04 to 99.92MPa at 25°C, from 16.08 to 62.04MPa at 30°C, from 10.00 to 22.70MPa at 40°C, and from 7.29 to 20.79MPa at 50°C).

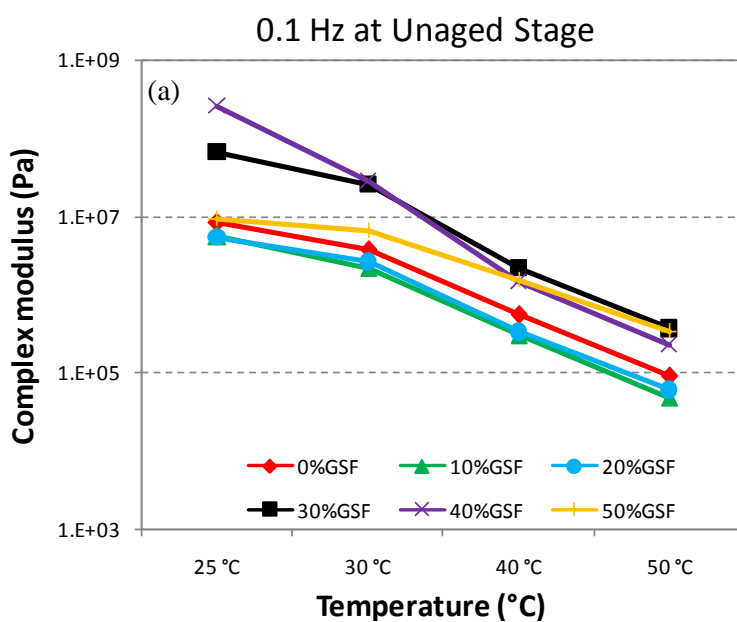
SEBs composed of B70/100 and variable amount of GSF at 0.1Hz;

Rheological parameter values at unaged stage and at 0.1Hz for the unaged base 70/100 bitumen and SEBs are presented in Table 6.60. In addition, the isochronal plots of complex modulus (G^*) and phase angle (δ) versus temperature at 0.1Hz for both are shown in Figure 6.65 (a) and (b) respectively. Unlike the conventional B70/100 straight bitumen properties, the isochronal plots show remarkable differences between 10%GSF and 20%GSF SEBs at each of the temperatures, and at a frequency as low as 0.1Hz. Compared to their respective base bitumen, the decrease in G^* for both SEBs is marked at the temperature domain, which illustrates the weakened elastic response of this extended binder pair. As was the case with the penetration and softening point tests, this decrease in complex modulus gives an obvious indication of the softening effect of 10% and 20%GSF extension. Therefore, laboratory test results demonstrate that 10% and 20%GSF SEBs will be more durable in terms of low temperature cracking. However, it should be noted that the results in the field may vary. For 30 and 40%GSF content SEBs, the significant increase in G^* occurs over the entire temperature domain, indicating an improved compatibility of the sulphur-bitumen system, and – as a consequence – enhanced rheological

characteristics. The complex modulus isochrones clearly demonstrate the increased complex modulus indicating the improved elastic response of these two sulphur-extended binders compared to their respective B70/100 base bitumen. What is more noticeable is the increased complex modulus regardless of temperature degree. This increase in elastic behavior over the entire temperature domain can be associated with the viscosity of the base bitumen. Because the viscosity is sufficiently low, the elastic network of the sulphur particles can affect the mechanical properties of the SEBs. Although a further increase in the amount of GSF caused a considerable change in the behavior of the SEB relative to its respective base bitumen at high temperatures, the same trend cannot be seen at low temperatures. The values of G^* for the SEB with 50%GSF and base bitumen at low temperature are almost identical.

Table 6.60 : Values of rheological parameters for the B70/100 base bitumen and SEB groups at 0.1Hz before aging.

Binder	Stage	Complex Modulus at 0.1 Hz (Pa)				Phase Angle at 0.1 Hz (degree)			
		25 °C	30 °C	40 °C	50 °C	25 °C	30 °C	40 °C	50 °C
B70/100	o	8.16E+06	3.66E+06	5.45E+05	8.93E+04	77.92	80.97	87.77	87.95
B70/100-10%GSF	o	5.50E+06	2.16E+06	2.94E+05	4.70E+04	78.43	79.67	85.23	86.66
B70/100-20%GSF	o	5.35E+06	2.59E+06	3.30E+05	5.94E+04	72.82	78.44	80.51	83.55
B70/100-30%GSF	o	6.54E+07	2.53E+07	2.14E+06	3.65E+05	51.34	60.42	76.47	80.73
B70/100-40%GSF	o	2.59E+08	2.80E+07	1.43E+06	2.26E+05	68.46	78.19	84.56	87.75
B70/100-50%GSF	o	9.14E+06	6.58E+06	1.53E+06	3.36E+05	59.82	73.80	79.26	82.97



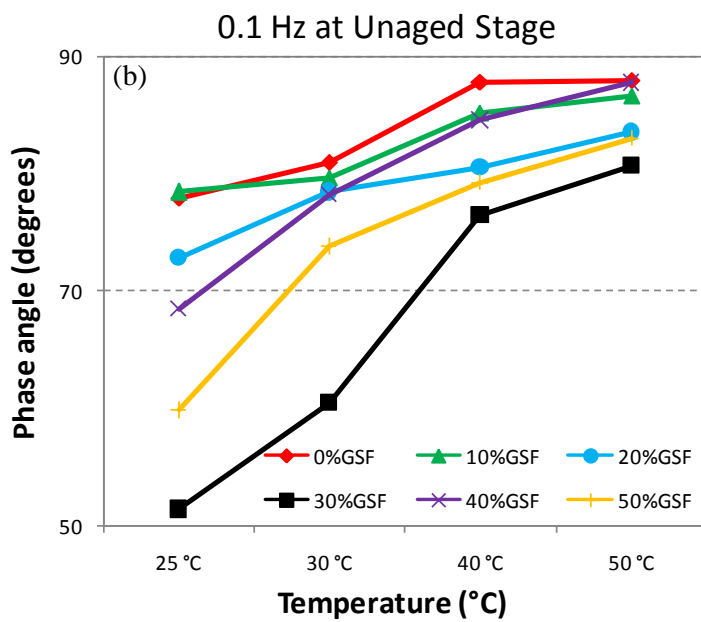


Figure 6.65 : Isochronal plots at 0.1Hz for neat B70/100 bitumen and SEB groups made of B70/100 bitumen before aging (a) Complex modulus (b) Phase angle.

Measurements of phase angle (δ) are generally considered to be more sensitive to chemical structure and, therefore, the extension of bitumen than complex modulus (Gordon, 2003b). The phase angle isochrones clearly show a relative change in δ with sulphur extension at each temperature. Although there is a slight difference between the values of the conventional bitumen and SEB with 10%GSF content, overall a significant reduction in δ occurs with further sulphur extension, particularly at 30%GSF. Whereas the phase angle of the straight B70/100 bitumen converges to 90° (*a δ value of exactly 90° corresponding to a perfect viscous behavior*) with increasing temperatures predominantly with viscous behavior, the presence of GSF remarkably enhances the elastic response of the extended binders.

The extension indices of G^* ($G^*_{\text{SEB}}/G^*_{\text{B70/100}}$) indicating relative changes in complex modulus for all five SEBs have been recorded at each temperature and at 0.1Hz in Table 6.61. The results indicate that there are more uniform differences in the extension indices of G^* especially for the first two SEBs. However with increasing GSF contents, this uniformity was lost and differences are more pronounced at low temperature (25°C). For instance, the extension indices of G^* are equal to 8.01 and 31.80 for the 30 and 40%GSF content SEBs respectively. Contrary to expectations, an additional amount of GSF (50%) did not cause an increase in the indices, while the gap between G^* values even seemed to decline.

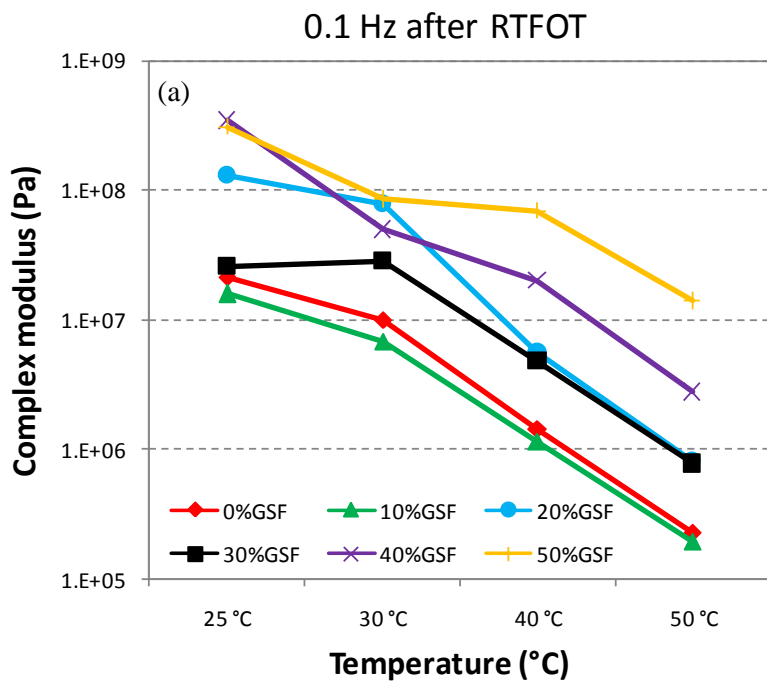
Table 6.61 : Relative changes in complex modulus for the B70/100 base bitumen and SEB groups at 0.1Hz before aging.

Binder	Stage	Extension Indices ($G^*_{SEB}/G^*_{B70/100}$) at 0.1 Hz			
		25 °C	30 °C	40 °C	50 °C
B70/100	o	1.00	1.00	1.00	1.00
B70/100-10%GSF	o	0.67	0.59	0.54	0.53
B70/100-20%GSF	o	0.66	0.71	0.61	0.66
B70/100-30%GSF	o	8.01	6.92	3.93	4.08
B70/100-40%GSF	o	31.80	7.67	2.62	2.53
B70/100-50%GSF	o	1.12	1.80	2.81	3.76

In order to reveal the aging effect, the rheological parameter values at 0.1Hz belonging to both the short-term aged base 70/100 bitumen and short-term aged SEB groups are given in the Table 6.62. In addition, isochronal plots of complex modulus (G^*) and phase angle (δ) versus temperature at 0.1Hz for both are shown in Figure 6.66 (a) and (b) respectively. Similar to its rheological behavior before aging, the 10%GSF content SEB demonstrated a less complex modulus than the neat bitumen. However for other SEBs, even the SEB with 20%GSF, a great increase in G^* is obvious. This increase in G^* can be attributed to two major facts: On the one hand, aging causes inevitable changes in the chemical components of pure bitumen. During the aging process, an alteration in both the quantity and quality of asphaltenes and resins is expected to occur. The increase in both asphaltenes and resins amounts is a direct result of the effect that aging has on the elastic properties of the bitumen (Zhang et al., 2010). Secondly, the rearrangement of sulphur particles in bitumen compounds during the aging process is supposed to increase the complex modulus of SEBs. Although they have different amount of GSF as an extender, the SEBs with 20 and 30%GSF seemed to have a nearly identical complex modulus at high temperatures.

Table 6.62 : Values of rheological parameters for the B70/100 base bitumen and SEB groups at 0.1Hz after short-term aging.

Binder	Stage	Complex Modulus at 0.1 Hz (Pa)				Phase Angle at 0.1 Hz (degree)			
		25 °C	30 °C	40 °C	50 °C	25 °C	30 °C	40 °C	50 °C
B70/100	r	2.15E+07	1.01E+07	1.46E+06	2.29E+05	70.39	73.53	84.32	86.27
B70/100-10%GSF	r	1.58E+07	6.78E+06	1.17E+06	1.95E+05	38.17	66.39	79.51	85.14
B70/100-20%GSF	r	1.30E+08	7.94E+07	5.55E+06	8.22E+05	30.80	68.56	70.94	79.28
B70/100-30%GSF	r	2.60E+07	2.85E+07	4.79E+06	7.83E+05	45.70	55.46	73.09	75.48
B70/100-40%GSF	r	3.45E+08	4.97E+07	2.00E+07	2.78E+06	27.69	34.35	64.28	77.05
B70/100-50%GSF	r	3.05E+08	8.51E+07	6.99E+07	1.40E+07	39.90	40.58	45.12	47.89



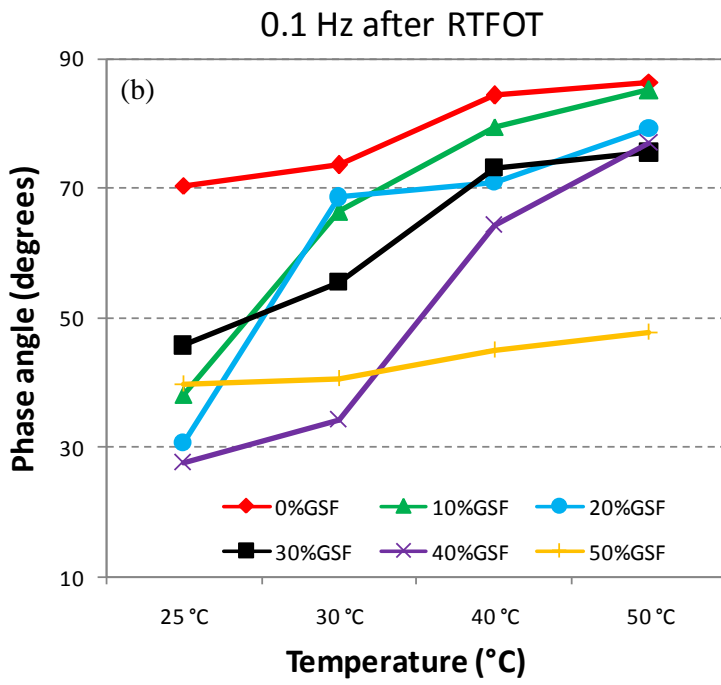


Figure 6.66 : Isochronal plots at 0.1Hz for neat B70/100 bitumen and SEB groups made of B70/100 bitumen after short-term aging. (a) Complex modulus and (b) Phase angle.

With RTFOT aging, the values of phase angle are decreased over the whole range and the phase angle curves are lowered correspondingly. These changes in values are noticeable. Even though the complex modulus curve of the SEB with 10%GSF content could not elevate over that of the neat bitumen, its phase angle curve is clearly lowered under that of the neat bitumen after short-term aging. For the short-term aged SEB with 20%GSF, an obvious plateau zone appears between 30 and 40°C. The pronounced plateau indicates the formation of an extreme sulphur network structure in bitumen. Among the all short-term aged samples, the SEB with 50%GSF seems the least sensitive to change in temperature since its phase angle curve becomes nearly flat due to its high percentage of GSF.

Table 6.63 displays both the extension indices of G^* ($G^*_{\text{SEB}}/G^*_{\text{B70/100}}$) and aging index parameter ($G^*_{\text{RTFOT}}/G^*_{\text{UNAGED}}$). It can be seen that the extension indices seems to be greater than 1.00 at each temperature (25 to 50°C) and at 0.1Hz for the all short-term extended binders, except the one containing 10%GSF, which points to the hardening of these SEBs following sulphur extension. Although the SEB with 10%GSF content considerably increased its complex modulus after short-term aging, this increase in the values does not surpass those of short-term aged neat bitumen.

Table 6.63 : Relative changes in complex modulus and aging index at 0.1Hz following short-term aging.

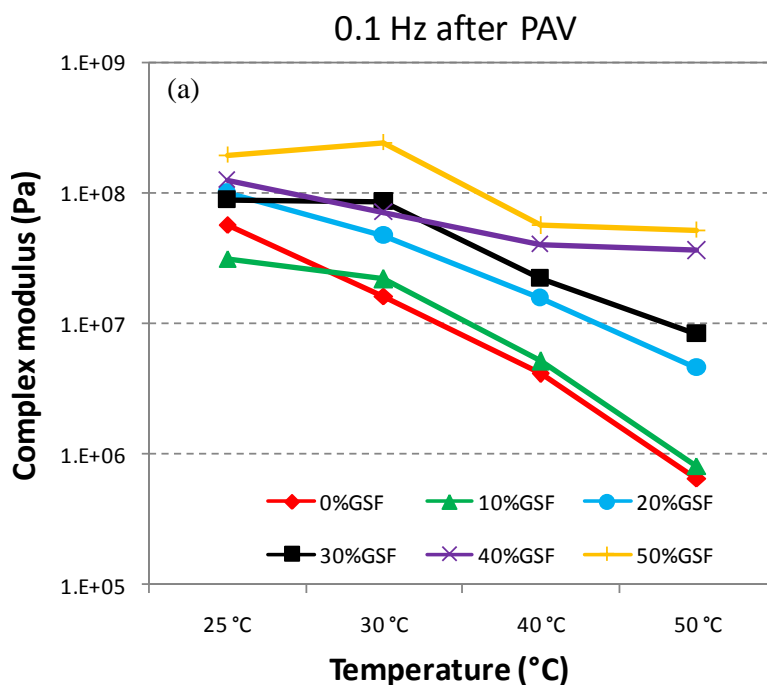
Binder	Stage	Extension Indices ($G^*_{SEB}/G^*_{B70/100}$) at 0.1 Hz				Aging Index (G^*_{RTFOT}/G^*_{UNAGED}) at 0.1Hz			
		25 °C	30 °C	40 °C	50 °C	25 °C	30 °C	40 °C	50 °C
B70/100	r	1.00	1.00	1.00	1.00	2.64	2.76	2.68	2.56
B70/100-10%GSF	r	0.74	0.67	0.80	0.85	2.88	3.13	3.96	4.14
B70/100-20%GSF	r	6.04	7.86	3.80	3.59	24.28	30.67	16.82	13.86
B70/100-30%GSF	r	1.20	2.82	3.28	3.42	0.40	1.13	2.24	2.15
B70/100-40%GSF	r	16.01	4.92	13.66	12.16	1.33	1.77	13.97	12.33
B70/100-50%GSF	r	14.14	8.42	47.86	61.32	33.32	12.92	45.65	41.81

As can be deduced from the same table, short-term aging yielded a uniform change on the complex modulus of neat bitumen since its aging index values over temperature domain are very close to each other: 2.64, 2.76, 2.68 and 2.56 respectively. Among all SEBs, the 30%GSF content SEB seems to have the fewest aging index parameters over temperature domain. However, the SEB with 50%GSF is clearly the most vulnerable to short-term aging in terms of aging index.

The influence of long-term aging on the rheological behavior of the neat B70/100 bitumen and SEB groups is shown in Figure 6.67 (a) and (b) and their values are given in Table 6.64. It can be seen that rheological parameters of long term-aged samples differ considerably from those of the both unaged and RTFOT aged samples. After PAV aging, there is an increase on the complex modulus and a reduction on the phase angle, indicating the improvement on the high-temperature performance. However, the evident increase in G^* and a remarkable decrease of the phase angle over the temperature domain after PAV aging are understandably greater than after RTFOT aging respectively, due to the prolonged aging process in the PAV. Unlike its behavior both before aging and after short-term aging, other than at low temperature the 10%GSF SEB did not have lower G^* values than those of pure bitumen. As a consequence, this proves that long-term aging ultimately led the 10%GSF extension to improve the rheological behavior of pure bitumen at 0.1Hz due to prolonged aging process. Considering their permanent values, among all SEBs, including the straight bitumen, the SEB containing 50%GSF is seen to have the highest complex modulus; 1.94E+08, 2.43E+08, 5.63E+07, and 5.20E+07Pa respectively.

Table 6.64 : Values of rheological parameters at 0.1Hz following sulphur extension.

Binder	Stage	Complex Modulus at 0.1Hz (Pa)				Phase Angle at 0.1 Hz (degree)			
		25 °C	30 °C	40 °C	50 °C	25 °C	30 °C	40 °C	50 °C
B70/100	p	5.73E+07	1.64E+07	4.11E+06	6.53E+05	43.19	52.31	75.59	82.44
B70/100-10%GSF	p	3.13E+07	2.19E+07	5.12E+06	8.14E+05	36.59	51.44	72.58	76.44
B70/100-20%GSF	p	1.02E+08	4.75E+07	1.59E+07	4.56E+06	47.16	36.52	44.60	55.72
B70/100-30%GSF	p	8.95E+07	8.56E+07	2.22E+07	8.43E+06	38.26	44.71	46.15	61.78
B70/100-40%GSF	p	1.26E+08	7.15E+07	4.05E+07	3.63E+07	43.96	45.50	46.67	44.62
B70/100-50%GSF	p	1.94E+08	2.43E+08	5.63E+07	5.20E+07	34.52	44.40	44.08	55.80



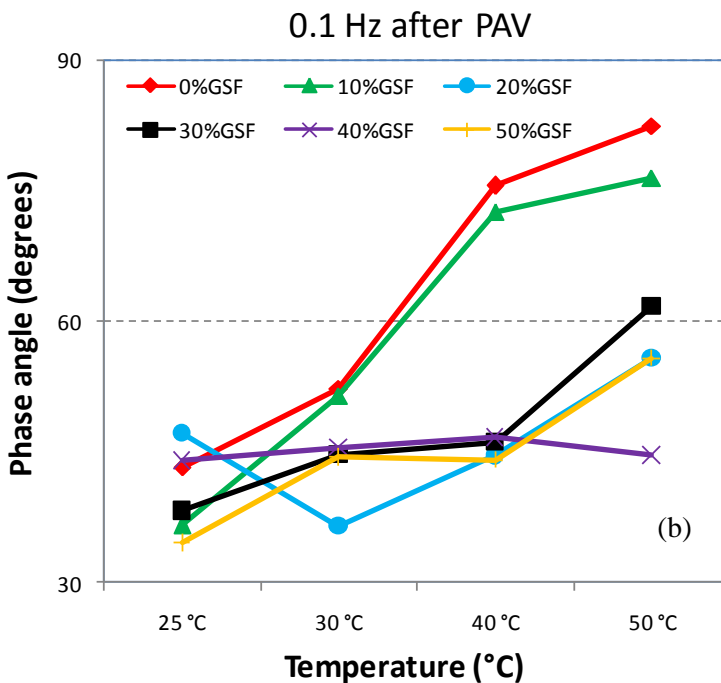


Figure 6.67 : Isochronal plots at 0.1Hz for neat B70/100 bitumen and SEB groups made of B70/100 bitumen after long-term aging. (a) Complex modulus and (b) Phase angle.

Owing to the sensibility of phase angle, the change in the chemical structure of the SEBs can be detected by the plot of phase angles versus temperature. In Figure 6.67 (b), the flat phase angle curve demonstrates the presence of two distinctive plateau regions. The first one is visible between 30 and 40°C for the SEBs with 30 and 50%GSF content. The second occurs over temperature domain for the SEB with 40%GSF content. These two plateaus clarify the formation of a significant elastic network of sulphur particles in bitumen matrix and reveal the insensibility of phase angle to temperature change. On the other hand, in case of 10%GSF content, the SEB whose rheological behavior remains very close to that of neat bitumen is susceptible to changes in temperature. This variation in the plots of phase angle versus temperature is unquestionably attributed to differing amounts of GSF and thus the further molecular interactions between sulphur particles and bitumen compounds (e.g. ratio of dispersion, dissolution, crystallization).

The extension indices of G^* ($G^*_{SEB}/G^*_{B70/100}$) and long-term aging index parameter (G^*_{PAV}/G^*_{UNAGED}) are given in Table 6.65. Since the B70/100-10%GSF seems to be similar to pure bitumen after long-term aging, its extension indices are very close to 1 (0.55, 1.34, 1.25, and 1.25 respectively). However, in terms of viscoelastic response of the binder, the increased extension indices with increasing amount of

GSF clearly reveal distinctions between the base bitumen and SEBs. In this sense, B70/100-50%GSF with its high extension indices amply illustrates the huge gap in complex modulus (3.39, 14.86, 13.69, and 79.53 respectively).

Table 6.65 : Relative changes in complex modulus and aging index at 0.1Hz following long-term aging.

Binder	Stage	Extension Indices ($G^*_{SEB}/G^*_{B70/100}$) at 0.1 Hz				Aging Index (G^*_{PAV}/G^*_{UNAGED}) at 0.1Hz			
		25 °C	30 °C	40 °C	50 °C	25 °C	30 °C	40 °C	50 °C
B70/100	p	1.00	1.00	1.00	1.00	7.03	4.48	7.54	7.32
B70/100-10%GSF	p	0.55	1.34	1.25	1.25	5.69	10.13	17.40	17.32
B70/100-20%GSF	p	1.78	2.90	3.86	6.98	19.01	18.33	48.14	76.84
B70/100-30%GSF	p	1.56	5.23	5.41	12.90	1.37	3.39	10.38	23.13
B70/100-40%GSF	p	2.19	4.37	9.84	55.48	0.48	2.55	28.34	160.56
B70/100-50%GSF	p	3.39	14.86	13.69	79.53	21.28	36.95	36.76	154.72

From the same table, it can be understood that there are irregular and substantial changes in the aging indexes of each SEB. In other words, the change in aging index with increasing temperature seems to occur in a kind of exponential way. This huge increase after long-term aging is believed to occur as a result of the formation of additional polysulfide bonds among bitumen compounds during the PAV process. However, the increase in aging index values for long-term aged pure bitumen remain relatively uniform and lower (7.03, 4.48, 7.54, and 7.32 respectively over temperature domain).

SEBs composed of B70/100 and variable amount of GSF at 0.2517Hz;

In order to clarify the effects of frequency change on both the base bitumen and SEB groups, the rheological properties of each sample before aging was investigated at a relatively higher frequency, 0.2517Hz. The obtained results are presented in Table 6.66 and the isochronal plots of complex modulus (G^*) and phase angles (δ) versus temperature domain are demonstrated in Figure 6.68 (a) and (b) respectively. Similar to 0.1Hz, 10 and 20%GSF utilization lowered the complex modulus curve of the base bitumen, thus indicating an improved viscous response of the base bitumen with sulphur extension, not only at 0.1Hz but also at 0.2517Hz. Even though this extended binder pair contains completely different amounts of GSF, the difference between their complex modulus curves is almost indistinguishable, as shown in Figure 6.68 (a). These results seem to confirm the drawn conclusions on the softening effect of sulphur extension up to 20% the amount of GSF.

There is a considerable change in complex modulus with further sulphur extension. In cases of 30 and/or 40%GSF utilization, the elevated complex modulus curves are quite distinctive, as shown in Figure 6.68 (a). This elevation can be related to the reaction of additional sulphur particles in bitumen matrix. At low portion of GSF (up to 20%) of sulphur particles are supposed to create fairly viscous network, but once the amount of GSF approaches to 30 and/or 40%, new additional sulphur particles will be capable of creating new polysulfide bonds that allow the SEB to enhance its rheological properties. Although increasing the amount of GSF up to 50%GSF yielded a marked increase in complex modulus between 40 and 50°C, identical to that seen for B70/100-30%GSF, the behavior at low and moderate temperature (25 to 30°C) does not differ from that of neat bitumen.

Consistent with complex modulus results, phase angles of both B70/100-10%GSF and B70/100-20%GSF are higher than that of the base bitumen. As can be seen in Figure 6.68 (b), the magnitude of the increase in phase angle is more obvious for 10%GSF content. Unlike its relatively lowered values at the lowest loading frequency (0.1Hz), this time phase angles of B70/100-20%GSF are elevated over that of base bitumen at 0.2517Hz.

Table 6.66 : Values of rheological parameters for the B70/100 base bitumen and SEB groups at 0.2517Hz before aging.

Binder	Stage	Complex Modulus at 0.2517 Hz (Pa)				Phase Angel at 0.2517 Hz (degree)			
		25 °C	30 °C	40 °C	50 °C	25 °C	30 °C	40 °C	50 °C
B70/100	o	1.90E+07	1.25E+07	1.34E+06	2.24E+05	62.29	66.49	81.58	89.06
B70/100-10%GSF	o	2.29E+07	4.58E+06	7.11E+05	1.16E+05	76.82	80.93	85.99	87.63
B70/100-20%GSF	o	1.26E+07	5.02E+06	7.25E+05	1.35E+05	67.74	73.81	82.02	82.66
B70/100-30%GSF	o	1.93E+08	3.50E+07	4.60E+06	8.11E+05	45.59	55.06	82.96	82.69
B70/100-40%GSF	o	3.12E+08	3.99E+07	3.45E+06	5.40E+05	35.80	54.74	82.65	89.00
B70/100-50%GSF	o	2.52E+07	1.27E+07	4.50E+06	7.73E+05	38.81	51.22	78.69	84.42

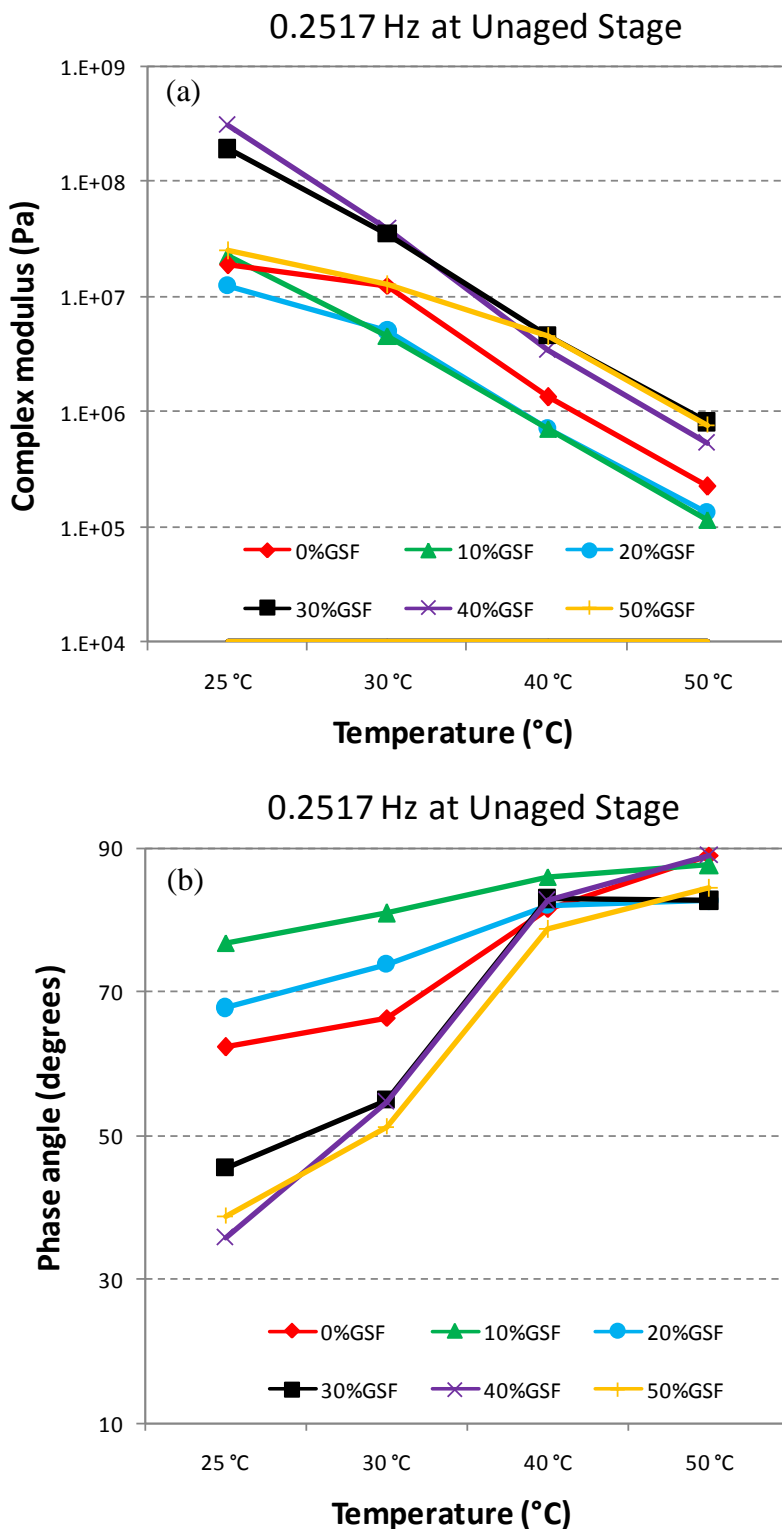


Figure 6.68 : Isochronal plots at 0.2517Hz for neat B70/100 bitumen and SEB groups made of B70/100 bitumen before aging. (a) Complex modulus and (b) Phase angle.

The other SEBs consisting of GSF over 20%, where the increased amount of sulphur considerably dominates the rheological behavior of the base bitumen, are shown to have relatively lower phase angles.

The extension indices of G^* ($G^*_{SEB}/G^*_{B70/100}$) measuring relative changes in complex modulus for all five SEBs have been recorded at each temperature and at 0.2517Hz in Table 6.67. Values of B70/100-20%GSF indicate that the magnitude of decrease in its complex modulus is similar at each temperature; 0.66, 0.40, 0.54, and 0.60 respectively. The behavior of the increase in extension indices with increasing further amount of GSF and increasing temperature is observed. However, in the cases of 30% and 40%GSF content, here the behavior of the G^* differs from that observed especially before 30°C in that the magnitude of the increase in G^* rises sharply due to the dominant effect of the sulphur phase.

Table 6.67 : Relative changes in complex modulus for the B70/100 base bitumen and SEB groups at 0.2517Hz before aging.

Binder	Stage	Extension Indices ($G^*_{SEB}/G^*_{B70/100}$) at 0.2517 Hz			
		25 °C	30 °C	40 °C	50 °C
B70/100	o	1.00	1.00	1.00	1.00
B70/100-10%GSF	o	1.21	0.37	0.53	0.52
B70/100-20%GSF	o	0.66	0.40	0.54	0.60
B70/100-30%GSF	o	10.13	2.80	3.43	3.62
B70/100-40%GSF	o	16.40	3.19	2.57	2.41
B70/100-50%GSF	o	1.33	1.02	3.36	3.45

The aging dependence of rheological behavior for base bitumen and SEB groups has been assessed at 0.2517Hz. The obtained results are presented in Table 6.68 and the isochronal plots of complex modulus (G^*) and phase angles (δ) versus temperature domain are demonstrated in Figure 6.69 (a) and (b) respectively. It is clear that after short term aging, the B70/100-10%GSF sample had a viscoelastic response (complex modulus) that was quite similar to that of neat bitumen. However, at temperatures higher than 30°C, even short-term aging could not cause its values to exceed those of neat bitumen. This illustrates an increased stubborn viscous response as indicated by the decreased G^* . On the other hand, plots (isotherms) for the SEBs with 40 and 50%GSF content demonstrate that extension of natural bitumen with these sulphur amounts resulted in fairly increased binder stiffness at short-term aged stage, however, 40%GSF extension appears to cause much more stiffness than 50%GSF extension does at moderate temperatures (30 and 40°C). After short-term aging, neat bitumen and the first trio of SEBs (with 10, 20, and 30%GSF) appear to have nearly

identical viscoelastic behavior at the temperature of 30°C. In other words, this temperature degree is a kind of intersection for those RTFOT-aged binders.

Taking the phase angle into consideration shows that following the short-term aging the curves of each of the SEBs – even those with 10 and 20% GSF – were lower than that of neat bitumen. Consistent with the trend observed at 0.1Hz, these results clarify that short-term aging lowers the phase angles of SEBs, indicating improved elasticity, which is potentially beneficial for resisting deformations. This stiffening effect caused by aging most probably occurs due to the redistribution of sulphur particles in the bitumen phase. Figure 6.69 (b) illustrates that the isochronal plot of phase angle belonging to R-B70/100-20%GSF is completely linear. The same figure also shows the phase angles of R-B70/100-50%GSF with a small-scale "plateau" observed between 30 and 40°C, where the values are relatively insensitive to temperature change.

Table 6.68 : Values of rheological parameters for the B70/100 base bitumen and SEB groups at 0.2517Hz after short-term aging.

Binder	Stage	Complex Modulus at 0.2517 Hz (Pa)				Phase Angle at 0.2517 Hz (degree)			
		25 °C	30 °C	40 °C	50 °C	25 °C	30 °C	40 °C	50 °C
B70/100	r	2.81E+07	1.69E+07	3.45E+06	5.55E+05	56.19	67.88	81.93	86.69
B70/100-10%GSF	r	3.53E+07	2.09E+07	2.56E+06	4.64E+05	56.81	59.09	79.81	84.56
B70/100-20%GSF	r	5.74E+07	1.63E+07	1.27E+07	1.80E+06	45.75	55.95	68.87	80.12
B70/100-30%GSF	r	2.13E+07	1.69E+07	7.83E+06	1.74E+06	40.68	52.97	68.51	74.90
B70/100-40%GSF	r	1.16E+08	1.67E+08	8.91E+07	5.35E+06	42.98	48.92	60.42	72.37
B70/100-50%GSF	r	3.25E+08	9.31E+07	5.43E+07	4.46E+07	41.00	51.24	55.15	75.60

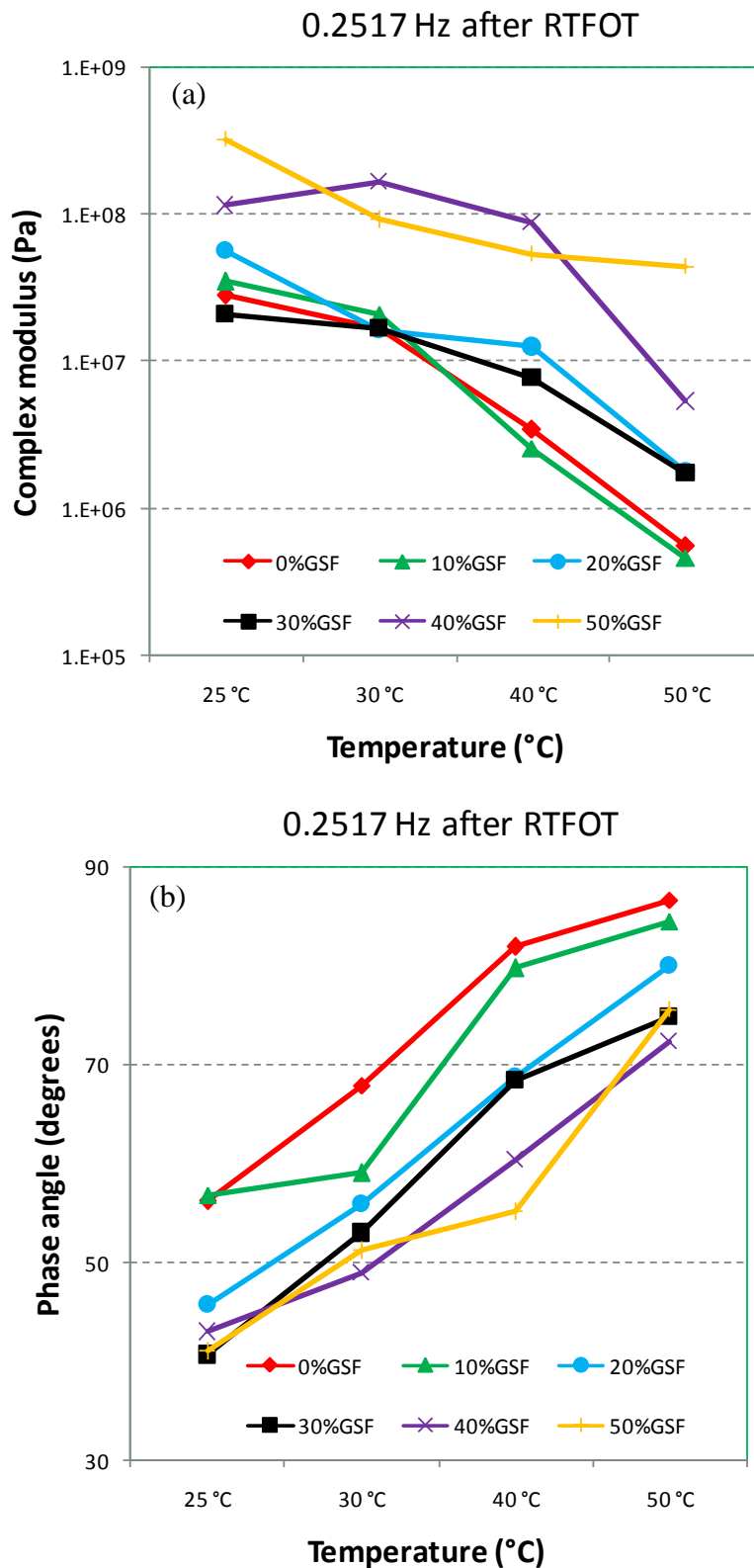


Figure 6.69 : Isochronal plots at 0.2517Hz for neat B70/100 bitumen and SEB groups made of B70/100 bitumen after short-term aging. (a) Complex modulus and (b) Phase angle.

In order to understand both the effects of sulphur extension and short-term aging, extension indices ($G^*_{\text{SEB}}/G^*_{\text{B70/100}}$) and aging index parameter ($G^*_{\text{RTFOT}}/G^*_{\text{UNAGED}}$)

are evaluated and given in Table 6.69. For the first trio of SEBs (with 10, 20, 30%GSF), the extension indices are relatively around 1, with some converge to 1, and most diverge from 1. On the other hand, for the last SEB pair (with 40 and 50%GSF) the extension indices are significantly distant from 1, indicating the presence of a huge gap between them and neat bitumen in terms of complex modulus at the short-term aging stage.

Table 6.69 : Relative changes in complex modulus and aging index at 0.2517Hz following short-term aging.

Binder	Stage	Extension Indices ($G^*_{SEB}/G^*_{B70/100}$) at 0.2517 Hz				Aging Index (G^*_{RTFOT}/G^*_{UNAGED}) at 0.2517Hz			
		25 °C	30 °C	40 °C	50 °C	25 °C	30 °C	40 °C	50 °C
B70/100	r	1.00	1.00	1.00	1.00	1.47	1.35	2.57	2.47
B70/100-10%GSF	r	1.26	1.23	0.74	0.84	1.54	4.56	3.59	4.01
B70/100-20%GSF	r	2.04	0.96	3.68	3.24	4.54	3.25	17.49	13.32
B70/100-30%GSF	r	0.76	1.00	2.27	3.14	0.11	0.48	1.70	2.14
B70/100-40%GSF	r	4.13	9.88	25.82	9.64	0.37	4.20	25.81	9.90
B70/100-50%GSF	r	11.57	5.49	15.73	80.39	12.86	7.32	12.05	57.69

In terms of deformation resisting performance, the short-term aging effect on GSF extension of base 70/100 penetration bitumen resulted in a sharp improvement of the complex modulus as shown by an increase in aging index. However, the opposite trend can be seen for the R-B70/100-30%GSF binder, where there is a slight decrease in complex modulus with short-term aging at 25 and 30°C. This effect can be attributed to the remodeling of present sulphur particles in bitumen matrix during RTFOT aging, which causes softer stiffness.

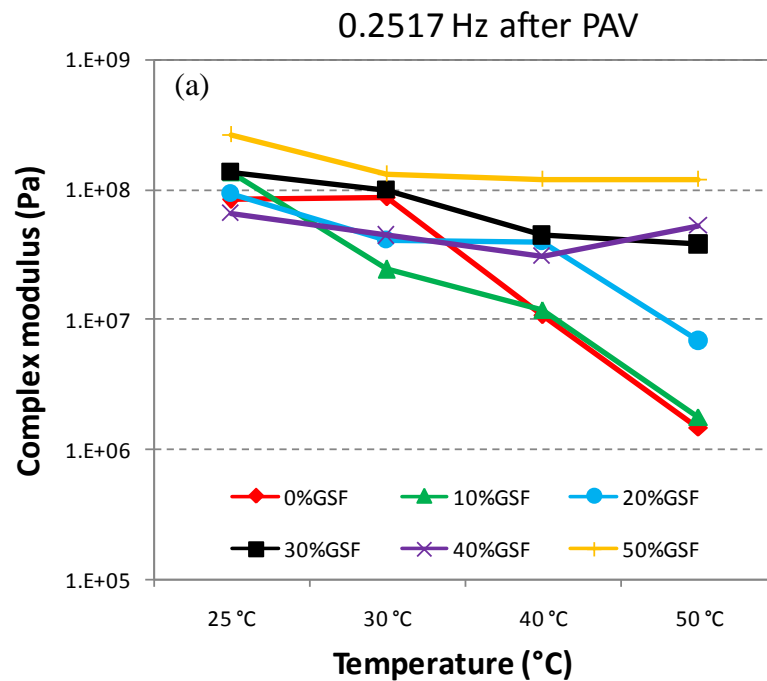
In order to investigate the influence of long-term aging on both the base bitumen and SEB groups, the dynamic shear rheometer (DSR) test was performed again on each PAV-aged sample at the same frequency, 0.2517Hz. The obtained results are presented in Table 6.70 and the isochronal plots of complex modulus (G^*) and phase angles (δ) versus temperature domain are demonstrated in Figure 6.70 (a) and (b) respectively. Excepting that with 10%GSF, the isochronal plots of all extended binders prove that they become less sensitive to temperature change once they have been exposed to long term aging. In other words, based on these preliminary laboratory results, when in service these SEBs will be sufficiently stable and thus able to keep their G^* constant in the face of increasing temperatures.

As the load frequency increased to 0.2517Hz, PAV aging caused a decrease in δ values and a shift towards more elastic response in sulphur-extended-binders. The

curves of both P-B70/100-10%GSF and P-B70/100-20%GSF appear to be completely parallel to that of long-term-aged base bitumen. An increased proportion of GSF resulted in further reduction in viscous response (lower phase angle) as illustrated by samples P-B70/100-40%GSF and P-B70/100-50%GSF. Figure 6.70 (b) also shows that this pair seems to have almost identical viscoelastic responses, particularly in the low to intermediate temperature regions (25-30°C). However, the gap between them becomes clearly distinctive with increasing temperature.

Table 6.70 : Values of rheological parameters for the B70/100 base bitumen and SEB groups at 0.2517Hz after long-term aging.

Binder	Stage	Complex Modulus at 0.2517Hz (Pa)				Phase Angle at 0.2517 Hz (degree)			
		25 °C	30 °C	40 °C	50 °C	25 °C	30 °C	40 °C	50 °C
B70/100	p	8.32E+07	8.67E+07	1.09E+07	1.48E+06	40.45	62.52	78.83	81.49
B70/100-10%GSF	p	1.35E+08	2.42E+07	1.19E+07	1.77E+06	21.16	51.22	64.22	76.00
B70/100-20%GSF	p	9.32E+07	4.11E+07	3.95E+07	6.79E+06	24.91	57.11	70.81	78.61
B70/100-30%GSF	p	1.37E+08	9.83E+07	4.42E+07	3.77E+07	43.32	39.54	54.83	83.57
B70/100-40%GSF	p	6.59E+07	4.41E+07	3.04E+07	5.27E+07	31.98	39.93	54.38	65.45
B70/100-50%GSF	p	2.67E+08	1.31E+08	1.20E+08	1.20E+08	32.59	40.57	41.40	68.53



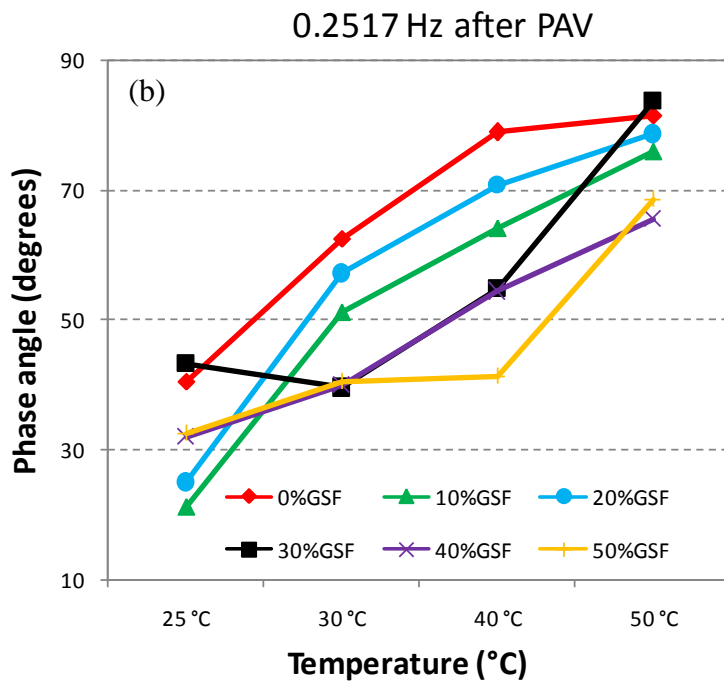


Figure 6.70 : Isochronal plots at 0.2517Hz for neat B70/100 bitumen and SEB groups made of B70/100 bitumen after long-term aging. (a) Complex modulus and (b) Phase angle.

The extension indices ($G^*_{SEB}/G^*_{B70/100}$) and long-term aging index parameter (G^*_{PAV}/G^*_{UNAGED}) are given in Table 6.71. After having been exposed to long-term aging, each SEB appears to have comparable extension indices at low and moderate temperatures (25 and 30°C). Although the P-B70/100-10%GSF continues to display similar viscoelastic response to that of long-term aged neat bitumen at increased temperatures, the difference for the other SEBs becomes more pronounced with increasing temperatures.

Table 6.71 : Relative changes in complex modulus and aging index at 0.2517Hz following long-term aging.

Binder	Stage	Extension Indices ($G^*_{SEB}/G^*_{B70/100}$) at 0.2517 Hz				Aging Index (G^*_{PAV}/G^*_{UNAGED}) at 0.2517Hz			
		25 °C	30 °C	40 °C	50 °C	25 °C	30 °C	40 °C	50 °C
B70/100	p	1.00	1.00	1.00	1.00	4.37	6.93	8.12	6.60
B70/100-10%GSF	p	1.62	0.28	1.09	1.20	5.87	5.28	16.68	15.31
B70/100-20%GSF	p	1.12	0.47	3.63	4.59	7.38	8.18	54.49	50.26
B70/100-30%GSF	p	1.64	1.13	4.06	25.51	0.71	2.81	9.61	46.54
B70/100-40%GSF	p	0.79	0.51	2.80	35.58	0.21	1.11	8.82	97.51
B70/100-50%GSF	p	3.20	1.52	11.00	81.11	10.56	10.35	26.59	155.35

By evaluating the magnitude of the increase in aging index of each binder after PAV aging, the evident increase in complex modulus is unquestionably greater than after

RTFOT aging due to the long aging process in the PAV. Similar to the trend observed at short-term aging stage, even PAV aging of the SEBs with 30 and 40%GSF did not cause an increase in their G^* at low temperatures; instead, the values for this pair remained low. This can be attributed to the presence of a strongly formed viscous network of sulphur particles in bitumen matrix. As a consequence, it is clear that at low loading frequencies (0.1 and 0.2517Hz), neither RTFOT nor PAV is sufficiently capable of degrading entire networks.

SEBs composed of B70/100 and variable amounts of GSF at 0.6329Hz;

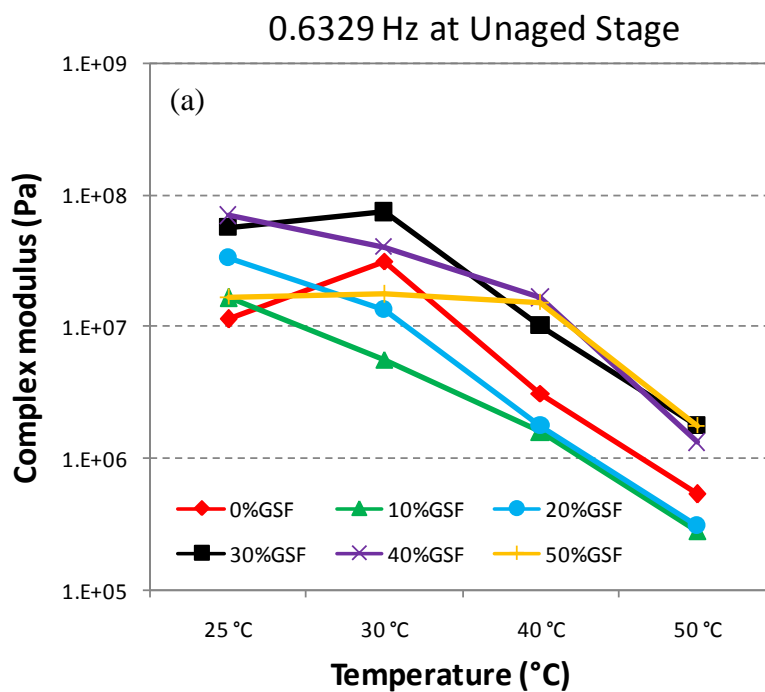
In order to investigate the effect of a further increase in loading frequency on both the base bitumen and SEB groups, the dynamic shear rheometer (DSR) test was re-performed on each unaged sample at the frequency of 0.6329Hz. The obtained results are presented in Table 6.72 and the isochronal plots of complex modulus (G^*) and phase angles (δ) versus temperature domain are demonstrated in Figure 6.71 (a) and (b) respectively. Increasing the loading frequency to 0.6329Hz did not change the viscoelastic behavior of the first two SEBs, as shown in Figure 6.71 (a). Similar to their trends observed at 0.1 and 0.2517Hz, 10 and 20%GSF content SEBs have lower complex modulus values, indicating that when compared to their respective base bitumen, they each tend to demonstrate a relatively viscous response, regardless of the temperature. However, the complex modulus, G^* plots (isotherms) for samples B70/100-30%GSF and B70/100-40%GSF demonstrate that the extension of natural 70/100 pen base bitumen with GSF resulted in increased binders stiffness, namely, a further elastic response. The further amount of GSF (50%) in neat bitumen appears to yield a moderate change in viscoelastic response, particularly in the low to intermediate temperature region (25-40°C); however, the gaps between B70/100-50%GSF and its respective base bitumen widen as the temperature approaches 50°C.

At increased loading frequency as high as 0.6329Hz, low GSF content SEBs seem to have similar phase angle curves. It is thus clear that although they include differing amounts of sulphur (10, 20, and 30%) these SEBs act in the same way with, not only each other, but also with neat bitumen in terms of viscoelastic behavior. However, when the GSF ratio in neat bitumen exceeds 30%, a distinctive reduction in phase angle occurs. The gap in elastic behavior is more obvious in case of 50%GSF extension. As may be observed, the extension of neat 70/100 penetration bitumen with a low amount of GSF (10 and 20%GSF) leads to a slight increase in the values

of phase angle due to a formed viscous network of sulphur particles. However, at further increases in GSF, the phase angle of neat bitumen begins to significantly decrease due to formed elastic network of sulphur particles, rather than that viscous network. These generated elastic networks seen at higher amounts of GSF lead the B70/100-40%GSF and B70/100-50%GSF to behave in a relatively elastic manner. Table 6.72 shows that the responses of 10 and 40%GSF content SEBs at 50°C are nearly viscous ($\delta = 88.49$ and 88.18 respectively), while the response tended to be more elastic as the test temperatures were reduced.

Table 6.72 : Values of rheological parameters for the B70/100 base bitumen and SEB groups at 0.6329Hz before aging.

Binder	Stage	Complex Modulus at 0.6329 Hz (Pa)				Phase Angle at 0.6329 Hz (degree)			
		25 °C	30 °C	40 °C	50 °C	25 °C	30 °C	40 °C	50 °C
B70/100	o	1.13E+07	3.12E+07	3.12E+06	5.32E+05	51.15	61.26	87.34	87.39
B70/100-10%GSF	o	1.65E+07	5.66E+06	1.57E+06	2.80E+05	53.25	72.65	85.76	88.49
B70/100-20%GSF	o	3.36E+07	1.34E+07	1.76E+06	3.07E+05	57.73	65.27	80.33	84.71
B70/100-30%GSF	o	5.63E+07	7.35E+07	1.02E+07	1.78E+06	55.05	73.01	82.38	81.66
B70/100-40%GSF	o	6.94E+07	4.02E+07	1.65E+07	1.31E+06	22.93	51.17	79.80	88.18
B70/100-50%GSF	o	1.69E+07	1.75E+07	1.53E+07	1.75E+06	27.98	14.40	35.90	86.78



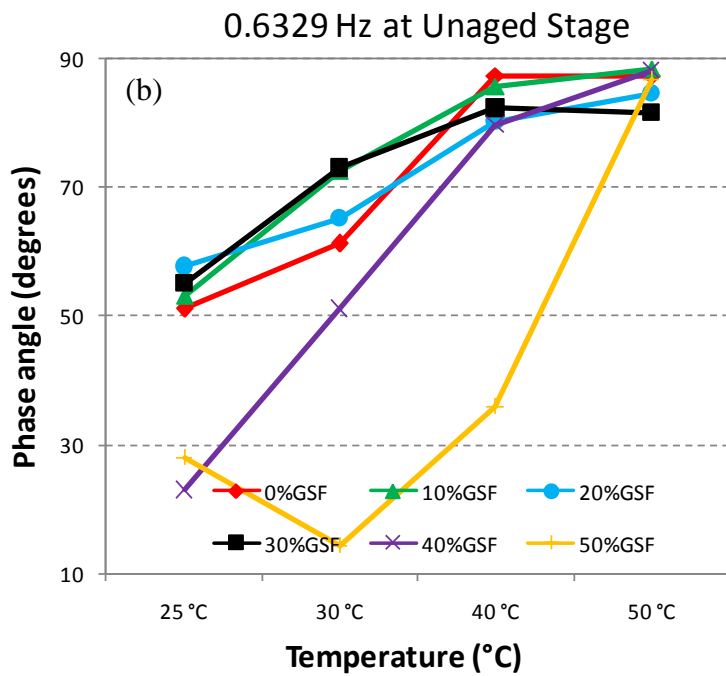


Figure 6.71 : Isochronal plots at 0.6329Hz for neat B70/100 bitumen and SEB groups made of B70/100 bitumen before aging. (a) Complex modulus and (b) Phase angle.

The extension indices of G^* ($G^*_{\text{SEB}}/G^*_{\text{B70/100}}$) measuring relative changes in complex modulus for all five SEBs have been recorded at each temperature and at 0.6329Hz and are displayed in Table 6.73. Consistent with the trends observed at 0.1 and 0.2517Hz, the extension indices of both B70/100-10%GSF and B70/100-20%GSF are lower than 1, excepting at low temperature (25°C). However, 30 and 40%GSF content SEBs have extension indices greater than 1, but the magnitude of change in these values is completely different at each temperature and there is no regularity. In case of further GSF extension (50%), these values become contradictory, since at low and high temperatures the values are fairly greater than 1, but less than 1 at 30°C.

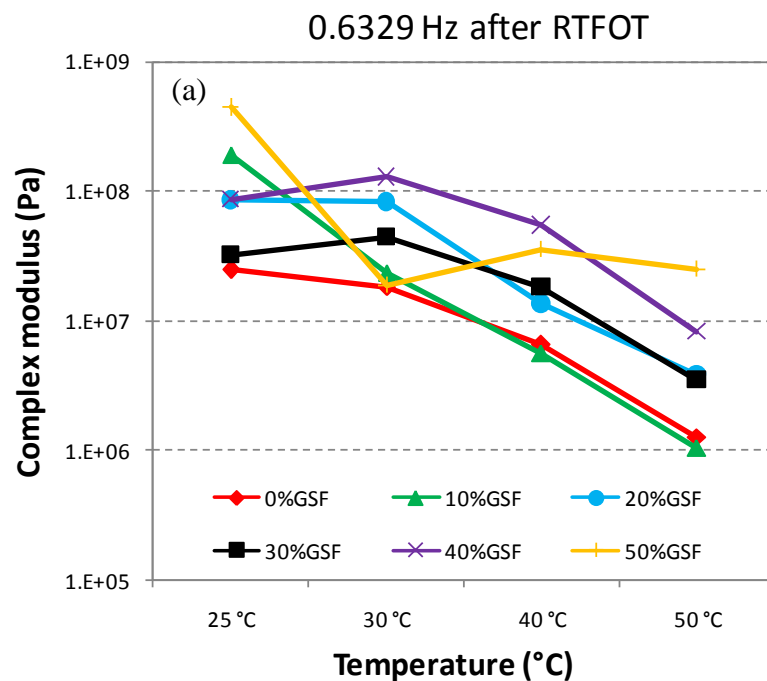
Table 6.73 : Relative changes in complex modulus for the B70/100 base bitumen and SEB groups at 0.6329Hz before aging.

Binder	Stage	Extension Indices ($G^*_{SEB}/G^*_{B70/100}$) at 0.6329 Hz			
		25 °C	30 °C	40 °C	50 °C
B70/100	o	1.00	1.00	1.00	1.00
B70/100-10%GSF	o	1.46	0.18	0.50	0.53
B70/100-20%GSF	o	2.97	0.43	0.56	0.58
B70/100-30%GSF	o	4.98	2.36	3.26	3.35
B70/100-40%GSF	o	6.14	1.29	5.27	2.45
B70/100-50%GSF	o	1.49	0.56	4.88	3.29

In order to evaluate the influence of short-term aging at 0.6329Hz on rheological behavior, the dynamic shear rheometer (DSR) test was re-conducted on the RTFOT-aged samples. The rheological parameter values at 0.6329Hz belonging to the both short-term aged base 70/100 bitumen and short-term aged SEB groups are given in Table 6.74. In addition, the isochronal plots of complex modulus (G^*) and phase angle (δ) versus temperature at 0.6329Hz for both of these cases are shown in Figure 6.72 (a) and (b) respectively. Short-term aging led the B70/100-10%GSF to demonstrate a marked increase in complex modulus over temperature domain, identical to that seen for short-term aged neat bitumen. Its rheological behavior at moderate and high temperature (30 to 50°C) does not differ from that of pure bitumen. However, similar to its unaged behavior, its complex modulus at 25°C is remarkably higher than that of neat bitumen. From this it can be concluded that short-term aging made this SEB relatively elastic. As can be observed in both Figure 6.72 (a) and Table 6.74, other short-term aged SEBs with further GSF content seem to increase their G^* values over temperature domain in relation to that corresponding to the non-extended sample. This was most significant for the 40%GSF concentration. It is worth mentioning that their curves at each temperature always remain superior to that of neat bitumen. However, the measurement of R-B70/100-50%GSF complex modulus at 30°C is particularly interesting, because at this point the value suddenly drops. This is probably attributed to the fact that it is sometimes difficult to fully highlight the effects of high amounts of sulphur on the viscoelastic properties of SEBs.

Table 6.74 : Values of rheological parameters for the B70/100 base bitumen and SEB groups at 0.6329Hz after short-term aging.

Binder	Stage	Complex Modulus at 0.6329 Hz (Pa)				Phase Angle at 0.6329 Hz (degree)			
		25 °C	30 °C	40 °C	50 °C	25 °C	30 °C	40 °C	50 °C
B70/100	r	2.48E+07	1.83E+07	6.56E+06	1.28E+06	42.27	52.80	80.30	87.81
B70/100-10%GSF	r	1.89E+08	2.38E+07	5.61E+06	1.05E+06	17.41	58.96	79.10	84.44
B70/100-20%GSF	r	8.51E+07	8.29E+07	1.35E+07	3.88E+06	32.85	41.32	58.42	78.60
B70/100-30%GSF	r	3.21E+07	4.41E+07	1.84E+07	3.50E+06	47.07	56.28	64.03	76.57
B70/100-40%GSF	r	8.66E+07	1.28E+08	5.44E+07	8.33E+06	40.50	39.71	48.91	83.79
B70/100-50%GSF	r	4.42E+08	1.87E+07	3.52E+07	2.50E+07	37.09	39.89	42.47	56.06



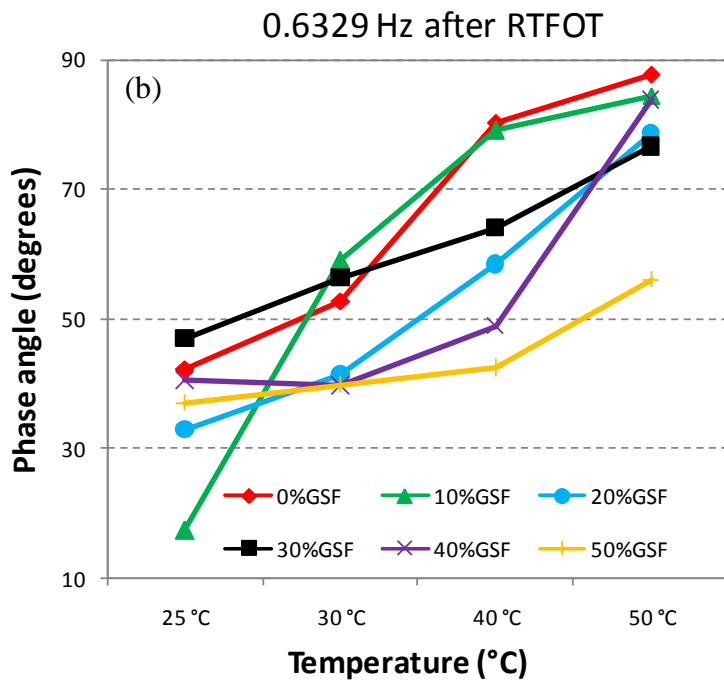


Figure 6.72 : Isochronal plots at 0.6329Hz for neat B70/100 bitumen and SEB groups made of B70/100 bitumen after short-term aging. (a) Complex modulus and (b) Phase angle.

Consistent with its complex modulus results, it must be pointed out that R-B70/100-10%GSF and short-term aged neat bitumen appear to have comparable phase angles, excepting at low temperature (25°C). Its increased complex modulus and reduced phase angle at 25°C serve as indicators of more elastic behavior compared to its respective base bitumen. The regular increase in the amount of GSF did not yield a regular decrease in phase angle. The curves of 30 and 40%GSF content SEBs are inferior to that of pure bitumen. As shown in Figure 6.72 (b), the curve of SEB with 50%GSF content shows a sort of intermediate plateau in δ which strongly highlights how the highest amount of sulphur strongly affects the properties of the straight 70/100 penetration bitumen.

In order to understand the effects of both sulphur extension and short-term aging, the extension indices ($G^*_{SEB}/G^*_{B70/100}$) and aging index parameter (G^*_{RTFOT}/G^*_{UNAGED}) are evaluated and given in Table 6.75. Extension indices of R-B70/100-10%GSF show that the values are sensitive to increases in temperature. The first value measured at 25°C appears remarkably greater than 1 (7.64). However, with increasing temperature the values tend to decrease regularly (1.30, 0.86, 0.82 respectively). Extension indices of other SEBs are always greater than 1, but the magnitudes of increase in G^* are completely various, sometimes slight and

sometimes severe, which means that there is no regularity. As stated before, a sharp drop in G^* of R-B70/100-50%GSF was observed at 30°C, but the value is still over 1 (1.02).

Table 6.75 : Relative changes in complex modulus and aging index at 0.6329Hz following short-term aging.

Binder	Stage	Extension Indices ($G^*_{SEB}/G^*_{B70/100}$) at 0.6329 Hz				Aging Index (G^*_{RTFOT}/G^*_{UNAGED}) at 0.6329Hz			
		25 °C	30 °C	40 °C	50 °C	25 °C	30 °C	40 °C	50 °C
B70/100	r	1.00	1.00	1.00	1.00	2.19	0.59	2.10	2.40
B70/100-10%GSF	r	7.64	1.30	0.86	0.82	11.43	4.21	3.56	3.77
B70/100-20%GSF	r	3.44	4.52	2.06	3.04	2.53	6.16	7.67	12.65
B70/100-30%GSF	r	1.30	2.41	2.80	2.75	0.57	0.60	1.80	1.97
B70/100-40%GSF	r	3.50	7.00	8.29	6.53	1.25	3.19	3.30	6.38
B70/100-50%GSF	r	17.85	1.02	5.37	19.63	26.17	1.07	2.31	14.29

Short-term aging led the neat bitumen to increase its initial complex modulus by as much as double at 25, 40 and 50°C, whereas it reduced the value by as much as half at 30°C. Short-term aging of R-B70/100-10%GSF seems to have its most impact at low temperatures, since the value (11.43) at 25°C is relatively greater than those observed at other temperatures.

There appears to be a regular increase in the values of aging index for R-B70/100-20%GSF and R-B70/100-40%GSF binders at elevated temperatures. The minimal effect of short-term aging among all SEBs, including the base bitumen, was also seen for the R-B70/100-30%GSF due to its lowest aging index values (0.57, 0.60, 1.80, and 1.97). Contrary to expectations of an increase in G^* after short-term aging, this SEB reduced its G^* nearly half at 25 and 30°C. This unexpected outcome may be due to the effect of short-term aging on sulphur particles. RTFOT most probably allowed the sulphur particles to create more viscous networks at those temperatures.

The rheological properties of the five SEB binders and control neat bitumen after PAV long-term aging were compared by producing isochronal plots at a reference loading temperature frequency of 0.6329Hz with increasing temperature as shown in Figure 6.73 (a) (complex modulus) and (b) (phase angle); their values are also given in Table 6.76. It can be seen that the rheological parameters of PAV-aged samples differ considerably from those of both the unaged and RTFOT aged samples. The obvious increase in the complex modulus and the reduction in the phase angle are indications of the improvement in high-temperature performance.

In terms of the complex modulus curves of the samples shown in Figure 6.73 (a), it is difficult to establish a direct link with the amount of GSF on the type of the binder. All long-term aged SEBs tend towards the different complex modulus versus temperature at 0.6329Hz, due to the high elastic response; however, over the central temperature region, the complex modulus isochronal curves of the both control neat bitumen and five SEB samples differ slightly. For the P-B70/100-40%GSF binder, the linearity of G^* values was lost at high temperature (50°C). Contrary to expectations, its complex modulus unexpectedly increased at 50°C. The most probable indication that the G^* value for this sample may be elevating at increased temperature can be seen for the heterogeneous mixing of sulphur particles and bitumen compounds at this high amount of GSF (40%).

Figure 6.73 (b) demonstrates that the curves of phase angle for each sample are almost parallel to each other. Since the slope of each curve is reduced, one can observe that after PAV-aging the SEB samples become relatively less sensitive to temperature changes. This insensitivity can be attributed to two major facts: On the one hand, the bitumen phase of already short-term aged SEBs is, this time, exposed to long-term aging. Hence, in addition to initial hardening via RTFOT, the bitumen phase became increasingly stiff due to the effects of long-term aging. Secondly, both physical and chemical bonds formed between the sulphur particles and the bitumen compounds became more stable, and so are better able to resist changes in temperature.

Table 6.76 : Values of rheological parameters for the B70/100 base bitumen and SEB groups at 0.6329Hz after long-term aging.

Binder	Stage	Complex Modulus at 0.6329Hz (Pa)				Phase Angle at 0.6329 Hz (degree)			
		25 °C	30 °C	40 °C	50 °C	25 °C	30 °C	40 °C	50 °C
B70/100	p	9.15E+07	8.08E+07	1.72E+07	3.03E+06	43.06	50.53	65.27	81.24
B70/100-10%GSF	p	3.78E+07	3.40E+07	1.11E+07	3.81E+06	49.26	57.52	65.92	80.55
B70/100-20%GSF	p	9.85E+07	4.13E+07	1.88E+07	9.15E+06	30.80	41.83	59.15	69.29
B70/100-30%GSF	p	5.82E+07	7.70E+07	1.87E+07	1.80E+07	38.33	47.55	49.75	68.96
B70/100-40%GSF	p	2.98E+08	4.29E+07	1.53E+07	3.22E+07	31.22	33.20	41.46	45.78
B70/100-50%GSF	p	5.74E+07	5.64E+07	2.31E+07	2.21E+07	26.06	34.04	47.89	56.47

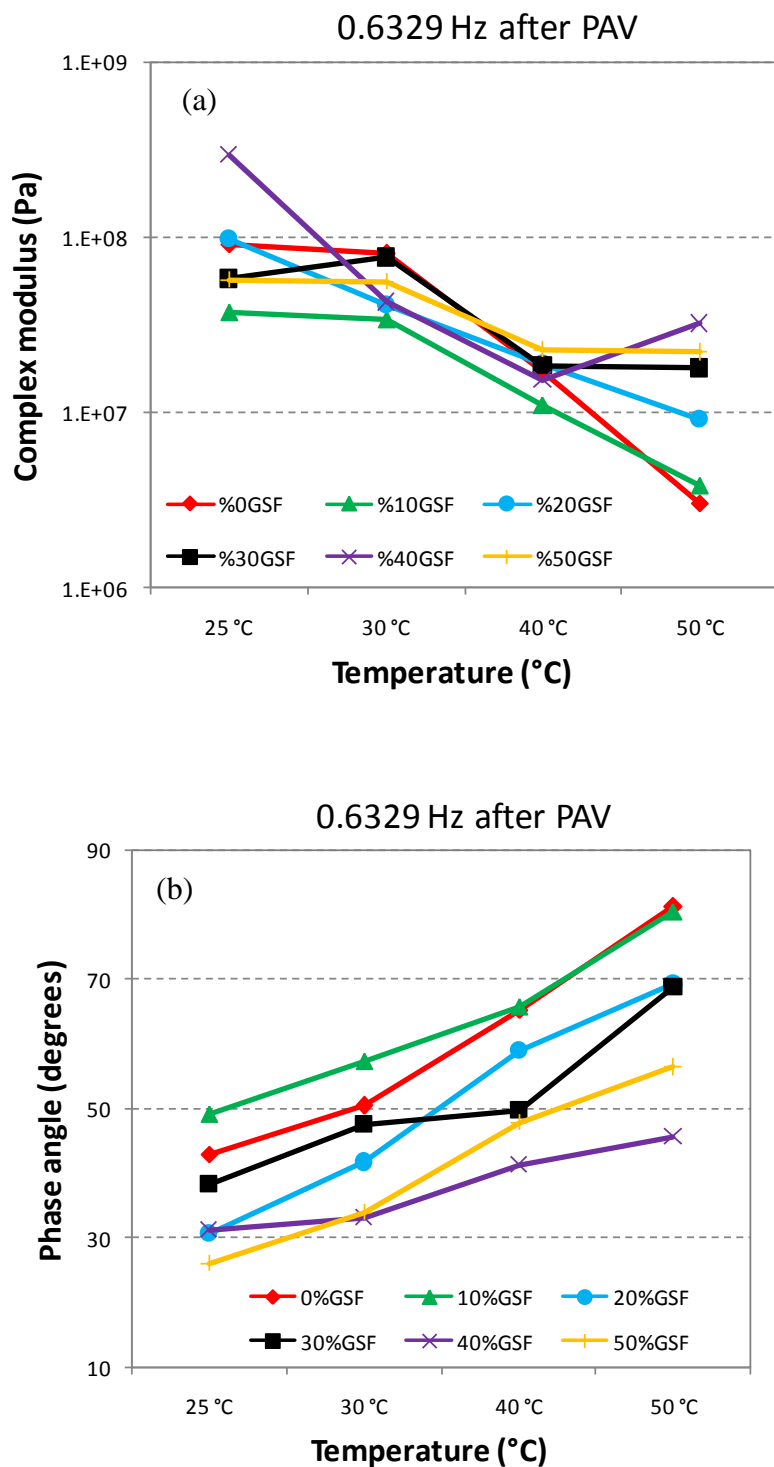


Figure 6.73 : Isochronal plots at 0.6329Hz for neat B70/100 bitumen and SEB groups made of B70/100 bitumen after long-term aging. (a) Complex modulus and (b) Phase angle.

The properties of the long-term aged base bitumen and the long-term aged SEBs of five different sulphur levels were compared and are shown in Table 6.77. At high temperature (50°C), the extension indices for each PAV-aged SEB are greater than 1, indicating that regardless of the amount of GSF sulphur particles, long-term aging of

the SEB led to an increase in G^* significantly at high temperature. This shows that the elasticity of the PAV-aged neat bitumen improved effectively at high temperature with the presence of sulphur particles. Taking the hot-climate areas into consideration, PAV aged SEBs simulating in-service binder will be capable of better withstanding potential deformations.

Table 6.77 : Relative changes in complex modulus and aging index at 0.6329Hz following long-term aging.

Binder	Stage	Extension Indices ($G^*_{SEB}/G^*_{B70/100}$) at 0.6329 Hz				Aging Index (G^*_{PAV}/G^*_{UNAGED}) at 0.6329Hz			
		25 °C	30 °C	40 °C	50 °C	25 °C	30 °C	40 °C	50 °C
B70/100	p	1.00	1.00	1.00	1.00	8.09	2.59	5.52	5.69
B70/100-10%GSF	p	0.41	0.42	0.64	1.26	2.29	6.00	7.04	13.65
B70/100-20%GSF	p	1.08	0.51	1.09	3.02	2.93	3.07	10.72	29.81
B70/100-30%GSF	p	0.64	0.95	1.08	5.93	1.03	1.05	1.83	10.09
B70/100-40%GSF	p	3.26	0.53	0.89	10.64	4.29	1.07	0.93	24.70
B70/100-50%GSF	p	0.63	0.70	1.34	7.28	3.40	3.22	1.51	12.59

Comparisons of the impacts of long term aging at 0.6329Hz on the rheological behaviors with neat bitumen and sulphur extended binders are quite interesting; these are shown in Table 6.77. The aging index for each binder indicates that the rheology of PAV-aged SEBs is strongly dependent on the extended amount of sulphur. As recorded in Table 6.77, at a moderate amount of GSF (30%GSF), the G^* value of SEB remains the closest to that of its unaged value since its aging index values are the lowest (1.03, 1.05, 1.83, and 10.09). In this case, after long term-aging, P-B70/100-30%GSF is seen to best maintain its rheological response related to its stable formation of network structure of sulphur. On the other hand, the aging index at relatively low amounts of GSF (10% and 20%) shows that after long-term aging these binders fundamentally change in their rheological behavior by a sort of exponential increase in G^* with increasing temperature. However, at relatively high amounts of GSF (40% and 50%), irregular changes in G^* were observed following the long-term aging.

SEBs composed of B70/100 and variable amounts of GSF at 4.0Hz:

In order to investigate the effect of ultimate loading frequency on both the base bitumen and SEB groups, in this study the dynamic shear rheometer (DSR) test was performed on each unaged sample at the frequency of 4.0Hz. The obtained results are presented in Table 6.78 and the isochronal plots of complex modulus (G^*) and phase

angles (δ) versus temperature domain are demonstrated in Figure 6.74 (a) and (b) respectively.

Consistent with their phase angle results, the complex modulus of SEBs with low levels of sulphur (10 and 20%) are lower than that of neat bitumen at 30, 40, and 50°C, indicating an increased viscous behavior. However, at low temperature and owing to their relatively higher G^* values, this SEB pair demonstrates more elasticity than that of neat bitumen.

In addition to $G^*/\sin\delta$, the slope of the logarithmic function of the complex modulus is another suggested factor for rutting sensitivity (Edwards and Redelius, 2003). Even though the slopes for the first four SEBs appear to be positive over temperature domain, the slope for B70/100-50%GSF is somewhat negative between 25 and 30°C as shown in Figure 6.74 (a). Increases in temperature did not remarkably change the rheological behavior of this SEB. A corresponding plateau effect appeared very clearly for its complex modulus, especially between 30 and 40°C. Compared with other SEBs, the B70/100-40%GSF have the highest positive slope value, indicating its higher temperature sensitivity.

Table 6.78 : Values of rheological parameters for the B70/100 base bitumen and SEB groups at 4.0Hz before aging.

Binder	Stage	Complex Modulus at 4.0 Hz (Pa)				Phase Angel at 4.0 Hz (degree)			
		25 °C	30 °C	40 °C	50 °C	25 °C	30 °C	40 °C	50 °C
B70/100	o	1.63E+07	2.40E+08	1.27E+07	2.81E+06	30.29	30.95	33.41	60.11
B70/100-10%GSF	o	2.69E+07	1.52E+07	6.53E+06	2.47E+06	62.79	68.51	71.64	73.53
B70/100-20%GSF	o	2.79E+07	2.26E+07	1.00E+07	1.51E+06	47.03	53.92	76.42	86.26
B70/100-30%GSF	o	8.91E+07	6.54E+07	3.03E+07	8.89E+06	30.21	58.05	77.45	77.05
B70/100-40%GSF	o	6.46E+08	1.22E+08	1.20E+07	6.55E+06	4.16	34.19	46.47	67.56
B70/100-50%GSF	o	8.86E+06	2.50E+07	2.06E+07	6.60E+06	36.90	31.25	31.08	42.11

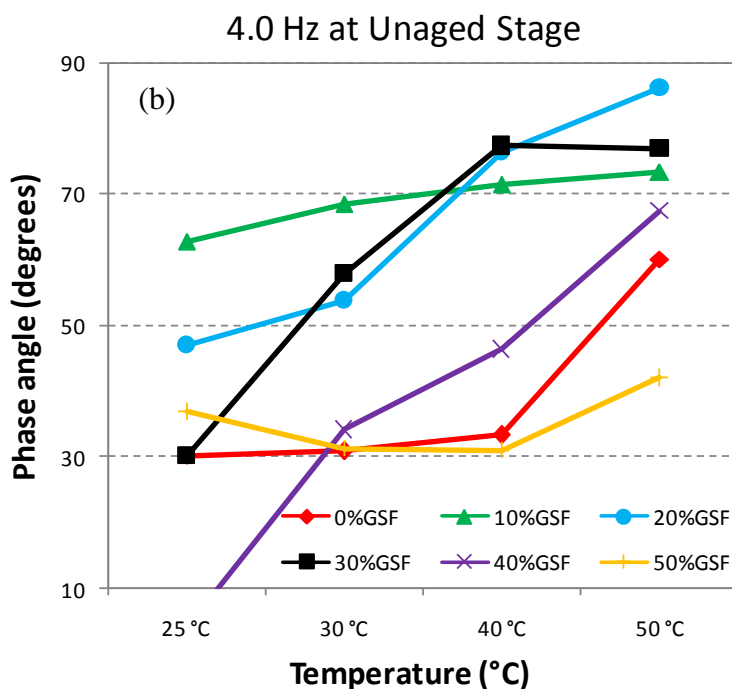
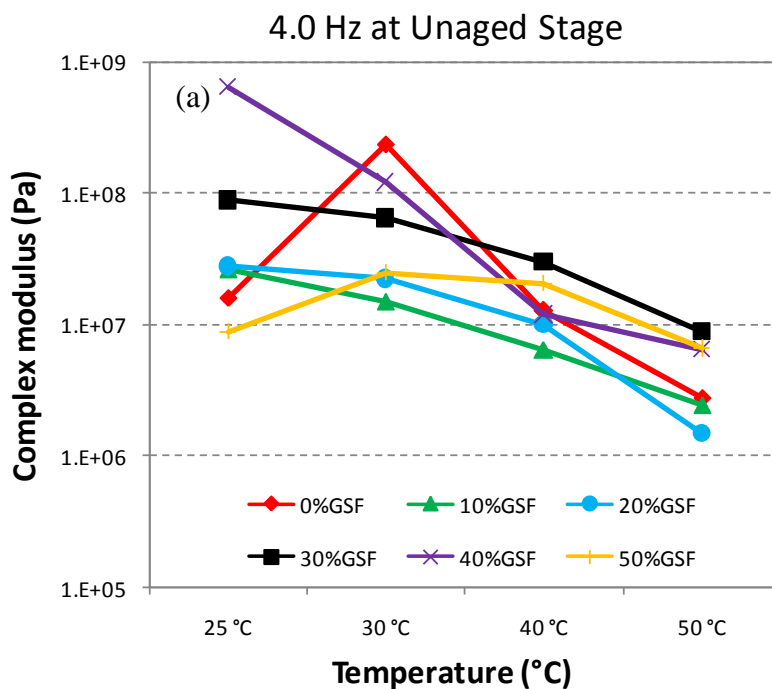


Figure 6.74 : Isochronal plots at 4.0Hz for neat B70/100 bitumen and SEB groups made of B70/100 bitumen before aging. (a) Complex modulus and (b) Phase angle.

As listed in Table 6.78, the increase in phase angle for nearly all binders containing different GSF level indicates that a lower elasticity begins to start at a low temperature (25°C). This indicates that at 4.0Hz loading frequency, adding sulphur to neat 70/100 penetration bitumen leads the binder to become relatively more viscous. This becomes more evident in the DSR analysis when comparisons are made of

lower amounts of GSF (10 and 20%). In line with previous lower frequency test results and other stiffness test results, these outcomes are meaningful, yet not surprising. This effect is not a desirable outcome and is an indication of declined elasticity, possibly causing a decreased resistance to deformation of an asphalt pavement. The 30%GSF content SEB sample showed a similar effect at low temperature (25°C), but a higher phase angle degree with increasing temperature. When the sulphur was extended to the 40%GSF level, the SEB indicates a rather sharp decrease in phase angle at 25°C, while the values are still remarkably greater than those of neat bitumen at other test temperatures. Excepting that at a low temperature, increasing the GSF level up to 50% resulted in improved elasticity. This very pronounced effect especially appeared at 50°C since the corresponding decrease in phase angle was registered up to 18 degree.

To sum up, the rheological effect of increasing loading frequency obtained by adding differing levels of sulphur to bitumen of penetration grade 70/100 leads us to the following conclusions: At 50°C, the G^* values of both unaged neat bitumen and unaged SEB groups tend to increase regularly with elevated loading frequency. At 40°C this regularity in increase begins to disappear at 1.596Hz for the SEBs with 40 and 50%GSF. After a slight decrease observed at this frequency, a following increase in G^* was then detected at 4.0Hz. Taking the other test temperatures (25 and 30°C) into consideration, the varying trend of G^* is generally inclined to increase with elevating loading frequency, even though some derangements were observed at intermediate loading frequencies in some of the samples. All in all, the magnitude and type of effects on binder rheology depend on both the bitumen itself and on the levels of extended sulphur.

Since the rheology sulphur-extended bitumen is strongly dependent on the utilized content of GSF, the extension indices of G^* ($G^*_{SEB}/G^*_{B70/100}$) measuring relative changes in complex modulus for all five SEBs have been recorded at each temperature and at 4.0Hz and are displayed in Table 6.79.

Table 6.79 : Relative changes in complex modulus for the B70/100 base bitumen and SEB groups at 4.0Hz before aging.

Binder	Stage	Extensive Indices ($G^*_{SEB}/G^*_{B70/100}$) at 4.0 Hz			
		25 °C	30 °C	40 °C	50 °C
B70/100	o	1.00	1.00	1.00	1.00
B70/100-10%GSF	o	1.65	0.06	0.51	0.88
B70/100-20%GSF	o	1.72	0.09	0.79	0.54
B70/100-30%GSF	o	5.48	0.27	2.38	3.17
B70/100-40%GSF	o	39.70	0.51	0.94	2.34
B70/100-50%GSF	o	0.54	0.10	1.62	2.35

As listed in Table 6.79, extensive indices at 25°C clearly increase with sulphur extensions up to 50%, thus indicating that the increasing GSF level enhances elasticity by the degree of formation of network structure in neat bitumen. However, a reverse effect is observed at the highest level (50%). Regardless of the amount of GSF, each SEB has lower extensive indices than 1.00 at 30°C, which can be regarded as a significant increase in the viscous behavior of neat bitumen in this study. For instance, the G^* value of 10%GSF content SEB is more than 16 times lower than that of the original bitumen at 30°C. At the highest test temperature in this study (50°C), SEBs with moderate and high content of GSF have extensive indices greater than 1.00, meaning that they surpass the base bitumen in enhanced and desired elastic behavior at high temperature.

The DSR test was conducted on the RTFOT-aged samples as a way to investigate the changes in both complex modulus and phase angle after short-term aging. Isochronal plots of G^* and δ at 4.0Hz for both base bitumen and SEB group in their RTFOT-aged conditions are shown in Figure 6.75 (a) and (b) and the measured values are listed in Table 6.80. As with the GSF extension of the base bitumen, there are distinct differences in the rheological characteristics of the samples after aging. Although R-B70/100-10%GSF shows a relatively increase in G^* at the lowest test temperature, the behavior at temperatures greater than 25°C differs from the short-aged neat bitumen. The same effect was also observed on the short-term aged 20%GSF content SEB at 30°C as presented in Table 6.80. As previously mentioned, low content sulphur extension caused the neat bitumen to soften. This trend remained the same for this SEB pair even after aging. The isochronal plot at 30%GSF content remains closer to that of the base bitumen between 25 and 40°C, at which point an

obvious plateau appeared for the same sample as illustrated in Figure 6.75 (a). This plateau in complex modulus is believed to be an indicator of the presence of sulphur elastic networks or entanglements in the neat bitumen. The significant difference in G^* is clearly seen by increasing the amount of GSF from 30 to 40%. The same effect is also marked at 50%GSF content. At these increased sulphur amounts, the G^* curves are all higher than those of neat bitumen in the tested temperature range, thus indicating enhanced elastic response for these samples.

Table 6.80 : Values of rheological parameters for the B70/100 base bitumen and SEB groups at 4.0Hz after short-term aging.

Binder	Stage	Complex Modulus at 4.0 Hz (Pa)				Phase Angel at 4.0 Hz (degree)			
		25 °C	30 °C	40 °C	50 °C	25 °C	30 °C	40 °C	50 °C
B70/100	r	2.13E+07	3.20E+07	1.74E+07	1.07E+07	59.17	66.75	70.30	71.59
B70/100-10%GSF	r	3.17E+07	1.02E+07	9.84E+06	6.40E+06	52.83	59.80	76.70	84.79
B70/100-20%GSF	r	1.19E+07	1.58E+07	1.84E+07	9.68E+06	28.89	57.92	63.25	71.43
B70/100-30%GSF	r	2.97E+07	2.72E+07	1.62E+07	1.62E+07	35.07	57.15	64.68	68.56
B70/100-40%GSF	r	7.84E+07	1.18E+08	4.75E+07	4.24E+07	51.86	57.04	71.22	74.67
B70/100-50%GSF	r	3.02E+08	8.92E+07	6.59E+07	2.92E+07	18.67	24.97	45.64	65.10

Figure 6.75 (b) displays the phase angle responses of both neat bitumen and SEB group after short-term aging. The 20, 30 and 50%GSF content SEB curves are all lower than those of neat bitumen over the test temperature range. The rest of the curves (belonging to SEB with 10 and 40%GSF) intersect with that of neat bitumen, showing a reduced phase angle at temperatures up to 40°C, but an increase after that point. In other words, RTFOT residues of the SEB with 10 and 40%GSF display an enhanced elasticity due to lower δ values before 40°C; however, an opposite trend in variations of phase angle is observed at temperatures greater than 40°C. Unlike other short-term aged SEBs, at each test temperature there is a substantial decrease in phase angle recorded for the SEB with 50%GSF. This pronounced effect on this sample can be attributed to both its aging process and to its high sulphur level. After RTFOT aging this high amount of sulphur in this SEB is assumed to manifest rheological behavior and cause an increase in its elastic behavior.

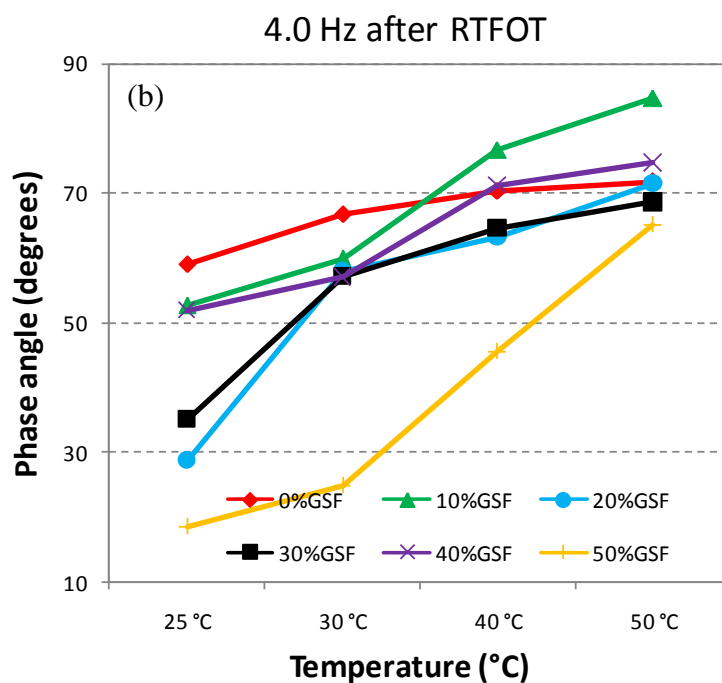
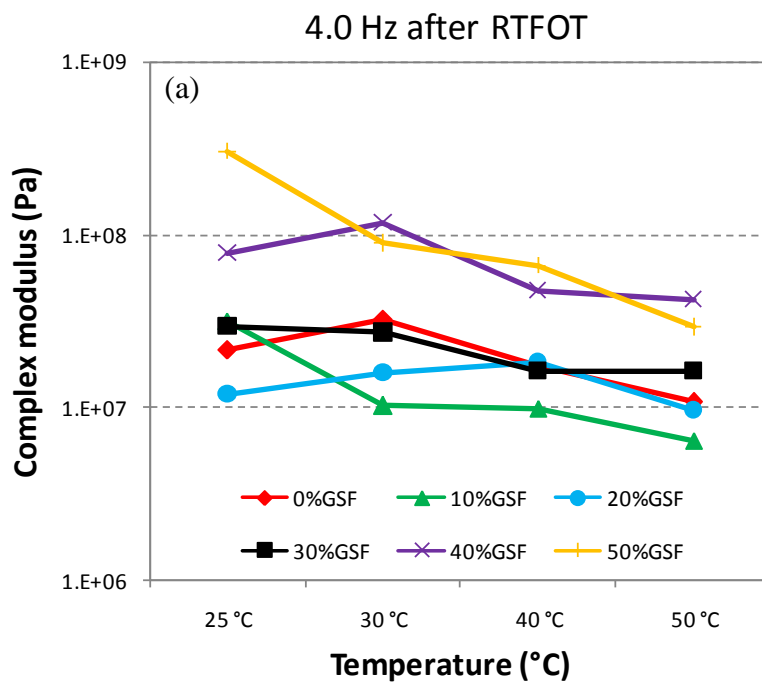


Figure 6.75 : Isochronal plots at 4.0Hz for neat B70/100 bitumen and SEB groups made of B70/100 bitumen after short-term aging. (a) Complex modulus and (b) Phase angle.

In order to investigate the effect of short-term aging on the level of sulphur extension, the extension indices of G^* ($G^*_{SEB}/G^*_{B70/100}$) measuring relative changes in viscoelastic response for all five SEBs have been recorded at each temperature and 4.0Hz and the results are displayed in Table 6.81. The results indicate that there are

significant differences in the extension indices of G^* among SEB groups and these differences are more pronounced at higher sulphur contents. At the lowest of GSF levels (10%) and at the lowest test temperature (25°C), extension indices greater than 1.00 indicate an increased stiffness of the RTFOT-aged base bitumen; however, the opposite becomes true at increasing temperature. The complex modulus for the RTFOT residue of neat bitumen is about 2 times higher than that of RTFOT residue of 20%GSF SEB between 25 and 30°C , whereas this pair shows similar linear viscoelastic behavior and functions with increasing temperature (Extension indices 1.06 and 0.90 at 40 and 50°C respectively). The marked increase in G^* for short-term aged SEBs starts with 40%GSF, indicating relatively higher elasticity. After RTFOT aging, a substantial amount of sulphur particles used as an extender in the neat bitumen most probably formed a kind of crystal, gel, or network structure, which then causes an enhanced elastic behavior in the binder. This becomes particularly more evident at 50%GSF content and at 25°C .

Table 6.81 : Relative changes in complex modulus and aging index at 4.0Hz following short-term aging.

Binder	Stage	Extensive Indices $G^*_{\text{SEB}}/G^*_{\text{B70/100}}$ at 4.0 Hz				Aging Index ($G^*_{\text{RTFOT}}/G^*_{\text{UNAGED}}$) at 4.0 Hz			
		25 °C	30 °C	40 °C	50 °C	25 °C	30 °C	40 °C	50 °C
B70/100	r	1.00	1.00	1.00	1.00	1.31	0.13	1.37	3.83
B70/100-10%GSF	r	1.48	0.32	0.56	0.60	1.18	0.67	1.51	2.59
B70/100-20%GSF	r	0.56	0.49	1.06	0.90	0.43	0.70	1.83	6.42
B70/100-30%GSF	r	1.39	0.85	0.93	1.51	0.33	0.42	0.54	1.82
B70/100-40%GSF	r	3.67	3.67	2.72	3.95	0.12	0.96	3.95	6.47
B70/100-50%GSF	r-	14.15	2.78	3.78	2.71	34.07	3.57	3.19	4.42

The aging index showing the changes in the rheological characteristics of 70/100 penetration bitumen and SEB group after aging is listed in Table 6.81. At 25°C , excepting the SEB with lowest and highest amount of GSF (10 and 50%), the remaining SEBs demonstrate a decrease in G^* after aging. This can be attributed to be a rearrangement (degradation) of sulphur particles into lower molecular weight fragments after aging, leading to a 'softening' of these SEBs. However this phenomenon is not evident for short-term aged neat bitumen, as the absence of any amount of GSF means that it cannot dominate the rheological behavior of the neat bitumen. On the other hand, at 30°C , not only is there a decrease in G^* in those SEBs containing an intermediate content of GSF, a decrease in G^* is also observed for neat bitumen and 10%GSF content SEB. Nevertheless, taking their aging index into

consideration reveals the fact that even though values are less than 1.00, they are still greater than those of neat bitumen. Hence, one can observe that short-term aging has a relatively higher impact on sulphur-extended-binders. As listed in the same table, within the testing temperature range, the aging index for the 50%GSF content SEB strongly remains greater than 1.00. This corresponding elevated G^* indicates the hardening effect of RTFOT. At increased temperatures, the effect of RTFOT on the sample is clearly marked as the increasing aging index. As can be seen in Table 6.81, excepting R-B70/100-30%GSF, the rest of the short-term aged samples have an aging index greater than 1.00 at 40°C.

Since the change in viscoelastic behavior after PAV aging differs from both RTFOT aged and unaged conditions, the values of the DSR test conducted on long-term aged samples are given in Table 6.82, and the isochronal plots of complex modulus and phase angle at 4.0Hz are displayed in Figure 6.76 (a) and (b) respectively. Even though long-term aging is expected to completely elevate the curves of SEBs with low sulphur levels (10 and 20%GSF) over that of their respective base bitumen, the scenario remains similar to that seen in their unaged and/or short-term aged conditions. As listed in Table 6.82, their G^* values are sometimes greater and sometimes lower than those of neat bitumen. Another noticeable finding is the considerable insensitivity in G^* values against temperature change for these two SEBs at the higher frequency of 4.0Hz. Regardless of aging conditions, this pair displays nearly horizontal G^* curves versus temperature domain as shown in Figure 6.74 (a), Figure 6.75 (a), and Figure 6.76 (a). For P-B70/100-30%GSF, although there are obvious decrease in G^* with increased temperature (above 30°C), the opposite trend is observed at low temperatures. The slope for complex modulus between 25 and 30°C is somewhat negative, indicating an enhanced elastic behavior. This unexpected outcome may be a direct result of the rearrangement of sulphur particles in neat bitumen during long-term aging. G^* curves belonging to PAV residues of SEB with 40 and 50%GSF are all higher than that of the neat bitumen, indicating that even at the ultimate loading frequency of 4.0Hz (in this study) and at high sulphur levels, SEBs are superior to their respective base bitumen in terms of enhanced elastic behavior. This marked increase in elastic response can be attributed to such parameters as the highest loading frequency, high sulphur content, and the impact of long-term aging. However, the presence of formed sulphur networks

proved by its micrographs (please see Chapter 6.3 Morphology Analysis Results pg. 291-294) is supposed to be the major effect on increased elastic behavior. As can be deduced from the Figure A.21 and Figure A.23 (pg. 337 and 339) these elastic networks are mainly seen on the upper surface of the binder.

As mentioned earlier, evaluations of phase angle are generally more sensitive to the chemical structure, and therefore the extension of bitumen, than complex modulus. Thus, δ is remeasured for each sample so as to reveal the impact of long-term aging on the chemical structure of SEBs. As displayed in Figure 6.76 (b), the phase angle isochrones of the first SEB clearly illustrate that at the lowest sulphur level (10%), the behavior of the extended binder remains close to that of the base bitumen in low temperature ranges (25-30°C). On the other hand, when the temperature is increased, the same SEB undergoes a fundamental change in its rheological behavior, displaying a substantial increase in its phase angle. Consistent with other stiffness results and as well as its decreased G^* values, this outcome is not insignificant.

Table 6.82 : Values of rheological parameters for the B70/100 base bitumen and SEB groups at 4.0Hz after long-term aging.

Binder	Stage	Complex Modulus at 4.0 Hz (Pa)				Phase Angel at 4.0 Hz (degree)			
		25 °C	30 °C	40 °C	50 °C	25 °C	30 °C	40 °C	50 °C
B70/100	p	2.46E+07	7.54E+07	2.08E+07	7.49E+06	50.04	65.73	57.35	65.20
B70/100-10%GSF	p	6.84E+07	3.26E+07	3.68E+07	1.14E+07	50.25	66.94	67.91	76.11
B70/100-20%GSF	p	1.62E+07	1.46E+07	1.05E+07	1.62E+07	25.75	27.96	61.18	72.99
B70/100-30%GSF	p	1.08E+07	1.33E+08	3.26E+07	1.65E+07	59.57	23.26	26.64	26.79
B70/100-40%GSF	p	1.11E+08	1.65E+08	1.32E+08	1.18E+07	34.63	43.22	50.27	53.25
B70/100-50%GSF	p	3.31E+08	2.11E+08	3.20E+07	2.94E+07	28.93	36.38	34.85	64.21

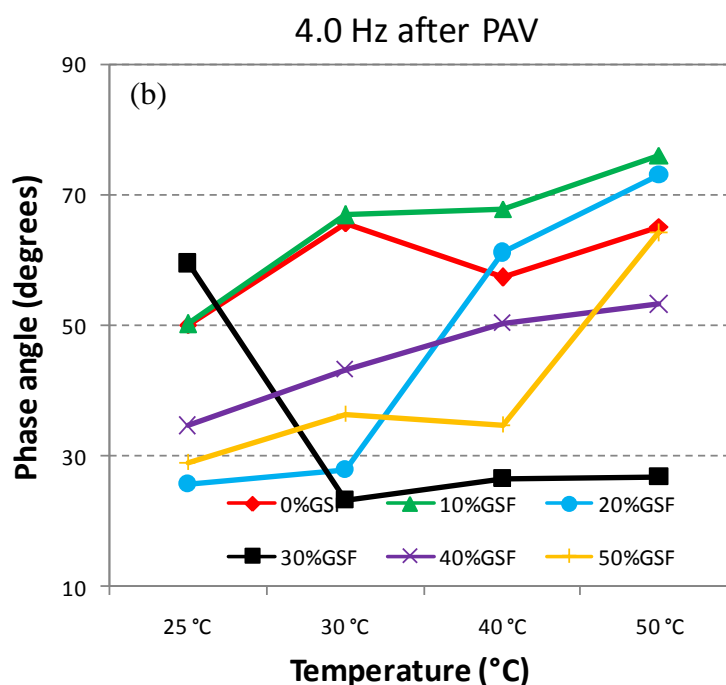
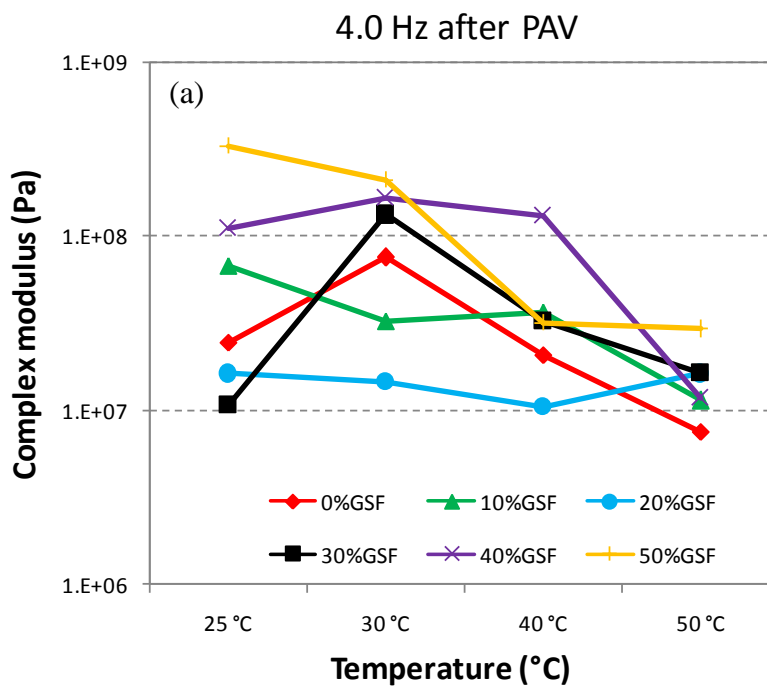


Figure 6.76 : Isochronal plots at 4.0Hz for neat B70/100 bitumen and SEB groups made of B70/100 bitumen after long-term aging. (a) Complex modulus and (b) Phase angle.

The second PAV-aged SEB (with 20%GSF) is observed to be more elastic than its respective base bitumen, particularly at low temperatures, whereas its viscoelastic response becomes more viscous due to its corresponding increase registered for the phase angle above 40°C. With a 30%GSF level content, the variation in phase angle

reconfirms the unexpected result seen in G^* values. As can be remembered, instead of declining, the G^* value of P-B70/100-30%GSF increased with increasing temperature. The trend towards this kind of viscoelastic response is similar for the phase angle trends. Instead of converging to viscous behavior when the temperature is increased from 25 to 30°C, this SEB displayed a more elastic behavior with a corresponding decrease in its phase angle recorded up to 36 degree. At further elevated test temperatures, an obvious plateau appears for the phase angle. This is a desirable phenomenon and an indication of improved resistance to deformation of an asphalt concrete (Edwards et al., 2006).

A marked decrease in phase angle for PAV-aged SEBs at each test temperature starts at the 40%GSF level, and becomes more pronounced for 50%GSF content SEB. In other words, the laboratory simulating long-term aging of these two SEBs using PAV results in differences in the rheological characteristics compared to their respective penetration grade bitumen. These high sulphur content extended binders show a shift towards more elastic behavior which is associated with pressure aging. This stiffening can be attributed to both high loading frequency (4.0Hz) and the degradation of the GSF particles after aging.

A comparison was made among the properties of the long-term aged base bitumen by long term aged SEBs with five different sulphur levels as shown in Table 6.83. Sulphur extension at 10%GSF could not yield a regular variation in G^* values of long-term aged neat bitumen. At increased temperatures, this value first increased then decreased, and eventually again increased. The DSR results and calculations of extensive indices demonstrate that long-term aged neat bitumen containing 20% sulphur (the SEB with 20%GSF) show lower elastic behavior values, with extensive indices lower than 1.00. This means that this SEB may be more sensitive to rutting. However, the same sample was observed to have improved elastic response at upper test temperature (50°C, at which extensive indices are equal to 2.17). In case of 30%GSF utilization, extensive indices seem to be greater than 1.00 at temperatures above 25°C, but apparently higher at 30°C than at 40°C. These results indicate obvious significant rheological differences between the base and extended bitumen at these elevated temperatures after long-term aging. This outcome can be attributed to the melting of present sulphur particles in bitumen phase. As expected, increasing the

amount of GSF from 30 to 40 or/and 50% in PAV-aged neat bitumen caused an obvious increase in its G^* values over temperature domain.

Table 6.83 : Relative changes in complex modulus and aging index at 4.0Hz following long-term aging.

Binder	Stage	Extensive Indices $G^*_{SEB}/G^*_{B70/100}$ at 4.0 Hz				Aging Index (G^*_{PAV}/G^*_{UNAGED}) at 4.0Hz			
		25 °C	30 °C	40 °C	50 °C	25 °C	30 °C	40 °C	50 °C
B70/100	p	1.00	1.00	1.00	1.00	1.51	0.31	1.63	2.67
B70/100-10%GSF	p	2.78	0.43	1.77	1.52	2.54	2.15	5.63	4.60
B70/100-20%GSF	p	0.66	0.19	0.51	2.17	0.58	0.65	1.05	10.77
B70/100-30%GSF	p	0.44	1.77	1.57	2.20	0.12	2.04	1.08	1.86
B70/100-40%GSF	p	4.50	2.19	6.37	1.57	0.17	1.35	11.02	1.80
B70/100-50%GSF	p	13.45	2.81	1.54	3.92	37.29	8.48	1.55	4.45

Rather remarkable results of the comparisons of the impact of long term aging at 4.0Hz on the rheological behaviors with neat bitumen and sulphur extended binders are shown in Table 6.83. The aging index for each binder indicates that the rheology of PAV residue of SEBs is not only dependent on the extended amount of sulphur, but also on the magnitude of the loading frequency. The scenario at 25°C after long-term aging is nearly identical to that observed in the RTFOT-aged samples. As previously mentioned, short-term aging caused a reduction in G^* values and an increase in viscous behavior in 20, 30, and 40%GSF content SEBs. This trend was again seen on the same samples. Although these samples underwent laboratory simulations of long term-aging via PAV, their G^* values did not increase and their viscoelastic behaviors did not become more elastic. However, similar to their behavior after short-term aging, the free-sulphur neat bitumen and SEBs with the lowest and highest content of GSF increased their complex modulus at 25°C (particularly P-B70/100-50%GSF with aging index value of 37.29). At 30°C, excepting that with 20%GSF, all PAV residue of SEBs have aging indexes greater than 1.00. The aging indexes at 40 and 50°C are greater than 1.00, indicating that at high test temperatures long-term aging has a significant influence on the viscoelastic behavior of the samples. At these elevated temperatures, regardless of sulphur level, each PAV residue seems to show a shift towards more elastic behavior under loading frequency of 4.0Hz. This phenomenon is more pronounced particularly for P-B70/100-40%GSF at 40°C and P-B70/100-20%GSF at 50°C (with value of 11.02 and 10.77 respectively).

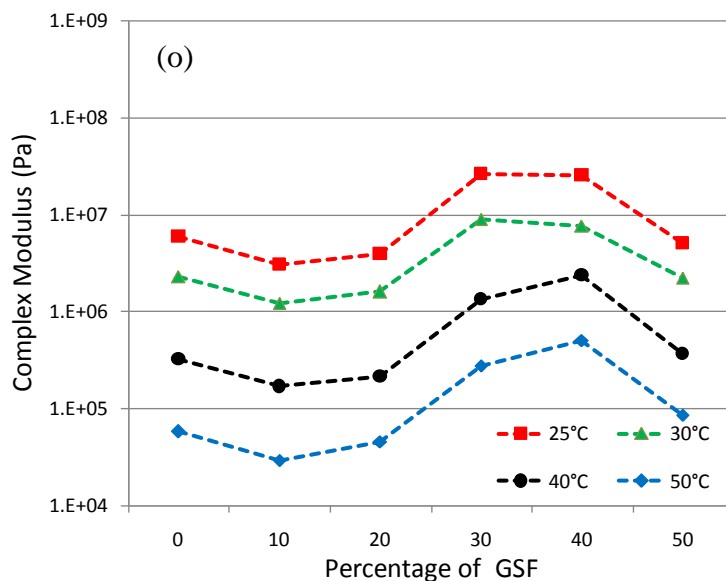
B100/150 and its derivatives

SEBs composed of B100/150 and variable amount of GSF: (0.1 and 1.59Hz)

Dynamic rheological properties

The major focus of DSR is to present two primary viscoelastic parameters of binders. The first one, giving the ratio of shear stress to maximum strain, complex modulus (G^*) is an indicator of the total resistance to deformation when the binder is subjected to shear loading. Phase angle (δ) ranging from 0 to 90° is the second major parameter used during testing to measure the lag between the applied shear stress and shear strain responses (Gordon, 2003b). Bituminous binder is a viscoelastic material; thus, δ is an excellent indicator of both its elastic and viscous behaviors. A δ value of exactly 0° points to a perfect elastic fit, whereas a δ value of exactly 90° corresponds to a perfect viscous fit. The reduced phase angle especially at higher temperatures enhances the elastic behavior of the binder.

The rheological behaviors of the extended of B100/150 at 0.1Hz before and after aging (both RTFOT and PAV) are depicted in Figure 6.77 (o), (r) and (p) and summarized in Table 6.84.



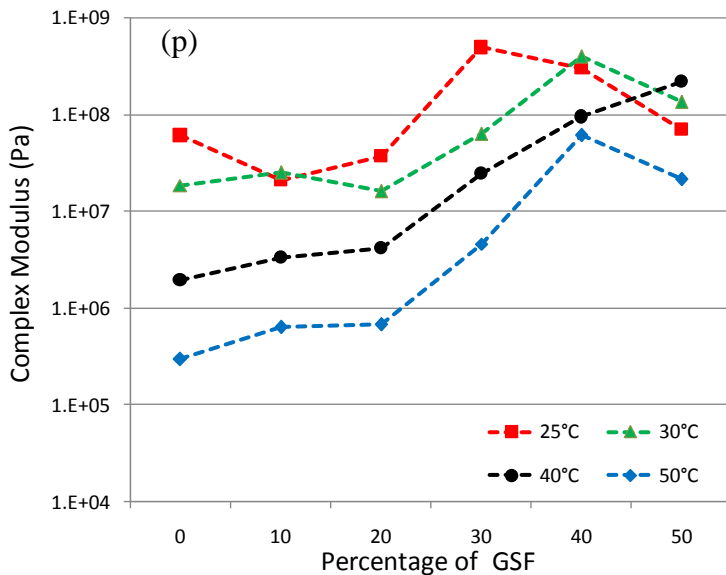
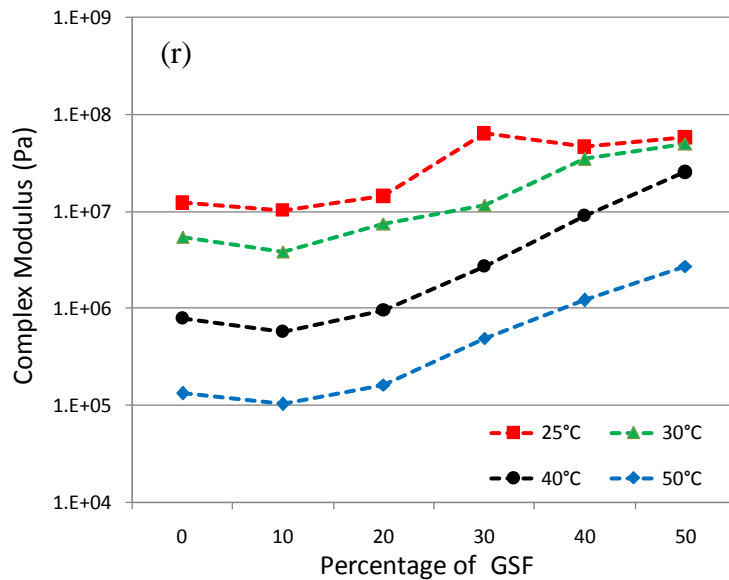


Figure 6.77 : Isochronal plots at 0.1Hz for un-aged, RTFOT and PAV aged B100/150 with various GSF amount (o), (r) and (p) respectively.

Before aging, all SEBs were measured (including neat bitumen). SEBs with 30 and 40% GSF were seen to have maximum G^* , whereas the 10% GSF replacement had the lowest G^* values at all temperatures. As shown in Figure 6.77 (o), the varying trend of G^* is clearly reduced with increasing temperatures. Increasing the temperature from 25 to 50°C caused G^* to be 99.03% for the neat bitumen. However, the value was lower (99.04, 98.85, 98.95, 98.05 and 98.32) for the 10, 20, 30, 40 and 50% GSF replacements separately and respectively. As a consequence, compared to the decrease of G^* for their base bitumen, a lower decrease of G^* for various SEBs (excepting the one including 10% GSF) reveals the fact that increases

in temperature only minimally affect the SEBs in terms of a complex modulus. More specifically, among all SEBs, the 40%GSF is least susceptible to temperatures, while the 10%GSF is most susceptible.

SEBs of 10 and 20%GSF content had lower G^* values, while the 50%GSF content SEB was found to exhibit nearly identical values at all temperatures. 30%GSF replacement increased G^* values of the neat bitumen 3.41, 2.93, 3.17 and 3.76 times at 25, 30, 40 and 50°C respectively. When GSF replacement increased to 40%, a similar response was generated in the value of G^* at 25 and 30°C; however, a distinctive differentiation was more pronounced at 40 and 50°C.

Table 6.84 : Changes in phase angle (δ) at 0.1 and 1.59Hz following GSF replacement and aging.

GSF Ratio	Stage	Phase Angle at 0.1 Hz (degree)				Phase Angle at 1.59 Hz (degree)			
		25 °C	30 °C	40 °C	50 °C	25 °C	30 °C	40 °C	50 °C
0%	o	79.00	80.79	87.63	88.75	51.07	62.20	61.34	85.52
	r	65.00	74.96	83.61	87.14	65.00	72.74	75.35	86.47
	p	55.30	70.42	79.48	85.51	49.40	47.03	59.22	86.26
10%	o	79.80	83.44	86.22	88.12	41.98	52.19	73.98	87.03
	r	68.73	74.73	84.05	86.33	55.34	65.86	79.11	86.05
	p	45.86	59.57	69.50	78.72	30.96	42.83	62.82	79.47
20%	o	80.46	80.32	81.53	84.30	44.45	71.25	80.15	87.27
	r	63.65	71.95	79.44	82.03	45.76	66.45	70.81	87.17
	p	46.80	57.23	67.88	76.00	59.92	28.49	55.94	85.53
30%	o	60.54	72.38	77.02	79.02	60.32	14.69	53.77	84.50
	r	52.07	58.54	70.34	77.70	12.65	67.49	74.01	85.39
	p	45.20	55.19	66.24	70.02	44.56	59.31	23.91	43.92
40%	o	61.24	72.84	75.53	77.11	17.77	52.62	50.05	83.18
	r	45.69	37.04	72.43	78.34	49.21	61.50	78.90	85.72
	p	24.25	31.74	30.07	63.57	44.68	46.11	49.40	51.63
50%	o	75.19	75.84	81.75	83.22	47.79	72.66	82.37	85.67
	r	50.75	55.06	69.86	74.23	45.25	46.12	49.36	54.51
	p	42.87	48.76	58.73	66.51	36.30	41.34	41.80	49.88

o, r, and p representing original age, short- and long-term aging respectively.

The phase angle (δ) values presented in Table 6.84 increased with increasing temperature. Conversely, increasing the GSF proportion up to 20% did not induce an appreciable change, but additional amounts of GSF – particularly 30 and 40% – showed a reduced δ at high temperatures. The decline of the phase angle for the SEBs containing 30 or 40%GSF indicates a higher elasticity, starting even at 25°C. This phenomenon demonstrates that 30 and/or 40%GSF proportions as a replacement may provide optimum dispersion and dissolution of sulphur particles and the crystalline structure in the bituminous binder. Increasing the temperature from 25 to

50°C increased δ 12.33% for the pure bitumen. Considering this increase ratio, the phase angle increased less for SEBs with 10, 20 and 50%GSF, but this trend was dissimilar for the 30 and 40%GSF content SEBs. Since an increase in their phase angle was evidently much higher, they can be confirmed to be the SEBs most affected at increased temperatures.

At 25 and 30°C, 0, 10 and 20%GSF volume SEBs showed a similar δ , whereas at 40 and 50°C, SEBs with zero and 10% and GSF had nearly identical δ , while the SEBs with 20 and 50%GSF were identical with each other. Demonstrating no dominant differences of δ between each other at all temperatures, SEBs with 30 and 40%GSF resulted in the lowest overall phase angle.

For rutting resistance at high temperatures, increased complex modulus (G^*) and low phase angle (δ) values are favorable because they are the mirror of a more elastic behavior (Lu and Isacsson, 1997; Huang, 2008). Corresponding to their promising G^* and δ , the 30 and 40%GSF volume SEBs are expected to demonstrate the utmost elastic response over the entire temperature range, specifically higher for SEBs with 40%GSF, and lower for those SEBs with 30%GSF at 40 and 50°C. Consistent with those previously reported stiffness results and compared to base bitumen, a 10%GSF replacement showed a marked decrease in G^* and a slight increase in δ . This means it will have a more viscous response.

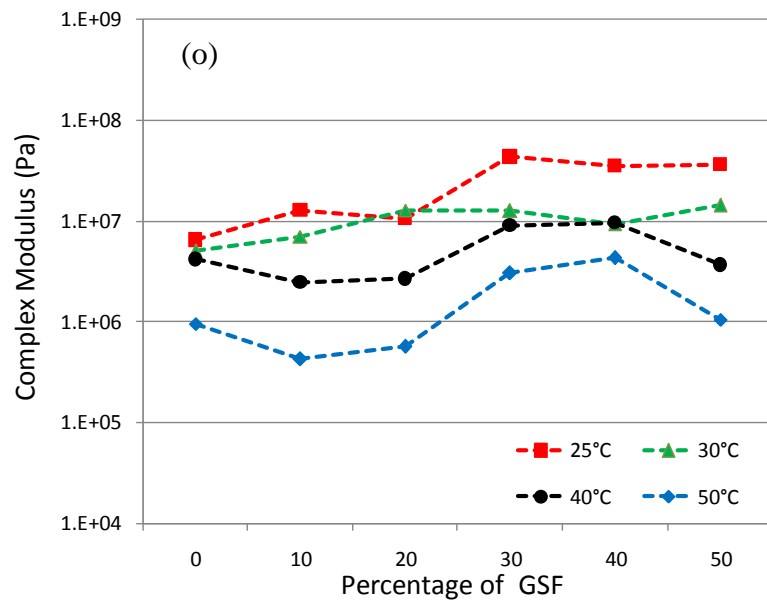
Figures 6.77 (r) and (p) depict the influence of aging on the rheological behavior of the base B100/150 bitumen and its extended binders. The effect of aging on the rheological behavior of SEB can be associated to two principal factors: The first key factor is related to the changes in chemical composition of the bitumen. During aging, evaporation of its soft components is inevitable and bitumen undergoes an increase in the amount and apparent molecular weight of the asphaltene after the capture of the oxygen molecules (Zhang et al., 2010). As a consequence, bitumen will have a tendency to increase its viscosity (Zhang et al., 2010). Secondly, due to its high molecular weight and its physical and chemical interactions with bitumen, the response of the sulphur to aging plays a major and different role in the rheological behavior of SEB.

Testing confirmed an irregular increase in G^* over the temperature range after RTFOT aging. In regards to the effects of short-term aging, of all the binders – including the base – the highest and lowest increase in G^* was typically observed with 50 and 30%GSF content SEBs respectively. The obvious increase in G^* after

PAV aging is greater than after RTFOT aging, owing to the prolonged aging process in the PAV.

Rather than a complex modulus, measurements of the phase angle are generally considered to be more sensitive to the chemical structure, and therefore the extension of the bitumen (Gordon, 2003b). As can be seen in Table 6.84 (r), after short-term aging, the loss of phase angle for the SEB with 40%GSF is very significant at 25 and 30°C. After PAV aging, this loss becomes more apparent, not only at 25 and 30°C but also at 40 and 50°C. It is clear that 40%GSF replacement decreases the phase angle value significantly, meaning that it brings elasticity to the base bitumen after both short and long-term aging.

Since higher frequencies represent a higher vehicle velocity, the viscoelastic behavior of the SEBs was investigated at 1.59Hz. Isochronal plots of complex modulus versus temperature at 1.59Hz for the SEBs and their base bitumen are depicted in Figure 6.78 (o), (r) and (p), and their phase angle values are summarized in Table 6.84.



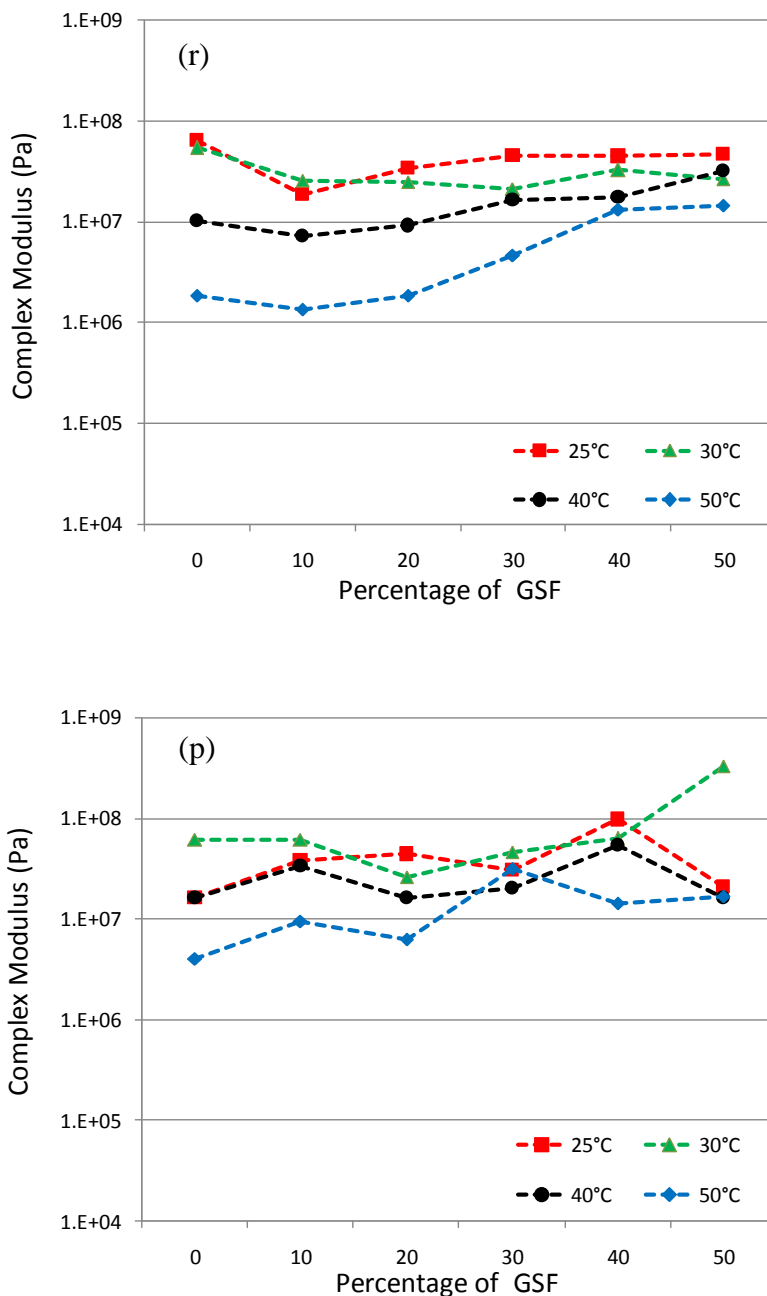


Figure 6.78 : Isochronal plots at 1.59Hz for un-aged, RTFOT and PAV aged B100/150 with various GSF amount (o), (r) and (p) respectively.

It can be seen that the rheology of the SEBs at 1.59Hz differs considerably from that at 0.1Hz. The higher the load frequency, the higher G^* values noted. Increased G^* of SEBs confirms a consistency with the trends observed in the increased elastic response to the higher load frequency, namely, higher vehicle velocity. Depending on the increase in frequency, the largest effect was shown on the 50, 20, 10, and 0%GSF SEBs at 25, 30, 40 and 50°C sequentially and separately. This case highlights the assumption that temperature will play a relatively minor role on G^* in case of an increase in GSF proportions.

Following the increase in frequency, there was a decrease in the phase angles of 40%GSF content SEB at 25°C, and 30%GSF content SEB at 30°C, while their elastic responses increased. At 40°C, both these SEBs continued to increase their elastic behavior, while a marginal effect on the phase angle was shown at 50°C for all of the binders.

Based on the test results performed at 1.59Hz, the most severe impact of short-term aging at 25 and 30°C appeared on the pure bitumen, which may indicate a higher rutting susceptibility. Similar results yielded at 0.1Hz demonstrate that this aging affect at higher temperatures (40 and 50°C) was more pronounced for the 50%GSF content SEB. Tests demonstrated that the 30%GSF content SEB was the least affected by RTFOT aging and also exhibited the most desirable viscoelastic behavior.

Of the short term-aged samples, the G^* increase in frequency yielded the most affect on pure bitumen, whereas sulphur replacement diminished this effect. Consistent with the scenario observed at 0.1Hz, short-term aging did also not regularly alter δ at 1.59Hz.

As previously mentioned regarding its vulnerability to aging, the phase angle of PAV residues at 1.59Hz were more evidently affected than their complex modulus. The general trend appeared to be a steady reduction in δ value at each temperature as the proportion of 30%GSF performed in the SEB. At 50°C, differentiation of the phase angel after PAV aging for the base bitumen and SEBs with 10 and 20%GSF remained relatively the same, whereas in the case of the further GSF replacement, the decrease in δ was reinforced, indicating a gain in rutting resistance at high temperatures.

When investigating the impact of increased frequency on PAV aged residues, the G^* of SEBs with a lower GSF (particularly 10%) remained nearly the same, whereas this effect became more prominent in the case of additional GSF replacement. To conclude, independent of aging, 30 and/or 40% sulphur replacement was found to significantly improve the rheology of the base bitumen at low and at high frequencies, when both G^* and δ are taken into consideration.

SEBs composed of B100/150 and variable amount of GSF; (0.2517 and 4.0Hz)

The rheological behaviors of the extended B100/150 at 0.2517 and 4.0Hz before and after aging (both RTFOT and PAV) have also been investigated. The logarithmic plots of complex modulus (G^*) varying at each test temperature versus sulphur amount, for all unaged samples are displayed in Figure 6.79 and 6.80. The values are then summarized in Table 6.85. Before aging, at low frequency (0.2517Hz) the highest complex modulus values are observed for both the neat bitumen and SEB group at the lowest test temperature (25°C) as compared with the other test temperatures. At this temperature, the lowest G^* values are obvious for the SEBs with lower amounts of sulphur, particularly so in the case of 20%GSF extension. Figure 6.79 illustrates that at 25°C, 10%GSF extension produces a significant decrease in the complex modulus of the neat bitumen and following the 20%GSF extension there is a further decrease in value. This decline in G^* may be attributed to an increment of the viscous component (G'') rather than elastic one (G'). Further information extracted from Table 6.85 clarifies that at 25°C, 10%GSF extension made complex modulus of original B100/150 bitumen reduce over five times (from 6.99E+07 to 1.29E+07Pa), whereas 20%GSF extension led the complex modulus of original B100/150 bitumen to reduce over thirteen times (from 6.99E+07 to 5.37E+06Pa). On the contrary, the highest value of the complex modulus found for the SEB with 40%GSF is due to its higher sulphur amount. As shown in Figure 6.79 and evidenced in Table 6.85, at 25°C the B100/150-40%GSF exhibit an enhanced elasticity as compared with its respective neat bitumen. As expected, this amount of sulphur in neat bitumen produced an increase in both the viscous and elastic component, but the variation of elastic one is clearly higher in amount; as a consequence, this SEB will retain, at low temperature, a higher elastic component as compared with the other sulphur-extended-binders as well as non-extended bitumen. It is important to underline how the contribution of increasing sulphur up to 30% on the whole product viscoelastic response is nearly negligible when the B100/150-30%GSF is taken into account. In this case, one can observe that this SEB is identical to neat bitumen in terms of rheological behavior at low temperature (G^* values: 6.99E+07 and 5.41E+07Pa for neat bitumen and this SEB respectively).

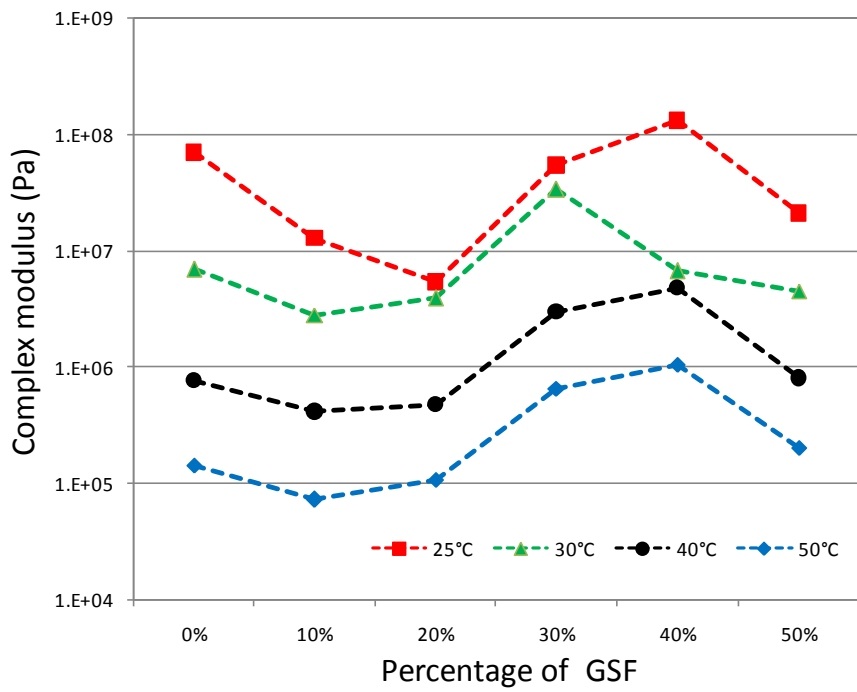


Figure 6.79 : Isochronal plots at 0.2517Hz for un-aged B100/150 with various GSF amount.

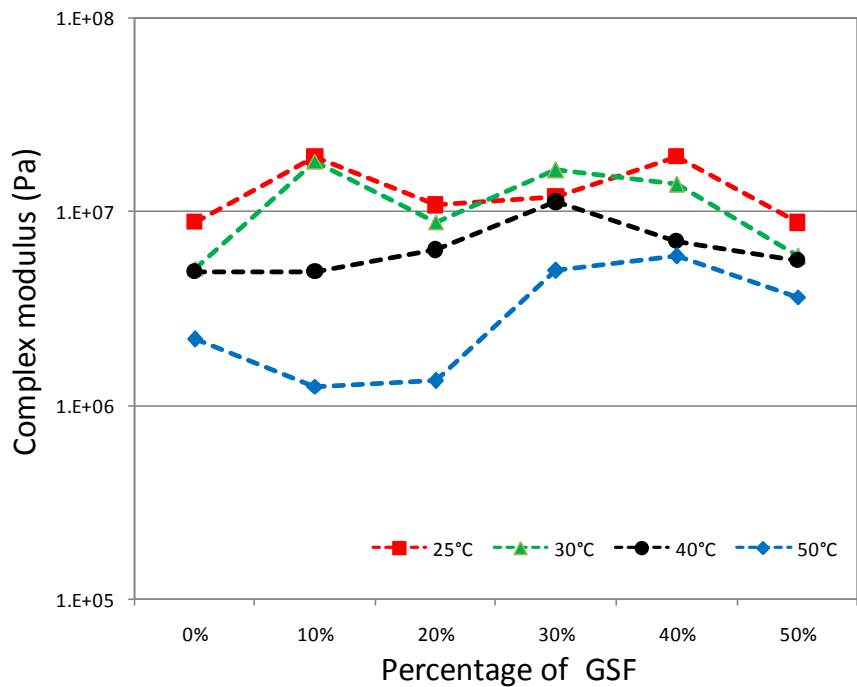


Figure 6.80 : Isochronal plots at 4.0Hz for un-aged B100/150 with various GSF amount.

In the case of SEB with 50%GSF, a softening effect is detected due to lower value of G^* . At this highest GSF content, the softening effect is believed to be related to the pronounced viscous component (G'') of the SEB. As illustrated in Figure A.35 (o1-o3) (please visit Chapter 6.3 Morphology Analysis Results and pg. 350) aggregated sulphur particles on the surface forming viscous networks are believed to be dominant to elastic networks.

Increasing the loading frequency from 0.2517 to 4.0Hz yielded a totally different response in viscoelastic behavior at 25°C. The rheological response, expressed by the G^* value, increased in amount when the SEBs with lower GSF content (10 and 20%) were studied. Owing to most probably high loading frequency, those SEBs seem to have improved elasticity with their elevated G^* values. However, the increase in loading frequency could not enhance the viscoelastic behavior of the other binders (including neat bitumen).

Comparing the G^* values of the SEBs at 4.0Hz points out that the first four SEBs exhibit more elastic behavior than their respective neat bitumen. However, similar to its behavior at 0.2517Hz, B100/150-50%GSF is still softer than non-extended bitumen at 4.0Hz due to its lower G^* value at 25°C. Nevertheless, the magnitude of gap between their complex modulus values is not as large as that seen in 0.2517Hz.

At 0.2517Hz loading frequency, increasing test temperature from 25 to 30°C lowered the logarithmic curve of complex modulus for each sample. The gap between the curves drawn at 25 and 30°C is obvious at low and high temperature ranges, whereas the magnitude of this gap lessens considerably at the medium temperature range. Despite the observed variations, these two curves seems to be almost parallel to each other, indicating that an increase in temperature lowered the G^* values but could not make a significant difference in rheological behavior of samples. Differing from 25°C, instead of the SEB with 40%GSF, among the all samples the SEB with 30%GSF demonstrates the maximum complex modulus values (3.37E+07Pa).

By contrast, the same increase in temperature at 4.0Hz somewhat resulted in different viscoelastic behavior particularly, for the SEB with 30%GSF. Instead of a decline in G^* values, an improved elastic behavior is clear for this sample due to its elevated complex modulus. This unexpected response can be attributed to contribution of sulphur particles existing in a gel-like form by means of increased

temperature. Overall, due most probably to the high loading frequency as 4.0Hz and the increase in temperature, regardless of the GSF proportions, every SEB appears to have higher complex modulus than their respective 100/150 penetration bitumen.

At 0.2517 and 4.0Hz loading frequency, the curves drawn at 40°C are placed under that of 25 and 30°C as shown in Figure 6.79 and 6.80. The isochronal plots of G^* at this temperature indicate that the level of sulphur extension is becoming more pronounced at 30 and 40%GSF level for 0.2517 and 4.0Hz respectively.

At 0.2517Hz, for the SEBs with 10 and 20%GSF, the scenario at 40°C did not differ from that previously seen at 25 and 30°C. This SEB pair again seemed to have shown a shift towards more viscous behavior. This remarkable increase in viscous response can be attributed to viscosity of the low amounts of sulphur particles in the neat bitumen. This amount, while low, is sufficient in allowing the viscous network to influence the mechanical properties of 100/150 penetration bitumen. Taking other traditional bitumen tests into consideration, we can state with certainty that these observed results are not coincident, conversely these rheological parameters for SEB with lower GSF content are strongly consistent with their own softening point, penetration, and viscosity grades. Hence, for these SEBs, a perfect correlation between complex modulus and conventional test results may be successfully used to characterize them.

The case at 4.0Hz and 40°C is a little different for low amounts of GSF utilization. At 10% sulphur extension, a decrease in G^* value is clearly negligible (from 4.94E+06 to 4.89E+06Pa). And unlike its behavior at 0.2517Hz, the complex modulus of the SEB with 20%GSF exceeded that of neat bitumen at 4.0Hz. The other SEBs also displayed enhanced elastic behavior with their elevated G^* values compared to their respective bitumen. However among all SEBs, the one with 30%GSF holds the highest value at 4.0Hz and 40°C.

As expected, at both loading frequencies (0.2517 and 4.0Hz), the logarithmic plots of complex modulus drawn at 50°C are lower than those of other test temperatures, indicating that the higher temperature reasonably caused a decline in G^* values. At 0.2517Hz loading frequency, the curve at 50°C is completely parallel to the previous one (the curve at 40°C), pointing out that despite the fact that the increase in temperature decreased their G^* values, overall similar phenomena were again

observed for the all samples. In the other words, at 50°C, the SEB with 10 and 20%GSF are more viscous compared to their respective bitumen, and the SEB with 40%GSF has the highest complex modulus value.

At 4.0Hz the SEBs with 10 and 20%GSF are seen for first time to have reduced G^* values compared to 100/150 penetration bitumen at 50°C. Even though these two binders were extended with different amounts of sulphur, they display nearly identical viscoelastic behavior due to their very close G^* values (1.25E+06 and 1.33E+06Pa respectively). Among all binders, including the neat bitumen, the SEB with 40%GSF demonstrates the utmost elastic behavior with its highest G^* value (5.89E+06Pa).

Table 6.85 : Changes in complex modulus (G^*) at 0.2517 and 4.0Hz following GSF replacement and aging.

GSF Ratio	Stage	Complex Modulus at 0.2517 Hz (Pa)				Complex Modulus at 4.0 Hz (Pa)			
		25 °C	30 °C	40 °C	50 °C	25 °C	30 °C	40 °C	50 °C
0%	o	6.99E+07	6.92E+06	7.63E+05	1.42E+05	8.84E+06	5.12E+06	4.94E+06	2.20E+06
	r	4.02E+07	1.02E+07	1.86E+06	3.17E+05	2.03E+07	1.73E+07	1.17E+07	5.45E+06
	p	6.61E+07	2.81E+07	4.31E+06	6.95E+05	4.91E+07	2.59E+07	2.43E+07	8.27E+06
10%	o	1.29E+07	2.78E+06	4.12E+05	7.21E+04	1.91E+07	1.82E+07	4.89E+06	1.25E+06
	r	2.24E+07	8.18E+06	1.35E+06	2.45E+05	1.62E+07	1.26E+07	1.85E+07	3.68E+06
	p	8.96E+07	5.05E+07	7.23E+06	1.45E+06	2.51E+07	1.54E+07	1.54E+07	9.51E+06
20%	o	5.37E+06	3.90E+06	4.74E+05	1.06E+05	1.08E+07	8.82E+06	6.34E+06	1.33E+06
	r	3.43E+07	2.35E+07	2.25E+06	3.63E+05	2.53E+07	1.48E+07	1.12E+07	4.10E+06
	p	4.10E+07	1.72E+07	8.08E+06	1.42E+06	3.51E+07	3.20E+07	3.60E+07	2.15E+07
30%	o	5.41E+07	3.37E+07	3.01E+06	6.49E+05	1.20E+07	1.65E+07	1.12E+07	4.97E+06
	r	6.07E+07	2.63E+07	4.82E+06	1.04E+06	1.69E+07	1.63E+07	1.99E+07	1.13E+07
	p	9.43E+07	9.03E+07	1.73E+07	1.36E+07	3.22E+07	1.64E+07	1.12E+07	1.62E+07
40%	o	1.31E+08	6.70E+06	4.85E+06	1.05E+06	1.94E+07	1.39E+07	7.04E+06	5.89E+06
	r	8.97E+07	5.84E+07	1.06E+07	2.49E+06	3.41E+07	1.31E+07	2.85E+07	1.03E+07
	p	3.13E+08	1.72E+08	1.40E+08	8.39E+07	1.39E+08	2.72E+07	1.60E+07	1.93E+07
50%	o	2.09E+07	4.51E+06	7.97E+05	2.00E+05	8.75E+06	5.87E+06	5.64E+06	3.63E+06
	r	1.30E+08	1.09E+08	8.70E+07	6.76E+06	1.92E+07	1.80E+07	1.22E+07	1.15E+07
	p	6.44E+07	6.14E+07	4.09E+07	1.74E+07	1.12E+07	1.27E+07	1.29E+07	1.15E+07

o, r, and p representing original age, short- and long-term aging respectively.

A higher complex modulus as well as lower phase angle values are expected following the aging process. However, it is worthy to point out that because such rheological parameters as complex modulus and phase angle are only related to the higher stiffness of the aged sample, they, by themselves, are not sufficient to guarantee the positive qualities of such residues, meaning a good elasticity and stiffness according to frequency or temperature (Mastrofini and Scarsella, 2000). Once the aging process has been performed, the temperature-dependent rheological

behavior of SEB reflects the individual contribution that neat bitumen and sulphur give to the total response.

The logarithmic plots of complex modulus (G^*) for all RTFOT-aged samples versus sulphur amount at 0.2517 and 4.0Hz and varying at each test temperature are displayed in Figure 6.81 and 6.82 respectively and the values are listed in Table 6.85. In addition, the aging index (G^*_r/G^*_o) for each residue is displayed in Table 6.86. Figure 6.81 illustrates that the hierarchy among logarithmic G^* curves did not change after RTFOT aging. In other words, the logarithmic curve drawn at 25°C presenting the highest G^* values is still located at the top and the logarithmic curve drawn at 50°C presenting the lowest G^* values is still located at the bottom, while the rest curves (at 30 and 40°C) are placed between them. On the contrary, at high frequency (4.0Hz), the same hierarchy for the first three curves is not observed as depicted in Figure 6.82. The curve of 50°C illustrating the lowest complex modulus values is placed at the bottom, whereas a regular change in complex modulus does not exist at other test temperatures.

Table 6.86 shows that at low frequency and the lowest test temperature (0.2517Hz and 25°C), an increased complex modulus is generally observed for the RTFOT aged samples as compared with the original ones. However, the opposite trend can be seen for the R-B100/150-40%GSF and short-term aged neat bitumen, where there is a slight decrease in complex modulus. Similarly, at high frequency (4.0Hz), short-term aging has a distinctive influence on the complex modulus at 25°C since both the elastic and viscous components are clearly affected by the RTFOT test. However, the opposite trend can be again seen for the R-B100/150-10%GSF due to fact that its aging index is less than 1.00, as evidenced in Table 6.86. This slight decrease in the complex modulus for R-B100/150-40%GSF at 0.2517Hz and R-B100/150-10%GSF at 4.0Hz (i.e. G'' increases more than G' after RTFOT) can be attributed to a more sol-like behavior of sulphur particles in bitumen phase after short-term aging.

The values of complex modulus measured at 0.2517Hz and 30°C after short-term aging are illustrated in Figure 6.81 and listed in Table 6.85. RTFOT aging led to an increase in their G^* values samples. After aging, the samples have relatively improved viscoelastic behavior compared with their original ones. The magnitude of increase in G^* varies regularly with an increase in the amount of GSF content. However, this regular variation is seen to disappear at 30% sulphur level since a

sudden drop in G^* value for R-B100/150-30%GSF is obvious at 30°C (aging index: 0.78).

Comparing its impact at 0.2517Hz and 30°C, RTFOT aging has relatively little influence on complex modulus at 4.0Hz and 30°C due to relatively lower aging index. In this sense, the elastic component as well as the viscous one may be said to have less affected at high loading frequency by RTFOT. The SEB with 10%GSF continued to demonstrate viscous behavior again, even though it was short-term aged. The influence of aging on the flow properties at 4.0Hz and 30°C appears to be least important at the medium-high sulphur level, when short-term aged SEBs (with 30 and 40%GSF) show nearly identical behavior with the original (aging index; 0.99 and 0.94 respectively).

From 30°C above, regardless of magnitude of loading frequency, short-term aging has a remarkable influence on the rheological behavior of binders, since all of them have an aging index greater than 1.00 as listed in Table 6.86. The values of the aging indexes reflect the positive aging resistance properties of the RTFOT residues. The much higher value of the aging index of RTFOT residue is a perfect indicator of a high degree of hardening. In this sense, with its great aging indexes at both low and high frequency as well as at both 40 and 50°C, the 50%GSF content SEB is the binder that is most sensitive to short-term aging process. Its highest amount of sulphur, considered mainly responsible for the formation of a more structured and aggregated elastic network in aged bitumen compounds, is believed to be the main cause of this enhanced elastic behavior.

The results illustrated in Figure 6.82 and listed in Table 6.85 indicate that RTFOT-aged SEBs with 30, 40, and 50%GSF display analogous flow properties at 4.0Hz and 50°C; their complex modulus values are very close to each other (1.13E+07, 1.03E+07, and 1.15E+07Pa respectively).

Table 6.86 : Showing the changes in complex modulus at 0.2517 and 4.0Hz following RTFOT and PAV aging.

GSF Ratio	Aging Indices	Changes in G^* following aging at 0.2517Hz				Changes in G^* following aging at 4.0Hz			
		25 °C	30 °C	40 °C	50 °C	25 °C	30 °C	40 °C	50 °C
0%	G^*_r/G^*_o	0.58	1.47	2.43	2.23	2.30	3.38	2.38	2.48
	G^*_p/G^*_o	0.95	4.06	5.65	4.90	5.56	5.07	4.91	3.77
10%	G^*_r/G^*_o	1.74	2.95	3.27	3.40	0.85	0.69	3.79	2.95
	G^*_p/G^*_o	4.00	6.17	5.36	5.90	1.55	1.22	0.83	2.58
20%	G^*_r/G^*_o	6.39	6.02	4.76	3.43	2.34	1.67	1.76	3.07
	G^*_p/G^*_o	7.62	4.42	17.05	13.35	3.25	3.63	5.68	16.10
30%	G^*_r/G^*_o	1.12	0.78	1.60	1.60	1.41	0.99	1.78	2.28
	G^*_p/G^*_o	1.74	2.68	5.76	21.05	2.68	0.99	0.99	3.26
40%	G^*_r/G^*_o	0.68	8.72	2.20	2.36	1.76	0.94	4.05	1.74
	G^*_p/G^*_o	2.38	25.73	28.95	79.82	7.15	1.96	2.27	3.28
50%	G^*_r/G^*_o	6.20	24.26	109.10	33.83	2.20	3.07	2.16	3.18
	G^*_p/G^*_o	3.08	13.61	51.34	87.13	1.27	2.17	2.29	3.17

o, r, and p representing original age, short- and long-term aging respectively.

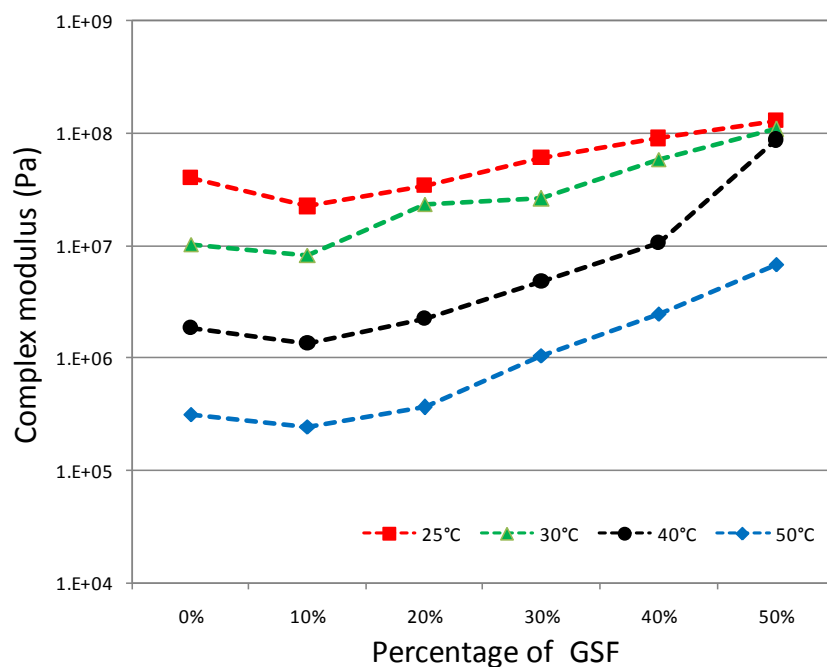


Figure 6.81 : Isochronal plots at 0.2517Hz for RTFOT-aged B100/150 with various GSF amount.

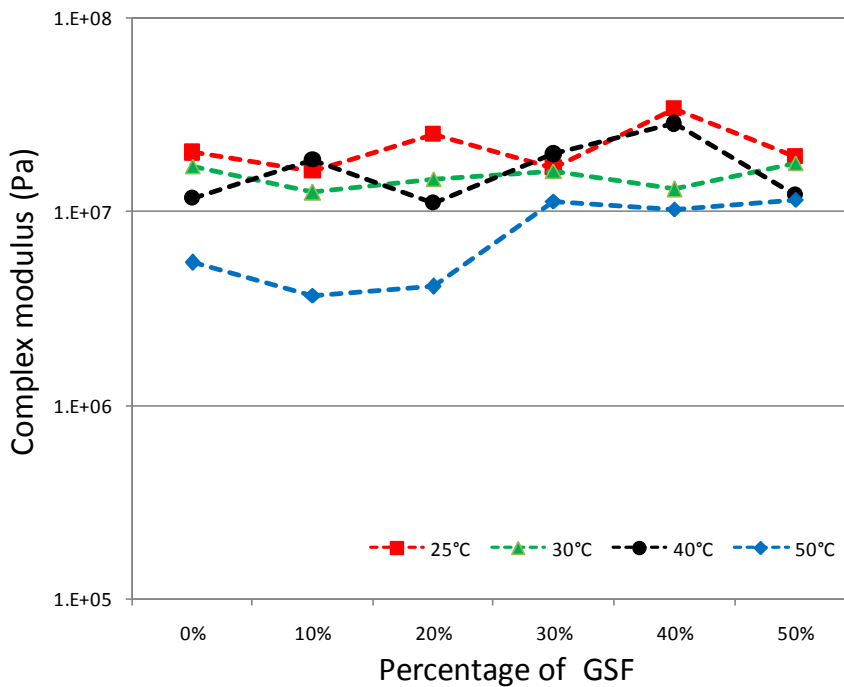


Figure 6.82 : Isochronal plots at 4.0Hz for RTFOT-aged B100/150 with various GSF amount.

In order to assess the quality of given PAV residue through long-term aging resistance, the rheological properties of each SEB are again investigated. As illustrated in Figure 6.83 and 6.84, long-term aging greatly influences complex modulus at both 0.2517 and 4.0Hz. It should be noted that the aging effect is strongly dependent not only on temperature range and the amount of GSF but also the aging process. Once the PAV test has been performed, the temperature-dependent rheological behaviors of SEBs, reflect the individual contribution that bitumen phase and sulphur phase gives to the total response.

Figure 6.83 proves that the previous trend observed at both original and RTFOT-aged stage regarding to hierarchy between thermal logarithmic curves did not change at PAV-aged stage. Similarly, the curve drawn at 25°C is again located at top of the graph illustrating higher G^* values, whereas the curve drawn at 50°C is again placed at bottom of the graph illustrating lower G^* values. The medium-temperature curves are then placed between them. However, comparing with those at the RTFOT-aging stage, the curves after PAV aging begin to near each other at elevated sulphur amounts, indicating SEBs at high GSF content display similar viscoelastic behavior, regardless of test temperature. On the other hand, this hierarchy is not observed at 4.0Hz, particularly from 20%GSF level above as demonstrated in Figure 6.84.

Table 6.86 shows that at low frequency and the lowest test temperature (0.2517Hz and 25°C), an increased complex modulus is observed for all PAV-aged SEBs as compared with the originals. After long-term aging, even the 40%GSF content SEB is observed to have improved its elastic behavior with an aging index (G^*_p/G^*o) greater than 1.00 (2.38). However, the scenario for neat bitumen remained the same. Despite being exposed to long-term aging, it still demonstrates a shift towards more viscous behavior. Owing to aging, this recorded small decrease in complex modulus for 100/150 penetration bitumen suggests that a variation from a more gel-like (elastic and more structured) to a more sol-like (viscous and less structured) behavior is occurring.

Increasing the loading frequency from 0.2517 to 4.0Hz at the same test temperature (25°C) yielded remarkable results on the PAV-aged samples. All long-term aged samples, including neat bitumen, were observed to increase their elasticity but not their viscous component due to their elevated G^* . Despite the fact that each sample seems to have an aging index greater than 1.00, the 40%GSF content SEB demonstrates the maximum value and indicates that it is the binder that is most sensitive to long term aging (aging index: 7.15).

When we looked at the effects of long-term aging we saw that when the test temperature was increased to 30°C at 0.2517Hz loading frequency, out of all the binders, including the base one, the highest and lowest magnitude of increase in G^* was typically observed with 40 and 30%GSF content SEBs. Nevertheless, as evidenced in Table 6.86, all long-term aged samples seem to have improved their elasticity owing to the prolonged aging process in PAV.

Table 6.85 points out that at 4.0Hz loading frequency neither RTFOT nor PAV aging played an observable role in viscoelastic behavior of the SEB with 30%GSF at 30°C. Since neither the elastic component nor the viscous component of this sample were affected by RTFOT or/and PAV, complex modulus remained nearly same (1.65E+07, 1.63E+07, and 1.64E+07Pa for original, RTFOT-aged stage, and PAV-aged stage respectively).

In investigations of the impact of increased frequency on PAV-aged SEB residues at 40°C, a considerable increase in G^* of samples with lower GSF (particularly 20%) was seen, whereas the opposite effect became even more prominent when GSF was

further utilized. Another interesting result is that it was assumed that there would be a variation in magnitude of aging index for 30%GSF content SEB when the temperature was increased from 30 to 40°C at 4.0Hz. However, this expectation was not met and the value remained the same (0.99). This same value remained almost consistent at different temperatures. In addition to this similarity, this sulphur-extended-binder shows analogous flow properties at 30 and 40°C before aging and after PAV aging.

The clear increase in G^* after PAV aging is not surprisingly greater than after RTFOT aging at 0.2517Hz and at 50°C owing to the prolonged aging process in the PAV. This hypothesis can also be adapted to high loading frequency if the exceptional response of the SEB with 10%GSF is ignored.

Table 6.86 shows that its RTFOT aging index is greater than the PAV ($G^*_r/G^*_o > G^*_p/G^*_o$). This phenomenon can be attributed to its determined elastic networks of sulphur particles formed during RTFOT process.

To conclude, it should be noted that changes arising from RTFOT or/and PAV aging in temperature susceptibility of the stiffness (G^*) of sulphur-extended-binders was found to depend on a combined effect of both neat bitumen hardening and degradation of sulphur particles.

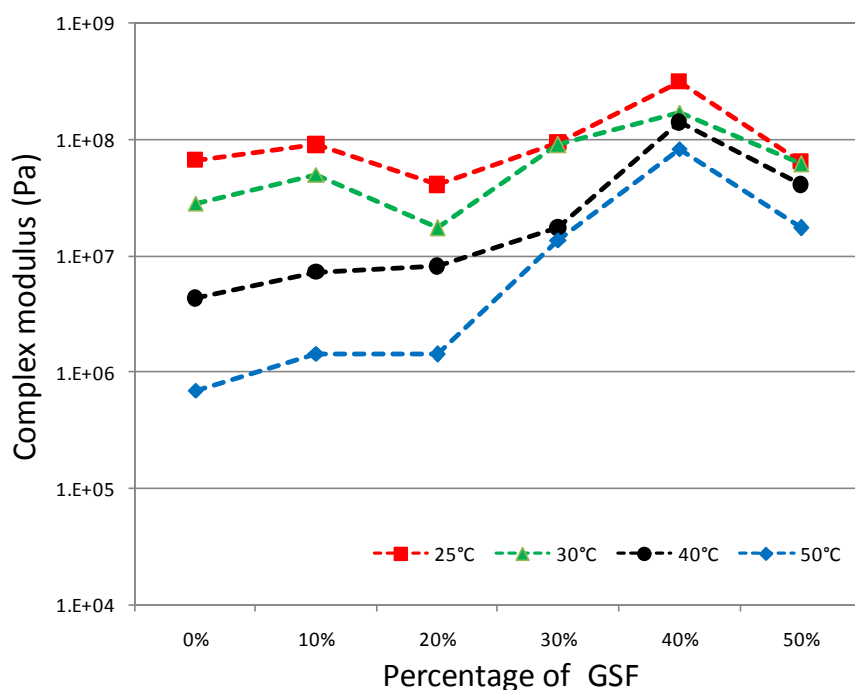


Figure 6.83 : Isochronal plots at 0.2517Hz for PAV-aged B100/150 with various GSF amount.

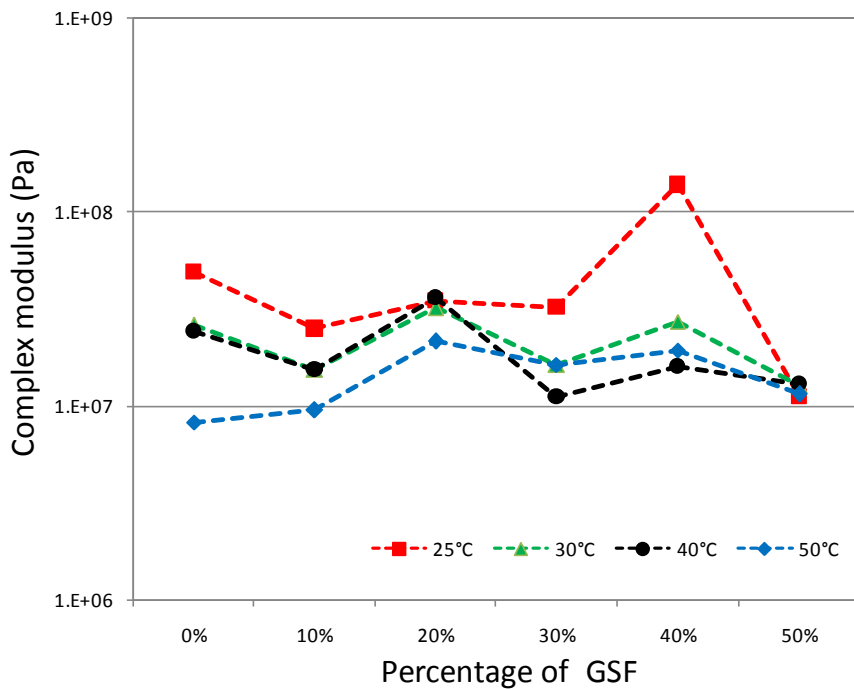


Figure 6.84 : Isochronal plots at 4.0Hz for PAV-aged B100/150 with various GSF amount.

The variations in second DSR parameter that is to say the phase angle (δ) values at 0.2517 and 4.0Hz are shown in Table 6.87.

Out of all original binders, the base has the lowest phase angle at 0.2517Hz and at 25°C, indicating that it is this binder that has the most promising elastic behavior. However, when the loading frequency was increased to 4.0Hz, a completely opposite effect was seen on the samples at the same test temperature; namely, original neat bitumen appears to be more likely to shift towards more viscous behavior, compared to sulphur-extended-binders. This result is an evolution of the sulphur fraction towards a more gel-like state at high loading frequency, giving the whole binder a more elastic character.

Consistent with their complex modulus values at 0.2517Hz, the increase in phase angles for the original 10 and 20%GSF content SEBs is meaningful at 30°C. Depending on the increase in frequency, the same samples are promising at the same temperature in terms of enhanced viscoelastic behavior compared to their respective base bitumen. It is obvious that gel-like states increase in parallel to increases in loading frequency.

Table 6.87 : Changes in phase angle (δ) at 0.2517 and 4.0Hz following GSF extension and aging.

GSF Ratio	Stage	Phase Angle at 0.2517 Hz (degree)				Phase Angle at 4.0 Hz (degree)			
		25 °C	30 °C	40 °C	50 °C	25 °C	30 °C	40 °C	50 °C
0%	<i>o</i>	42.45	76.67	87.52	89.11	43.92	45.32	56.51	59.21
	<i>r</i>	65.00	78.67	84.07	87.41	30.12	38.19	54.29	83.17
	<i>p</i>	55.49	69.41	79.65	85.29	40.10	4.74	74.79	87.30
10%	<i>o</i>	73.38	80.84	87.42	88.15	33.32	51.78	72.11	80.38
	<i>r</i>	68.00	76.45	83.20	86.29	46.17	49.87	26.98	69.87
	<i>p</i>	42.90	55.53	71.68	77.87	20.10	48.95	61.02	78.19
20%	<i>o</i>	86.54	79.51	83.18	83.31	37.12	56.46	54.06	77.63
	<i>r</i>	55.07	65.88	79.50	81.89	40.64	45.73	56.39	86.29
	<i>p</i>	60.77	69.41	72.83	74.30	18.76	39.90	71.21	76.63
30%	<i>o</i>	56.64	67.27	78.12	80.10	32.20	35.53	39.43	62.40
	<i>r</i>	67.14	78.54	79.23	80.00	27.06	32.93	53.50	58.74
	<i>p</i>	36.48	54.62	41.33	66.90	19.93	31.77	36.65	73.92
40%	<i>o</i>	55.20	60.76	67.01	74.70	30.22	45.69	69.70	83.79
	<i>r</i>	42.25	53.34	59.24	79.99	43.11	47.03	59.22	41.07
	<i>p</i>	37.54	64.78	61.56	57.72	15.69	20.75	35.86	53.86
50%	<i>o</i>	58.70	76.14	82.93	84.01	30.04	35.28	70.67	76.16
	<i>r</i>	32.08	53.88	64.46	72.97	32.57	39.64	31.93	52.51
	<i>p</i>	47.17	46.99	51.60	56.69	14.62	21.99	28.54	54.79

o, r, and p representing original age, short- and long-term aging respectively.

As can be seen in Table 6.87, after short-term aging, the loss of phase angle at 40°C for the 50%GSF content SEB is very significant at both loading frequencies.

At 50°C and at 0.2517Hz, there are only minimal variations in phase angle variations due to RTFOT aging of neat bitumen and of 10, 20 and 30%GSF content SEBs, all of which show that good aging resistance is minimal (passing from 89.11 to 87.41 for neat bitumen, from 88.15 to 86.29 for the SEB with 10%GSF, from 83.31 to 81.89 for the SEB with 20%GSF, and from 80.10 to 80.00 for the SEB with 20%GSF). On the other hand, under the same test temperature and the same loading frequency, PAV aging produced a remarkable decrease in phase angles of the samples: following the long-term aging all binders become harder as compared with the original and RTFOT-aged samples. Increasing the loading frequency from 0.2517 to 4.0Hz at 50°C generally yielded a decrease in phase angle of samples regardless of aging.

To sum up, a good equilibrium between stiffness and elasticity is important to assure good performances, both at high and low temperatures, giving the binder enough flexibility so that it does not crack at low temperature and enough rigidity so that it does not flow at high temperatures (Mastrofini and Scarsella, 2000).

SEBs composed of B100/150 and variable amount of GSF at 0.6329Hz;

Rheological parameter values at unaged stages and at 0.6329Hz for the unaged base 100/150 bitumen and SEBs are presented in Table 6.88. In addition, the isochronal plots of complex modulus (G^*) and phase angle (δ) versus temperature at 0.6329Hz for both are shown in Figure 6.85 (a) and (b) respectively.

Before aging, a marked decrease in complex modulus (G^*) at each test temperature is obtained in neat bitumen by the extension of low sulphur content (10 and 20%GSF). Consistent with those previously reported results, the extension of neat bitumen with low amounts of GSF (10 and 20%GSF) decreases the complex modulus significantly, meaning that low level sulphur extensions confer viscous behavior to the base bitumen. Further increase in the sulphur level caused increased complex modulus. However, the benefit of sulphur on rheology seems to disappear in case of 50%GSF extension, particular at medium and high temperature ranges.

Table 6.88 : Values of rheological parameters for the B100/150 base bitumen and SEB groups at 0.6329Hz before aging.

Binder	Stage	Complex Modulus at 0.6329 Hz (Pa)				Phase Angle at 0.6329 Hz (degree)			
		25 °C	30 °C	40 °C	50 °C	25 °C	30 °C	40 °C	50 °C
B100/150	o	5.41E+07	2.03E+07	2.17E+06	3.51E+05	51.00	55.53	85.24	88.10
B100/150-10%GSF	o	1.49E+07	7.20E+06	9.05E+05	1.76E+05	53.36	68.23	86.39	88.79
B100/150-20%GSF	o	2.06E+07	7.66E+06	1.15E+06	2.47E+05	44.34	75.01	83.81	83.78
B100/150-30%GSF	o	7.07E+07	2.96E+07	6.13E+06	1.43E+06	57.09	69.72	70.48	82.22
B100/150-40%GSF	o	7.07E+07	2.14E+07	1.65E+07	2.11E+06	43.53	44.37	69.62	79.25
B100/150-50%GSF	o	9.55E+07	1.14E+07	1.76E+06	4.57E+05	38.63	37.94	84.51	85.71

Phase angle is another very important rheological parameter for bituminous binders. The desired effect of sulphur extension is to provide a sulphur network that imparts elastic stability at higher temperatures and this is indicated by a decrease in phase angle. It is clear that the utilization of GSF at high levels in 100/150 penetration bitumen decreases the phase angle (or loss tangent) value significantly, meaning that a sulphur extension that exceeds 30% brings elasticity to the base bitumen. It is assumed that the formation of elastic networks in bitumen phase is most probably responsible for more stiffened binder owing to relatively high sulphur presence.

On the contrary, aside from the decreased stiffness at each temperature, 10% sulphur extension causes an elevated phase angle in original neat bitumen, as shown in both Table 6.88 and Figure 6.85 (b).

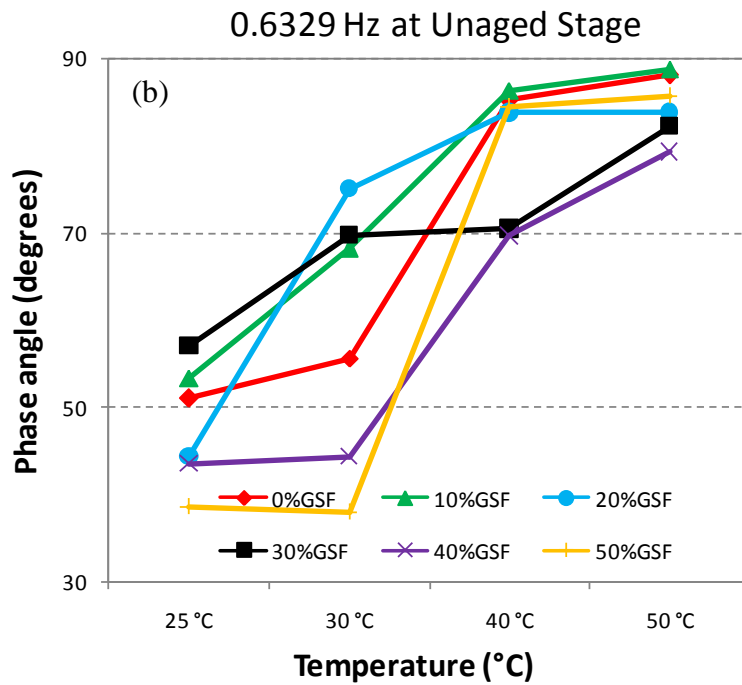
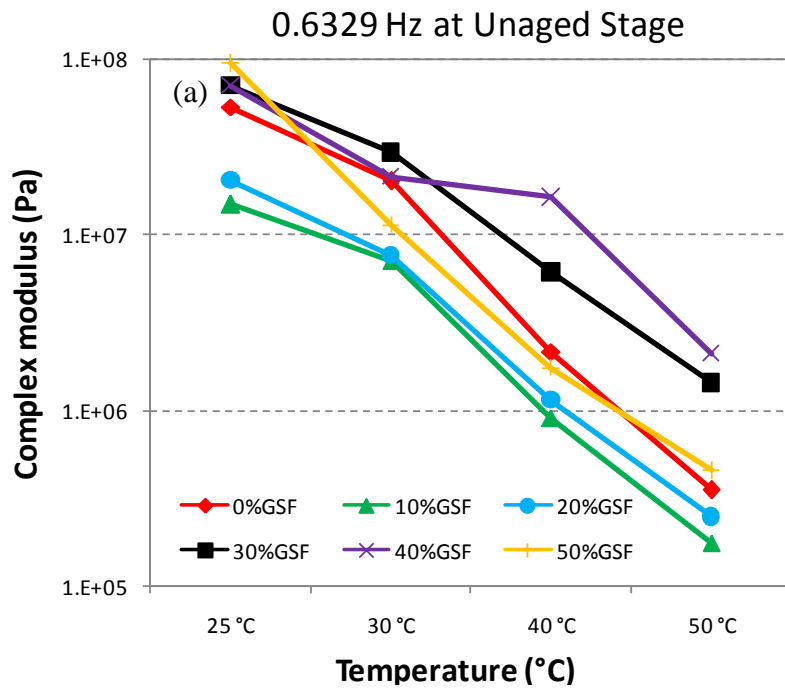


Figure 6.85 : Isochronal plots at 0.6329Hz for neat B100/150 bitumen and SEB groups made of B100/150 bitumen before aging. (a) Complex modulus and (b) Phase angle.

The extension indices of G^* ($G^*_{\text{SEB}}/G^*_{\text{B100/150}}$), indicating relative changes in complex modulus for all five SEBs, have been recorded at each temperature and at 0.6329Hz in Table 6.89. For unaged 100/150 penetration bitumen, it is often the case that low volume (10 and/or 20%) additions of sulphur to the binder at each test

temperature indicates extension indices less than 1.00, emphasizing the lowered complex modulus. In fact, at low temperatures, both the elastic modulus and viscosity of bitumen are high, making it difficult for bitumen to flow before breaking. As a result, it is easier for binders to reach their failure stress upon deformation in cold weather, and this causes thermal cracking to the pavement (Ruan et al., 2003). In this sense, the extension of neat 100/150 penetration bitumen at 10 and/or 20% sulphur levels will be favorable when the cold climate conditions in cold regions are considered.

The benefit of increased stiffness derived from further amounts of sulphur appears to be based on extension indices greater than 1.00.

Table 6.89 : Relative changes in complex modulus for the B100/150 base bitumen and SEB groups at 0.6329Hz before aging.

Binder	Stage	Extension Indices ($G^*_{SEB}/G^*_{B100/150}$) at 0.6329 Hz			
		25 °C	30 °C	40 °C	50 °C
B100/150	unaged	1.00	1.00	1.00	1.00
B100/150-10%GSF	unaged	0.28	0.35	0.42	0.50
B100/150-20%GSF	unaged	0.38	0.38	0.53	0.70
B100/150-30%GSF	unaged	1.31	1.45	2.82	4.08
B100/150-40%GSF	unaged	1.31	1.05	7.59	6.00
B100/150-50%GSF	unaged	1.77	0.56	0.81	1.30

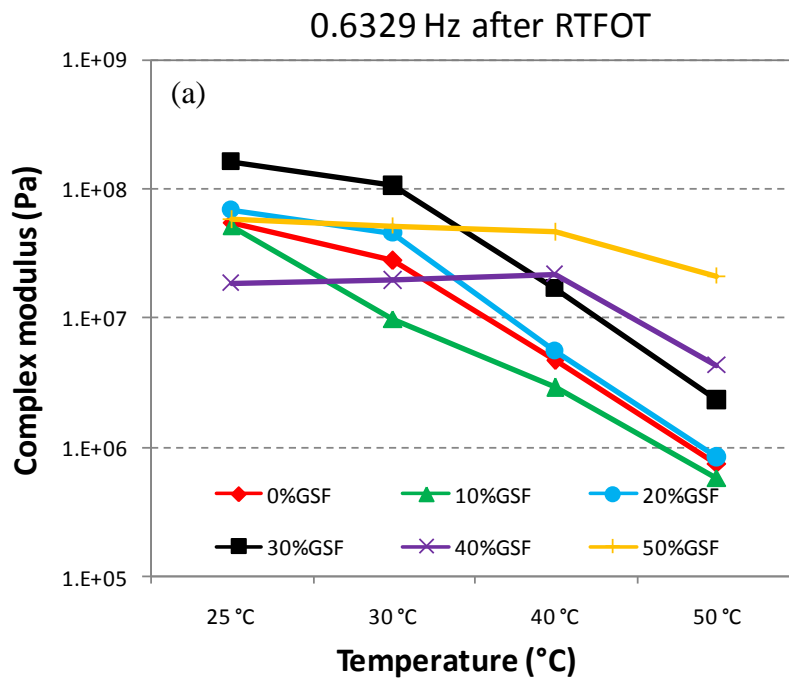
In order to reveal the aging effect, the rheological parameter values at 0.6329Hz of both the short-term aged base 100/150 bitumen and short-term aged SEB groups are given in Table 6.90. In addition, the isochronal plots of complex modulus (G^*) and phase angle (δ) versus temperature at 0.6329Hz of both are shown in Figure 6.86 (a) and (b) respectively.

After RTFOT aging, the effect of sulphur extension on the variation of the complex modulus and phase angle is more pronounced compared with the unaged binders, indicating – most likely – the rearrangement of sulphur particles in bitumen phase by means of the aging process. In addition to their re-distribution in bitumen phase, a decrease in molecular size of sulphur particles, as proved by morphological analysis via SEM (Scanning Electron Microscope) (please see Chapter 6.3 Morphology Analysis) plays a considerable role in the rheology of aged SEBs. On the other hand,

the contribution of aged bitumen phase to the entire rheology of the binder should be seriously considered.

Table 6.90 : Values of rheological parameters for the B100/150 base bitumen and SEB groups at 0.6329Hz after short-term aging.

Binder	Stage	Complex Modulus at 0.6329 Hz (Pa)				Phase Angle at 0.6329 Hz (degree)			
		25 °C	30 °C	40 °C	50 °C	25 °C	30 °C	40 °C	50 °C
B100/150	r	5.51E+07	2.78E+07	4.68E+06	7.49E+05	45.00	52.62	83.84	87.62
B100/150-10%GSF	r	5.11E+07	9.93E+06	2.91E+06	5.82E+05	54.32	77.87	86.30	87.77
B100/150-20%GSF	r	6.86E+07	4.50E+07	5.55E+06	8.36E+05	53.75	71.48	78.90	83.53
B100/150-30%GSF	r	1.62E+08	1.06E+08	1.69E+07	2.31E+06	24.18	54.19	70.58	79.03
B100/150-40%GSF	r	1.86E+07	1.96E+07	2.19E+07	4.35E+06	50.91	41.08	46.49	72.03
B100/150-50%GSF	r	5.77E+07	5.19E+07	4.62E+07	2.10E+07	40.15	43.67	42.75	56.16



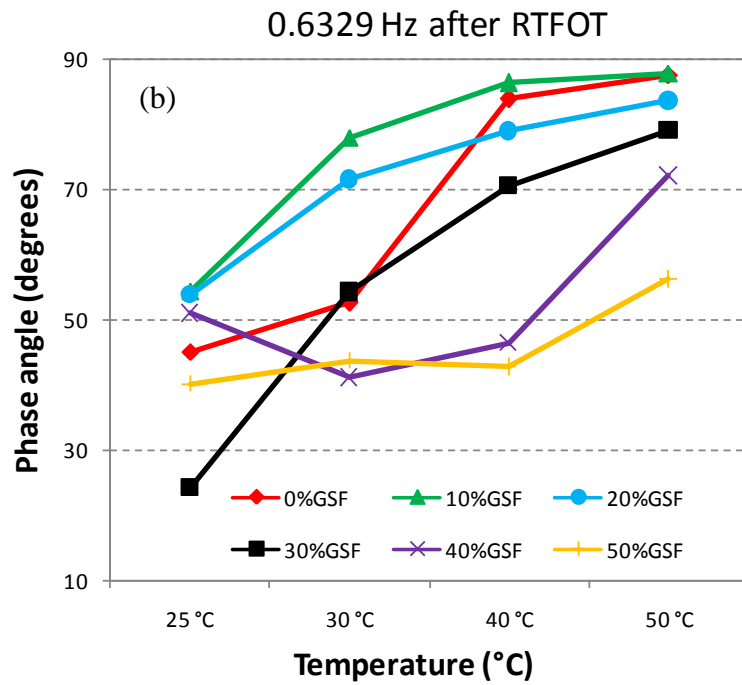


Figure 6.86 : Isochronal plots at 0.6329Hz for neat B100/150 bitumen and SEB groups made of B100/150 bitumen after short-term aging. (a) Complex modulus and (b) Phase angle.

RTFOT aging results in a considerable shift of the entire phase angle curve in the direction of more elastic (relatively less viscous) behavior (Figure 6.86 (b)), indicating that a variation from a more sol-like (viscous and less structured) to a more gel-like (elastic and more structured) behavior has occurred. Two possible reasons for this variation in sulphur extension benefit are: (1) with short-term aging, sulphur particles in bitumen are degraded into smaller molecules causing the bitumen-sulphur interactions considerably rise up and as a result, hardening effect occurs on the ultimate binder, and (2) the viscosity and the stiffness of the 100/150 penetration bitumen are increased significantly due to oxidation.

Table 6.91 displays both the extension indices of G^* ($G^*_{SEB}/G^*_{B100/150}$) and aging index parameter (G^*_{RTFOT}/G^*_{UNAGED}).

Table 6.91 : Relative changes in complex modulus and aging index following short-term aging at 0.6329Hz.

Binder	Stage	Extension Indices ($G^*_{SEB}/G^*_{B100/150}$) at 0.6329 Hz				Aging Index (G^*_{RTFOT}/G^*_{UNAGED}) at 0.6329Hz			
		25 °C	30 °C	40 °C	50 °C	25 °C	30 °C	40 °C	50 °C
B100/150	r	1.00	1.00	1.00	1.00	1.02	1.37	2.15	2.13
B100/150-10%GSF	r	0.93	0.36	0.62	0.78	3.42	1.38	3.21	3.30
B100/150-20%GSF	r	1.25	1.62	1.19	1.12	3.33	5.87	4.83	3.38
B100/150-30%GSF	r	2.95	3.79	3.61	3.09	2.30	3.57	2.75	1.62
B100/150-40%GSF	r	0.34	0.70	4.68	5.81	0.26	0.91	1.33	2.07
B100/150-50%GSF	r	1.05	1.87	9.89	28.09	0.60	4.54	26.31	46.03

The influence of long-term aging on the rheological behavior of the neat B100/150 bitumen and SEB groups is shown in Figure 6.87 (a) and (b) and their values are given in Table 6.92. Long-term aging enhances elasticity much more than RTFOT-aging. Thus, PAV-aged SEBs demonstrate promising dynamic-mechanical properties. The reason for the yielded stiffening for long-term aged SEBs is that the sulphur-extension results in an increase in both the in-phase and out-of-phase components of G^* (G' and G'' respectively), but the relative amounts of increase are totally different.

Table 6.92 : Values of rheological parameters for the B100/150 base bitumen and SEB groups at 0.6329Hz after long-term aging.

Binder	Stage	Complex Modulus at 0.6329Hz (Pa)				Phase Angle at 0.6329 Hz (degree)			
		25 °C	30 °C	40 °C	50 °C	25 °C	30 °C	40 °C	50 °C
B100/150	p	3.19E+07	1.92E+07	1.02E+07	1.57E+06	40.43	60.50	81.74	86.63
B100/150-10%GSF	p	6.01E+07	3.74E+07	1.91E+07	3.10E+06	40.28	23.44	65.87	80.78
B100/150-20%GSF	p	5.82E+07	3.57E+07	2.03E+07	2.96E+06	15.54	35.08	62.63	75.70
B100/150-30%GSF	p	1.15E+08	6.55E+07	3.76E+07	2.26E+07	40.79	46.49	53.02	63.17
B100/150-40%GSF	p	1.81E+08	1.40E+08	1.44E+08	1.15E+08	27.29	25.95	21.78	24.65
B100/150-50%GSF	p	1.17E+08	9.37E+07	9.39E+07	5.19E+07	14.24	51.97	65.70	80.69

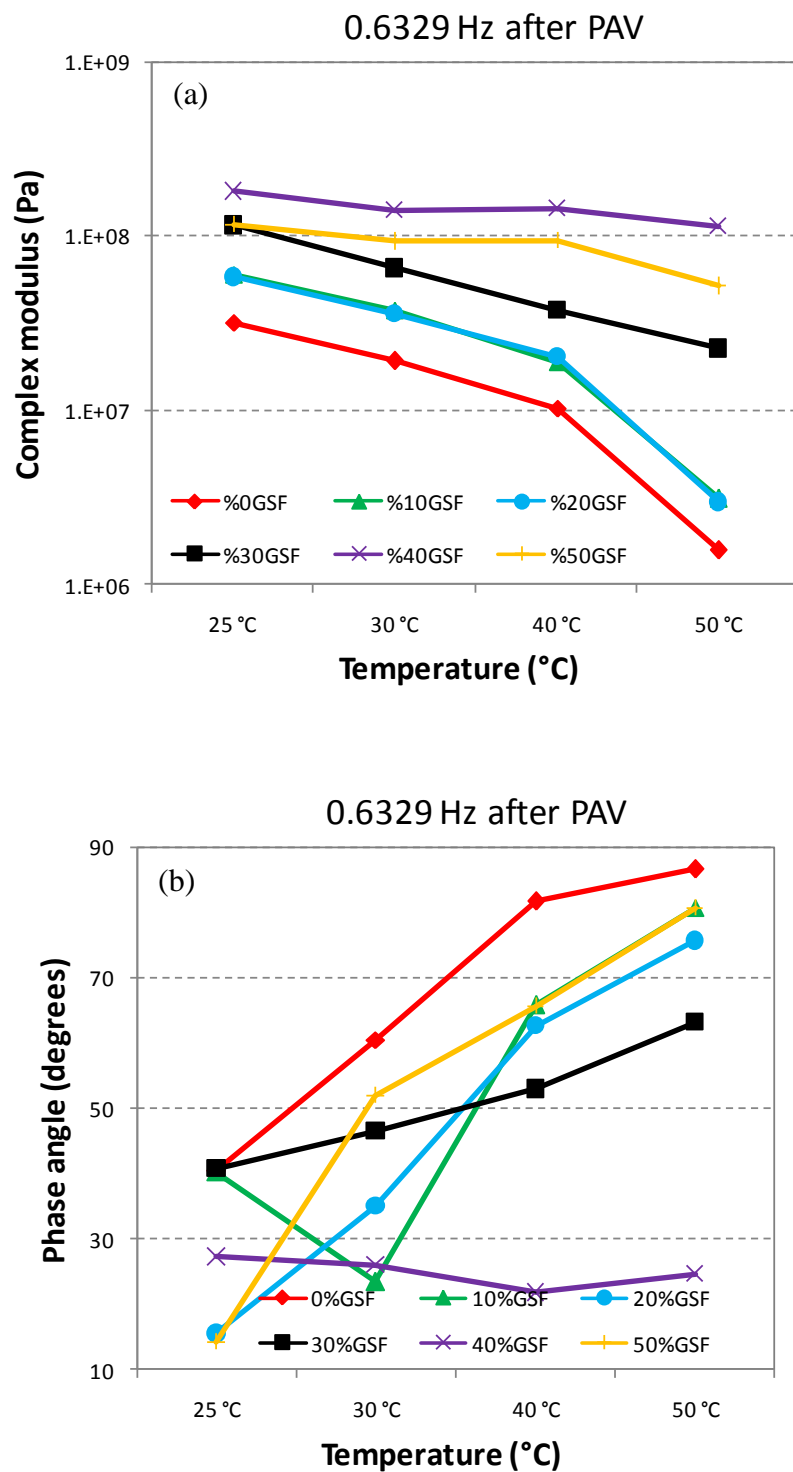


Figure 6.87 : Isochronal plots at 0.6329Hz for neat B100/150 bitumen and SEB groups made of B100/150 bitumen after long-term aging. (a) Complex modulus and (b) Phase angle.

The extension indices of G^* ($G^*_{\text{SEB}}/G^*_{\text{B100/150}}$) and long-term aging index parameter ($G^*_{\text{PAV}}/G^*_{\text{UNAGED}}$) are given in Table 6.93.

Table 6.93 : Relative changes in complex modulus and aging index following long-term aging at 0.6329Hz.

Binder	Stage	Extension Indices ($G^*_{SEB}/G^*_{B100/150}$) at 0.6329 Hz				Aging Index (G^*_{PAV}/G^*_{UNAGED}) at 0.6329Hz			
		25 °C	30 °C	40 °C	50 °C	25 °C	30 °C	40 °C	50 °C
B100/150	p	1.00	1.00	1.00	1.00	0.59	0.94	4.71	4.48
B100/150-10%GSF	p	1.89	1.95	1.87	1.97	4.03	5.20	21.11	17.59
B100/150-20%GSF	p	1.83	1.86	1.98	1.88	2.83	4.65	17.67	11.99
B100/150-30%GSF	p	3.62	3.41	3.67	14.39	1.63	2.21	6.13	15.81
B100/150-40%GSF	p	5.67	7.31	14.07	73.05	2.55	6.56	8.74	54.58
B100/150-50%GSF	p	3.67	4.88	9.17	32.99	1.23	8.19	53.41	113.62

B160/220 and its derivatives

The dependence of the rheological behavior of B160/220 and B160/220-extended binders with varying sulphur levels on different loading frequencies (0.1-4.0Hz) at 25°C have been evaluated and the results are shown in Table 6.94. The isochronal plots of complex modulus and phase angle are depicted in Figure 6.88 (a-f). 25°C is determined since it is usually applied to evaluate the performance of asphaltic concrete pavement in moderate climate region.

The complex modulus and phase angle curves at unaged stage (Figure 6.88 (a) and (b)) illustrate that a marginal decrease in complex modulus (softening) and a common increase in phase angle (increasing viscous response) occur when the neat 160/220 penetration bitumen is replaced with 10%GSF. These results accord with previous traditional tests and reveal once again that low sulphur content in bitumen tends to lower binder stiffness. The resistance against cracking at low temperature is also expected to improve considerably. Additionally, compared to B160/220 control bitumen, SEBs (with 20, 30, 40 and 50%GSF) have increased G^* and decreased δ values over the entire frequency range. Figure 6.88 (a) and (b) show that a sulphuric extension of 160/220 penetration bitumen starts to increase the complex modulus and decrease the phase angle values at 20% sulphur level. These changes in rheological behavior are particularly more noticeable at high frequencies. Any further increase in sulphur amount causes an apparent plateau effect on G^* values and continued to decrease phase angle values. It should be noted that B160/220-40%GSF does not considerably alter its G^* values with increasing loading frequency. As shown in Table 6.94, the complex modulus values for this SEB are 2.56E+07, 2.17E+07, 2.04E+07, 2.19E+07 and 2.21E+07 and 2.21E+07Pa at 0.1, 0.2517, 0.6329, 1.596 and 4.0Hz respectively. Of these four SEBs, the 50%GSF SEB seems to be the most

promising as a way to control bitumen, since it tends to have the highest complex modulus and the lowest phase angle values (except at 1.596Hz) at each test frequency.

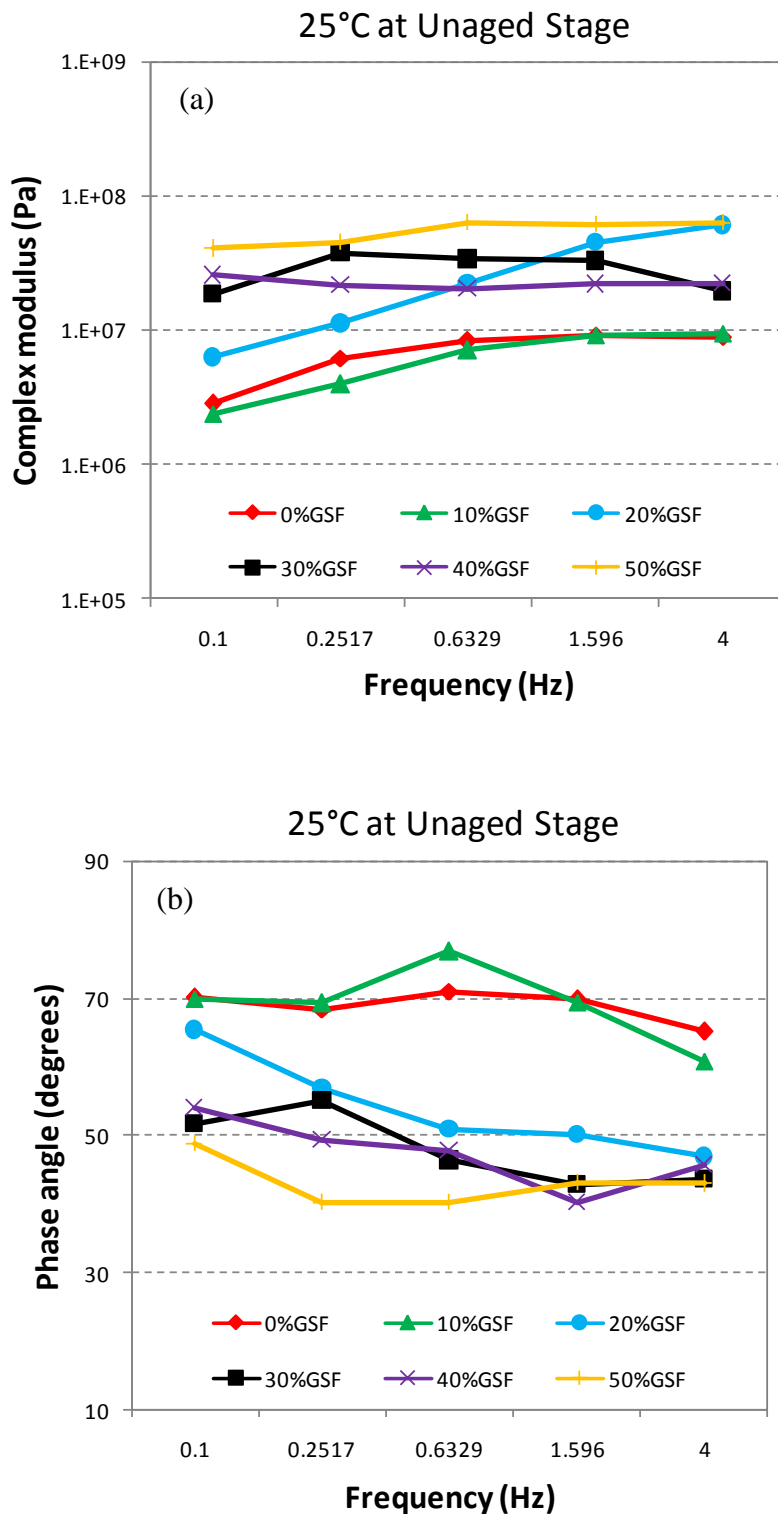
To sum up, the obtained results indicate that sulphuric extension of B160/220 stiffens the ultimate binder at the unaged stage. However, it should be noted that replacing neat bitumen with low sulphur (10%) removes the stiffening effect that higher quantities of sulphur provide. This result agrees with the previous results obtained in this study.

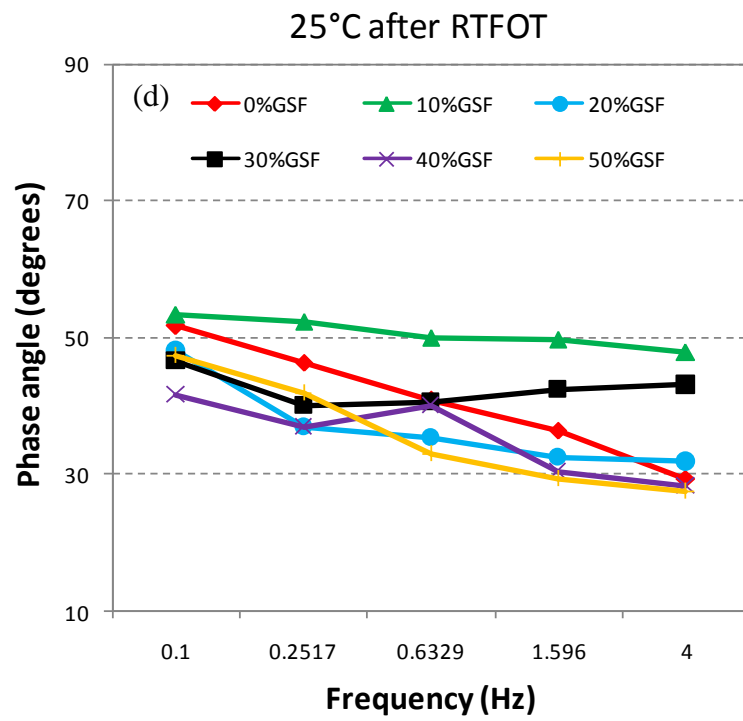
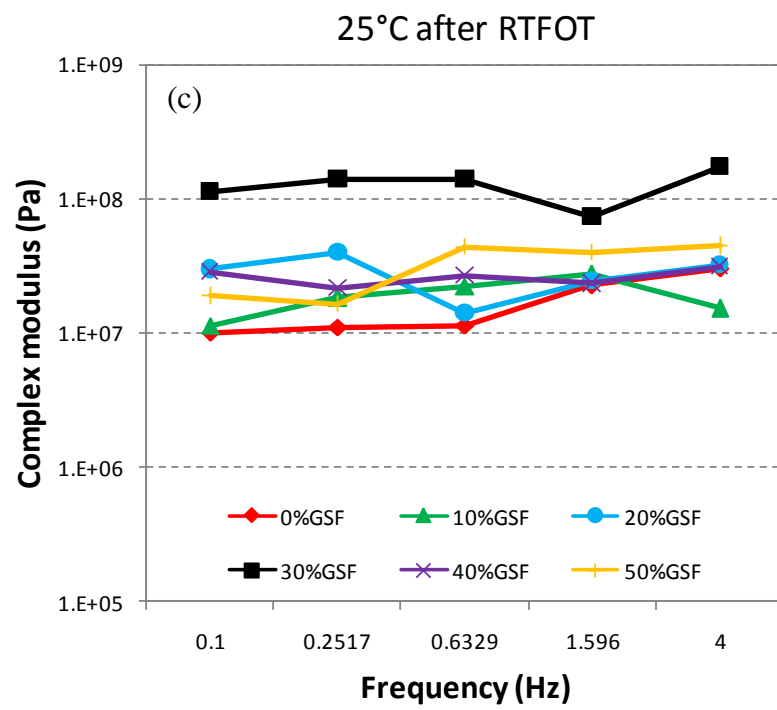
Table 6.94 : Rheological values of B160/220 base bitumen and B160/220-sulphur-extended-binders at a reference temperature of 25°C before aging, after RTFOT- and PAV-aging.

UN-AGED STAGE				RTFOT STAGE				PAV STAGE				
	Temp. °C	Frequency Hz	Phase Angle °	Complex Modulus Pa	Temp. °C	Frequency Hz	Phase Angle °	Complex Modulus Pa	Temp. °C	Frequency Hz	Phase Angle °	Complex Modulus Pa
0%GSF	25	0.1	70.13	2.82E+06	25	0.1	51.75	1.00E+07	25	0.1	64.51	8.71E+07
	25	0.2517	68.45	6.17E+06	25	0.2517	46.36	1.09E+07	25	0.2517	60.91	1.03E+08
	25	0.6329	71.08	8.25E+06	25	0.6329	40.81	1.13E+07	25	0.6329	54.62	1.55E+08
	25	1.596	69.89	9.16E+06	25	1.596	36.46	2.27E+07	25	1.596	55.19	1.63E+08
	25	4	65.20	8.83E+06	25	4	29.42	3.04E+07	25	4	44.04	1.71E+08
10%GSF	25	0.1	69.93	2.37E+06	25	0.1	53.39	1.14E+07	25	0.1	45.24	1.88E+08
	25	0.2517	69.35	3.93E+06	25	0.2517	52.41	1.82E+07	25	0.2517	45.12	1.98E+08
	25	0.6329	76.90	7.10E+06	25	0.6329	50.08	2.21E+07	25	0.6329	46.84	2.04E+08
	25	1.596	69.52	9.25E+06	25	1.596	49.74	2.72E+07	25	1.596	44.26	2.03E+08
	25	4	60.94	9.53E+06	25	4	47.90	1.52E+07	25	4	32.65	2.01E+08
20%GSF	25	0.1	65.46	6.28E+06	25	0.1	48.08	2.97E+07	25	0.1	58.30	2.22E+08
	25	0.2517	57.00	1.12E+07	25	0.2517	36.98	3.98E+07	25	0.2517	54.68	2.05E+08
	25	0.6329	50.97	2.24E+07	25	0.6329	35.51	1.41E+07	25	0.6329	53.31	2.24E+08
	25	1.596	50.16	4.52E+07	25	1.596	32.55	2.44E+07	25	1.596	52.70	2.29E+08
	25	4	46.95	6.01E+07	25	4	31.90	3.23E+07	25	4	44.32	2.64E+08
30%GSF	25	0.1	51.69	1.87E+07	25	0.1	46.67	1.12E+08	25	0.1	46.97	3.03E+08
	25	0.2517	55.20	3.76E+07	25	0.2517	40.05	1.39E+08	25	0.2517	47.44	3.79E+08
	25	0.6329	46.38	3.37E+07	25	0.6329	40.60	1.40E+08	25	0.6329	44.95	4.41E+08
	25	1.596	42.91	3.27E+07	25	1.596	42.44	7.36E+07	25	1.596	37.49	3.31E+08
	25	4	43.62	1.94E+07	25	4	43.16	1.75E+08	25	4	32.08	3.31E+08
40%GSF	25	0.1	54.08	2.56E+07	25	0.1	41.78	2.85E+07	25	0.1	39.42	6.22E+07
	25	0.2517	49.40	2.17E+07	25	0.2517	37.02	2.18E+07	25	0.2517	40.80	7.25E+07
	25	0.6329	47.85	2.04E+07	25	0.6329	40.16	2.69E+07	25	0.6329	33.90	9.26E+07
	25	1.596	40.24	2.19E+07	25	1.596	30.48	2.34E+07	25	1.596	34.81	1.02E+08
	25	4	45.70	2.21E+07	25	4	28.38	3.11E+07	25	4	32.89	1.54E+08
50%GSF	25	0.1	48.88	4.05E+07	25	0.1	47.43	1.89E+07	25	0.1	45.11	2.83E+08
	25	0.2517	40.38	4.52E+07	25	0.2517	41.98	1.66E+07	25	0.2517	39.34	2.45E+08
	25	0.6329	40.25	6.25E+07	25	0.6329	33.17	4.37E+07	25	0.6329	29.15	3.31E+08
	25	1.596	43.18	6.14E+07	25	1.596	29.42	4.02E+07	25	1.596	31.30	2.95E+08
	25	4	43.03	6.25E+07	25	4	27.59	4.44E+07	25	4	22.95	3.24E+08

As binders undergo oxidative aging, their flow behavior becomes more complex or non-Newtonian. In other words, binder hardening increases the stiffness and modulus

of binders and lowers the strain required to cause cracking. Therefore, it is imperative that the rheological properties of binders after oxidative aging be painstakingly investigated to understand the binder hardness acquired during the service life of the pavement (Huang et al., 2011). In this respect, in order to investigate and understand the effect of aging on sulphuric extension of B160/220 at 25°C the DSR test was also conducted on RTFOT and PAV residues.





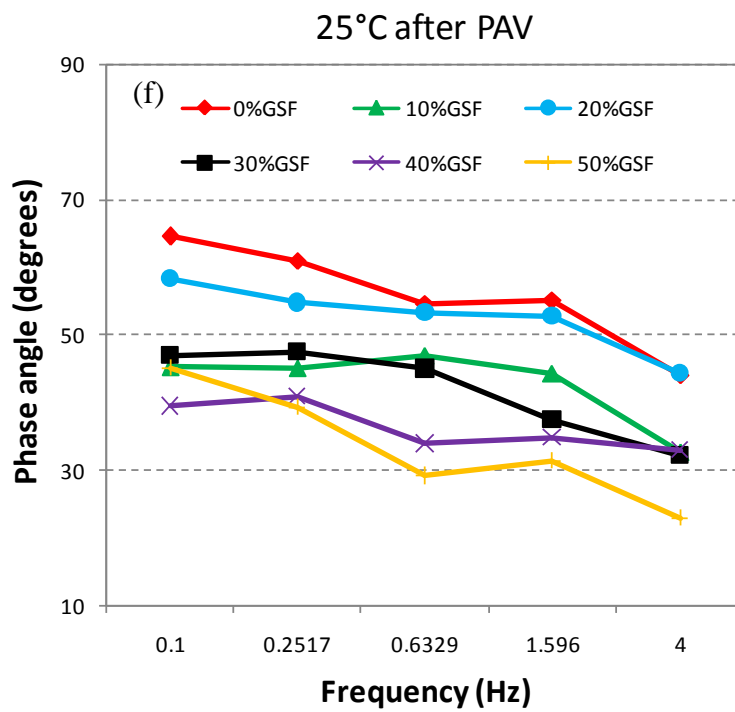
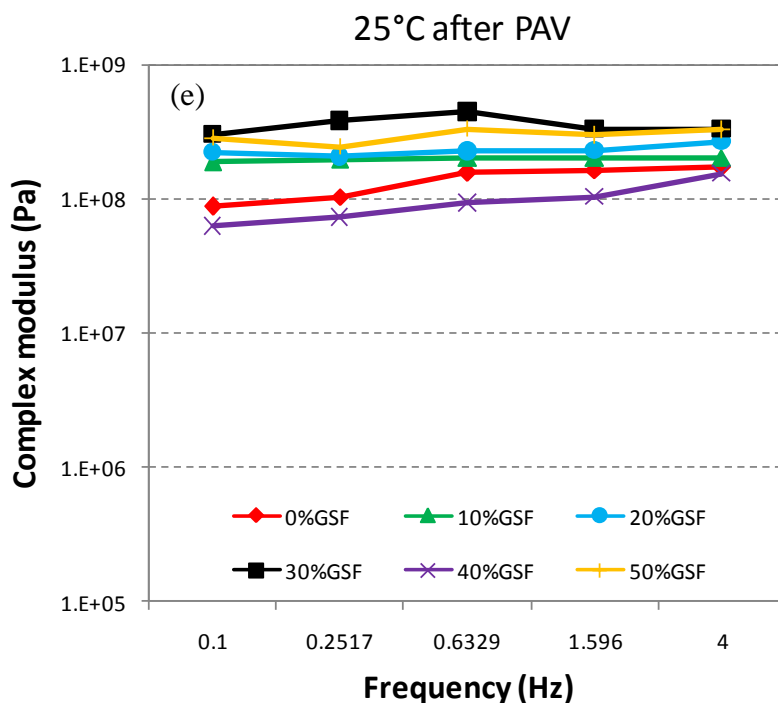


Figure 6.88 : The isochronal plots of complex modulus and phase angle versus loading frequency for B160/220 and B160/220-sulphur-extended-binders at a reference temperature of 25°C (loading frequency sweep, 0.1-4.0Hz). (a) and (b) Before aging. (c) and (d) After RTFOT-aging. (e) and (f) After PAV-aging.

As listed in Table 6.94, complex modulus generally increases and phase angle decreases with RTFOT aging. This kind of behavior is similar to the rheological characteristics of a conventional binder under the action of temperature and loading parameters in which the modulus increases as loading frequency increases and phase angle decreases as loading frequency increases. For the SEB with 20%GSF at higher loading frequencies (0.6329, 1.596 and 4.0Hz) and the SEB with 50%GSF at entire frequency domain, the situation is exceptional in terms of complex modulus. Instead of increasing their values, the aforementioned SEBs decreased their complex modulus values after RTFOT aging. The most probable reason can be the breakdown of the initial sulphur-carbon bonds that were exposed to the high temperature of RTFOT process (163°C). On the other hand, differing from these results, their phase angle values seemed to decrease, which once more again reinforces the approach that variation in the phase angle and complex modulus after aging could be different. Overall, the R-B160/220-40%GSF appears to be the least affected binder after short-term aging since its G^* values are very close to its values at the unaged stage. Table 6.94 clarifies that after RTFOT aging its complex modulus values are only 1.11, 1.00, and 1.32, 1.07 and 1.40 times higher at 0.1, 0.2517, 0.6329, 1.596, and 4.0Hz respectively.

The rheological properties of the long-term aged specimens are presented in Figure 6.88 (e) and (f) in terms of isochronal plots of complex modulus and phase angle respectively. Major increases in G^* at entire frequency domain are unquestionably the effect of long-term aging. In addition, there is considerable evidence of extreme sulphuric extension regardless of loading frequency with the approach of a plateau region indicative of a dominant sulphur networks. Hence, one can observe that once exposed to long-term aging, SEBs can be more durable to changes in loading frequency. In addition to the dominant sulphur network, this phenomenon can also be attributed to strengthening of present sulphur-carbon bonds during PAV aging. Another remarkable effect of PAV aging on G^* values is that there is a relatively smaller gap between the values of long-term aged SEBs.

PAV aging is also expected to have a great impact on phase angle values; however the decrease was almost comparable with that attained from RTFOT aging. The decrease in phase angles where the elastic response is greater proves the tendency of

the sulphur particles to form a continuous elastic network when dissolved/dispersed in the bitumen matrix.

Comparisons of the rheological behaviors of SEBs with those of conventional B160/220 bitumen at 30°C provide interesting results. Relative to this, evaluations of the frequency dependency of the B160/220-sulphur extended binders and B160/220 in terms of complex modulus and phase angle have been carried out. The absolute values of G^* and δ before aging, after aging (both short- and long-term aging) are listed in Table 6.95 and then the isochronal plots are displayed in Figure 6.89 (a-f).

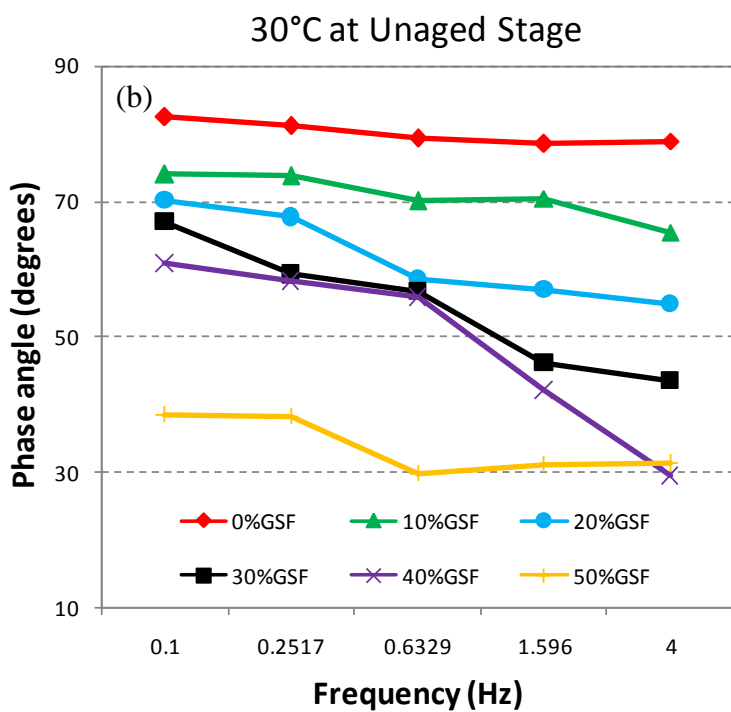
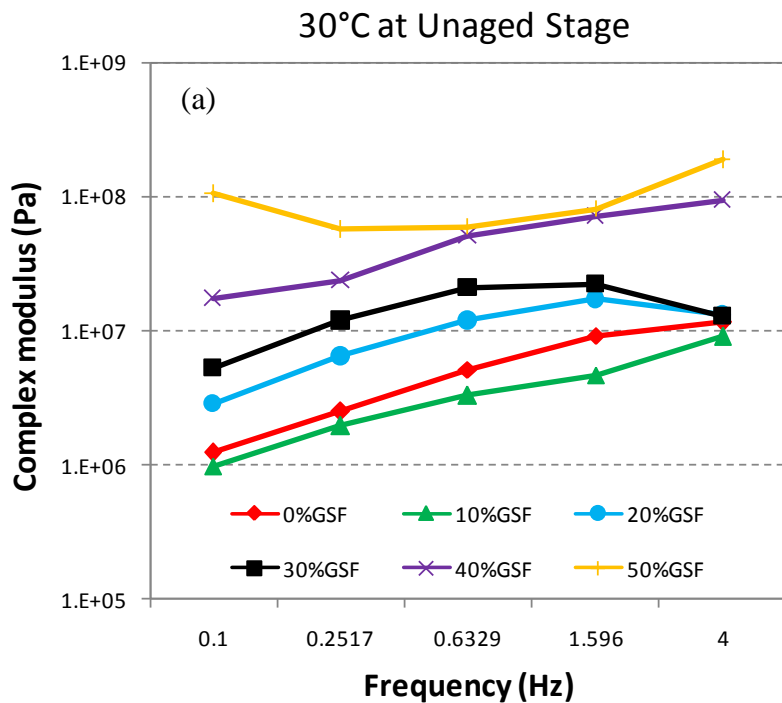
At the unaged stage, sulphuric extension at 10% level decreases the G^* of the original bitumen considerably at each frequency, while δ of the original bitumen dramatically decreases at the same time. As listed in Table 6.95, the phase angle (δ) of the conventional bitumen ranges from around 79 to around 83° at entire frequency loading. In this case, the stored energy per cycle of deformation becomes negligible, so the neat B160/220 bitumen displays almost pure viscous liquid behavior with unremarkable elasticity even at 30°C. However, the varying trend of δ began to slow when conventional bitumen was replaced by 10%GSF. The simultaneous decrease in G^* and δ can be considered to be a kind of paradox. Actually, this phenomenon is not surprising as, firstly, the phase angle is more sensitive to the sulphuric extension of B160/220 than G^* and, secondly the background information previously presented in this study indicates that sulphuric extension at the 10% level differs remarkably in regard to both traditional and rheological characteristics as a function of the compatibility of the different sulphur-bitumen reactions.

The rheology of sulphur-extended binder is considerably dependent on replaced content of sulphur. As recorded in Figure 6.89 (a), after replacement with a sufficient content of granular sulphur ($\geq 20\%$) the ultimate binders change fundamentally in their rheological behavior by a substantial increase in complex modulus. However, a decrease in phase angle begins even at low amounts of GSF (10%), and continues to decrease with further sulphuric extension. In these cases, the rheological response of the SEBs may be related to the formation of network structure of sulphur particles. The sequence of isochronal plots in both figures (Figure 6.89 (a) and (b)) reveals the hierarchy, namely regular variation of rheological parameters with increasing amount of GSF.

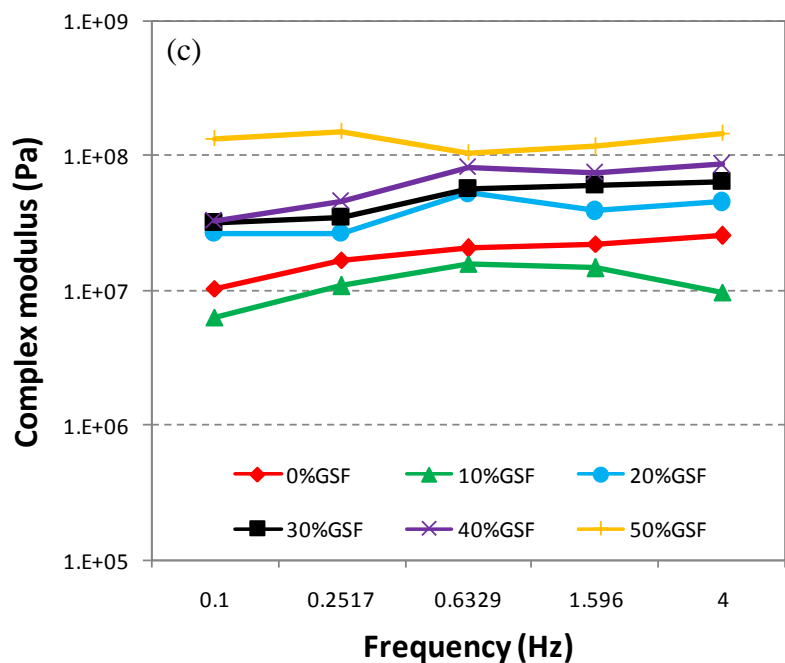
Table 6.95 : Rheological values of B160/220 base bitumen and B160/220-sulphur-extended-binders at a reference temperature of 30°C before aging, after RTFOT- and PAV-aging.

	UN-AGED STAGE				RTFOT STAGE				PAV STAGE			
	Temp. °C	Frequency Hz	Phase Angle °	Complex Modulus Pa	Temp. °C	Frequency Hz	Phase Angle °	Complex Modulus Pa	Temp. °C	Frequency Hz	Phase Angle °	Complex Modulus Pa
0%GSF	30	0.1	82.38	1.24E+06	30	0.1	59.16	1.03E+07	30	0.1	49.81	1.08E+07
	30	0.2517	81.12	2.51E+06	30	0.2517	45.68	1.70E+07	30	0.2517	46.71	1.58E+07
	30	0.6329	79.28	5.10E+06	30	0.6329	46.30	2.06E+07	30	0.6329	43.71	2.97E+07
	30	1.596	78.48	9.12E+06	30	1.596	44.80	2.21E+07	30	1.596	45.67	2.56E+07
	30	4	78.78	1.16E+07	30	4	41.74	2.55E+07	30	4	41.61	3.99E+07
10%GSF	Temp. Frequency °C Hz	Phase Angle °	Complex Modulus Pa	Temp. Frequency °C Hz	Phase Angle °	Complex Modulus Pa	Temp. Frequency °C Hz	Phase Angle °	Complex Modulus Pa	Temp. Frequency °C Hz	Phase Angle °	Complex Modulus Pa
	30 0.1	73.94	9.75E+05	30 0.1	61.48	6.40E+06	30 0.1	69.55	2.51E+07	30 0.1	69.30	3.34E+07
	30 0.2517	73.68	1.96E+06	30 0.2517	58.93	1.09E+07	30 0.2517	56.66	4.52E+07	30 0.2517	56.39	5.72E+07
	30 0.6329	70.00	3.30E+06	30 0.6329	52.78	1.60E+07	30 0.6329	36.62	1.13E+08	30 0.6329	36.39	2.29E+07
	30 1.596	70.36	4.64E+06	30 1.596	48.65	1.47E+07	30 1.596	37.48	1.20E+08	30 1.596	37.25	1.92E+07
20%GSF	Temp. Frequency °C Hz	Phase Angle °	Complex Modulus Pa	Temp. Frequency °C Hz	Phase Angle °	Complex Modulus Pa	Temp. Frequency °C Hz	Phase Angle °	Complex Modulus Pa	Temp. Frequency °C Hz	Phase Angle °	Complex Modulus Pa
	30 0.1	70.07	2.88E+06	30 0.1	54.61	2.68E+07	30 0.1	42.25	9.70E+07	30 0.1	42.02	1.35E+08
	30 0.2517	67.62	6.43E+06	30 0.2517	52.98	2.69E+07	30 0.2517	42.96	1.35E+08	30 0.2517	42.73	2.29E+07
	30 0.6329	58.47	1.19E+07	30 0.6329	49.65	5.34E+07	30 0.6329	36.62	1.13E+08	30 0.6329	36.39	2.29E+07
	30 1.596	56.96	1.71E+07	30 1.596	52.52	3.92E+07	30 1.596	37.48	1.20E+08	30 1.596	37.25	1.92E+07
30%GSF	Temp. Frequency °C Hz	Phase Angle °	Complex Modulus Pa	Temp. Frequency °C Hz	Phase Angle °	Complex Modulus Pa	Temp. Frequency °C Hz	Phase Angle °	Complex Modulus Pa	Temp. Frequency °C Hz	Phase Angle °	Complex Modulus Pa
	30 0.1	66.91	5.33E+06	30 0.1	48.25	3.18E+07	30 0.1	49.96	3.97E+07	30 0.1	41.52	2.94E+07
	30 0.2517	59.21	1.19E+07	30 0.2517	42.09	3.52E+07	30 0.2517	36.95	2.29E+07	30 0.2517	36.39	3.09E+07
	30 0.6329	56.73	2.09E+07	30 0.6329	42.90	5.68E+07	30 0.6329	37.38	1.92E+07	30 0.6329	35.86	3.73E+07
	30 1.596	46.08	2.23E+07	30 1.596	38.29	6.04E+07	30 1.596	27.20	1.49E+08	30 1.596	24.00	8.53E+08
40%GSF	Temp. Frequency °C Hz	Phase Angle °	Complex Modulus Pa	Temp. Frequency °C Hz	Phase Angle °	Complex Modulus Pa	Temp. Frequency °C Hz	Phase Angle °	Complex Modulus Pa	Temp. Frequency °C Hz	Phase Angle °	Complex Modulus Pa
	30 0.1	60.73	1.75E+07	30 0.1	55.38	3.32E+07	30 0.1	39.42	5.19E+07	30 0.1	30.95	6.29E+07
	30 0.2517	58.18	2.38E+07	30 0.2517	55.82	4.61E+07	30 0.2517	33.26	3.09E+07	30 0.2517	30.49	1.62E+07
	30 0.6329	55.72	5.07E+07	30 0.6329	47.36	8.29E+07	30 0.6329	29.83	3.35E+07	30 0.6329	24.00	8.53E+08
	30 1.596	42.05	7.08E+07	30 1.596	41.60	7.50E+07	30 1.596	33.26	3.09E+07	30 1.596	30.49	1.62E+07
50%GSF	Temp. Frequency °C Hz	Phase Angle °	Complex Modulus Pa	Temp. Frequency °C Hz	Phase Angle °	Complex Modulus Pa	Temp. Frequency °C Hz	Phase Angle °	Complex Modulus Pa	Temp. Frequency °C Hz	Phase Angle °	Complex Modulus Pa
	30 0.1	38.40	1.05E+08	30 0.1	58.92	1.34E+08	30 0.1	39.41	1.67E+08	30 0.1	39.44	1.84E+08
	30 0.2517	38.19	5.69E+07	30 0.2517	42.82	1.52E+08	30 0.2517	40.24	3.64E+08	30 0.2517	39.44	1.84E+08
	30 0.6329	29.70	5.90E+07	30 0.6329	40.00	1.05E+08	30 0.6329	33.26	3.09E+07	30 0.6329	30.49	1.62E+07
	30 1.596	31.11	8.02E+07	30 1.596	30.31	1.17E+08	30 1.596	33.26	3.09E+07	30 1.596	30.49	1.62E+07

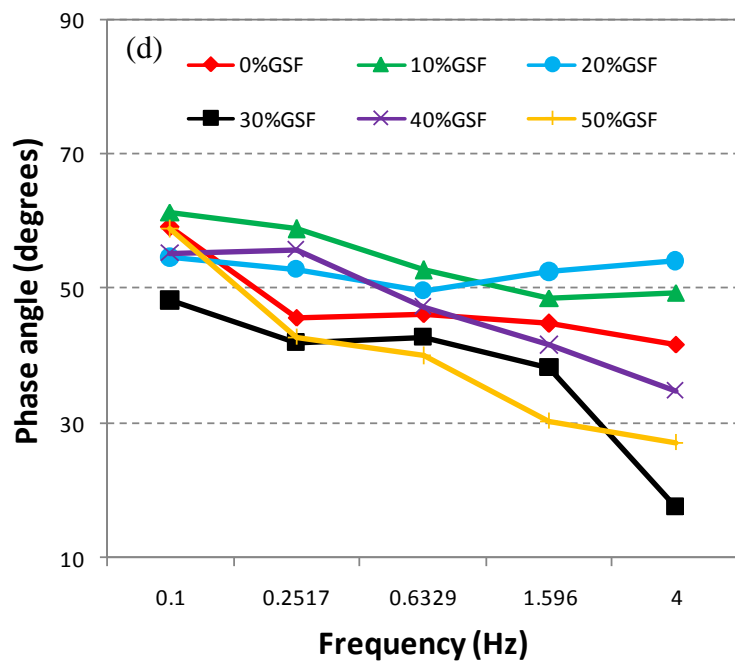
Considering the complex modulus, G^* , plots (isotherms) for B160/220-30%GSF, B160/220-40%GSF, and B160/220-50%GSF demonstrate that the further sulphuric extension of neat bitumen resulted in increased binder stiffness; however the 50%GSF content SEB appeared to be much stiffer than the others. Consistent with trends observed in the viscoelastic response, G^* values generally increased as loading frequency increased (exceptions are 20 and 30%GSF content SEBs at high frequency and 50%GSF content SEB at low frequency).



30°C after RTFOT



30°C after RTFOT



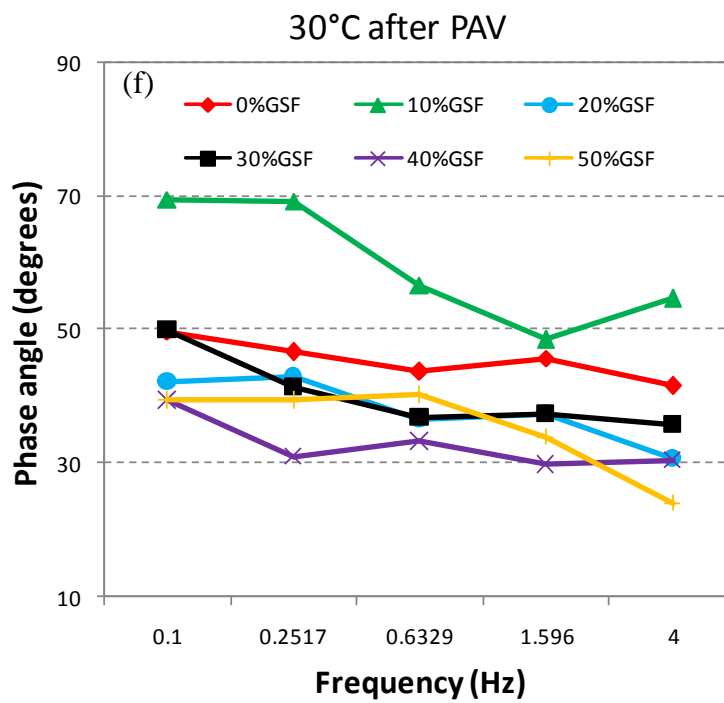
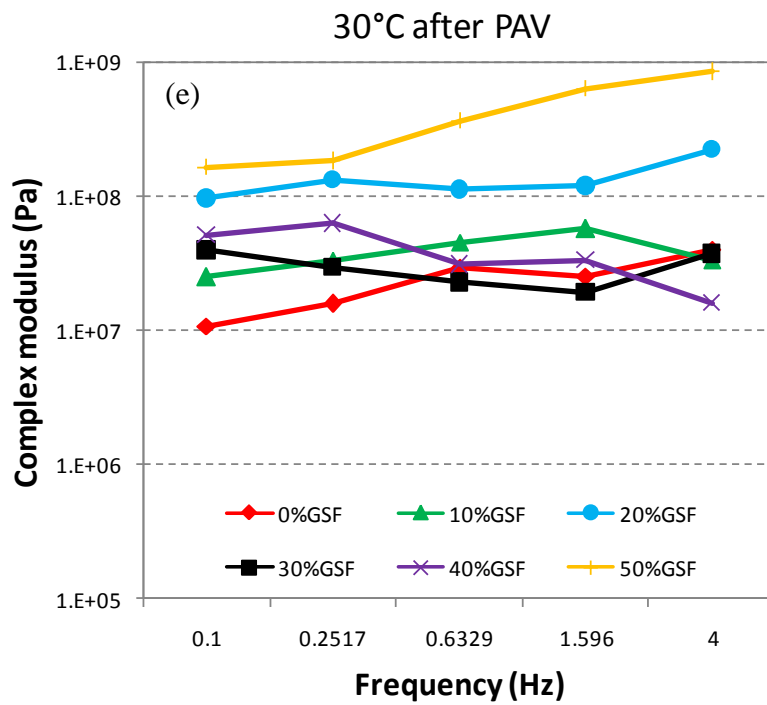


Figure 6.89 : The isochronal plots of complex modulus and phase angle versus loading frequency for B160/220 and B160/220-sulphur-extended-binders at a reference temperature of 30°C (loading frequency sweep, 0.1-4.0Hz). (a) and (b) Before aging. (c) and (d) After RTFOT-aging. (e) and (f) After PAV-aging.

The DSR test was also carried out on RTFOT residues as a means to evaluate and understand the impact of short-term aging on sulphuric extension of B160/220 at 30°C. Compared with the effect of sulphuric extension on the viscoelastic response of neat bitumen at unaged stage, Figure 6.89 (c) shows that the short-term aging increased the complex modulus values fairly (which indicates increased elastic response), with a "plateau" observed between 0.1 and 4.0Hz, where the complex modulus values were relatively insensitive to frequency change. In addition to aging, an increased proportion of GSF resulted in a further increase in elastic response (higher G^*), as illustrated by 40 and 50%GSF content SEBs.

On the other hand, the trend for 10%GSF SEB is totally different. Even though RTFOT aging increased its G^* values considerably, the magnitude in the increase did not exceed the G^* values of short-term aged neat bitumen. Its isochronal plot still lies under that of neat bitumen as displayed in Figure 6.89 (c). In accordance with its G^* values, the δ values of R-B160/220-10%GSF appeared to be higher than those of the 160/220 penetration bitumen; the δ values of this SEB ranging from 61.48 to 49.44° always exceeded those of the neat bitumen which ranged from 59.16 to 41.74°.

It is well known that the long-term aging that occurs during the service life of pavement leads to an increase of elastic response of the binder. Hence, the viscoelastic behaviors of PAV-aged specimens were evaluated via the DSR test. As recorded in Table 6.95, the magnitudes of increase in G^* values for the SEBs with 10, 20 and 50%GSF are greater than those observed after RTFOT aging. On the other hand, the other two SEBs (with 30 and 40%GSF) did not further increase their G^* values, particularly at higher frequencies. Phase angle curves in Figure 6.89 (f) indicate that a plateau region from 39.41 to 40.24° (0.1 – 0.6329Hz) appeared for the 50%GSF content SEB. Similarly, the 30%GSF content SEB has a clear plateau region from 35.86 to 36.95° (0.6329 – 4.0Hz). These two plateau regions that follow long-term aging are clear indications of the presence of sulphur networks in the extended binder.

Overall, the obtained results show the potential benefits offered by B160/220-sulphur-extended-binders when contrasted with neat bitumen, as indicated by enhanced mechanical properties at 30°C (higher complex modulus and lower phase angle, indicating improved elasticity which is potentially beneficial for resisting deformation).

The frequency dependency of the B160/220 and B160/20-sulphur-extended binders in terms of complex modulus and phase angle has been assessed at a reference temperature of 40°C. The absolute values of G^* and δ before aging and after aging (short- and long-term aging) are listed in Table 6.96 and then the isochronal plots are presented in Figure 6.90 (a-f).

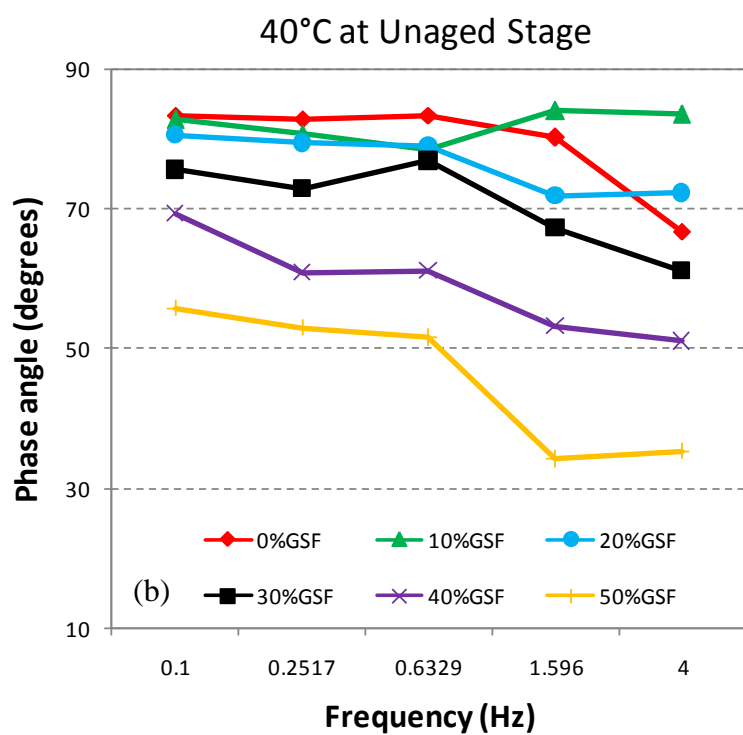
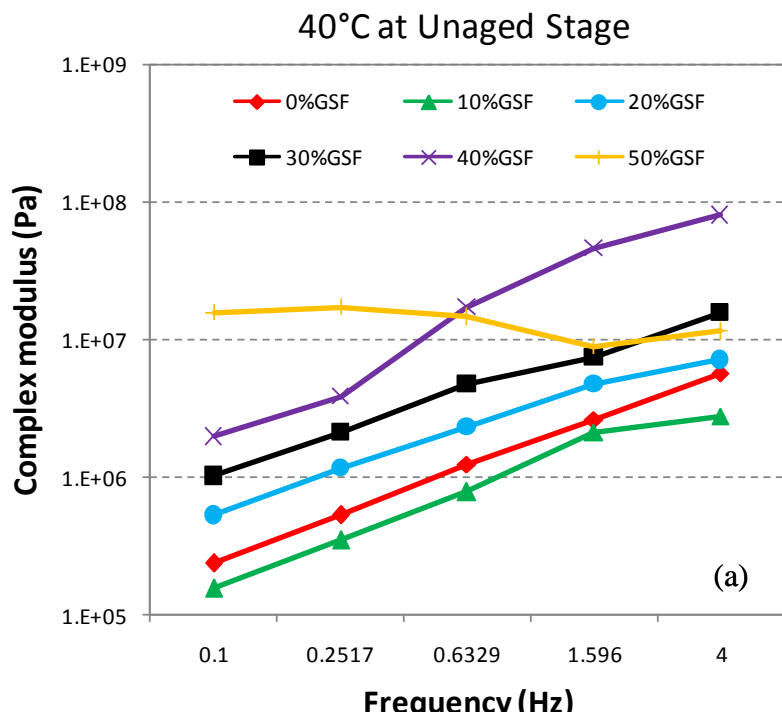
At the unaged stage, the rheological behavior of 10%GSF content SEB differs considerable from the other SEBs, as well as the conventional bitumen, with this relatively soft binder having consistently the lowest G^* values over the entire frequency domain (Figure 6.90 (a)). The elevated complex modulus curves explain an increase in complex modulus (stiffening and increasing elastic response) with increasing weight of the GSF. These changes are noticeable and relatively alter the shape of rheological response of the traditional 160/220 penetration bitumen. The effect of blending 50% by weight of the granular sulphur with 50% by weight of the B160/220 bitumen does not increase the overall complex modulus values further compared to the B160/220-40%GSF. This is unexpected, as the complex modulus curve of the B160/220-50%GSF would be expected to lie over that of the SEB with 40%GSF. One probable reason for the unexpected viscoelastic response of this binder can be the lack of compatibility (stability) between the sulphur particles and bitumen components at excessive GSF level (50%), while the hindering effect of increasing shear frequency on the further poly-sulphuric bonds may be the second reason for this outcome. Therefore the most significant influence of sulphuric extension at 50% seen in Figure 6.90 (a) is that the generated binder has a lower frequency susceptibility compared to both the other SEBs and the straight bitumen.

The rheological nature of the extended binders, as shown through the phase angle curves in Figure 6.90 (b), differ remarkably from those of the conventional bitumen. Although the 10%GSF content SEB shows a continuous decrease of phase angle at low frequency range similar to that found for both neat bitumen and the B160/220-20%GSF, its response is predominantly viscous in nature with phase angles between 80° and 90° over the majority of the increased frequency domain. On the other hand, the increase in sulphur level yielded a gradual reduction in phase angle.

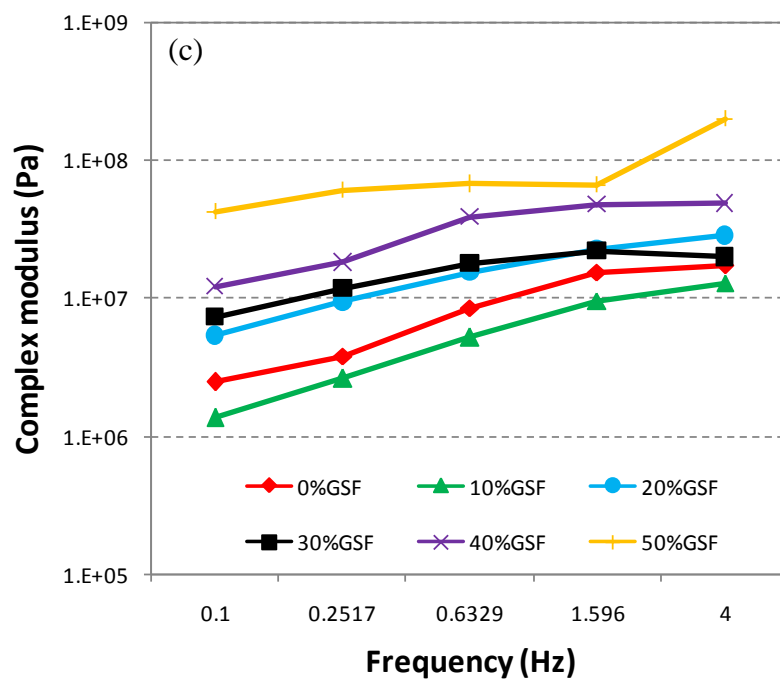
Table 6.96 : Rheological values of B160/220 base bitumen and B160/220-sulphur-extended-binders at a reference temperature of 40°C before aging, after RTFOT- and PAV-aging.

UN-AGED STAGE				RTFOT STAGE				PAV STAGE				
	Temp. °C	Frequency Hz	Phase Angle °	Complex Modulus Pa	Temp. °C	Frequency Hz	Phase Angle °	Complex Modulus Pa	Temp. °C	Frequency Hz	Phase Angle °	Complex Modulus Pa
0%GSF	40	0.1	83.43	2.35E+05	40	0.1	65.50	2.45E+06	40	0.1	63.79	6.90E+06
	40	0.2517	83.00	5.28E+05	40	0.2517	65.61	3.77E+06	40	0.2517	56.60	9.00E+06
	40	0.6329	83.48	1.23E+06	40	0.6329	59.53	8.42E+06	40	0.6329	51.75	1.06E+07
	40	1.596	80.31	2.63E+06	40	1.596	66.11	1.53E+07	40	1.596	43.82	1.13E+07
	40	4	66.87	5.63E+06	40	4	47.33	1.73E+07	40	4	38.91	1.62E+07
10%GSF	Temp. Frequency °C Hz	Phase Angle °	Complex Modulus Pa	Temp. Frequency °C Hz	Phase Angle °	Complex Modulus Pa	Temp. Frequency °C Hz	Phase Angle °	Complex Modulus Pa	Temp. Frequency °C Hz	Phase Angle °	Complex Modulus Pa
	40	0.1	82.81	1.55E+05	40	0.1	71.78	1.35E+06	40	0.1	48.97	2.80E+07
	40	0.2517	80.84	3.48E+05	40	0.2517	66.59	2.60E+06	40	0.2517	45.35	2.98E+07
	40	0.6329	78.62	7.80E+05	40	0.6329	63.84	5.17E+06	40	0.6329	39.28	4.26E+07
	40	1.596	84.10	2.13E+06	40	1.596	73.75	9.50E+06	40	1.596	30.44	3.31E+07
20%GSF	Temp. Frequency °C Hz	Phase Angle °	Complex Modulus Pa	Temp. Frequency °C Hz	Phase Angle °	Complex Modulus Pa	Temp. Frequency °C Hz	Phase Angle °	Complex Modulus Pa	Temp. Frequency °C Hz	Phase Angle °	Complex Modulus Pa
	40	0.1	80.68	5.26E+05	40	0.1	62.81	5.32E+06	40	0.1	67.15	1.27E+07
	40	0.2517	79.51	1.16E+06	40	0.2517	55.52	9.37E+06	40	0.2517	65.02	1.30E+07
	40	0.6329	78.97	2.30E+06	40	0.6329	55.76	1.53E+07	40	0.6329	60.93	1.50E+07
	40	1.596	71.97	4.77E+06	40	1.596	50.48	2.27E+07	40	1.596	50.17	1.35E+07
30%GSF	Temp. Frequency °C Hz	Phase Angle °	Complex Modulus Pa	Temp. Frequency °C Hz	Phase Angle °	Complex Modulus Pa	Temp. Frequency °C Hz	Phase Angle °	Complex Modulus Pa	Temp. Frequency °C Hz	Phase Angle °	Complex Modulus Pa
	40	0.1	75.64	1.02E+06	40	0.1	55.16	7.30E+06	40	0.1	58.99	1.87E+07
	40	0.2517	72.99	2.10E+06	40	0.2517	54.71	1.17E+07	40	0.2517	55.77	1.96E+07
	40	0.6329	76.93	4.70E+06	40	0.6329	51.53	1.77E+07	40	0.6329	48.12	1.84E+07
	40	1.596	67.35	7.43E+06	40	1.596	48.28	2.21E+07	40	1.596	39.72	2.11E+07
40%GSF	Temp. Frequency °C Hz	Phase Angle °	Complex Modulus Pa	Temp. Frequency °C Hz	Phase Angle °	Complex Modulus Pa	Temp. Frequency °C Hz	Phase Angle °	Complex Modulus Pa	Temp. Frequency °C Hz	Phase Angle °	Complex Modulus Pa
	40	0.1	69.40	1.96E+06	40	0.1	53.27	1.21E+07	40	0.1	46.09	2.42E+07
	40	0.2517	61.01	3.86E+06	40	0.2517	48.22	1.81E+07	40	0.2517	39.21	4.89E+07
	40	0.6329	61.27	1.71E+07	40	0.6329	47.34	3.86E+07	40	0.6329	37.86	3.88E+07
	40	1.596	53.21	4.59E+07	40	1.596	45.15	4.78E+07	40	1.596	32.28	3.42E+07
50%GSF	Temp. Frequency °C Hz	Phase Angle °	Complex Modulus Pa	Temp. Frequency °C Hz	Phase Angle °	Complex Modulus Pa	Temp. Frequency °C Hz	Phase Angle °	Complex Modulus Pa	Temp. Frequency °C Hz	Phase Angle °	Complex Modulus Pa
	40	0.1	55.80	1.55E+07	40	0.1	43.21	4.23E+07	40	0.1	50.68	3.59E+07
	40	0.2517	53.01	1.70E+07	40	0.2517	42.54	6.11E+07	40	0.2517	49.62	5.47E+07
	40	0.6329	51.63	1.46E+07	40	0.6329	39.65	6.74E+07	40	0.6329	42.89	5.65E+07
	40	1.596	34.21	8.84E+06	40	1.596	33.03	6.61E+07	40	1.596	38.25	1.06E+08
	40	4	35.44	1.14E+07	40	4	29.75	1.98E+08	40	4	32.97	1.57E+08

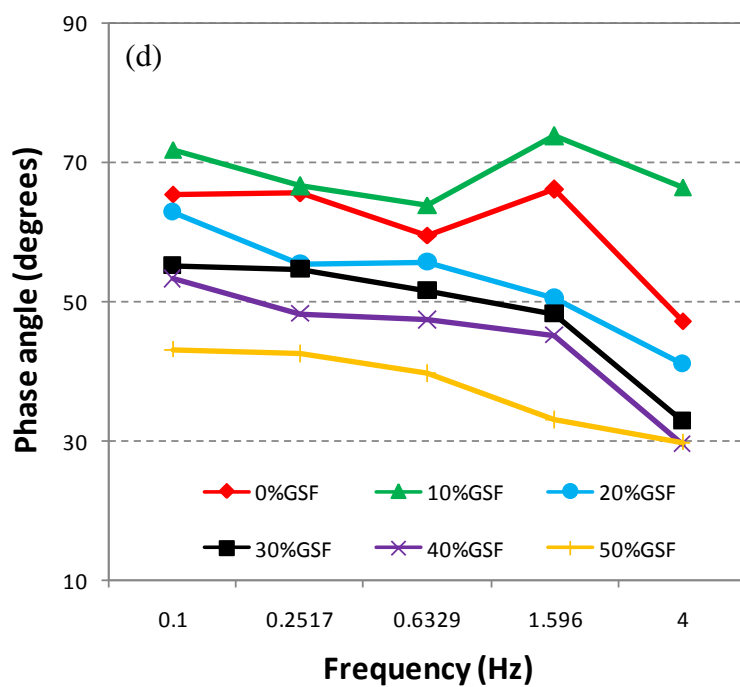
As can be seen in Table 6.96, with the exceptional behavior of the 40%GSF content SEB at 4.0Hz, the evident increase in complex modulus values for all binders after aging is reasonable due to oxidative exposure during the laboratory simulation of short-term aging via RTFOT. It is assumed that the oxidative aging strengthened the poly-sulphuric networks and converted some of the physical bonds to chemical ones. Once again, as with its results at other reference test temperatures, owing to its low G^* values, the 10%GSF content SEB does not compete with neat bitumen.



40°C after RTFOT



40°C after RTFOT



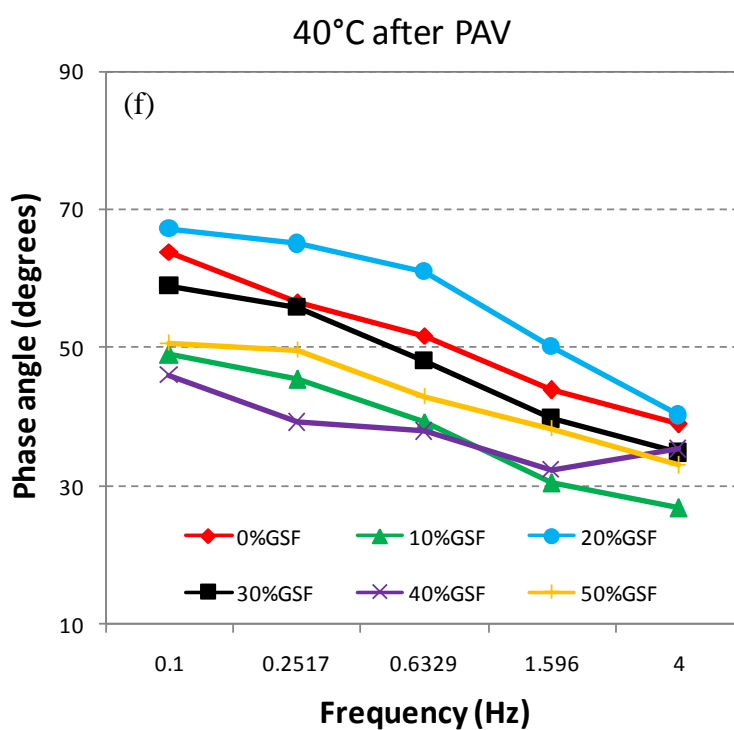
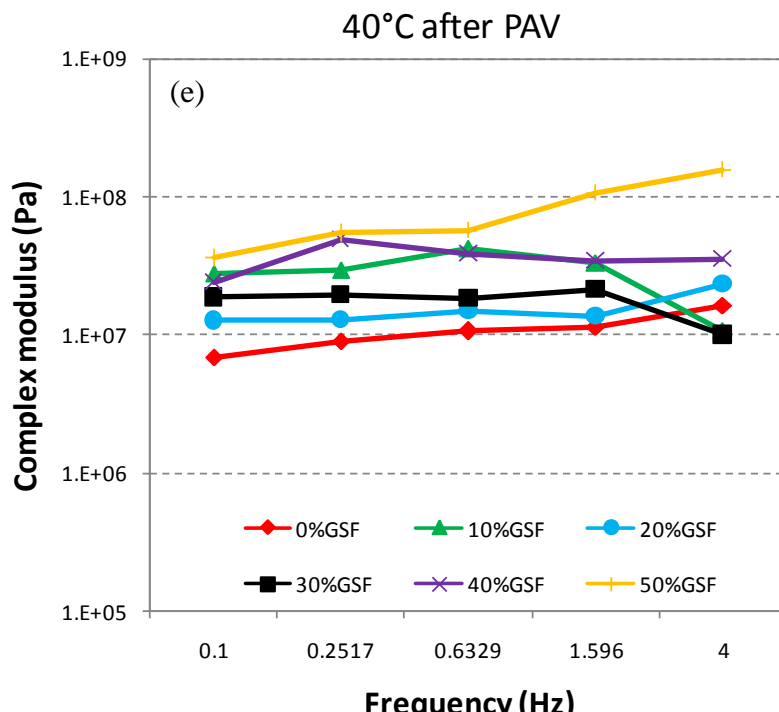


Figure 6.90 : The isochronal plots of complex modulus and phase angle versus loading frequency for B160/220 and B160/220-sulphur-extended-binders at a reference temperature of 40°C (loading frequency sweep, 0.1-4.0Hz). (a) and (b) Before aging. (c) and (d) After RTFOT-aging. (e) and (f) After PAV-aging.

Taking the complex modulus curves of other aged SEBs into consideration, the 30%GSF content SEB has comparable G^* values to the relatively softer 20%GSF content SEB within a frequency range from 0.1 to 1.596Hz. Despite this, this binder does appear to be softer than 20%GSF content SEB at the high frequency of 4.0Hz. A further increase of sulphuric extension in neat bitumen resulted in more improved elasticity due to elevated G^* values.

The viscoelastic behavior of 10%GSF content SEB tends to be substantially different from that of neat bitumen in its phase angles, initially decreasing with increasing frequency, moving from a viscous to a slight elastic rheological response, and then increasing before finally decreasing again. These obtained results from unaged and RTFOT-aged stage show that 10%GSF content SEB can neither partly nor completely replicate the rheological properties of conventional bitumen in terms of rutting resistance, which is evidenced by its relatively lower complex modulus and higher phase angle values as a function of frequency. Therefore, instead of trying to create an alternative binder by 10% sulphuric extension, it will be much more better for modifying (soften) stiffer grade bitumen via 10% sulphuric extension.

The rheological properties of the long-term aged specimens are presented in Figure 6.90 (e) and (f) in terms of isochronal plots of complex modulus and phase angle respectively. Rather than increasing G^* values further, PAV aging appears to make binders more resistant to varying loading frequencies. This supposition is also supported by the relatively smooth curves seen in Figure 6.90 (e). Furthermore, compared to their results at unaged and RTFOT-stage, the SEBs exhibit a relatively closer resemblance to each other after long-term aging. In other words, the gap between the G^* curves of PAV-aged SEBs declines, even though they remain very different from each other structurally. In addition, it is seen that PAV-aging greatly elevates the G^* values of 10%GSF content SEB, eventually situating its G^* curve over that of neat bitumen. This indicates that, after aging, this binder displays a more elastic response compared to neat 160/220 penetration bitumen.

The variations of the phase angle curves in Figure 6.90 (f) also confirm the benefits of sulphuric extension due to the considerable increase in elastic response compared to the 160/220 penetration bitumen (excepting the 20%GSF extension).

The dependence of the rheological behavior of B160/220 and B160/220-extended binders with varying sulphur levels on different loading frequencies (0.1-4.0Hz) at 50°C has been evaluated and the results are shown in Table 6.97. The isochronal plots of complex modulus and phase angle are depicted in Figure 6.91 (a-f). 50°C is an important temperature since it is usually applied to evaluate the performance of asphaltic concrete pavement in hot climate region.

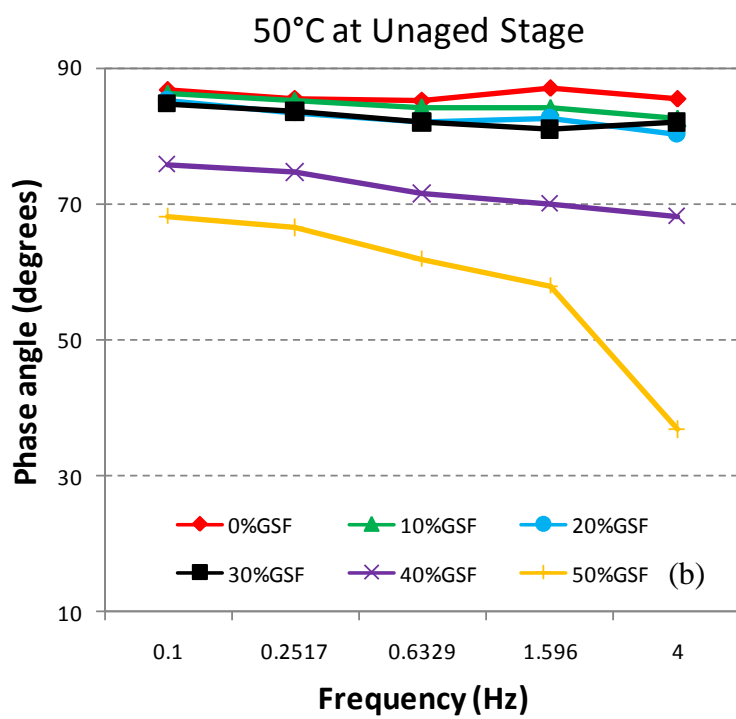
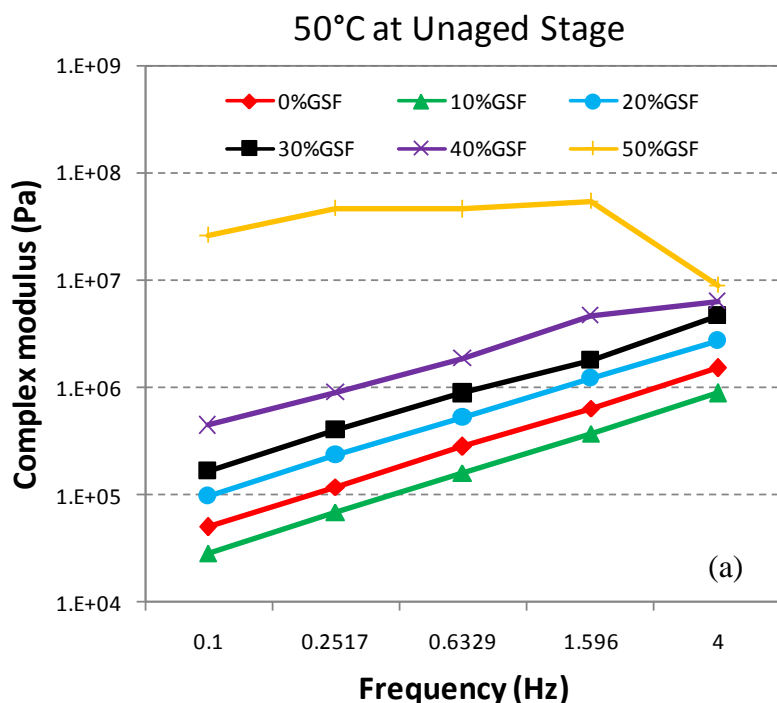
As shown in Figure 6.91 (a), the lower isochronal plot of complex modulus versus frequency seen in the 10%GSF content SEB prior to aging explains the formation of viscous sulphur networks in straight bitumen. It is believed that at this low quantity, the sulphur particles are not sufficiently able to create strong physical and chemical bonds with each other, and thus move freely in the bitumen matrix leading to an increase in viscous response. The high-temperature performance of the base 160/220 penetration bitumen can be improved by increasing the amount of sulphur extension from 10 up to 20%, as shown by the increase in the complex modulus as listed in Table 6.97. Further increasing the amount of sulphur leads to the varying trend in the rheology to become more obvious, while also improving high-temperature performance. The physical and chemical interactions that occur result in a decline in the size of the sulphur globes in size, and the dissolution and dispersion of more sulphur particles. Additionally, poly-sulphuric networks are believed to have been formed in the bitumen phase, thus resulting in this enhanced elasticity.

An evaluation of the phase angle values reveals that extending the sulphur up to 30% does not yield a significant variation. On the other hand, in the isochronal plots of complex modulus versus frequency, the reduced phase angle values of the sulphur-extended binder can be observed only at high sulphur levels. From 30 to 40%GSF, the phase angle values decrease quickly; whereas by 50%GSF, the sulphur-extended-binder displays the lowest δ values with increasing the shear frequency, which becomes apparent at 4.0Hz. What is more interesting is that the aforementioned binder is clearly becoming more susceptible to dynamic shear due to the degradation of some of the poly-sulphuric networks with increasing shear frequency. This is depicted in Figure 6.91 (b).

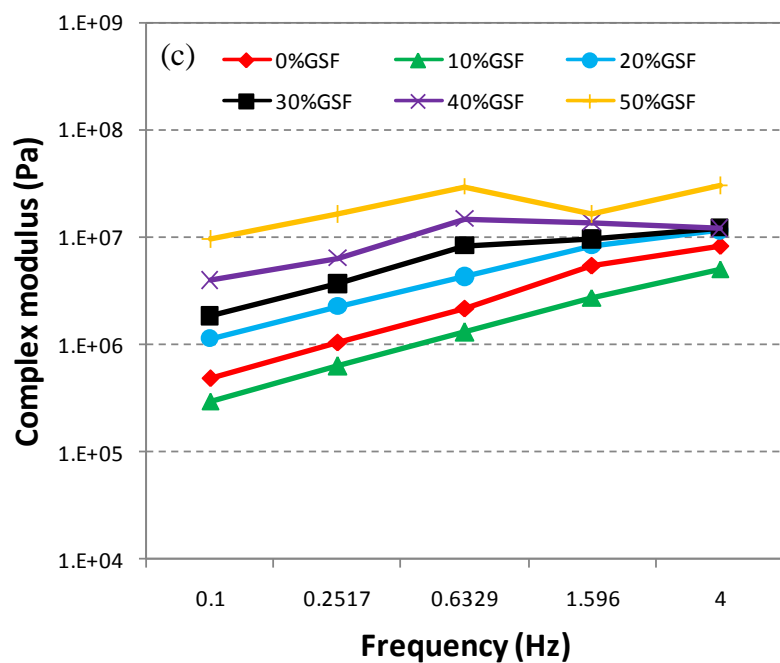
Table 6.97 : Rheological values of B160/220 base bitumen and B160/220-sulphur-extended-binders at a reference temperature of 50°C before aging, after RTFOT- and PAV-aging.

	UN-AGED STAGE				RTFOT STAGE				PAV STAGE			
	Temp. °C	Frequency Hz	Phase Angle °	Complex Modulus Pa	Temp. °C	Frequency Hz	Phase Angle °	Complex Modulus Pa	Temp. °C	Frequency Hz	Phase Angle °	Complex Modulus Pa
0%GSF	50	0.1	86.72	4.98E+04	50	0.1	75.06	4.93E+05	50	0.1	68.16	1.47E+06
	50	0.2517	85.47	1.19E+05	50	0.2517	75.25	1.06E+06	50	0.2517	67.34	2.78E+06
	50	0.6329	85.13	2.80E+05	50	0.6329	74.74	2.17E+06	50	0.6329	70.35	5.31E+06
	50	1.596	87.11	6.45E+05	50	1.596	75.46	5.50E+06	50	1.596	67.86	8.07E+06
	50	4	85.55	1.52E+06	50	4	71.28	8.37E+06	50	4	60.00	1.12E+07
10%GSF	50	0.1	86.28	2.90E+04	50	0.1	75.59	2.99E+05	50	0.1	64.96	6.82E+06
	50	0.2517	85.22	6.90E+04	50	0.2517	74.04	6.26E+05	50	0.2517	55.53	9.50E+06
	50	0.6329	84.05	1.62E+05	50	0.6329	73.41	1.30E+06	50	0.6329	63.80	8.83E+06
	50	1.596	84.23	3.75E+05	50	1.596	78.52	2.74E+06	50	1.596	55.85	9.11E+06
	50	4	82.53	8.88E+05	50	4	79.45	4.98E+06	50	4	55.03	1.41E+07
20%GSF	50	0.1	85.25	9.79E+04	50	0.1	69.92	1.13E+06	50	0.1	59.96	7.58E+06
	50	0.2517	83.35	2.35E+05	50	0.2517	66.31	2.23E+06	50	0.2517	46.79	1.68E+07
	50	0.6329	82.10	5.30E+05	50	0.6329	65.32	4.23E+06	50	0.6329	41.46	2.05E+07
	50	1.596	82.56	1.21E+06	50	1.596	64.12	8.38E+06	50	1.596	40.02	1.64E+07
	50	4	80.20	2.76E+06	50	4	60.42	1.14E+07	50	4	29.55	5.02E+07
30%GSF	50	0.1	84.61	1.69E+05	50	0.1	68.21	1.84E+06	50	0.1	51.88	1.70E+07
	50	0.2517	83.53	4.03E+05	50	0.2517	64.17	3.64E+06	50	0.2517	37.16	1.79E+07
	50	0.6329	81.96	8.87E+05	50	0.6329	63.74	8.18E+06	50	0.6329	45.08	1.83E+07
	50	1.596	80.86	1.81E+06	50	1.596	67.35	9.44E+06	50	1.596	45.24	2.01E+07
	50	4	81.90	4.62E+06	50	4	48.11	1.22E+07	50	4	41.20	1.62E+07
40%GSF	50	0.1	75.81	4.42E+05	50	0.1	61.91	3.92E+06	50	0.1	40.47	1.49E+07
	50	0.2517	74.62	9.03E+05	50	0.2517	60.08	6.40E+06	50	0.2517	36.91	1.57E+07
	50	0.6329	71.43	1.86E+06	50	0.6329	61.12	1.46E+07	50	0.6329	37.92	1.35E+07
	50	1.596	69.94	4.65E+06	50	1.596	59.07	1.35E+07	50	1.596	37.83	1.41E+07
	50	4	68.08	6.38E+06	50	4	46.15	1.19E+07	50	4	30.03	3.72E+07
50%GSF	50	0.1	68.20	2.60E+07	50	0.1	58.78	9.52E+06	50	0.1	40.77	2.83E+07
	50	0.2517	66.43	4.65E+07	50	0.2517	59.79	1.61E+07	50	0.2517	42.69	3.77E+07
	50	0.6329	61.86	4.52E+07	50	0.6329	52.18	2.93E+07	50	0.6329	38.46	3.95E+07
	50	1.596	57.97	5.39E+07	50	1.596	51.97	1.62E+07	50	1.596	39.07	2.29E+07
	50	4	36.79	8.89E+06	50	4	41.58	2.98E+07	50	4	33.47	7.05E+07

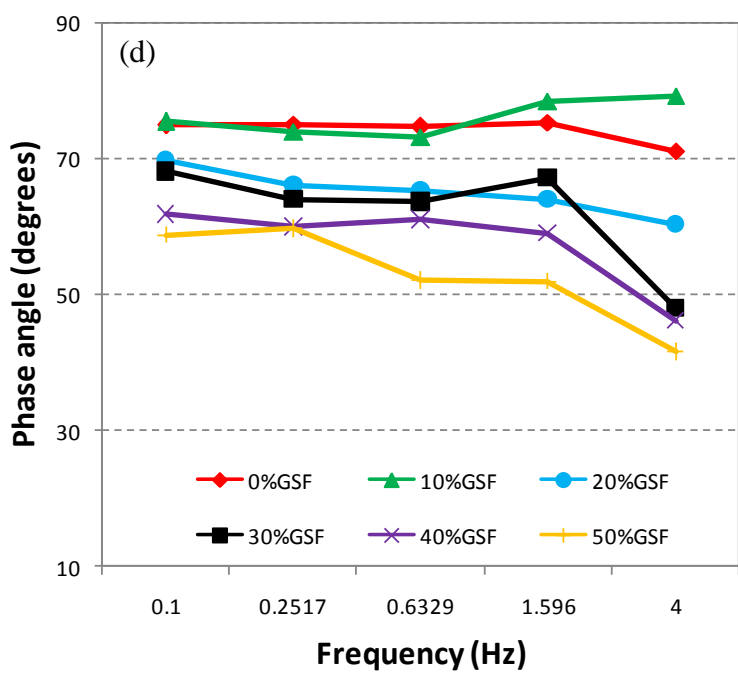
The expected increase in elastic behavior is detected after short-term aging; this trend becomes very apparent when the sulphur levels are increased up to 40wt%. On the other hand, the opposite effect is observed for the 50%GSF content SEB. The breakdown of the initially formed networks and/or decomposition of the sulphur dispersed in bitumen during laboratory simulations of short-term aging via RTFOT may be the main reasons leading to decrease in its G^* values. Similar to its rheological behavior before aging, the 10%GSF content SEB continued to display a less complex modulus than the free-sulphur bitumen (Figure 6.91 (c)). This once more again reinforces the approach that the variation in the viscoelastic properties of the aged straight bitumen strongly depends on the level of sulphur present.



50°C after RTFOT



50°C after RTFOT



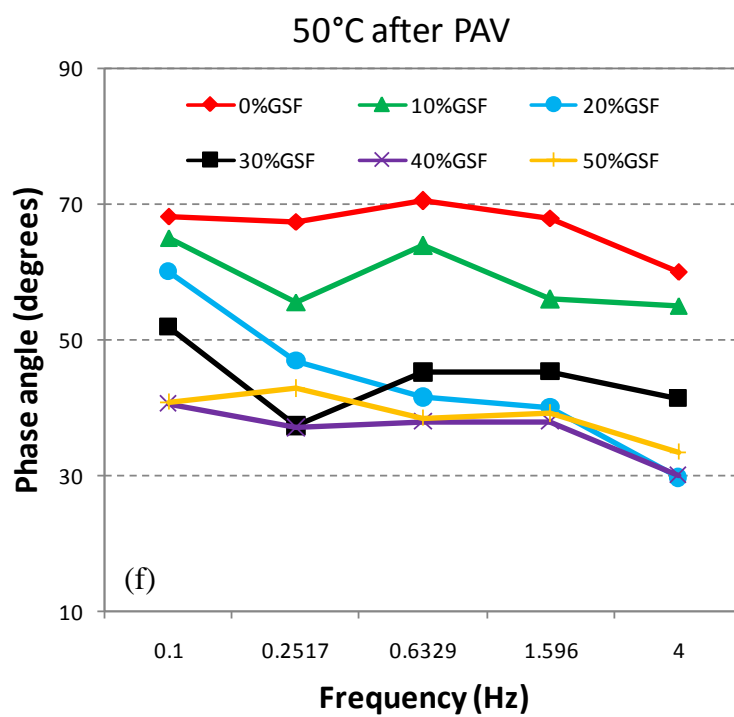
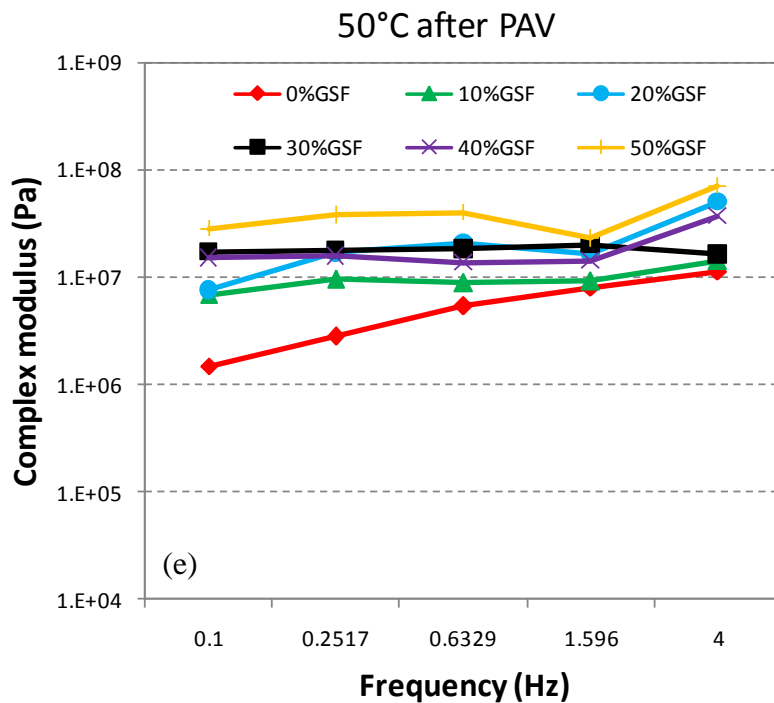


Figure 6.91 : The isochronal plots of complex modulus and phase angle versus loading frequency for B160/220 and B160/220-sulphur-extended-binders at a reference temperature of 50°C (loading frequency sweep, 0.1-4.0Hz). (a) and (b) Before aging. (c) and (d) After RTFOT-aging. (e) and (f) After PAV-aging.

Evaluations of the phase angle values after RTFOT aging indicates that owing to some variations, the obtained results are not in agreement with the G^* values. For instance, even though the δ curve of the 10%GSF content SEB is expected to have been higher than that of base bitumen over the entire frequency range, it actually was lower at low and intermediate frequency ranges. Furthermore, the sequence of δ curves is not similar to the sequence that was seen before aging. As depicted in Figure 6.91 (d), the δ value of 30%GSF content SEB is somewhat greater than that of the 20%GSF content SEB at 1.596Hz. These awkward outcomes can be explained in two ways: On the one hand, δ measurements are generally more sensitive to chemical composition than they are to the complex modulus of the sulphuric extension of bitumen (Gordon, 2003b). Secondly, RTFOT aging has a considerable influence on the variation of phase angle.

After PAV aging, there is a continuation and augmentation of the improved complex modulus of the sulphur-extended binders thanks to the further occurrences of elastic sulphur networks under pressure aging. Figure 6.91 (e) demonstrates that the difference in complex modulus among the SEBs is reduced over the entire frequency range. Furthermore, prolonged aging most likely serves to strengthen the stability of sulphur particle bonds; as a consequence, the susceptibility of the B160/220-sulphur-extended binders to change in shear frequency is alleviated to a considerable extent as proved by the pronounced plateau of their complex modulus plots. Other remarks on the effect of PAV aging regard the cases of 10 and 50%GSF content SEBs. The viscous behavior of the 10%GSF content SEB is eventually lost and this binder shifts towards toward more elastic response compared to neat bitumen. However, even prolonged aging did not increase the initial G^* values of the 50%GSF content SEB.

In the analysis for the isochronal plots of phase angle versus loading frequency it was noted that the influence of PAV aging on the structural characteristics of the sulphur-extended binders is almost similar to that by RTFOT aging, with the exception of minor variations. For instance, differing from both the unaged and RTFOT-aged stage, the δ curve of the 10%GSF content SEB lowered under that of the neat bitumen and the δ curve of the 50%GSF content SEB does not place at the bottom after long-term aging. In addition, the variation in phase angle values among the SEBs relatively increases further over the entire frequency range, compared to the results subsequent to RTFOT aging (Figure 6.91 (f)).

6.2.4 Bending beam rheometer (BBR) results

In order to investigate the influence of aging on the low temperature creep behavior of the SEBs, the long-term aged test was followed by the conducting of a bending beam rheometer (BBR ATS, Applied Test Systems, Inc, USA) creep test. This was carried out on each PAV-residue at two low different temperatures in accordance with ASTM D6648.

Two indices, the creep stiffness modulus (S) and stiffness change rate (m -value) determined from the BBR test, were deemed suitable for evaluating the relative thermal cracking performance of bituminous binder in the field (Ramadhan et al., 1998). However, it was concluded through the validation of performance prediction models of bituminous binders and paving mixtures that the binder specification alone does not assure enough thermal cracking performance, and other mixture characteristics may have a significant effect on thermal cracking performance for a specific bituminous binder (Lyton et al., 1994).

Since SHRP specifications call for the creep stiffness to be lower than 300MPa and the m -value to be greater than 0.300 at the 60th second to minimize low-temperature cracking, each long-term aged SEB residue was tested at two low different temperatures (0 and -6°C); both of which were selected to meet those requirements. High creep stiffness most probably led the asphalt layers to become brittle. This then leads to unavoidable cracking. Adversely, a high value of creep rate means that the binder will be more prone to disperse energy due to its rapid changing stiffness. The obtained results are summarized in Table 6.98 and graphically presented from Figures 6.92 to 6.100.

Table 6.98 : A-short-brief of BBR results.

Sample	BBR Results at 0°C		BBR Results at -6°C	
	Stiffness (MPa)	<i>m</i> -value	Stiffness (MPa)	<i>m</i> -value
B50/70-0%GSF	120.7688	0.573990	202.3186	0.516078
B50/70-10%GSF	55.1120	0.396614	120.6765	0.351887
B50/70-20%GSF	72.4704	0.345638	203.1288	0.469844
B50/70-30%GSF	99.1090	0.309508	147.5209	0.282068
B50/70-40%GSF	92.8471	0.359545	140.0123	0.321952
B50/70-50%GSF	80.4054	0.278899	91.6630	0.265332
B70/100-0%GSF	41.0085	0.455871	86.9746	0.383853
B70/100-10%GSF	34.2126	0.468644	64.9136	0.379006
B70/100-20%GSF	46.6242	0.361868	112.4626	0.370713
B70/100-30%GSF	40.6767	0.353212	103.6449	0.326963
B70/100-40%GSF	52.5614	0.314183	102.8170	0.288397
B70/100-50%GSF	58.9271	0.283813	94.2754	0.262336
B100/150-0%GSF	23.3502	0.403805	65.3581	0.408827
B100/150-10%GSF	23.0799	0.395921	59.6844	0.393339
B100/150-20%GSF	31.0118	0.407049	72.8397	0.366812
B100/150-30%GSF	42.9103	0.383991	60.7984	0.369818
B100/150-40%GSF	39.7573	0.351084	70.8814	0.314706
B100/150-50%GSF	37.1613	0.327044	65.9511	0.297924
B160/220-0%GSF	unreadable	unreadable	25.5614	0.392467
B160/220-10%GSF	unreadable	unreadable	26.6806	0.377206
B160/220-20%GSF	unreadable	unreadable	38.5230	0.361610
B160/220-30%GSF	unreadable	unreadable	33.4868	0.307970
B160/220-40%GSF	unreadable	unreadable	41.2976	0.345516
B160/220-50%GSF	unreadable	unreadable	28.9439	0.282087

From the table and following figures, we can obtain the following conclusions:

SEBs composed of B50/70 and variable amount of GSF;

The control bitumen (B50/70-0%GSF) demonstrated the highest creep stiffness (S) at 0°C temperature and highest *m*-value at the temperature of both 0 and -6°C. A replacement of 10%GSF clearly improved the low temperature cracking resistance of the pure B50/70 bitumen, as shown by the declined creep stiffness at both temperatures. However, this extension also resulted in declining its *m*-values, but these values still remained higher than 0.300. For the B50/70-30%GSF the *m*-value was at threshold point at 0°C but unpromising at -6°C. For the B50/70-50%GSF, in spite of its acceptable stiffness at both temperatures, the *m*-value was seen to be less than 0.300, which implies the low-temperature cracking resistance of the B50/70-50%GSF declines through vulcanization, a chemical process that converts natural

rubber or related polymers into more durable materials via the addition of sulphur (Ghosh et al., 2003). Thus, the declined low-temperature cracking resistance of B50/70-50%GSF was most probably caused by the formation of carbon-sulphur bonds. The opposite result can be found for the B50/70-40%GSF at both temperatures. As can be seen from Table 6.98, there is a clear decline in creep stiffness declines and an increase in the *m*-value of the 40%GSF replacement, indicating that the low temperature cracking resistance has improved.

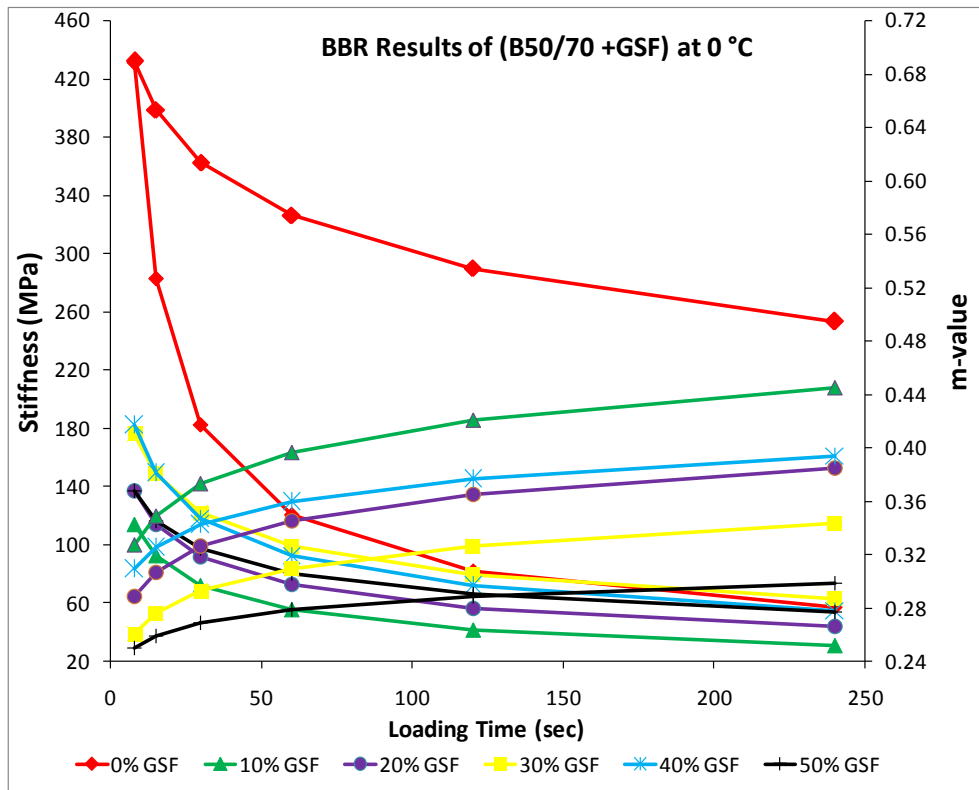


Figure 6.92 : Showing BBR results of (B50/70+GSF) residues at 0°C.

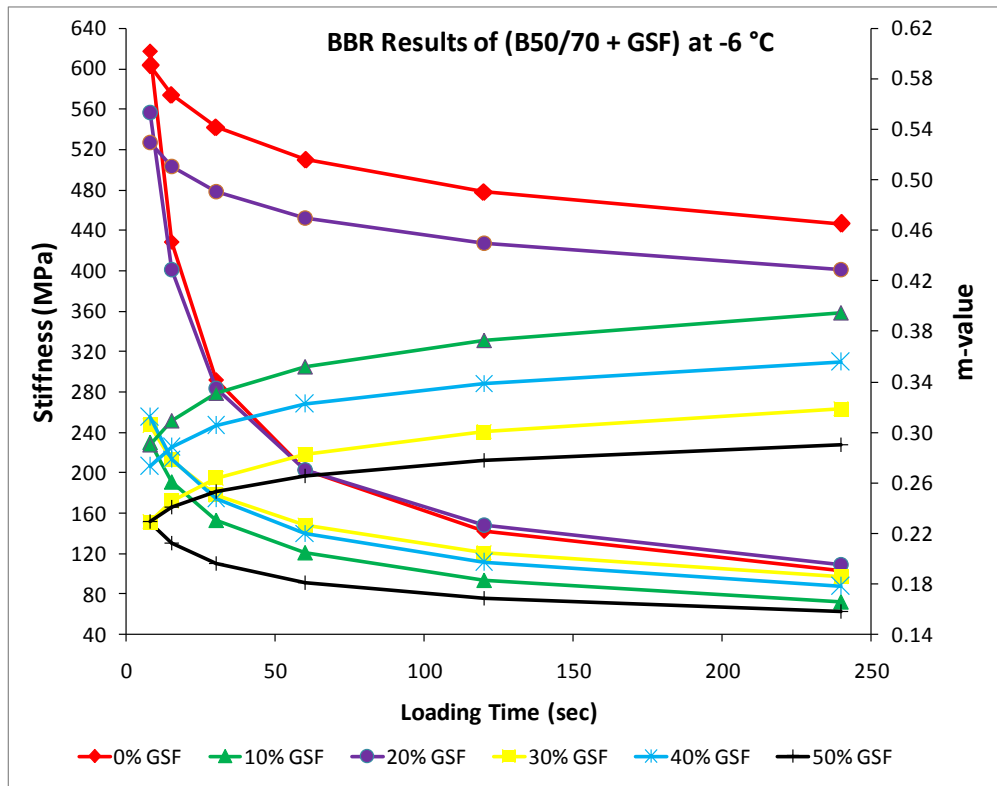


Figure 6.93 : Showing BBR results of (B50/70+GSF) residues at -6°C.

SEBs composed of B70/100 and variable amount of GSF;

In case of 10%GSF replacement, the creep stiffness of pure B70/100 became smaller and its *m*-value became greater. This is an indication that when B70/100 bitumen is substituted with 10%GSF, the new binder B70/100-10%GSF will become less hard and its relaxation capability will increase at a temperature of 0°C. This is also true for the same SEB at the temperature of -6°C, except now its *m*-value has decreased. The opposite result can be found for the B70/100-20%GSF at both temperatures. As can be seen from Table 6.98, there is a clear increase in creep stiffness and decrease in the *m*-value decreases in the case of 20%GSF replacement; this indicates that the low temperature cracking resistance of B70/100-20%GSF is not superior to that of pure B70/100, but is still within acceptable ranges. Any additional GSF replacement causes a gradual decrease in *m*-value at both 0 and -6°C, and a gradual increase in creep stiffness at 0°C, but a decrease at -6°C when compared with B70/100-20%GSF. Although its creep stiffness is still convenient at either 0 or -6°C, B70/100-50%GSF does not meet the requirement of pavement performance at both temperatures due to its lower *m*-value, which is lower than 0.300. B70/100-30%GSF is promising as a binder than can meet thermal cracking performance requirement at both temperatures, but B70/100-40%GSF can only meet this requirement at -6°C.

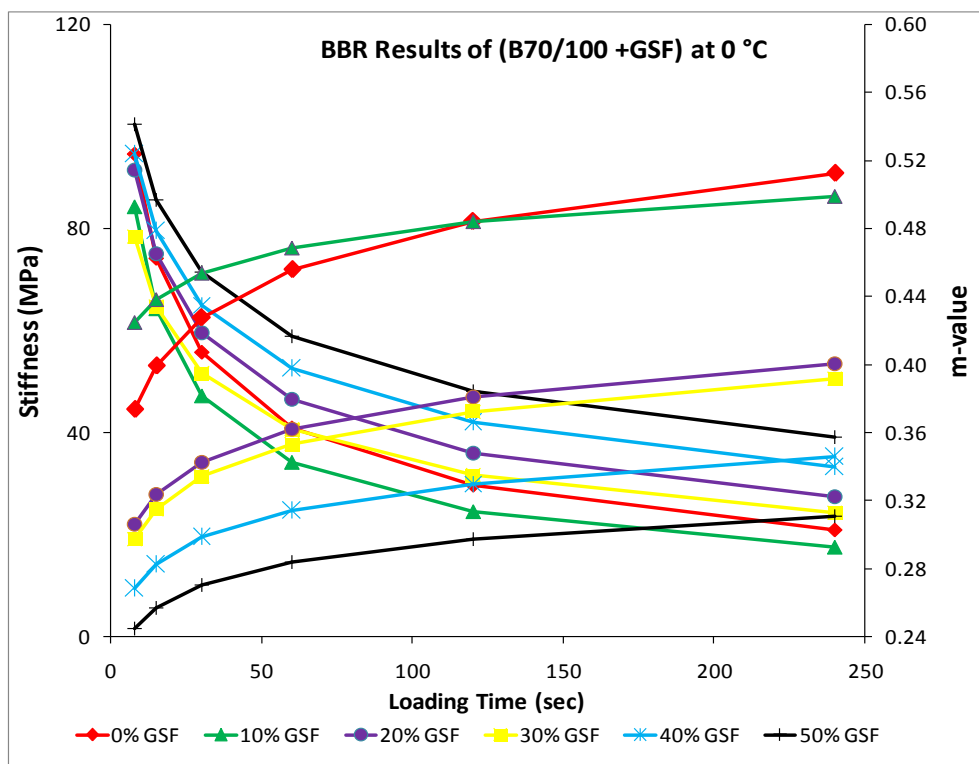


Figure 6.94 : Showing BBR results of (B70/100+GSF) residues at 0°C.

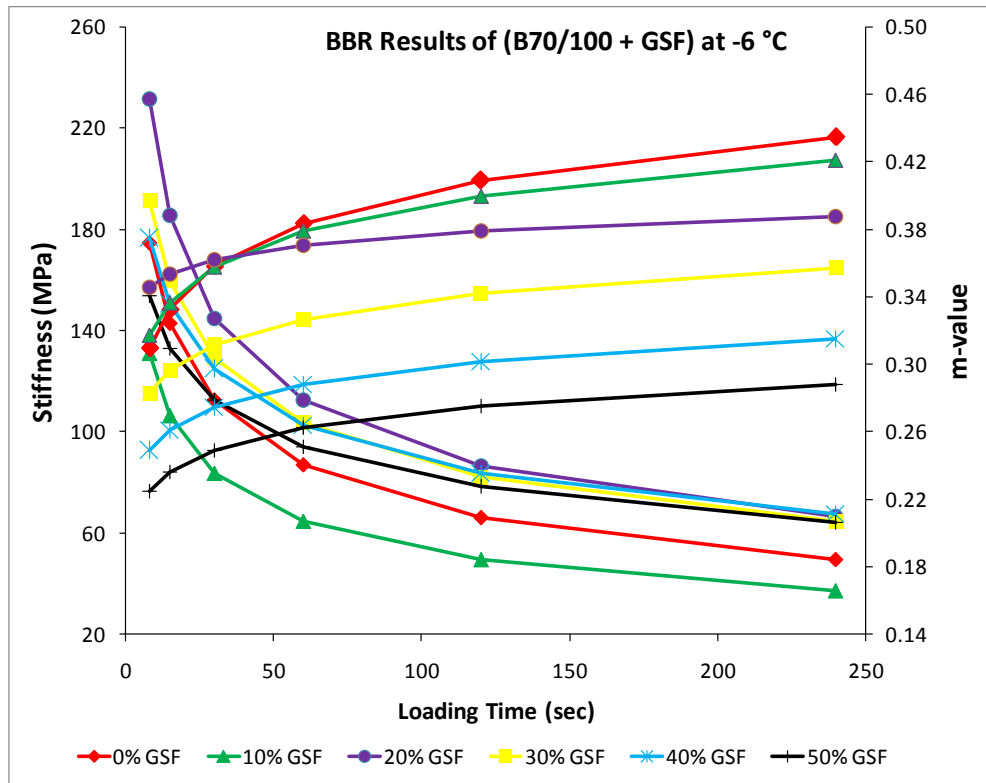


Figure 6.95 : Showing BBR results of (B70/100+GSF) residues at -6°C.

SEBs composed of B100/150 and variable amount of GSF;

It was found that when 10% of the conventional B100/150 bitumen is replaced with GSF, its low temperature cracking resistance showed almost no change, as clearly shown by the lack of change in creep stiffness and *m*-value at both temperatures. As the amount of GSF increased to 20%, the creep stiffness also had a tendency to increase at both temperatures. Despite this, the *m*-value increased at 0°C, exceeding that value for f pure bitumen, but decreased at -6°C. The creep stiffness value of 50% GSF content SEB is almost identical to that of pure B100/150 bitumen at the temperature of -6°C, but its *m*-value is lower and, therefore, unacceptable.

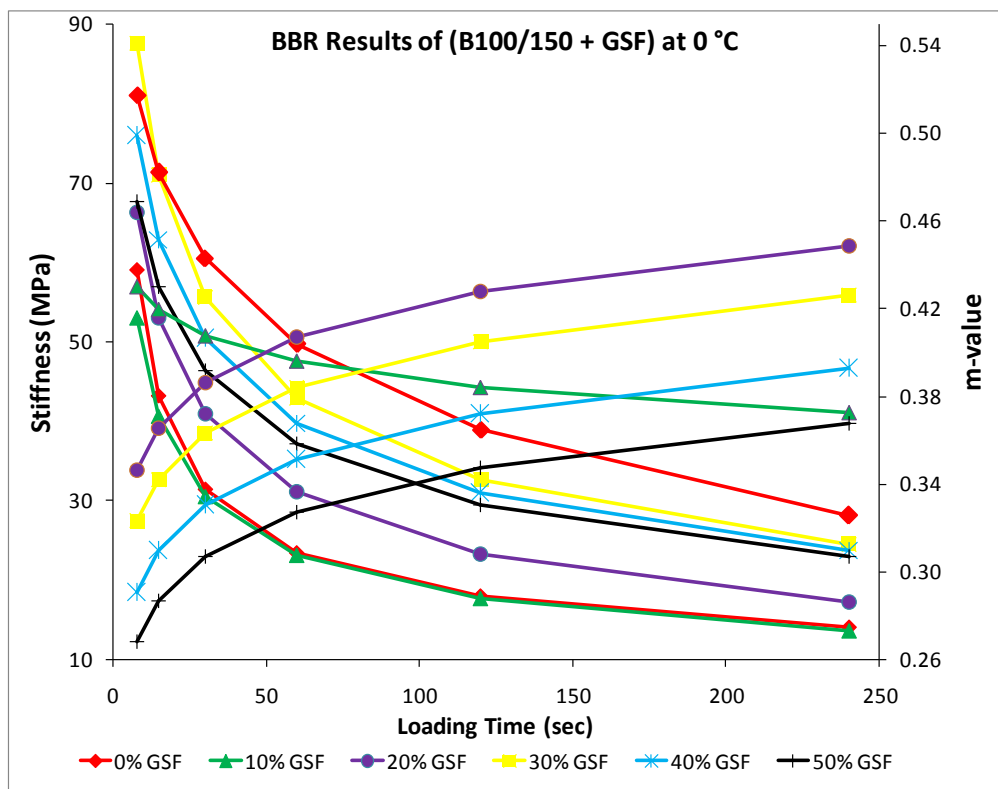


Figure 6.96 : Showing BBR results of (B100/150+GSF) residues at 0°C.

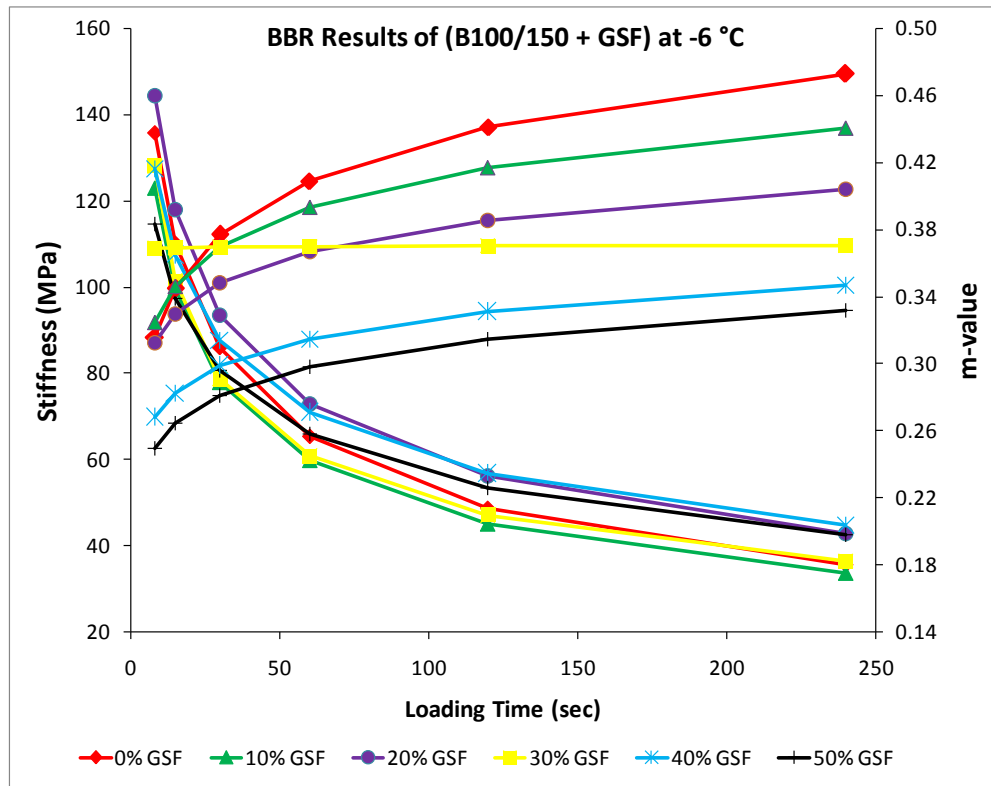


Figure 6.97 : Showing BBR results of (B100/150+GSF) residues at -6°C.

SEBs composed of B160/220 and variable amount of GSF;

Since it is already softer as compared with other pure bitumens in terms of consistency, the new SEBs that are derivatives of B160/220 are also expected to have less consistency. As expected, those samples had higher deflection (greater than 4.000mm); hence, two indices from the BBR test creep stiffness and *m*-value could not be obtained at the temperature of 0°C, as shown in following Figure 6.98.

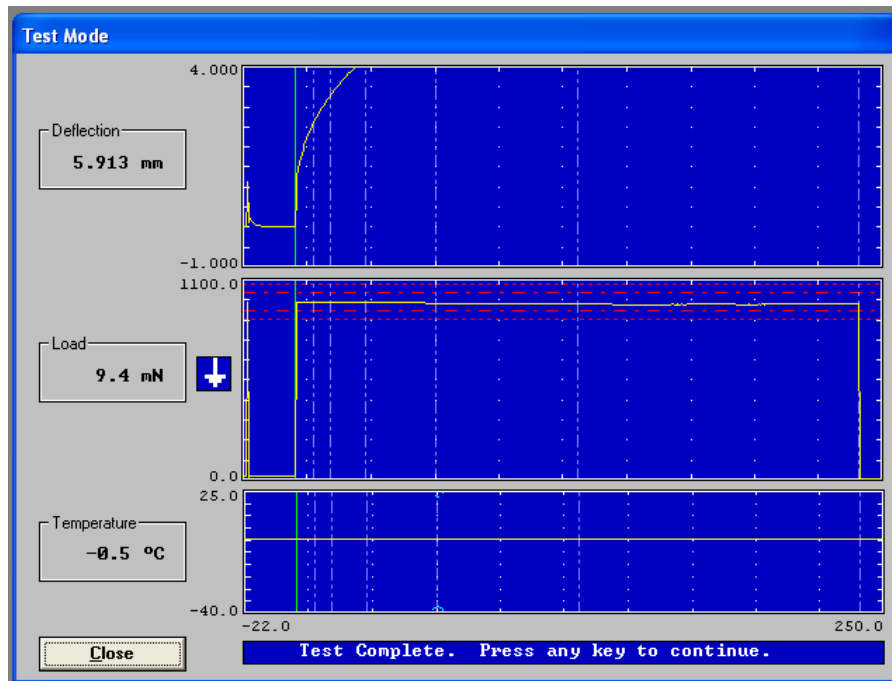


Figure 6.98 : Showing great deflection of (B160/220+GSF) residues at 0°C.

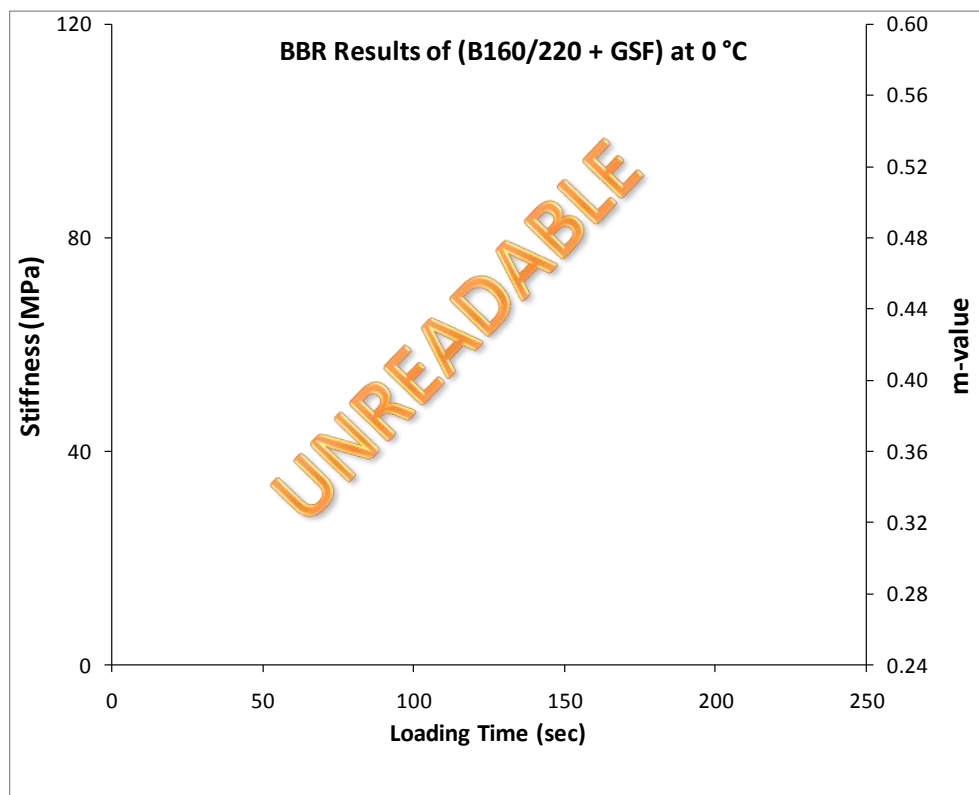


Figure 6.99 : Showing BBR results of (B160/220+GSF) residues at 0°C.

At the temperature of -6°C, the pure B160/220 bitumen demonstrated the lowest creep stiffness and the greatest *m*-value. In other words, at that temperature no single

GSF replacement is capable of improving upon pure B160/220 bitumen's low-temperature cracking resistance. Even in the case of 50%GSF replacement, the B160/220 bitumen will not be able to fulfill the determined requirements due to its low m -value (<0.300). No additional GSF replacements caused any regular changes in either creep stiffness or m -value. At times, these replacements caused a decrease or, at other times, an increase. The m -value of another critical SEB, B160/220-30%GSF, is almost at the threshold point but still remains promising. Among all SEBs, the derivatives of B160/220 at the temperature of -6°C had the least creep stiffness of each GSF replacement.

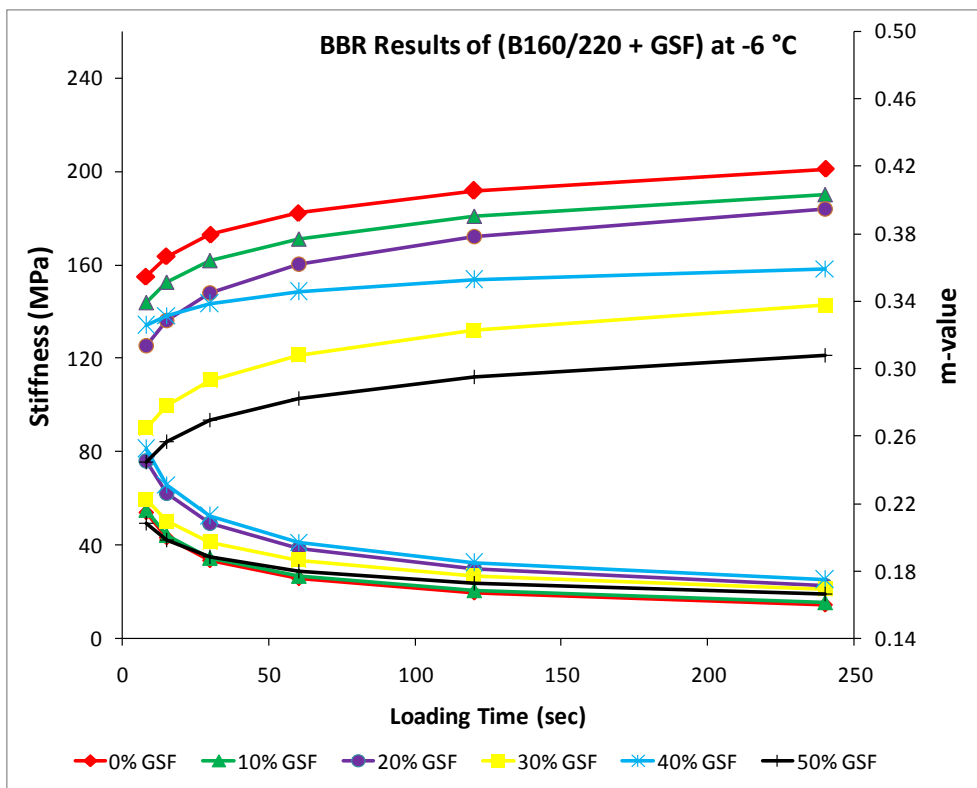


Figure 6.100 : Showing BBR results of (B160/220+GSF) residues at -6°C.

To sum up, regardless of pure and original bitumen type, the SEBs produced by 50%GSF replacement have relatively low and unacceptable (except B100/150-50%GSF) m -values at both 0 and -6°C as compared with pure bitumen. Increasing GSF replacements did not significantly improve the pure bitumen's creep stiffness, sometimes making them increase and sometimes decrease. Likewise, despite the fact that m -value had a general tendency to decrease as the percentage of GSF replacement was increased, it also sometimes increased. However, its alteration was not regular.

In conclusion, the results obtained in this study showed that, various GSF replacements failed to have a regular and positive effect on pure bitumen's low temperature thermal cracking performance.

6.3 Morphology Analysis Results

The compatibility between bitumen and sulphur is critical to the properties of SEBs. Based on the type of the neat bitumen and amount of GSF, three fundamental events are expected to occur subsequent to the replacement of bitumen with sulphur. A particular amount of the replaced sulphur reacts with the bitumen, another dissolves in the bitumen, and the rest forms a crystalline structure (Kennepohl and Miller, 1978; Rennie, 1979). All these states of the sulphur ultimately determine the fate of the SEBs. In this study, the morphologies of the SEBs before and after aging (both RTFOT and PAV) were investigated using SEM by characterizing distribution, shape and fineness of the sulphur in bitumen matrix. Furthermore, according to the spectrum processing, each sample was analyzed to evaluate the volume of carbon (C) and sulphur (S) elements present in terms of both weight and atomic percentages. The obtained values are summarized in Table 6.99. The morphology of the neat B50/70 bitumen and its derivative SEBs with separate GSF content before and after aging are shown in Figure A.1, Figure A.3, Figure A.5, Figure A.7, Figure A.9, and Figure A.11 respectively. The pale regions of the images correspond to the sulphur-rich phase; the dark areas represent the bitumen-rich phase.

SEBs composed of B50/70 and variable amount of GSF;

The microscopic compatibility between sulphur and B50/70 grade bitumen was investigated to reveal the morphological properties of SEBs before and after both short- and long-term aging. For the 10%GSF included sample, fine sulphur particles invisibly dissolved in a continuous and dominant bitumen phase, as can be seen in Figure A.3 (o1 and o2). Comparisons with the unaged stage demonstrate that after RTFOT aging the dissolved sulphur particles increased their size and began to be clearly visible. This is shown in Figure A.3 (r1, r2, and r3). However, the influence of long-term aging led the sulphur particles to once again decline in size, with their outlines becoming very homogenous. This suggests a further dissolution of GSF and a further improvement in the compatibility between GSF and bitumen over time. This is presented in Figure A.3 (p1, p2, and p3).

Inspection of the micrographs (Figure A.5 (o1, o2, and o3)) of the 20%GSF content SEB reveals that, in addition to the dissolved fine particles, coarse particles of sulphur are also present in the bituminous phase. As seen on the SEM micrographs, however, their radii range between 5 and 10 μ m, which is negligible because it is evident that these large aggregates of sulphur particles are mostly localized on the surface of bitumen. The short-term aging effect is displayed in Figure A.5 (r1, r2, and r3). After exposing the 20%GSF SEB to RTFOT, the light dots in the pictures representing the swelling of the dissolved sulphur particles became distinctive. Once the same SEB is subjected to long-term aging, a small proportion of the sulphur usually segregated into small regions on the bitumen phase, as shown in Figure A.5 (p1, p2, and p3).

For the 30%GSF SEB, the morphological natures of the sulphur-rich phase and bitumen-rich phases before and after aging are illustrated in Figure A.7 (o1-o3, r1-r3, and p1-p3). Secured in the continuous matrix formed by the bitumen, the sulphur exhibited a biphasic morphology. The barely visible small light spots demonstrate the presence of dissolved sulphur and coarse, irregular shape sulphur particles, thereby signifying dispersed sulphur. When compared to the unaged stage of the same SEB, after short-term aging the coarse particles substantially disappeared, demonstrating an increase in dissolved sulphur proportion and a very homogenous matrix. Therefore, the major effect of short-term aging on the morphology of the SEB is the homogeneous distribution of sulphur in bitumen matrix. There is also a further improvement in the compatibility between sulphur and bitumen, most probably with further aging due to the severe degradation of GSF. After PAV aging, the giant sulphur particles seem to have appeared on the upper surface of the bitumen phase.

In the case of 40%GSF replacement, the morphological views for unaged, short- and long-term aged stages are given in Figure A.9 (o1-o3, r1-r3, and p1-p3). The presence of dominant coarse sulphur particle reveals that the the unaged SEB has an irregular surface. This most probably stems from an excessive sulphur amount that exceeds the optimum replacement capacity of the neat bitumen. Views captured particularly at the magnification of X1000 demonstrate that sulphur particles have a tendency to create fishbone-looking crystalline structures after the SEB was subjected to RTFOT. Further aging did not paint a different picture.

An increase of the sulphur content to 50% yielded different pictures in terms of morphology. The views belonging to unaged, short- and long-term aged sample are given in Figure A.11 (o1-o3, r1-r3, and p1-p3). At the initial stage, sulphur exhibited a multiphasic morphology. A remarkable amount of sulphur dissolved in the bitumen matrix developed a colloidal form, while the rest heterogeneously dispersed in terms of size. Among the all SEBs with various GSF amounts, this is the first time that giant sulphur particles with a radius over $10\mu\text{m}$ are present. After short-term aging, the morphology changed from that of coarse sulphur particles to a crystalline structure; this verifies the assumption that the compatibility between the GSF and bitumen increases over time. The views captured at the magnification of X40 and X500 clarify that this cream-like crystalline structure dominates the upper surface of the bitumen. However, as a consequence of a prolonged aging time in PAV, there was an obvious break-down in the network between surface sulphur aggregation, and the size of the crystalline structure was seen to decline.

Finally, a spectrum processing analysis was carried out to reveal the amounts of carbon (C) and sulphur (S) contents in terms of both weight and atomic percentages for each sample (Figure A.2, Figure A.4, Figure A.6, Figure A.8, Figure A.10, and Figure A.12). The obtained values are briefly summarized in Table 99.

Table 6.99 : Element analyses for the series of B50/70 before and after aging.

Sample	Stage	Element	Weight (%)	Atomic (%)
B50/70-0%GSF	Un-aged	Carbon	100	100
		Sulphur	-	-
	RTFOT-aged	Carbon	100	100
		Sulphur	-	-
	PAV-aged	Carbon	94.93	98.04
		Sulphur	5.07	1.96
B50/70-10%GSF	Un-aged	Carbon	91.09	96.47
		Sulphur	8.91	3.53
	RTFOT-aged	Carbon	72.98	87.82
		Sulphur	27.02	12.18
	PAV-aged	Carbon	94.39	97.82
		Sulphur	5.61	2.18
B50/70-20%GSF	Un-aged	Carbon	82.95	92.85
		Sulphur	17.05	7.15
	RTFOT-aged	Carbon	82.83	92.79
		Sulphur	17.17	7.21
	PAV-aged	Carbon	85.40	93.98
		Sulphur	14.60	6.02
B50/70-30%GSF	Un-aged	Carbon	70.68	86.55
		Sulphur	29.32	13.45
	RTFOT-aged	Carbon	81.33	92.08
		Sulphur	18.67	7.92
	PAV-aged	Carbon	46.83	70.16
		Sulphur	53.17	29.84
B50/70-40%GSF	Un-aged	Carbon	68.59	85.36
		Sulphur	31.41	14.64
	RTFOT-aged	Carbon	50.99	73.53
		Sulphur	49.01	26.47
	PAV-aged	Carbon	58.87	79.26
		Sulphur	41.13	20.74
B50/70-50%GSF	Un-aged	Carbon	92.53	97.06
		Sulphur	7.47	2.94
	RTFOT-aged	Carbon	69.91	86.12
		Sulphur	30.09	13.88
	PAV-aged	Carbon	61.29	80.87
		Sulphur	38.71	19.13

SEBs composed of B70/100 and variable amount of GSF;

In the examination of the extended B70/100 grade bitumen, image analysis was used to reveal the morphological properties of SEBs before and after both short- and long-term aging. It should be noted that in these micrographs all horizontal bars represent a length of 10 μ m; the light phase shows sulphur, and the dark phase shows bitumen.

Figure A.15 (o1-o3, r1-r3, and p1-p3) shows the original, short-term aged, and long-term aged micrographs of the 10%GSF SEB. Prior to aging, the dispersed, irregular shaped sulphur particles seemed to have created an aggregation on the upper surface, whereas the fine sulphur particles dissolved in bitumen matrix were barely visible. It is noteworthy to point that at the unaged stage both physical and chemical reactions between sulphur particles and bitumen compounds play major roles in bond development. Following short-term aging, the diameter of surface sulphur aggregation displays a tendency to decrease. This change in size is most probably due to the transition of some dispersed sulphur particles into a colloidal form. Compared with Figure A.15 (r1-r3), the numbers of sulphur particles dispersed in bitumen substantially increase and their sizes decrease, apparently after PAV aging, as shown in Figure A.15 (p1-p3). These outcomes imply the further degradation of GSF and a further improvement in the compatibility between sulphur and bitumen.

The morphological change of the B70/100-20%GSF binder before and after aging is shown in Figure A.17 (o1-o3), (r1-r3) and (p1-p3). Prior to aging, as shown in Figure A.17 (o1-o3), a wide range of light colored sulphur aggregations are pronounced on the upper surface. Zooming into the surface reveals that these aggregations consist of homogeneous and moderate-sized sulphur particles. In addition to the bitumen reactions of varying amounts, RTFOT aging played two major roles in the development of a biphasic morphology of the sulphur. On the one hand, owing to oxidative aging, a substantial amount of dissolved fine sulphur particles were seen to have swollen and became visible; secondly, the high temperature test led the bitumen to absorb a considerable amount of the coarse sulphur particles previously located on the upper surface. As depicted in Figure A.17 (p1-p3), the remaining coarse particles seemed to have condensed, grown in size, and to have increased their dimensions up to 30 μ m.

Inspection of the micrographs (Figure A.19 (o1, o2, and o3)) for the 30%GSF content SEB reveals that, in addition to the fine sulphur particles embedded in the bitumen-rich phase, an essential amount of coarse particles are also present on the surface. The dissolution ratio of the sulphur in bitumen is unquestionably related with the blending temperature and the dissolution efficiency of the sulphur (Petrossi et al., 1972). As previously mentioned, granular shape, 2-3mm diameter sulphur was utilized for replacement during the preparation of the SEB samples. Close attention was paid to the blending temperature so as to prevent possible emissions of poisonous SO₂ and H₂S gases. To this end, a temperature constant of 140°C was assigned. Rather than increasing the blending temperature, it was considered that decreasing the diameter of sulphur particles would better fill the miscibility gap between the sulphur particles and 70/100 grade bitumen compounds. The short-term aging effect is exhibited in Figure A.19 (r1, r2, and r3). Morphologies indicate that cream-like coarse sulphur particles previously seen in the unaged stage have now nearly disappeared, hence the same SEB would be relatively more homogeneous after RTFOT aging. Even though a single and unstable cluster made up of huge sulphur particles is detected on the surface, one may observe that short-term aging also provides improved compatibility between the sulphur particles and the bitumen compounds. Lastly, the outcomes of long-term aging on the same SEB are given in Figure A.19 (p1, p2, and p3). Compared to RTFOT aged images, further sulphur crystalline structure aggregations reoccurred. Previous research on the subject highlighted the fact that while there were fewer problems arising from low crystallization, the coarsening of the crystals has to be considered in terms of their great effect on SEB behavior.

Results from SEM images (Figure A.21 (o1-o3, r1-r3, and p1-p3)) illustrated that an increase of the GSF content up to 40% promoted a variety of morphology. At the unaged stage, in-surface zooming reveals that sulphur particles variously exist in bitumen phase. On the one hand, fine sulphur globes with diameters smaller than 1μm are homogeneously dissolved and, secondly, moderate-sized particles are fairly distributed in bitumen matrix. The rest has clearly formed a crystalline structure on the surface. It should be mentioned that an invisible and remarkable portion of GSF is already on its way to creating both physical and chemical bonds with major bitumen compounds (such as saturates, aromatics, resins and etc.)

Previous studies stated that untransformed, but reacted and dissolved sulphur particles of 5-10 μm in diameter have a fairly homogeneous distribution, and characterize the fundamental morphology of the SEB (Fairbrother et al., 1955).

Following short-term aging via RTFOT, the needle-like, surface sulphur particles can be seen in Figure A.21 (r1-r3). Inspection of the micrographs (Figure A. 21 (p1-p3)) demonstrate that further PAV aging resulted in increasing the number of these crystals forming a cream-like structure on the top surface.

Increasing the sulphur content to 50% yielded different pictures in terms of morphology. The views belonging to unaged, short- and long-term aged sample were given in Figure A.23 (o1-o3, r1-r3, and p1-p3). At the unaged stage, Figure A.23 (o1-o3) indicates that extensive phase separation takes place in the case of 50%GSF replacement. In fact, the upper part seems to consist of a fluorescent sulphur-rich matrix in the presence of dark bitumen-rich matrix. The fact that the dispersed sulphur particles are of irregular shape suggests that the bitumen compounds and the sulphur particles are no longer miscible and that interfacial adhesion has lowered. After short-term aging, the coarse particles appear to have converted to needle-like sulphur crystals, as depicted in Figure A.23 (r1-r3). Once the same SEB is subjected to long-term aging, these heterogeneous structure needle-like sulphur crystals form small clusters in the matrix.

The above-mentioned results recommend that the GSF content of 50% is most probably the upper limit for sulphur extension of the neat 70/100 grade bitumen, since bitumen compounds can no longer absorb the sulphur particle.

Finally, in the spectrum processing, each sample was analyzed to evaluate the volume of carbon (C) and sulphur (S) elements present in terms of both weight and atomic percentages (Figure A.14, Figure A.16, Figure A.18, Figure A.20, Figure A.22, and Figure A.24). The obtained values are summarized in Table 6.100.

Table 6.100 : Element analyses for the series of B70/100 before and after aging.

Sample	Stage	Element	Weight (%)	Atomic (%)
B70/100-0%GSF	Un-aged	Carbon	97.64	99.10
		Sulphur	2.36	0.90
	RTFOT-aged	Carbon	100	100
		Sulphur	-	-
	PAV-aged	Carbon	97.49	99.05
		Sulphur	2.51	0.95
	Un-aged	Carbon	71.20	86.84
		Sulphur	28.80	13.16
	RTFOT-aged	Carbon	50.92	73.47
B70/100-10%GSF		Sulphur	49.08	26.53
	PAV-aged	Carbon	62.79	81.84
		Sulphur	37.21	18.16
	Un-aged	Carbon	63.14	82.05
		Sulphur	36.86	17.95
	RTFOT-aged	Carbon	85.03	93.81
		Sulphur	14.97	6.19
	PAV-aged	Carbon	76.95	89.91
		Sulphur	23.05	10.09
B70/100-20%GSF	Un-aged	Carbon	62.86	81.88
		Sulphur	37.14	18.12
	RTFOT-aged	Carbon	72.41	87.51
		Sulphur	27.59	12.49
	PAV-aged	Carbon	75.50	89.16
		Sulphur	24.50	10.84
	Un-aged	Carbon	78.87	90.88
		Sulphur	21.13	9.12
	RTFOT-aged	Carbon	65.31	83.41
B70/100-30%GSF		Sulphur	34.69	16.59
	PAV-aged	Carbon	72.21	87.40
		Sulphur	27.79	12.60
	Un-aged	Carbon	64.59	82.96
		Sulphur	35.41	17.04
	RTFOT-aged	Carbon	67.51	84.72
		Sulphur	32.49	15.28
	PAV-aged	Carbon	58.38	78.92
		Sulphur	41.62	21.08

SEBs composed of B100/150 and variable amount of GSF;

For the O-B100/150-10%GSF, a dominant continuous bitumen phase with dissolved GSF can be seen in Figure A.27 (o1-o3). Among the SEBs with different GSF amounts, the 10%GSF sample revealed the finest dissolution of sulphur. The effects of aging on the morphology are demonstrated in Figure A.27 (r1-r3) and (p1-p3). Compared with the unaged stage, the number of sulphur particles dissolved in bitumen decreased and their sizes increased after the RTFOT aging, as shown in Figure A.27 (r1-r3). In Figure A.27 (p1-p3), it can be seen that the dissolved particle sizes tend to decline in continuous bitumen after PAV aging, which reinforces the assumption of dissolution of GSF and the improvement of the compatibility between GSF and bitumen over time. The morphological change of the B100/150 bitumen with 20%GSF content before and after aging is shown in Figure A.29 (o1-o3), (r1-r3) and (p1-p3). Before aging, as shown in Figure A.29 (o1-o3), two different phases of sulphur can be observed. Compared with the dissolved fine sulphur particles shown in Figure A.27 (o1-o3), the dispersed sulphur particles can be also detected in Figure A.29 (o1-o3). After aging, these dispersed particles seem to create icy-looking crystalline structures as seen in Figure A.29 (r1-r3) and (p1-p3). Compared with 20%GSF, the 30%GSF replacement did not result in any remarkable morphological differentiation at the unaged and RTFOT aged stages, as shown in Figure A.31 (o1-o3) and (r1-r3). However, after PAV aging, coarse sulphur particles started to be visible. The effects of 40%GSF replacement are shown in Figure A.33 (o1-o3), (r1-r3) and (p1-p3). Owing to its additional amounts, homogeneous distribution of dispersed sulphur particles started to disappear and coarse particles were first seen at the unaged stage. RTFOT aging paved the way for these particles to increase their size. After PAV aging, even though these giant particles appeared to diminish, icy-looking crystalline structures began to dominate a substantial part of the whole matrix. Although Figure A.35 (o1-o3) illustrates that further GSF replacement does not deteriorate the homogeneity of dissolved and dispersed sulphur, after aging it can be confirmed that B100/150 with 50%GSF easily decomposes over time.

Finally, the spectrum processing analysis was conducted to evaluate the volumes of carbon (C) and sulphur (S) elements in terms of both weight and atomic percentages for each sample (Figure A.26, Figure A.28, Figure A.30, Figure A.32, Figure A.34, and Figure A.36). The obtained values are briefly summarized in Table 6.101.

Table 6.101 : Element analyses for the series of B100/150 before and after aging.

Sample	Stage	Element	Weight (%)	Atomic (%)
B100/150-0%GSF	Un-aged	Carbon	100	100
		Sulphur	-	-
	RTFOT-aged	Carbon	100	100
		Sulphur	-	-
	PAV-aged	Carbon	100	100
		Sulphur	-	-
	Un-aged	Carbon	92.06	96.87
		Sulphur	7.94	3.13
	RTFOT-aged	Carbon	68.23	85.15
B100/150-10%GSF		Sulphur	31.77	14.85
	PAV-aged	Carbon	90.15	96.07
		Sulphur	9.85	3.93
	Un-aged	Carbon	79.13	91.01
		Sulphur	20.87	8.99
	RTFOT-aged	Carbon	61.88	81.25
B100/150-20%GSF		Sulphur	38.12	18.75
	PAV-aged	Carbon	46.95	70.26
		Sulphur	53.05	29.74
	Un-aged	Carbon	76.63	89.75
		Sulphur	23.37	10.25
	RTFOT-aged	Carbon	66.41	84.07
B100/150-30%GSF		Sulphur	33.59	15.93
	PAV-aged	Carbon	77.75	90.32
		Sulphur	22.25	9.68
	Un-aged	Carbon	81.29	92.06
		Sulphur	18.71	7.94
	RTFOT-aged	Carbon	59.36	79.59
B100/150-40%GSF		Sulphur	40.64	20.41
	PAV-aged	Carbon	77.45	90.17
		Sulphur	22.55	9.83
	Un-aged	Carbon	66.79	84.30
		Sulphur	33.21	15.70
	RTFOT-aged	Carbon	50.87	73.44
B100/150-50%GSF		Sulphur	49.13	26.56
	PAV-aged	Carbon	61.88	81.25
		Sulphur	38.12	18.75

SEBs composed of B160/220 and variable amount of GSF;

Image analysis was used to study the morphology of extended B160/220 grade bitumen in order to characterize the nature of the continuous phase and the fineness of the dispersion of the discontinuous phase. It should be noted that, similar to previous pictures, also in these images all horizontal bars represent a length of 10 μm ; the light phase represents sulphur, while the dark phase represents bitumen.

Figure A.39 (o1-o3, r1-r3, and p1-p3) shows the original, short-term aged, and long-term aged micrographs of the 10%GSF content SEB. Prior to aging, the white sulphur particles finely dissolved in the dark bitumen, indicating that the 10%GSF easily dispersed in the bitumen. Following RTFOT, "jellyfish-like" sulphur aggregations appeared on the surface. By zooming in, this filamentous sulphur network structure can be easily seen. The amount of this jelly-fish like surface aggregation increased after prolonged PAV aging.

The morphological views for unaged, short- and long-term aged stage 20%GSF replacement are given in Figure A.41 (o1-o3, r1-r3, and p1-p3). This picture remained content with an increase in GSF content and the sulphur particles continued to dissolve uniformly in bitumen matrix. However, dissimilar to the 10%GSF, here only a handful of crystalline structures were detected on the surface. Following short-term aging, the sulphur particles increased in size from approximately 0.01 μm to 10 μm , suggesting that sulphur promotes a noticeable irregular surface.

The texture of a road surface is determined by both macro and micro scales. In terms of macro scale road-hold, when the road surface is wet the water in the contact area between the tire and the road surface has to be quickly removed, especially at higher vehicle speeds. The macro texture is dominantly determined by the size of the aggregate particles at the road surface. On the other hand, the micro texture is determined by the roughness and angularity of the surface of the aggregate particles. The micro texture ensures the removal of the last traces of water from those locations where high contact pressures between the aggregate and the tire are present. Based on the image analysis, at this stage the groundbreaking challenge that needs to be addressed will be the possibility that 20%GSF replacement may contribute to the kinds of road surface textures that are important for road-hold. However, it should be noted that this approach should be both logical and only based on those images obtained in this study; hence there is more to do on this aspect.

Long-term aging led to a detection of uniform dissolution of fine sulphur particles. When the GSF proportion was increased to 30%, very small sulphur globules continued to dissolve uniformly in bitumen matrix, as shown in Figure A.43 (o1-o3). This fairly homogenous dispersion of GSF was assumed to be the primary reason why the 30%GSF content SEB showed a large increase in the complex modulus, indicating a favorable resistance to rutting. This outcome allows us to unquestionably claim that an amount of 30%GSF is an appropriate replacement for B160/220 grade bitumen in terms of both morphology and rheology. The influence of aging on the same SEB is given in Figure A.43 (r1-r3 and p1-p3). From the images, it is clear that short-term aging leads to a superficial gel formation. Then, the long-term PAV simulated aging led to a tendency for the same SEB to convert this superficial gel formation to a crystalline structure.

Results from SEM pictures (Figure A.45 (o1-o3, r1-r3, and p1-p3)) illustrate that an increase of the GSF content up to 40% promoted a variety of morphology. At the unaged stage, the consequences of the multiphase nature sulphur particles are their heterogeneous dispersion in size, leading to a probable instability and their tendency to microscopically and/or macroscopically separate under the circumstance of particularly at high temperatures and in the absence of stirring. Moreover, once the aforementioned SEB is subjected to RTFOT aging, the huge, nearly 50 μ m sulphur particles begin to aggregate superficially. Any further aging would pave the way of these particles to considerably dominate the upper surface.

Compared with 40%GSF, the 50%GSF replacement did not result in any remarkable morphological differentiation at the unaged, and both RTFOT and PAV aged stages, as shown in Figure A.47 (o1-o3), (r1-r3), and (p1-p3).

To conclude, independent of aging, among the SEBs with different GSF amounts, a 30%GSF replacement was found to significantly develop a favorable compatibility with the neat B160/220 when morphological approach is taken into consideration. Finally, according to the spectrum processing, each sample was analyzed to evaluate the volumes of carbon (C) and sulphur (S) elements present in terms of both weight and atomic percentages (Figure A.38, Figure A.40, Figure A.42, Figure A.44, Figure A.46, and Figure A.48). The obtained values are summarized in Table 6.102.

Table 6.102 : Element analyses for the series of B160/220 before and after aging.

Sample	Stage	Element	Weight (%)	Atomic (%)
B160/220-0%GSF	Un-aged	Carbon	100	100
		Sulphur	-	-
	RTFOT-aged	Carbon	100	100
		Sulphur	-	-
	PAV-aged	Carbon	100	100
		Sulphur	-	-
	Un-aged	Carbon	92.06	96.87
		Sulphur	7.94	3.13
	RTFOT-aged	Carbon	68.23	85.15
B160/220-10%GSF		Sulphur	31.77	14.85
	PAV-aged	Carbon	90.15	96.07
		Sulphur	9.85	3.93
	Un-aged	Carbon	79.13	91.01
		Sulphur	20.87	8.99
	RTFOT-aged	Carbon	61.88	81.25
B160/220-20%GSF		Sulphur	38.12	18.75
	PAV-aged	Carbon	46.95	70.26
		Sulphur	53.05	29.74
	Un-aged	Carbon	76.63	89.75
		Sulphur	23.37	10.25
	RTFOT-aged	Carbon	66.41	84.07
B160/220-30%GSF		Sulphur	33.59	15.93
	PAV-aged	Carbon	77.75	90.32
		Sulphur	22.25	9.68
	Un-aged	Carbon	81.29	92.06
		Sulphur	18.71	7.94
	RTFOT-aged	Carbon	59.36	79.59
B160/220-40%GSF		Sulphur	40.64	20.41
	PAV-aged	Carbon	77.45	90.17
		Sulphur	22.55	9.83
	Un-aged	Carbon	66.79	84.30
		Sulphur	33.21	15.70
	RTFOT-aged	Carbon	50.87	73.44
B160/220-50%GSF		Sulphur	49.13	26.56
	PAV-aged	Carbon	61.88	81.25
		Sulphur	38.12	18.75

7. COST ANALYSIS

Based on the NYSDOT Average Posted Prices (item 698.01 and 698.04), the unit cost of asphalt (performance graded binder) is 617 dollars per ton (New York State Department of Transportation, 2015). Currently, the price of sulphur in the US ranges from \$129 to \$136 per ton (U.S. Department of the Interior U.S. Geological Survey, 2015). Hence, at the time this thesis was completed (December, 2015), 30% and 40% sulphur replacement could result in a \$145 and \$194 price decrease per ton in the total binder cost respectively. Furthermore, owing to the decrease in viscosity grades, sulphur replacement in bituminous binder could facilitate a relatively lower range of both mixing and compaction temperatures. It is still too early to make certain definitive judgments, but if successful, SEB can be a stunning advantage particularly for non-oil and/or low-oil producing countries that have an abundant supply of sulphur.

8. CONCLUSIONS

From this study, the following conclusions were drawn on the basis of the obtained test results: the traditional test results revealed that a significant reduction in penetration and a great increase in the softening point were observed for each type of bitumen replaced with varying GSF proportions (except 10%) at both the un-aged and short-term aged stages. On the other hand, replacing the bitumen with a 10% GSF showed the lowest hardening effect expressed in terms of a softening point, penetration and viscosity. This scenario provides possible solutions to resolving the issues concerning finding a replacement material that is more resistance to cracking, especially at lower temperatures. Furthermore, considering especially their lower viscosity grades, any SEB with 10%GSF will present a favorable potential for future warm asphalt production.

Creep stiffness and rates were measured so as to determine in which way sulphur replacement affects the behavior of SEB at low temperatures. The obtained results demonstrated that sulphur amounts lower than 50% generally caused SEB to fulfill required thermal cracking performance standards at low temperatures. Varying GSF replacements enhanced the viscoelastic parameters of current binders. At low temperatures the 10%GSF utilization especially creates more viscous behavior (lower G^* and higher δ means more flexibility consistent with its hardness results) and is favored to resist cracking. On the other hand, 30 and/or 40%GSF replacements can bring more elastic behavior to the base bitumen particularly at high temperatures (higher G^* and lower δ hence more elasticity) and are very promising for resisting deformation. Morphological analysis was also in close approximation with both traditional and rheological results in terms of displaying the sulphur dispersion, dissolution and crystalline structure throughout the neat bitumen.

In addition to these preliminary findings, the second set of field experiments – as a further study – is planned to conduct for the observation of the performance under actual conditions. A-100-meter section of highway is planned to be paved with HMA

using the new binder (GSF substituted bitumen) and another 100 meter highway section is planned to be paved with BST with the new adhesive binder. Prior to actual construction, periodical drillings of sample cores at 3, 6, and 12 month intervals will be performed to observe performance of these pavement sections.

As the world marches into the 21st century, nearly all of its road pavements are still made from asphalt, a material made from oil. Eventually, all the nations of the world will begin to suffer from the domination of fossil fuels on their economies. It is imperative that we find an alternative and sustainable binder, or – at the very least – are able to replace a considerable proportion of the current material. The purpose of this study has been to conduct an in-depth and integrated study relative to potential sulphur replacement in bituminous binders. Although obtained conventional test results and rheological characteristics demonstrate encouraging potentials of sulphur-extended-binders, it should be noted that there is more to do on this subject, especially in terms of the topic's environmental aspects.

REFERENCES

- Al-Otaishan, A.T. and Terrel, R.L.** (1980). Material characteristics and predicted performance of sulphur-asphalt mixtures from in-service pavements, Proceedings of the Association of Asphalt Paving Technologists, pg: 252-265.
- Amsterdam, E.V.** (2008). Construction materials for civil engineering, 4th Edition, pg. 134-140.
- Anderson, D.A., Christensen, D.W., Bahia, H.U., Dongre, R., Sharma, M.G., Antle, C.E., and Button, J.** (1994). Binder characterization and evaluation. Vol. 3, Physical Characterization, Strategic Highway Research Program Report No. SHRP-A-369, National Research Council, Washington, D.C.
- Anderson, D., Youtcheff, J., and Zupanick, M.** (2000). Asphalt binders, TRB Committee on Characteristics of Bituminous Materials, TRB Millennium Paper Series.
- Asphalt Institute** (1998). Construction of hot mix asphalt pavements, Second Edition, Lexington, Kentucky.
- Asphalt Institute** (2001). Superpave mix design (SP-2), pp. 128.
- Asphalt Institute** (2003). Performance graded asphalt binder specification and testing, Superpave Series No. 1 (SP-1), 3rd Edition, Lexington, KY.
- Asphalt Institute** (2006). Laboratory mixing and compaction temperatures, Asphalt Institute Executive Offices and Research Center, Asphalt Institute Technical Bulletin, Lexington, KY, USA.
- Asphalt Institute** (2007). State of-knowledge on the use of sulfur-extended asphalt (SEA).
- ASTM** (2001). Standards, American Society for Testing and Materials.
- Awanti, S.S., Amarnath, M.S., and Veeraragavan, A.** (2008). Laboratory evaluation of SBS modified bituminous paving mix, Journal of Materials in Civil Engineering, doi: [http://dx.doi.org/10.1061/\(ASCE\)0899-1561\(2008\)20:4\(327\)](http://dx.doi.org/10.1061/(ASCE)0899-1561(2008)20:4(327)), Vol. 20, No. 4, pp. 327-330.

Bahia, H.U. and Anderson, D.A. (1994). The pressure ageing vessel (PAV): A test to simulate rheological changes due to field ageing. Physical Properties of Asphalt Cement Binders Conf., American Society for Testing and Materials, Dallas/Fort Worth Airport, Texas, 67-88.

Bahia, H.U. and Anderson, D.A. (1995a). Strategic highway research program binder rheological parameters: Background and comparison with conventional properties. Transportation Research Record 1488, TRB, National Research Council, Washington, DC, pp. 32-39.

Bahia, H.U. and Anderson, D.A. (1995b). The development of the bending beam rheometer; Basics and critical evaluation of the rheometer, Physical Properties of Asphalt Cement Binders: ASTM STP 1241, John C. Hardin, Ed., American Society for Testing and Materials, Philadelphia, PA., pp. 28-50.

Bahia, H.U., Hislop, W.P., and Zhai, H. (1998). Classification of asphalt binders into simple and complex binders. Association of Asphalt Paving Technologists (AAPT), Vol. 63.

Bahia, H.U., Hanson, D.I., Zeng, M., Zhai, H., Khatri, M.A., and Anderson, R.M. (2001). Characterisation of modified asphalt binders in Superpave mix design. National Cooperative Highway Research Program (NCHRP), Rep. No. 459, National Academy Press, Washington DC.

Bell, C.A. and Sosnovske, D. (1994). Ageing: Binder validation. SHRP report, Rep. No. SHRP-A-384, National Research Council, Washington DC.

Bencowitz, I. and Boe, E.S. (1938). The sulfur asphalt binder concept, American Society for Testing Materials, Proceeding, Vol. 38, No. 2, pp.539.

Blanco, R., Rodriguez, R., Garduno, M.G., and Castano, V.M. (1996). Rheological properties of styrene-butadiene copolymer reinforced asphalt. J. Appl. Polym. Sci., Volume 61, Issue 9, pp. 1493–1501.

Blażejowski, K., Olszacki, J., and Peciakowski, H. (2014). Bitumen handbook, Orlen Asfalt, pp 32.

Brennan, M.J. and O'Flaherty, C.A. (2002). Material used in road pavements, chapter 5 and chapter 6.

Chen, J.S. and Huang, C.C. (2007). Fundamental characterization of SBS-modified asphalt mixed with sulfur. Journal of Applied Polymer Science, 103(5), 2817-2825.

Chen, W.F. and Richard Liew, J.Y. (2002). The civil engineering handbook, Second edition, Chapter 45, Bituminous materials and mixtures, CRC Press, Print ISBN: 978-0-8493-0958-8, eBook ISBN: 978-1-4200-4121-7.

- COST 333** (1999). Bituminous materials and hydraulically bound materials. Development of New Bituminous Pavement Design Method, European commission, Brussels, Belgium, pp. 115-172.
- Courval, G.J., and Akili, W.A.D.D.A.H.** (1982). Sulfur asphalt binder properties by the sliding plate rheometer. Asphalt Paving Technol, 51, 222.
- Cremllyn, R.J.** (1996). An introduction to organosulfur chemistry. John Wiley and Sons Ltd. Chichester, United Kingdom, ISBN: 0471955124.
- Deniz, M.T.** (2009). The usage of granular sulphur with bitumen as a binder and its effect on the permanent deformations, PhD Thesis, ITU, Istanbul.
- Devlet Planlama Teşkilatı (DPT),** (2001). Fosfat-Kükürt-Alunit, Sekizinci Beş Yıllık Kalkınma Planı, Madencilik Özel İhtisas Komisyonu Raporu, Cilt I, Ankara.
- Diew, W.Y.** (2001a). Penetration of bituminous materials. School of Civil and Structural Engineering, Nanyang Technological University.
- Diew, W.Y.** (2001b). Pavement materials. School of Civil and Structural Engineering, Nanyang Technological University.
- Domke, C.H., Liu, M., Davison, R.R., Bullin, J.A., and Glover, C.J.** (1997). Study of Strategic Highway Research Program pressure ageing vessel procedure using low-temperature ageing experiments and asphalt kinetics. Transportation Research Record, (no. 1586), pp. 10-15.
- Edwards, Y. and Redelius, P.** (2003). Rheological effects of waxes in bitumen. Energy Fuels, 17(3), pp.511-20, doi: 10.1021/ef020202b
- Edwards, Y., Tasdemir, Y., and Isacsson, U.** (2006). Rheological effects of commercial waxes and polyphosphoric acid in bitumen 160/220-high and medium temperature performance, Journal of Construction and Building Materials, doi:10.1016/j.conbuildmat.2006.07.012, 21(10) pp. 1899–1908.
- Elseifi, M.A., Flintsch, G.W., and Al-Qadi, I.L.** (2003). Quantitative effect of elastomeric modification on binder performance at intermediate and high temperatures. Journal of Materials in Civil Engineering, Vol.15, No.1 pp.32-40, doi: [http://dx.doi.org/10.1061/\(ASCE\)0899-1561\(2003\)15:1\(32\)](http://dx.doi.org/10.1061/(ASCE)0899-1561(2003)15:1(32))
- Er, T.**, (2003). Asfalt kaplamalarda sülfür kullanımı, Yüksek Lisans Tezi, İstanbul Teknik Üniversitesi, Fen Bilimleri Enstitüsü, İstanbul.
- Exxon** (1997). Shift study of pulmonary function and symptoms in workers exposed to asphalt fumes. Final report submitted to Asphalt Industry Oversight Committee. East Millstone, NJ, Exxon Biomedical Sciences, Inc. Report No: 97TP31.

Fairbrother, F., et al. (1955). Journal of Polymer Science, Vol. 14, pp. 4599.

Fu, H., Xie, L., Dou, D., Li, L., Yu, M., and Yao, S. (2007). Storage stability and compatibility of asphalt binder modified by SBS graft copolymer, Journal of Construction and Building Materials, 21(7), pp. 1528-1533.

Fwa, T. F. (2005). The Handbook of Highway Engineering, CRC Press, Chapter 7, Highway Materials, p.7.10.

Gardner, D.M. and Frankel, G.K. (1956). J. Am. Chem. Soc., 78, 3279.

Ghosh, P., Katare, S., Patkar, P., Caruthers, J.M., Venkatasubramanian, V., and Walker, K.A. (2003). Sulfur vulcanization of natural rubber for benzothiazole accelerated formulations: From reaction mechanisms to a rational kinetic model. Rubber Chemistry and Technology, 76(3), pp.592-693.

Gordon, D.A. (2003a). State of the art report on ageing test methods for bituminous pavement materials. International Journal of Pavement Engineering, 4(3), pp. 165-176.

Gordon, D.A. (2003b). Rheological properties of styrene butadiene styrene polymer modified road bitumens. Journal of Fuel, 82(14), pp. 1709-1719.

Griffin, R.L., Miles, T.K., and Penther, C.J. (1955). Microfilm durability test for asphalt. Proceedings of the Association of Asphalt Paving Technologists 24, 31.

Hagos, E.T. (2008). The effect of ageing on binder properties of porous asphalt concrete. Master of Science in Transport and Road Engineering, Delft University of Technology, Netherland.

Heukelom, W. (1973). Improved nomographs for bitumen, Shell Bitumen Review, 43, pp. 8-9.

Huang, S.C. (2008). Rubber concentrations on rheology of aged asphalts binders. Journal of Materials in Civil Engineering, 10.1061/(ASCE)0899-1561(2008)20:3(221).

Huang, S.C., Miknis, F.P., Schuster, W., Salmans, S., Farrar, M., and Boysen, R. (2011). Rheological and chemical properties of hydrated lime and polyphosphoric acid-modified asphalts with long-term aging. Journal of Materials in Civil Engineering, Vol. 23, No. 5, pg: 628-637. doi: [http://dx.doi.org/10.1061/\(ASCE\)MT.1943-5533.0000219](http://dx.doi.org/10.1061/(ASCE)MT.1943-5533.0000219)

Illston, J.M. and Domone, L.J. (2001). Construction Materials, Their Nature and Behaviour, Third Edition, Spon Press, Taylor&Francis Group, London and New York.

- Imants, D.** (1977). Sulfur as an asphalt diluent and a mix filler, Advances in Chemistry Series, No. 165, New Uses of Sulfur, American Chemical Society.
- Isaccson, U. and Lu, X.** (1999). Laboratory investigation of polymer modified bitumen. Association of Asphalt Paving Technologists (AAPT), Vol. 68, pp. 35-63.
- Ishai, I., Brule, B., Vaniscote, J.C., and Ramond, G.** (1988). Some rheological and physio-chemical aspects of long term asphalt durability. Association of Asphalt Paving Technologists (AAPT), Vol. 57, Viking Press Inc.
- Ishai, I. and Yuval, R.** (2002). Reformulation of asphalt cements for paving, Journal of Transportation Engineering, 10.1061/(ASCE)0733-947X(2002)128:2(111), Vol. 128, No. 2, pp. 111-122.
- Jian-Shiu Chen, P.E., Min-Chih Liao, and Ming-Shen Shiah** (2002). Asphalt modified by styrene-butadiene-styrene triblock copolymer: Morphology and model. Journal of Materials in Civil Engineering, doi: [http://dx.doi.org/10.1061/\(ASCE\)0899-1561\(2002\)14:3\(224\)](http://dx.doi.org/10.1061/(ASCE)0899-1561(2002)14:3(224)), 14(3), pp. 224-229.
- Jimenez, R.A. and Stokes, K.J.** (1981). Effects of heat and air on the viscosity of sulfur-asphalt mixtures. Proceedings Association of Asphalt Paving Technologists, Vol.50, pp. 467-479.
- Kennedy, T.W., Haas, R., Smith, P., Kennepohl, G.A., Hignell, E.T.** (1977). Engineering evaluation of sulphur-asphalt mixtures. Transportation Research Board Research Record, Issue Number: 659, ISSN: 0361-1981, pp 12-17.
- Kennedy, T.W., Huber, G.A., Harrigan, E.T., Cominsky, R.J., Hughes, C.S., Von Quintus, H., and Moulthrop, J.S.** (1994). Superior performing asphalt pavements (Superpave): The Product of the SHRP Asphalt Research Program. Report SHRP A-410, Strategic Highway Research Program, Washington, D.C.
- Kennepohl, G.J.A., Logan, A., and Bean, D.C.** (1974). Sulphur-asphalt binders in paving mixes, Canadian Sulphur Symposium, Calgary, Alberta.
- Kennepohl, G.J.A., Logan, A., and Bean, D.C.** (1975). Conventional paving mixes with sulphur-asphalt binders, Proceedings Association of Asphalt Paving Technologists, Vol.44, pp. 485-505.
- Kennepohl, G.J.A. and Miller, L.J.** (1978). Sulphur asphalt binder technology for pavements. American Chemical Society, Washington, D.C.
- Kett, I.** (1998). Asphalt materials and mix design manual, William Andrew Publisher, pp. 54-55

- Kumar, P., Mehndiratta, H., and Singh, K.** (2010). Comparative Study of Rheological Behavior of Modified Binders for High-Temperature Areas. *Journal of Materials in Civil Engineering*, 10.1061/(ASCE)MT.1943-5533.0000099, 22(10), pp. 978-984.
- Kutney, G.** (2007). Sulfur: history, technology, applications & industry. Toronto: ChemTec Publications. ISBN 978-1-895198-37-9.OCLC 79256100, p. 43.
- Lepe, A.P., Boza, F.M., Gallegos, C., González, O., Muñoz, M.E., and Santamaría, A.** (2003). Influence of the processing conditions on the rheological behaviour of polymer-modified bitumen. *Fuel*, Vol. 82, pp. 1339-1348.
- Lesueur, D., Gerard, J.F., Claudy, P., Letoffe, J.M., Martin, D., and Planche, J.P.** (1998). Polymer modified asphalts as viscoelastic emulsions. *Journal of Rheology*, 42(5), pp. 1059–1074.
- Lu, X. and Isacsson, U.** (1997). Rheological characterization of styrene-butadiene-styrene copolymer modified bitumens. *Journal of Construction and Building Materials*, 11(1), 23-32.
- Lu, X. and Isacsson, U.** (1998). Chemical and rheological evaluation of ageing properties of SBS polymer modified bitumen. *Fuel*, 77(9–10), 961–972.
- Lubbers, H.E.** (1985). Bitumen in de weg-en waterbouw. Nederlands Adviesbureau voor bitumentoppassingen.
- Lytton, R.L., Saylak, D., and Pickett, D.E.** (1977). Predictions of sulphur-asphalt pavement performance with VESYS IIM. Proceedings of the Fourth International Conference on Structural Design of Asphalt Pavements, University of Michigan, Ann Arbor, Michigan.
- Lytton, R.L., Uzan, J., Fernando, E.G., Rougue, R., Hiltunen, D., and Stoffels, S.M.** (1994). Development and validation of performance prediction models and specifications for asphalt binder and paving mixes. SHRP-A-357, Nat. Res. Council, Washington, D.C.
- Maccarrone, S., Holleran, G., and Gnanseelan, G.P.** (1995). Properties of polymer modified binders and relationship to mix and pavement performance. *Journal of the Association of Asphalt Paving Technologists*, Vol. 64, pp. 209–240.
- Maden Tetkik ve Arama Enstitüsü** (1984). Türkiye küktür envanteri, Maden Tetkik ve Arama Enstitüsü Yayınlarından, No: 190, Ankara.

- Marasteanu, M.O. and Clyne, T.R.** (2006). Rheological characterization of asphalt emulsions residues, *Journal of Materials in Civil Engineering*, Vol. 18, No. 3, pp. 398-407, doi: [http://dx.doi.org/10.1061/\(ASCE\)0899-1561\(2006\)18:3\(398\)](http://dx.doi.org/10.1061/(ASCE)0899-1561(2006)18:3(398)).
- Mastrofini, D. and Scarsella, M.** (2000). The application of rheology to the evaluation of bitumen ageing. *Journal of Fuel*, Vol. 79, pp. 1005-1015
- Mathew, T.V. and Rao, K.V.K.** (2006). Introduction to transportation engineering, Chapter 23, Pavement Materials: Bitumen.
- McBee, W.C., Sullivan, T.A., and Izatt, J.O.** (1980). State-of-the-art guideline manual for design, quality control, and construction of sulfur-extended asphalt (SEA) pavements. FHWA-IP-80-14, Implementation Package, Prepared by US Department of Interior Bureau of Mines with The Sulphur Institute.
- Mes, B.** (2003). Ontrafeling van verouderingseigenschappen van bitumen in ZOAB (in Dutch). MSc thesis, Rijkswaterstaat, Road and Hydraulic Engineering Institute (DWW).
- Meyers, M.A. and Chawla, K.K.** (1999). Mechanical behavior of materials. New Jersey, USA:Prentice-Hall, pp. 98-103.
- Michler, G.H.** (1996). Electron microscopic investigations of morphology and structure formation of polymers. *Journal of Macromolecular Science*, B35, pp. 329–355.
- Murphy, M., O'Mahony, M., Lycett, C., and Jamieson, I.** (2001). Recycled polymers for use as bitumen modifiers, *Journal of Materials in Civil Engineering*, 13(4), pp.306-314.
- Nehb, W. and Vydra, K.** (2006). Sulfur, Ullmann's Encyclopedia of Industrial Chemistry, doi: 10.1002/14356007.a25_507.pub2
- New York State Department of Transportation.** (2015).
<https://www.dot.ny.gov/main/business-center/contractors/construction-division/fuel-asphalt-steel-price-adjustments>
- Oliver, J.W.H. and Tredrea, P.F.** (1997). The change in properties of polymer modified binders with simulated field exposure. Association of Asphalt Paving Technologists (AAPT), Vol. 66.
- Özgüner, A.M.** (2005). Sulphur, Maden Tetkik ve Arama Genel Müdürlüğü Yayınlarından, Ankara.
- Parmeggiani, G.** (2000). Nitrogen rolling thin film oven test laboratory testing proposals. Euroasphalt and Eurobitume Congress, Barcelona.

Pavement Interactive (2012).

http://training.ce.washington.edu/pgi/Modules/03_materials/033_body.htm#penetration_grading

Pavement Interactive (2013).

<http://www.pavementinteractive.org>

Peralta, J., Williams, R.C., Rover, M., and Silva, H.M.R.D.D. (2012). Development of a rubber-modified fractionated bio-oil for use as noncrude petroleum binder in flexible pavements. Transportation Research Circular E-C165: Alternative Binders.

Petersen, J.C., Robertson, R.E., Branthaver, J.F., Harnsberger, P.M., Duvall, J.J., Kim, S.S., Anderson, D.A., Christensen, D.W., Bahia, H.U., Dongre, R., Antle, C.E., and Sharma, M.G. (1994). Binder characterization and evaluation; Volume 4, Test Methods, Strategic Highway Research Program Report No. SHRP-A-370, National Research Council, Washington, D.C.

Peterson, J.C. (2000). Chemical composition of asphalt as related to asphalt durability. Included in series Asphaltenes and Asphalts, 2. Developments in Petroleum Science, 40B. Elsevier, USA.

Petrossi, U., Bocca, P.L., and Pacor, P. (1972). Reactions and technological properties of sulfur-treated asphalt. Ind. Eng. Chem. Prod. Res. Dev., 11:214.

Pfeiffer, J.P.H. and Van Doormal P.M. (1936). The rheological properties of asphaltic bitumens. *J. Instn Petrol. Tech.*, 22(152), 414-440.

Ramadhan, R.H., Al-Abdul Wahhab, H.I., Asi, I.M., and Al-Dubabe, I.A. (1998). Evaluation of Arabian asphalt binder for low-temperature cracking, *Journal of Materials in Civil Engineering*, Vol. 10, No. 1, pp. 26-33.

Ramaiah, S., D'Angelo, J., and Dongre, R. (2004). Evaluation of modified german rotating flask. *Transportation Research Record*, (1875), pp. 80-88.

Read, J. and Whiteoak, D. (2003). The Shell Bitumen Handbook, 5th Edition, Shell Bitumen, Surrey, UK.

Rennie, W.J. (1979). Sulphur asphalts, New uses for sulphur technology Series No. 2, Sulphur Development Institute of Canada, p. 1-13.

Roberts, F.L., Kandhal, P.S., Brown, E.R., Lee, D.Y., and Kennedy, T.W. (1996). Hot mix asphalt materials, mixture design and construction, second edition, NAPA Research and Education Foundation, Lanham, MD.

- Ruan, Y., Davison, R.R., and Glover, C.J.** (2003). The effect of long-term oxidation on the rheological properties of polymer modified asphalts, *Fuel*, 82(14), pp.1763-1773.
- SAIMM** (2015). 5th Sulphur and sulphuric acid 2015 conference, The Southern African Institute of Mining and Metallurgy, Southern Sun Elangeni Maharani, KwaZulu-Natal, South Africa.
- Shalaby, A.** (2001). Modelling short-term ageing of asphalt binders using the rolling thin film oven test, *Canadian Journal of Civil Engineering* 29 (1), pp.135-144.
- Shui, H.F., et al.** (1998). Study on the ageing kinetics of paving asphalt. *J. East China University of Sci. Technol.* 24(4), pp.399.
- Sirin, O., Shih, C.T., Tia, M., and Ruth, B.E.** (1998). Development of a modified rotavapor apparatus and method for short-term ageing of modified asphalts. *Transportation Research Record* 1638, pp.72–84, Washington, D.C.
- Stevenson, F.J.** (1986). Cycles in soil carbon, nitrogen, phosphorus, sulfur, micronutrients. John Wiley & Sons, New York.
- Strickland, D., Colange, J., Shaw, P., and Pugh, N.** (2008). A study of the low-temperature properties of sulphur extended asphalt mixtures, Canadian Technical Asphalt Association.
- Sulphur Institute** (2011). An introduction to sulphur.
<http://www.sulphurinstitute.org/learnmore/sulphur101.cfm>
- Şener, F. and Özgüner, A.** (2000). Kimya sanayi hammaddeleri (Kükürt), Sekizinci Beş Yıllık Kalkınma Planı, DPT, ISBN 975 – 19 – 2822 – 2, Ankara.
- Taha, R., Ali, G., and Delwar, M.** (1998). Evaluation of coke-dust modified asphalt using Superpave, *Journal of Materials in Civil Engineering*, doi: [http://dx.doi.org/10.1061/\(ASCE\)0899-1561\(1998\)10:3\(174\)](http://dx.doi.org/10.1061/(ASCE)0899-1561(1998)10:3(174)), Vol. 10, No. 3, pp. 174-179.
- Texas Gulf Sulphur Company** (1957). Modern sulphur mining, pp. 21.
- Trudinger, P.A.** (1975). The biogeochemistry of sulphur. In: K.D. McLachlan (Ed.), Sulphur in Australian Agriculture. Sydney Univ. Press, Sydney. pp. 11-20.
- University of Washington** (2010). 7 Flexible pavement distresses.
- U.S. Department of the Interior, U.S. Geological Survey.** (2015). Mineral Commodity Summaries 2015, pg. 157.

Verhasselt, A.F. (2002). Long term ageing-simulation by RCAT ageing test. International Conference on Asphalt Pavements (ICAP). Copenhagen, Denmark.

Whorlow, R.W. (1980). Rheological techniques, Chichester, West Sussex, England: Ellis Horwood Ltd.

Wikipedia (2014). The free encyclopedia, <https://www.wikipedia.org/>

Wu, S., Mo, L., Cong, P., Yu, J., and Luo, X. (2007). Flammability and rheological behavior of mixed flame retardant modified asphalt binders. *Fuel*, 87(1), pp. 120-124, doi: 10.1016/j.fuel.2007.03.039

Yayla, N. (2002). Karayolu mühendisliği, Birsen Yayınevi, p. 2-8

Zaniewski, J.P. and Pumphrey, M.E. (2004). Evaluation of performance graded asphalt binder equipment and testing protocol. Asphalt Technology Program, Department of Civil and Environmental Engineering, Morgantown, West Virginia.

Zhang, F., Yu, J., and Wu, S. (2010). Effect of ageing on rheological properties of storage-stable SBS/sulphur-modified asphalts. *Journal of Hazardous Materials*, 182(1-3), 507-517.

Zhao, F.J., Wu, J., and McGrath, S.P. (1996). Humic Substances in Terrestrial Ecosystems Chapter 12—Soil Organic Sulphur and its Turnover, Elsevier Science, doi:10.1016/B978-044481516-3/50013-X, pp. 467-506.

APPENDICES

APPENDIX A: SEM Images

APPENDIX A

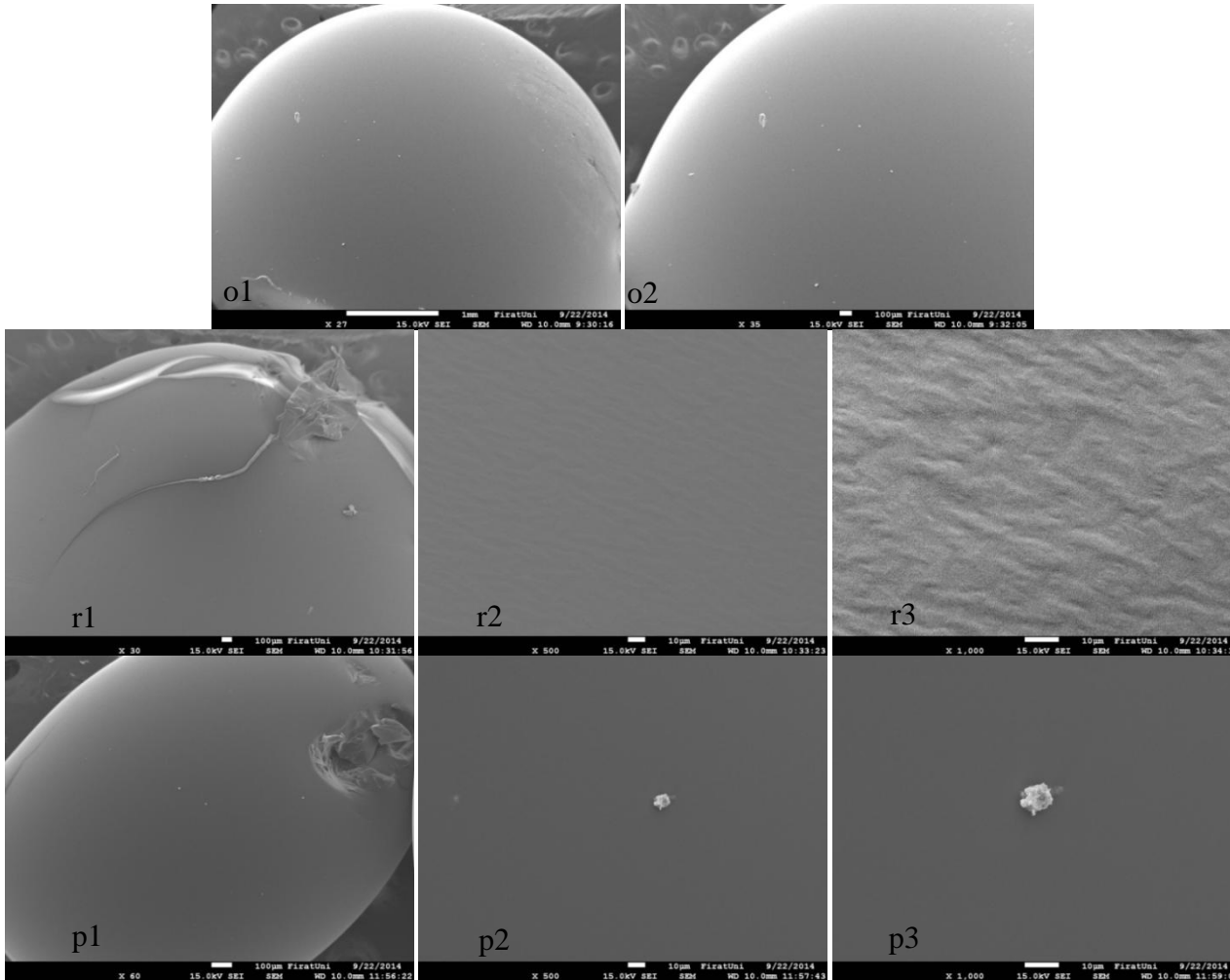


Figure A.1 : Showing images of B50/70-0%GSF (o1 and o2 at the un-aged stage, r1, r2 and r3 at the RTFOT-aged stage and p1, p2 and p3 at the PAV-aged stage).

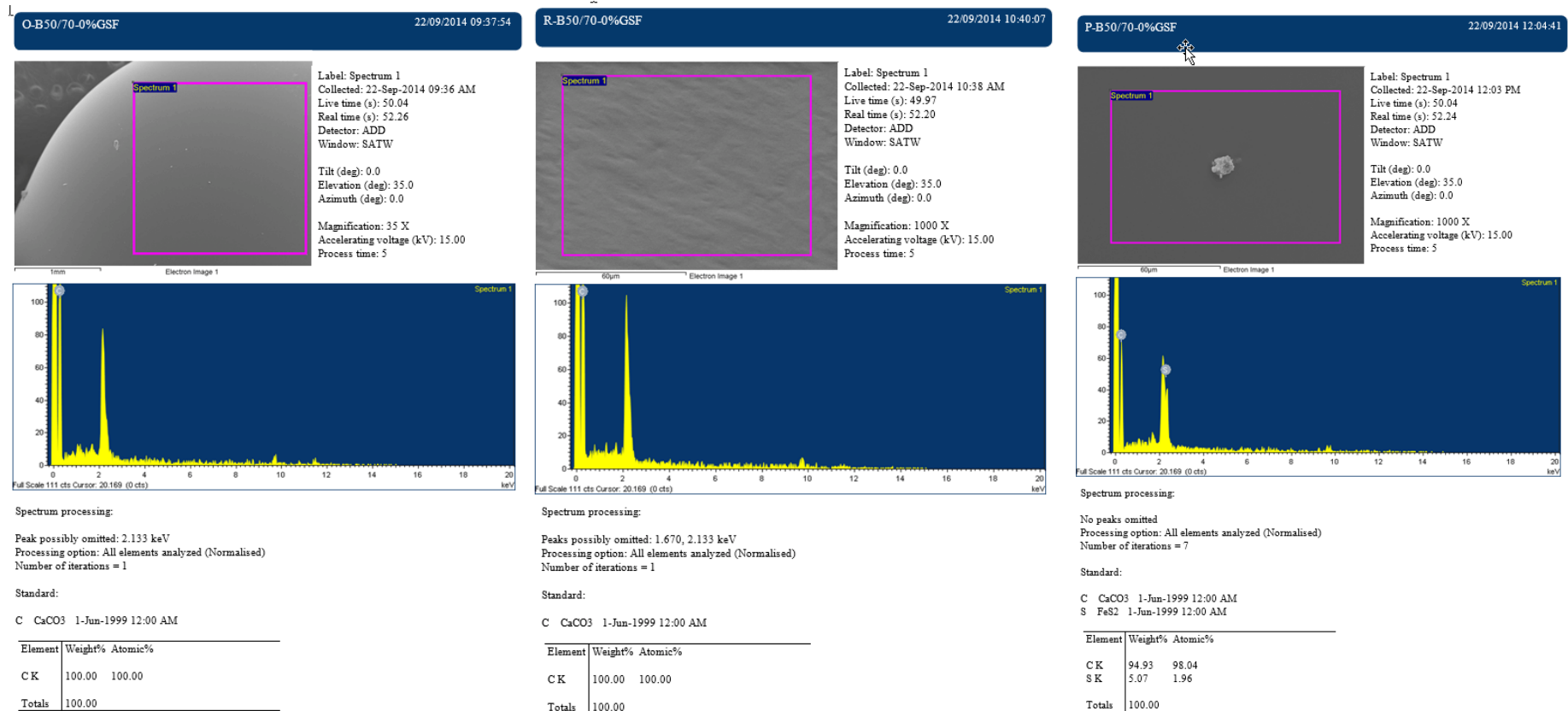


Figure A.2 : Showing element analysis of B50/70-0%GSF.

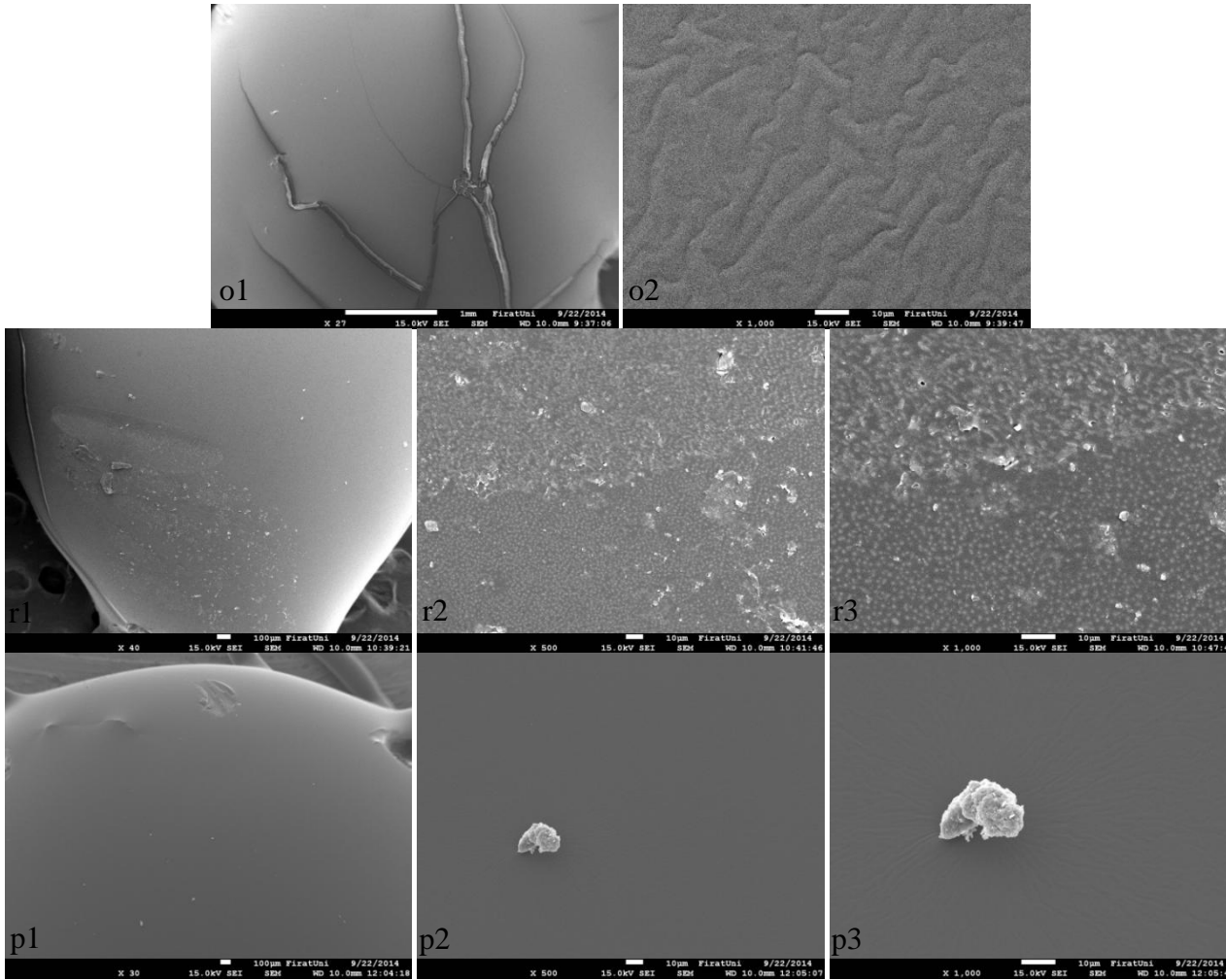
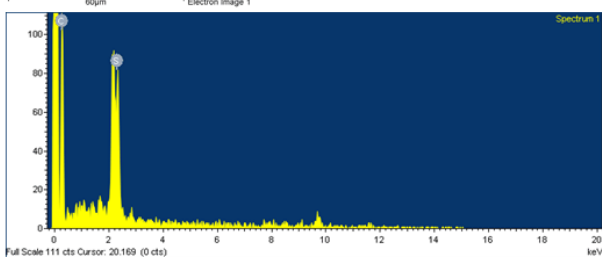
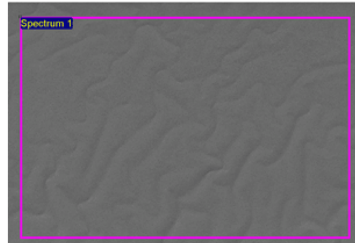


Figure A.3 : Showing images of B50/70-10%GSF (o1 and o2 at the un-aged stage, r1, r2 and r3 at the RTFOT-aged stage and p1, p2 and p3 at the PAV-aged stage).

O-B50/70-10%GSF 22/09/2014 09:45:12



Spectrum processing:

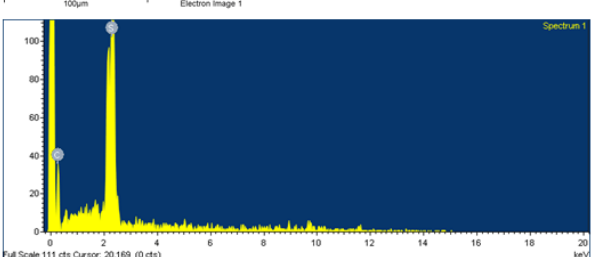
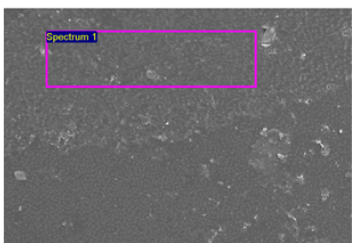
No peaks omitted
Processing option: All elements analyzed (Normalised)
Number of iterations = 11

Standard:

C CaCO₃ 1-Jun-1999 12:00 AM
S FeS₂ 1-Jun-1999 12:00 AM

Element	Weight%	Atomic%
CK	91.09	96.47
SK	8.91	3.53
Totals	100.00	

R-B50/70-10%GSF 22/09/2014 10:49:03



Spectrum processing:

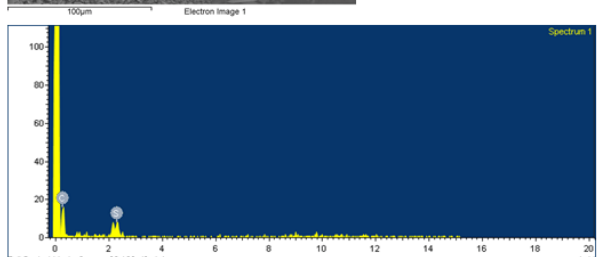
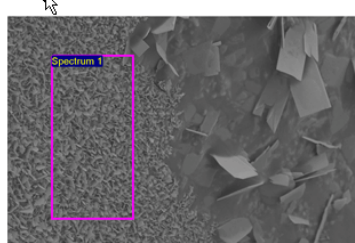
No peaks omitted
Processing option: All elements analyzed (Normalised)
Number of iterations = 8

Standard:

C CaCO₃ 1-Jun-1999 12:00 AM
S FeS₂ 1-Jun-1999 12:00 AM

Element	Weight%	Atomic%
CK	72.98	87.82
SK	27.02	12.18
Totals	100.00	

P-B50/70-10%GSF 22/09/2014 10:24:48



Spectrum processing:

No peaks omitted
Processing option: All elements analyzed (Normalised)
Number of iterations = 6

Standard:

C CaCO₃ 1-Jun-1999 12:00 AM
S FeS₂ 1-Jun-1999 12:00 AM

Element	Weight%	Atomic%
CK	94.39	97.82
SK	5.61	2.18
Totals	100.00	

Figure A.4 : Showing element analysis of B50/70-10%GSF.

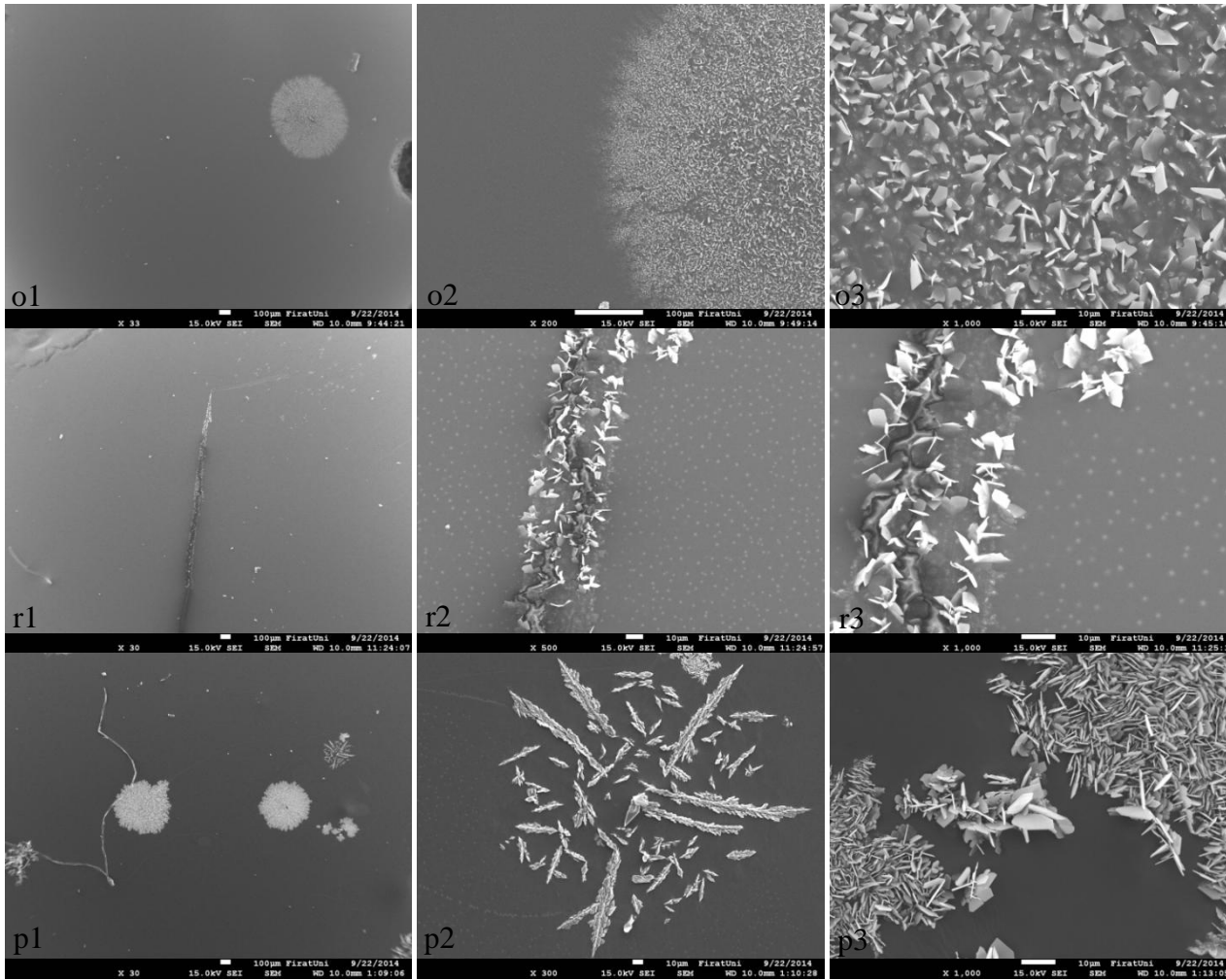


Figure A.5 : Showing images of B50/70-20% GSF (o1, o2 and o3 at the un-aged stage, r1, r2 and r3 at the RTFOT-aged stage and p1, p2 and p3 at the PAV-aged stage).

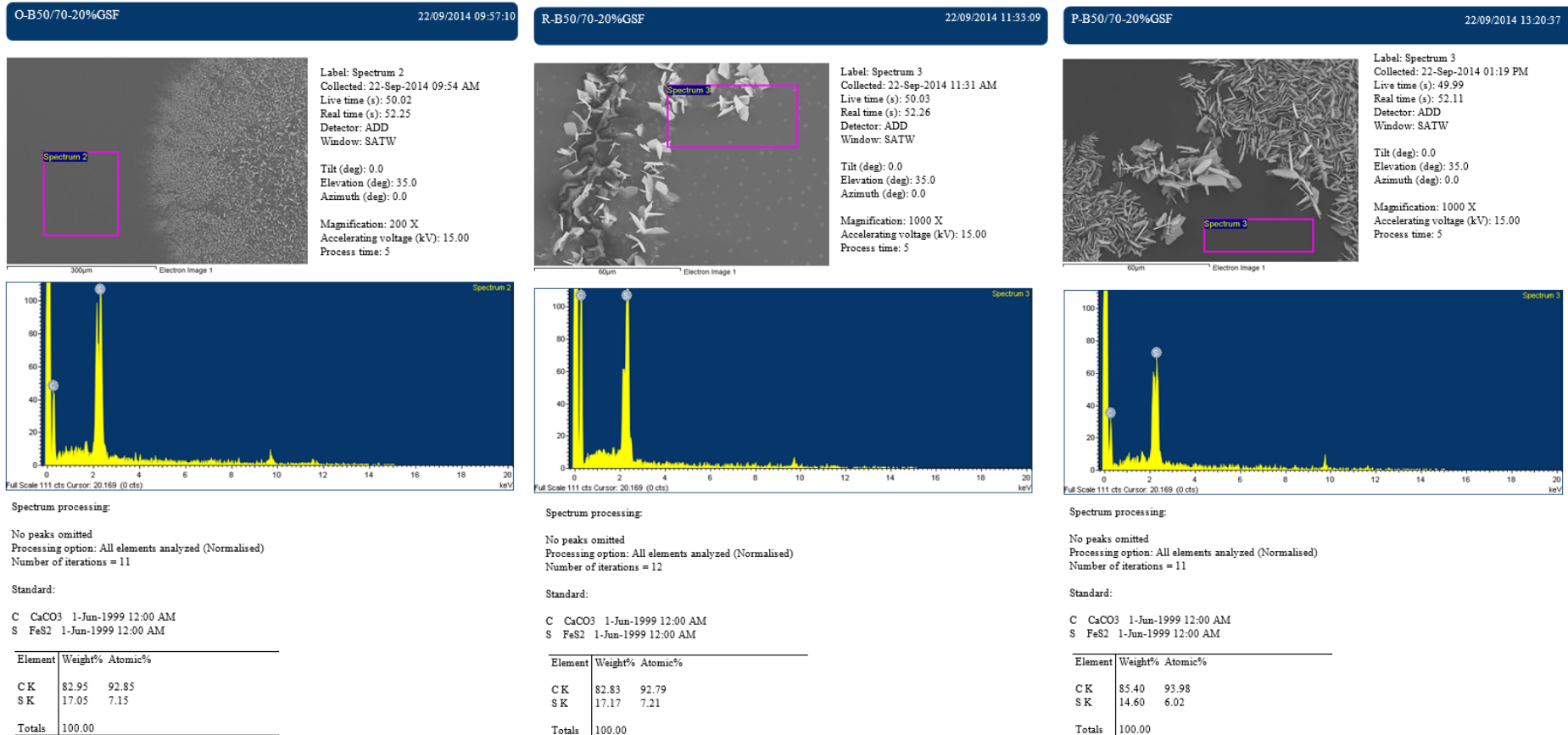


Figure A.6 : Showing element analysis of B50/70-20%GSF.

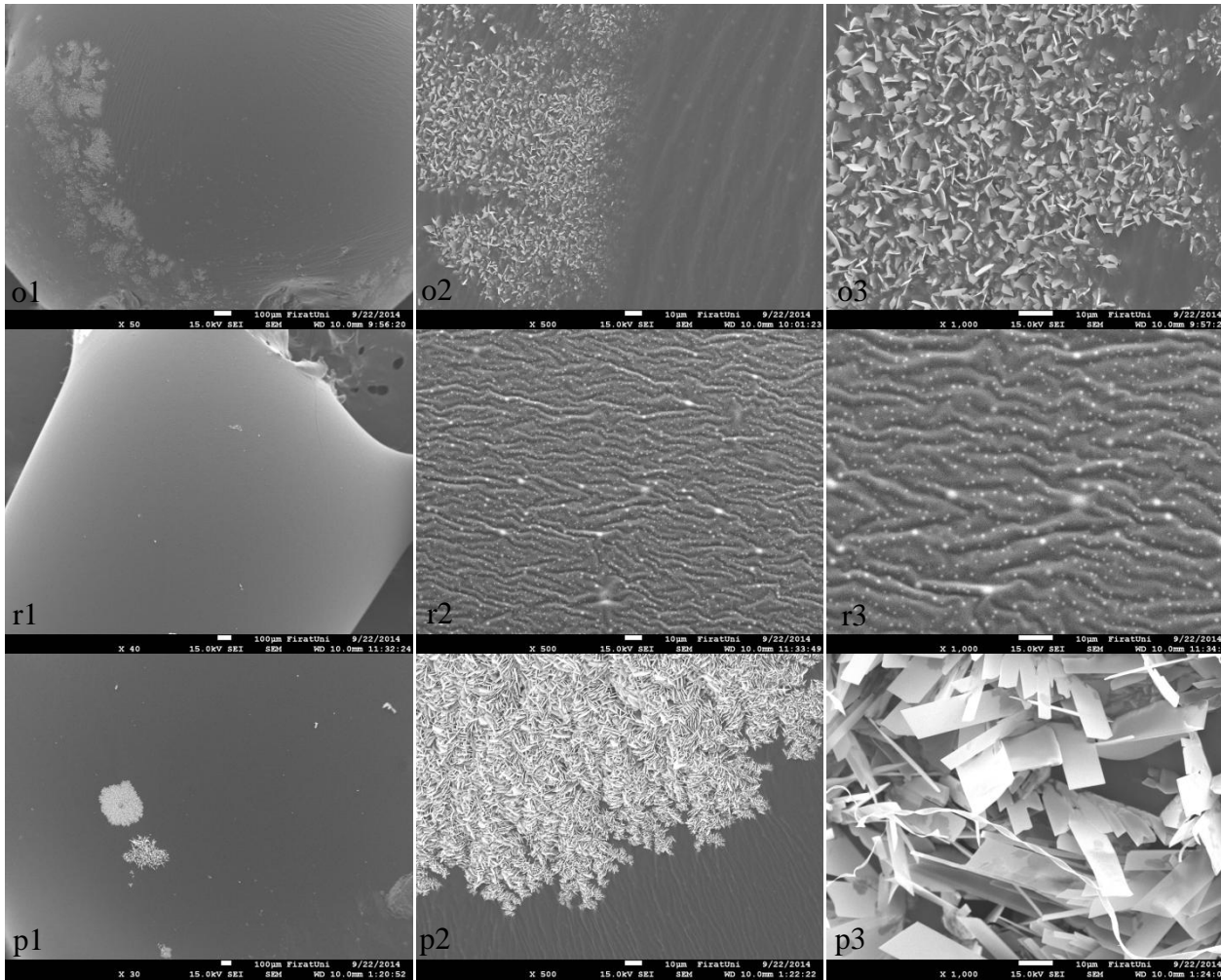
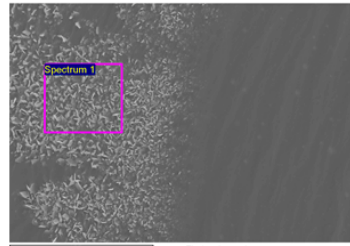


Figure A.7 : Showing images of B50/70-30% GSF (o1, o2 and o3 at the un-aged stage, r1, r2 and r3 at the RTFOT-aged stage and p1, p2 and p3 at the PAV-aged stage).

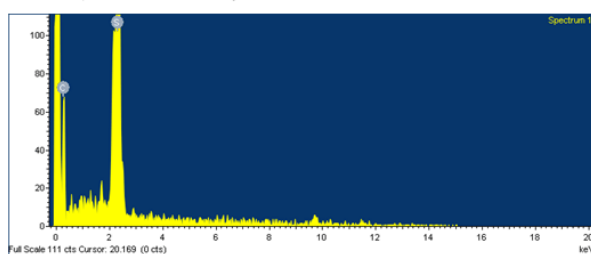
O-B20/70-30%GSF 22/09/2014 10:08:51



Label: Spectrum 1
Collected: 22-Sep-2014 10:05 AM
Live time (s): 50.02
Real time (s): 52.23
Detector: ADD
Window: SATW

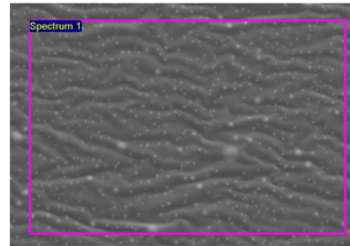
Tilt (deg): 0.0
Elevation (deg): 35.0
Azimuth (deg): 0.0

Magnification: 500 X
Accelerating voltage (kV): 15.00
Process time: 5



Element	Weight%	Atomic%
C K	70.68	86.55
S K	29.32	13.45
Totals	100.00	

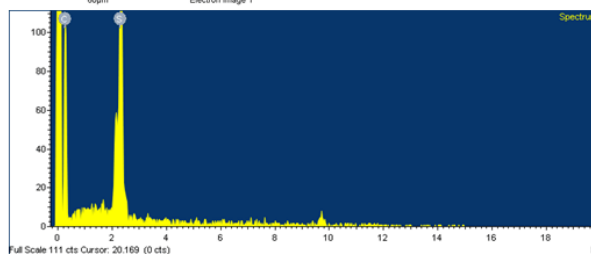
R-B50/70-30%GSF 22/09/2014 11:39:52



Label: Spectrum 1
Collected: 22-Sep-2014 11:38 AM
Live time (s): 50.03
Real time (s): 52.35
Detector: ADD
Window: SATW

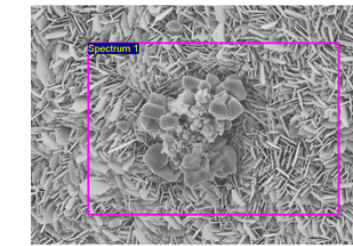
Tilt (deg): 0.0
Elevation (deg): 35.0
Azimuth (deg): 0.0

Magnification: 1000 X
Accelerating voltage (kV): 15.00
Process time: 5



Element	Weight%	Atomic%
C CaCO ₃	1-Jun-1999 12:00 AM	
S FeS ₂	1-Jun-1999 12:00 AM	
Totals	100.00	

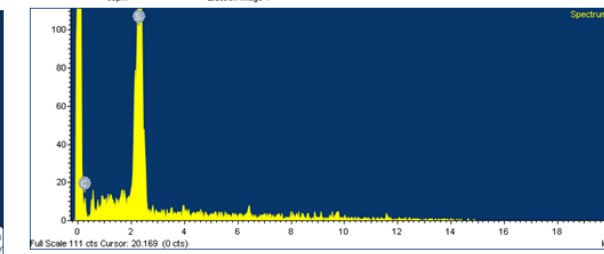
L-PB50/70-30%GSF 22/09/2014 13:32:53



Label: Spectrum 1
Collected: 22-Sep-2014 01:31 PM
Live time (s): 49.97
Real time (s): 52.24
Detector: ADD
Window: SATW

Tilt (deg): 0.0
Elevation (deg): 35.0
Azimuth (deg): 0.0

Magnification: 1000 X
Accelerating voltage (kV): 15.00
Process time: 5



Element	Weight%	Atomic%
C CaCO ₃	1-Jun-1999 12:00 AM	
S FeS ₂	1-Jun-1999 12:00 AM	
Totals	100.00	

Figure A.8 : Showing element analysis of B50/70-30%GSF.

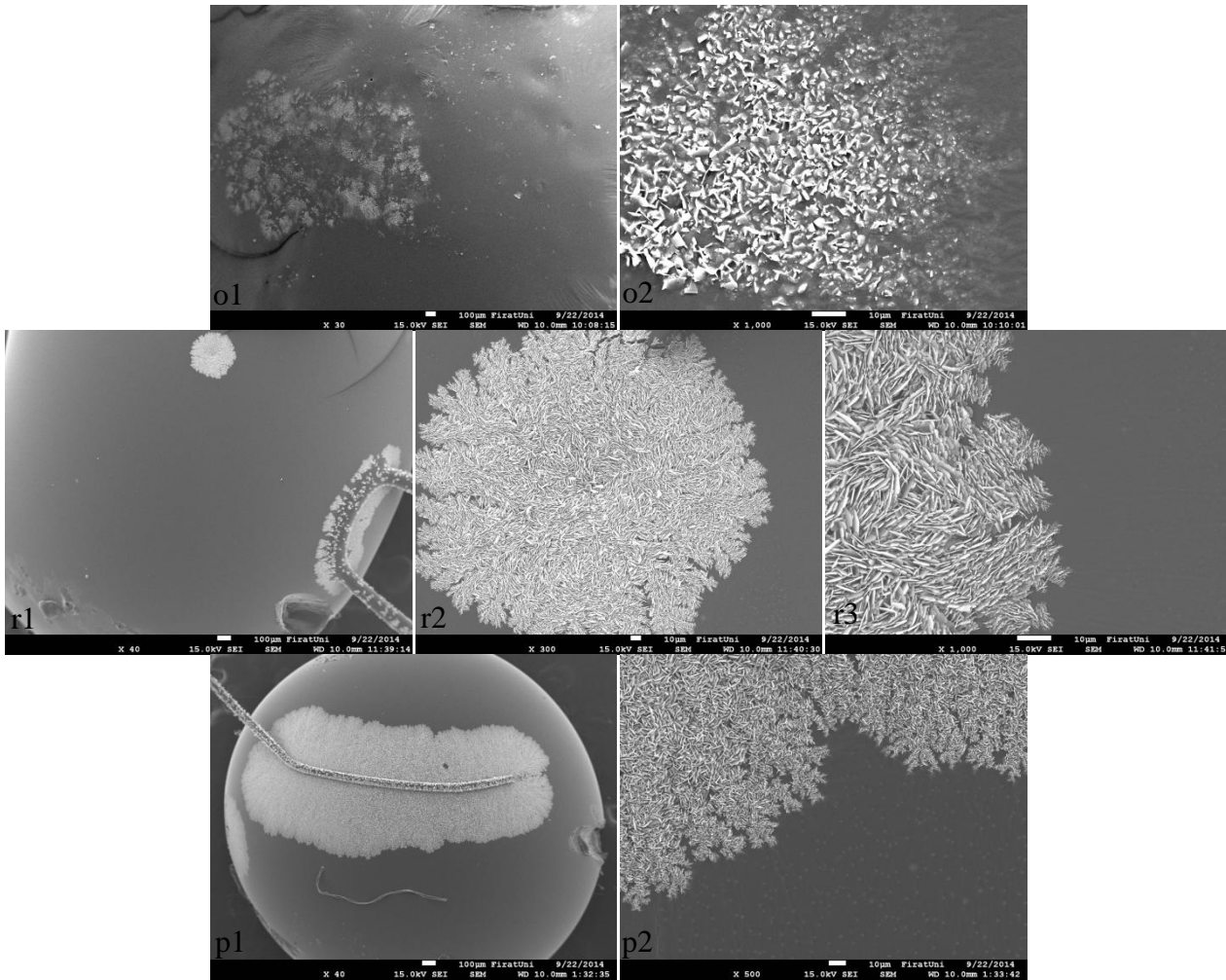


Figure A.9 : Showing images of B50/70-40% GSF (o1 and o2 at the un-aged stage, r1, r2 and r3 at the RTFOT-aged stage and p1 and p2 at the PAV-aged stage).

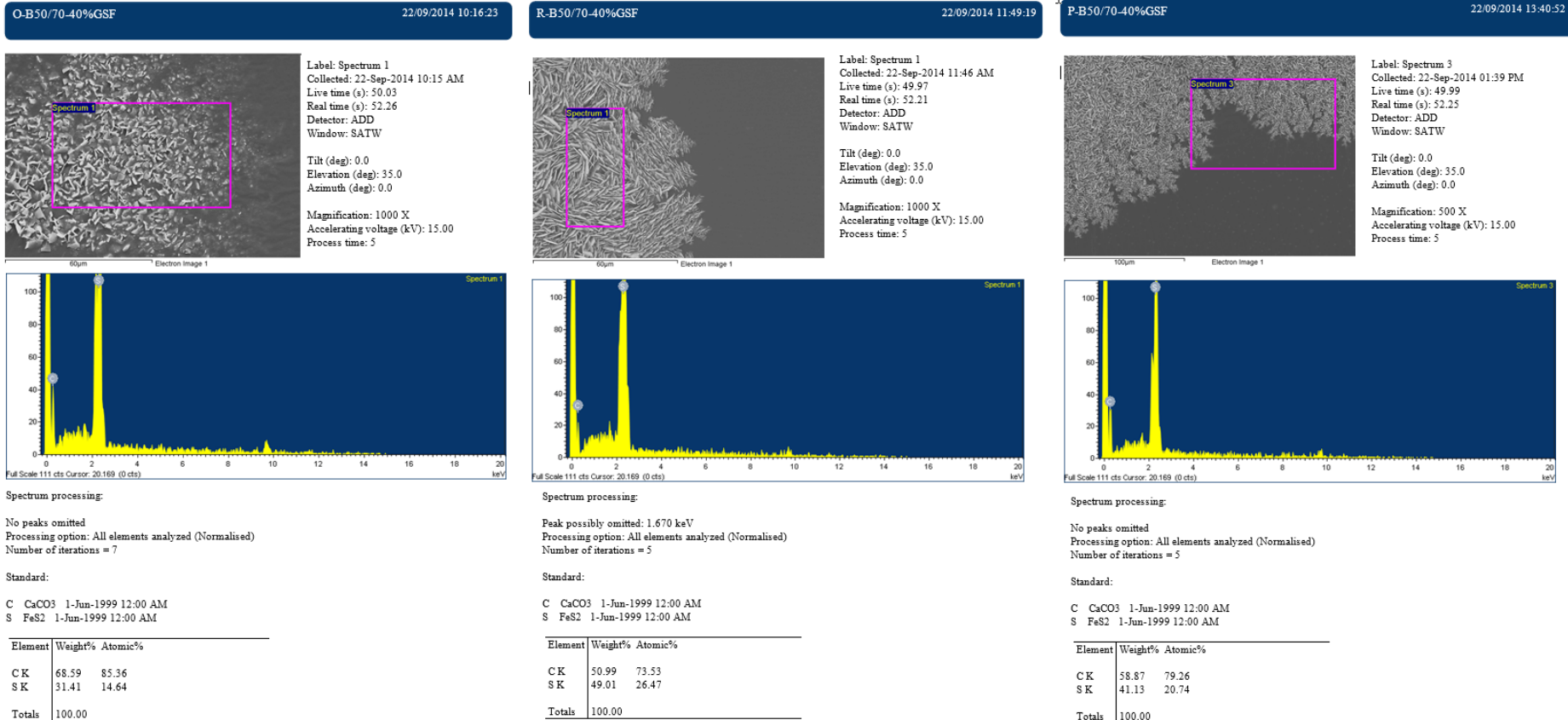


Figure A.10 : Showing element analysis of B50/70-40%GSF.

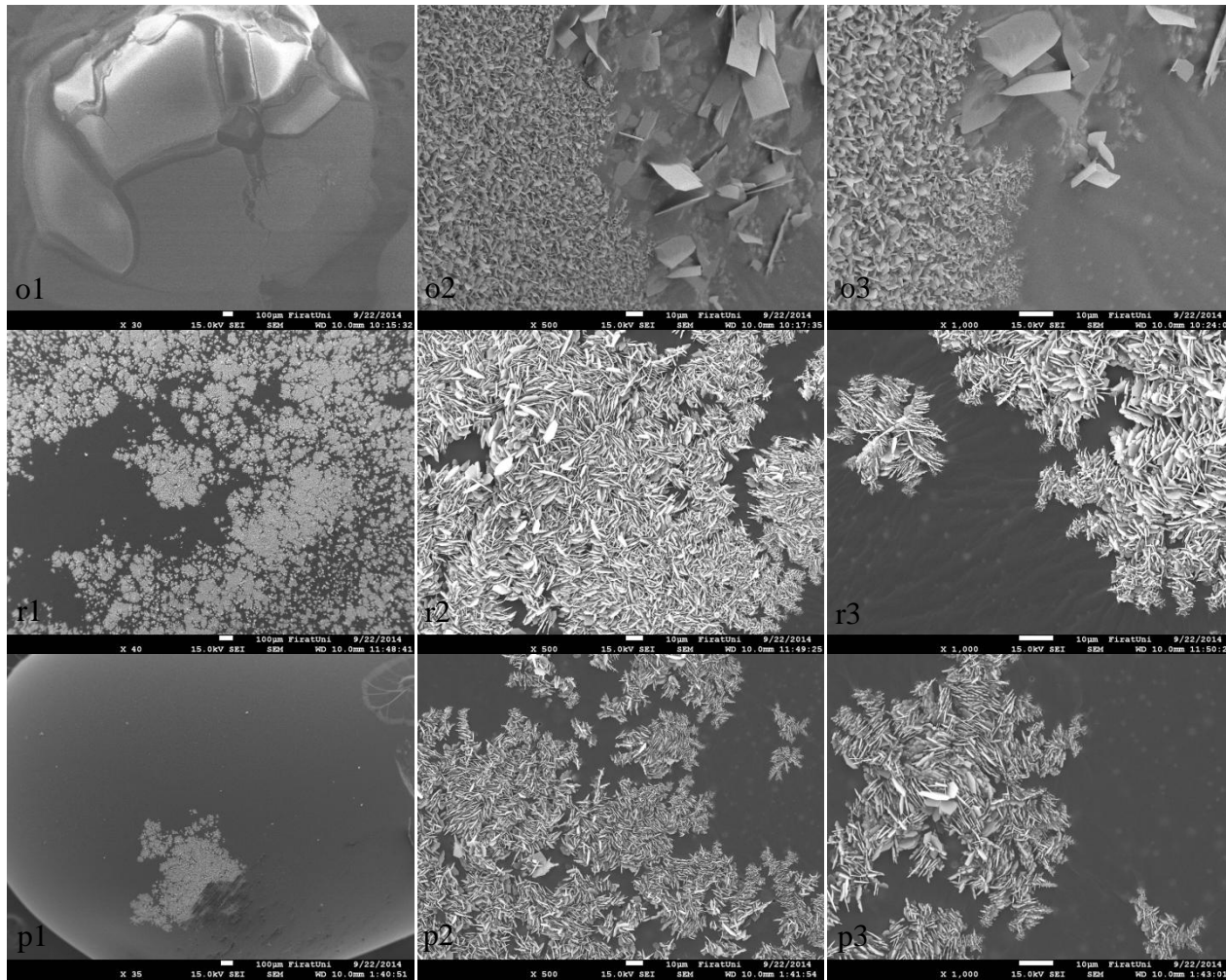


Figure A.11 : Showing images of B50/70-50%GSF (o1, o2 and o3 at the un-aged stage, r1, r2 and r3 at the RTFOT-aged stage and p1, p2 and p3 at the PAV-aged stage).

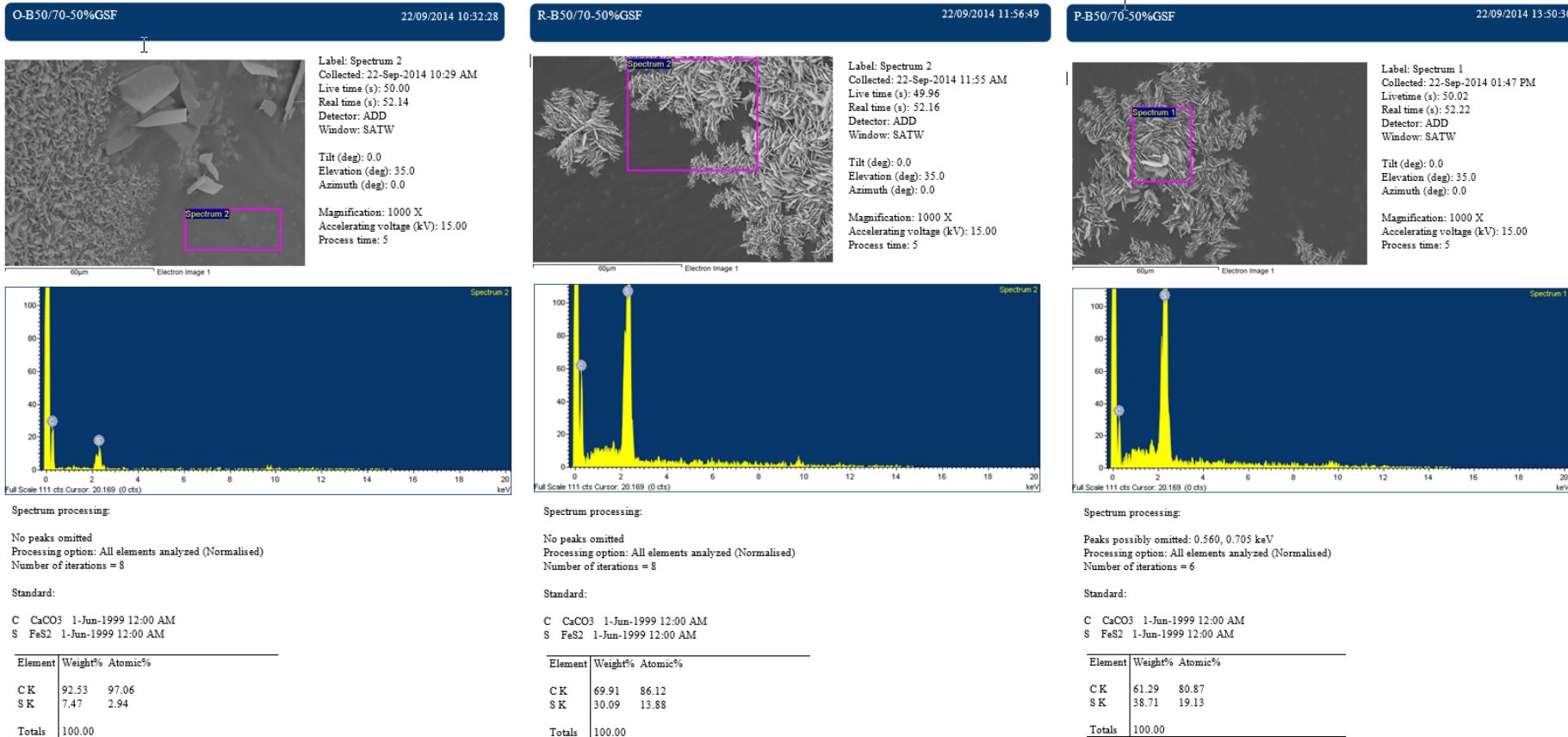


Figure A.12 : Showing element analysis of B50/70-50%GSF.

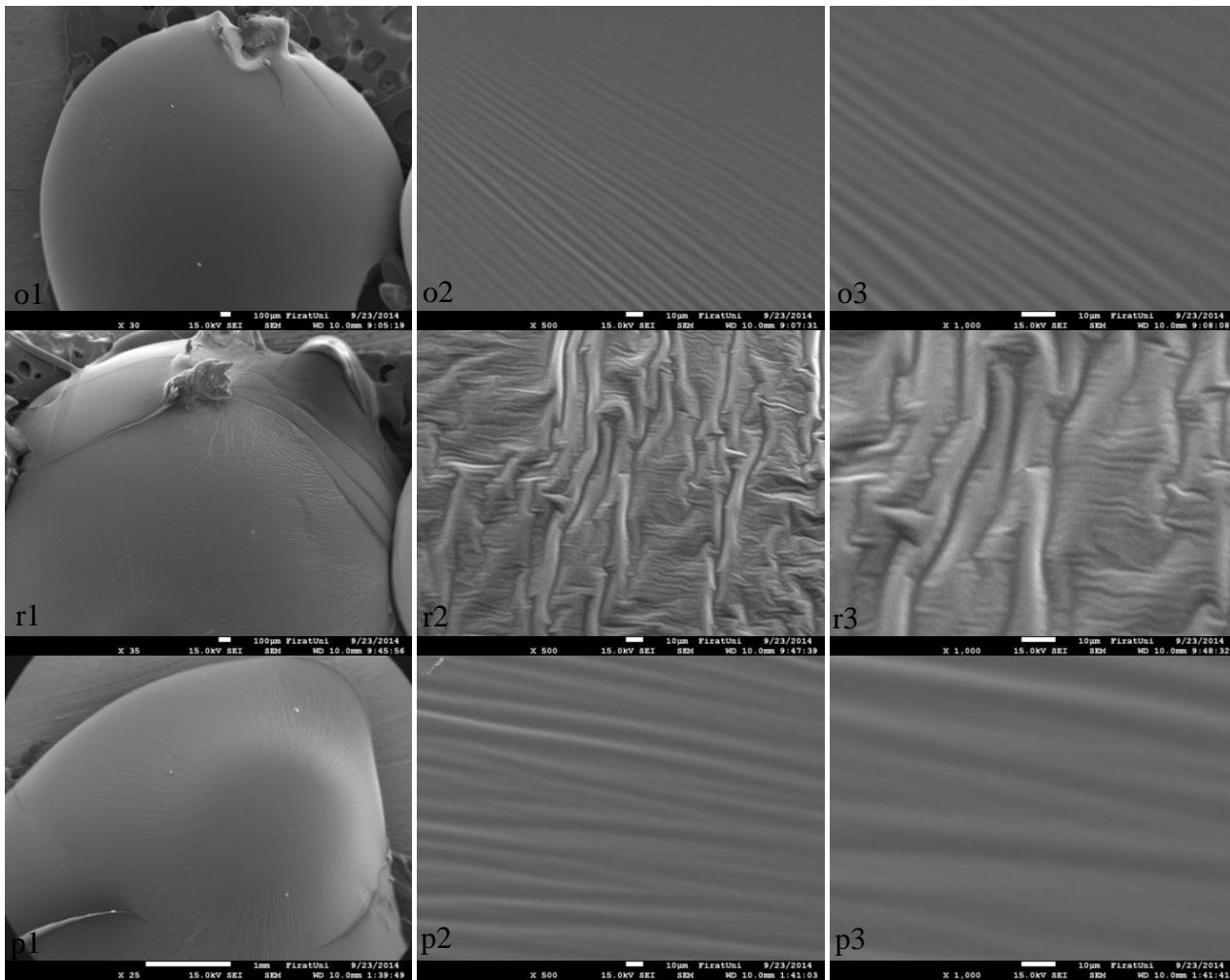


Figure A.13 : Showing images of B70/100-0%GSF (o1, o2 and o3 at the un-aged stage, r1, r2 and r3 at the RTFOT-aged stage and p1, p2 and p3 at the PAV-aged stage).

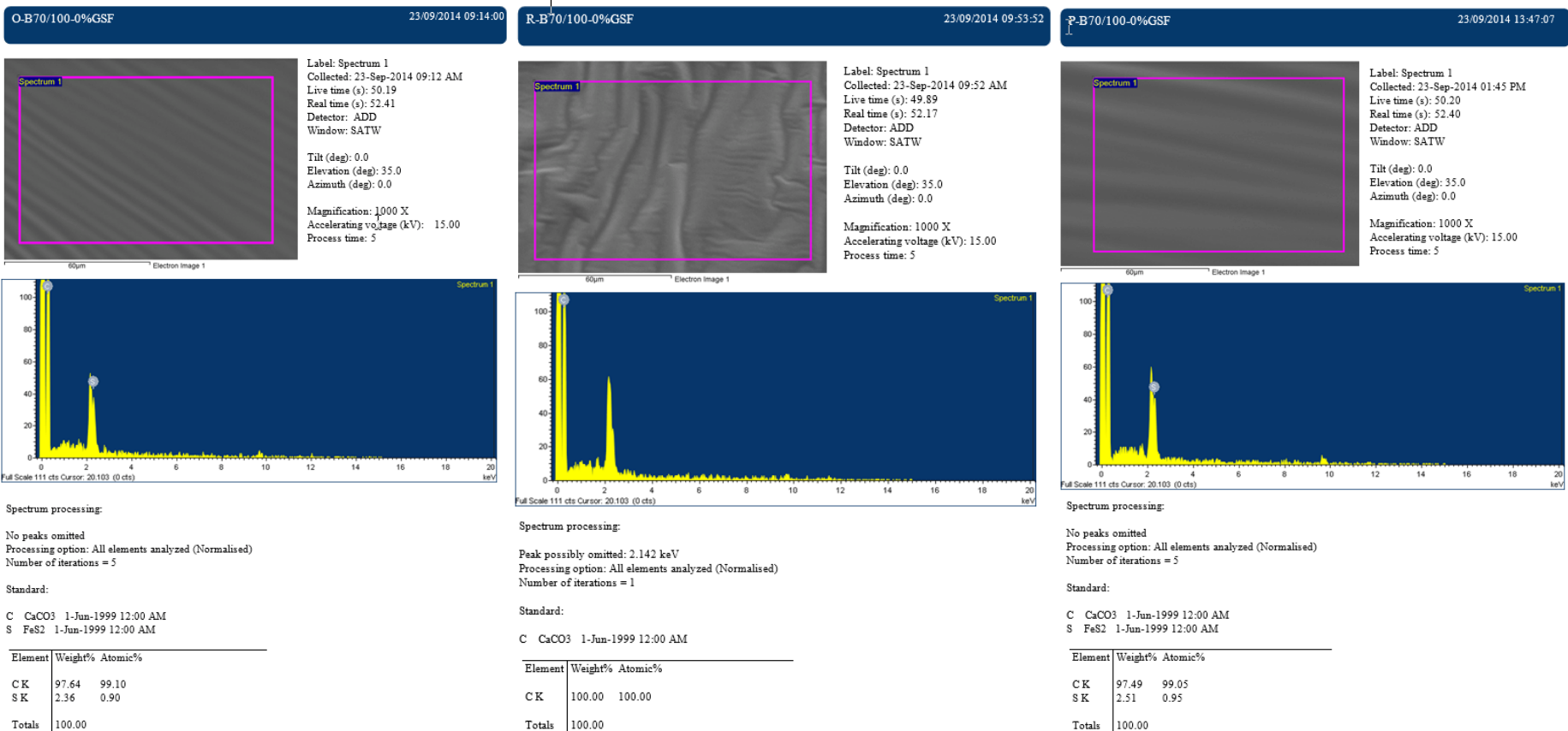


Figure A.14 : Showing element analysis of B70/100-0%GSF.

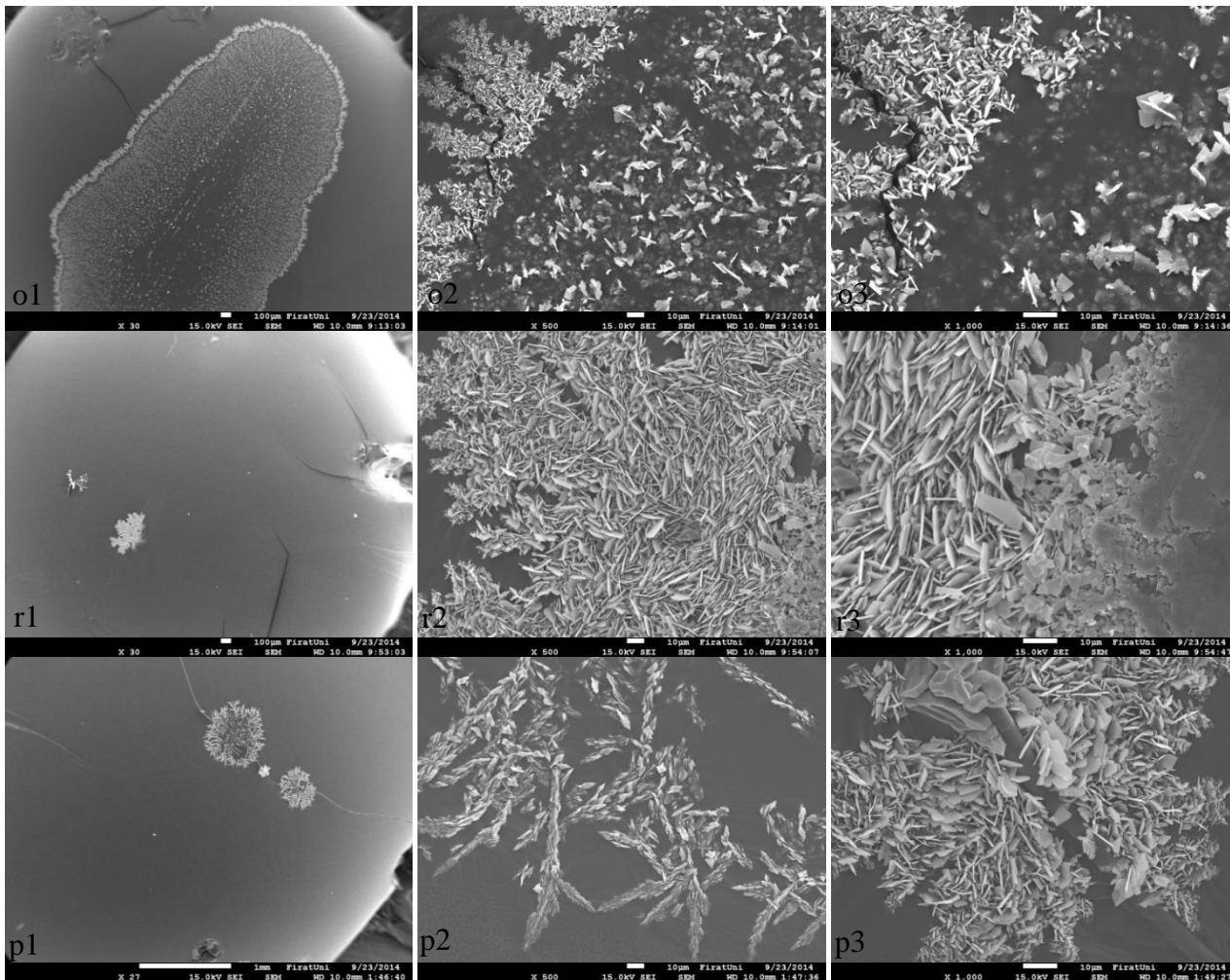


Figure A.15 : Showing images of B70/100-10%GSF (o1, o2 and o3 at the un-aged stage, r1, r2 and r3 at the RTFOT-aged stage and p1, p2 and p3 at the PAV-aged stage).

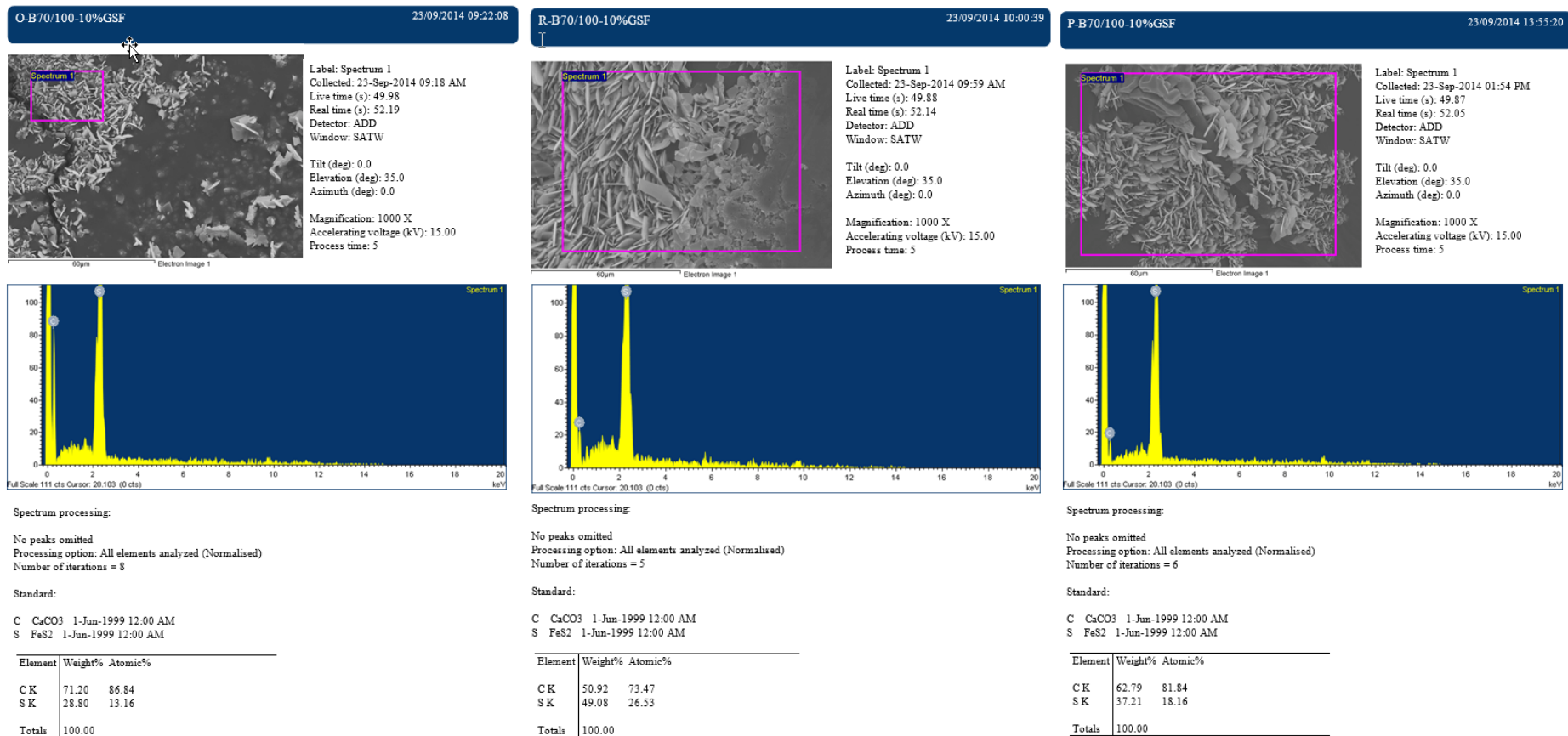


Figure A.16 : Showing element analysis of B70/100-10%GSF.

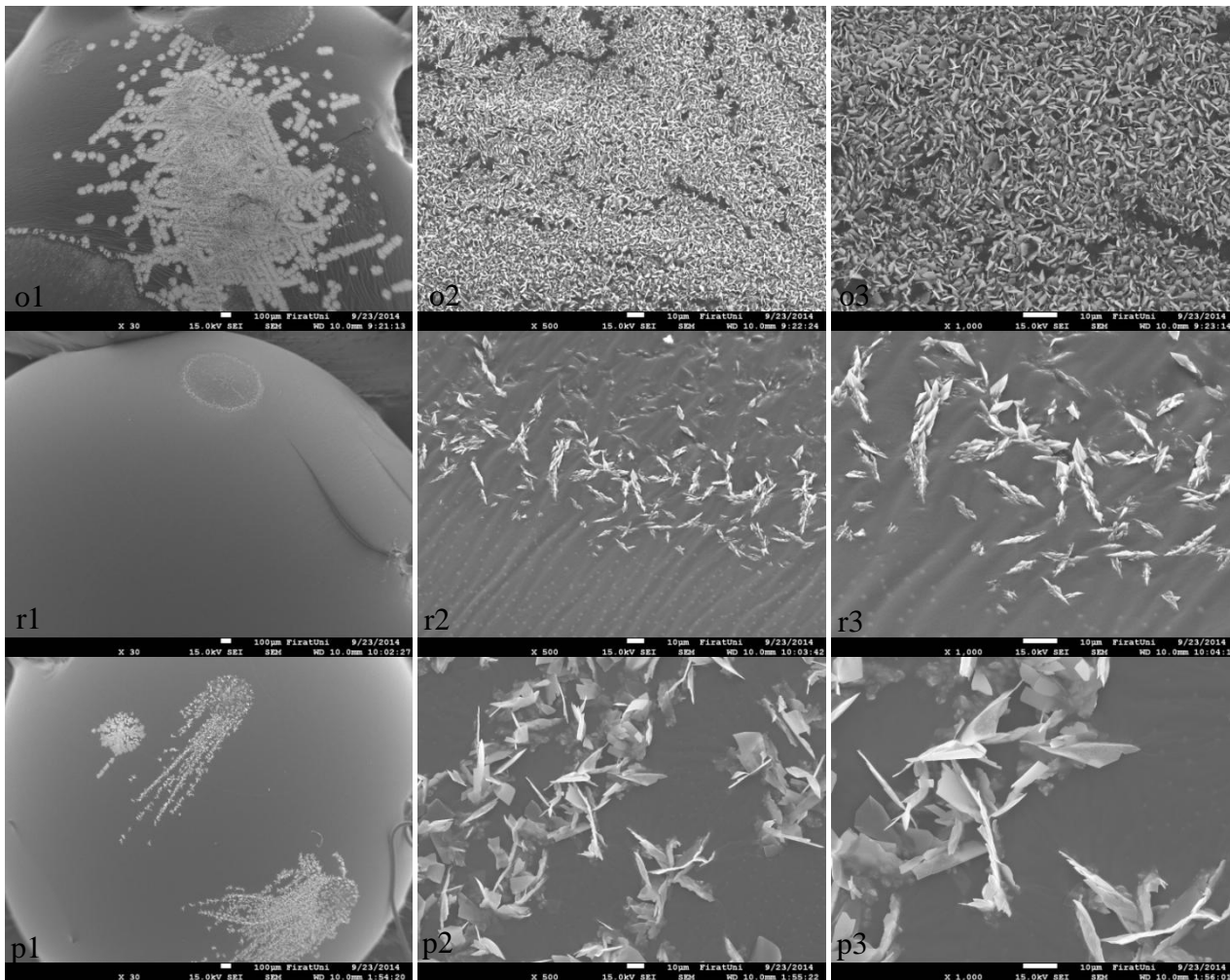
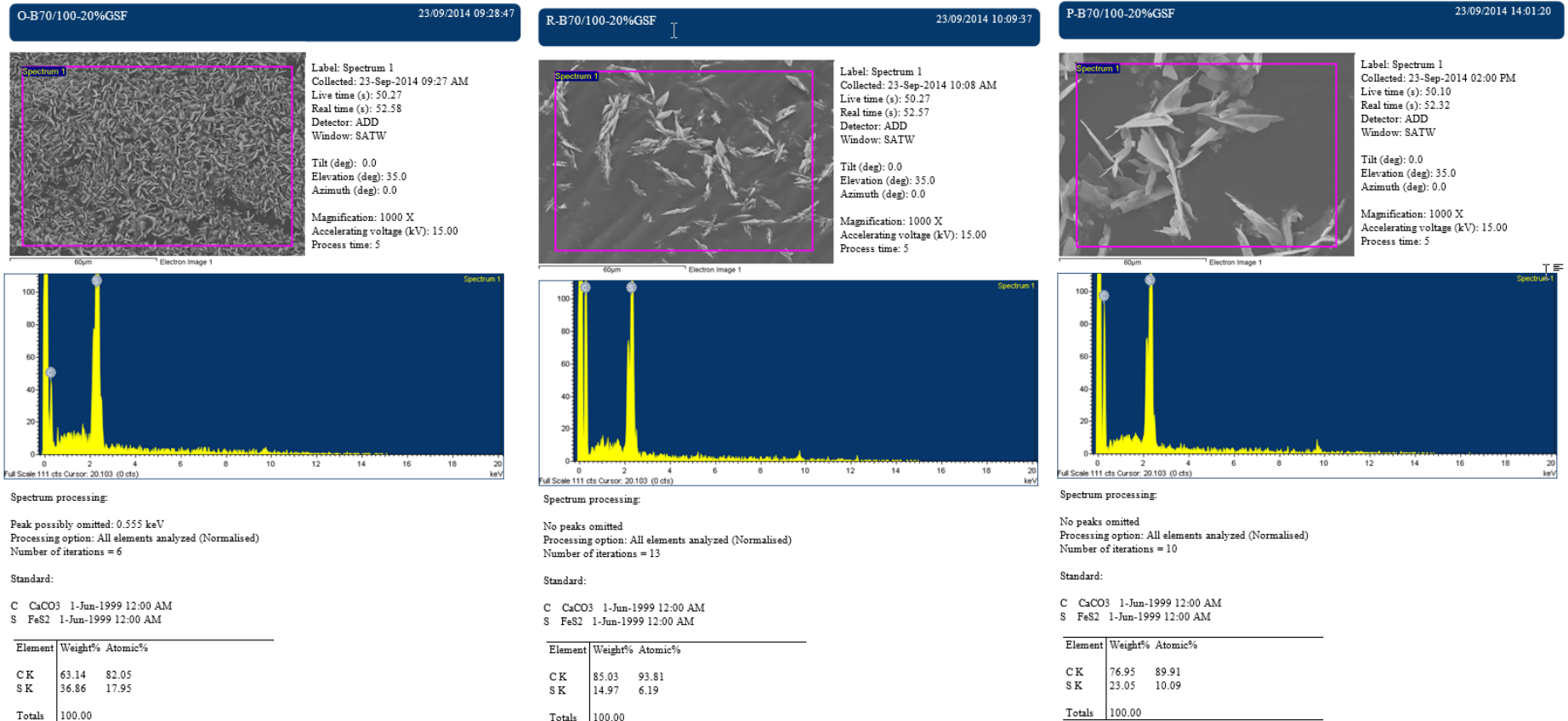


Figure A.17 : Showing images of B70/100-20%GSF (o1, o2 and o3 at the un-aged stage, r1, r2 and r3 at the RTFOT-aged stage and p1, p2 and p3 at the PAV-aged stage).



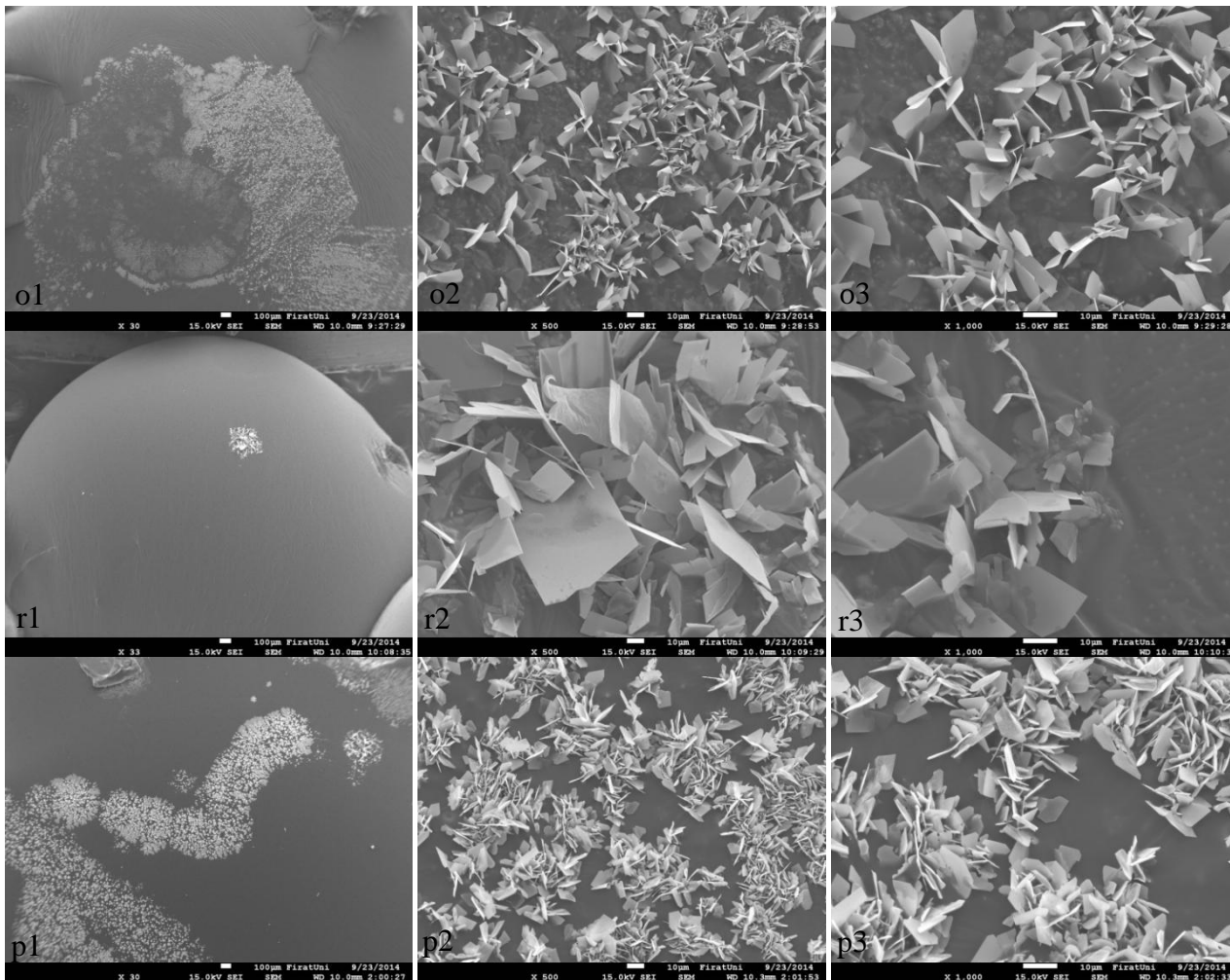
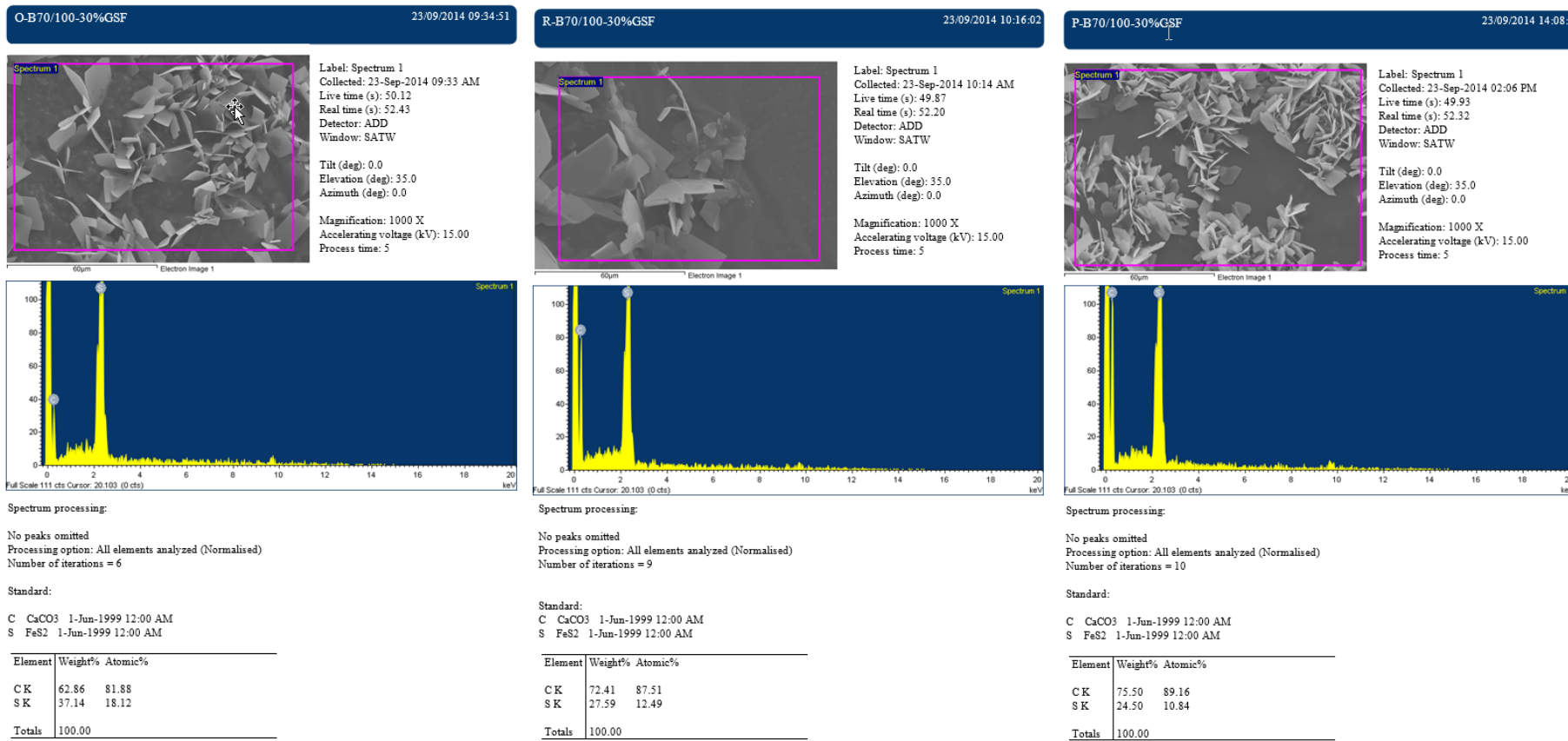


Figure A.19 : Showing images of B70/100-30%GSF (o1, o2 and o3 at the un-aged stage, r1, r2 and r3 at the RTFOT-aged stage and p1, p2 and p3 at the PAV-aged stage).



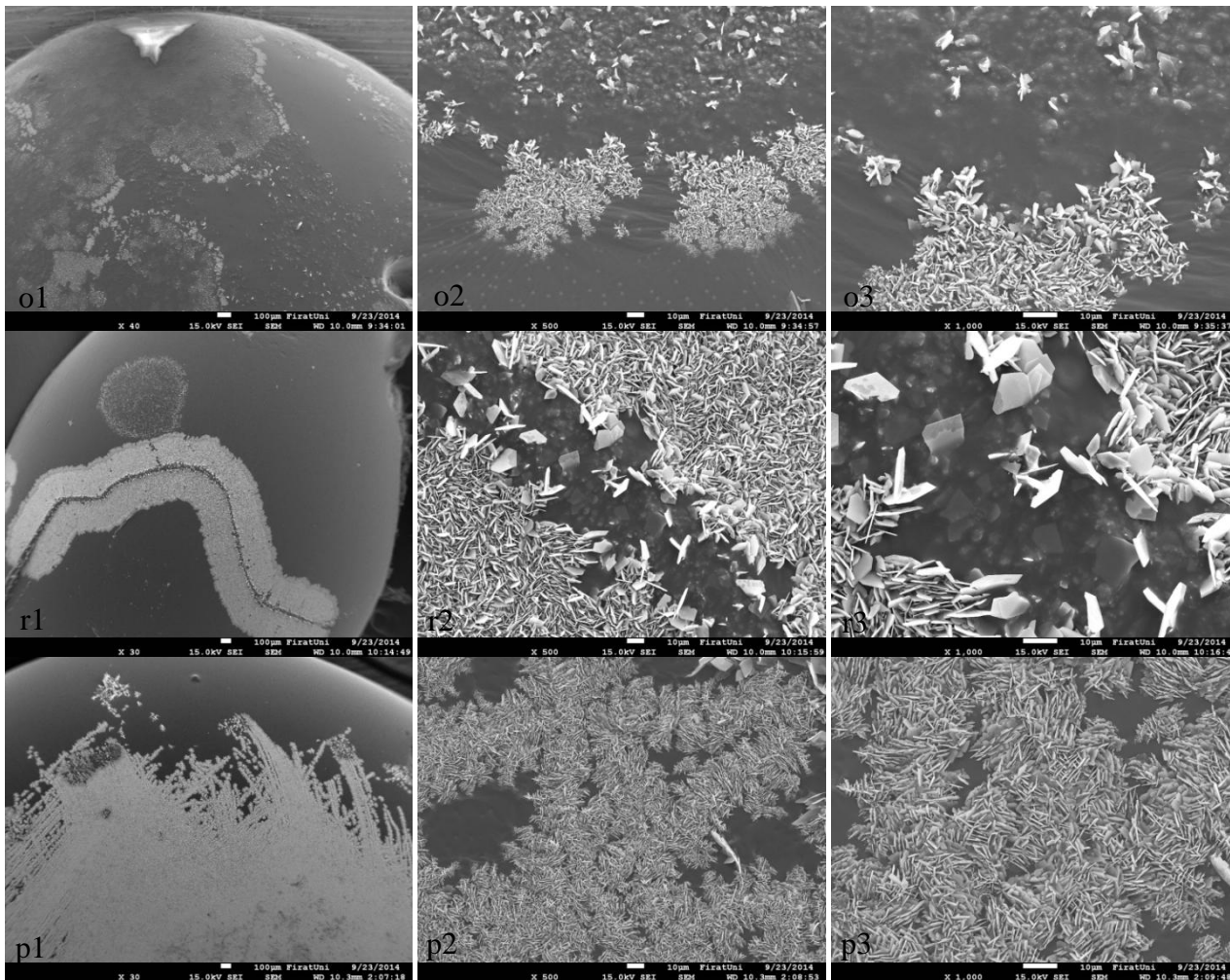


Figure A.21 : Showing images of B70/100-40%GSF (o1, o2 and o3 at the un-aged stage, r1, r2 and r3 at the RTFOT-aged stage and p1, p2 and p3 at the PAV-aged stage).

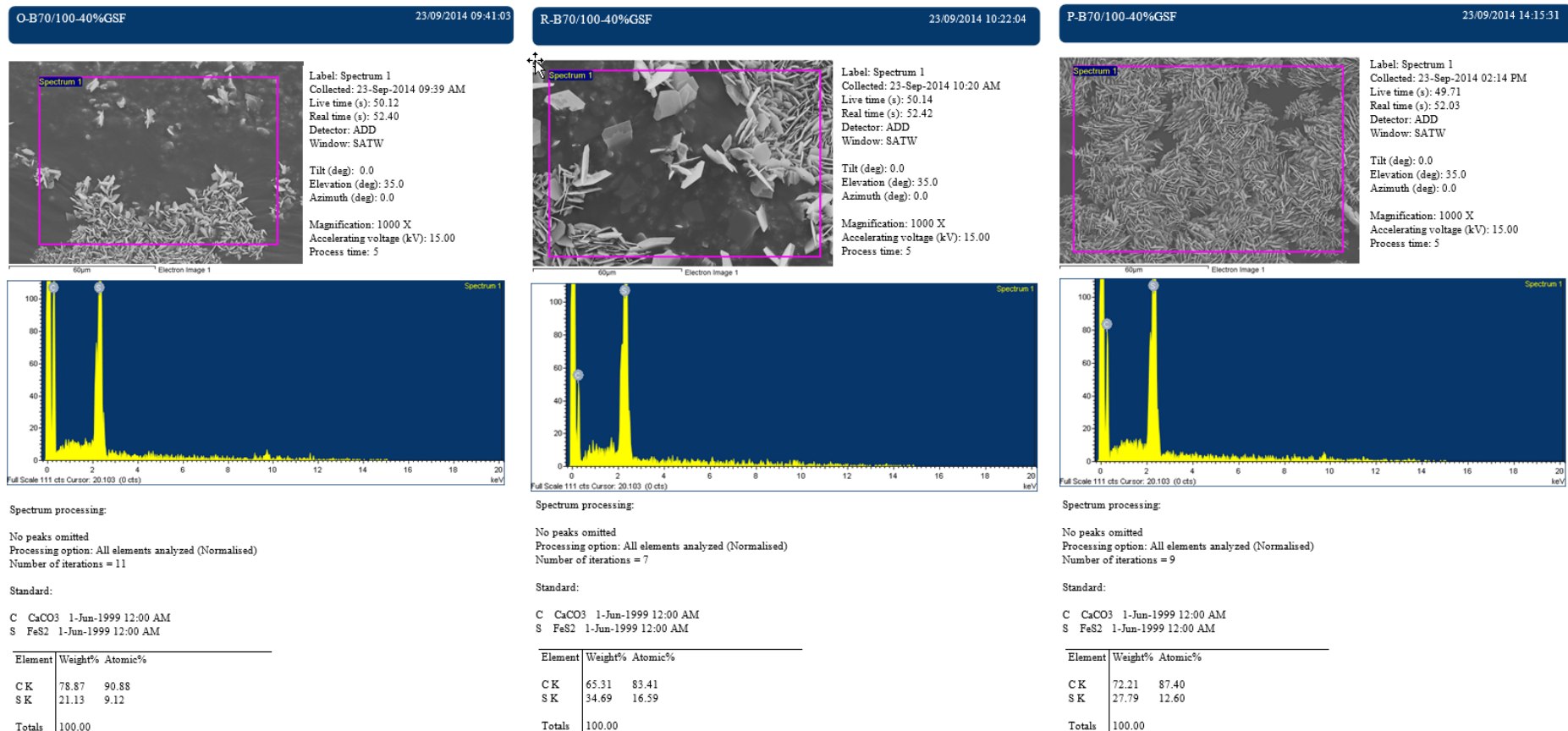


Figure A.22 : Showing element analysis of B70/100-40%GSF.

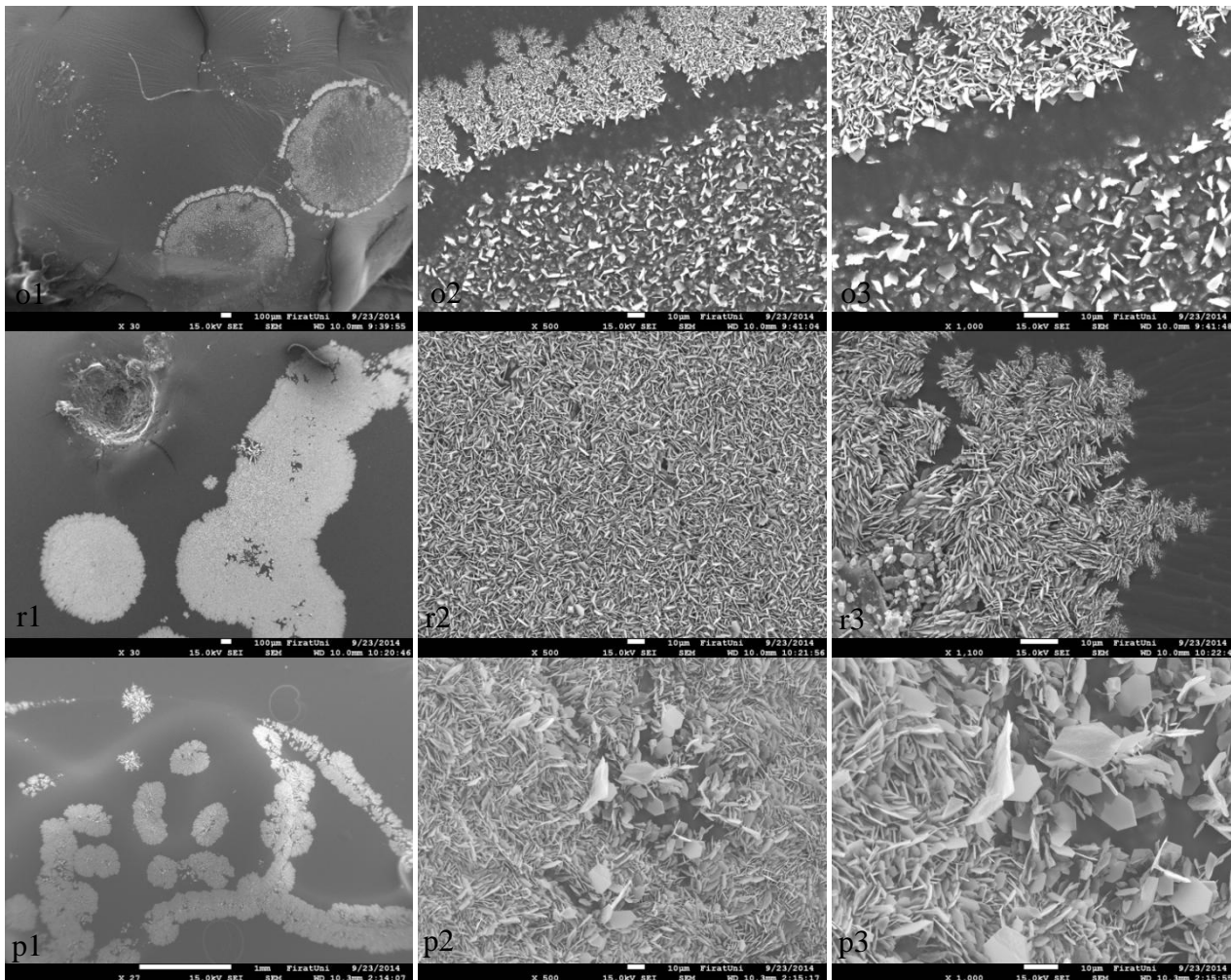


Figure A.23 : Showing images of B70/100-50% GSF (o1, o2 and o3 at the un-aged stage, r1, r2 and r3 at the RTFOT-aged stage and p1, p2 and p3 at the PAV-aged stage).

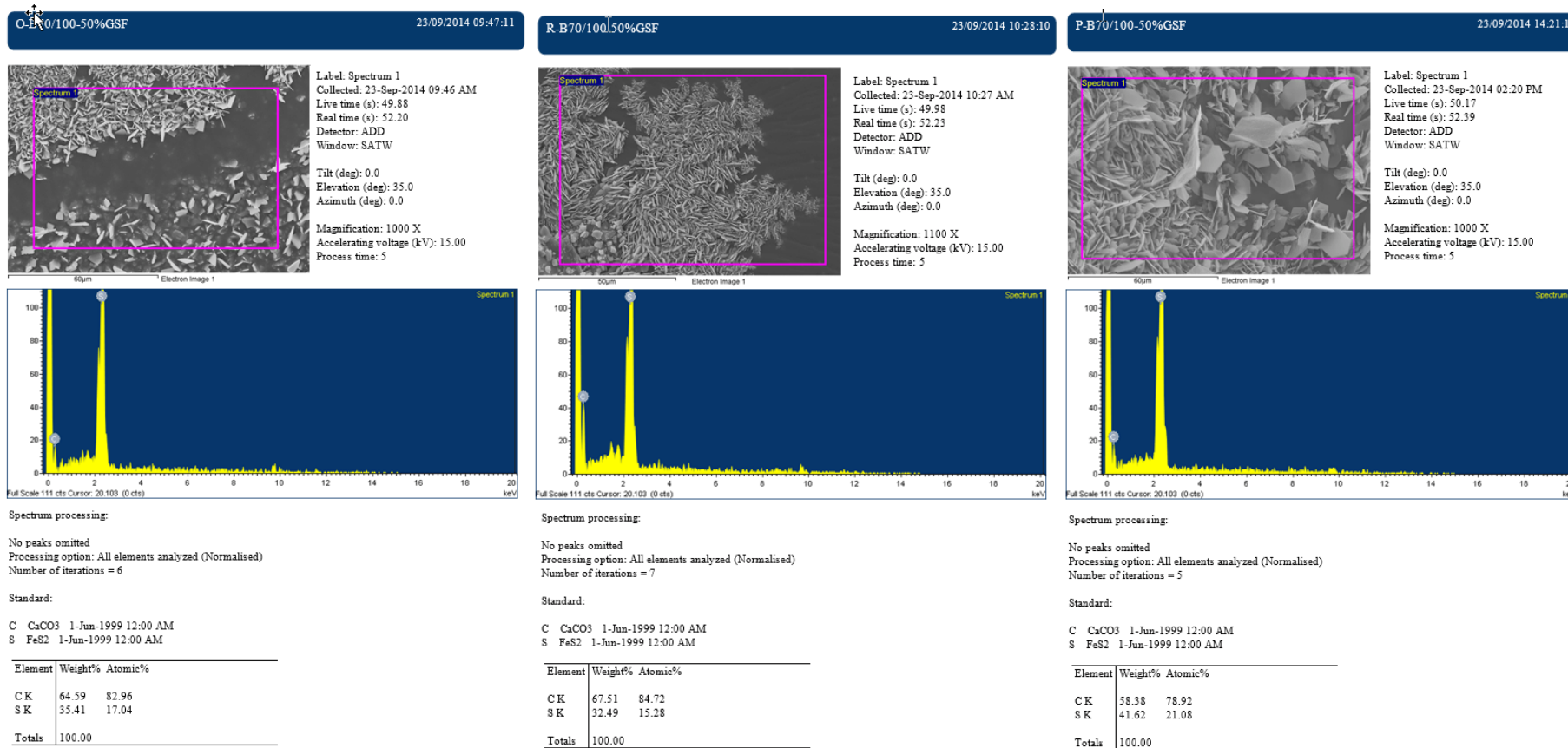


Figure A.24 : Showing element analysis of B70/100-50%GSF.

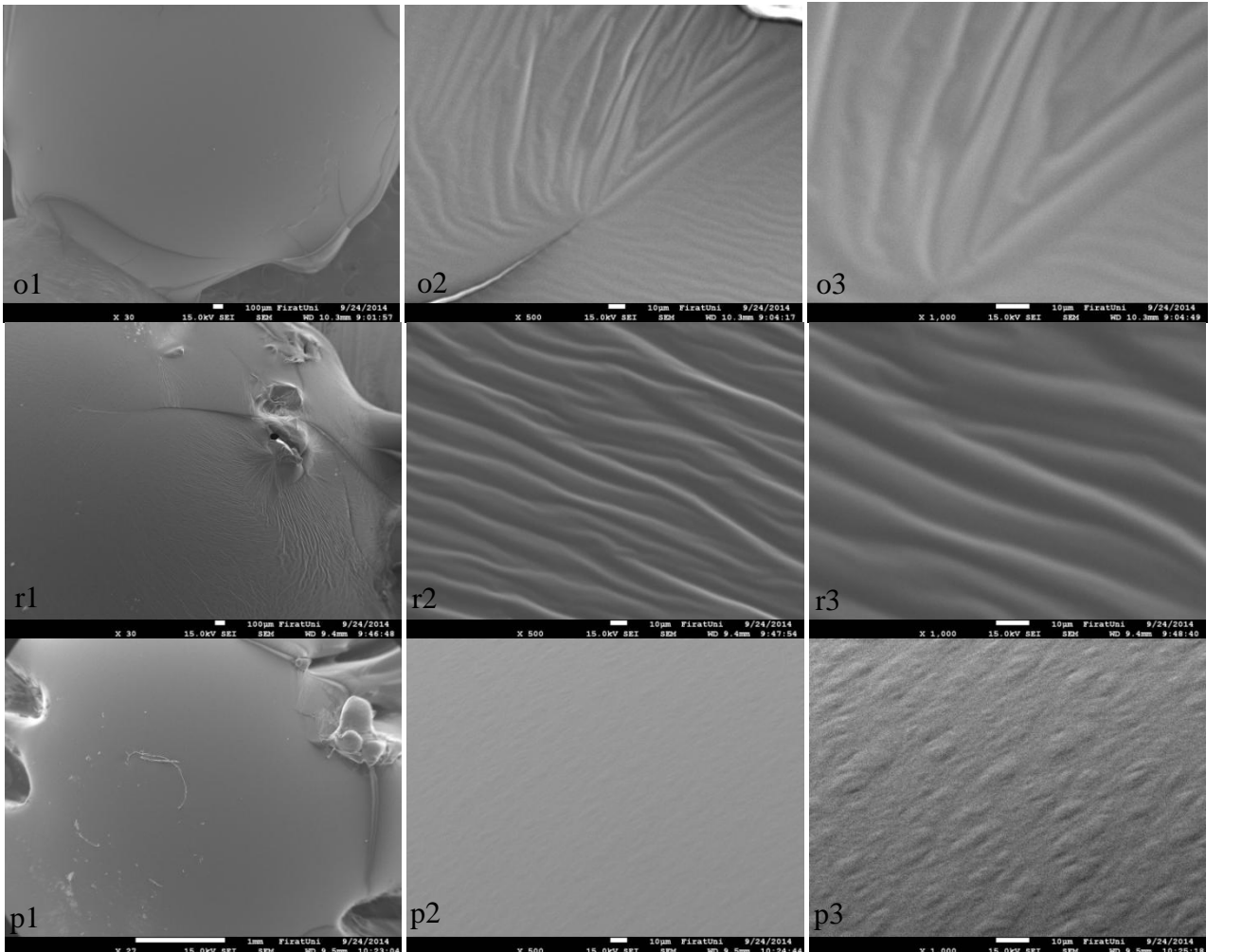
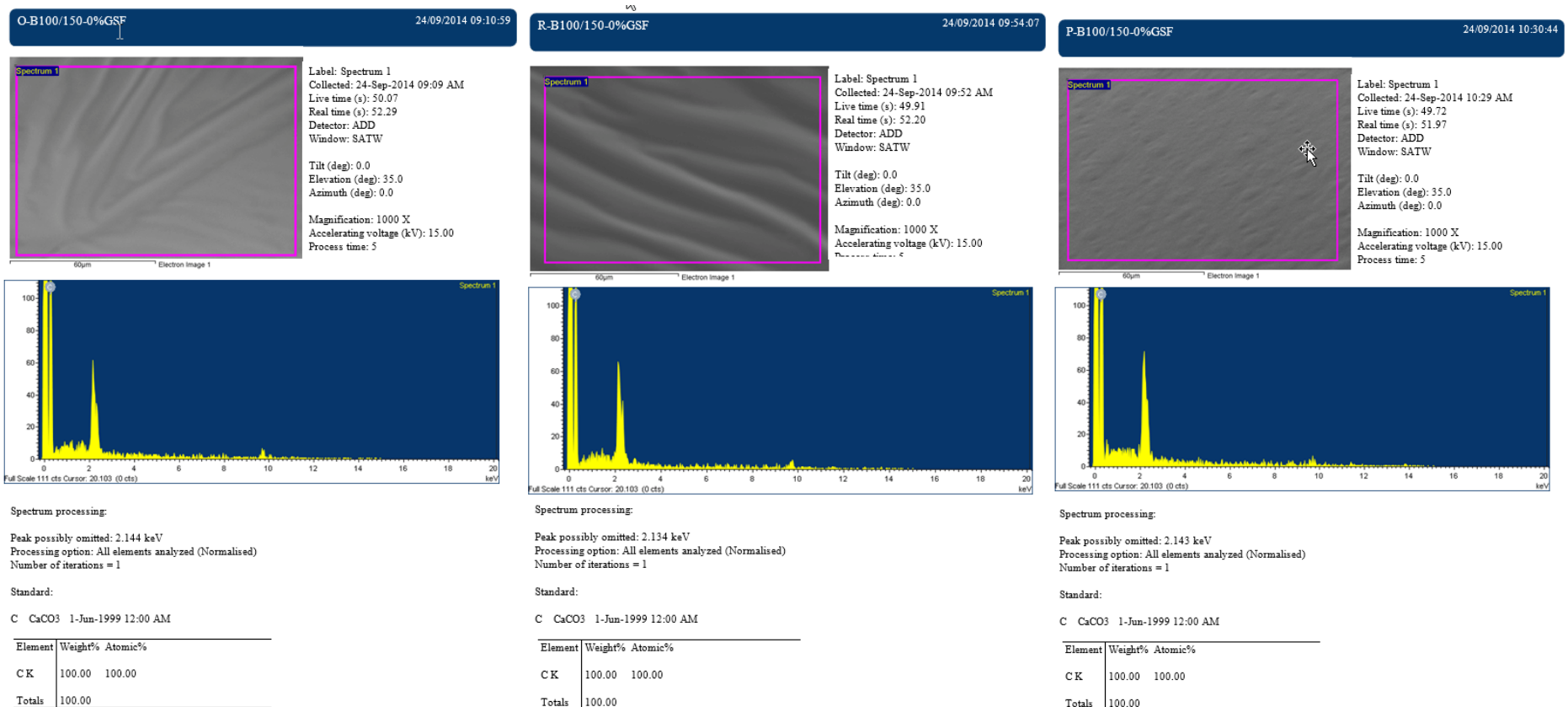


Figure A.25 : Showing images of B100/150-0% GSF (o1, o2 and o3 at the un-aged stage, r1, r2 and r3 at the RTFOT-aged stage and p1, p2 and p3 at the PAV-aged stage).



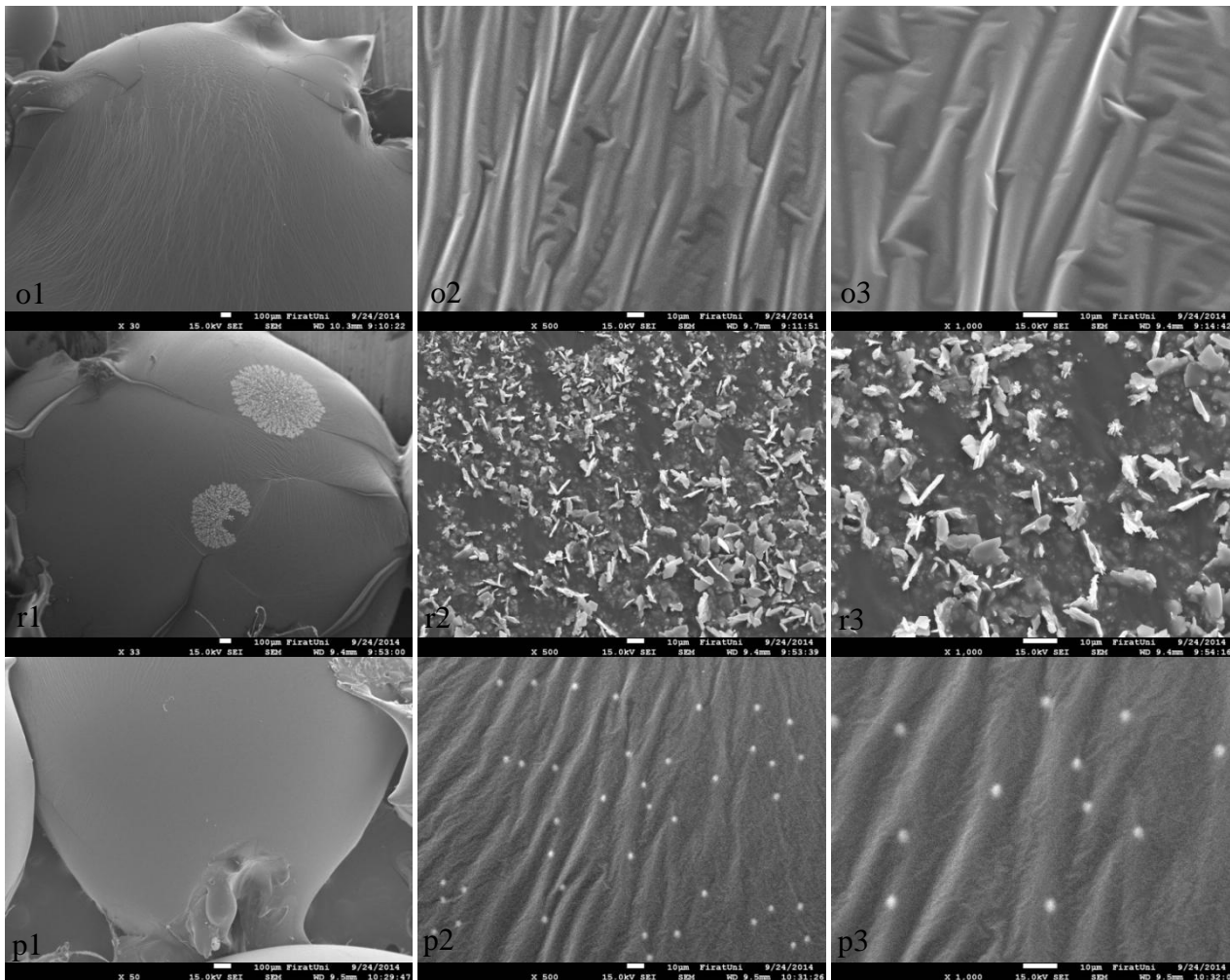
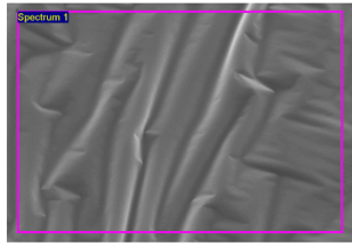


Figure A.27 : Showing images of B100/150-10%GSF (o1, o2 and o3 at the un-aged stage, r1, r2 and r3 at the RTFOT-aged stage and p1, p2 and p3 at the PAV-aged stage).

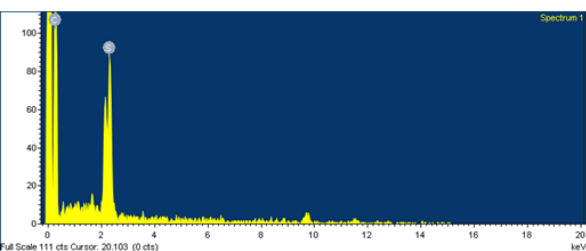
O-B100/150-10%GSF 24/09/2014 09:20:09



Spectrum 1
Label: Spectrum 1
Collected: 24-Sep-2014 09:18 AM
Live time (s): 50.23
Real time (s): 52.56
Detector: ADD
Window: SATW

Tilt (deg): 0.0
Elevation (deg): 35.0
Azimuth (deg): 0.0

Magnification: 1000 X
Accelerating voltage (kV): 15.00
Process time: 5



Spectrum processing:

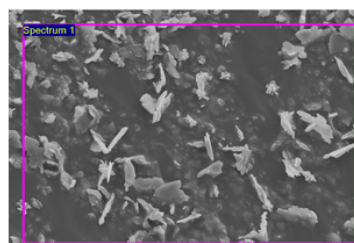
No peaks omitted
Processing option: All elements analyzed (Normalised)
Number of iterations = 11

Standard:

C CaCO₃ 1-Jun-1999 12:00 AM
S FeS₂ 1-Jun-1999 12:00 AM

Element	Weight%	Atomic%
C K	92.06	96.87
S K	7.94	3.13
Totals	100.00	

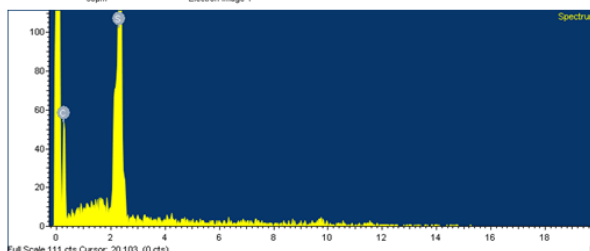
R-B100/150-10%GSF 24/09/2014 09:59:36



Spectrum 1
Label: Spectrum 1
Collected: 24-Sep-2014 09:58 AM
Live time (s): 49.86
Real time (s): 52.14
Detector: ADD
Window: SATW

Tilt (deg): 0.0
Elevation (deg): 35.0
Azimuth (deg): 0.0

Magnification: 1000 X
Accelerating voltage (kV): 15.00
Process time: 5



Spectrum processing:

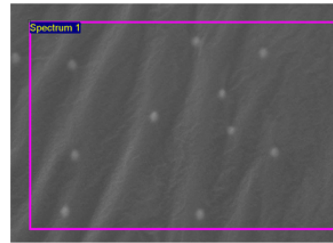
No peaks omitted
Processing option: All elements analyzed (Normalised)
Number of iterations = 8

Standard:

C CaCO₃ 1-Jun-1999 12:00 AM
S FeS₂ 1-Jun-1999 12:00 AM

Element	Weight%	Atomic%
C K	68.23	85.15
S K	31.77	14.85
Totals	100.00	

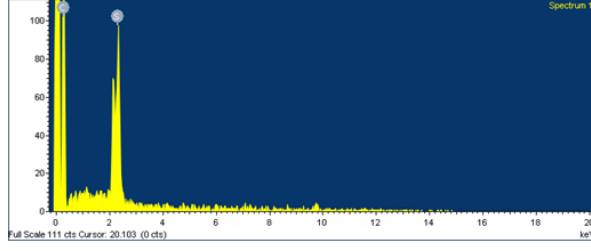
P-B100/150-10%GSF 24/09/2014 10:37:19



Spectrum 1
Label: Spectrum 1
Collected: 24-Sep-2014 10:36 AM
Live time (s): 50.01
Real time (s): 52.24
Detector: ADD
Window: SATW

Tilt (deg): 0.0
Elevation (deg): 35.0
Azimuth (deg): 0.0

Magnification: 1000 X
Accelerating voltage (kV): 15.00
Process time: 5



Spectrum processing:

No peaks omitted
Processing option: All elements analyzed (Normalised)
Number of iterations = 11

Standard:

C CaCO₃ 1-Jun-1999 12:00 AM
S FeS₂ 1-Jun-1999 12:00 AM

Element	Weight%	Atomic%
C K	90.15	96.07
S K	9.85	3.93
Totals	100.00	

Figure A.28 : Showing element analysis of B100/150-10%GSF.

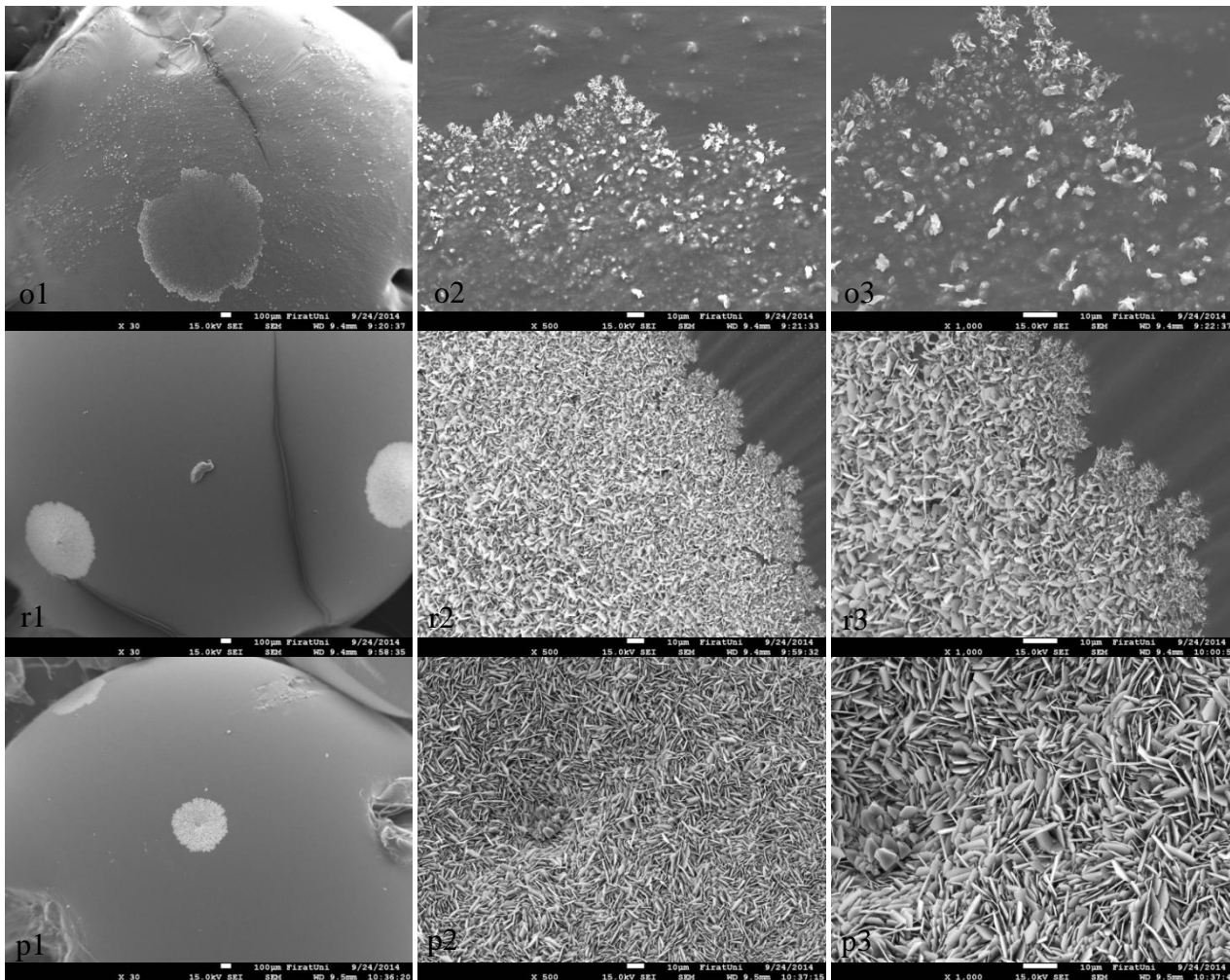


Figure A.29 : Showing images of B100/150-20%GSF (o1, o2 and o3 at the un-aged stage, r1, r2 and r3 at the RTFOT-aged stage and p1, p2 and p3 at the PAV-aged stage).

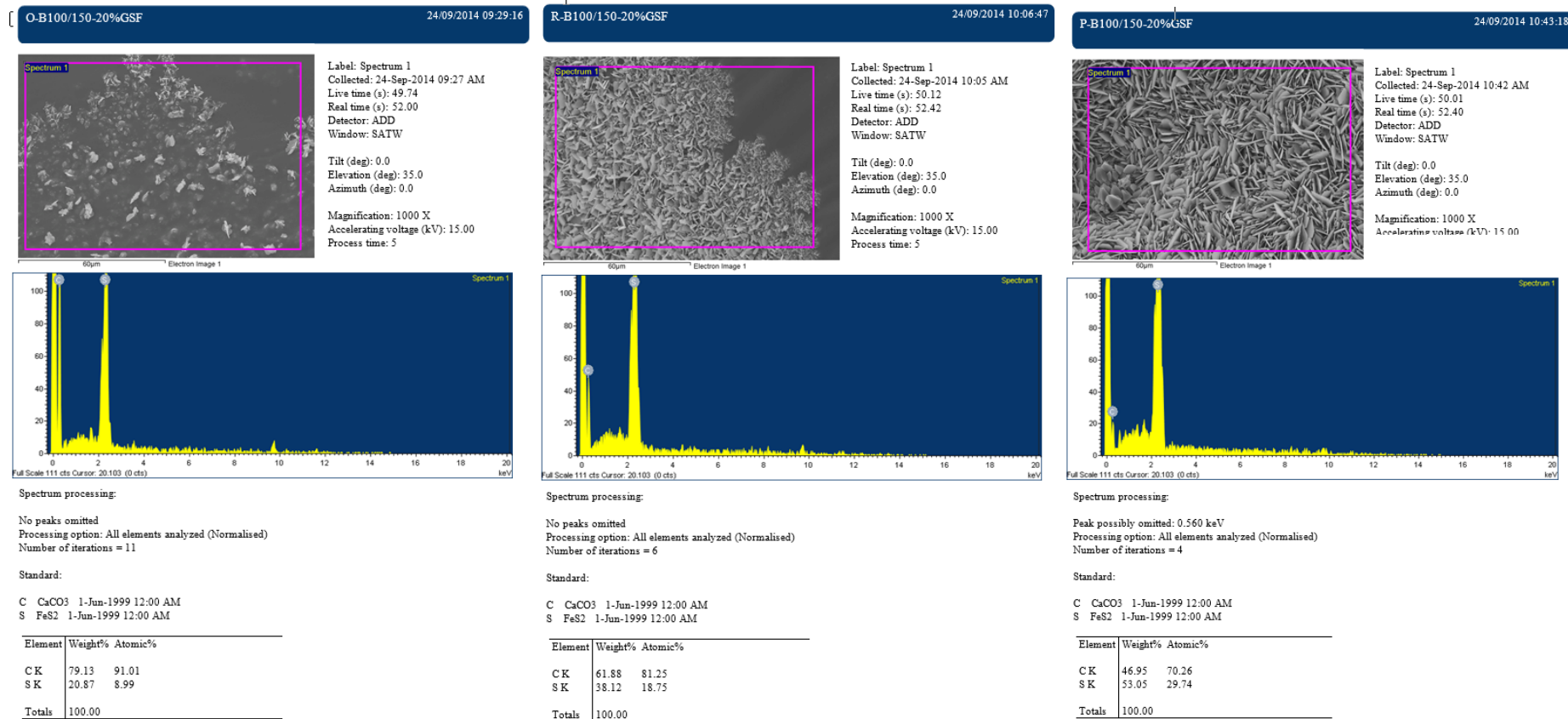


Figure A.30 : Showing element analysis of B100/150-20%GSF.

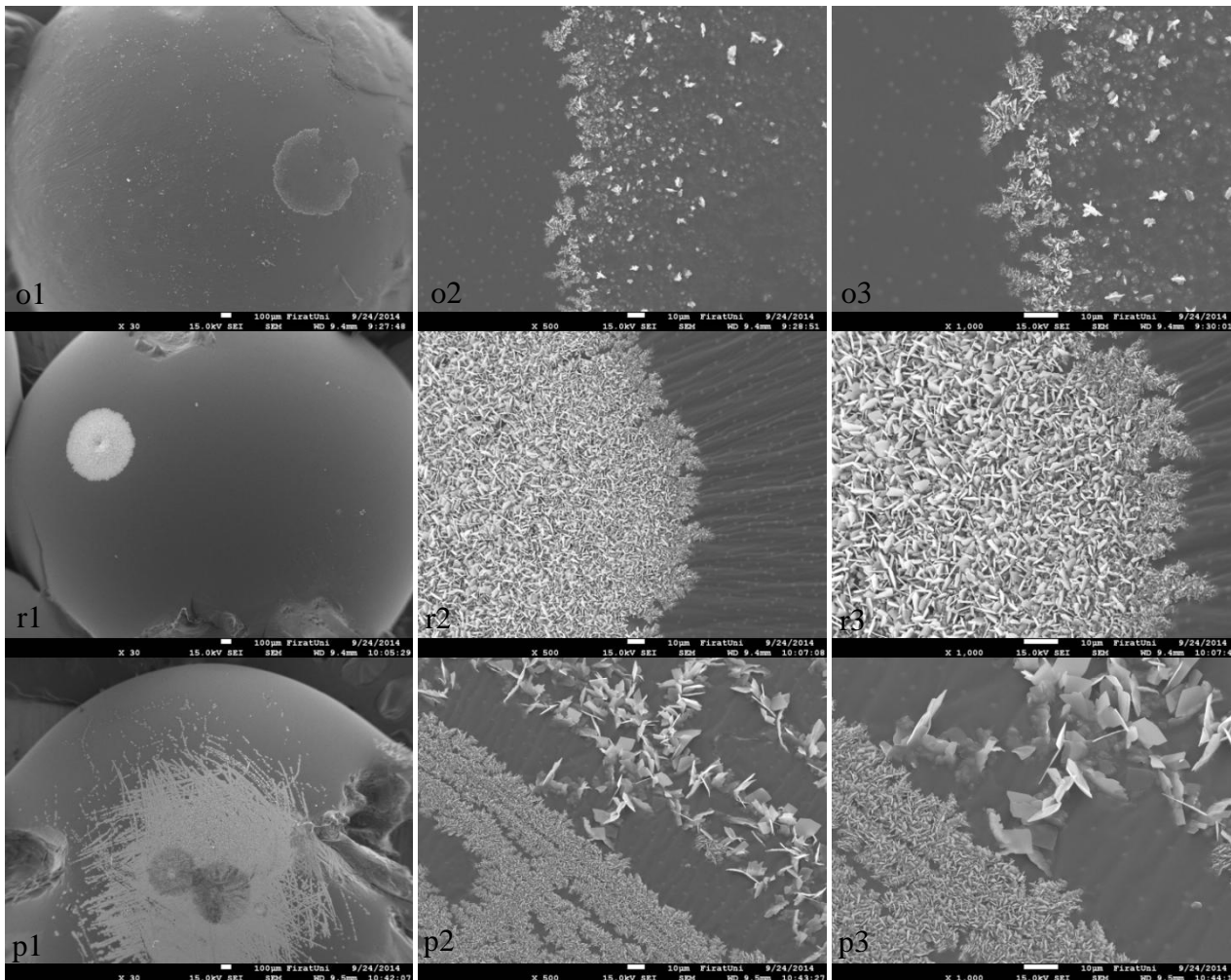


Figure A.31 : Showing images of B100/150-30%GSF (o1, o2 and o3 at the un-aged stage, r1, r2 and r3 at the RTFOT-aged stage and p1, p2 and p3 at the PAV-aged stage).

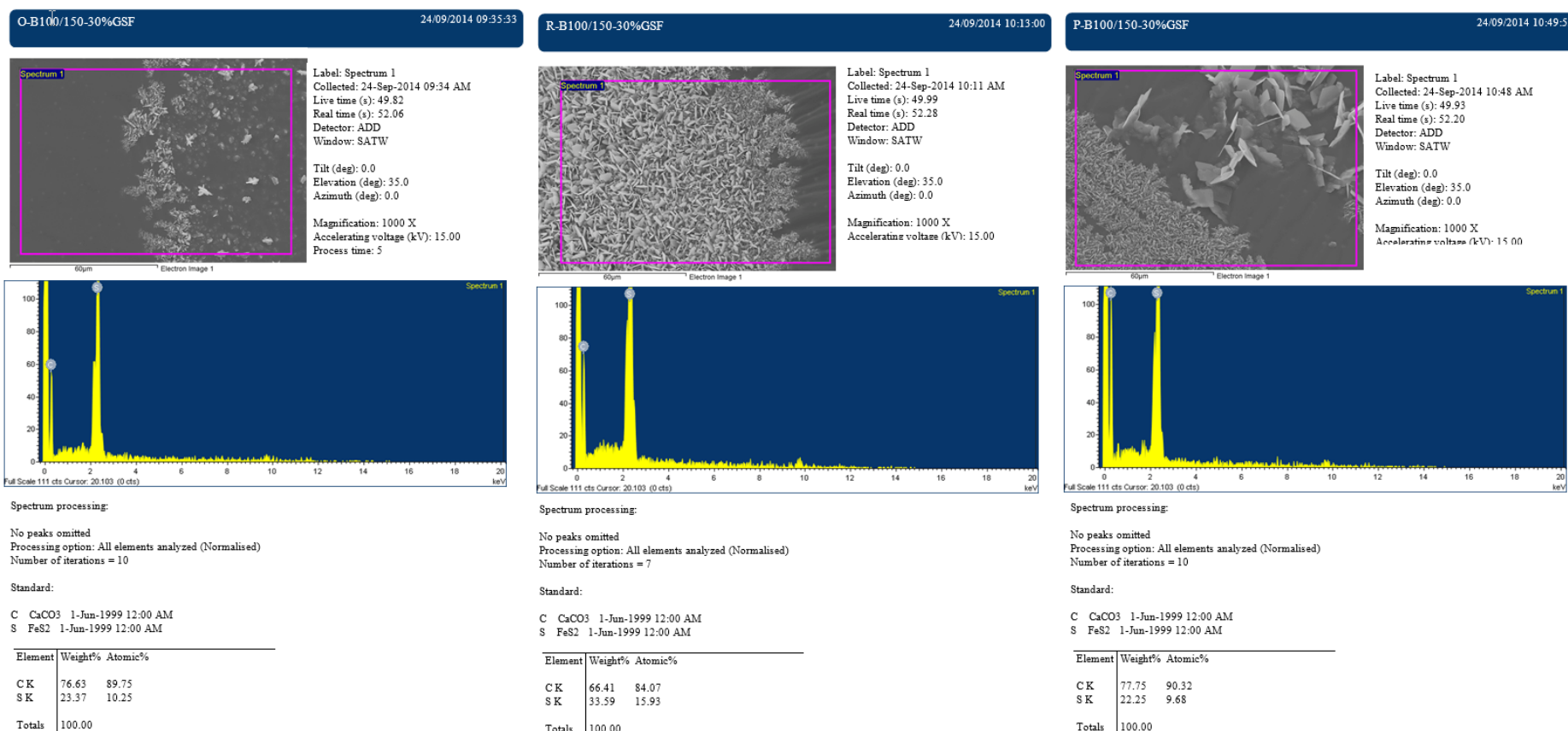


Figure A.32 : Showing element analysis of B100/150-30%GSF.

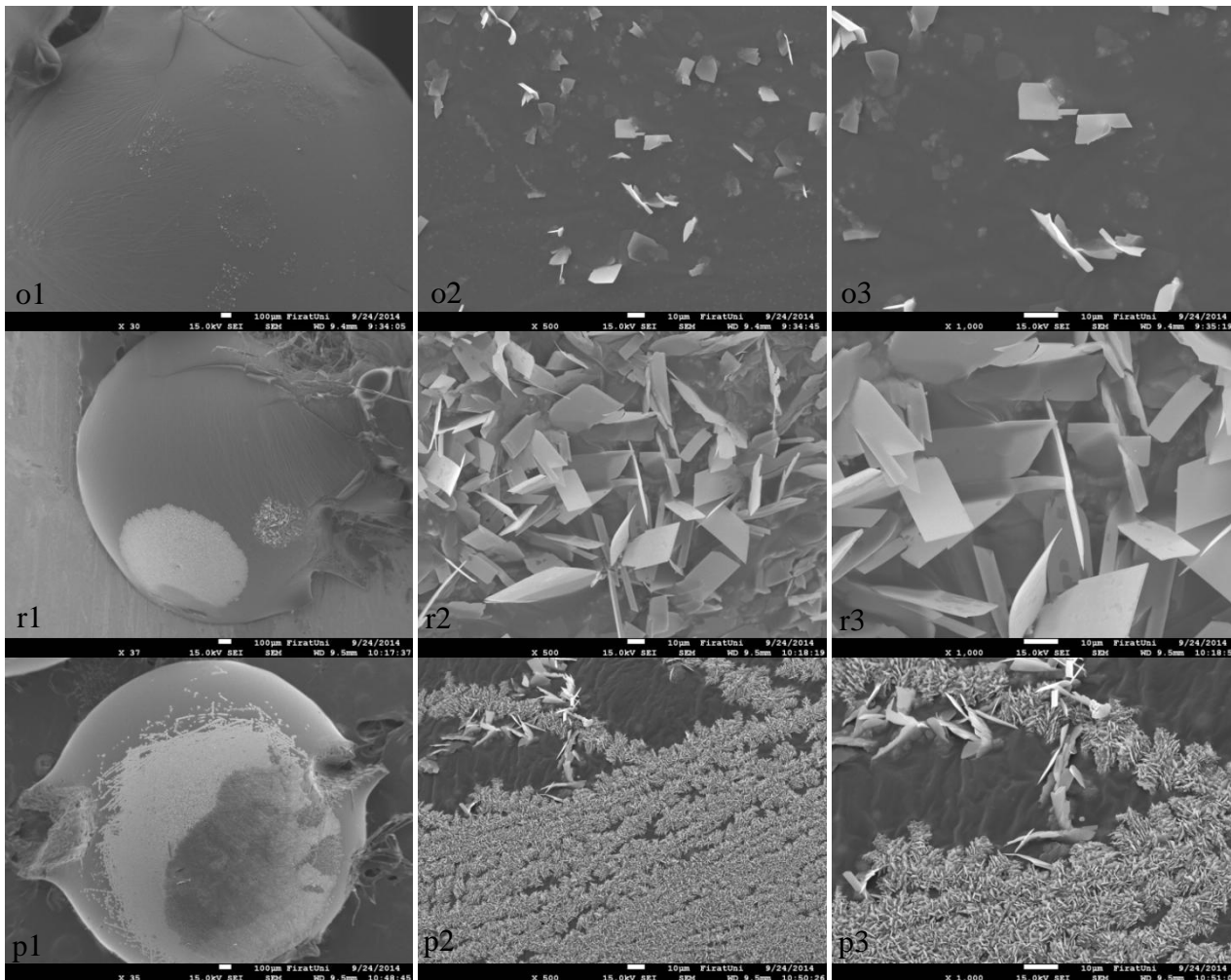
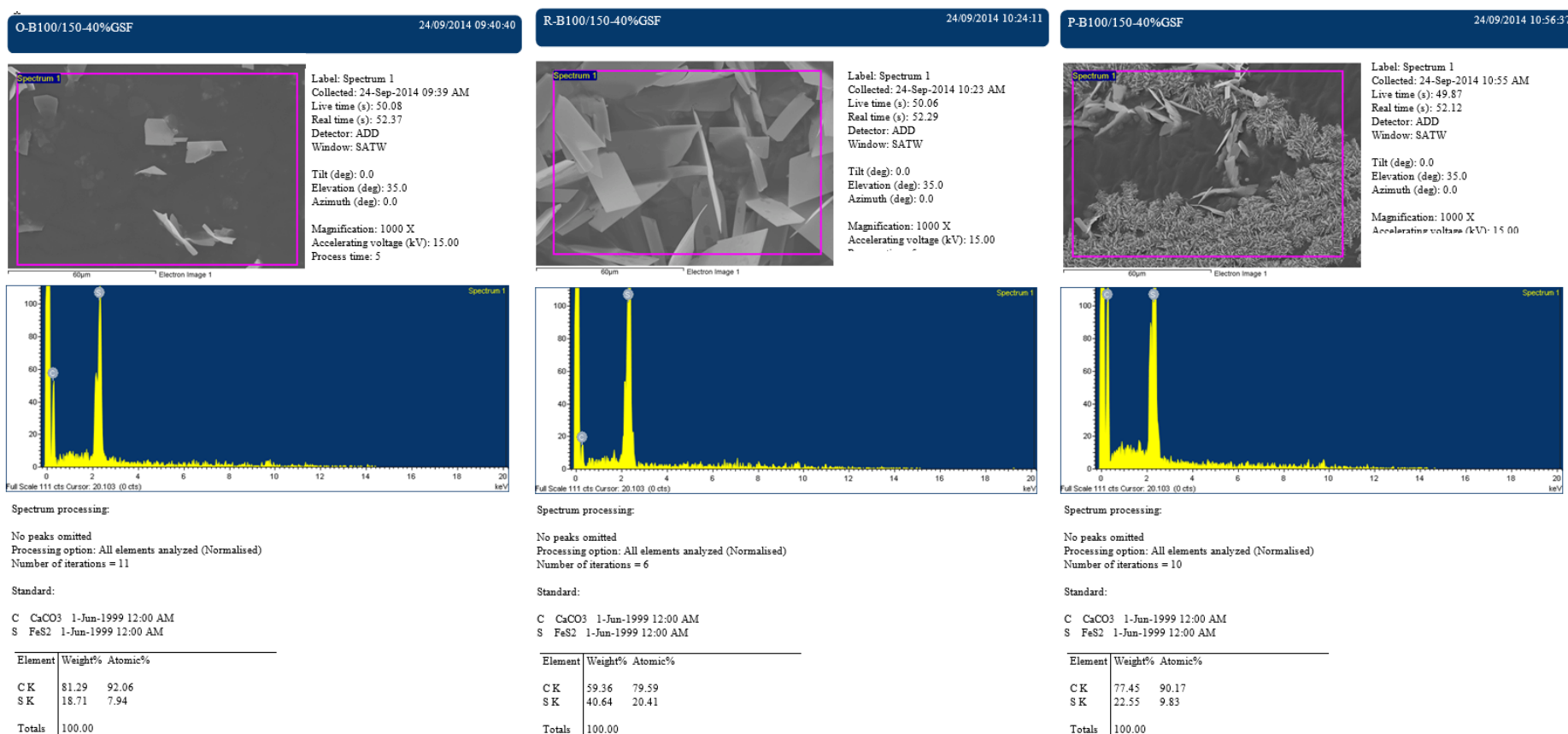


Figure A.33 : Showing images of B100/150-40%GSF (o1, o2 and o3 at the un-aged stage, r1, r2 and r3 at the RTFOT-aged stage and p1, p2 and p3 at the PAV-aged stage).



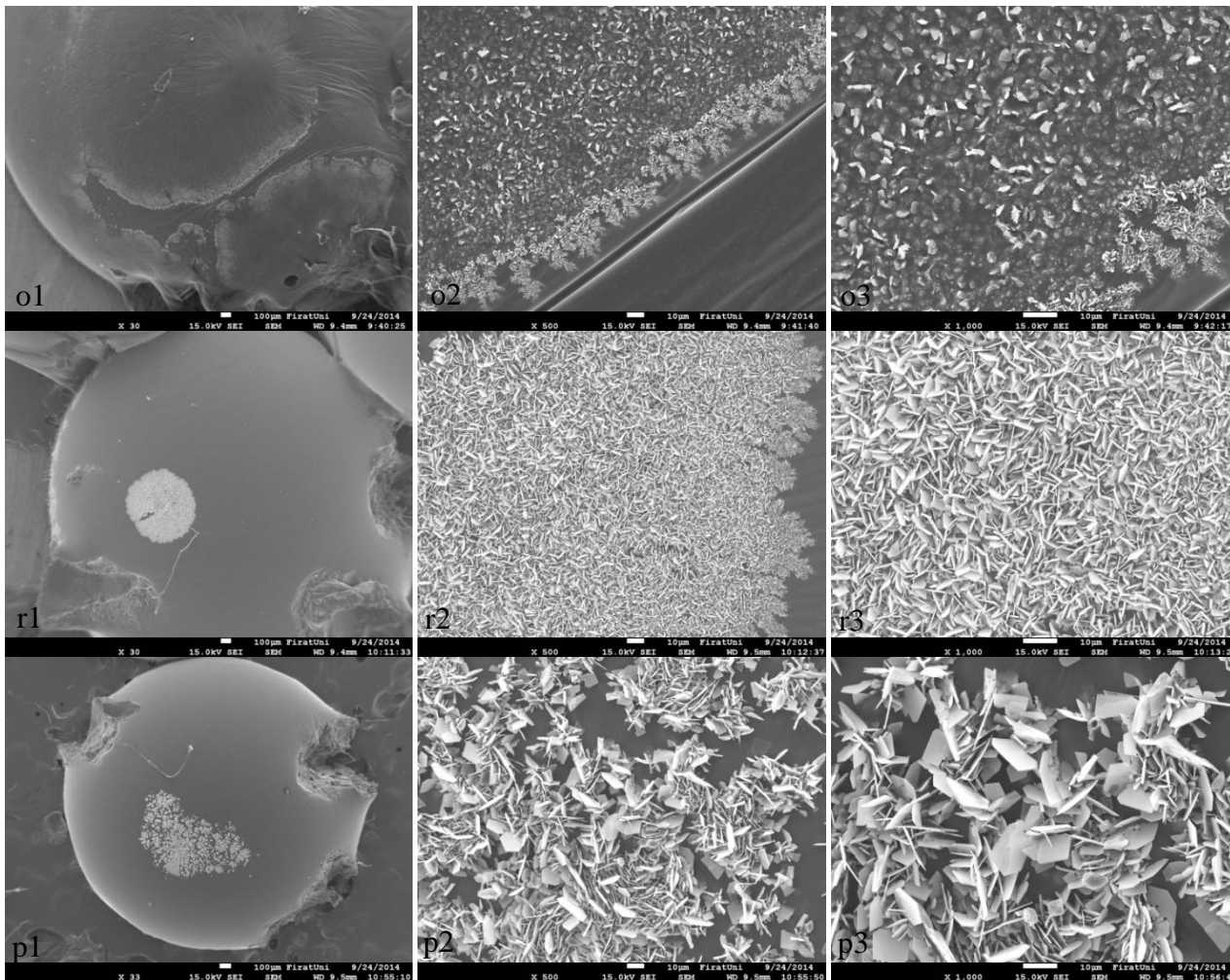


Figure A.35 : Showing images of B100/150-50%GSF (o1, o2 and o3 at the un-aged stage, r1, r2 and r3 at the RTFOT-aged stage and p1, p2 and p3 at the PAV-aged stage).

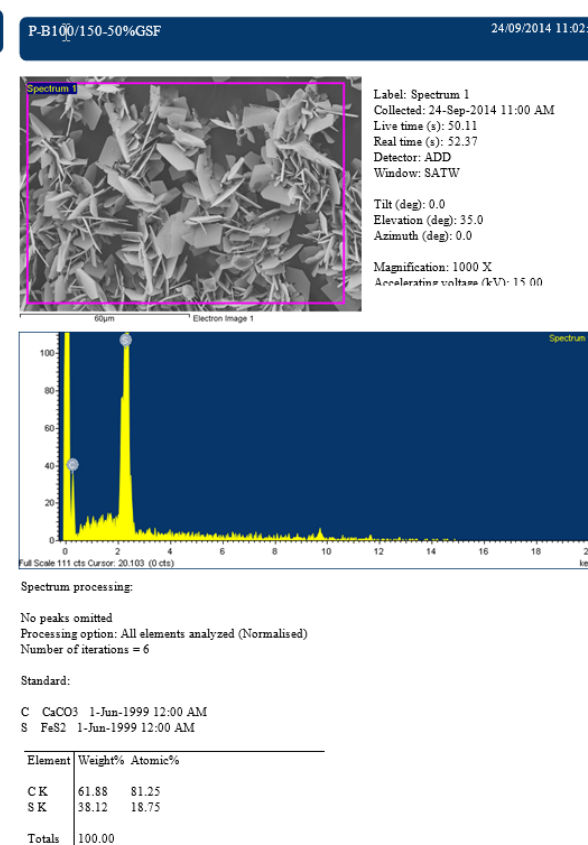
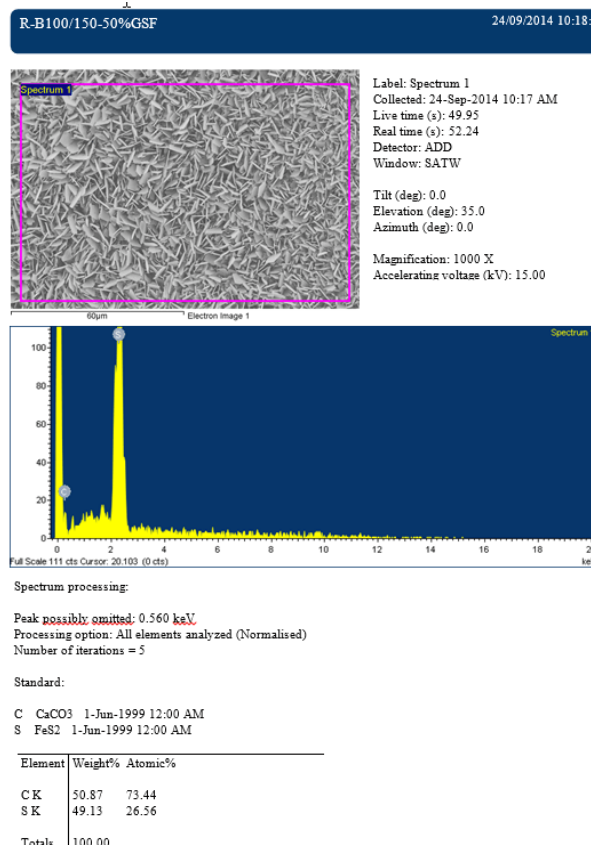
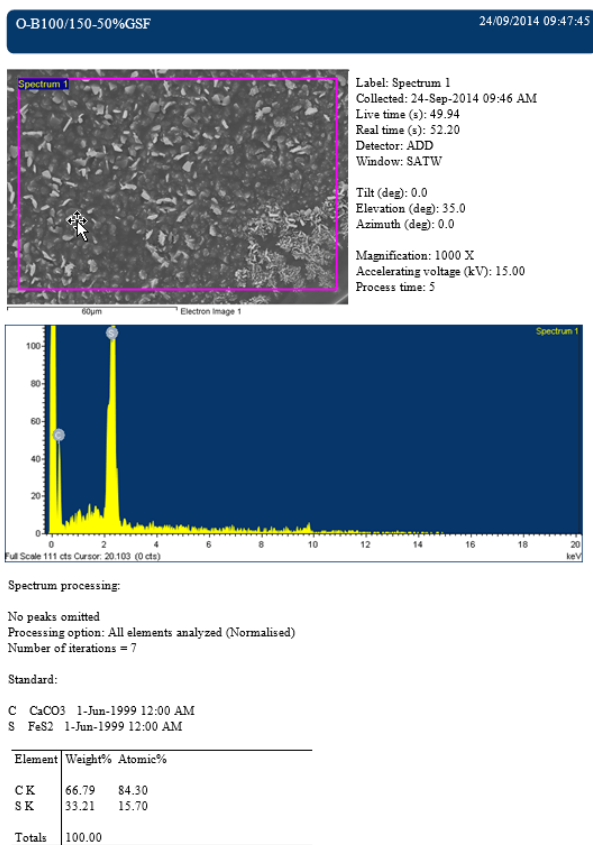


Figure A.36 : Showing element analysis of B100/150-50%GSF.

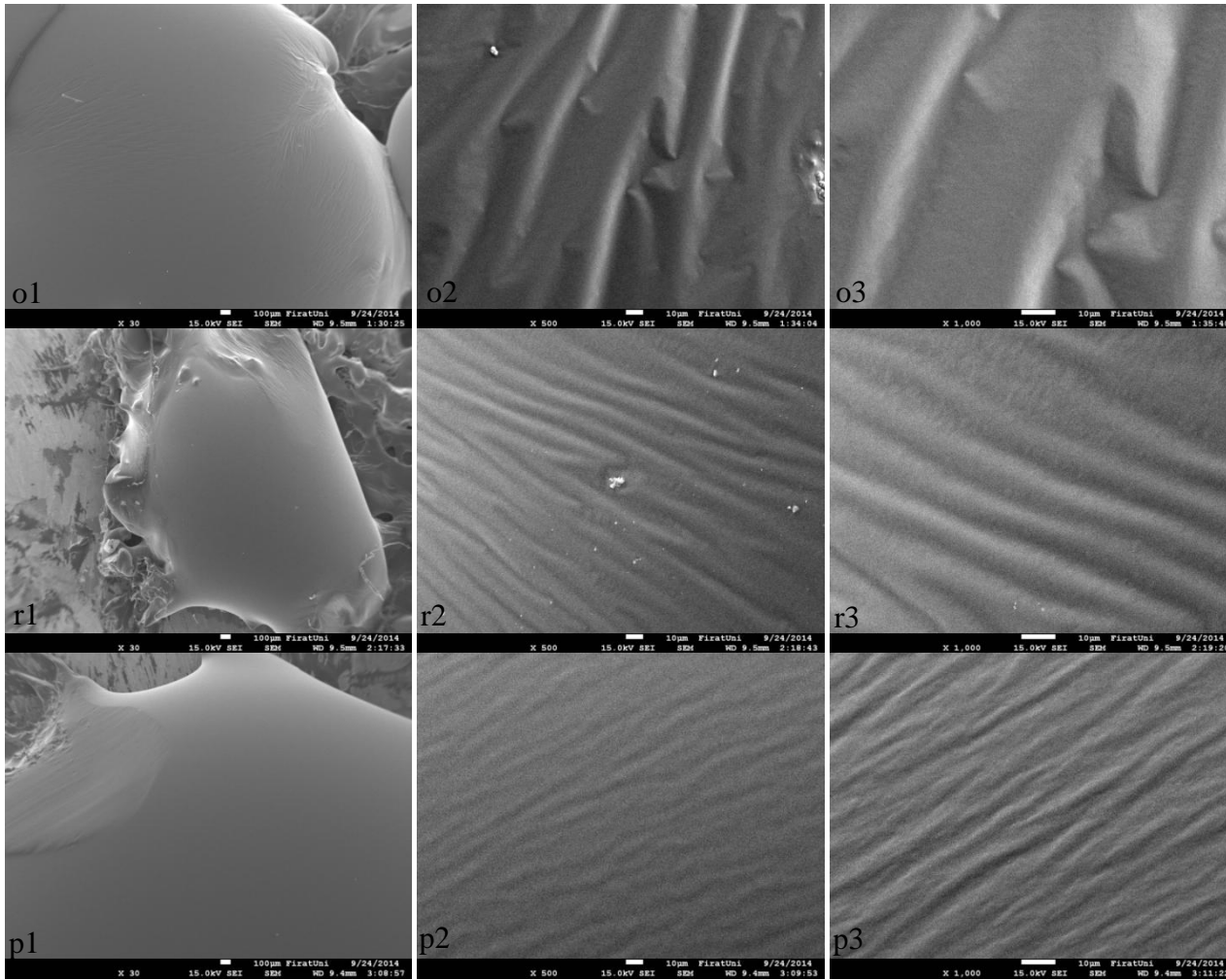


Figure A.37 : Showing images of B160/220-0% GSF (o1, o2 and o3 at the un-aged stage, r1, r2 and r3 at the RTFOT-aged stage and p1, p2 and p3 at the PAV-aged stage).

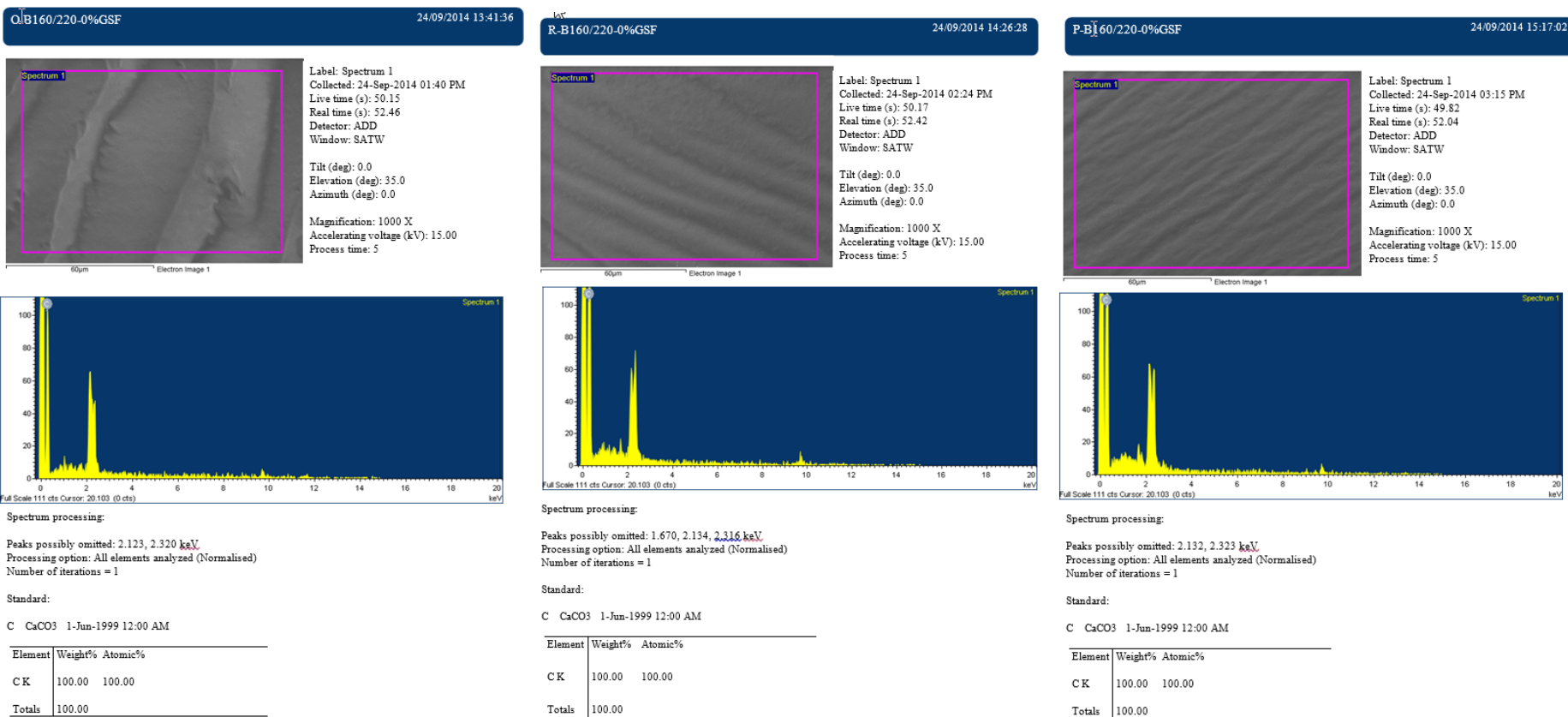


Figure A.38 : Showing element analysis of B160/220-0%GSF.

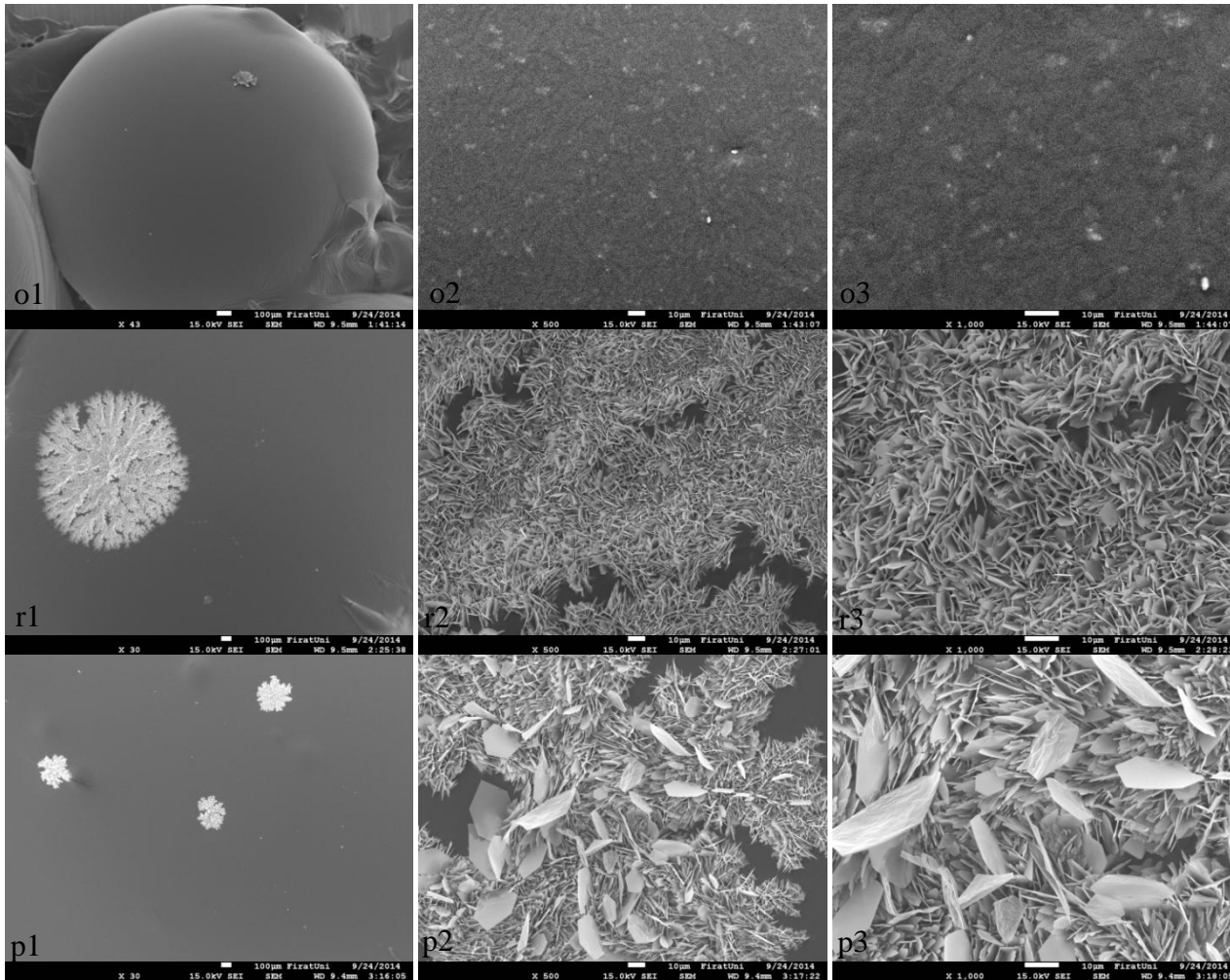
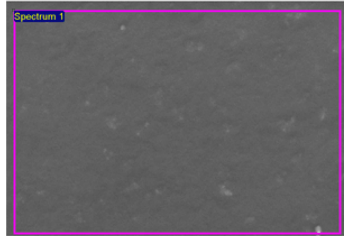


Figure A.39 : Showing images of B160/220-10%GSF (o1, o2 and o3 at the un-aged stage, r1, r2 and r3 at the RTFOT-aged stage and p1, p2 and p3 at the PAV-aged stage).

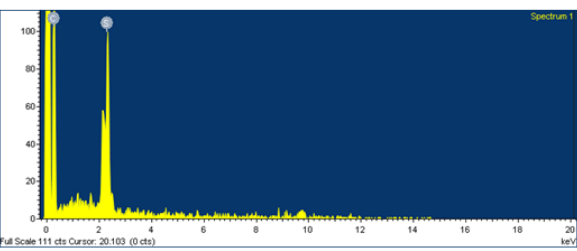
O-B160/220-10%GSF 24/09/2014 13:49:41



Label: Spectrum 1
Collected: 24-Sep-2014 01:48 PM
Live time (s): 50.08
Real time (s): 52.35
Detector: ADD
Window: SATW

Tilt (deg): 0.0
Elevation (deg): 35.0
Azimuth (deg): 0.0

Magnification: 1000 X
Accelerating voltage (kV): 15.00
Process time: 5



Spectrum processing:

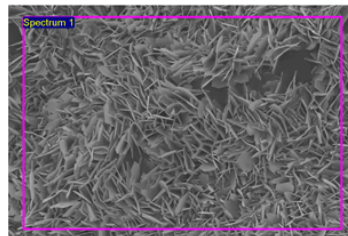
No peaks omitted
Processing option: All elements analyzed (Normalised)
Number of iterations = 12

Standard:

C CaCO₃ 1-Jun-1999 12:00 AM
S FeS₂ 1-Jun-1999 12:00 AM

Element	Weight%	Atomic%
CK	88.36	95.30
SK	11.64	4.70
Totals	100.00	

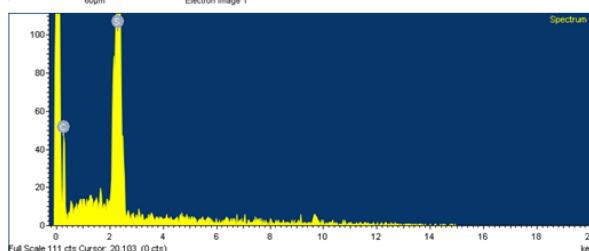
R-B160/220-10%GSF 24/09/2014 14:33:46



Label: Spectrum 1
Collected: 24-Sep-2014 02:32 PM
Live time (s): 50.20
Real time (s): 52.48
Detector: ADD
Window: SATW

Tilt (deg): 0.0
Elevation (deg): 35.0
Azimuth (deg): 0.0

Magnification: 1000 X
Accelerating voltage (kV): 15.00
Process time: 5



Spectrum processing:

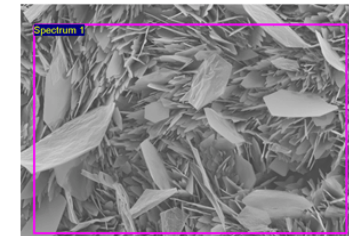
Peak possibly omitted: 1.640 keV
Processing option: All elements analyzed (Normalised)
Number of iterations = 6

Standard:

C CaCO₃ 1-Jun-1999 12:00 AM
S FeS₂ 1-Jun-1999 12:00 AM

Element	Weight%	Atomic%
CK	60.03	80.04
SK	39.97	19.96
Totals	100.00	

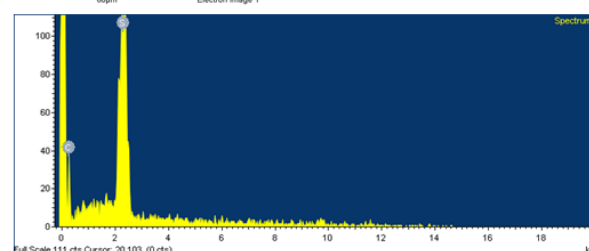
P-B160/220-10%GSF 24/09/2014 15:23:36



Label: Spectrum 1
Collected: 24-Sep-2014 03:22 PM
Live time (s): 49.74
Real time (s): 52.12
Detector: ADD
Window: SATW

Tilt (deg): 0.0
Elevation (deg): 35.0
Azimuth (deg): 0.0

Magnification: 1000 X
Accelerating voltage (kV): 15.00
Process time: 5



Spectrum processing:

No peaks omitted
Processing option: All elements analyzed (Normalised)
Number of iterations = 5

Standard:

C CaCO₃ 1-Jun-1999 12:00 AM
S FeS₂ 1-Jun-1999 12:00 AM

Element	Weight%	Atomic%
CK	55.63	77.00
SK	44.37	23.00
Totals	100.00	

Figure A.40 : Showing element analysis of B160/220-10%GSF.

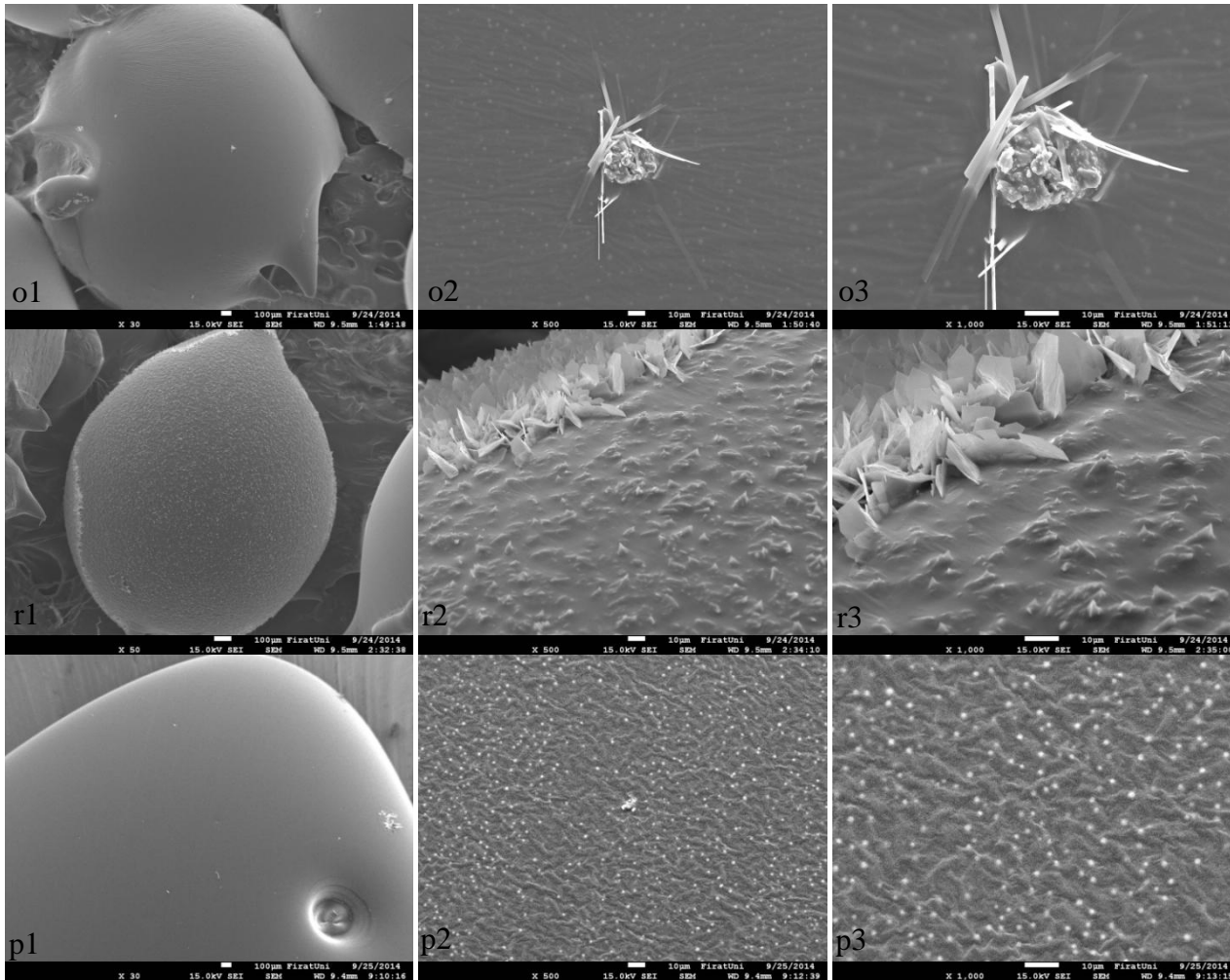
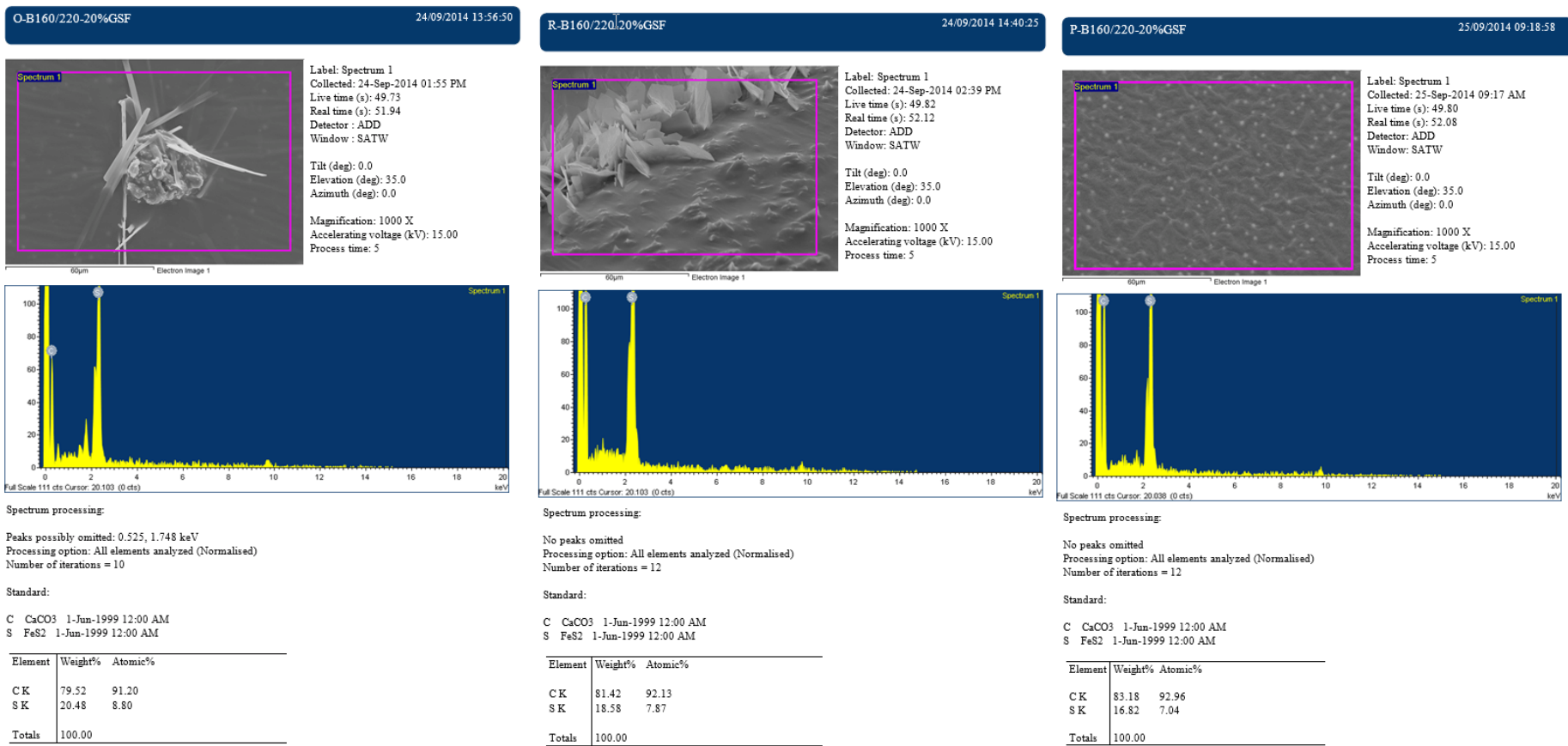


Figure A.41 : Showing images of B160/220-20%GSF (o1, o2 and o3 at the un-aged stage, r1, r2 and r3 at the RTFOT-aged stage and p1, p2 and p3 at the PAV-aged stage).



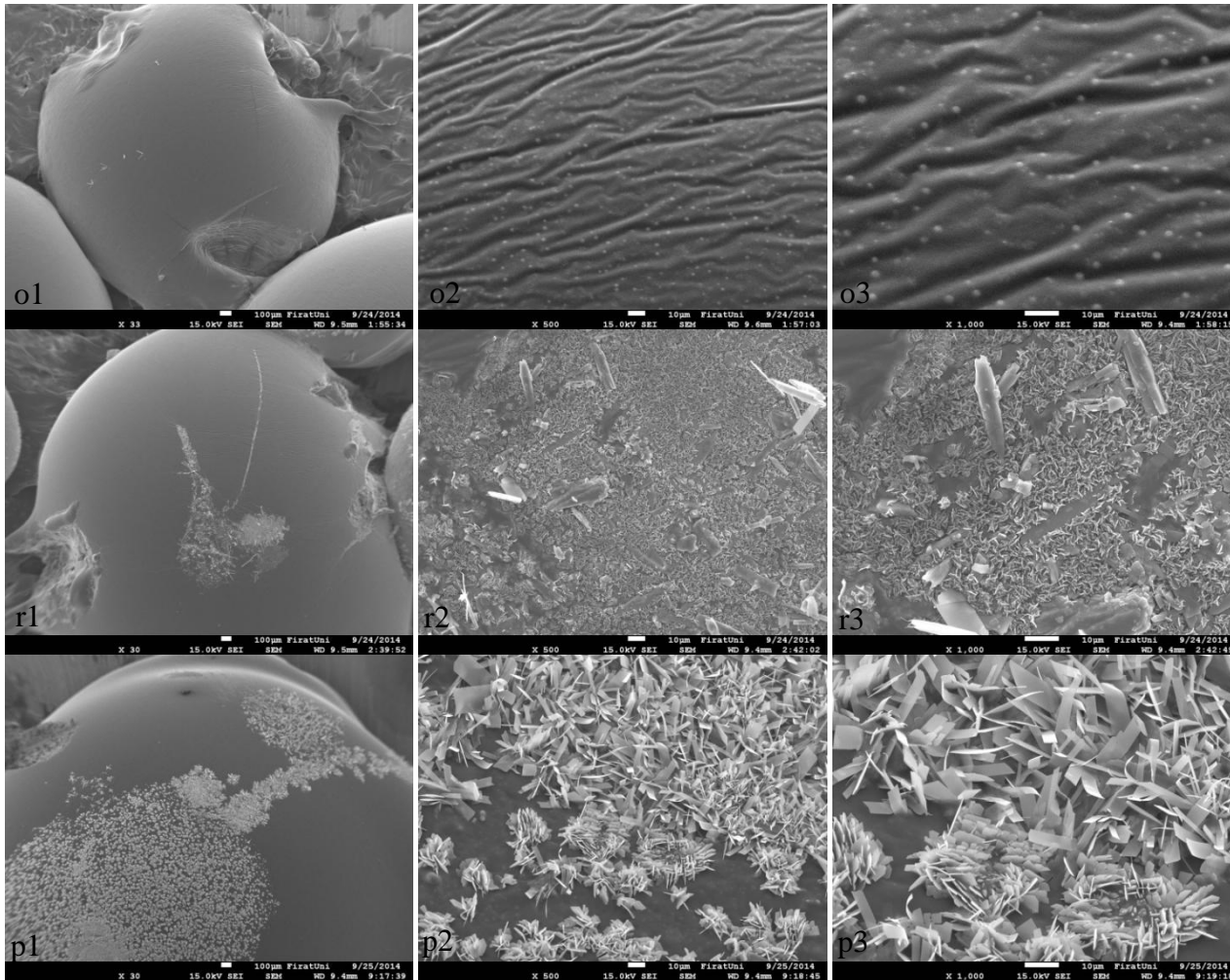


Figure A.43 : Showing images of B160/220-30% GSF (o1, o2 and o3 at the un-aged stage, r1, r2 and r3 at the RTFOT-aged stage and p1, p2 and p3 at the PAV-aged stage).

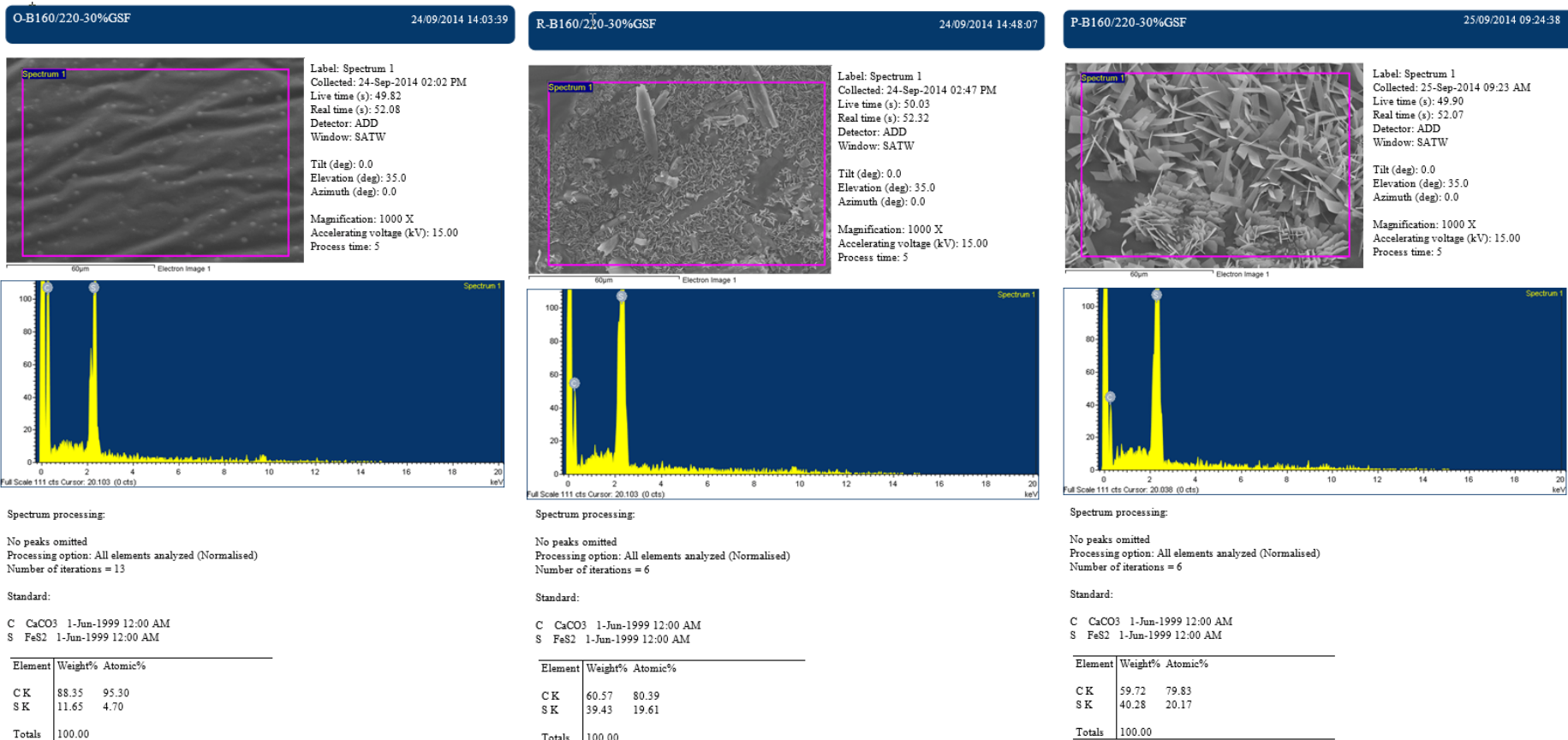


Figure A.44 : Showing element analysis of B160/220-30%GSF.

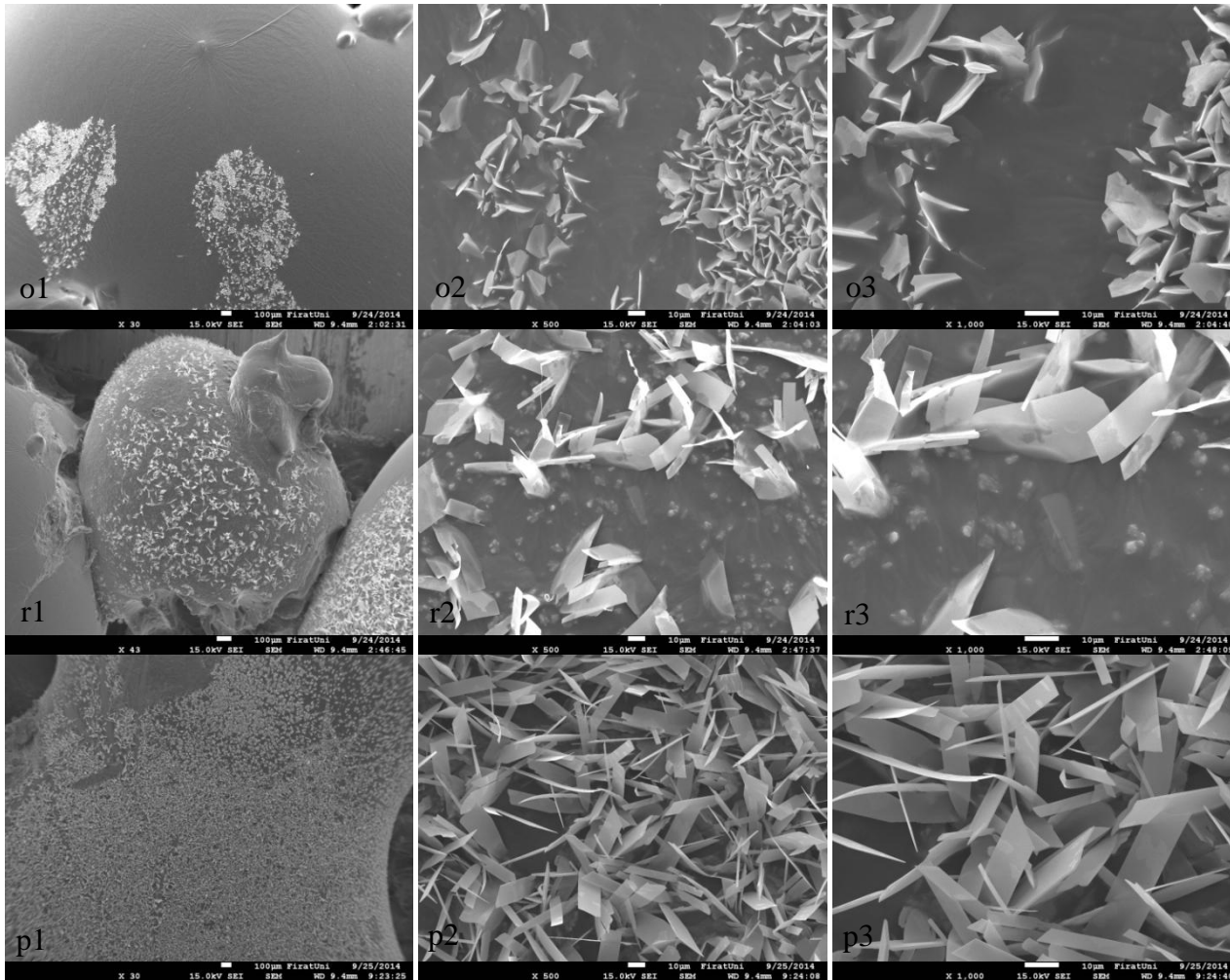


Figure A.45 : Showing images of B160/220-40% GSF (o1, o2 and o3 at the un-aged stage, r1, r2 and r3 at the RTFOT-aged stage and p1, p2 and p3 at the PAV-aged stage).

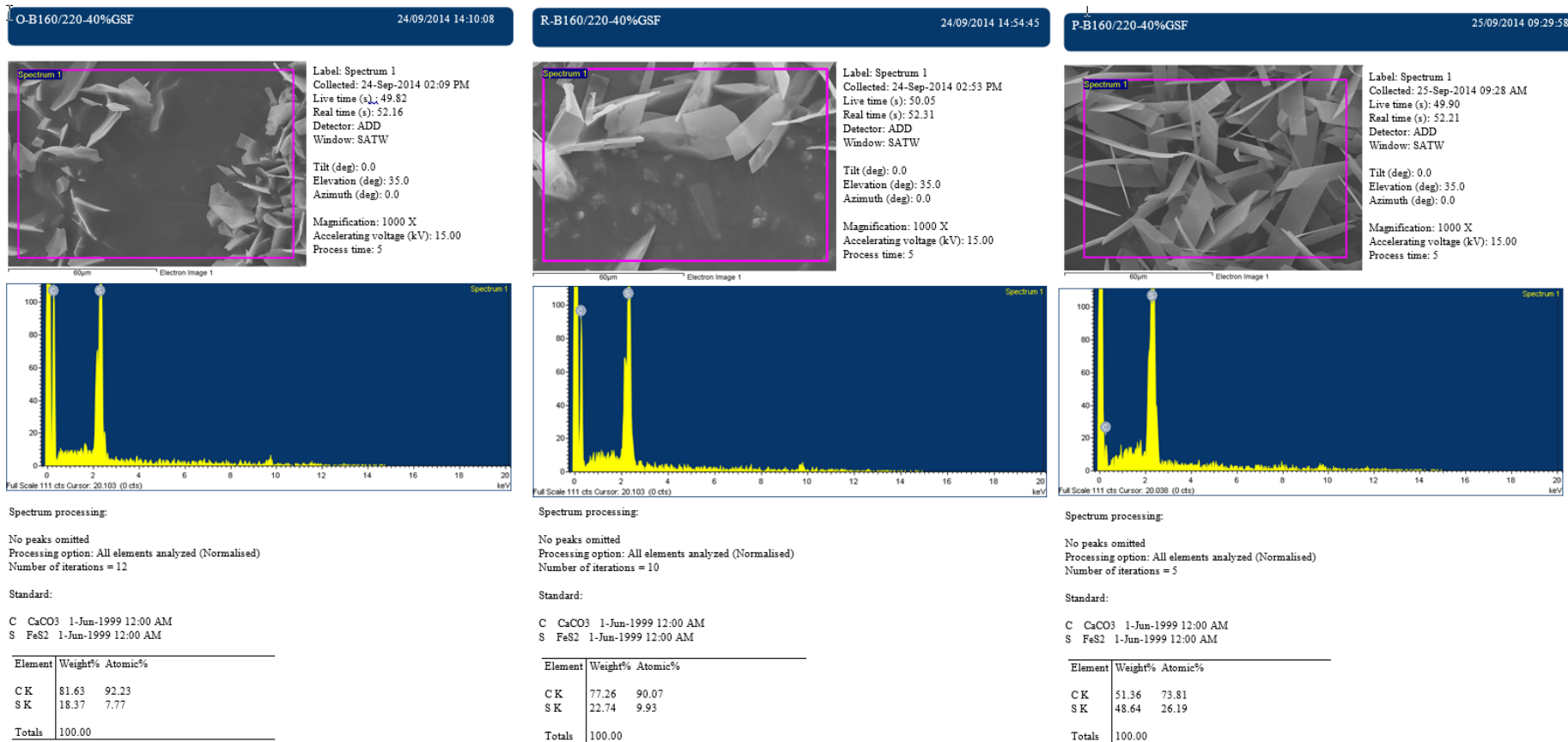


Figure A.46 : Showing element analysis of B160/220-40%GSF.

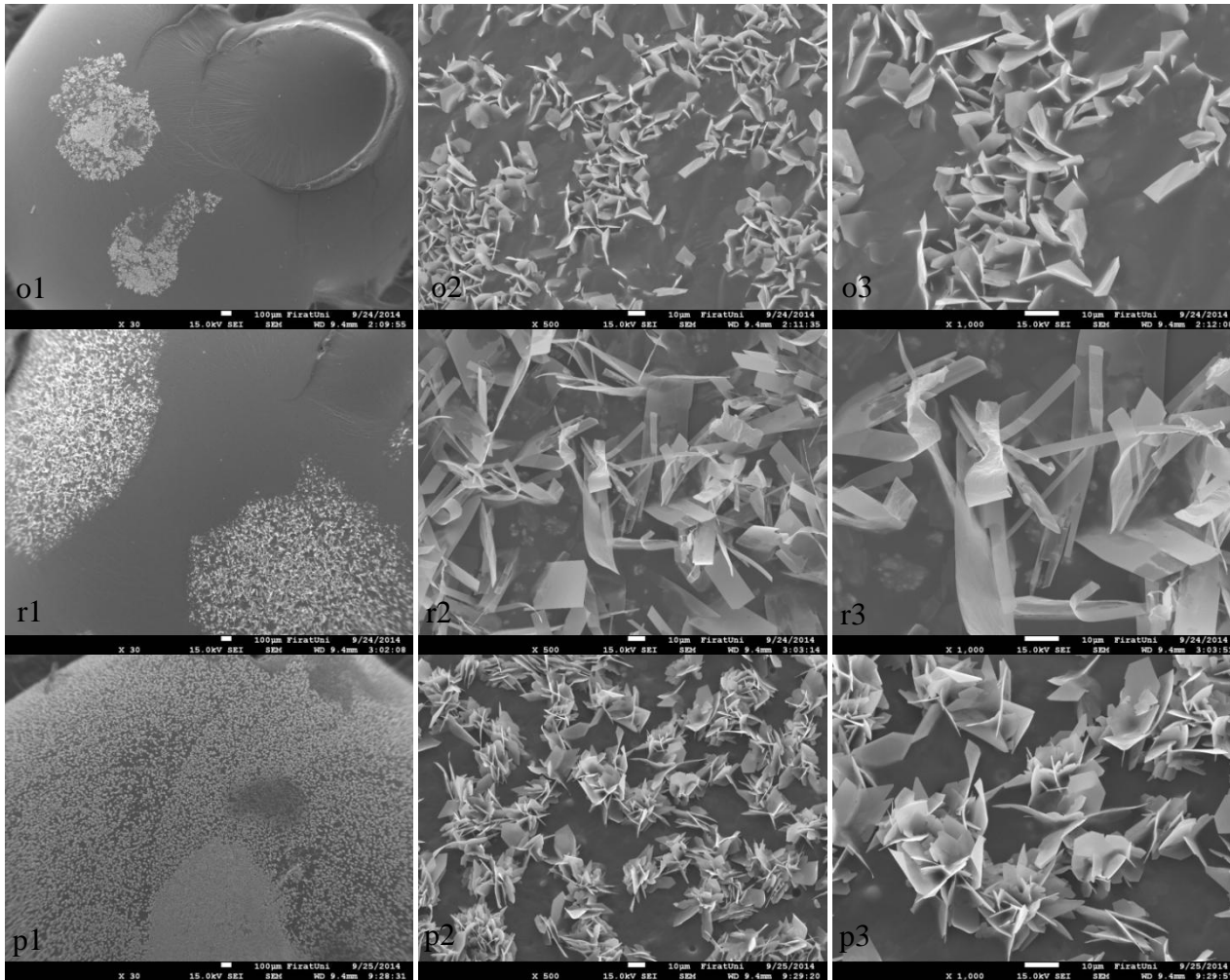


Figure A.47 : Showing images of B160/220-50%GSF (o1, o2 and o3 at the un-aged stage, r1, r2 and r3 at the RTFOT-aged stage and p1, p2 and p3 at the PAV-aged stage).

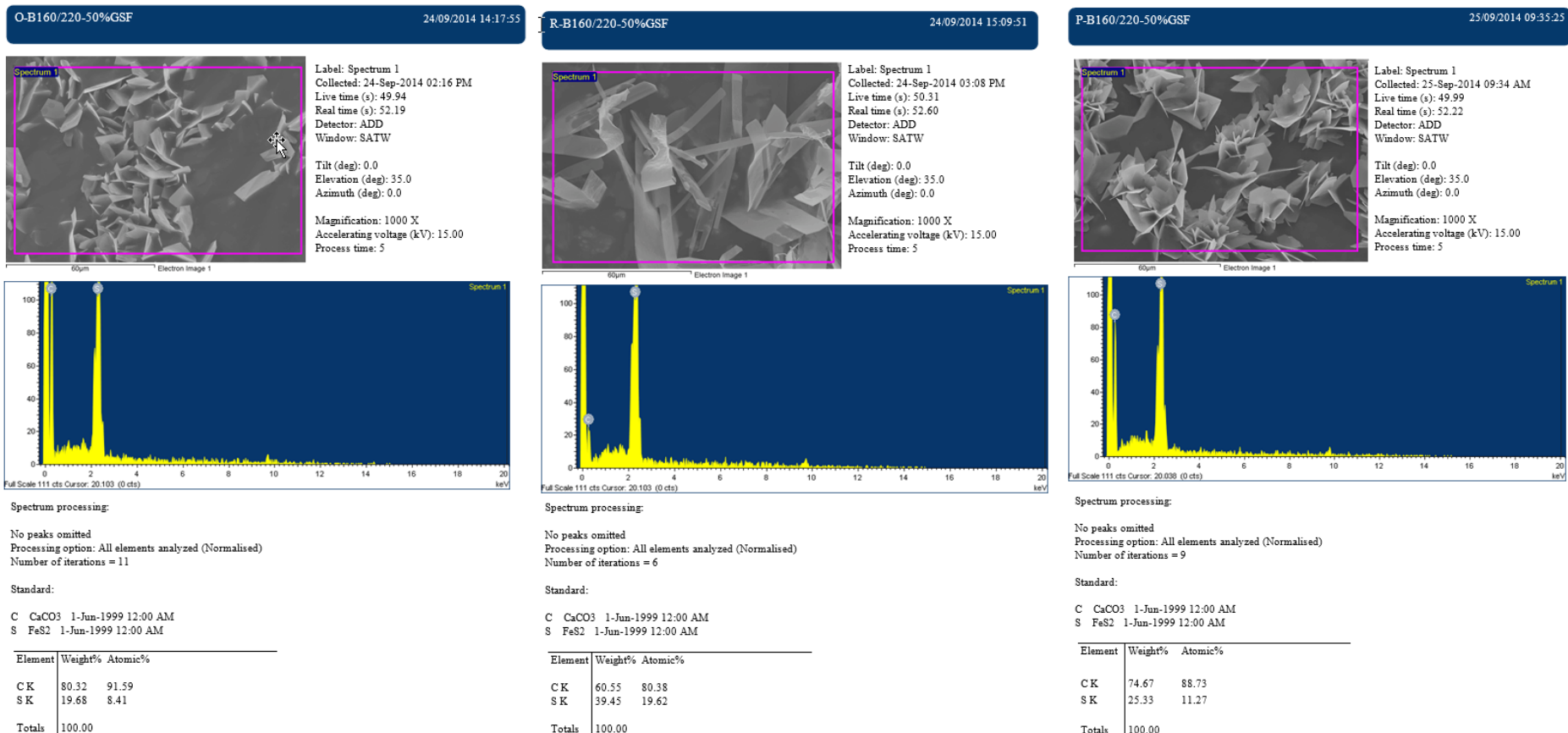


Figure A.48 : Showing element analysis of B160/220-50%GSF.

CURRICULUM VITAE



Name Surname: Abdulgazi GEDIK

Place and Date of Birth: Elazig 15.04.1982

E-Mail: gedikab@hotmail.com

EDUCATION:

B.Sc.: 2005, Istanbul Technical University (ITU), Civil Engineering

M.Sc.: 2008, Istanbul Technical University (ITU), Transport Engineering Program

PROFESSIONAL EXPERIENCE AND REWARDS:

I have been working as a field quality engineer for Turkish Directorate of Highways (KGM) since 2007.

PUBLICATIONS, PRESENTATIONS AND PATENTS ON THE THESIS:

Gedik, A. and Lav, A. (2013). Sulphur Utilization in Asphaltic Concrete Pavements, Proceedings of the 2013 Airfield & Highway Pavement Conference, Los Angeles, California, June 9-12, 2013, pp. 1175-1191, doi: 10.1061/9780784413005.099

Gedik, A. and Lav, A. (2016). "Determining Optimum Sulfur Content as Alternative Binder Additive in Asphaltic Concrete Pavements." *Journal of Materials in Civil Engineering*, doi: 10.1061/(ASCE)MT.1943-5533.0001527, 04016040

Gedik, A. and Lav, A. (2016). "Analytical, Morphological and Rheological Behavior of Sulphur-Extended-Binder." *Canadian Journal of Civil Engineering*, doi: 10.1139/cjce-2015-0409

